TECHNICAL **EBOOK**

cadence®



# RF Electronics: Design and Simulation

## Featuring Cadence AWR Software

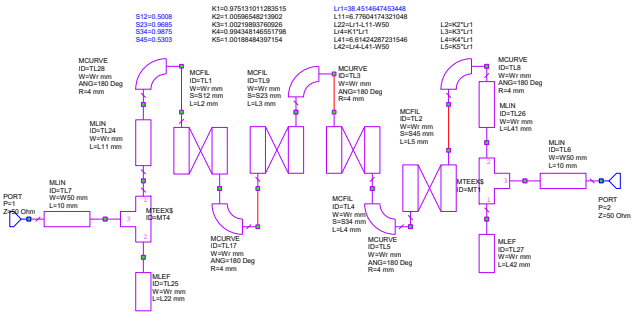
This eBook is a comprehensive RF design course, including lecture notes and lab examples, intended for final year undergraduate or masters students. The materials cover RF simulation, transformers, transmission lines, mixers, oscillators, filters, and amplifiers.

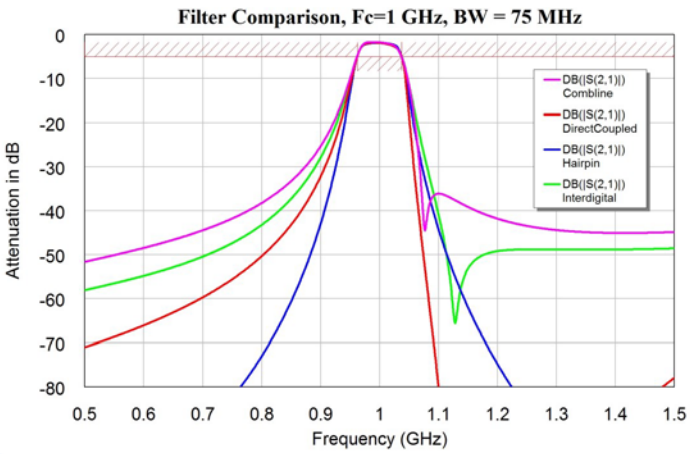
## Contents

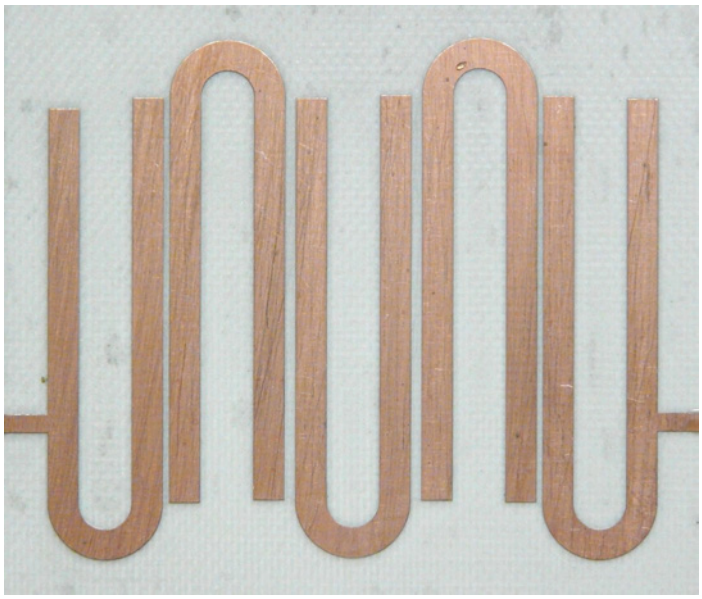

Chapter 1: Introduction ..... 1
Chapter 2: Chapter Computer Simulation ..... 5
Chapter 3: Transformers and Hybrids ..... 50
Chapter 4: Transmission Line Transformers and Hybrids ..... 64
Chapter 5: Frequency Mixers ..... 109
Chapter 6: Oscillators ..... 173
Chapter 7: RF Filters ..... 208
Chapter 8: Amplifiers: Stability, Noise and Gain ..... 275
Chapter 9: Impedance Matching of Power Amplifiers ..... 304
Chapter 10: Operational Amplifiers ..... 340
Chapter 11: Circuit Manufacture ..... 364
Appendix 1: Importing Local Vendor and XML Libraries ..... 385
Appendix 2: Producing Graphs using AWR DE ..... 389

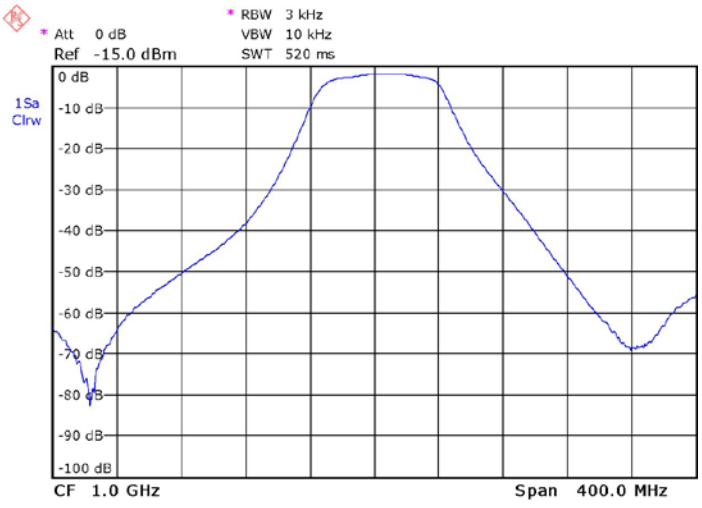
# RF Electronics:

## Design and Simulation








Cornelis J. Kikkert

James Cook University

Townsville, Queensland, Australia

# **RF Electronics** Design and Simulation

**Publisher: James Cook University, Townsville, Queensland, Australia, 4811. http://www.jcu.edu.au**

**2022 Edition, Copyright © 2022 C. J. Kikkert, ISBN 978-0-6486803-9-0.**

This is 4th edition of this book. The earlier editions were: The 2018 edition, ISBN 978-0-9954470-8-0, the 2015 Edition, ISBN 978-0-9942333-0-1 and the 2013 edition, ISBN 978-0-9873109-3-4.

**All rights reserved. No part of this publication may be reproduced or distributed, in any form or by any means, without the prior permission of Cornelis J. Kikkert.**

All web pages linked from the references were accessed and checked to be correct in May 2022.

The accompanying AWR DE project files are also Copyright © 2022 C. J. Kikkert, ISBN 978-0-6486803-9-0. All or part of their content may also be copyrighted under earlier editions of this book. C. J. Kikkert grants readers of this book permission to use these project files and to modify them, in order to gain an understanding of the material presented in this publication. The text contained in the “Design Notes” of the project files may not be altered or removed from the project files.

The mentioning of any commercial companies in this book is not done as an endorsement. They are mentioned purely in order to better describe the material presented in this book.

Cadence Design Systems Inc. (owners of AWR) has been given a licence to distribute this publication and the accompanying project files through the University Program of Cadence AWR. For details, please see their web site

https://www.cadence.com/en_US/home/company/cadence-academic-network/educators/education-kits.html#rf

A catalogue record for this book is available from the James Cook Library.

# RF Electronics

## Design and Simulation

**Cornelis J. Kikkert**

James Cook University

Townsville, Queensland, Australia

2022 Edition

# Contents


Page

**Preface** III

Contents III
Preface X
Acknowledgement XI
About the Author XII

**Chapter 1: Introduction** 1

RF Electronics Design 1
Computer Simulation 3
References 4

**Chapter 2: Computer Simulation** 5

Introduction 5
Basic Operation 6
Example 2.1: Low Pass Filter 6
Equations in AWR DE 10
Optimisation 11
Example 2.2: Diplexer 11
Device Models 16
Linear Models 16
Non-Linear Models 18
Example 2.3: Low Noise Amplifier 23
Determination of Transmission Line Parameters 24
Nonlinear Time Based Simulation 27
Time Domain Transient Circuit Simulation 28
Example 2.4: Buck DC-DC Converter 28
Harmonic Balance Circuit Simulation 33
Black Box Matching of Circuits to Measurements 35
Example 2.5: Bandpass T Matching Network 35
S Parameter Measurements 37
Impedance Measurements 40
Summary 48
References 48

**Chapter 3: Transformers and Hybrids** 50

Introduction 50
Wideband Transformers 51
Example 3.1: RF Transformer Design 52
Bifilar and Trifilar Windings 53
Transmission line transformers with ferrite cores 54
Transformer Hybrids 56
Power Combiner / Splitter 57
Wilkinson Transformer Hybrid 58
Example 3.2 Wilkinson Transformer Hybrid Design 59

| | Page |
|---|---|
| Transmission Line Hybrid with Ferrite Cores | 61 |
| Many Way Hybrids | 62 |
| References | 63 |
| **Chapter 4: Transmission Line Transformers and Hybrids** | **64** |
| Introduction | 64 |
| Example 4.1: Bandwidth Calculation | 65 |
| Wilkinson Transmission Line Hybrid | 67 |
| Compensated Wilkinson Hybrid | 72 |
| Unequal Split Wilkinson Hybrid | 73 |
| Wideband Wilkinson Hybrid | 73 |
| Example 4.2: 90 to 270 MHz Wilkinson Hybrid | 74 |
| Quarter Wave Hybrid or 1.5 λ Rat-race hybrid | 78 |
| Branchline Coupler | 80 |
| Backward Travelling Wave Hybrid | 88 |
| Edge Coupled Lines | 88 |
| Example 4.3: 20 dB Coupler | 89 |
| Lange Coupler | 93 |
| Broadside Coupled Lines | 94 |
| Example 4.4: 100 Watt 3 dB Broadside Coupler | 96 |
| Coaxial Couplers | 98 |
| Transmitter Power Meters | 98 |
| Transmission Line Baluns | 98 |
| Marchand Balun | 99 |
| Marchand Balun Realisation | 101 |
| Parallel Line Balun Realisation | 104 |
| Wireline and Wirepac Couplers | |
| References | 107 |
| **Chapter 5: Frequency Mixers** | **109** |
| Introduction | 109 |
| Definition of Terms | 110 |
| Conversion Loss | 110 |
| Isolation | 111 |
| Compression Point | 111 |
| Dynamic Range | 112 |
| Two-tone Third Order Intermodulation Distortion | 112 |
| Third Order Intercept Point | 113 |
| LO Level | 114 |
| Example 5.1: Mixer LO Level Calculation | 115 |
| Ideal Multiplier | 115 |
| Single Diode Mixer | 117 |
| Computer Simulation of Mixers | 119 |
| Balanced Mixer | 125 |
| Double Balanced Mixer | 129 |
| Mixer Terminations | 137 |
| Triple Balanced Mixer and High Level BDM | 140 |
| Microwave Mixers | 143 |

Page

Transmission line Balanced Mixer 144
Branchline Coupler Balanced Mixer 145
Basic Operation 146
Hardware Realisation 148
180°Hybrid Microwave DBM 153
Active Single Transistor Mixer 155
Frater-Gilbert Cell Active Mixer 156
Quadrature (IQ) Mixers 161
Active IQ Mixers 163
Image Reject Mixers 163
Passive IQ Mixers 166
Examples of Commercial Active Mixers 167
LTCC Mixers 168
MMIC Mixers 169
Other Mixers 169
Additional Resources 169
References 170
Abbreviations 171

**Chapter 6: Oscillators 173**

Principles of Oscillators 173
Oscillator Types 173
Positive Feedback Oscillators 173
Oscillator Design Process 174
Frequency Selective Networks 175
Colpitts Oscillator Design Procedure 176
Step 1: Select an amplifier type 176
Step 2: Design an amplifier 177
Step 3: Design a resonator 178
Step 4: Linear Oscillator Analysis 179
Step 5: Nonlinear Oscillator Analysis 179
Hartley Oscillator 182
Practical Inductors 186
Example 6.1: Low Phase Noise Oscillator Design 187
Low Phase Noise Colpitts Oscillator 187
Low Phase Noise Hartley Oscillator 188
Crystal Oscillators 190
Example 6.2: Crystal Oscillator Design 190
RF and Microwave Oscillators 193
Example 6.3: 1 GHz Microstrip Oscillator Design 194
Dual Resonator Oscillator 199
Design Improvements 201
Phase Locked Loops 205
Frequency Locked Loop 206
References 206

Page

**Chapter 7: RF Filters** 208

Introduction 208
Electrical Filters 208
Acoustic Filters 208
Filter Design Revision 208
Filter Tables 209
Butterworth Filters 210
Bessel Filter 212
Chebyshev Filter 213
Cauer-Chebyshev Filter 213
Reflectionless Filters 215
RF Lowpass Filter Design 219
Bandpass Filter Design 224
LC Bandpass Filters 224
Low-Pass to Band-Pass Transformation 224
LC Coupled Resonator Filter 225
HF Filters 231
Cauer-Chebyshev Bandpass Filters 233
Parallel Coupled-Line Filter 233
Example 7.1: 1 GHz, 70 MHz Bandwidth Filter 233
Hairpin Filter 236
Helical Filters 240
Example 7.2: 100 MHz, 1 MHz Bandwidth Filter 241
Interdigital Filters 244
Round Rod Interdigital Filters 245
PCB Interdigital Filters 246
Example 7.3: 1GHz, 70 MHz Bandwidth Filter 247
Direct Coupled Resonator Filters 252
Example 7.4: 1 GHz, 500 MHz Bandwidth Filter 253
Fine Tuning the Filter 255
Microstrip Filter Comparison 257
EM Simulation 262
Coaxial Filters 269
Ceramic Filters 272
SAW Filters 273
References 273

**Chapter 8: Amplifiers: Stability, Noise and Gain** 275

Introduction 275
MMIC 275
Requirement for Stability 277
Smith Chart Revision 277
Scattering Parameter Revision 278
Stability 280
Stability Circles 281
Unconditional Stability 282
Conditional Stability 282

| | Page |
|---|---|
| Stability Factors: Measures of Stability | 282 |
| Design for Maximum Gain | 283 |
| Amplifier Noise Figure | 283 |
| Examples | 284 |
| Example 8.1 BGB707 MMIC | 284 |
| Example 8.2 PMA-5453 MMIC | 289 |
| Example 8.3 Bipolar Transistor | 291 |
| Improving Amplifier Noise Figure and Stability | 295 |
| Bandwidth Limiting using Reflectionless Filters | 295 |
| Resistors at Output | 297 |
| Conclusion | 302 |
| References | 302 |
| Abbreviations | 302 |
| **Chapter 9: Impedance Matching of Power Amplifiers** | **304** |
| Introduction | 304 |
| RF Power Device Impedances | 304 |
| Large Signal Parameters | 305 |
| Types of Matching | 305 |
| Transformer Matching | 305 |
| LC Matching | 305 |
| Transmission Line Matching | 305 |
| Choice of Components and Q value | 305 |
| LC Matching | 306 |
| PI Network | 307 |
| Low Pass T Network | 308 |
| Bandpass L Network | 309 |
| Bandpass T Network | 309 |
| Capacitive Impedance Transformer | 310 |
| Example 9.1: 150 MHz, 35W Amplifier | 311 |
| PI Network | 313 |
| Low Pass T Network | 314 |
| Bandpass L Network | 314 |
| Bandpass T Network | 315 |
| Capacitive Impedance Transformer | 315 |
| Transformer Matching | 317 |
| Transmission-Line Matching | 318 |
| Broadband Matching | 320 |
| Example 9.2: Broadband Amplifier Using S Parameters | 324 |
| Example 9.3: Broadband Amplifier Using Device Models | 332 |
| References | 339 |
| **Chapter 10: Operational Amplifiers** | **340** |
| Introduction | 340 |
| Voltage Feedback Theory | 340 |
| Current Feedback Theory | 241 |
| Current and Voltage Feedback Amplifier Comparison | 342 |
| Example 10.1: High Impedance 0.01 - 20MHz Amplifier | 343 |

| | Page |
|---|---|
| High Impedance Input Stage | 344 |
| Other OpAmp Stages | 346 |
| Hardware Realisation | 348 |
| Amplifier Protection | 349 |
| Low Noise Designs using Operational Amplifiers | 351 |
| Example 10.2: Amplifier Design for Noise Performance | 297 |
| Oscillator using Operational Amplifiers | 357 |
| Limitation of Simulations | 362 |
| References | 363 |
| **Chapter 11: Circuit Manufacture** | **364** |
| Introduction | 364 |
| Subtractive Process: Conductive Track Removal | 364 |
| Additive Process: Depositing Tracks and Vias | 364 |
| Printed Circuit Board Materials | 365 |
| Conventional PCB Substrates | 365 |
| Paper and Resin Substrates; FR2 and FR3 | 365 |
| Fibreglass and Epoxy Substrates; FR4, FR408, IS400 | 366 |
| Microwave and RF Printed Circuit Board Materials | 367 |
| RT/duroid | 367 |
| RO3000 and RO3200 (PTFE/Ceramic Laminates) | 368 |
| RO4000 | 368 |
| Other Laminates | 369 |
| Multilayer Boards | 369 |
| Non-Clad Substrates | 370 |
| Alumina Substrates | 370 |
| Other Substrates | 371 |
| Manufacturing | 371 |
| Layout Hints | 371 |
| Etching | 372 |
| Manufacturing using a PCB Milling Machine | 373 |
| Manufacturing using Laser Ablation | 373 |
| Thin Film | 373 |
| Thick Film | 375 |
| Printing Screens | 375 |
| Pastes (Inks) | 376 |
| RF Applications of Thick Film Circuits | 377 |
| Manufacturing using 3D printing | 377 |
| Low Temperature Cofired Ceramic (LTCC) | 379 |
| MMIC Fabrication | 380 |
| References | 382 |
| **Appendix 1: Importing Local Vendor and XML Libraries** | **385** |
| Local Vendor Libraries | 385 |
| Importing Spice Device Models | 386 |
| References | 388 |

Page

**Appendix 2: Producing Graphs using AWR DE** **389**

Generating Plots 389

References 392

# Preface

The material presented in this book evolved from teaching analogue electronics courses at James Cook University (JCU) over many years. When I started teaching, electronics design, computer simulation tools were non-existent and most of the design optimisation was done by replacing components in hardware. It was a big step forward when EESOF became available in the mid 1980's. The computer simulation tools have progressed enormously since then. Early in my career, I was given the following advice for designing electronic circuits. "Get the circuit to work and then start taking components out. Put back the one that stops the circuit from working." This is a silly statement, since in a proper design removing any component will stop if from working, but it does illustrate the goal of any designer: *Design a circuit that will work first time, according to specification. It must do so reliably and at as low a cost as possible.* Since labour is expensive, the circuits also should not require any adjustments after manufacture in order that they meet the specifications.

Using the computer simulation used in this book, we can now design our analogue electronic circuits such that they satisfy all these conditions. We can change active device parameters in the simulation, to ensure that variations in performance during manufacturing do not cause the circuit to fail to meet the specifications. We can check that the circuit will meet specifications under any permitted temperature, power supply and input signal variations. For RF circuits, we can, by simulation, change microwave PCB substrates for lower cost FR4 type substrates to verify if the circuit still performs correctly with the lower cost substrate. For consumer or space critical applications, the computer simulation tools used in this book will allow Low Temperature Cofired Ceramic (LTCC) or MMIC circuits to be designed. With those circuits, one cannot open them up to change components. They must be correct right from the start.

During the last 20 years, much of the analogue electronics in radio and TV receivers has been replaced with digital electronics, causing a change in the operating frequency of analogue electronic designs. There has been a rapid growth in the number of radio transmitters and receivers used. Many developed countries now have more mobile phones than people. Most smart-phones and computers use WLAN/WiFi to access the internet. WLAN/WiFi, Bluetooth, Wireless Gigabit, WiMax, Zigbee, W-CDMA, LTE and 5G are all relatively new communication systems using microwave (above 1 GHz) frequency bands. At present, there is a rapid growth in automotive radars for collision prevention and autonomous vehicle operation. IoT and Electricity Demand Side Management will result in most consumer devices having WiFi or similar communication technology, to control their operation or advise the owner of a fridge that the milk bottle is empty. Because of increasing demand for radio spectrum, the operating frequencies are getting higher and the transmitters need to have a higher spectral cleanliness.

This explosion in microwave system applications requires a matching RF and microwave electronic design capability from our engineers. More stringent filtering is required and less intermodulation distortion is permitted from amplifiers, to ensure systems do not interfere with each other. 20 years ago, most electronic designs using microwave frequencies were for military, instrumentation, or high-end communication applications, such as microwave radio links operated by Telcos. Now most microwave designs are for consumer applications. As a result, the emphasis on reducing the cost of both the circuit and the design has become more important. RF and microwave circuit simulation play a significant part in this cost reduction.

It is important for Universities to realise however, that computer simulation of an electronic design is not the end-point, but only a step in the realisation of the production of hardware that operates as required. That is why in this book, firstly computer simulation has been used to enhance the understanding by students and designers of the properties and limitations of their designs, and secondly many photographs and measured performance of the hardware realisation of these designs presented have been included. I hope that the material presented in this book will increase the RF and microwave design skills of many students and practicing designers.

This whole book is suitable for teaching RF and microwave electronic design in the final year of an undergraduate Bachelor Degree program or as a course in a postgraduate program. Chapter 2 can be used at earlier years of a Bachelor Degree program to teach the principles of computer simulation, the design of analogue electronic circuits and passive circuit analysis. These computer simulation techniques are not limited to RF and Microwave frequencies. For that reason, chapter 2 includes examples operating below 100 kHz. The modelling of mains (50/60 Hz) power distribution transformers, described in chapter 2, could not have been done without the optimisation capability of AWR DE.

Unless otherwise indicated, any of the hardware shown in photographs, have been designed by the author and produced by him with assistance from JCU and technical staff. There are some photos of hardware from unknown manufacturers (UM). Those have been labelled with (UM).

This fourth (2022) edition includes new material on couplers, mixers and advances in 3D printing of PCB's and Device models, as well as many other updates, such as changing examples to use currently available devices. A new appendix on plotting using AWR DE is also included. As a result, this edition is 66 pages larger than the 2018 edition.

This fourth edition used AWR DE V16 project files; as a result, many figures have been updated to reflect the slight changes in appearance from earlier versions.

## Acknowledgment

I thank my wife Maxine for her patience and tolerance of my absences over many years, as I fulfil my desire to teach students the art of electronic design, being absorbed in research in the design of instrumentation and communication equipment. I thank her for being able to spend a lot of my time in writing and updating this book and the accompanying project files, even in my "retirement".

I thank my colleagues at James Cook University, for their encouragement and feedback on the course that resulted in this book. I thank AWR for making their software available for teaching at James Cook University. Without that, this book could not have been written. I thank Dane Collins and Sherry Hess from AWRCorp, for the novel step that we took in distributing this book on their web site. That allows this book to be used by many more students. I thank the late Prof Mike Heimlich, from Macquarie University, who peer reviewed the first edition of this book and made many very valuable comments. I thank the AWR support staff, for helping me when I could not get some of the project files to work correctly. I thank Cadence and their staff; David Vye, for firstly providing project files for modelling amplifier performance and secondly, together with David Junkin and Kira Jones continuing the vision of making this book readily available to university staff and students around the world. Finally, I thank Prof. Mohan Jacob from James Cook University, and Dr. Sudipta Chakraborty from Macquarie University who both peer reviewed this edition of the book. Their comments have been incredibly valuable and resulted in this book being much better than the draft version.

## About the Author

Cornelis Jan Kikkert obtained his BE and PhD from Adelaide University in 1968 and 1972 respectively. He is a Chartered Professional Engineer, a Fellow of Engineers Australia and a Life Senior Member of IEEE. He was a lecturer at Adelaide University for 3 years and was at James Cook University in Townsville for 37 years, as a Lecturer, Senior Lecturer, Associate Professor and 7 years as Head of Electrical and Computer Engineering.

He "retired" in 2010 to have more time for research. Since 2010, he is an Adjunct Associate Professor at both James Cook University and The University of Adelaide.

He has more than 50-year experience in the design of electronics for communication equipment, broadcast transmitters, satellite beacon receivers, weather satellite receivers and many other applications, as well as the design of electronic instrumentation for measuring RF and microwave signals.

In addition to this book, he is the author of more than 100 peer-reviewed papers, 4 book chapters and an inventor on 8 patents.

Email Keith.Kikkert@jcu.edu.au, Keith.Kikkert@adelaide.edu.au.

June 2022

# Chapter 1

# Introduction

## RF Electronics Design

The Radio Frequency (RF) spectrum range is normally considered to include frequencies from 30 MHz to 300 GHz. That frequency range is further divided into Very High Frequency (VHF), Ultra High Frequency (UHF), Super High Frequency (SHF) and Extremely High Frequency (EHF) as shown in figure 1.1. The Tremendously High Frequency (THF) or Terahertz frequency band requires design techniques that are not covered by this book.

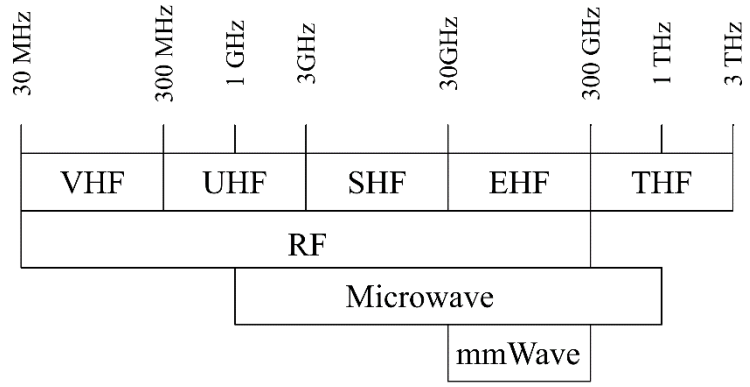



Figure 1.1 RF Spectrum Bands.

RF electronic designs require different techniques than electronic designs at lower frequency since:

1 The resistors, capacitors and inductors used do not necessarily behave like ideal components. In particular, leads on resistors and capacitors have an inductance associated with them, which can easily dominate.

2 The wavelength of the signals is comparable to the size of components used. This presents some challenges and some opportunities.

3 The track lengths may be a significant fraction of a wavelength, allowing Microstrip-lines or Striplines, to be used as elements for filters, couplers, impedance matching circuits etc.

4 The tracks on the circuit boards should be seen as transmission lines with a characteristic impedance, chosen such that the transmission line and the devices connected to it, satisfy the circuit specifications at all the required frequencies. Conventional printed circuit boards are lossy at high frequencies. Circuit boards for RF and Microwave frequencies normally use low loss materials and have carefully controlled thicknesses, to provide constant impedances for transmission lines.

5 For EHF designs, the wavelength is comparable to the package size of IC's used to realise the circuit, so that filters, couplers, impedance matching circuits and antennas, can be realises in silicon as part of the IC.

At lower frequencies, many of the analogue circuits are being replaced with digital circuits. Analogue circuit design techniques are used for much of the circuitry in any transmitter and receiver circuit used in Radio, TV, Microwave, Mobile Phone, Wireless LAN etc. Digital techniques, such as software-defined radio, digital predistortion and digital signal processing techniques are increasingly being used to enhance the performance, reduce the cost and make the transmitters and receivers more flexible.

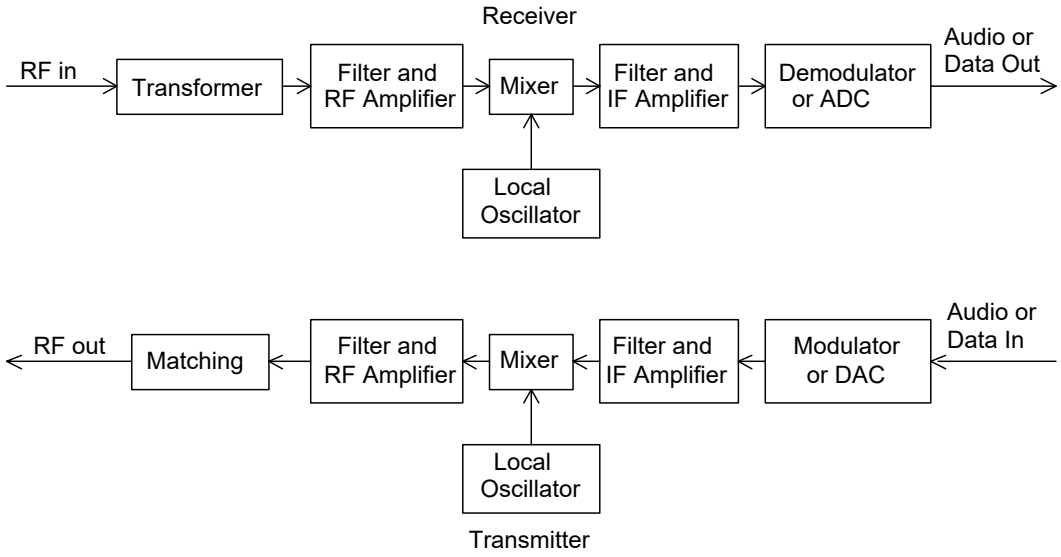



Figure 1.2. Typical Transmitter and Receiver Block Diagram.

A traditional block diagram of a receiver and a transmitter is shown in figure 1.2. The basic building blocks in this diagram are RF Transformer, Mixer, RF and IF amplifier, Local Oscillator and a demodulator or detector. In this course, we will look at many of these elements in detail.

For consumer devices with large production runs, such as mobile phones and USB dongles for Digital TV, Bluetooth or WLAN, many of the blocks in figure 1.2, are combined in one package, which contains one or more ICs. A typical example of this is a Bluetooth dongle, shown in figure 1.3. All the RF functions, including the 2.5 GHz transmitter and receiver, all the protocol handling and the USB interface are contained in the two IC's on figure 1.3. The antenna is included, as an element on the PCB, as the zigzag track on the left. Note that the end of that track is not connected. For efficient radiation, the length of the track is close to a quarter wavelength.

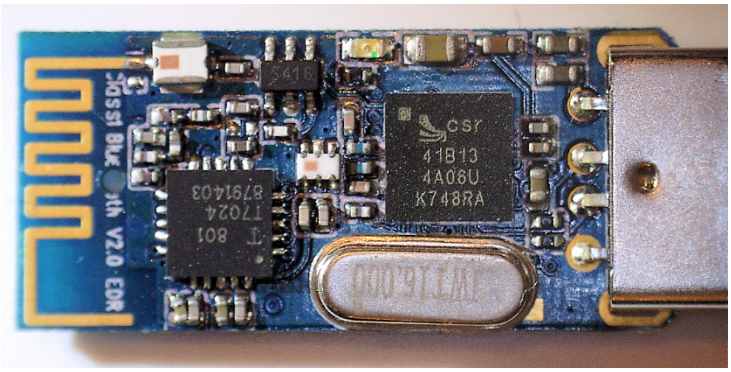



Figure 1.3. Typical Consumer RF Module. (Unbranded Bluetooth USB Adapter)

For many applications, such IC's may be too expensive for the small number of circuits to be produced, or the performance that can be obtained from an IC cannot meet the required specifications, such as output power or adjacent carrier rejection. For high power applications such as transmitters, IC's alone cannot meet the impedance matching and power demands. As a result, a discrete implementation is often required. This book deals with the design of such RF circuits.

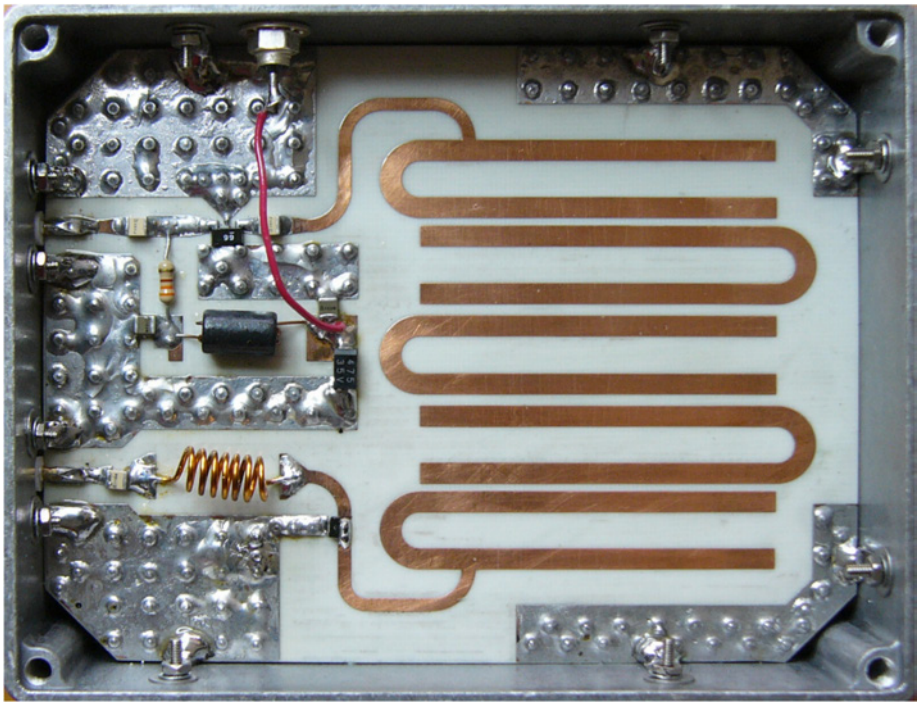


Figure 1.4. Harmonic Multiplier, to produce 810 MHz from 162 MHz. [1].

Figure 1.4 is a typical example and shows a harmonic multiplier for a Satellite Beacon Receiver built at James Cook University. The input is a 162 MHz signal and the output is the 5$^{th}$ harmonic at 810 MHz. The active device is a Microwave Monolithic IC (MMIC) amplifier. Currently wireless services operate at frequencies of 1.8 GHz for mobile phones, 2.5 GHz for Bluetooth and WLAN and 5 GHz for WLAN. In many cases, IC's specially designed for these applications can be used at other frequencies. The designer should keep this in mind as it can reduce the cost of specialised circuits.

This book does not specifically deal with the design of RF IC's. The techniques described here are directly applicable to the design of RF IC's and have even been used through microwave and up to millimetre-wave [2 - 4], since those need to allow for the IC to be comparable with the wavelength for GHz frequency designs. In addition, the chapters on amplifiers and oscillators allow for the design of circuits, which can be directly implemented in RF IC's.

## Computer Simulation

For any commercial design, it is important to produce a properly functioning design as quickly as possible. Ideally, there should be just one design iteration, it should be correct and reliable with the first realisation, since any further design-iterations will cost more money and will delay the time before product comes to market, thus reducing any competitive advantage.

Computer simulation allows most aspects of the design to be investigated and optimised quickly before any hardware is produced. The modern computer simulation tools are very good and generally allow a correctly functioning design to be produced first time. The main commercial computer simulation systems are:
1) EEsof, which was purchased by Hewlett-Packard, then spun off as Agilent and is now Keysight PathWave Design [5] comprising Advanced System Design (ADS**),** GoldenGate RFIC Simulator (EMDS), EMPro 3D and other packages.
2) AWR Design Environment software [6] comprising Microwave Office (MWO), Visual Systems Simulator (VSS), Analogue Office, AXIEM, Analyst and other packages. AWR was purchased by National Instruments in 2011 and by Cadence in 2019.
3) Other RF simulation companies are Ansoft and Cadence.
Both PathWave and AWRDE perform well, and both allow linear and non-linear circuit analysis, using steady state and time-domain circuit simulation, as well as the more detailed electromagnetic simulation of circuits. The author has used both EEsof EDA and AWR DE for many years. In the author's experience, AWR DE is easier for the students to learn and as a result, AWR DE has been used in the RF electronics course and entry-level electronics and circuit simulation courses at James Cook University. The authors lecture notes for the RF electronics course form the basis of this book. Chapter 2 has deliberately been written to allow it to be used for both advanced RF electronics courses and entry-level courses.

Both the Keysight and Cadence AWR software allow the design and simulation of RF IC's. Depending on quantities and manufacturing technology, it can be expensive to manufacture an RF IC. The author encourages the RF designs by the students to be manufactured, to allow the students hardware experience in measurement and fault-finding of RF circuits, as well as providing feedback on their designs. As a result, this book concentrates on using commercial PCB substrates for components like couplers, combiners and filters and using commercial transistors and IC's in active RF designs.

The AWR DE project files for each figure in this book are included with this book and are available for download from the AWR web site [6]. For the 2022 edition of this book, AWR DE version V16 has been used for all the simulations.

## References

1. Kikkert, C. J. "The design of a Ka band satellite beacon receiver". Sixth International Conference on Information, Communications and Signal Processing (ICICS 2007), Singapore, 10-13 Dec, Publisher IEEE.
2. Analog/RF IntgCkts, RFIC Designer's notes, https://analog.intgckts.com/
3. Analog Devices RF and Microwave, https://www.analog.com/en/products/rf-microwave.html
4. WiFi Alliance, http://www.wi-fi.org/
5. Keysight Technologies EEsof Electronic Design Automation (EDA) software, http://www.keysight.com/find/eesof
6. Cadence AWR Corp: AWR Design Environment http://www.awrcorp.com/

# Chapter 2

# Computer Simulation

## Introduction

There are many circuit-simulation programmes available. Most of these use SPICE models, which include all relevant parameters. At lower frequencies, programmes like the commercial "Multisim" program are useful, but for RF circuits, frequency-domain computer simulation tools are much more computationally efficient for steady state analysis than SPICE based programmes. Frequency-domain computer simulation tools also allow transmission lines to be used as elements and are able to evaluate Intermodulation (IM) distortion caused by two closely spaced tones. Typical examples of RF circuit simulation software are Pathwave EDA by Keysight Technologies [1] and AWR Design Environment (AWR DE) [2].

AWR DE contains five very different simulation programs: Microwave Office (MWO), which is used for circuit simulation. This chapter describes its use for circuit simulation. The second part is Visual System Simulation (VSS), which is used to simulate whole systems. VSS is typically used to simulate communication systems to determine the performance of different modulation techniques. The third part is Analog Office, which is used for RF-IC design. The fourth part is AXIEM, which is used for 3D planar electromagnetic (EM) simulation, and the fifth part is Analyst, which is a full 3D EM simulation software. This is a very powerful computer simulation suite. During operation of the AWR DE software, all the different component MWO [3], VSS, Analog Office, AXIEM and APLAC that have valid licences, are all available. In some instances, more than one of these AWR DE components are used at the same time, the generic name AWR DE is used in this book, unless a specific component is mentioned. For the 2020 edition of this book, AWR DE version 15 is used for all the simulations.

AWR DE is very good for both RF and lower frequency simulations. Many RF transistors and diodes devices models are available for both linear models and non-linear (Transient or Harmonic Balance) models. In addition, the required model parameters can often be downloaded from the device manufacturer's web site. For microwave frequencies, the device models used and the modern communication simulation programmes are very accurate, resulting in a good agreement between the computer simulations and the resulting hardware. For Terahertz frequencies, foundry models are often not accurate enough and one may have to develop their own models.

The linear models treat any passive and active devices as "linear" devices and use conventional circuit analysis techniques to solve the equations for the circuit to be simulated. As a result, the simulation is fast, but it will not deal with non-linear effects such as those that occur in a mixer, oscillator or amplifier. Applying optimisation techniques to the linear simulation of the circuit allows the best performance to be obtained quickly. Simulation of non-linear circuits can be done in two ways: Firstly, Harmonic Balance is a frequency-based, steady state analysis that uses non-linear differential equations to model the devices and then uses a linear combination of excitation tones to balance currents and voltages to satisfy Kirchhoff's law. Examples of this are the simulation of the harmonics produced by an oscillator. Secondly, transient time domain simulation using SPICE models can be used to analyse the non-linear behaviour of a circuit. Examples of this are the simulation of an oscillator starting up.

Nonlinear circuit simulation is described in detail later in this chapter, using example 2.4: Buck DC-DC Converter.

Computer simulation is a powerful tool for ensuring that a circuit has been designed to perform correctly. It is best practice for commercial designs to firstly check the circuit under the ideal design conditions and then check that the circuit still performs correctly for all realistic component tolerances variations. Since the production of a PCB, containing an RF circuit is quite expensive it is always good practice to first fully simulate the circuit using both EM and circuit simulation. Inadequate simulation may result in a design fault being discovered in the hardware after it is built, resulting in costly delays. Even though modern computer simulation tools are very good, they are no substitute for good design by an experienced designer. Even then, one will often find something that was not known and was not considered in the simulation, especially at RF and microwave frequencies, that can seriously affect the circuit's performance. The computer simulation process is illustrated by some examples.

# Basic Operation

## *Example 2.1: Low-Pass Filter*

Design a 4th order low-pass filter and a high-pass filter to have a cut off frequency of 250 MHz and an impedance level of 75 Ω, and in the second example combine these filters to form a VHF-UHF TV antenna diplexer. The Coaxial cables used for TV antennae are 75 Ω impedance. Hence, 75 Ω is used for the impedance of this diplexer.

For Butterworth filters [4] the design equations for L and C are well known and obtained using the Cauer topology realisation for Butterworth polynomials and are used for the filter tables of [5] for these filters. The components are [4]:

$$C_i = \frac{1}{\pi F_c R} Sin\left(\frac{(2i-1)\pi}{2n}\right) \quad i = 1,3,5,\ldots \qquad \text{Eqn. 2.1}$$

$$L_i = \frac{R}{\pi F_c} Sin\left(\frac{(2i-1)\pi}{2n}\right) \quad i = 2,4,6,\ldots \qquad \text{Eqn. 2.2}$$

Where R is the desired load impedance and $F_c$ is the cut off frequency. Later in this chapter, it is shown how these equations can be used directly in AWR DE. The high-pass filter is obtained using the standard low-pass to high-pass transformation described in most filter textbooks, such as section 5.4 of Zverev [5] and section 2.6 of Huelsman [6]. The low-pass to high-pass transformation simply results in the normalised L and C values being swapped and replacing L with C and C with L in the circuit. As can be seen by comparing figures 2.3 or 2.7 with figure 2.8.

These equations can easily be entered into a spreadsheet, to give the results for the 250 MHz filter shown in table 2.1. This spreadsheet is also included in the zip file containing all the AWR DE project files used in this chapter.

We now enter these values into MWO. To do this we must create the required project as follows:

Open AWR DE. This will then open up a blank project as shown in figure 2.1.

Select *Project* ⇒ *Add Schematic* ⇒ *New Schematic* and name the Schematic "LowPass". Then type CNTL+L or select the Element window at the bottom left of the Design Environment window and select *Lumped Elements* ⇒ *Capacitor* and drag the CAP symbol into the circuit schematic as shown in figure 2.2.

Table 2.1. Spreadsheet results for Butterworth filter element values.

| | | | | | |
|---|---|---|---|---|---|
| Terminating Impedance | 75 Ω | | | | |
| Frequency | 250 MHz | | | | |
| Filter Order | 4 | | | | |
| | | Element Values: (Ω, F, H) | | | |
| Component | Number | Normalised Impedance | Low-pass | | High-pass | |
| Rs, Rn | 1 | | R | 75 | R | 75 |
| (from eqn. 2.1) | Component 1 | 0.765367 | C | 6.497E-12 | L | 6.23838E-08 |
| (from eqn. 2.2) | Component 2 | 1.847759 | L | 8.822E-08 | C | 4.59382E-12 |
| (from eqn. 2.1) | Component 3 | 1.847759 | C | 1.568E-11 | L | 2.58402E-08 |
| (from eqn. 2.2) | Component 4 | 0.765367 | L | 3.654E-08 | C | 1.10905E-11 |

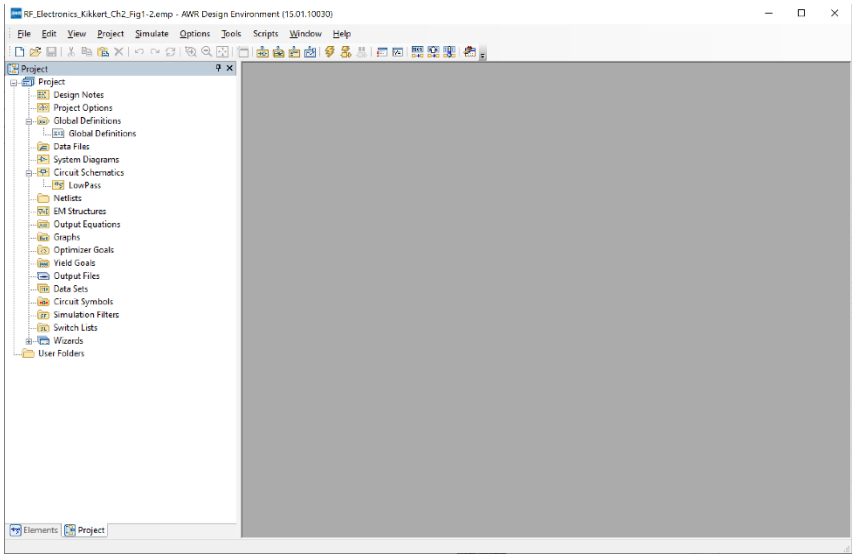



Figure 2.1. MWO blank project screen.

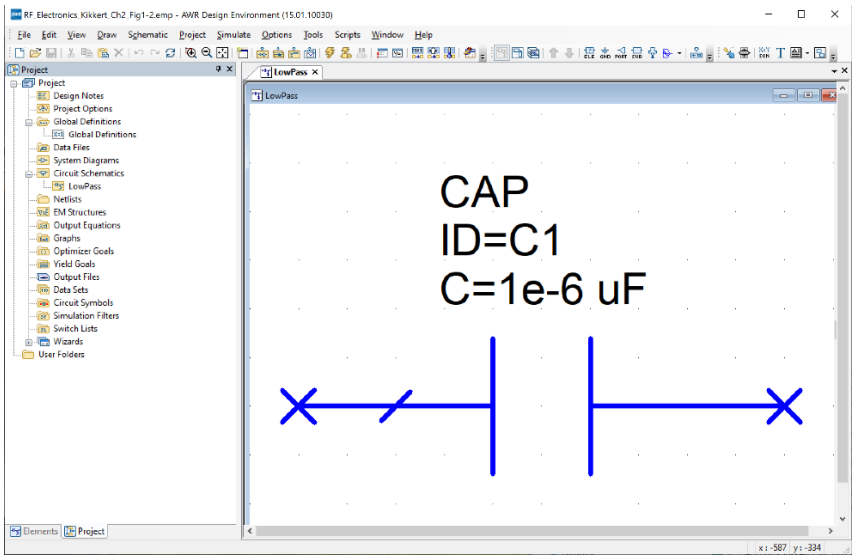



Figure 2.2. Capacitor placed.

Now place all the other capacitors and inductors in the correct location. When placing the component, a right mouse click rotates the component. Selecting the port symbol from the mini toolbar, or selecting *Draw* ⇒ *Add Port* allows the input and output ports to be added to the circuit. *Draw* ⇒ *Add Ground* allows a ground connection to be added. Double Left Click on a component or on the property's text in the schematic, allows the required value for that component to be entered. Repeat this for all the other components to result in the final circuit as shown in figure 2.3.

Note that normally filters are designed with the smallest number of inductors, so that odd order filters with the end elements being capacitors are far more common.

**Practical Note:** The filters are to be used as part of a diplexer, consisting of a high-pass and a low-pass filter in parallel. The high-pass filter must not short out the low-pass filter at low frequencies and the low-pass filter must not short out the high-pass filter at high frequencies, so that an open circuit input impedance is required in the stopband of these filters. This is achieved with the first (series) element being an inductor for the low-pass filter, and the first element being a capacitor for the high-pass filter.

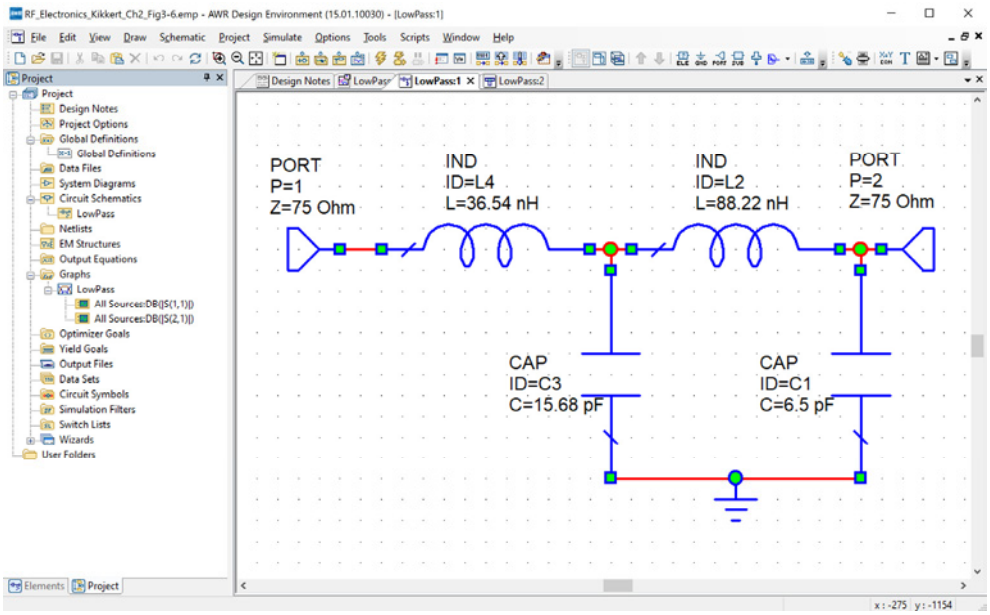



Figure 2.3. Low-pass filter circuit.

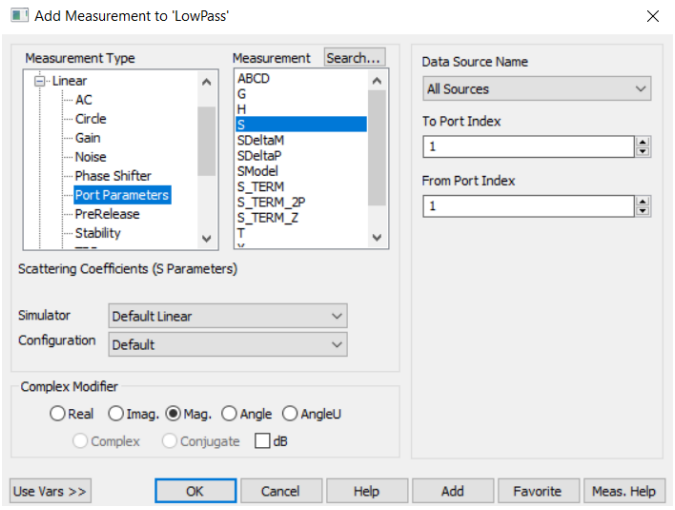



Figure 2.4. "*Add Measurement*" window.

Select the project window again and select Graph and right mouse click and select add measurement. This opens the window shown in figure 2.4. RF devices are normally specified by the Scattering (S) parameters. These are described in more detail in chapter 8 and equations 8.3 to 8.12. Pozar [7] in section 4.3 gives a detailed description of S parameters. They give a simple performance measurement of the circuit. $S_{11}$ and $S_{22}$ are the input and output return loss, indicating how well the device is matched. $S_{21}$ and $S_{12}$ are the forward and reverse gains. Select *Linear Measurement type* ⇒ *Port Parameter* and *S parameter* to obtain S parameter measurements of the filter, as shown in figure 2.4. Save the project as "LowPassFilter" to keep these values. Since this circuit is to be connected using TV Coaxial cable, ensure that the impedance of the ports is changed from the default value of 50 Ω to 75 Ω.

Now set the operating frequency range using the *Project options* entry in the left bar. Set the *Global Units frequency* to MHz and then set the operating frequency range in the *Frequencies* window as shown in figure 2.5.

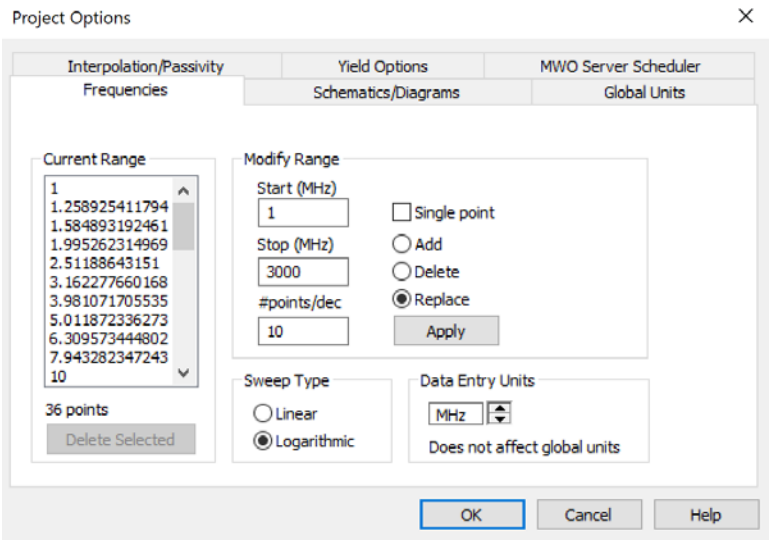



Figure 2.5. Project frequencies.

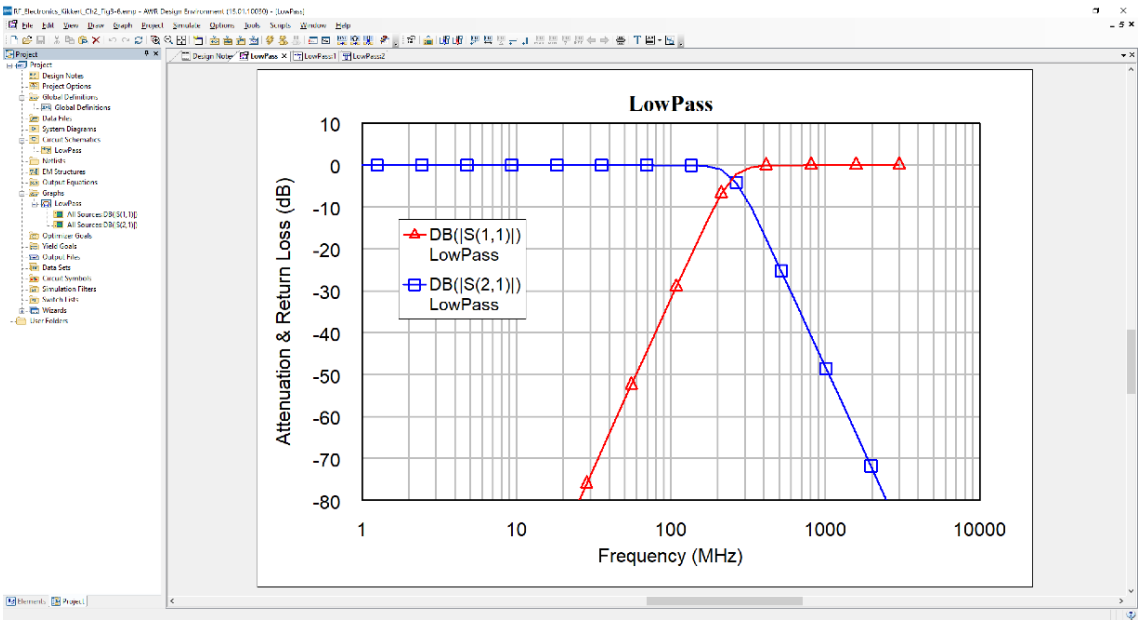



Figure 2.6. Frequency response of the low-pass filter.

Select *Simulate* ⇒ *Analyse* to give the required frequency response as shown in figure 2.6. The scales, line thickness and other parameters of the graph can be set from inside the Graph Property toolbar, (the left element of the right toolbar shown in the blue top area in figure 2.6), or the properties can be accessed by right clicking inside the Low Pass graph and selecting *Properties*.

In figure 2.6, the blue graph is the transfer function $S_{21}$ and the magenta one is the input reflection coefficient $S_{11}$.

## Equations in AWR DE

It is possible to use variables and equations either as global variables for the whole project or as part of an individual circuit diagram. This allows greater control over the filter parameters and avoids having to use a spreadsheet to calculate the filter element values. For instance, by making the cut off frequency a variable, the filter can easily be tuned to achieve a required cut off frequency. The cut off frequency can be tuned or optimised to meet required specifications. The resulting circuit diagram is shown in figure 2.7. The variables can be placed in any order, but any variable specification must be above the use of that variable. The resistance R and frequency variable $F_c$ must thus be on top, since those are used by C1, L2, C3 and L4. The equations are added to the circuit diagram using: *Draw* ⇒ *Add Equation*, and then placing the equation location on the circuit diagram. Variables, which AWR DE cannot find, either globally or in the current schematic, are shown in red. Any corrective action may simply be the moving around of a variable to satisfy this top to bottom flow requirements. The full list of built in functions is shown in section 8.5.3 of the 2010 AWR DE users-guide, available by selecting Help on the pull down menu. Variables can be tuned manually or be changed automatically as part of optimisation by selecting Properties and then enabling the Tune and/or Optimize check boxes. If needed the range of values can be constrained to specified upper and lower values. It is desirable to constrain R, L and C from becoming negative.

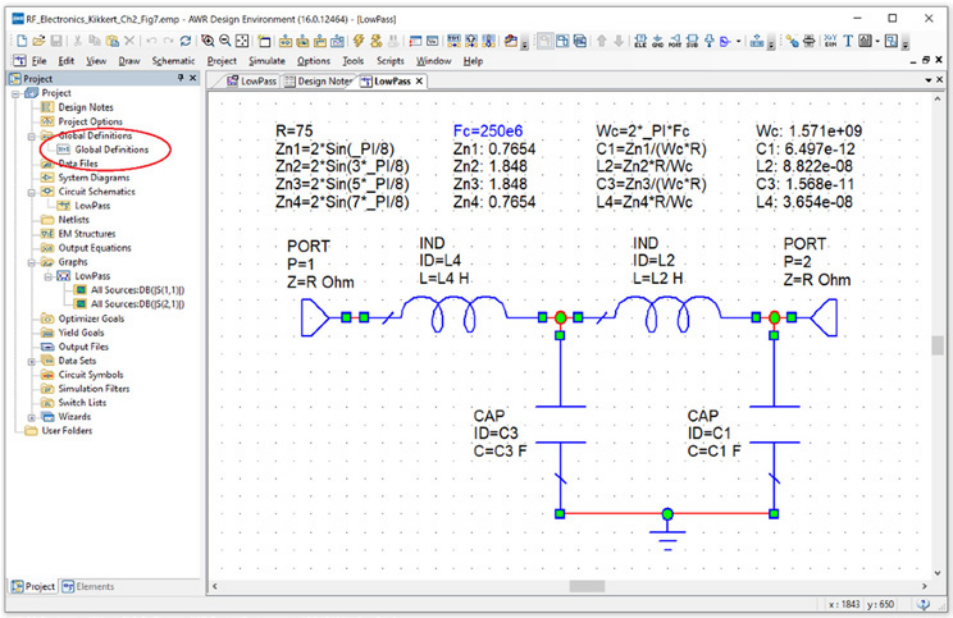



Figure 2.7. Tuneable filter.

Any variables or equations whose variables can be tuned are displayed in a blue font as shown in figure 2.7. Circuit values can either be shown as base values, such as H, F or

Hz or as convenient values, such as µH, nH, nF, pF, MHz or GHz. If the base values are used, then equations such as equations 2.1 and 2.2 can be used. If convenient units are used, then the appropriate multipliers need to be included in the equations to result in say pF for the capacitance, when a frequency in MHz is entered. When convenient units are used, all the graphs will have the x-axis in the convenient (MHz) units. If the same equations or the same variables are shared in more than one circuit, it is better to locate the equations in the Global Definitions window shown in the left pane of figure 2.7. Those equations are then available to all circuits.

In figure 2.7, the thickness of the lines can be changed by selecting *Options* ⇒ *Environment Options* ⇒ *Schematics/Diagrams* and setting Symbol Thickness to 10 then setting OK. It is also possible to have equations using the output parameters of a circuit. This is demonstrated in example 5, Bandpass T Matching Network, of this chapter.

# Optimisation

## *Example 2.2: Diplexer*

It is required to design a Diplexer to permit VHF and UHF TV signals to be received by separate antennae and then combined, for use by a TV. In Australia the VHF TV frequencies range from 46 MHz to 230 MHz and the UHF TV frequencies range from 527 MHz to 820 MHz. Similar frequency ranges are used in other countries. For this example, 250 MHz is used as the boundary between VHF and UHF. As a result, $S_{21}$ (low-pass transfer function) is to be greater than -3 dB for frequencies below 250 MHz and $S_{31}$ (high-pass transfer function) is to be greater than -3 dB for frequencies above 250 MHz. A low pass filter with a cut off frequency of 250 MHz, as shown in figure 2.6 is used for the VHF signals and a high-pass filter with a cut off frequency of 250 MHz, is used for the UHF signals. These two filters are then connected as shown in figure 2.9. The same circuit can be used as a splitter, to separate FM radio and VHF TV signals from UHF TV signals. A diplexer consists of a low-pass filter selecting the low frequency components and a high-pass filter selecting the high frequency components.

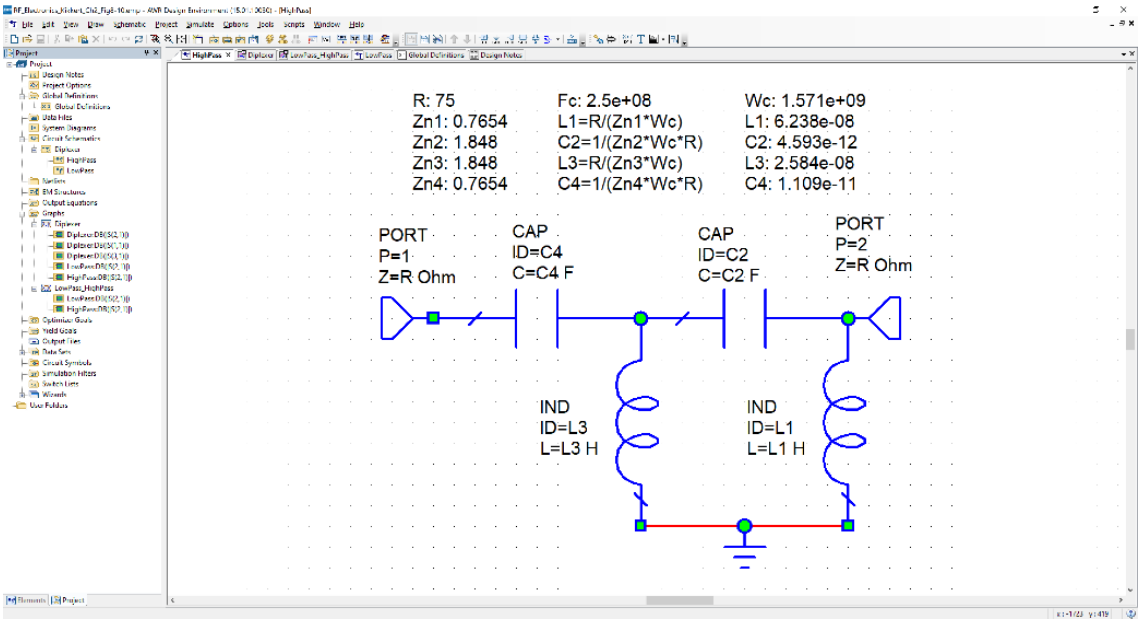



Figure 2.8. High-pass filter.

The easiest way to produce the diplexer is to produce a separate high-pass filter and then use that and the low-pass filter as sub-circuits to produce the diplexer. The low–pass filter can be the Butterworth low-pass filter of figure 2.7. The high-pass filter shown in figure 2.8, uses the component values from table 2.1. The full diplexer is shown in figure 2.9, and the resulting S parameter frequency response is shown in figure 2.10.

**Practical Note:** Since the high-pass filter and low-pass filter are in parallel, the low-pass filter must have an open-circuit input impedance at high frequencies and the high-pass filter must have an open circuit input impedance at low frequencies. This is achieved by using filters that have the first element as a series element for the input.

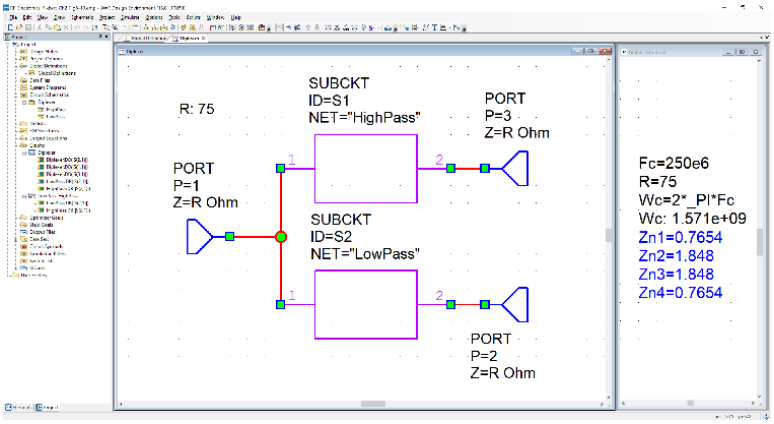



Figure 2.9. Diplexer using low-pass and high-pass sub-circuits.

In this example, one could optimise each of the 8 individual components of the high-pass and low-pass filters. To facilitate the optimisation, it is desirable to keep the number of parameters to be optimised as small as possible, and optimise the 4 values Zn1 to Zn4, shown in figure 2.9. These are located in the Global Definitions and are used to calculate the element values for both the high-pass and low-pass filters, using the equations in figures 2.7 and 2.9. The corner frequency Fc and Impedance R, are also located in the Global Definitions to allow those to be changed without affecting the optimisation.

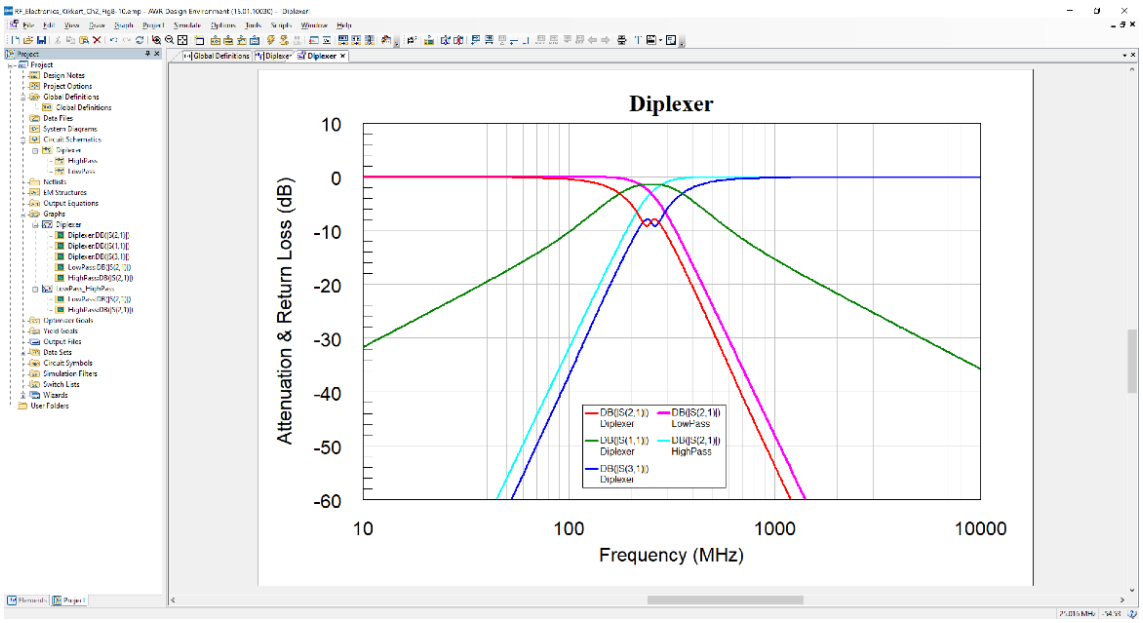



Figure 2.10. Frequency response of the diplexer.

As can be seen from figure 2.10, return loss ($S_{11}$) is only -1.4 dB near the cut off frequency of the filters so that the input is poorly matched. By comparing the blue curve of the low-pass filter by itself, with the cyan curve of the low-pass filter as part of the diplexer, it can be seen that there is a significant interaction between the low-pass and high-pass filters. There is a similar degradation in performance of the high-pass filter, as shown by the red and magenta traces. One can use the optimisation capability to improve the performance of the diplexer at the crossover frequency range. The first task is to specify the optimisation goals. For this design, the requirements are that $S_{11}$ is less than -20 dB over the entire VHF and UHF TV frequency range.

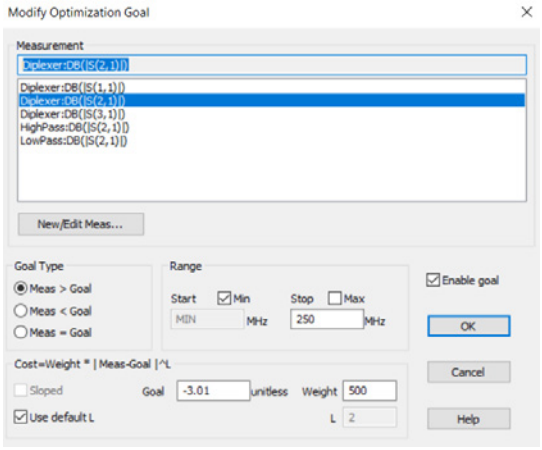



Figure 2.11. Specification of optimisation goals.

These optimisation goals are entered in the optimisation goal function as shown in figure 2.11. Double click on the elements to be optimised and select the “optimize” checkbox in the element options window, for the component or the variable linked to a component as shown in figures 2.7 and 2.8, to ensure that the element can be optimised. In addition, some attenuation limits at 100 MHz and -35 dB and 625 MHz and -35 dB, for $S_{21}$ and $S_{31}$ can be added, to prevent the components being changed so that all frequencies are passed by both the high-pass and low-pass networks. Finally, the $S_{11}$ limit is set to -45 dB to ensure a near perfect match over the entire frequency band. Often the optimisation limits are changed during the optimisation process, to ensure the best performance to be obtained for the final network. For most circuits a higher return loss is normally acceptable, however this network will optimise in one-step to meet these limits. The weighting of the pass-band optimisation limits for $S_{21}$ and $S_{31}$ are made 1000 since the typical errors are much smaller than the error in $S_{11}$, which is given a weighting of 1 to give comparable errors at the start, thus ensuring that all limits receive sufficient optimisation effort.

Select *Simulate* $\Rightarrow$ *Optimise* to start the optimisation. For this optimisation, "Simplex Optimisation" is a good optimisation method to use and the optimisation will reach its goal in one-step. Figure 2.12 shows the optimisation starting performance with the optimisation goals and the Optimizer panel. A logarithmic frequency scale is used since that will clearly show the straight lines of the 80dB/decade stopband attenuation. Figure 2.13(top) shows the optimisation criteria and the performance after the optimisation has been completed. It can be seen that the diplexer meets all the required specifications and that it is even possible to meet a -45 dB return loss on $S_{11}$. Less than 300 iterations of the "Simplex Optimisation" are required to obtain the final values. Changing the $S_{11}$ optimisation limit to -60 dB, allows $S_{11}$ to be reduced even further, as shown in Figure 2.13(bottom).

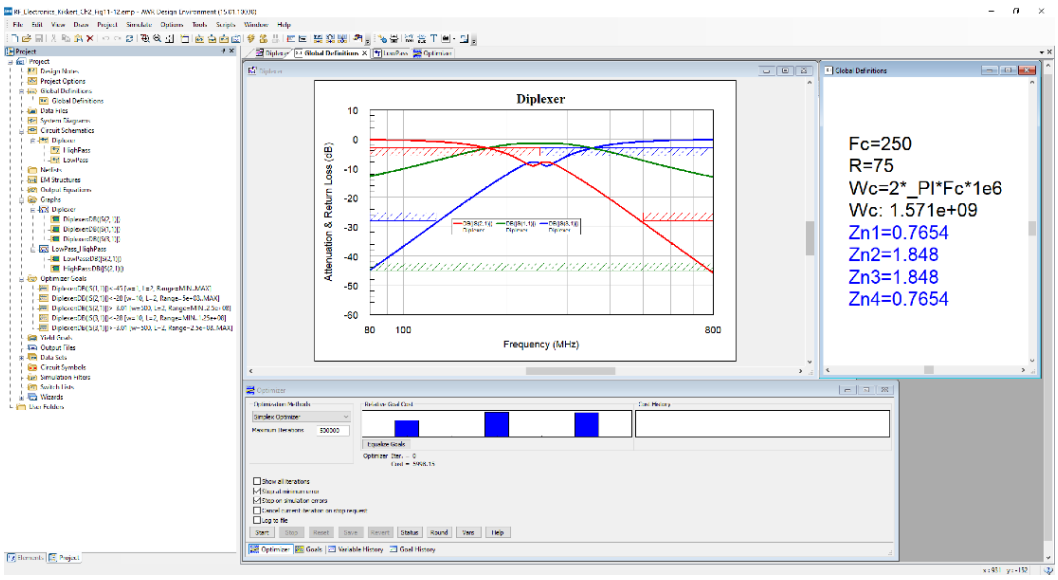
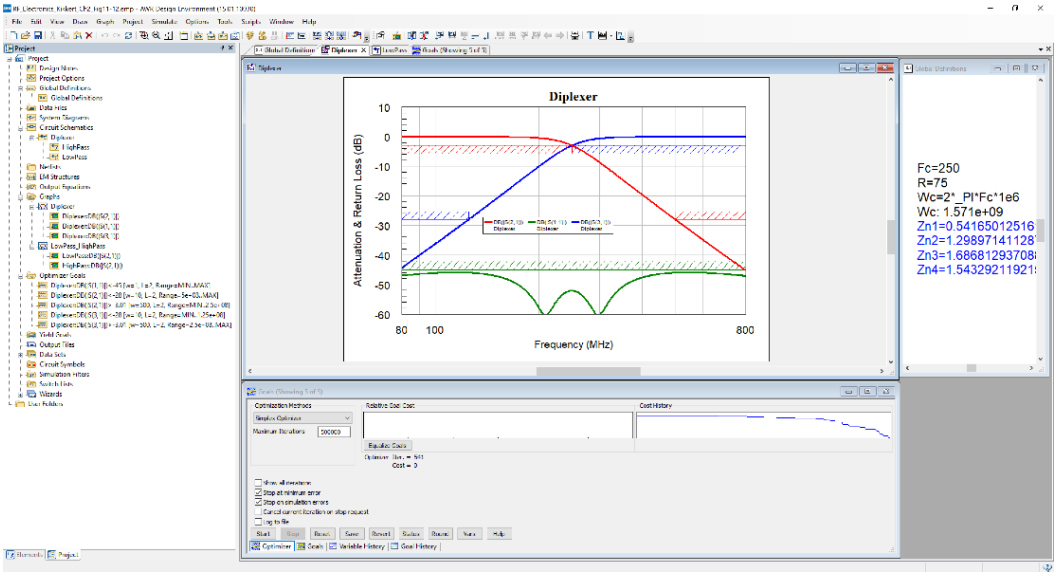



Figure 2.12. Optimisation criteria and the diplexer performance before optimisation.



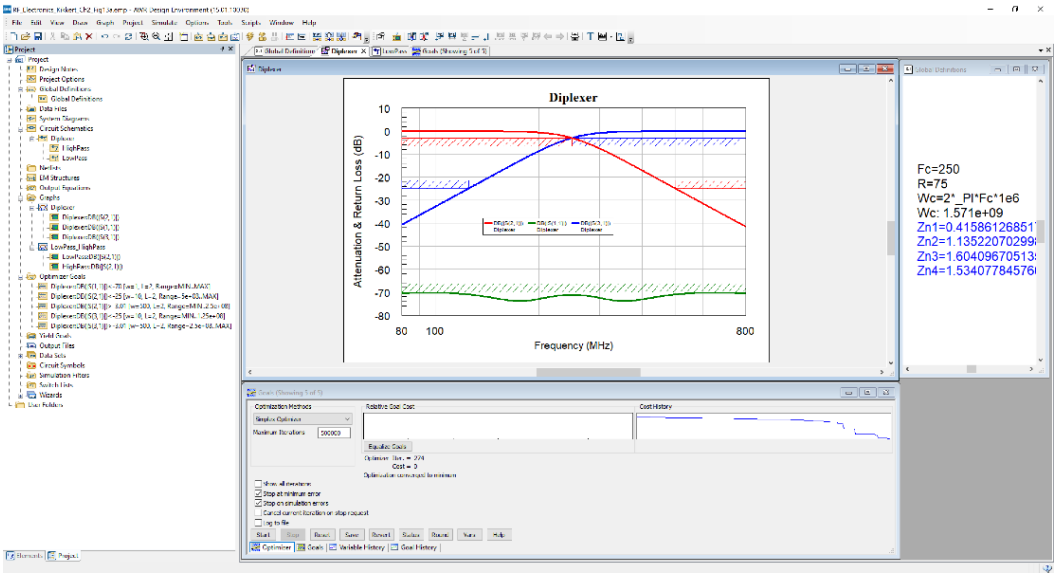




Figure 2.13. Diplexer performance after optimisation. Top 45dB, bottom 70dB for S11.

For the -70dB optimisation of S11, the stopband attenuation limits need to be reduced slightly from -28 dB to -25 dB. It then becomes a choice whether a better S11 or a higher stopband attenuation is more important. Zn1 reduces more but Zn4 does not change much when going from -45 dB for S11 to -70dB.

This diplexer is also used in Application Note AN-M-OPT-DPX-2020.2.6.pdf [8] to investigate the speed of operation of different optimization routines in AWR DE V14.

When the cost function does not decrease, it is worthwhile to change some conditions since the optimisation may be stuck in a local minimum rather than the global minimum for the cost function. Changing the weight for one or more of the goals or changing the optimisation function may get the optimisation out of the local minimum. The “random local” optimiser is good for a complex optimisation function that will exist close to the global optimum condition. Other optimisation methods, such as Simulated Local Annealing or Discrete Local Search can also be tried to ensure the optimisation is not stuck in a local minimum. It may even be necessary to alternate between several optimisation strategies and change optimisation limits and weights in order to ensure that a good performance is obtained. For this example, a Discrete Local Search will not produce a good optimisation, however for complex problems [9] it gives better results than the Simplex Optimisation. It is thus important to try different optimisation techniques to obtain the best results. A good overview of each optimisation method can be found in section 2.6.9 of the AWR DE Simulation and Analysis Guide and in Application Note AN-M-OPT-DPX-2020.2.6.pdf [8].

The component values of the filter after optimisation with a -70 dB $S_{11}$ return loss for the low-pass sub-circuit are shown in figure 2.14 and those for the high-pass sub-circuit are shown in figure 2.15. Note that the component values are significantly different from the starting values using the Butterworth filter table values. The component values are very practical, so that the diplexer can easily be made.

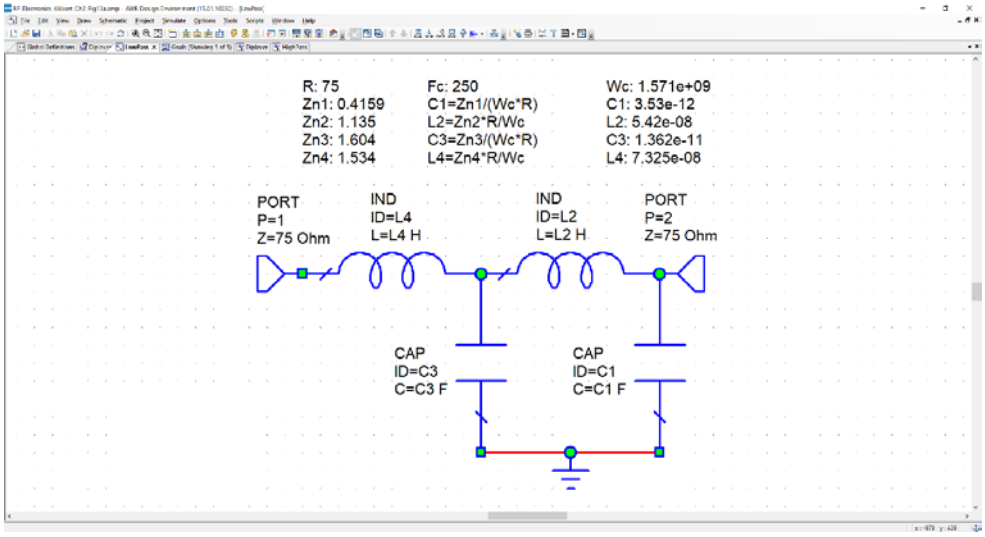



Figure 2.14. Final low-pass filter for diplexer.

It is possible to replace the inductors using Microstrip lines as shown in figures 7.10 and 7.11 of Chapter 7. Using Microstrip lines allows this diplexer to be made on a low cost FR3 or FR4 PCB using only capacitors and Microstrip lines. If this is done then the length and impedances of the Microstrip lines must be further optimised to meet the same specifications as this diplexer, since figures 7.10 and 7.11 show that Microstrip lines

behave different from inductors when their line length becomes comparable to a quarter wavelength.

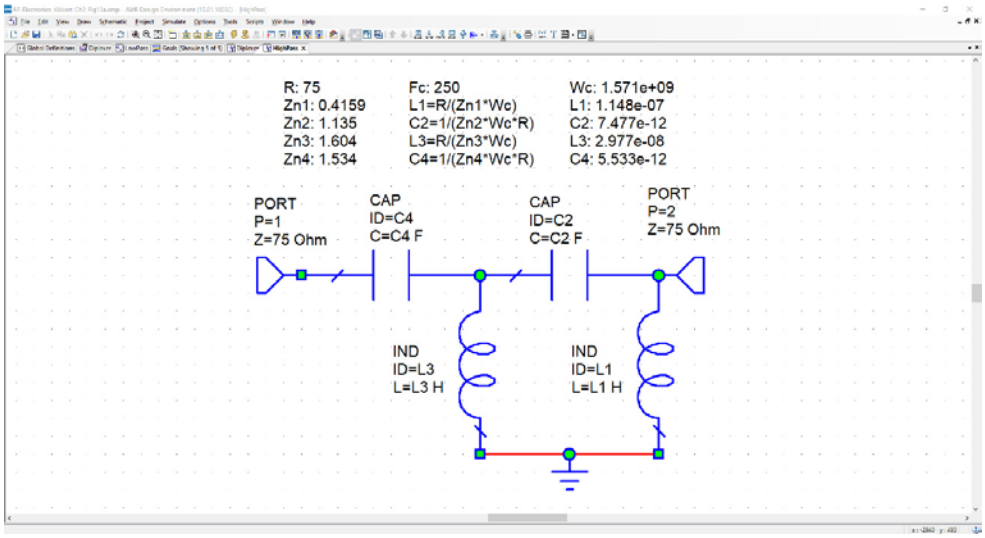



Figure 2.15. Final high-pass filter for diplexer.

# Device Models

As RF devices become more complex, the circuit simulation software must also become more complex in order to be able to accurately simulate these new RF devices.

## *Linear Models*

Several different types of transistor models can be used. The simplest ones are linear analytical models, such as the Hybrid, Pi or T models used in basic electronic design subjects. Such models are used for teaching basic electronics at many Universities. For these models, MWO treats the transistor as a linear device and only an AC analysis can be performed. Figure 2.16 shows how a simple Hybrid Pi model can be realised in AWR. Saving that schematic, as *Hybrid Pi*, allows that then to be imported in another schematic by selecting *Draw* ⇒ *Add Subcircuit* and then selecting *Hybrid Pi* and placing the subcircuit in the new circuit diagram. Since this is a bipolar transistor model it is desirable to change the Symbol by clicking on properties of the subcircuit and the selecting symbol and then selecting BJT@system.syf as the symbol. In AWR DE, it is thus easy to produce a model of an element and incorporate those elements in a circuit.

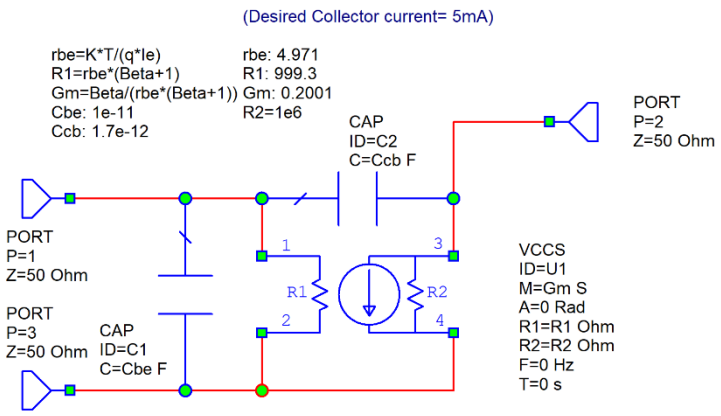



Figure 2.16. Hybrid Pi Transistor Model.

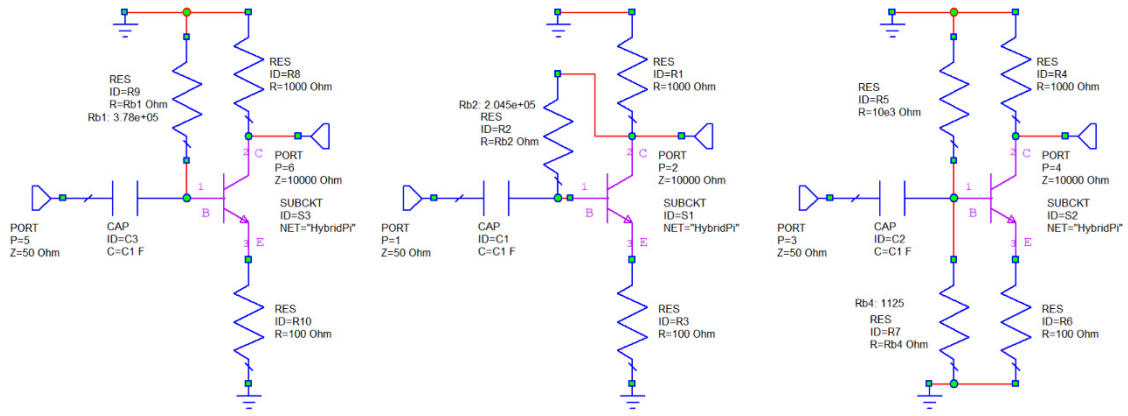
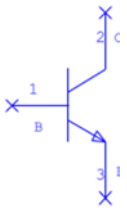



Figure 2.17. Bias stabilisation of Transistor amplifiers.

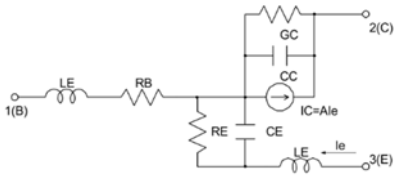
Figure 2.17 shows three transistor circuits that are often used to demonstrate bias stabilisation. The left circuit uses no bias stabilisation, the middle circuit uses collector bias stabilisation and the right circuit used emitter bias stabilisation. These circuits all use the Hybrid Pi transistor model of figure 2.16. The effect of changing the transistor gain Beta can be investigated by selecting *Simulate* $\Rightarrow$ *Tune*, and then vary Beta and to observe the effect of the changes. In addition, the input voltage can be changed and the resulting change in output can be seen.

## Bipolar Transistor (Closed Form): BIP

### Symbol




### Equivalent Circuit




### Parameters

| Name | Description | Unit Type | Default |
|---|---|---|---|
| ID | Element ID | Text | B1 |
| A | Magnitude of DC current gain (alpha) | | 0.8 |
| T | Current gain time delay | Time | 0 ns |
| F | -3dB frequency for current gain | Frequency | 0 GHz |
| CC | Collector capacitance | Capacitance | 0 pF |
| GC | Collector conductance | Conductance | 0 S |
| RB | Base resistance | Resistance | 1 ohm |
| LB | Base inductance | Inductance | 0 nH |
| CE | Emitter capacitance | Capacitance | 0 pF |
| RE | Emitter resistance | Resistance | 1 ohm |
| LE | Emitter inductance | Inductance | 0 nH |

Figure 2.18. BIP circuit of the closed form transistor model from AWR DE [10].

Since the Hybrid, Pi or T models are linear AC only models; DC voltages, bias stability or clipping of the amplifier cannot be observed. The manufacturers data sheet [11] for the BC546 BJT transistor, gives Ccb = 1.7 pF and Cbe = 10 pF. Using those values in figure 2.16 results in a similar frequency response to that obtained in figure 2.24.

AWR DE includes advanced Hybrid Pi (HYBPI) and T (BIP) models, which include lead inductances as part of the *Linear Devices* circuit elements. As an example, the BIP linear model of a transistor, shown in figure 2.18. The lead inductances are normally ignored for lower frequency models. The user must determine the element parameters for the device used from equations, like used in figure 2.16, the manufacturer's data sheets or measurements.

S parameter measurements of circuits and devices, can be made at RF and microwave frequencies and allow S parameter models to be used as part of simulations. For example placing the uPC8181TB MMIC amplifier from Renesas in a circuit, by selecting *Element ⇒ Libraries ⇒ AWR Web site ⇒ Parts by Type ⇒ Data ⇒ Renesas ⇒ IC ⇒ 1_Wide_Band_Amp ⇒ uPC8181TB Vcc=Vout=3V Icc=23mA*. Inserts a 2-port subcircuit in the circuit schematic that contains an S parameter file for the model. As shown in table 6.1 in example 6.3 in Chapter 6, for some MMIC's only S parameter performance data are available. In Chapter 9, figure 9.6 shows that for high power active devices, large signal S parameters are often specified. S parameters are a linear measurement based representation of a device, and just like the T and Hybrid Pi transistor model, those models assume the correct biasing has been satisfied and these linear models cannot handle clipping caused by the output signal being large.

## Nonlinear Models

The second type are non-linear analytical models. MWO includes Angelov, Gummel-Poon, Parker-Skellern, SPICE, Statz and Volterra based transistor models. Simulation Program with Integrated Circuit Emphasis (SPICE) based models can accurately model both the linear and non-linear parameters of a device. SPICE models are available for simple devices like resistors, capacitors, inductors, transistors and diodes or complex devices like MMIC's and operational amplifiers. The original versions of SPICE [12] are covered by a permissive BSD licence. However, since the release of SPICE1 in 1973, many different companies developed their different versions of SPICE models. Some of those are HSPICE and PSPICE (owned by Cadence). Some semiconductor manufacturers developed their own SPICE simulation software for their own devices. Analog Devices developed LTSpice [13], Texas Instruments developed TinaTI [14] are examples of these. This lack of compatibility means that many SPICE device models will not easily import into programmes like AWR DE. To overcome this, in 1996 the Compact Model Coalition was formed to promote standardization of compact model formulation and their interfaces, with the aim of allowing the complying SPICE models to be used in different simulation software. AWR is a member of the CMC. In 2013 the Silicon Integration Initiative (Si2) [15] took over the operation of the CMC. NXP has developed SiMKit [16] is a simulator-independent compact transistor model library. Connections for different simulators are handled through adapters that provide the right interfacing to those simulators. The latest releases of AWR DE, includes circuit element libraries with CMC Models, SimKit 4.7 Models, APLAC models, IC Foundary Process Design Kit (PDK) models as well as both SPICE and S parameter models of many devices. These libraries can be seen by selecting *Circuit Elements ⇒ Libraries ⇒ AWR web site.*

These non-linear models permit an accurate analysis of a transistor circuit. The Gummel-Poon Transistor model [17] included in AWR DE has the circuit diagram shown in figure 2.19. The model includes some device non-linearity and is significantly more complex than the BIP model shown in figure 2.18. Details of the Gummel-Poon model for a BC546 transistor can be seen by selecting *Circuit Elements ⇒ Libraries ⇒ AWR web site ⇒ Parts by Type ⇒ Nonlinear ⇒ Zetex ⇒ GBJT ⇒ NPN ⇒ BC546bp*, and placing the

transistor in a circuit diagram. Selecting the device and then selecting properties opens up the properties window. Select *2nd* opens up the secondary parameters window as shown in figure 2.20.

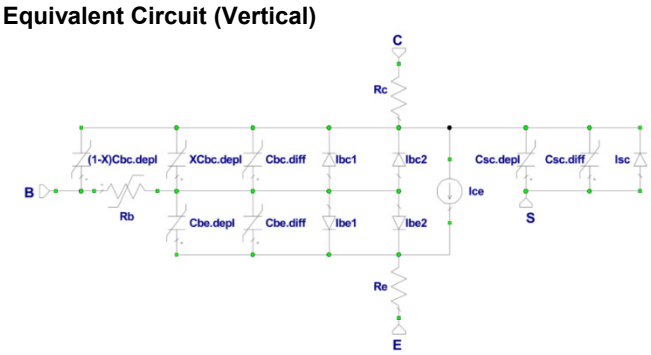



Figure 2.19. Circuit diagram of the Gummel-Poon Transistor model From AWR DE.

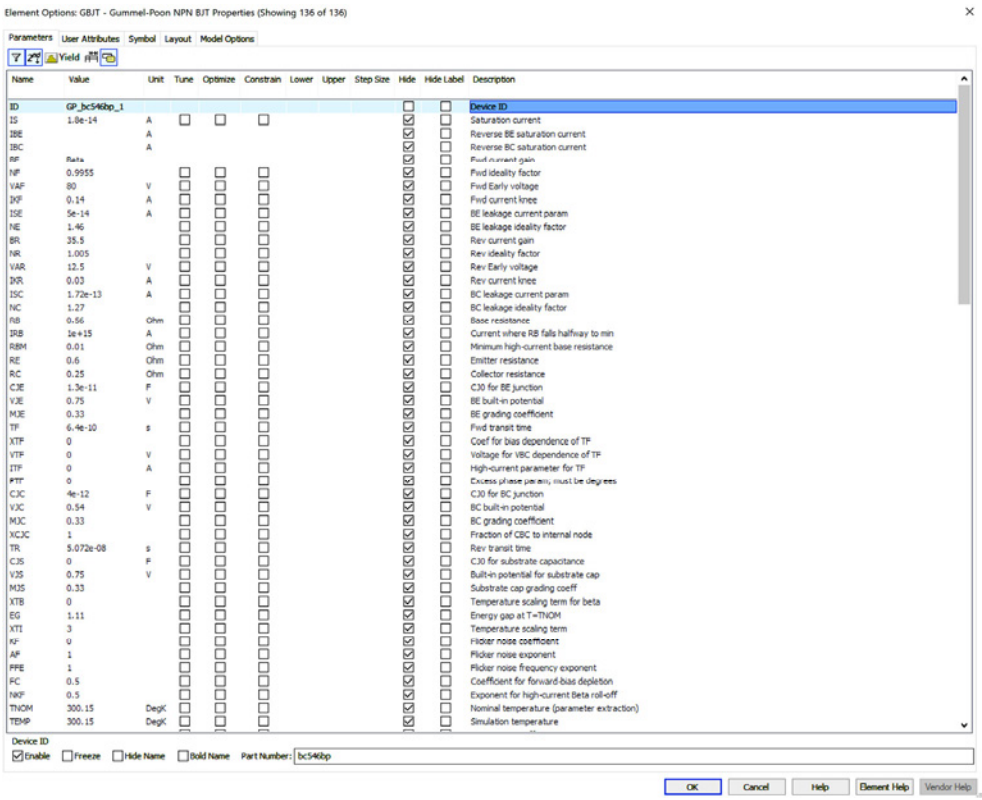



Figure 2.20. Parameters of a BC546 Gummel-Poon transistor model.

Using an existing transistor as a starting point or the Gummer-Poon model available at *Circuit Elements* ⇒ *Nonlinear* ⇒ *BJT* ⇒ *GBJT*, the model for another transistor can be produced by editing the secondary parameters and then saving that with a new name.

For some transistors, instead of the device parameters of figure 2.20, a SPICE netlist, imported as a data file, is included in the AWR device libraries from the web site. As an example a BFP720 transistor SPICE file can be used by selecting *Elements* ⇒ *Libraries* ⇒ **AWR web site* ⇒ *Parts by Type* ⇒ *Nonlinear* ⇒ *Infineon* ⇒ *RF Bipolar Transistors* ⇒ *Ultra Low Noise SiGe:C Transistors up to 12 GHz.* That transistor is used in figure 2.25. The netlist for the BFP720 transistor is the SPICE based Gummel-Poon model realisation:

```
! ************************************************************
! Infineon Technologies AG
! GUMMEL-POON MODEL IN SPICE 2G6 SYNTAX
! VALID UP TO 12 GHZ
! >>> BFP720 <<<
! (C) 2012 Infineon Technologies AG
! Version 3.1 JULY 2012
! ************************************************************
! .OPTION TNOM=25  C, GMIN= 1.00e-12
! BFP720 C B E1 E2
DIM
  TEMP  C
  FREQ  HZ
   RES  OH
  COND  /OH
   IND  H
   CAP  F
   LNG  M
  TIME  SEC
   ANG  DEG
   VOL  V
   CUR  A
   PWR  DBM
CKT
!
CAP 22 33 ID="CBEPAR" C=1.673e-13
CAP 22 11 ID="CBCPAR" C=4.302e-14
CAP 11 33 ID="CCEPAR" C=1.457e-13
IND 22 20 ID="LB" L=7.12e-10
IND 33 30 ID="LE" L=7.9e-11
IND 11 10 ID="LC" L=7.12e-10
CAP 20 30 ID="CBEPCK" C=6e-14
CAP 20 10 ID="CBCPCK" C=1.222e-15
CAP 10 30 ID="CCEPCK" C=6e-14
IND 20 2 ID="LBX" L=3.02e-10
IND 30 34 ID="LEX" L=2.217e-11
IND 10 1 ID="LCX" L=3.02e-10
!
RES 33 55 ID="RPS" R=0.1365
RES 55 30 ID="RSub" R=800
RES 34 3 ID="RE1" R=0.001
RES 34 4 ID="RE2" R=0.001
!
GBJT 22 11 33 55 ID="Q1" TNOM=25 IS=7.621e-16 BF=646.8 NF=1.017 VAF=120.2 &
   IKF=0.08618 ISE=1.782e-14 NE=2 BR=90.95 NR=1.012 &
   VAR=1.455 IKR=0.008585 ISC=2.278e-14 NC=1.5 RB=7.151 &
   IRB=0 RBM=1.031 RE=0.321 RC=5.9 XTB=-2.407 EG=1.11 &
   XTI=0.3 CJE=6.754e-14 VJE=1.064 MJE=0.1384 TF=2.611e-12 &
   XTF=3.2 VTF=2.294 ITF=0.7341 PTF=0.1 CJC=4.36e-14 &
   VJC=1.073 MJC=0.9219 XCJC=0.5 TR=2.035e-09 CJS=7.013e-14 &
   MJS=0.09104 VJS=1.063 FC=0.5 KF=3.4e-12 AF=1.5
!
SDIODE 55 11 ID="Diode_sub" IS=4.085e-15 N=1.02 RS=800 CJ0=4e-14 &
   BV=1e+15
! ************************************************************
DEF4P 1 2 3 4 "BFP720"
```

Many PSPICE device models are available as part of the Cadence OrCad software and SPICE models can also be obtained from several websites [18-21].

High frequency models, which include the effects of the components being mounted on PCB substrates, are available through the optional Modelithics libraries. The Modelithics EXEMPLAR library covers a reduced set of component and a free licence for educational

use by Universities for this library can be obtained from their web site [22]. The linear models for resistors, capacitors and inductors include the effects of surface mount pads, leads and substrates, to permit accurate modelling of the components at microwave frequencies. Non-linear models for active devices are also included.

The technique for importing SPICE files into AWR DE, is shown in appendix 1. Alternately, one can simply change the format by entering the BFP720 parameter values shown above into the secondary parameters window shown in figure 2.20 for the Gummel-Poon transistor and then renaming and saving the device. If needed circuit symbols can also be changed, by right clicking on the device and then selecting *Symbol* to select the desired symbol to be linked.

Figure 2.21 shows the circuit diagrams for the amplifiers shown in figure 2.17, but using nonlinear models instead. The first and very critical step of any transistor design is the biasing. By right clicking on the circuit-schematic and selecting "Add Annotation" and then selecting "DCVA_N" will provide voltages at all the nodes in the circuit, to enable the biasing voltages to be checked and compared with the design values. The node voltage annotation is shown in figure 2.21. To save simulation time, *Data Sets*, results from simulation are stored. If after simulation, the annotation is not shown in the schematic, delete any *Data Sets* from the project and re-simulate the project to refresh the annotation. Similarly, currents in and out of all the nodes can also be shown. The biasing resistors for the 3 circuits are adjusted to give 7 V at the collectors. Those resistor values were then used in figure 2.17 to provide an accurate comparison between the linear and nonlinear model.

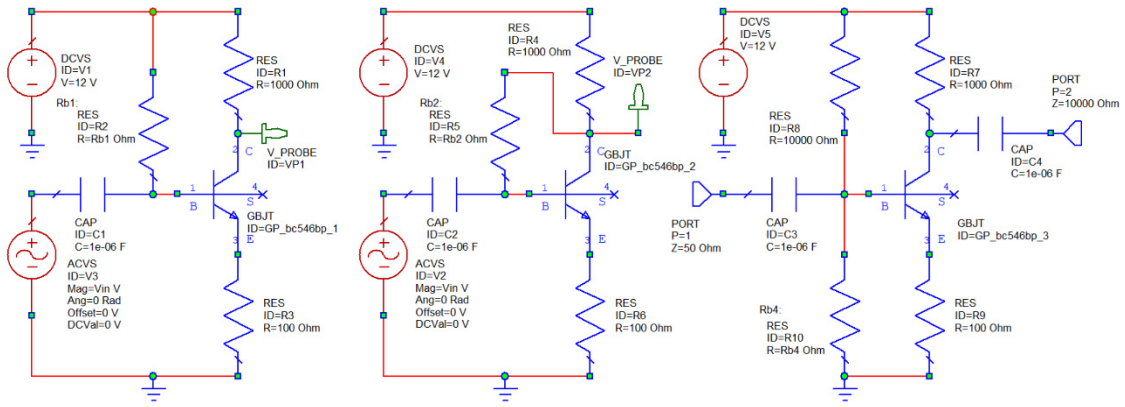



Figure 2.21. Nonlinear simulation of amplifiers of figure 2.17.

The left 2 circuits in Figure 2.21 shows the circuit configuration for the time response shown in figures 2.22 and 2.23. The right circuit in figure 2.21, shows how these circuits can be changed to obtain the frequency responses shown in figure 2.24. For figures 2.22 and 2.23 an input voltage of 0.6Vp and *APLAC Trans* simulators are used. The *APLAC Trans* simulator provides a more accurate waveform simulation than can be obtained using harmonic balance simulators. To plot the time waveforms, Right click on Graphs, and create a new graph. Add a new measurement and select *Nonlinear* ⇒ *Voltage* ⇒ *Vtime* and then select the desired Data Source Name, Measurement Component and Sweep Frequency to be shown. For a frequency plot of the voltage gain select *Linear* ⇒ *Voltage* ⇒ *VGT* and then select the desired Data Source Name, ports and dB Magnitude.

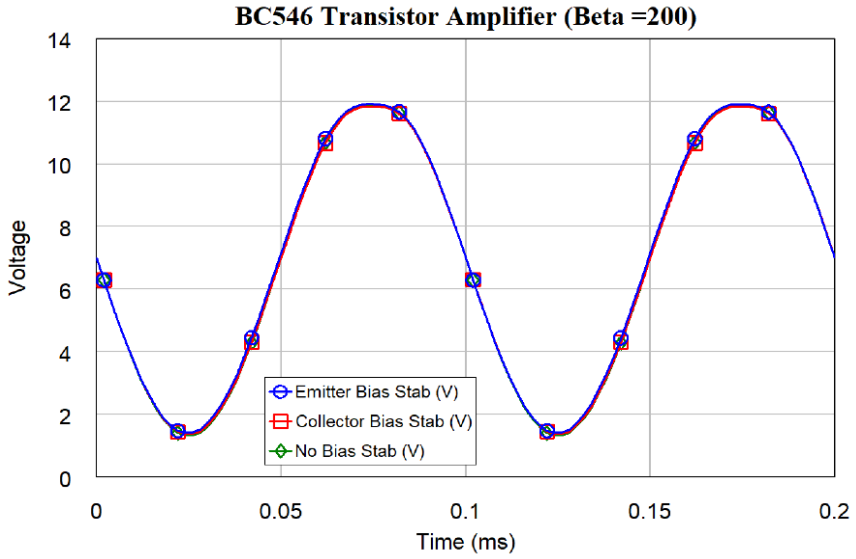



Figure 2.22. Waveform of amplifiers of figure 2.21 with Beta=200.

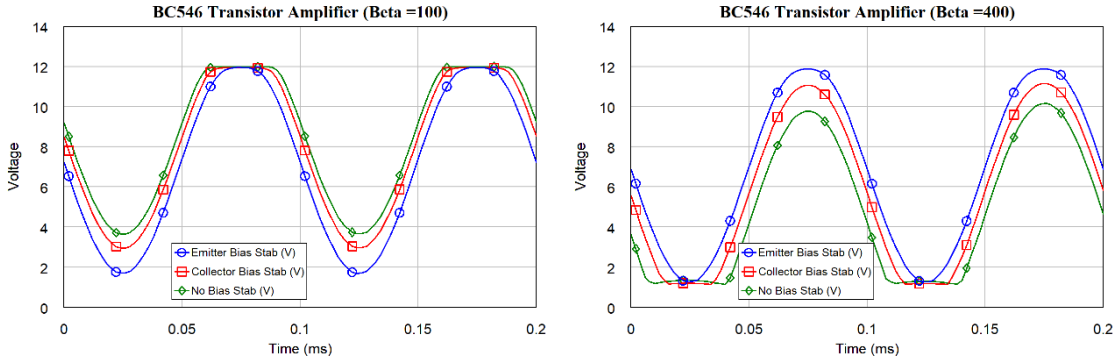



Figure 2.23. Waveform for circuits of figure 2.21 when Beta changes.

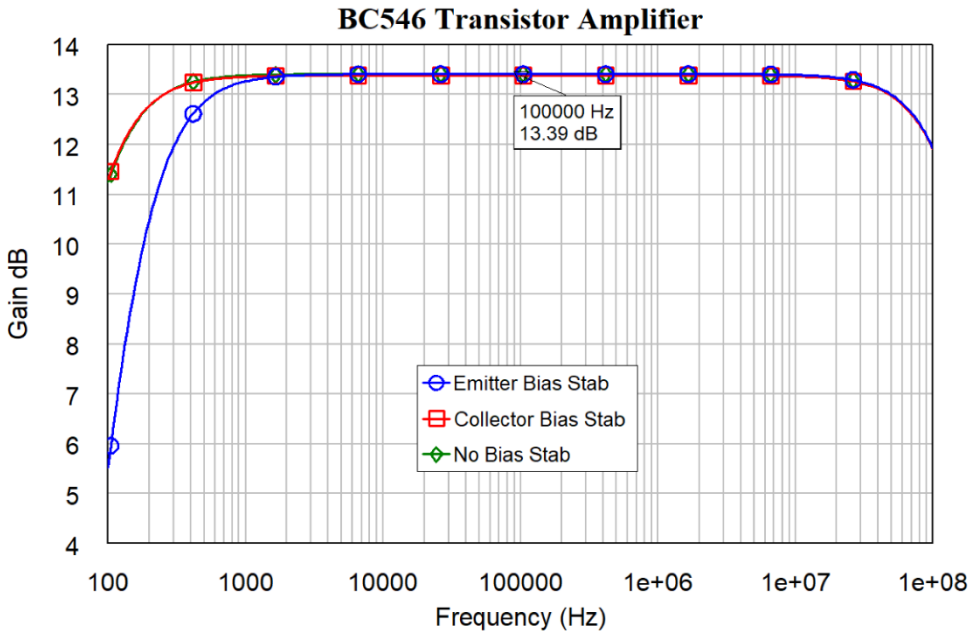



Figure 2.24. Frequency response of amplifiers of figure 2.21.

The transistor gain, Beta, can be tuned to observe the biasing voltage changes that occur when the value of Beta changes. The Emitter stabilisation provides good stability when Beta changes. Frequency Response of these amplifiers for Beta=200 is shown in fig 2.24. Note that the Emitter Bias Stabilised amplifier has a lower input impedance and thus a higher low frequency corner frequency.

## *Example 2.3: Low Noise Amplifier*

The non-linear models are now applied to the design and simulation of a low noise amplifier. The design is to use a BFP720 Silicon Germanium Carbon (SiGe:C) NPN Hetero-junction transistor. The SPICE transistor model can be obtained from the AWR Vendor Library from *Parts By Type* ⇨ *Nonlinear* ⇨ *Infineon* ⇨ *RF Bipolar Transistors* ⇨ Ultra *Low Noise SiGe:C Transistors up to 12 GHz* ⇨ *BFR720*. Add the part to the schematic. The transistor package has two emitter leads, if desired the transistor symbol can be changed by right clicking on the transistor block and selecting properties. Then select symbol *NPN_hbt@APLAC.syf* to replace the 4 terminal block with a double emitter transistor symbol, as shown in figure 2.25. If desired, instead of using Web access to insert the transistor model, the Vendor Library Parts can be installed locally, using the procedure outlined in Appendix 1 and the same parts can then be selected from this locally installed library.

With the package having two emitters, it is difficult to realise emitter stabilisation at >1 GHz. As a result, collector stabilisation is implemented. One of the biasing resistors (Rb) is adjusted to provide a collector current of 10 mA. To obtain a low noise figure, an inductor is used to decouple the biasing. The frequency response of the amplifier has a peak at 4 GHz and adding a 0.7pF capacitor at the output provides a flat frequency response. Increasing the collector current provides a higher gain and a flatter frequency response. The resulting amplifier schematic is shown in figure 2.25. The node voltage annotation is shown. For the microwave amplifier of figure 2.25, the maximum possible gain is required and the emitters are connected to ground. The maximum collector current is 25 mA, so that a 13 mA quiescent collector current is safe. That is also the collector current used for the parameters specified in the data sheet [23]. The resistors Rb can be adjusted to ensure that the quiescent collector current of 10 mA is obtained. As is normal for RF and microwave amplifiers, 50 Ω source and load impedances are used.

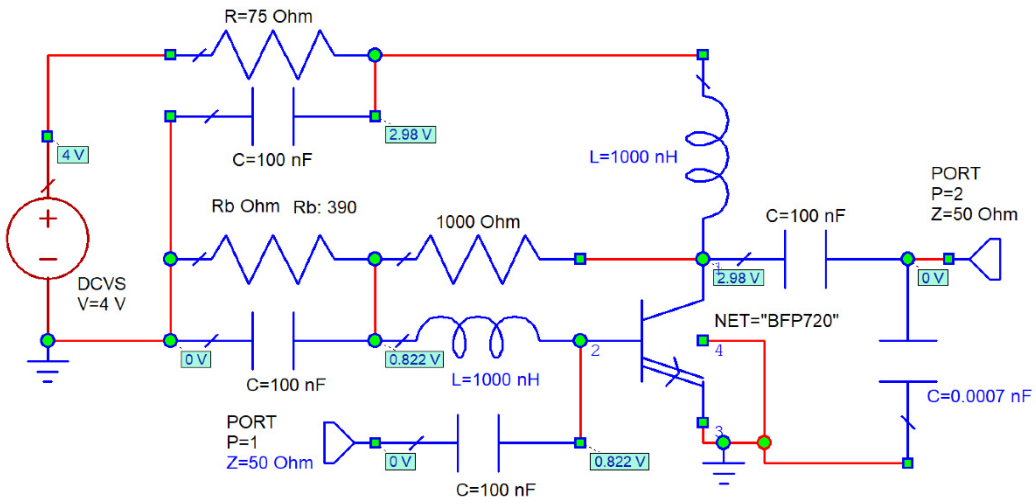



Figure 2.25. Transistor amplifier circuit diagram.

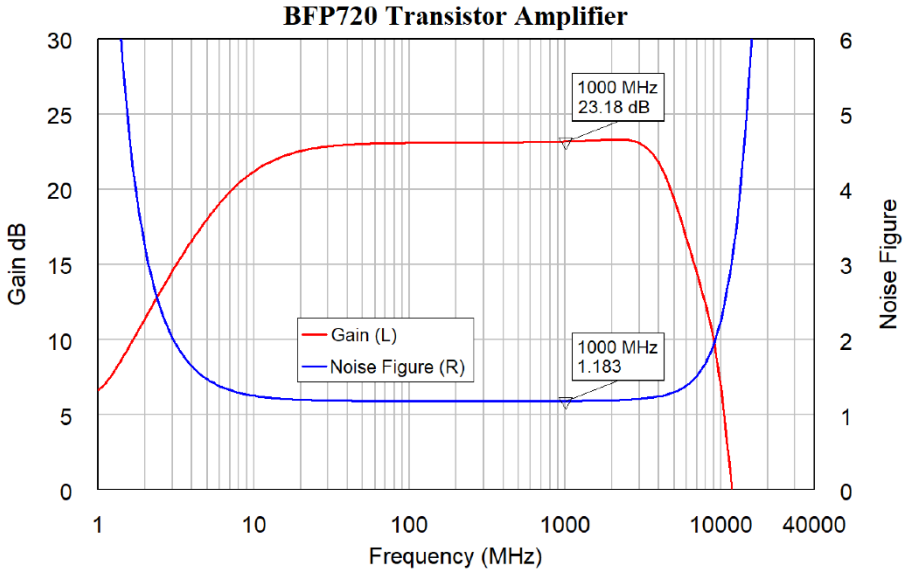



Figure 2.26. Frequency response of the amplifier of figure 2.25.

The gain measurement in figure 2.26 is made using *Linear* ⇒ *Gain* ⇒ VGT to provide the voltage gain from port 1 to port 2. To provide a flat frequency response above 1 GHz, a 0.7 pF capacitor is added across the output. Plotting S11 and S22 for the 50 Ω input and output ports in figure 2.25, shows that this does not provide a good input and output return loss. This results in a gain that is 2 dB less than the data sheet specification. The 50 Ω source and load impedance is not optimum for a low noise figure and as a result, the noise figure is 0.6 dB worse than the data sheet specification. Chapter 8 "Amplifiers: Stability, Noise and Gain" shows how good noise figures can be obtained and Chapter 9 "Impedance matching of Power Amplifiers" shows how the input and output impedances can be matched for a good 50 Ω return loss and best amplifier gain. To prevent having to wait for transients to die down, harmonic balance simulation is preferable for the waveform simulations of this amplifier.

For most transistors, the effect of supply voltage, temperature, and component variations can be investigated, to ensure that the design works properly for all expected component tolerances. However not all device models include a temperature model.

## Determination of Transmission Line Parameters

In many applications, a printed circuit layout using microwave printed circuit board materials needs to be made. The widths and lengths required can be determined. For earlier versions of AWR, a program TXLine, which can be downloaded from the AWR website had to be used to calculate microstrip line parameters. With the current version of AWR DE, the line parameters can be determined by right clicking on a transmission line and selecting synthesise to open the Transmission Line Calculator. TX line and the Transmission Line Calculator cover most of the different coupled lines or strip lines available. In many cases, it is more convenient to use the schematic circuit realisation of the transmission line models to determine the required line parameters, rather than using the Transmission Line Calculator. Figure 2.27 shows a Microstrip line, which we want to be a quarter wavelength long with a 50 Ω impedance at 1 GHz.

Figure 2.27 uses a Rogers RO4003 substrate, with a dielectric constant of 3.38, a loss tangent of 0.0027, a substrate thickness of 0.8128 mm and 35 micron (1 oz.) copper

cladding, as specified in MSUB. To calculate the line width required for a 50 Ω impedance and a quarter wavelength line length at 1 GHz, right-click on the MLIN element in the project of figure 2.27 and select *Synthesize*. That then opens the Transmission Line Calculator window shown in figure 2.28.

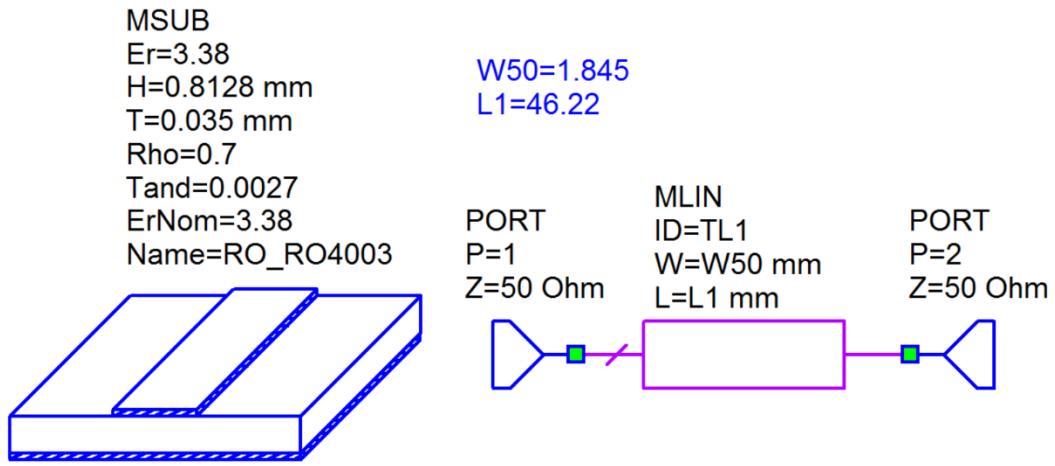



Figure 2.27. Basic Microstrip line circuit.

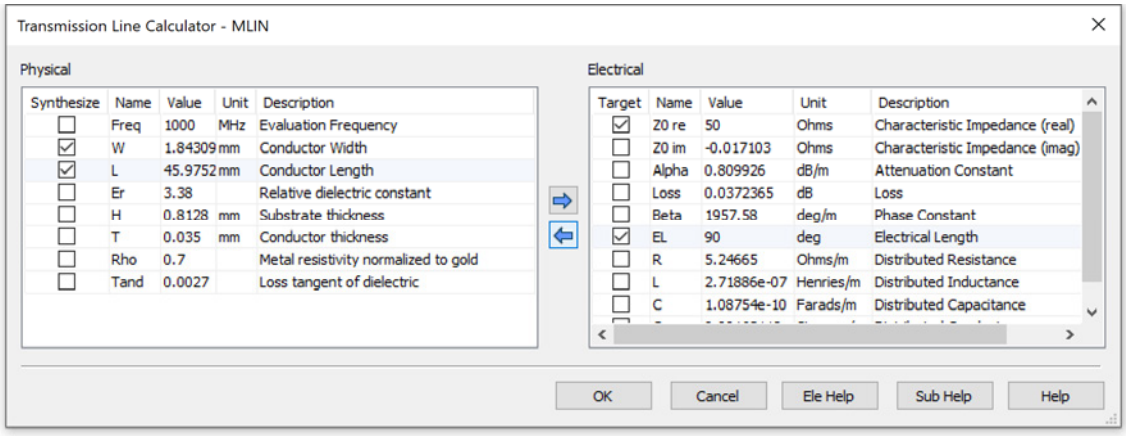



Figure 2.28. Transmission Line Calculator Window.

In the *Transmission Line Calculator* on the Electrical side, change the Z0 re value to 50 Ohms and the EL value to 90 degrees and select those as targets. In the left hand Physical side, select W and L in Synthesize. Then click ⇦ to perform the calculation. The width is calculated as 1.84309 mm and the length as 45.975mm. Selecting OK puts those values in the schematic for W and L. If needed we can copy those values to variables W50 and L90 to use in other schematics.

The same line width determination can be done by making some very simple test circuits and optimising the relevant parameters. For figure 2.27, when the line is exactly 50 Ω, then the return loss ($S_{11}$) is very small regardless of frequency, as described in Chapter 4 "Transmission Line Transformers and Hybrids" of this book. Optimising the line width to give the lowest return loss $S_{11}$ at 1GHz, results in a 1.84314193242188 mm line width and a return loss of 69.34 dB. That width is close to the result from the Transmission Line Calculator.

When the length of a quarter wavelength long line needs to be determined, then the circuit of figure 2.29 can be used. The open circuited stub will reflect as a short-circuit, when

the length of the stub is one quarter wavelength. An open circuit effect of the line is included by using an MLEF line element. The T junction can be included to ensure that the actual layout, including the required junctions, performs exactly as required. Using the width as determined in figures 2.27 or 2.28, the length is now tuned or optimised to produce a notch at the required frequency, as shown in figure 2.30. The quarter wavelength line length at 1 GHz is optimised as 45.851736743757 mm, which is close to the result from the Transmission Line Calculator.

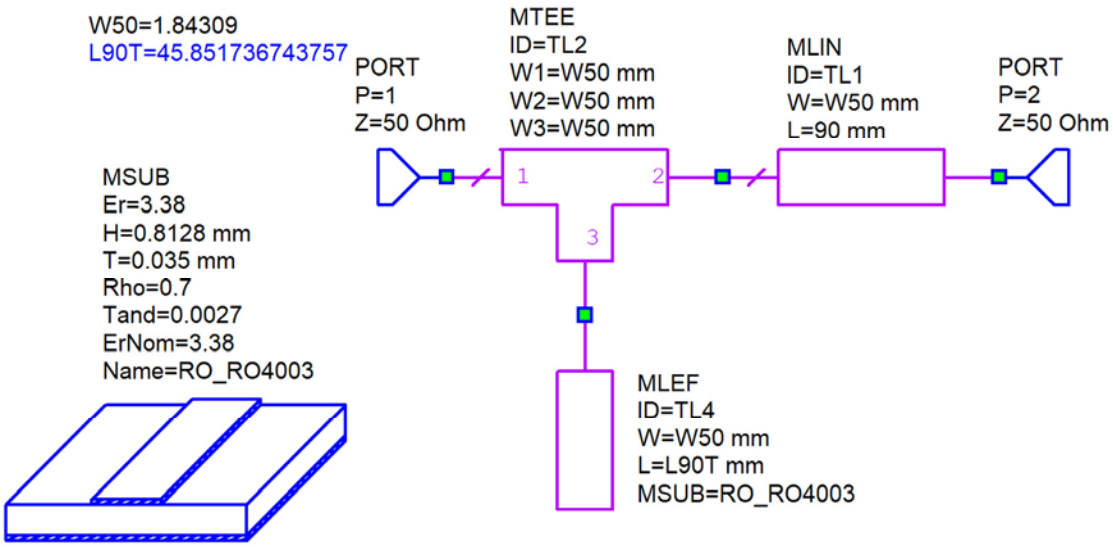



Figure 2.29. Circuit for determining the length of one-quarter wavelength.

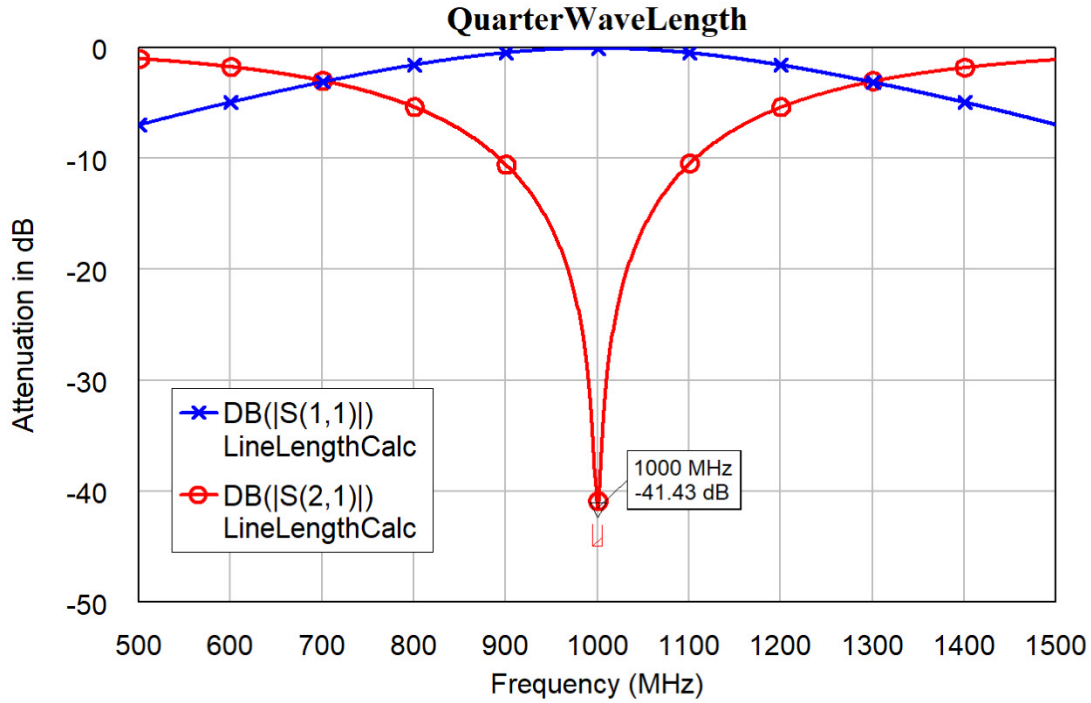



Figure 2.30. Frequency response of the circuit in figure 2.29.

For many circuits, simple test circuits like those of figures 2.27 and 2.29 can be used to determine the basic parameters of Stripline or Microstrip lines that can then be used as part of a more complex circuit. This is used in several places throughout this book.

This technique is very useful for obtaining the correct length when the stub has bends in it, as is the case for the design of a Branchline coupler with folded lines to reduce the size, as described in Chapter 4 " Transmission Line Transformers and Hybrids" of this book

## Nonlinear Time Based Simulation

Many electronic circuits are nonlinear. For example, frequency mixers described in chapter 5 use nonlinear properties of diodes to produce the frequency shifting of RF signals used in most radio and TV receivers. The output amplitude of oscillators described in chapter 6, is determined by the saturation of the active devices. Power amplifiers, described in chapter 9, are normally operated at power levels where the active devices are operating close to saturation and are thus operating in nonlinear regions. The ability to analyse the effect of the nonlinear operation of circuits is thus an important part of any design.

There are two types of nonlinear time-based simulation. The first type is time domain based **transient** simulation, like the classical Laplace transform based circuit analysis for linear circuits. The time waveforms produced by computer simulation programs such as Multisim, Microcap and LTSPICE use SPICE time based simulation. AWR DE includes transient time based simulation using APLAC® or the optional HSPICE® and Spectre® software. Transient analysis, begins at time t = 0 and assumes that only DC sources are connected to the circuit to be analysed, before that time. At time t = 0 a stimulus is applied and the resulting current and voltage waveforms are determined at ports or test points. The transient simulators start with the largest possible time increment and reduce that time increment automatically if the results are not accurate enough. If needed the automatic time increment selection can be overridden. See Basic_Transient.emp project in the MWO/AO /Examples [24] for an example included with the AWR DE software. It is desirable to read the help file AWR DE *Simulation and Analysis Guide > Transient Analysis > Transient Analysis Basics* (Section 7.1) [25], included with AWR DE software for additional information if needed. These help files contain much more detail than what is needed for this book. Transient analysis is useful for determining the transient time and voltage waveforms of a circuit.

The second type is Harmonic Balance (HB). This is a frequency based, **steady state** analysis that uses non-linear differential equations to model the devices and then uses a linear combination of excitation tones to balance currents and voltages to satisfy Kirchhoff's law. The inputs applied to the circuit are one or two tone signals, whose amplitudes or frequency can be swept if needed. The amplitude, phase and frequency at the ports or test points in the circuit, as determined by HB can be used to calculate the corresponding time waveforms.

HB has a lower noise floor than transient time simulation and is thus better for determining harmonics. Examples of harmonic balance simulations are shown in Chapter 5 "Mixers" and Chapter 6 "Oscillators" of this book. Harmonic Balance provides a fast simulation of the most common RF circuit analysis; the steady state operation of non-linear circuits, and it is able to easily display the corresponding time waveforms and spectra. Harmonic Balance is thus used more often than transient time domain simulation.

AWR DE comes with a built-in HB analyser and more recently with the APLAC ™ simulator, which includes both HB and transient analysis simulation.

## *Time Domain Transient Circuit Simulation*

The time domain transient analysis is illustrated with the simulation of a Buck DC-DC converter, used in many power supplies. For this circuit the maximum voltages and currents in the start-up transients are important as well as the steady state operations. This example is used to show both transient and harmonic balance analysis operation.

### Example 2.4: Buck DC-DC Converter

The specifications are for the buck converter to change $V_{in}$ = 48 Volt DC to $V_{out}$ = 12 Volt DC. A maximum output current of 5 Amp is required. MOSFETs have low ON resistance and result in a high efficiency converter design. An IRF9530 – SiHF9530 100V, 12A, P Channel Power MOSFET, with an ON resistance of 0.3 Ω is chosen. The PSPICE model for that is readily available from the Vishay web site [26]. Change the extension from .lib to .cir and import it in AWR DE. A switching frequency of 100 kHz, is chosen to keep the filter elements small while minimising switching losses.

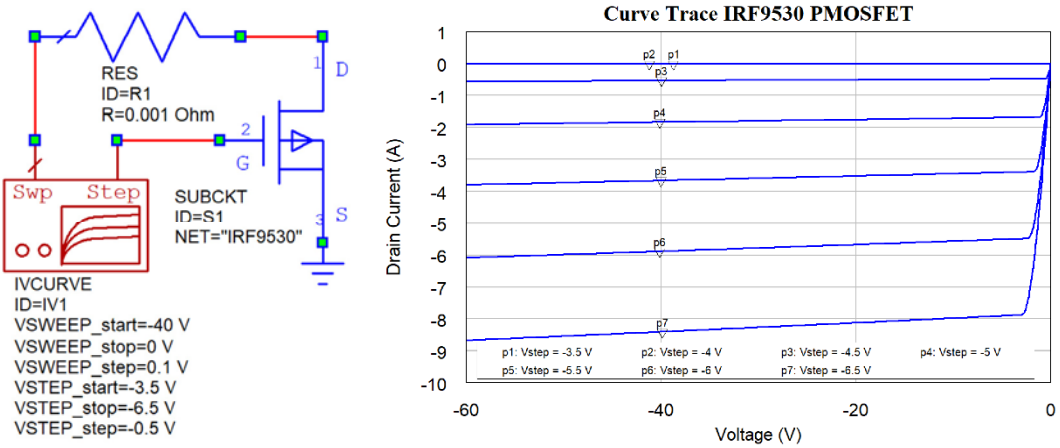



Figure 2.31. Curve tracer use and output for IRF9530, SiHF9530 PMOSFET.

AWR DE allows the transistor's IV curves versus bias current to be plotted using the IVCURVE measuring device. Figure 2.31 shows that for a 6 Amp drain current, and a -48 V, drain source voltage, a > 6 Vpp gate voltage is required. Varying the gate drive voltage in the simulation shows that a 10 Vpp gate drive is required to switch the MOSFET hard ON and this minimise the losses in the converter. For a 5 A nominal output current, the nominal load resistor must be 12/5 = 2.4 ohm. A minimum current of $I_{min}$ = 0.2 A is required, corresponding to a maximum load resistance of 60 Ω.

$$D = \frac{V_{out}+V_{diode}}{V_{in}+V_{diode}} \qquad \text{Eqn. 2.3}$$

$$L \geq \frac{t_{on}}{2I_{min}}(V_{in} - V_{out}) \qquad \text{Eqn. 2.4}$$

$$V_{ppr} = V_{out}\frac{T_S^2(1-D)}{8LC} \qquad \text{Eqn. 2.5}$$

If the diode voltage drop is 0.5V, then equation 2.3 shows that the duty cycle D = 0.2577. For a 100 kHz switching frequency, that results in an ON time $t_{on}$ = 2.577 µs. Equation 2.4 then results in a minimum inductance of 232 µH. For a peak-to-peak ripple voltage $V_{ppr}$ = 50 mV, a $C_{min}$ = 9.6 µF is required. In the simulation of the Buck Converter $L_{min}$ = 240 µH and $C_{min}$ = 10 µF are used. For realistic results, a 0.1 Ω resistive loss is included for the inductor. That results in a 0.5 V drop across the inductor and a

corresponding reduction in output voltage. Changing $t_{on}$ to 2.67 µs, results in 12V for a 2.4 Ω load. The 10 µF capacitance and the nominal resistance result in a Q of 0.24, so that the transient response of the output voltage has minimal overshoot. The corresponding circuit of the buck converter is shown in figure 2.32.

In figure 2.32, Voltage probes have been used for the measurement points. They are not really needed since VP1 is the same as the voltage at node 1 of the inductor, SRL.RL1@1 and VP2 is the same as SRL.RL1@2. The use of voltage probes makes it easier to identify the measurement locations.

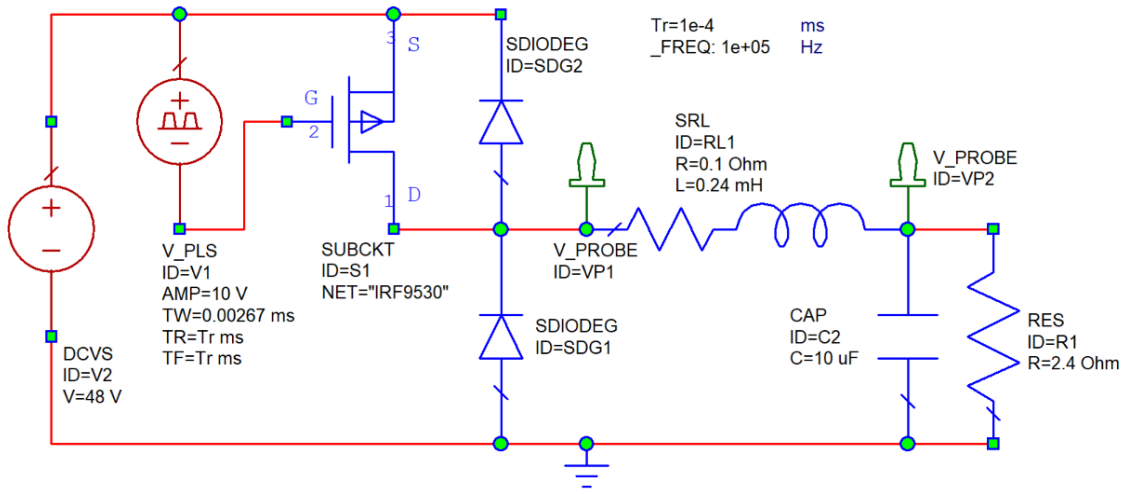



Figure 2.32. Buck DC-DC converter circuit.

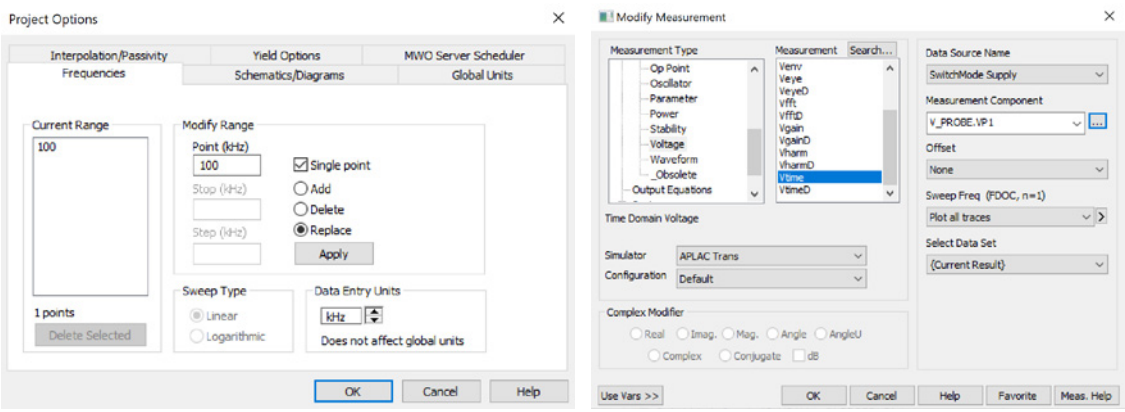



Figure 2.33. Frequency setting (L) and measurement type window (R) for transient simulation.

To specify the measurement points, select *Nonlinear* and *Current* and *Itime* for current measurements versus time and Voltage and Vtime for voltage measurements versus time. Ensure that the simulator selected is *Aplac Trans* for the transient analysis required, as shown on the right in figure 2.33. This then turns on the APLAC transient analysis and turns off any HB analysis for that measurement. Then select the location of the voltage or current to be measured, by double clicking on the small window showing "..." next to "Measurement Component" in figure 2.33(R). This then shows the circuit diagram of figure 2.32 and allows the selection of the component or lead where the current or voltage is to be measured and plotted.

For the simulation, the first step is to set the frequency of operation by setting the frequencies in the project options as a single frequency of 100 kHz as shown in figure 2.33. Setting this frequency automatically controls the time steps used in the simulation

in order to obtain an accurate solution. It is possible to do simulations for multiple operating frequencies of the Buck converter. However, that results in overlapping output plots, so single frequencies are best. The next step is to ensure that the length of the simulation is correct. In this example, we want to analyse the transient response and settling of the output voltage. For the maximum load resistance of 60 Ω, the transient response takes 1.5 ms. Corresponding to 150 periods of the 100 kHz pulse generator V_PLS, are required. Since a 48V supply is switched, it is also necessary to increase the *Maximum Voltage or Current Change* from the default value of 1 to 100 in this *APLAC Sim* window of figure 2.34(L).

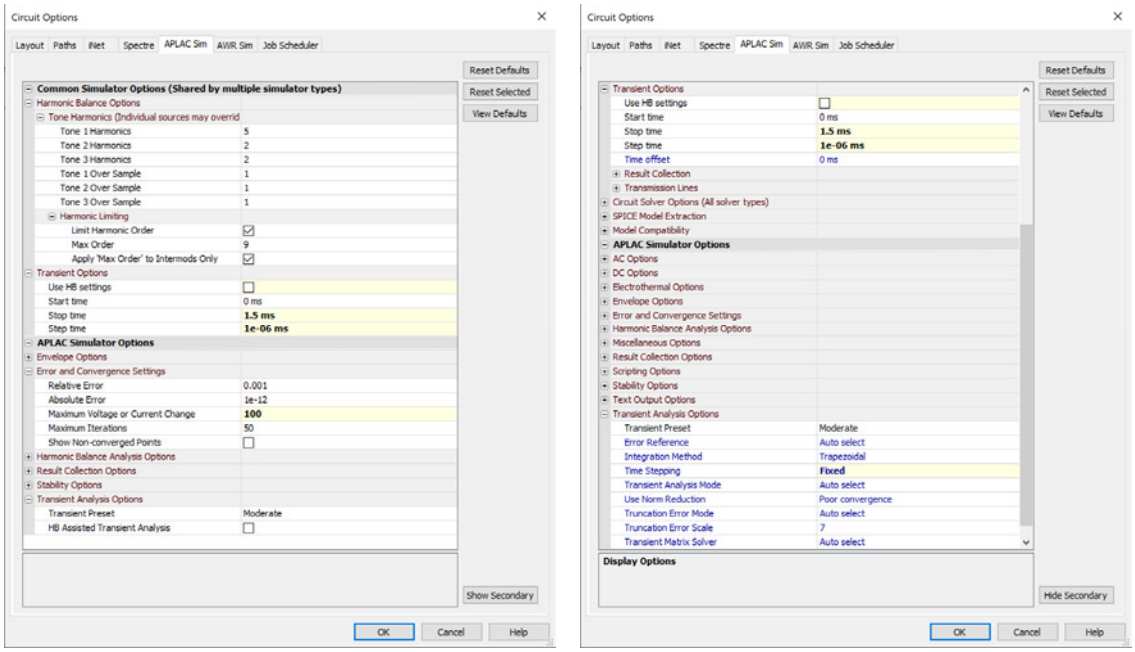



Figure 2.34. Circuit Option settings primary (L) and secondary (R) for transient analysis.

Normally, the time stepping is varied to ensure accurate results then changes occur. In this simulation that results in ringing when timing is changed by APLAC. To avoid this in *APLAC Sim* window in Circuit Options, select *Show Secondary* as shown in figure 2.34(R) and in Transient Analysis Options, for Time Stepping select Fixed. Then set the Time step values in Transient Options. Set the simulation Stop time to 1.5 ms and set step time to 0.01 µs or 1e-5 ms. If the step time is set too large, the simulation will not be accurate and the output voltage may decrease as the On time $t_{on}$ (TW) is increased, instead of increasing as $t_{on}$ is increased. If the step time is too small, the simulation will take long to complete. The settings in the project files for figure 2.31-2.40 incorporates these settings. By making variables or elements tuneable, the effect of their variation can easily be investigated. For the calculated ON time of 2.567 µs, the switching delays result in a steady state output voltage for the converter of 11.52 V. The 0.5 V lower than expected voltage is caused by the 0.5 V drop due to the 0.1 Ω resistance of the inductor. Changing the ON time of the pulse generator to 2.67 µs results in a close to 12V output with little overshoot and ripple at the 5A output current, as shown in figure 2.35.

If the simulation of a circuit like the one in figure 2.32 fails, it may be possible to complete it by selecting *Options* ⇒ *Default Circuit options* ⇒ *APLAC Sim* ⇒ *Show Secondary.* Then for the *APLAC Simulation Options* ⇒ *AC Options* or *DC Options,* change the settings for the *Matrix Solver* from *Auto Select* to one of the other settings like *Aplac Sparse*. Other changes like reducing the step-time, may also assist in the completion.

For many simulations using imported SPICE models, warnings like “Value of (SDIODE!_S1_D3.RS) < RMin (changed to 10.000u)” may be shown. If preferred, they can be removed by changing RS in the line “SDIODE 5 0 ID="D3" IS=1e-10 N=0.4 RS=3e-06 BV=1e+15” in the original PSPICE file from RS=3e-06 to RS=10e-06.

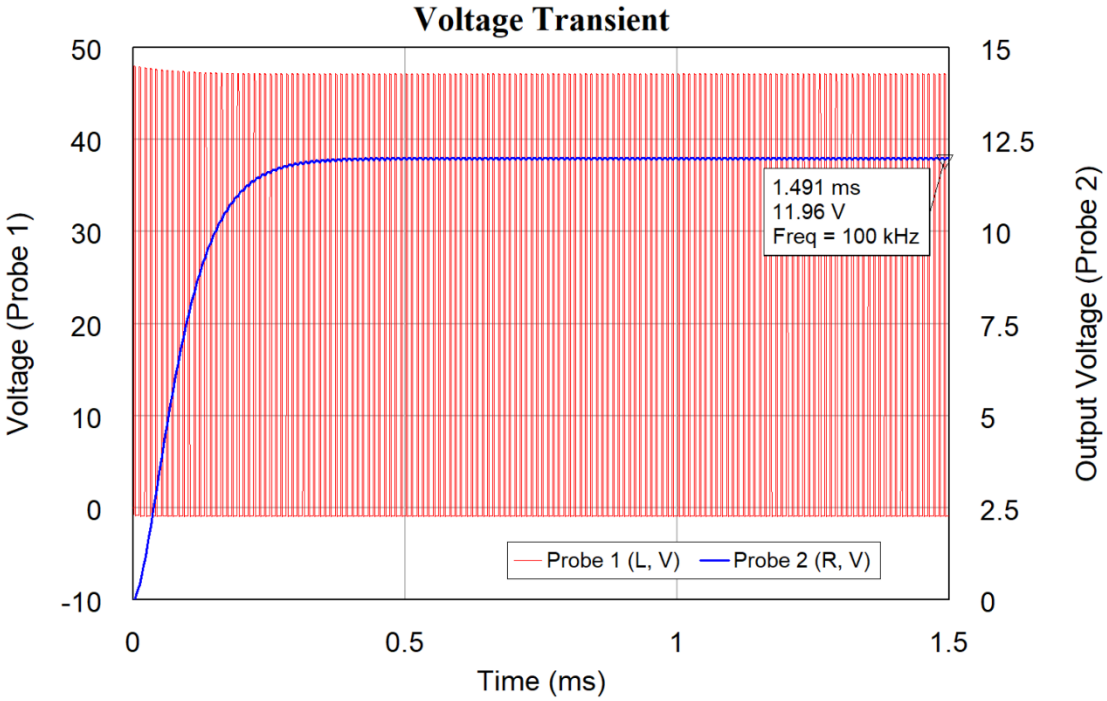



Figure 2.35. Buck Converter voltage waveforms at probes and pulse generator.

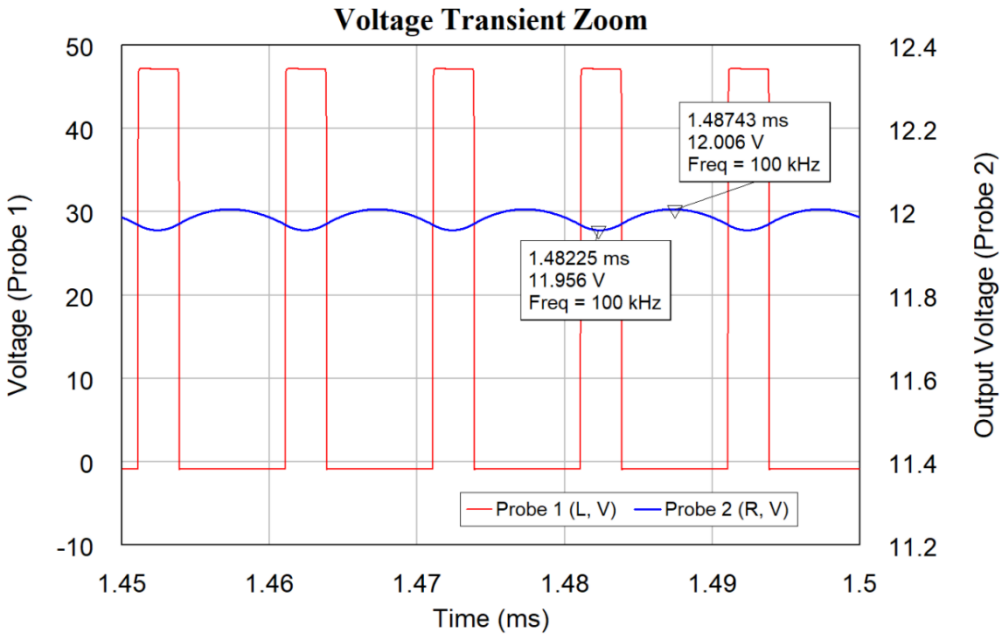



Figure 2.36. Close-up of steady state voltage of figure 2.35.

The output voltage has a small steady state ripple, which can be seen plotting the time waveforms from 1.45 to 1.5 ms. Plotting the output voltage (VP2) on the right axis allows the voltage scale to be magnified. The steady state output voltage as obtained by the transient analysis is close to 12 V as shown in figure 2.36. The current waveforms of the buck converter of figure 2.32 are shown in figures 2.37 and 2.38.

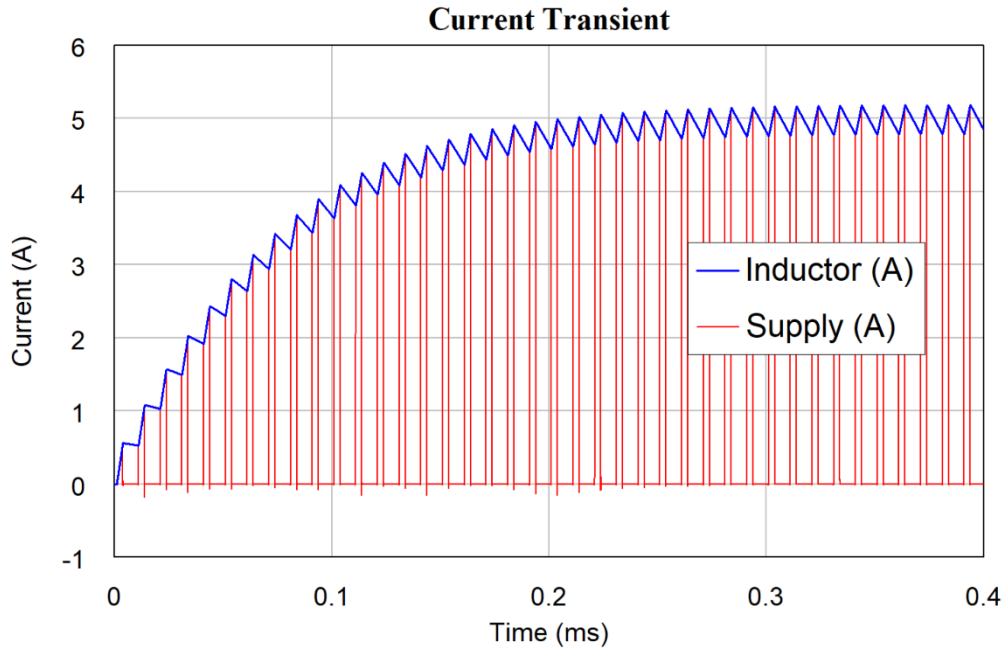



Figure 2.37. Buck Converter current waveforms with $R_L$=2.4 Ω.

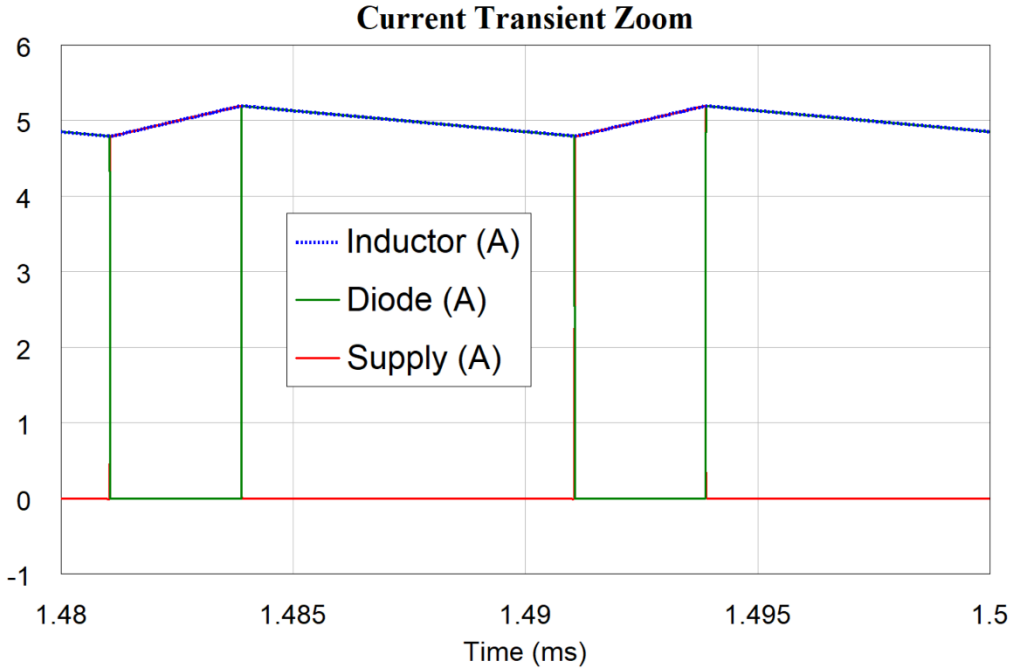



Figure 2.38. Buck Converter, expanded time current waveforms with $R_L$=2.4 Ω.

Changing the load resistor from 2.4 Ω to 120 Ω causes a larger transient output voltage overshoot and results in the converter operating in a discontinuous conduction mode as shown in figure 2.39. The plot of voltage waveforms similar to figure 2.35, show some damped high frequency oscillations, when the transistor switches OFF, as shown in figure 2.40, with the expanded time waveforms on the right. This figure also shows that the output voltage has an overshoot to 10.8V, which may be too high for safe operation of any hardware connected to the DC-DC converter. This simulation is done with the time and step settings of figure 2.34 (L). Using the Use HB settings produces slightly different results and may not clearly show the oscillations.

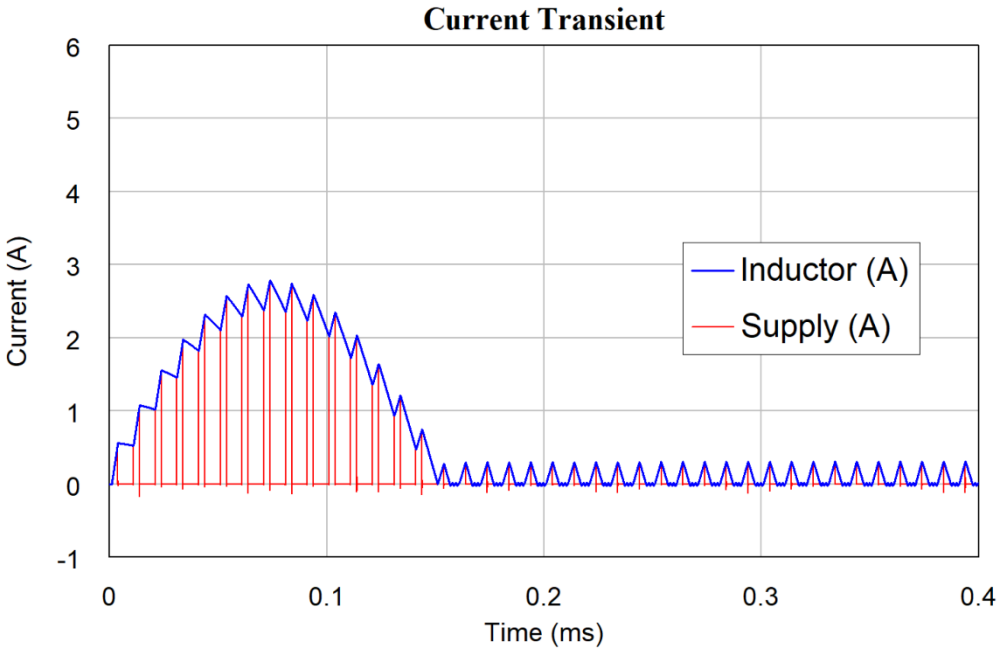



Figure 2.39. Buck Converter current waveforms with $R_L$=120 Ω.

Observing the steady state transient output similar to figure 2.36, shows that the output voltage has a peak of 24.3V. Extending the simulation time to 6 ms results in an output voltage of 17.54 V at 2 ms, 17.23 V at 4 ms and 17.20 V at 6 ms. The voltage increase is due to the discontinuous conduction mode. This voltage may cause damage to any 12 V loads. These simulations are thus useful to design hardware that produces the correct output voltage regardless of the output current drawn. For this application, that requires the pulse width TW in figure 2.32 to be controlled by the output voltage.

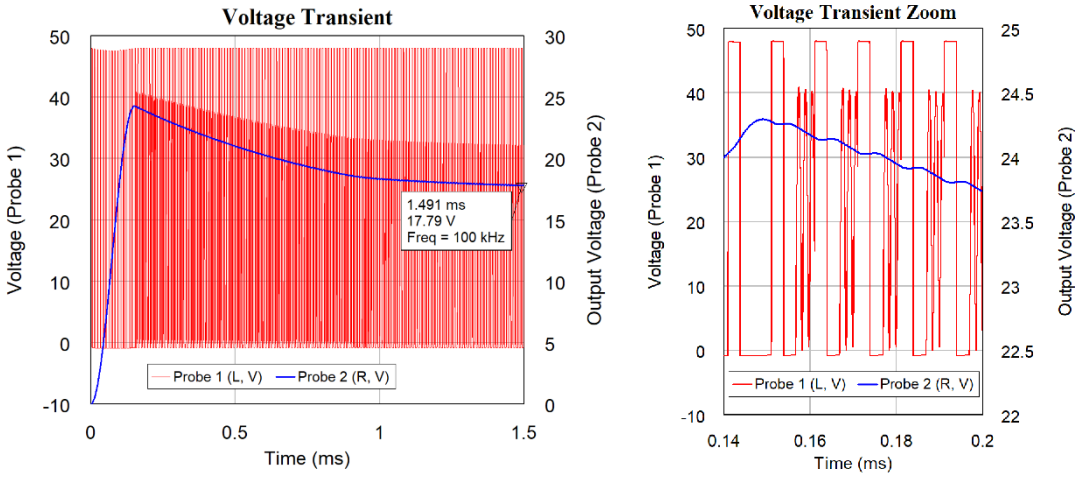



Figure 2.40. Buck Converter voltage waveforms with $R_L$=120 Ω.

## *Harmonic Balance Circuit Simulation*

Harmonic balance (HB) is used in chapter 5, to determine the conversion loss and waveforms of mixers, it allows the variations of gain with signal amplitude in an amplifier to be calculated and it allows all the harmonics produced by the oscillator to be determined. Using the appropriate non-linear amplifier models, HB allows the inter-modulation distortion of an amplifier to be determined as a function of output power. Because HB simulation takes significantly longer to complete, most designs are initially

done using linear simulation models and then the final design is optimised using the harmonic balance models. HB simulation produces steady state results only.

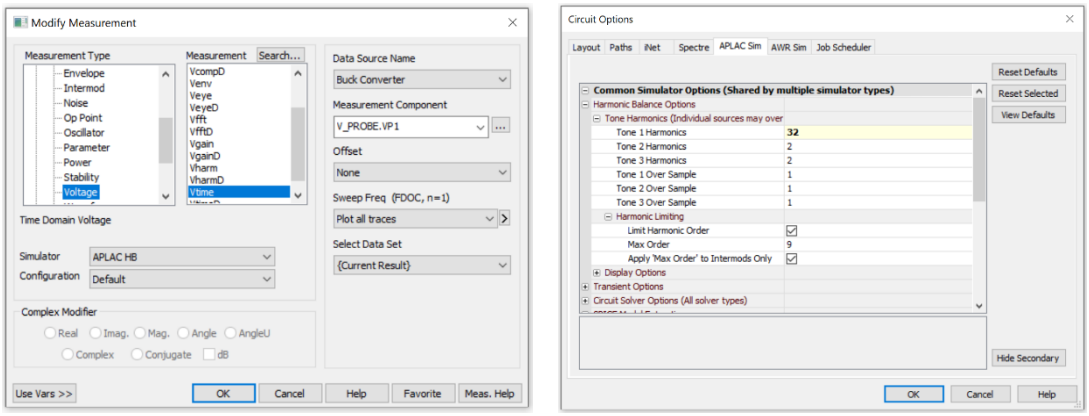



Figure 2.41. Harmonic Balance option windows.

Harmonic balance simulation can be carried out by simply changing the properties of the measurements of the voltage transient analysis graph from APLAC Trans to APLAC HB, as shown on the left of figure 2.41. Since the input waveform is a square wave, the number of tone harmonics to be used needs to increase. Select *Options* ⇒ *Default Circuit Options* ⇒ *Harmonic Balance*, and then increase the number of harmonics to 32 as shown in as shown on the right of figure 2.41.

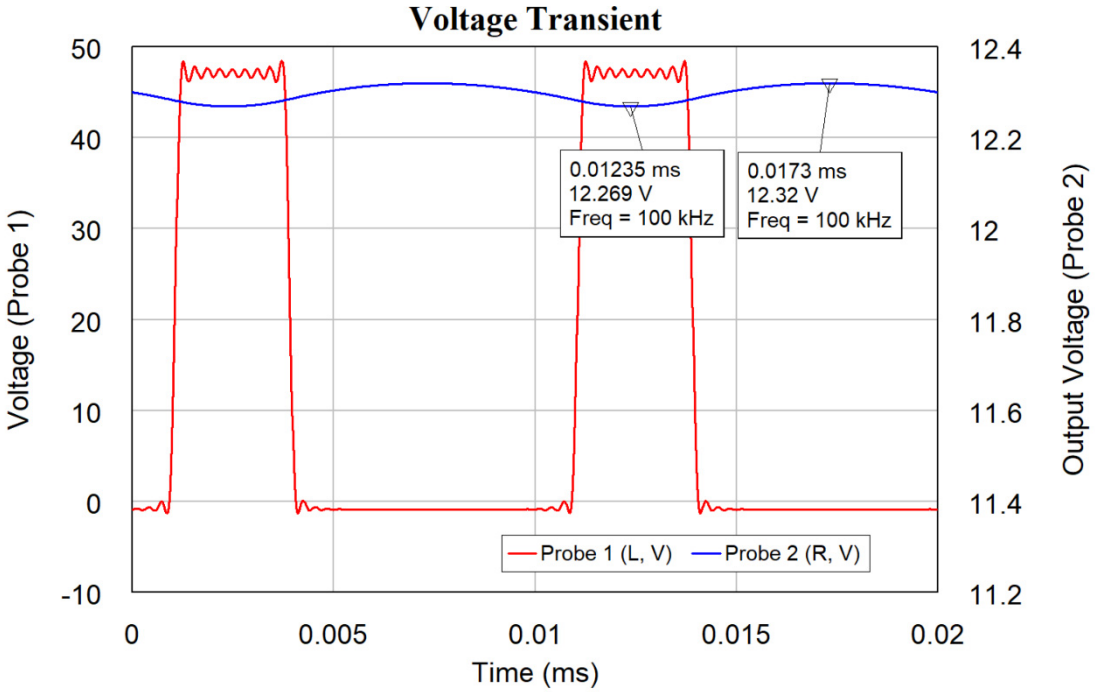



Figure 2.42. Waveforms for the circuit of figure 2.43 using Harmonic Balance.

Figure 2.42 shows the voltage waveform resulting from the Harmonic Balance simulation, using 32 harmonics. The time scale corresponds to 2 steady-state cycles of the input waveform. The output voltage level is slightly higher than the one obtained using the time domain simulation, as shown in figure 2.36. Having a lower number of harmonics results in a more distorted square waveform and a higher output voltage. The convergence depends on the number of harmonics and the waveform duty cycle. The

project file for figure 2.42 uses a pulse width TW=2.67 μs and 32 harmonics for the harmonic balance simulation. That project file will not converge for >48 harmonics. When $R_L$ = 120 Ω, high frequency oscillations occur in the transient response as shown in figure 2.40. As a result, the harmonic balance simulation fails to converge. For most RF circuits, square waves are not used, so that a high number of harmonics is not required to represent the waveforms accurately. As a result, convergence is normally achieved.

The transient analysis fully includes all nonlinearities specified in the device parameters and accurately incorporates unexpected conditions like the oscillations shown in figure 2.40. Accurate nonlinear analysis as described here is thus essential in ensuring a design operates fully as required over all expected input and load conditions. The Transient and Harmonic Balance simulations give very similar steady state results, but for <32 harmonics, APLAC HB simulation is normally quicker.

## Black Box Matching of Circuits to Measurements

Sometimes one needs to model an existing device, without having direct access to all the elements making up that circuit. An example [9,27] is the development of a model can be used to model a mains power distribution transformer, at frequencies up to 5 MHz, so that one knows the impedances the transformer presents at Power Line Carrier frequencies (up to 150 kHz), which are used for Smart Grid applications or determining the effects of lightning through power networks. A single-phase power distribution transformer has 2 terminals for its low voltage (LV) winding, 2 terminals for its medium voltage (MV) winding and a terminal for the metal case of the transformer, a total of 5 terminals. A 3-phase power distribution transformer has 3 LV phase terminals, 3 MV terminals, a Neutral terminal and a case, a total of 8 terminals. To simplify the model, each LV phase winding and each MV winding is assumed to be identical. So that a similar model to the single phase transformer results, as shown in [27].

One can measure the impedances seen between any 2 of the 5 terminals of a single phase transformer. As shown in [9], a sufficiently accurate model can be developed using 5 measurements, rather than the 10 possible measurements that can be made between the 5 terminals. The problem now becomes how to match the components in the model to those impedance measurements. One could write down equations for the impedances that can be seen in each of the 5 measurement points and solve the resulting complex equations to obtain the component values. Since the impedances of the inductances and capacitances change with frequency, solving these equations is an exceedingly difficult task.

It is possible to guess a circuit configuration and use MWO and optimisation tools, to "solve" the simultaneous equations by optimisation and match the circuit elements to the measurements. To illustrate this technique, the process is performed on a relatively simple network.

### *Example 2.5: Bandpass T Matching Network*

A simple Bandpass T matching network described in Chapter 9 "Impedance Matching of Power Amplifiers" of this book is used to illustrate the impedance matching process. These networks are used to match power transistors to 50 Ω loads. For this example, an input matching network is chosen to match a device with an input impedance of $X_D$ = 5 + j 0.9 Ω to a source with $X_L$ = 50 Ω at 150 MHz with a Q of 3.5. The equations in Chapter 9 are entered into the Global Definitions window, as shown in figure 2.43. Two versions of the circuit are shown in figures 2.44 and 2.45 respectively. Lbt, Cbt1 and Cbt2 are the

component value variables evaluated from the equations in the Global Definitions window.

```
Band  Pass T
Rl=50      Q=3.5        TwoPi=2*_Pl
Rd=5       Xd=0.9       Fm=150

Wm=TwoPi*Fm*1e6                    Ld=Xd/Wm
A2=((Rd*(1+Q*Q)/Rl) -1)            A=Sqrt(A2)
B=Rd*(1+Q*Q)                       Qmin=sqrt(Rl/Rd-1)

Xlbt= (Rd*Q - Xd)                  Lbt=Xlbt/Wm
Xcbt2=Rl*A                         Cbt2= 1/(Wm*Xcbt2)
Xcbt1=B/(Q-A)                      Cbt1= 1/(Wm*Xcbt1)
```

Figure 2.43. Bandpass T equations in *Global Definitions* window.

Figure 2.44 uses a voltage controlled voltage source to implement the impedance of the source and is only included to show the complex source impedance of transistor can be realised. The Voltage Controlled Voltage Source, resistor R1 and inductor L1, provide the same impedance as the transistor. Figure 2.45 implements that complex impedance as part of port 1. The component values are calculated to be Lbt = 17.61 nH, Cbt1 = 46.92 pF and Cbt2 = 37.22 pF. In addition, the components were assigned typical Q values of 100 for the inductor and 300 for the capacitors. Figure 2.46 shows the resulting frequency response of the network of figure 2.45. The impedance match is very good at 150 MHz and is better if ideal elements are used.

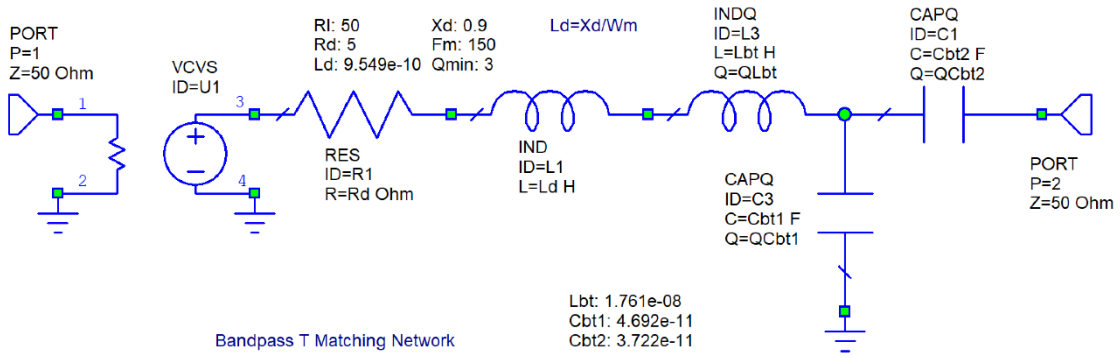



Figure 2.44. Calculated Bandpass T matching network with VCVS impedance matching.

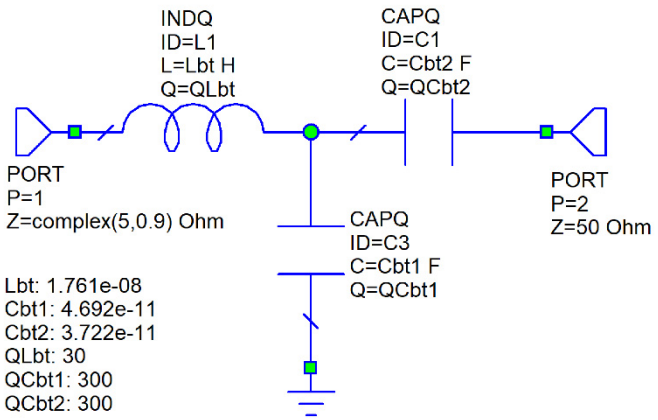



Figure 2.45. Calculated Bandpass T matching network with Port source impedance matching.

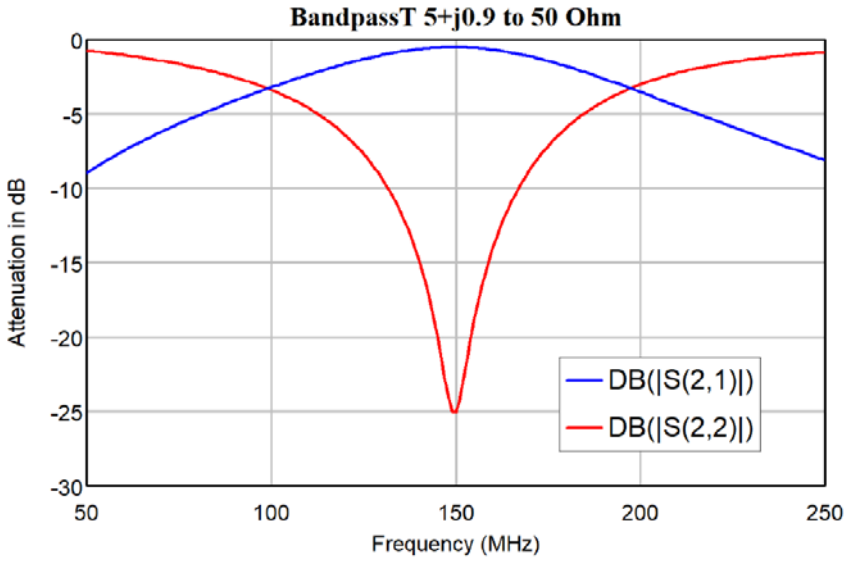



Figure 2.46. Frequency response of the calculated Bandpass T matching network.

## S Parameter Measurements

The network of figure 2.45 is used to generate an S parameter file. Such a data file is similar to S parameter data obtained from a network analyser. This file is obtained by exporting the trace data of a table-graph containing the complex S parameters of the circuit in figure 2.45. This can be saved as a text file. Change the .txt extension to .S2p to denote a 2-port S parameter file. This file can then be imported as a Touchstone file, by right clicking on *Data Files* and selecting *Import Data File* or by using the *Project* ⇒ *Add Data File* ⇒ *Import Data File* dropdown menu. This data file can be named "Measurements". The Touchstone heading "#MHz S RI" needs to be added, to denote that the frequency is in MHz , it is an S parameter file and the data are Real and Imaginary values. "R 50" denotes that a 50 Ω source and load impedance is used. That is the default.

The Touchstone file format for a 2-port S parameter network typically is as follows:

```
# GHZ S RI R 50
f1 ReS11 ImS11  ReS21 ImS21  ReS12 ImS12  ReS22 ImS22
f2 ReS11 ImS11  ReS21 ImS21  ReS12 ImS12  ReS22 ImS22
f3 ReS11 ImS11  ReS21 ImS21  ReS12 ImS12  ReS22 ImS22
```

In addition the heading lines of text need to be denoted as comments by inserting a "!" at the beginning of the line. The resulting Touchstone file is as shown in table 2.2. To keep the number of lines in this table small a 10 MHz frequency increment is chosen in the project options, resulting in 21 frequencies being used. In practice, many more frequencies would be used. This table is produced by calculating the S parameters for the network of figure 2.45 when the port impedances are 50 Ω.

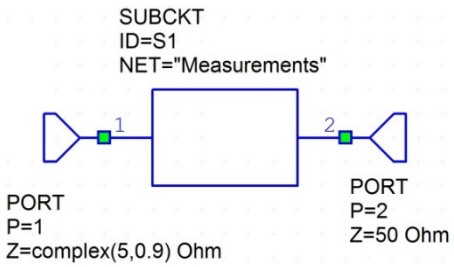



Figure 2.47. Circuit containing the Measurements Touchstone file.

The data in table 2.2 is used in a new circuit, by right clicking on *Circuit Schematics* and selecting *New Schematic* and giving that a suitable name like "Measured_Ckt". Select Draw ⇒ Add Subcircuit and for the Subcircuit select the Measurements Touchstone file. Add ports to result in the circuit shown in figure 2.47.

Table 2.2. Bandpass T, S parameters of figure 2.45 when Port Z=50 Ω.

| !1 | 2 | 3 | 4 | 5 | 6 | 7 | 8 | 9 |
|---|---|---|---|---|---|---|---|---|
| #MHz S RI | | | | | | | | |
| !Freq | S(1,1) (Real) | (Imag) | S(2,1) (Real) | (Imag) | S(1,2) (Real) | (Imag) | S(2,2) (Real) | (Imag) |
| 50 | -0.243196 | -0.731472 | 0.59059 | 0.130582 | 0.59059 | 0.130582 | 0.550605 | -0.561518 |
| 60 | -0.375925 | -0.65411 | 0.624213 | 0.0449708 | 0.624213 | 0.0449708 | 0.484718 | -0.598862 |
| 70 | -0.47541 | -0.575551 | 0.634624 | -0.0349784 | 0.634624 | -0.0349784 | 0.425575 | -0.633207 |
| 80 | -0.552339 | -0.499376 | 0.628902 | -0.10684 | 0.628902 | -0.10684 | 0.370205 | -0.66539 |
| 90 | -0.613449 | -0.426228 | 0.61193 | -0.170042 | 0.61193 | -0.170042 | 0.316886 | -0.695395 |
| 100 | -0.662903 | -0.355774 | 0.587119 | -0.224755 | 0.587119 | -0.224755 | 0.264712 | -0.722954 |
| 110 | -0.703262 | -0.287473 | 0.556924 | -0.271444 | 0.556924 | -0.271444 | 0.213273 | -0.747795 |
| 120 | -0.736122 | -0.220851 | 0.523162 | -0.310684 | 0.523162 | -0.310684 | 0.162454 | -0.769717 |
| 130 | -0.762495 | -0.155588 | 0.487214 | -0.343089 | 0.487214 | -0.343089 | 0.112306 | -0.788613 |
| 140 | -0.783052 | -0.0915112 | 0.450145 | -0.369279 | 0.450145 | -0.369279 | 0.0629657 | -0.804466 |
| 150 | -0.79827 | -0.0285797 | 0.412785 | -0.38986 | 0.412785 | -0.38986 | 0.0146048 | -0.817331 |
| 160 | -0.808518 | 0.0331546 | 0.375778 | -0.405423 | 0.375778 | -0.405423 | -0.0325988 | -0.827327 |
| 170 | -0.814116 | 0.0935747 | 0.339618 | -0.416533 | 0.339618 | -0.416533 | -0.0784796 | -0.834611 |
| 180 | -0.81536 | 0.152526 | 0.30468 | -0.423723 | 0.30468 | -0.423723 | -0.122895 | -0.839373 |
| 190 | -0.812541 | 0.209837 | 0.271237 | -0.427495 | 0.271237 | -0.427495 | -0.16573 | -0.84182 |
| 200 | -0.805953 | 0.265335 | 0.239481 | -0.428314 | 0.239481 | -0.428314 | -0.206899 | -0.842168 |
| 210 | -0.795895 | 0.31886 | 0.209536 | -0.426606 | 0.209536 | -0.426606 | -0.246341 | -0.840633 |
| 220 | -0.782667 | 0.37027 | 0.181472 | -0.422762 | 0.181472 | -0.422762 | -0.284025 | -0.837429 |
| 230 | -0.766573 | 0.419448 | 0.155312 | -0.417133 | 0.155312 | -0.417133 | -0.319939 | -0.832757 |
| 240 | -0.747909 | 0.466301 | 0.131047 | -0.410032 | 0.131047 | -0.410032 | -0.354093 | -0.826812 |
| 250 | -0.726969 | 0.510764 | 0.108637 | -0.40174 | 0.108637 | -0.40174 | -0.386513 | -0.81977 |

Sometimes one needs to develop a circuit model corresponding to measured data. In most cases, one has to develop a circuit schematic based on physical properties of frequency behaviour. To develop a Bandpass T matching network model of the measured data of table 2.2, the circuit is known, but component values are not known. To develop a model of the network, a suitable circuit diagram is developed, with trial guesses for the component values. As shown in figure 2.48, the components are guessed to be 1 pF for the capacitors and 1 nH for the inductor. A value of 100 is used for the initial Q values.

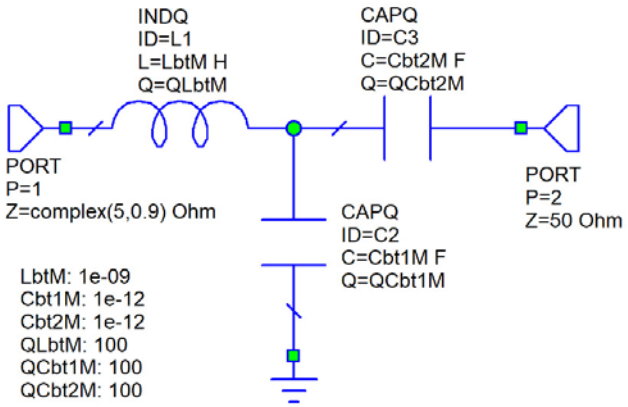



Figure 2.48. Bandpass T matching network initial guess.

The model needs to be tuned or optimised to ensure its S parameters match the measurements for all S parameters and all frequencies. To achieve this error equations are produced, like the equations 2.5 shown below for $S_{11}$.

```
MoS11Re = Bandpass T Model:Re(S(1,1))
MoS11Im = Bandpass T Model:Im(S(1,1))
MeS11Re = Measured_Ckt:Re(S(1,1))
MeS11Im = Measured_Ckt:Im(S(1,1))
MeS11 = Complex(MeS11Re,MeS11Im)
MoS11 = Complex(MoS11Re,MoS11Im)
ES11C = (MeS11-MoS11)/(MeS11+MoS11)
```

Eqn. 2.5

MoS11Re is the real part of $S_{11}$ of the Bandpass T model. The format on the right hand side of the = sign is exactly like the format of measurements used in graphs. ES11C is the normalised Error of the $S_{11}$ parameters in Complex form. Similar equations are produced for $S_{21}$, $S_{12}$, and $S_{22}$.

Since the impedance measurements only exist at the frequencies shown in table 2.2, the project frequencies must be set to the same values, so that the error equations can be evaluated. Section 13: Scripts of the AWRDE users Guide has details on scripts and how to write new ones. Fortunately, the required Match_Proj_Freq_to_Datafile_Freq script is one, which is already included in AWR DE. That script is accessed from *Scripts* ⇒ *Simulation* menu. This script requires a Touchstone data file containing the relevant frequency values. Since that Touchstone file is already included in the project, the project frequencies are then set to the values in table 2.2, so that the optimisation can be done.

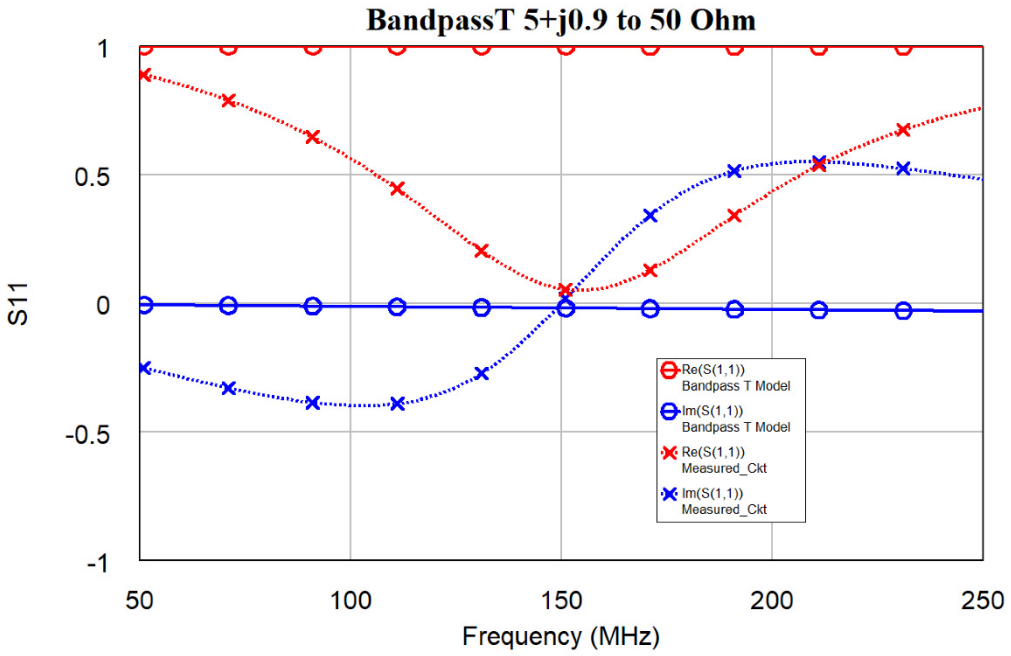



Figure 2.49. $S_{11}$ for Bandpass T model and measurements before optimisation.

Figure 2.49 shows S11 from both the model of figure 2.48 and the measurements of table 2.2 as a function of frequency. As expected, our initial values are not correct and there is a significant difference between the guessed and required values. The 3 element values in figure 2.48 and the three Q values are allowed to change under optimisation. The real and imaginary parts of ES11C and the corresponding error equations for S21, S12, and S22 with desired values of zero are set as optimiser goals.

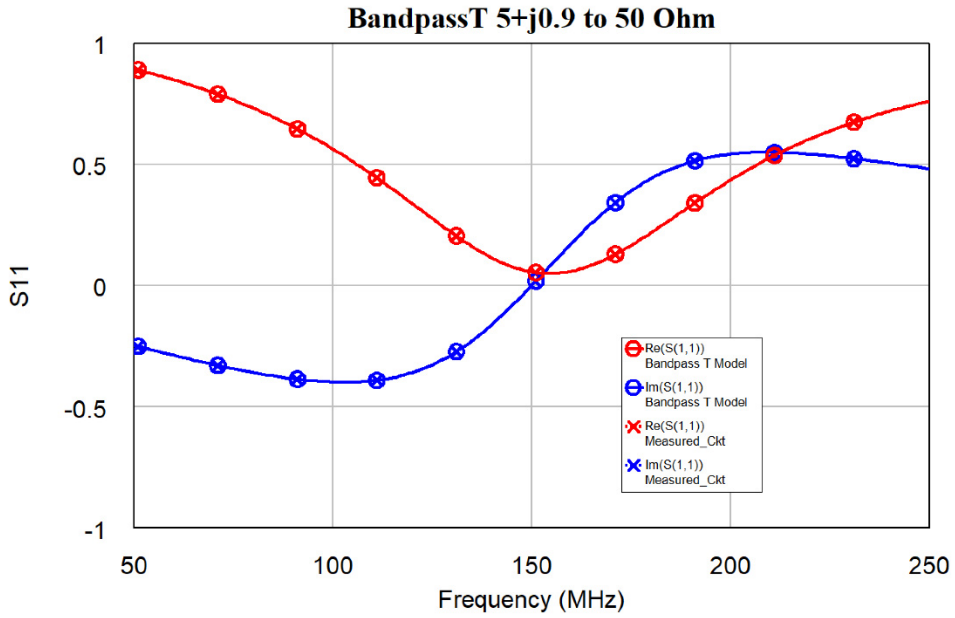



Figure 2.50. $S_{11}$ for Bandpass T model and measurements after optimisation.

Running the optimiser quickly reduces the errors to very close to zero and results in both the model and the measurement having the same S parameters as shown for $S_{11}$ in figure 2.50. The component values of the Bandpass T network model shown in figure 2.48, have changed to perfectly match the values shown in figure 3.45.

Touchstone files as data files have the advantage that AWR DE knows what the frequency units are i.e. Hz, kHz, MHz or GHz. The frequencies in the Touchstone file can also be used to set the frequencies for the project, using the Match_Proj_Freq_to_Datafile_Freq script.

## Impedance Measurements

For Touchstone files and multiport networks, all the relevant parameters $S_{11}$, $S_{21}$, $S_{12}$, and $S_{22}$ for all the ports must be contained in the Touchstone file. It is possible to develop suitable models for many port networks using less than all the required measurements. The three phase mains distribution transformer model developed by [27] and described at the end of this chapter is one example.

To illustrate this, the Bandpass T transformer model described above is also developed using impedance measurements, made by measuring impedances between each of the 3 terminals of the network of figure 2.48. Similarly, to the S parameter measurements described above, the impedances are calculated by AWR DE and saved as a data file.

The Bandpass T network has 3 terminals and the impedances between each of those terminals can be measured using Mixed Mode Converter (MMCONV) elements in AWR DE, as shown in figure 2.51. The differential (*Diff*) port (1) on the MMCONV, measures the difference in the voltages and currents between terminals 3 and 4 of the MMCONV. To prevent the impedances connected to the Common mode (*Comm*) terminals (2) of the MMCONV to affect the measured impedances, the Common mode terminals on the MMCONV must be left an open circuit. The MMCONV element provides an isolation, so that the impedance at ports 1 to 3, do not affect the measured impedances. For the analysis to be performed without errors, one point in the circuit needs to be earthed, as shown in figure 2.51.

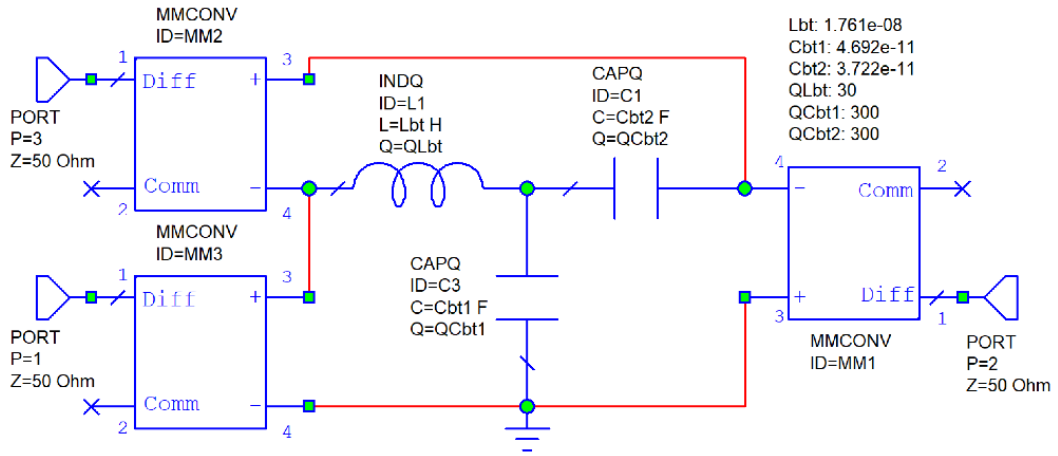



Figure 2.51. Measuring Impedances of Bandpass T matching network.

The resulting impedances can be plotted in AWR DE, and exported to a text file. This table is in a format that allows it to be directly imported into AWR DE as a data file for use and plotting. Simply select the graph or table to be plotted and click: *Graph ⇒ Export Trace Data*. Then select the file location and file name of the resulting text file. In these files a line starting with "!" denotes a comment. Adding comment lines are useful for showing what values are being imported into the project.

Table 2.3 shows a text file with impedances produced by the circuit shown in figure 2.51. The first few lines beginning with "!" are added for clarity. To keep the number of lines in this table small a 10 MHz frequency increment is chosen in the project options, resulting in 21 frequencies being used. In practice, many more frequencies would be used.

Table 2.3. Bandpass T impedances of figure 2.51

| ! | Port1 | | Port12 | | Port2 | |
|---|---|---|---|---|---|---|
| !1 | 2 | 3 | 4 | 5 | 6 | 7 |
| !(Hz) | Ohm | Rad | Ohm | Rad | Ohm | Rad |
| !Freq | \|Z(1,1)\| | Ang | \|Z(1,1)\| | Ang | \|Z(1,1) | \|Ang |
| 5e+007 | 62.3068 | -1.55103 | 79.9836 | -1.55319 | 153.34 | -1.5608 |
| 6e+007 | 49.8955 | -1.55026 | 64.6261 | -1.55305 | 127.785 | -1.56246 |
| 7e+007 | 40.7142 | -1.5487 | 53.3402 | -1.55224 | 109.531 | -1.56365 |
| 8e+007 | 33.5517 | -1.5464 | 44.5991 | -1.5509 | 95.8405 | -1.56455 |
| 9e+007 | 27.7353 | -1.54329 | 37.5547 | -1.54903 | 85.1919 | -1.56524 |
| 1e+008 | 22.8613 | -1.53917 | 31.6981 | -1.54659 | 76.673 | -1.5658 |
| 1.1e+008 | 18.6729 | -1.53365 | 26.7054 | -1.54346 | 69.7028 | -1.56625 |
| 1.2e+008 | 14.999 | -1.52604 | 22.3608 | -1.53941 | 63.8944 | -1.56663 |
| 1.3e+008 | 11.7215 | -1.515 | 18.515 | -1.53407 | 58.9795 | -1.56695 |
| 1.4e+008 | 8.75645 | -1.49766 | 15.0612 | -1.5268 | 54.7667 | -1.56722 |
| 1.5e+008 | 6.0441 | -1.46659 | 11.9217 | -1.51639 | 51.1157 | -1.56746 |
| 1.6e+008 | 3.54601 | -1.39517 | 9.03836 | -1.50028 | 47.921 | -1.56767 |
| 1.7e+008 | 1.29202 | -1.07732 | 6.36831 | -1.47213 | 45.1021 | -1.56786 |
| 1.8e+008 | 1.23578 | 1.05858 | 3.88314 | -1.41062 | 42.5965 | -1.56802 |
| 1.9e+008 | 3.2318 | 1.38396 | 1.59862 | -1.17756 | 40.3546 | -1.56816 |
| 2e+008 | 5.20895 | 1.45618 | 0.968778 | 0.893954 | 38.3368 | -1.5683 |
| 2.1e+008 | 7.11364 | 1.48751 | 2.94209 | 1.36479 | 36.5113 | -1.56842 |
| 2.2e+008 | 8.94914 | 1.505 | 4.9482 | 1.44975 | 34.8517 | -1.56852 |
| 2.3e+008 | 10.7227 | 1.51618 | 6.88928 | 1.48451 | 33.3364 | -1.56862 |
| 2.4e+008 | 12.4415 | 1.52394 | 8.76478 | 1.50338 | 31.9474 | -1.56871 |
| 2.5e+008 | 14.1117 | 1.52965 | 10.5805 | 1.51524 | 30.6695 | -1.5688 |

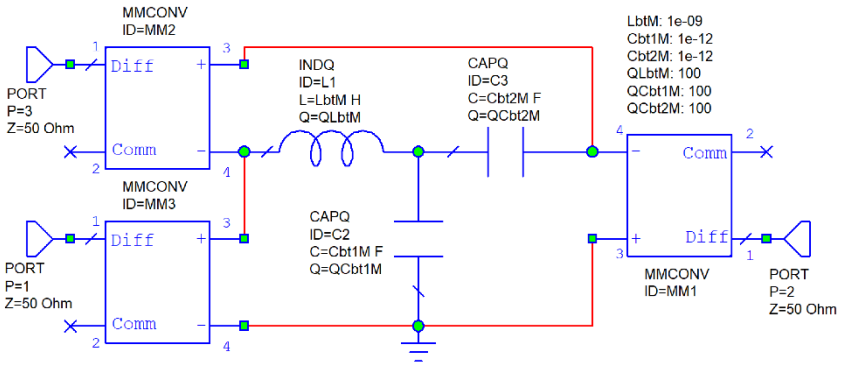



Figure 2.52. Initial Bandpass T matching network model.

When one needs to develop a model of an unknown network, impedance measurements will need to be made between all terminals of that network and a table similar to the one shown in table 2.3, for the impedances of figure 2.51, is then produced using those measurements. To develop a model of the network, the same trial guesses for the component values as shown in figure 2.48 are used, as shown in figure 2.52. As before these initial guessed values, will change during the network optimisation.

To import measured data, a spreadsheet containing the measurements is normally imported as a data file. As AWR DE does not easily recognise frequency units other than Hz, when.txt data files are used, it is easiest to use Base Units (Hz, Henry and Farad) for the error calculations. As a result, the measurements that are imported as data files may need to be changed to contain Base Units values. A Text Data file is imported in the same way as Touchstone files, by right clicking on *Data Files* and selecting *Import Data File* or by using the *Project* ⇒ *Add Data File* ⇒ *Import Data File* dropdown menu. Again, it is worthwhile to add some comments and headings with each line starting with a "!". In this example, the impedance data produced as table 2.3 is used as the measurement file.

It is slightly more difficult to use a text data file in AWR DE than it is to use a Touchstone file. This data can be imported into the project, using the following equations 2.6 in the global definitions:

```
MeFreq = Col(datafile("Measurements"),1)
MeP1Z11M = Col(datafile("Measurements"),2)
MeP1Z11Ph = Col(datafile("Measurements"),3)
MeP12Z11M = Col(datafile("Measurements"),4)
MeP12Z11Ph = Col(datafile("Measurements"),5)
MeP2Z11M = Col(datafile("Measurements"),6)
MeP2Z11Ph = Col(datafile("Measurements"),7)
```

Eqn. 2.6

*MeFreq*, are the measurement frequencies, *MeP1Z11M* is the measured Port 1 impedance magnitude, *MeP1Z11Ph* is the measured Port 1 impedance phase and so on. These variables can now be used, to set up the error equations shown in figure 2.53, which correspond to a normalised difference between the measured impedances and those obtained from the impedance seen at ports 1 to 3.

In figure 2.53 EP1Z11M is the error for the magnitude of Z11 for Port 1, MeP11Z11M is the measured value of the magnitude of Z11 for Port 1and MoP11Z11M is the magnitude of Z11 for Port 1 of the model. EP1Z11P is the error for the phase of Z11 for Port 1, MeP11Z11P is the measured value of the phase of Z11 of Port 1 and MoP11Z11P is the phase of Z11 for Port 1 of the model.

LC Matching Networks
Rl: 50
Rd: 5 Fm: 150 A: 0.5701
Xd: 0.9 Qmin: 3 B: 66.25
Ld: 9.549e-10

Band Pass T
Lbt: 1.761e-8 LbtM: 1e-9
Cbt2: 3.722e-11 Cbt1M: 1e-12
Cbt1: 4.692e-11 Cbt2M: 1e-12

MoP1Z11M = BandpassTModel:|Z(1,1)|
MoP1Z11Ph = BandpassTModel:Ang(Z(1,1))
EP1Z11M = (MeP1Z11M-MoP1Z11M)/(MeP1Z11M+MoP1Z11M)
EP1Z11Ph = (MeP1Z11Ph-MoP1Z11Ph)

MoP2Z11M = BandpassTModel:|Z(2,2)|
MoP2Z11Ph = BandpassTModel:Ang(Z(2,2))
EP2Z11M = (MeP2Z11M-MoP2Z11M)/(MeP2Z11M+MoP2Z11M)
EP2Z11Ph = (MeP2Z11Ph-MoP2Z11Ph)

MoP12Z11M = BandpassTModel:|Z(3,3)|
MoP12Z11Ph = BandpassTModel:Ang(Z(3,3))
EP12Z11M = (MeP12Z11M-MoP12Z11M)/(MeP12Z11M+MoP12Z11M)
EP12Z11Ph = (MeP12Z11Ph-MoP12Z11Ph)

Figure 2.53. Error equations in *Output Equations Window* of AWR DE project.

Similar equations are used for ports 2 and 3 of the networks in figures 2.51 and 2.52. These error equations are used as part of the optimisation process, where the component values of the black box model are optimised to minimise the values of these error equations.

Since the impedance measurements only exist at the frequencies shown in table 2.3, the project frequencies must again be set, as described above, to the same values, using the Match_Proj_Freq_to_Datafile_Freq script. That script is accessed from *Scripts* ⇒ *Simulation* menu. This script requires a Touchstone data file containing the relevant frequency values. For the S parameter data, the Touchstone file was part of the project. That is not the case now, so that a simple dummy Touchstone file containing the frequency values must now be produced from the measurements in table 2.3.

Import the data from table 2.3 into a spreadsheet program. In many cases, the relevant data already exists in a spreadsheet. Make a new sheet in the spreadsheet program and paste the measurement frequency data into the first column, corresponding to the frequencies at which the equations are to be evaluated. Then add 8 columns containing a zero, to represent the 4 complex S parameter values (one entry for magnitude and one for angle) required by Touchstone files. Create a new Touchstone file in the AWR DE project by right clicking on Data Files and select Touchstone File option. The Touchstone like spreadsheet data is then pasted in that Touchstone data file and the text "#Hz S MA R 50" is added as the first line to produce the Touchstone data file shown in table 2.4.

Table 2.4. Touchstone file for setting the project frequencies.

| | | | | | | | | |
|---|---|---|---|---|---|---|---|---|
| #Hz S MA R 50 | | | | | | | | |
| 5e+007 | 0 | 0 | 0 | 0 | 0 | 0 | 0 | 0 |
| 6e+007 | 0 | 0 | 0 | 0 | 0 | 0 | 0 | 0 |
| 7e+007 | 0 | 0 | 0 | 0 | 0 | 0 | 0 | 0 |
| 8e+007 | 0 | 0 | 0 | 0 | 0 | 0 | 0 | 0 |
| 9e+007 | 0 | 0 | 0 | 0 | 0 | 0 | 0 | 0 |
| 1e+008 | 0 | 0 | 0 | 0 | 0 | 0 | 0 | 0 |
| 1.1e+008 | 0 | 0 | 0 | 0 | 0 | 0 | 0 | 0 |
| 1.2e+008 | 0 | 0 | 0 | 0 | 0 | 0 | 0 | 0 |
| 1.3e+008 | 0 | 0 | 0 | 0 | 0 | 0 | 0 | 0 |
| 1.4e+008 | 0 | 0 | 0 | 0 | 0 | 0 | 0 | 0 |
| 1.5e+008 | 0 | 0 | 0 | 0 | 0 | 0 | 0 | 0 |
| 1.6e+008 | 0 | 0 | 0 | 0 | 0 | 0 | 0 | 0 |
| 1.7e+008 | 0 | 0 | 0 | 0 | 0 | 0 | 0 | 0 |
| 1.8e+008 | 0 | 0 | 0 | 0 | 0 | 0 | 0 | 0 |
| 1.9e+008 | 0 | 0 | 0 | 0 | 0 | 0 | 0 | 0 |
| 2e+008 | 0 | 0 | 0 | 0 | 0 | 0 | 0 | 0 |
| 2.1e+008 | 0 | 0 | 0 | 0 | 0 | 0 | 0 | 0 |
| 2.2e+008 | 0 | 0 | 0 | 0 | 0 | 0 | 0 | 0 |
| 2.3e+008 | 0 | 0 | 0 | 0 | 0 | 0 | 0 | 0 |
| 2.4e+008 | 0 | 0 | 0 | 0 | 0 | 0 | 0 | 0 |
| 2.5e+008 | 0 | 0 | 0 | 0 | 0 | 0 | 0 | 0 |

The line beginning with # is a header, specifying the parameters to be used. # MHz, denotes that the frequencies are in MHz, Hz denotes the frequencies are in Hz. S denotes that this is an S parameter file,

MA indicates that the complex data is in polar form (magnitude, angle), the angle of which is always in units of degrees;

Selecting Select *Scripts* ⇒ *Simulation* ⇒ *Match_Proj_Freq_to_Datafile_Freq* will set the project frequencies to the ones in the Touchstone file of table 2.4. In many cases automatic measurements are made on the network to be determined so that more than one thousand measurements result. The frequency setting script described above is then the only practical way to match the project frequencies to the measurements. Once the project frequencies have been set to correspond to the measured frequencies, the Touchstone file can be deleted from the project if desired.

Figures 2.54 and 2.55 compare the impedance measurements of the calculated Bandpass T circuit of figure 2.51 and those of the model using the starting values in figure 2.52. The curves with the markers, i.e. the top two curves in figure 2.54 and the bottom two curves in figure 2.55, are the starting impedances of the model. The curves without the markers are the impedances of the Bandpass T circuit. There are thus significant differences between the circuit and the model at the start of the optimisation.

Optimisation goals are set to reduce the phase and magnitude errors to zero. The circuit simulator is then set to optimise the guessed component values to minimise the error equations shown in figure 2.53.

In this application, the simplex optimiser results in a fast optimisation, to produce the results, in figures 2.56 and 2.57. These figures compare the impedance measurements of the calculated Bandpass T circuit of figure 2.51with that of the model of figure 2.52 and show that after optimisation, the impedances for the calculated Bandpass T matching network are exactly the same values, as those of the modelled network.

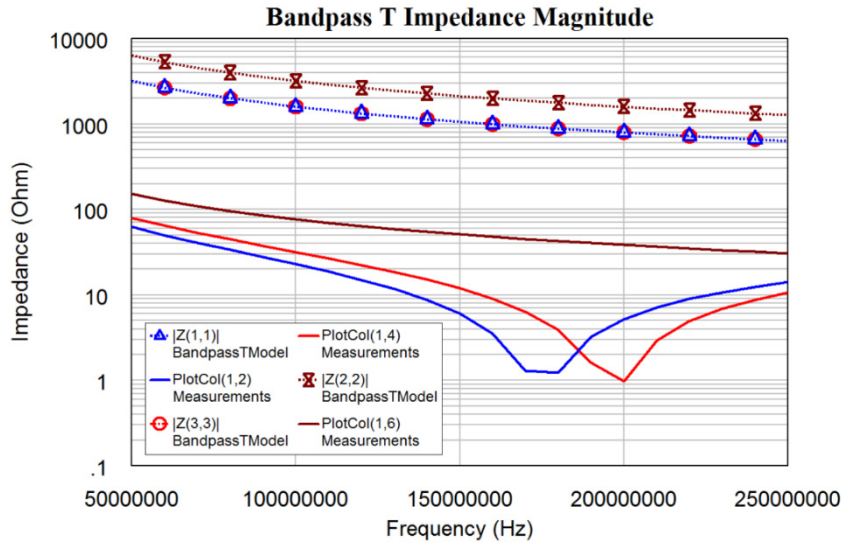



Figure 2.54. Starting impedance magnitude comparison of circuits of figures 2.51 and 2.52.

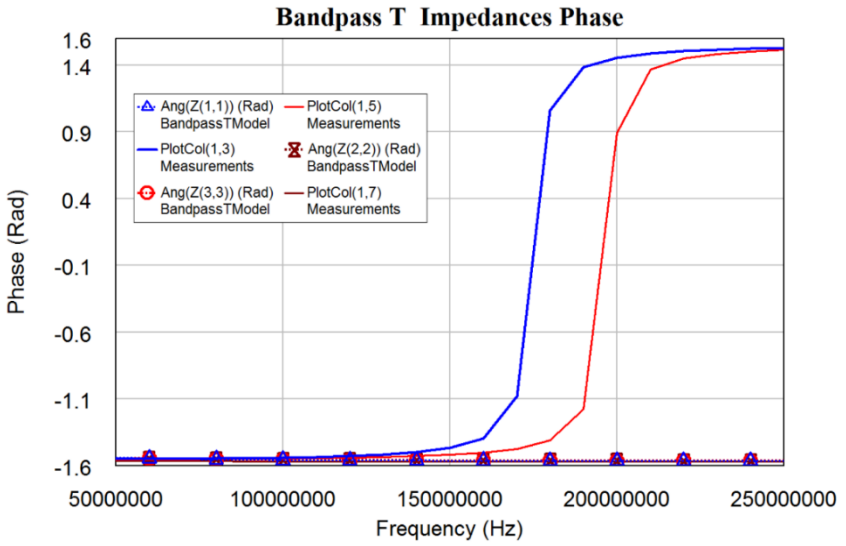



Figure 2.55. Starting impedance phase comparison of circuits of figures 2.51 and 2.52.

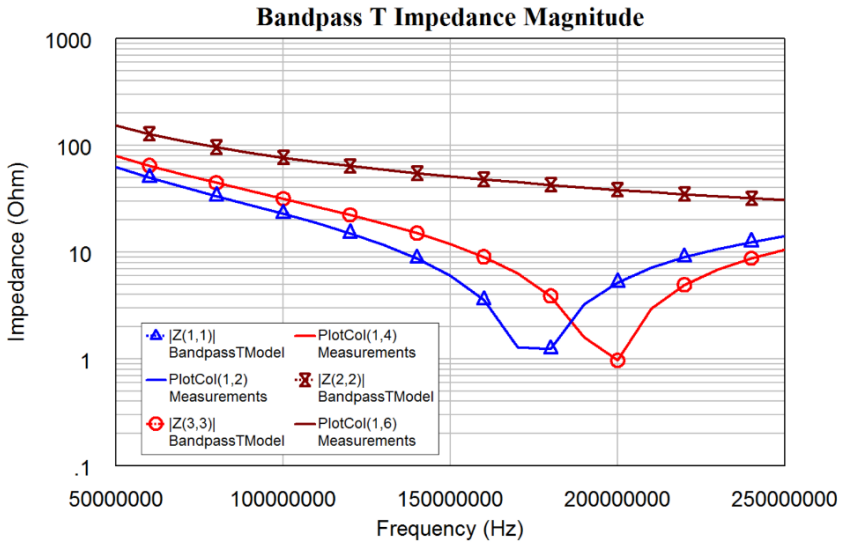



Figure 2.56. Impedance magnitude comparison after optimisation.

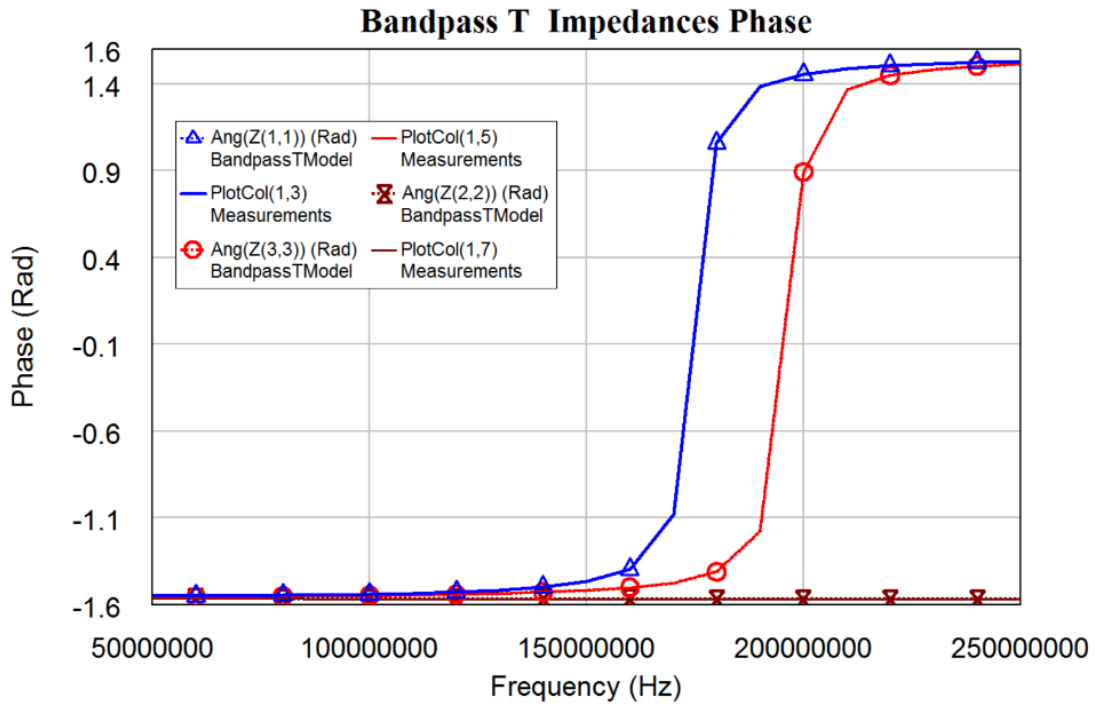



Figure 2.57. Impedance phase comparison after optimisation.

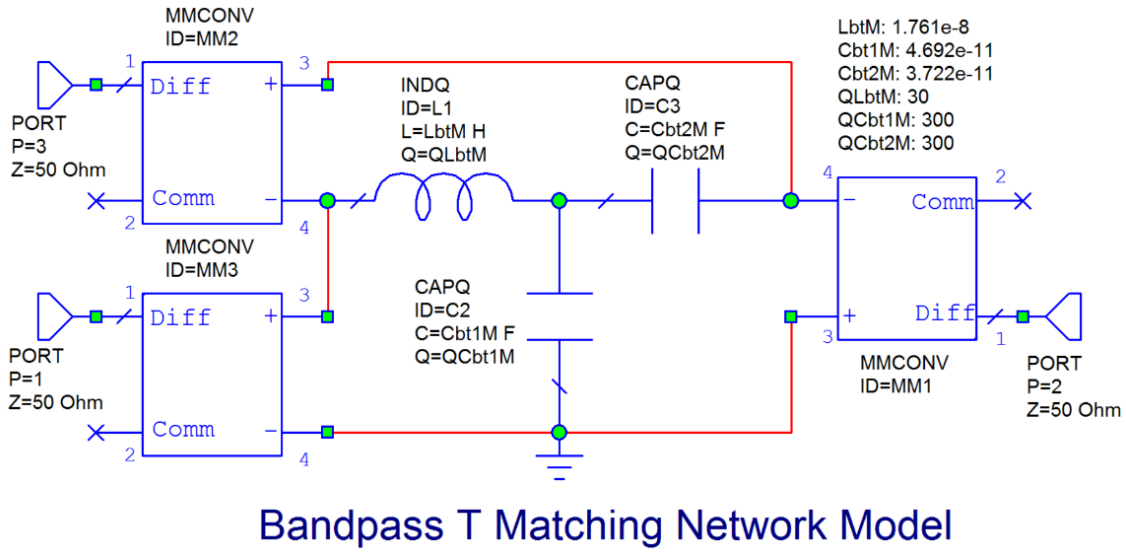



Figure 2.58. Bandpass T Matching network model after optimisation.

Both the magnitude and the phase response of the calculated circuit and the model match exactly. The components and their Q values of the circuit model, after optimisation are shown in figure 2.58 and exactly match the component values of the Bandpass T network of figure 2.45, showing that we have perfectly modelled the circuit from impedance measurements only.

One application of this technique is the modelling of mains power transformers for use at 50 kHz to 150 kHz Power Line Carrier (PLC) frequencies. This technique was successfully applied to single-phase transformers and three phase transformers to allow low cost coupling networks, to couple the PLC signals onto the High Voltage power lines to be designed. These coupling networks rely on the transformer circuit model developed using this technique for part of the coupling network [9, 27].

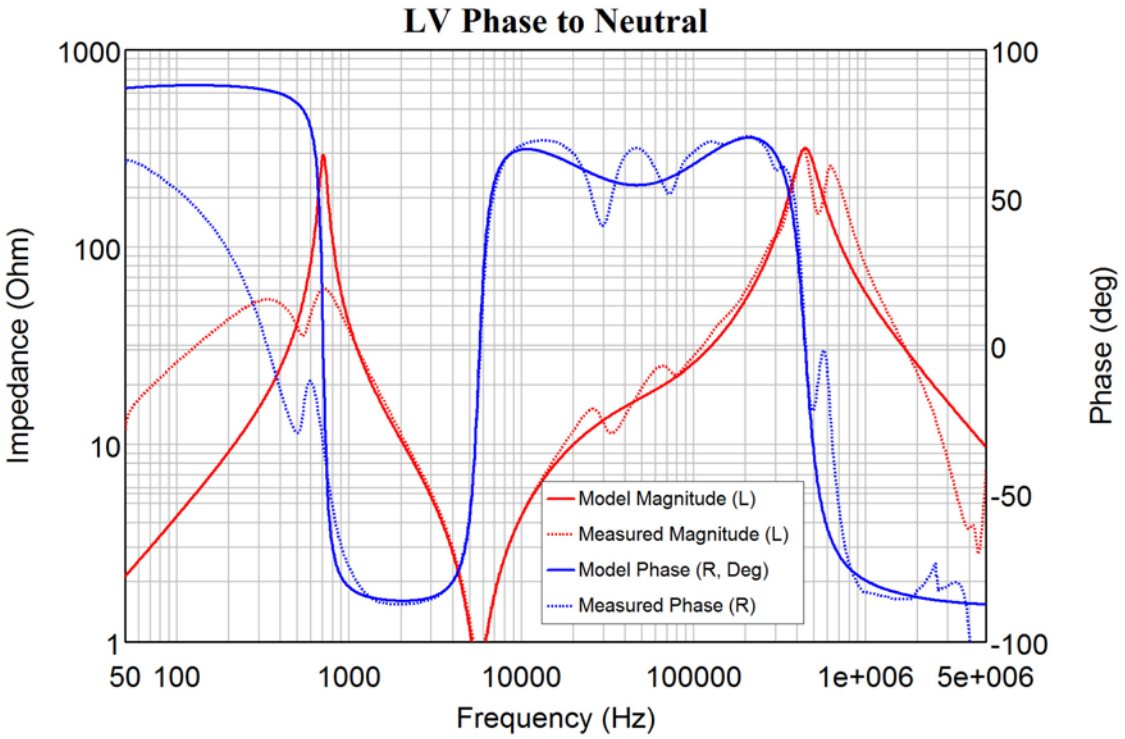



Figure 2.59. Comparison of measured and modelled low voltage winding impedances of a 200 kVA mains power distribution transformer. (Fig 7 of [9])

Figures 2.59 and 2.60 show the results from this technique being applied to the modelling of a power distribution transformer at power line carrier (PLC) frequencies, for Smart Grid applications [9]. One thousand impedance measurements are made on each of the 23 selected combinations of 10 terminals, using frequencies from 50 Hz to 5 MHz. A 3-phase model is developed and the circuit values are then matched, to provide the best match to the measurements. The actual circuit model required is far more complex than the model used and as a result, a good match is obtained for 10 kHz to 400 kHz frequencies used for PLC, but a poorer match is obtained at 50 Hz to 500 Hz. Without using this black box impedance matching technique, a suitable transformer model could not be developed.

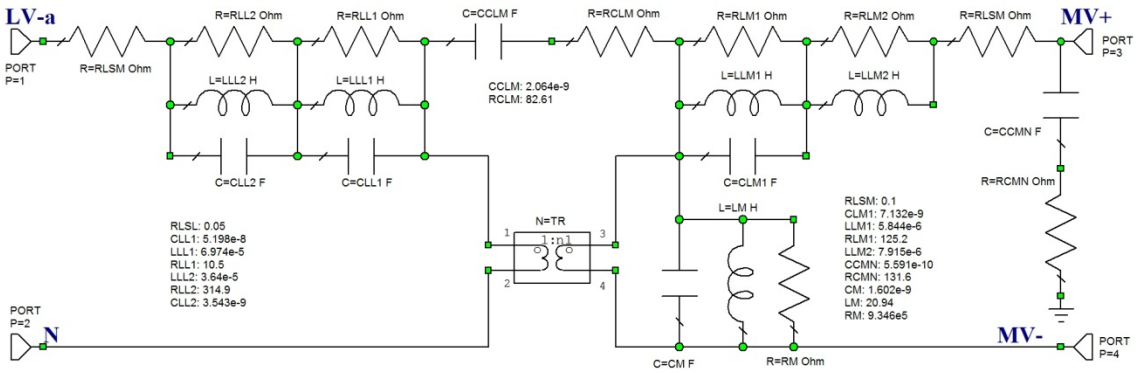



Figure 2.60. One phase of the 3-phase transformer circuit model. (Fig 6 of ref [27])

Figure 2.60 shows one phase of this three-phase transformer model. In addition, coupling between each of the windings to the transformer case are included in the full model. These

circuits are much more complex than the circuits of figures 2.51 and 2.52, but the same optimisation techniques are used.

## Summary

This chapter has introduced some basic aspects of computer simulation using the AWR DE and APLAC components of the AWR Design Environment. In the rest of this book, the computer simulation will be expanded with both linear and non-linear applications and examples.

AWR DE has a good interactive help capability, with specific information available for every circuit element or measurement. The interactive element help can be accessed by right clicking on the element and selecting "Element Help". In addition, the examples included with the AWR DE software will assist in understanding the operation of computer simulation software for electronic circuits at all frequencies.

## References


1. Keysight Technologies Pathwave Design software, https://www.keysight.com/au/en/products/software/pathwave-design-software.html
2. Cadence AWR Software: AWR Design Environment, https://www.awr.com/awr-software/products
3. Microwave Office https://www.awr.com/awr-software/products/microwave-office
4. Butterworth Filters; http://en.wikipedia.org/wiki/Butterworth_filter
5. Zverev, A. I. "Handbook of filter Synthesis", Book Publisher John Wiley & sons 1967.
6. Huelsman, L. P. "Active and Passive Analog Filter Design", McGraw-Hill,1993.
7. Pozar, D. M. *"Microwave Engineering"* 3rd Edition, Wiley, 2005, Section 4.3.
8. Kikkert, C. J. "Optimization Study of a Diplexer" https://www.awr.com/resource-library/optimization-study-diplexer.
9. Kikkert C. J. "A PLC Frequency Model of 3 Phase Power Distribution Transformers", SmartGridComm2012, 5-8 November 2012, Tainan City, Taiwan.
10. AWR Corp. "Element Help files: MWO/AO Element Catalog > Linear Devices >Bipolar Transistor (Closed Form): BIP".
11. ON Semi, BC546 data sheet. https://www.onsemi.com/products/discretes-drivers/general-purpose-and-low-vcesat-transistors/bc546
12. Nagel, L. W, and Pederson, D. O., *SPICE (Simulation Program with Integrated Circuit Emphasis)*, Memorandum No. ERL-M382, University of California, Berkeley, Apr. 1973
13. Analog Devices LTspice https://www.analog.com/en/design-center/design-tools-and-calculators/ltspice-simulator.html
14. Texas Instruments Tina-TI https://www.ti.com/tool/TINA-TI
15. Compact Model Coalition https://si2.org/cmc/
16. NXP SiMKit https://www.nxp.com/design/software/models/simkit:SIMKIT
17. AWR Corp. "Element Help files: MWO/AO Element Catalog>Nonlinear> Gummel-Poon BJT:GBJT".
18. 5SPICE: web site has links to many SPICE model web sites. http://www.5spice.com/html/links-tutorials.html
19. Microchip AN1297 "Microchip's Op Amp Spice Macro Models", http://ww1.microchip.com/downloads/en/AppNotes/01297a.pdf

20. ON Semi Discrete PSPICE Models: https://www.onsemi.com/support/design-resources/models
21. Infineon: http://www.infineon.com/cms/en/tools/
22. Modelithics University Program, https://www.modelithics.com/home/university
23. BFP720 Data-Sheet https://www.infineon.com/cms/en/product/rf/rf-transistor/low-noise-rf-transistors/bfp720/
24. AWR Corp, MWO/AO /Examples "Basic_Transient.emp project"
25. AWR Corp, AWR DE Help files Section 7.1 "Transient Analysis Basics".
26. Vishay, SiHF9530 PSpice model https://www.vishay.com/docs/90306/sihf9530.lib
27. Kikkert C. J. "Modelling Power Transformers for the Design of SWER line Coupling Networks.", 1st IEEE International Conference on Smart Grid Communications (SMARTGRIDCOMM 2010), October 4-6, Maryland USA.

# Chapter 3

# Transformers and Hybrids

## Introduction

At RF frequencies, Transformers are used to:

1 Invert signals by producing a 180-degree phase shift.

2 Change Impedances, to ensure that devices are matched correctly, thus ensuring that most of the power is transferred into or out of the devices.

3 Change balanced signals from a TV antenna to unbalanced signals for transmission using coaxial cables and connecting to a TV set.

4 Change unbalanced signals to balanced ones for use in mixers.

5 Provide DC isolation and permit DC and RF signals to be carried on the same coaxial cable for masthead amplifiers and other remote powered applications.

RF Transformers differ from audio and 50 Hz mains transformers in that:

1 Ferrites are normally used for the magnetic material.

2 The windings may be an appreciable fraction of the wavelength.

3 Capacitive coupling between the primary and secondary windings and the self-capacitance of the windings must be taken into account. The capacitance between the windings, extends the frequency response, but at a 1:1 turns ratio. The self-capacitance of the windings causes resonances.

4 The transformers may need to operate over several decades of frequency.

5 At VHF frequencies and above, transmission lines may be used as transformers, without the use of ferrites. Such transformers operate over a relatively small frequency range.

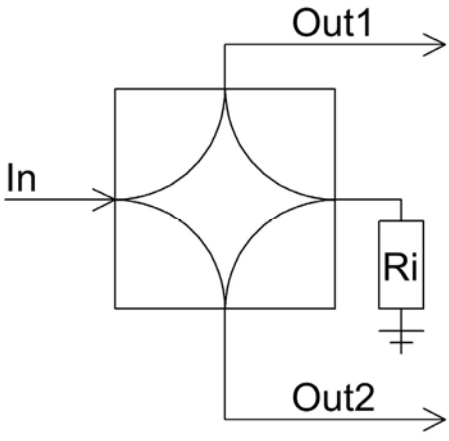



Figure 3.1. Hybrid symbol.

Hybrids are used to split or combine signals, while providing isolation between those signals.

Figure 3.1 shows the commonly used symbol for a hybrid. The input signal is divided equally between Out1 and Out2. Out1 and Out2 are isolated from each other. This allows us to drive two amplifiers, thereby improving amplifier stability and increasing the output power handling capability.

The power-handling capability of RF transistors operating up to 1 GHz can be as high as 100 Watt. Figure 3.2 shows how two such 100 Watt amplifiers, together with two hybrids can be used to produce a 200 Watt amplifier. This also gives some redundancy against failure of an amplifier. For an ideal hybrid, if one amplifier fails, the output will drop by 6 dB, with the power from the remaining amplifier being split between the antenna and the resistive load at the output hybrid, but the system still operates. For higher

power output requirements, many of these modules can be combined in a similar manner. As a result, solid-state amplifier modules with output powers of several kW can be made.

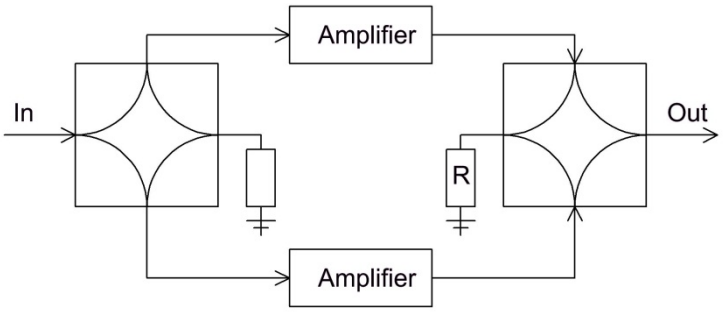



Figure 3.2. Parallel operation of amplifiers.

At VHF frequencies the hybrids are normally made using transmission lines. At lower frequencies, the hybrids can be made using transformers. Most telephone handsets, operating at audio frequencies, have either a transformer hybrid or an active hybrid using an Application Specific Integrated Circuit, (ASIC).

## Wideband Transformers

For a conventional ferrite transformer, the upper length of the winding is limited to approximately 10% of the wavelength. At 1 GHz the wavelength is 300 mm and the maximum winding length is thus 30 mm. If the windings are like a transmission line, as used in TV baluns shown in figures 3.7 and 3.8, this limit does not apply. The corresponding lower limit [1] is:

$$l_{min} = \frac{R_l}{2(1+\mu_r)f_{min}} \qquad \text{Eqn. 3.1}$$

Where $R_l$ is load impedance in Ohm, $f_{min}$ is the lowest operating frequency of the transformer in MHz and $l_{min}$ is the length of the winding in metres. For a Neosid F14 material with a $\mu_r$ of 220, operating at 1 MHz in a 50 Ω system, the minimum winding length is thus 113 mm. This minimum winding length should be allowed for in the design of transformers made using ferrites.

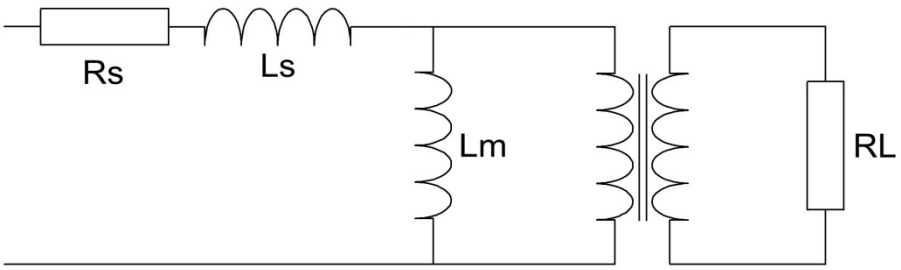



Figure 3.3. Simplified RF transformer model.

Transformers can be designed using the above equations, however by considering the simple conventional transformer model [2] shown in Figure 3.3, containing a Leakage inductance Ls and a Magnetising inductance Lm, the optimum number of turns required for RF transformers can be easily determined. To simplify the calculations assume that the transformer has a 1:1 turns-ratio, so that the load $R_L$ is also the load reflected into the primary. For other turns ratios, the load impedance reflected into the primary, is the impedance used for calculations.

At low frequency, the Magnetising inductance Lm shunts the output load. The lower cut off frequency is thus when $j\omega L_M = R_L$. At high frequencies, the Leakage inductance is in series with the output. The upper cut off frequency is thus when $j\omega L_S = R_L$.

For the model of figure 3.3, the leakage inductance can most easily be measured by short-circuiting the secondary winding of the transformer. Under those conditions the input impedance of the transformer is $R_s + j\omega L_S$. When the transformer is open circuited, the input impedance is $R_s + j\omega L_S + j\omega L_M$. Since $L_m$ is typically 1000 times larger than $L_s$, the leakage inductance can be ignored as part of the lower frequency calculation. This simple model does not include inter-winding and self-capacitances, but for many applications, it is accurate enough as $R_s$ often governs the upper cut-off frequency ($F_{high}$).

If one normally wants to operate the transformer at a frequency $F_c$ then it is desirable to make this $F_c = \sqrt{F_{low} F_{high}}$ where $F_{low}$ and $F_{high}$ are the upper and lower cut off frequencies of the transformer. As described above, the upper and lower cut off frequencies are determined by the leakage and magnetising inductance respectively.

The input impedance of the transformer at the centre frequency is thus:

$$Z_c = \sqrt{Z_{Ls} Z_{Lm}} = \sqrt{\omega L_s \omega L_m} \qquad \text{Eqn. 3.2}$$

For a 50 Ω system, one wants this $Z_c$ to be 50 Ω. Under those conditions $R_s + j\omega L_S$ is much smaller than $R_L$ and $j\omega L_M$ is much larger than $R_L$, so that virtually all the input power is transferred to the output.

Since the inductance is proportional to the number of turns squared, the characteristic impedance of the transformer is also proportional to the number of turns squared. The number of turns chosen for the transformer winding is such that the characteristic impedance of the transformer matches the system impedance. Since in many cases the detailed properties of the ferrite may not be known, the characteristic impedance is most easily determined by winding a trial-winding on the transformer and using the measured open and short circuited impedances to then calculate the correct number of turns required.

In practice, the magnetising inductance has some losses associated with it and the resistive losses of the windings are in series with the leakage inductance. The resistive losses are normally very small. Since the inductance is proportional to the frequency, at the upper and lower frequency limits the inductance dominates, so that in the calculation for the upper and lower frequency limits, the resistive part of the measured input impedance can be ignored.

## *Example 3.1: RF Transformer Design*

An RF isolation transformer operating at 1 MHz and a 50 Ω impedance is required. To determine the number of turns required on a ferrite toroid, wind a bifilar trial winding on it. At the desired centre frequency, determine the leakage inductance of the transformer by measuring the input impedance with the secondary winding short-circuited. Then determine the magnetising inductance by measuring the input impedance with the secondary winding open-circuited. For an 11 turn bifilar trial winding, at 1 MHz, the short circuit impedance is $Z_{Ls} = j0.4\ \Omega$, corresponding to a leakage inductance of 64 nH. The open circuit input impedance is $Z_{Lm} = j400\ \Omega$, corresponding to a magnetising inductance of 64 μH. From equation 3.2, the characteristic impedance is thus $Z_c = \sqrt{(400 \times 0.4)} = 12.65\ \Omega$.

The inductance and impedance is proportional to the square of the number of turns. Thus, for the required 50 Ω transformer impedance, we need 11 x √(50/12.65) = 21.8 turns. The number if turns needs to be an integer. The 22 turn winding one will thus have a leakage inductance of 256 nH and a magnetising inductance of 256 μH. The number of turns for 1 Ω, N1 =11 x √(1/12.65) = 3.093 is a useful parameter that can be used for calculating the number of turns required for different impedances. For an impedance Z, the number of turns required is Nz = N1√ Z.

The ratio of the open circuit to the short circuit impedance is 1000:1. The ratio of the upper and lower cut off frequency is thus also 1000:1, with the centre frequency being at the geometric mean of the upper and lower cut off frequencies. The upper cut off frequency is thus 1MHz*√(1000) = 32 MHz. The lower cut off is 1MHz/√(1000) = 32 KHz.

The measured performance normally agrees closely with the calculated one. The actual upper corner frequency is often a little lower than the calculated one, since the losses in the ferrite increase non-linearly with frequency and are thus proportionally higher at the centre frequency, where the measurements of the leakage and magnetising inductance are made. RF transformers using bifilar and trifilar windings operate well at frequencies up to several GHz.

## *Bifilar and Trifilar Windings*

For a bifilar winding, two wires are twisted together to form a primary and secondary winding of a transformer, with close capacitive coupling between the windings, which result in a wide frequency response. Bifilar windings are used for inverting transformers. Trifilar windings use three wires twisted together as shown in figures 3.4 and 3.5. Trifilar windings are used for Baluns (Balanced-Unbalanced transformers) [3] and for transformers with a 4:1 impedance transformation ratio, as shown in figure 3.4. For most TV antennae, the output from the antenna is a balanced signal, on two active wires carrying signals of opposite polarity. For low loss transmission without interference, a coaxial cable is normally used to transmit this signal between the antenna and the TV set. A Balun is used to convert the balanced signals from the antenna to the match the unbalanced signal for the coaxial cable.

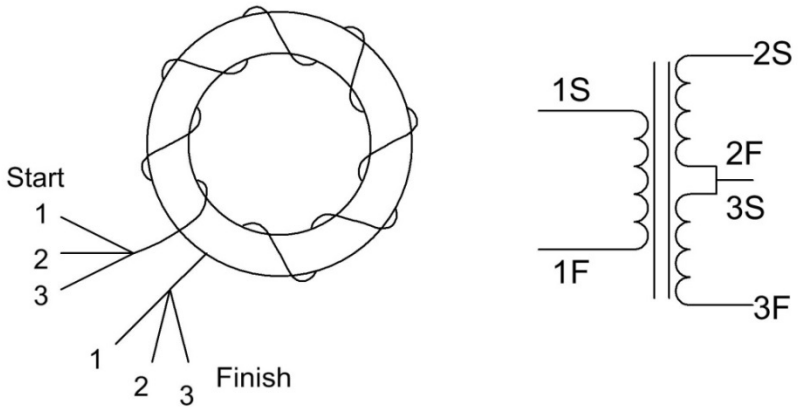



Figure 3.4. Trifilar winding diagram.

If port 2F-3S is earthed in figure 3.4, then the transformer is a balanced to unbalanced transformer, called Balun. For a 75 Ω input impedance, a 300 Ω output-impedance is obtained. Such a Balun is often used in TV antenna systems.

To construct a bifilar of trifilar winding, take the required number of wires, in parallel, put one end in a vice and the other in the chuck of a hand drill and turn the operate the drill until the required amount of twisting has been done. The inter-winding capacitance can be controlled by selecting the insulation thickness on the wires. Winding self-capacitance can be minimised by using a single layer winding. Figure 3.5 shows a typical bifilar and pentafilar transformer using single layer windings. Such transformers typically have a 3 decade frequency bandwidth.

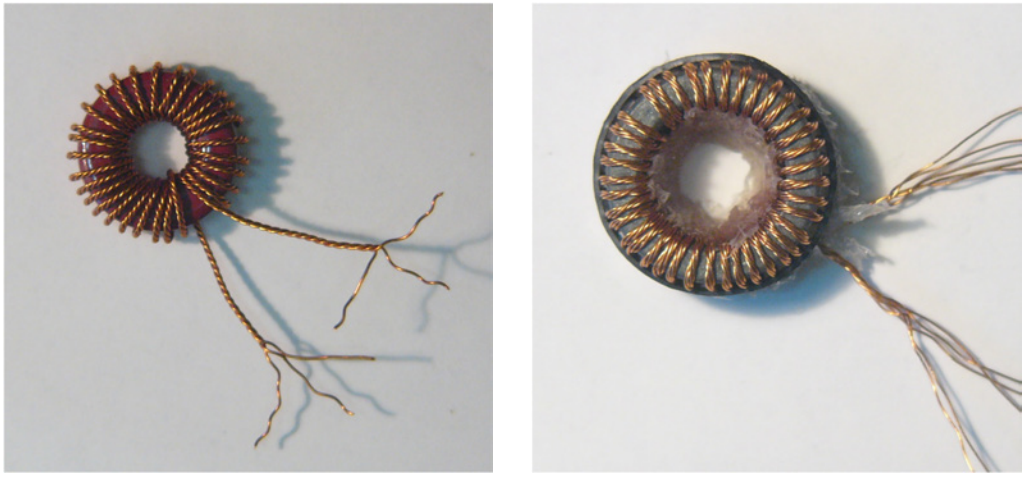


Figure 3.5. A trifilar wound RF Transformer (left) and a pentafilar transformer (right).

For instrumentation grade double balanced mixers a very good balance in the output signals is required, then an additional core, as shown in figure 3.6, can be added [3]. This provides winding 1 with a balanced input, thus causing the impedances at 2S to be exactly the same as those at 3F. Often the cost of the additional core is not justified.

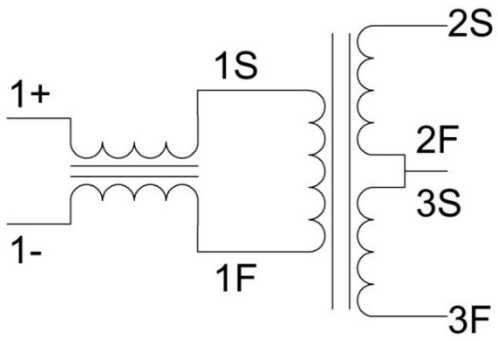



Figure 3.6. Balun with improved output balance.

## Transmission Line Transformers with Ferrite Cores

At high frequencies, the primary and secondary windings are sometimes wound using transmission lines, as shown in Figures 3.7. This then uses inter-winding capacitances to use capacitive coupling at high frequency and magnetic coupling at lower frequency thus extending the bandwidth, significantly above what can be obtained using the construction technique of figures 3.4 and 3.5. For the 75 Ω system, shown in figure 3.7, the characteristic impedance for the transmission lines used for the windings are 150 Ω. There is thus no reflection at the junction, where the two lines are connected in parallel. The two transmission lines are in series at the right hand side and the balanced output then form a 300 Ω system. Since the same propagation delay occurs through both the top and

bottom transmission lines, the + and – signals are perfectly balanced at all frequencies. The corresponding hardware is shown in figure 3.8

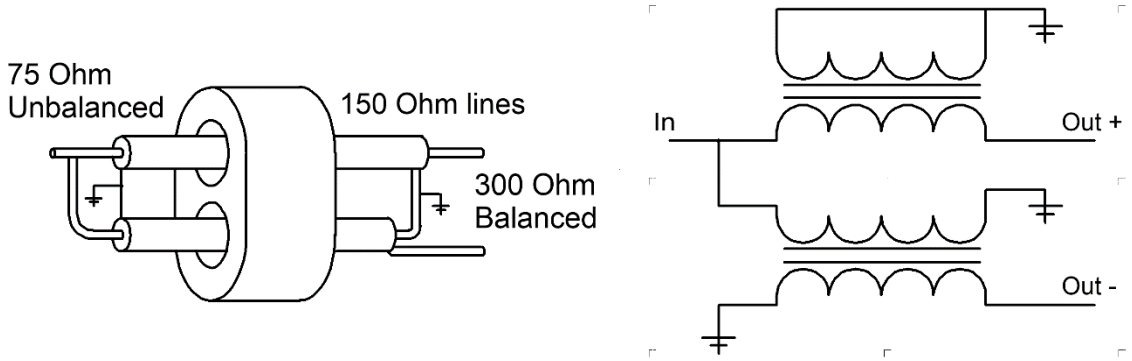



Figure 3.7. Diagram of transformers with ferrites and transmission lines.

The determination of the number of turns required for this transformer is the same as that for the bifilar or trifilar winding outlined above. The lower corner frequency is determined by the magnetising inductance. The upper corner frequency is determined by the losses in the ferrite. For the transmission-line transformer the winding length is no longer limited to be less than 10% of the wavelength, as both outputs have the same propagation delay through the transmission line. Typically, these cores are wound on low loss ferrites, giving them very high upper cut-off frequencies.

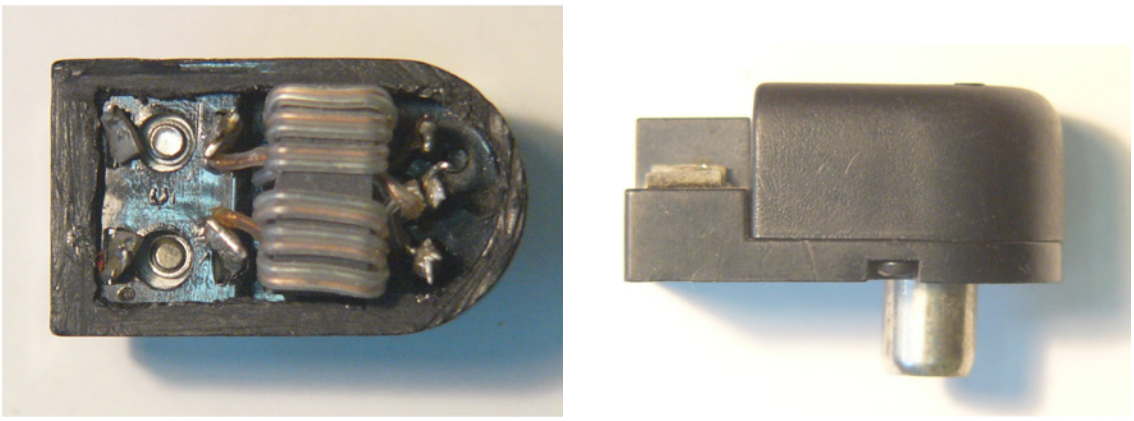
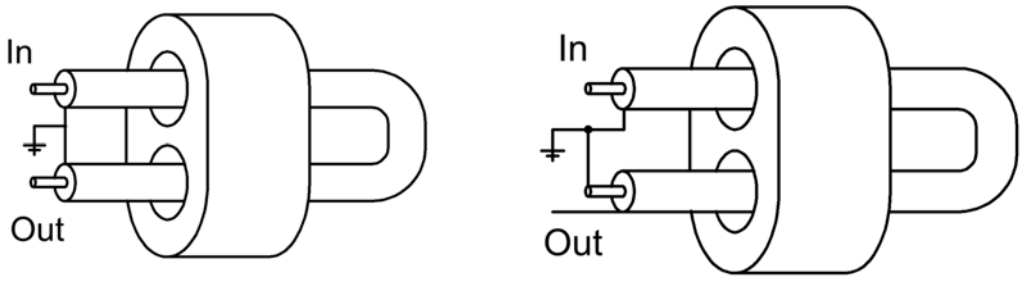


Figure 3.8. TV Balun using Ferrite RF transformer and transmission line windings.

Figure 3.8 shows a TV balun (*Bal*anced to *Un*balanced) transformer, corresponding to the circuit diagram in figure 3.7. This allows a typical dipole antenna, which has a balanced output of 300 Ω impedance to be connected to a 75 Ω coaxial cable, for a low loss connection to a TV. The transmission line balun is an ideal match at high frequencies and the ferrite provides the isolation at low frequency.

By simply wrapping a coaxial lead around a ferrite or steel former, a non-inverting transformer, like figure 3.9, is obtained. This will provide isolation between both ends of the coaxial cable. Such a lead is useful in preventing earth loops for μV measurements.

A transformer, using transmission lines for the windings, can be used as an isolating transformer, by connecting opposite sides of the transmission line to ground as indicated in figure 3.10. The lower frequency of this transformer is determined by the magnetising inductance of the former. This can be increased by simply adding more cores or having the transmission line go through the hole in the core many times.




## Transformer Hybrids

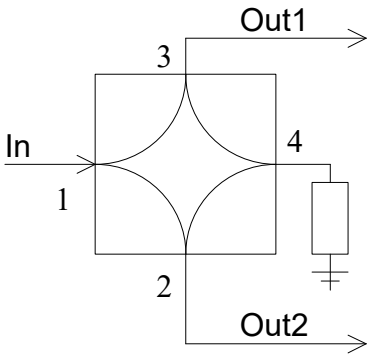



Figure 3.11. Hybrid.

In a hybrid, the input power at port 1 is split two ways to adjacent ports 2 and 3. Port 4, opposite the input port is isolated from the input port, and should have no energy going to it. A hybrid can thus be used as a power splitter.

Hybrids are normally symmetrical and bi-directional. Port 2 can thus also be used as an input, and under those conditions, half the power appears at port 1 and the other half appears at port 4. Under these conditions, port 3 is isolated. If we now apply another input signal at port 3, that will also split two ways with half appearing at port 1 and the other half at port 4. For most hybrids, the phase angle at port 4 is 180 degrees out of phase for inputs at either port 2 or port 3, so that if equal signals are applied to ports 2 and 3, the sum of the signals will appear at port 1 and the difference will appear at port 4. If the signals applied to port 2 and port 3 are the same, the powers are combined at port 1. A hybrid can thus be used as a power combiner as well.

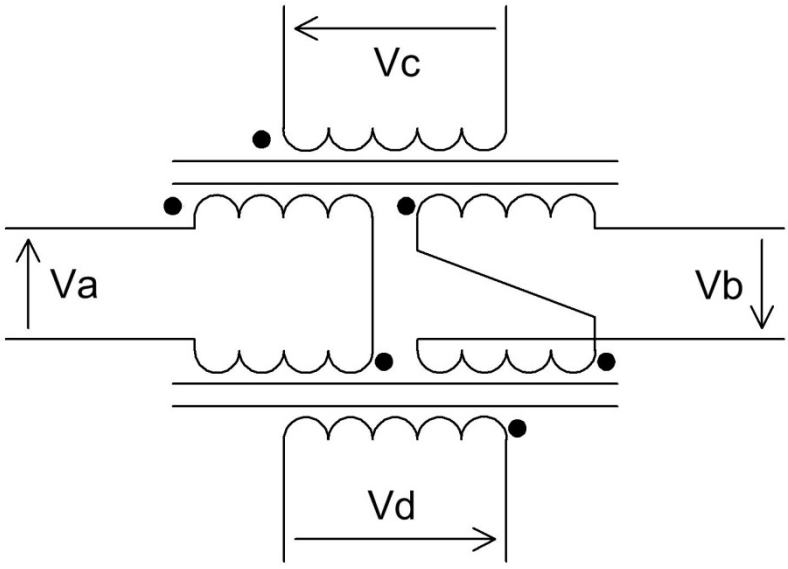



Figure 3.12. Audio transformer hybrid.

Transformer hybrids like the ones in figure 3.12 are used in telephony networks, where the signals to and from the normal telephone are sent in both directions on two wires.

Assume that all the windings on the transformers have the same number of turns. For the Audio transformer hybrid in figure 3.12, the voltages at each of the ports are related as:

$$\begin{aligned} Va &= Vc + Vd \\ Vb &= Vc - Vd \\ 2Vc &= Va + Vb \\ 2Vd &= Va - Vb \end{aligned} \qquad \text{Eqn. 3.3}$$

By changing the turns ratio to 0.707, the same equations are obtained for all the ports:

$$\begin{aligned} Va &= 0.707Vc + 0.707Vd \\ Vb &= 0.707Vc - 0.707Vd \\ Vc &= 0.707Va + 0.707Vb \\ Vd &= 0.707Va - 0.707Vb \end{aligned} \qquad \text{Eqn. 3.4}$$

This ensures that the impedance levels in each port are the same. Note that Va does not couple into Vb and Vc does not couple into Vd and vice versa. A 40 dB isolation is typical under properly matched conditions.

Figure 3.13 shows how this audio hybrid can be wired up for use with amplifiers to produce a bi-directional amplifier, to amplify signals travelling in both directions along a wire. If the 2-wire circuit is not terminated properly, then part of the energy travelling out of this amplifier will be reflected and come back as input to the amplifier and be amplified again. If the gain of the amplifier is A dB and the isolation is B dB, then the singing margin is 2×(B-A). The singing margin is the gain around the amplifier/hybrid loop. If the gain around the loop is more than 0 dB, then oscillations will occur. In practice, the singing margin should be better than 6 dB. We should thus have more than 6 dB loss around the loop, even in the worst conditions.

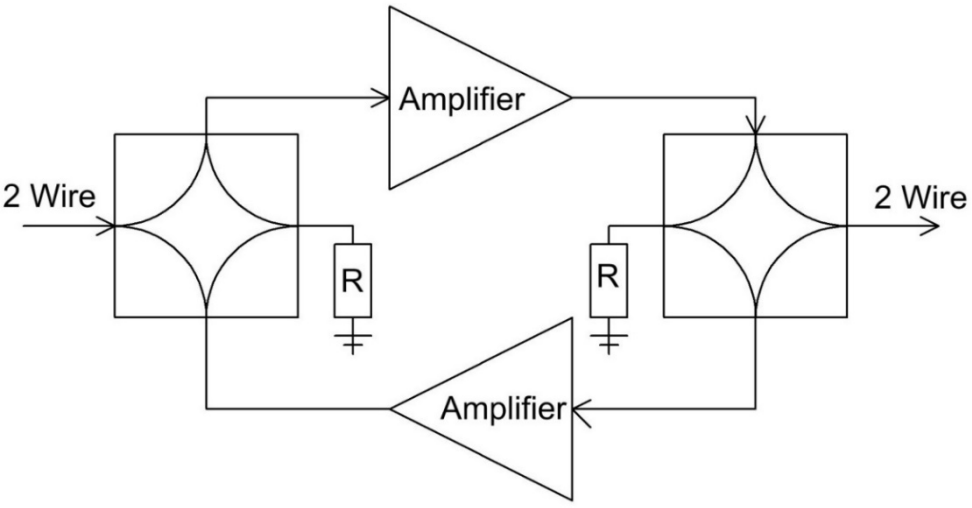



Figure 3.13. Bi-directional amplifier.

## Power Combiner / Splitter

In a power combiner or power splitter, the terminating port is not brought out. The power combiner or power splitter is thus a 3-port device. Since linear passive devices are bi-directional, the same device can be used as both a power splitter and a power combiner. Often these devices are still called a hybrid. A common transformer based power splitter is a Wilkinson Hybrid. The two-way power splitters sold by department stores to permit two TVs to be operated from one antenna are Wilkinson Hybrids.

## *Wilkinson Transformer Hybrid*

Figure 3.14 shows the circuit diagram of a Wilkinson Transformer Hybrid. It has two transformers, the left one combines signals A and B into C and the tight one changes to impedance of this signal C to the required output impedance. If the same voltage input is applied to both ports A and B, then there is no voltage drop across the terminating resistor or transformer and port C is at same voltage as ports A and B. If the impedance levels for ports A and B are $Z_0$, then for power conservation, the impedance level at port C must be ½ $Z_0$. For those situations where the output impedance should be $Z_0$ then a 3:2 turns ratio transformer will change the impedance level by 2.25, which is close enough to 2:1.

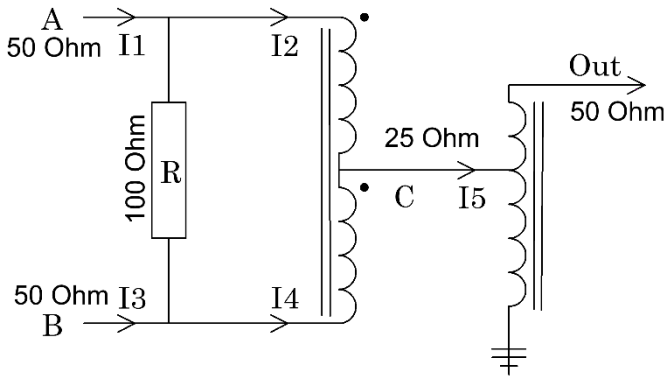



Figure 3.14. Wilkinson Transformer Hybrid.

If a voltage is applied to port A and 0 Volt is applied to port B, then the voltage at port C is ½ of that at port A. If the input current at port A entering the transformer is $I_2$, then through transformer action an equal and opposite current is flowing through the bottom part of the transformer, so that $I_2 = I_4$, under all conditions. If the load impedance at port C is ½ $Z_0$ as before then the input impedance seen at port A at the input of the transformer is 2 $Z_0$ since the transformer has a 2:1 turns ratio and a 4:1 impedance transformation ratio, since at port C one has half the voltage and twice the current.

Consider figure 3.14. For complete isolation between ports A and B, if a signal is applied at port A then the voltage at port B is zero, so that $I_3 = 0$. The current $I_4$ must thus flow through the resistor. The value of R required for complete isolation between ports A and B can now be calculated. The voltage across the resistor is:

$$V_a = \frac{I_4}{R} = \frac{I_2}{2Z_0} \qquad \text{Eqn. 3.5}$$

Since $I_2 = I_4$, we must have $R = 2Z_0$ to achieve isolation between both input ports. Under those conditions the impedance seen at the input port A is $Z_0$, being the transformer input impedance of $2Z_0$ in parallel with the terminating resistor of $2Z_0$.

If this hybrid is used as a power splitter and the loads on ports A and B are matched, then no current will flow through the terminating resistor. Under those conditions that can be removed, at the expense of a poor isolation if unequal loads are present. For a power combiner in an antenna systems, where the output from two identical antenna elements are combined, a hybrid can be used that does not contain any isolating resistor, since the signals arriving at each of the antennae is identical and as a result no power is dissipated in the isolating resistor.

The Wilkinson transformer hybrids are commercially available as wideband power-splitters and power-combiners manufactured by companies such as Mini-Circuits.

The conventional TV splitter is a cut down version of the Wilkinson hybrid. Since the cable losses will mask any unequal loads, the terminating resistor is not normally present and since impedance variations can be tolerated, no output transformer is used. The omission of those components reduces the cost for this consumer-oriented circuit.

If a Wilkinson Transformer hybrid is used to combine the output from two transmitters, any unbalance will be dissipated in the resistor R. For two 100 Watt transmitters, 50 Watt will be dissipated in the resistor and 50 Watt will be radiated if one of the amplifiers fails. The resistor must thus be selected with this power requirement in mind.

## *Example 3.2: Wilkinson Transformer Hybrid Design*

The transformer on the left of figure 3.14 combines signals A and B. If an input is applied to port A but no input is applied to port B, then for a 50 Ω impedance at port A, the transformer must provide a 100 Ω impedance, since it is in parallel with the 100 Ω resistor. The impedance at port C is thus 25 Ω, since both windings on that transformer are the same. The transformer on the right provides an impedance transformation from 25 Ω to 50 Ω. If we use the same toroidal core as was used in example 3.1, then the required number of turns can easily be calculated. That transformer at 1 MHz, had N1 = 3.093. and a 1000:1 bandwidth.

For a 25 Ω winding, N25 = N1√(25) turns = 15.46 turns are required. Since this has to be an integer number, 16 turns are used. The left transformer will thus have a bifilar winding with 16 turns on it. The leakage inductance will then be 125.8 nH and the magnetising inductance will be 125.8 µH. The 25 Ω to 50 Ω impedance transformation transformer will have a 2:3 turns ratio auto-transformer, with a total number of 21.87 turns. This can be obtained with a 7 turn trifilar winding, so that the 25 Ω winding will consist of two 7 turn windings in series and the 50 Ω winding will have the three 7 turn windings in series. The resulting leakage inductance is 251.6 nH and the magnetising inductance is 251.6 µH.

To simulate the Wilkinson hybrid in Cadence AWR DE, ideal transformer elements XFMR are used. To make this into a practical model, the transformer representation in figure 3.3 meeds to be used. The transformer on the left of figure 3.15 has two 25 Ω windings in series. The corresponding leakage and magnetising inductances are calculated in figure 3.15 as Ls25 and Lm25. The transformer on the right of figure 3.15 provides a 25 Ω to 50 Ω impedance transformation. Its leakage and magnetising inductances are calculated in figure 3.15 as Ls50 and Lm50.

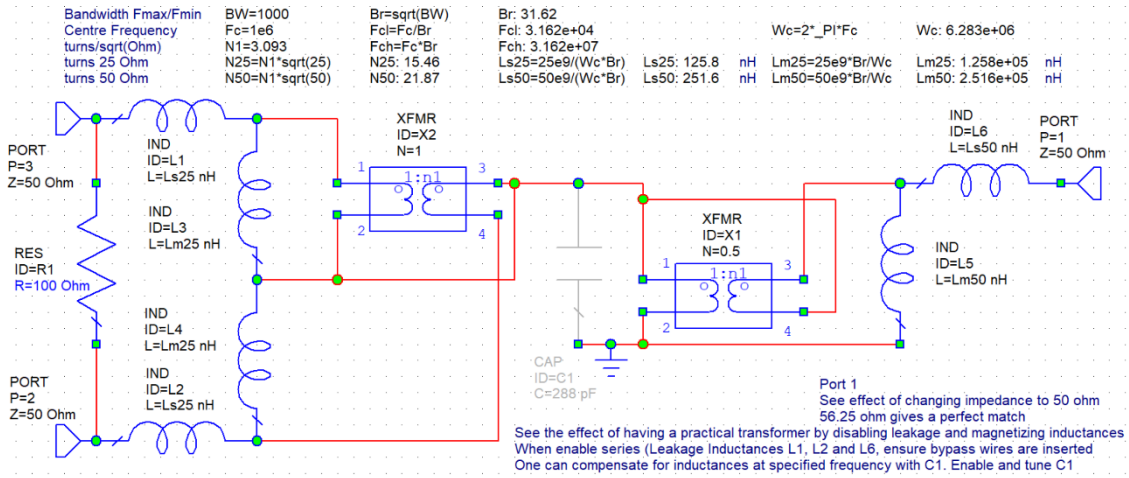



Figure 3.15. Wilkinson Hybrid model for computer simulation.

Figure 3.16 shows the corresponding frequency response. It can be seen that a good isolation and return loss on all ports is obtained at the design frequency of 1 MHz. Constructing this hybrid normally results in a close agreement with the simulation and typically result in a three decade frequency bandwidth.

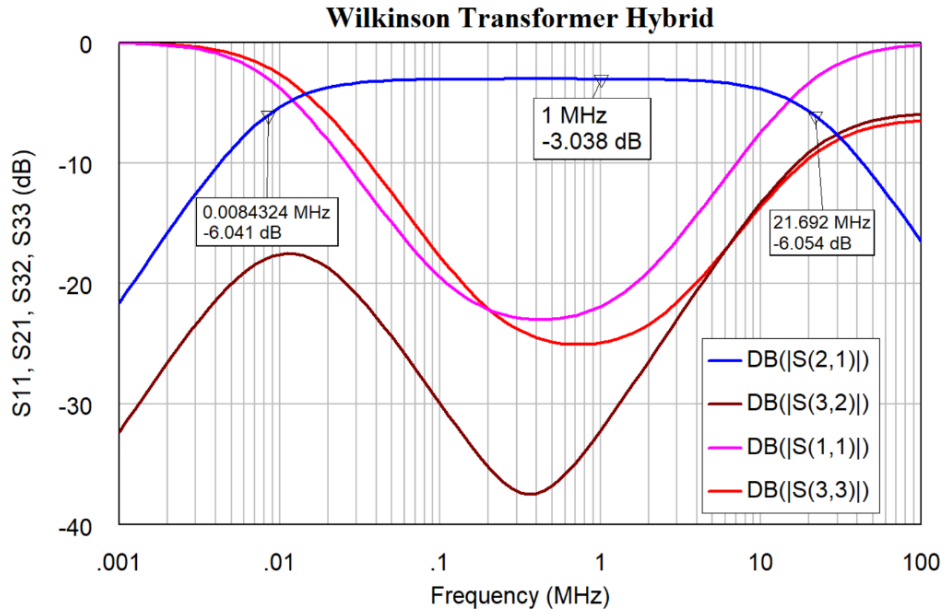



Figure 3.16. Simulated performance of Wilkinson Hybrid.

The 25 Ω to 50 Ω impedance transformation requires a $\sqrt{2} = 1.414$ turns ratio. A 2 to 3 turns ratio is the nearest. For a 25 Ω impedance on the 2x7 turn winding the 3x7 turn winding corresponds to a 56.25 Ω impedance. Tuning the Port 1 impedance to 65.25 Ω results in a better isolation. In addition, the return loss from all ports can be improved by tuning a capacitor at the junction of the two transformers, to partially cancel the leakage and magnetising inductances at some frequencies. That also increases the bandwidth. Figure 3.17 shows the resulting performance.

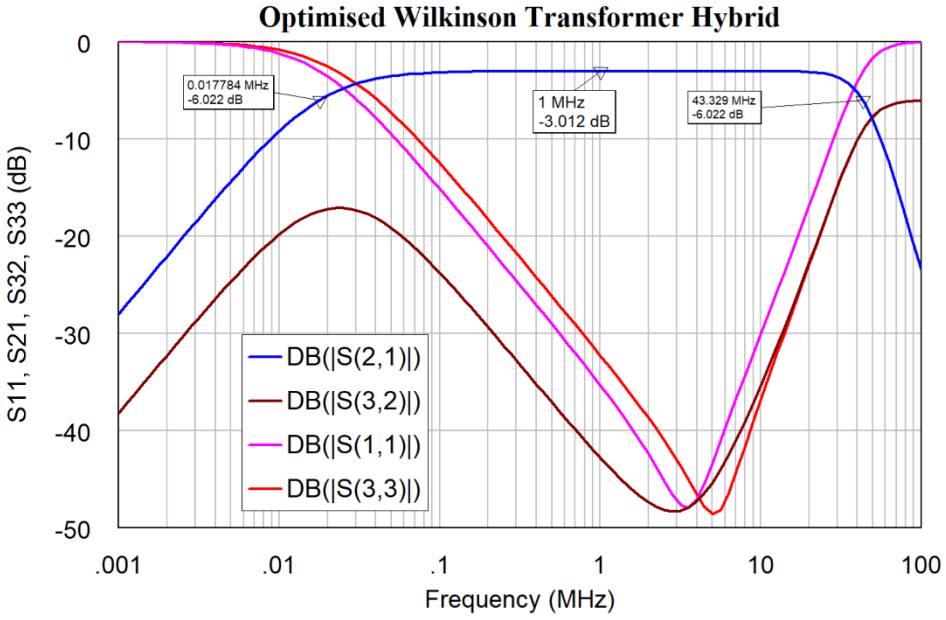



Figure 3.17. Performance of the optimised Wilkinson Hybrid.

## Transmission Line Hybrid with Ferrite Cores

A simple hybrid made using standard 50 Ω transmission line hybrid and ferrite cores is shown in figures 3.18 to 3.20. If the impedance at A and B is $Z_0$ then at C the impedance is $\frac{1}{2}Z_0$. The impedance seen when B=0 is $2\times(\frac{1}{2}Z_0)=Z_0$ . The power dissipated in the load resistor is the power associated with the difference in the input signals. For high power operation, the rating of that resistor must be carefully considered. If the input at A and B are the same then no power will be dissipated in the load resistor.

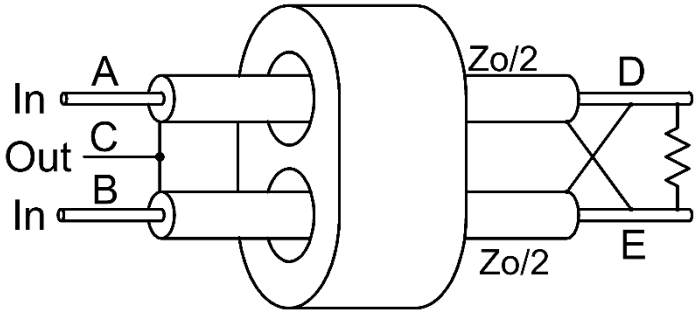



Figure 3.18. Hybrid with ferrite cores.

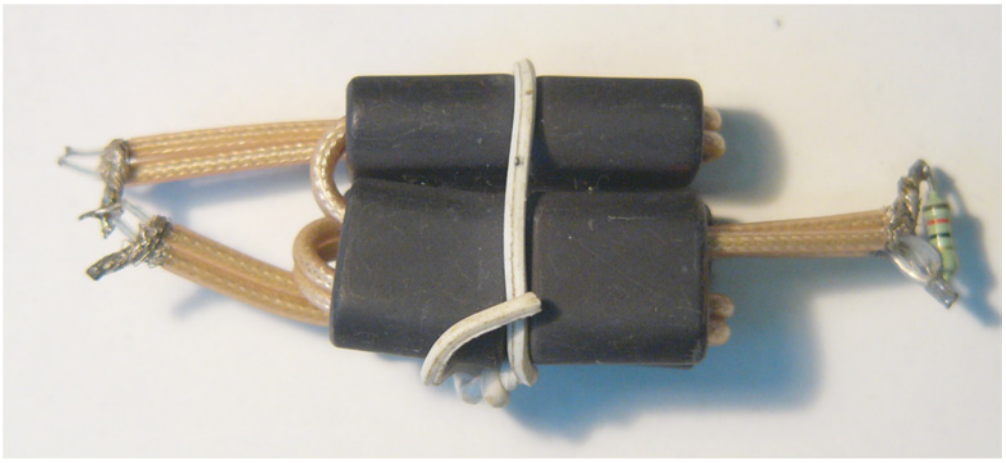


Figure 3.19. Circuit of hybrid in figure 3.18

The realisation of the hybrid is shown in figure 3.19 and the circuit can be analysed using the circuit representation in figure 3.20. In figure 3.19, the 25 Ω transmission lines are obtained by having two 50 Ω transmission lines in parallel.

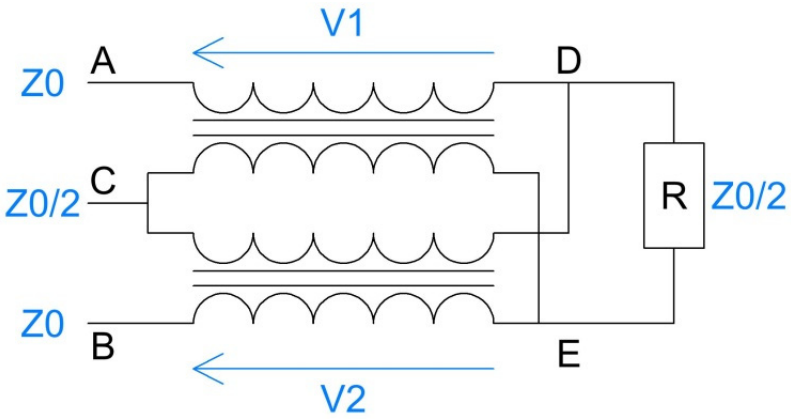



Figure 3.20. Circuit of hybrid in figure 3.18.

The equations for this hybrid are:

$$V_a - V_d = V_1$$
$$V_c - V_e = V_1 \qquad \text{Eqn. 3.6}$$
$$V_c - V_d = V_2$$
$$V_b - V_e = V_2$$

Subtracting the first two equations and the last two equations and adding the resulting equations gives:

$$V_c = \frac{V_a + V_b}{2} \qquad \text{Eqn. 3.7}$$

Now consider the conditions required for isolation. If $V_b=0$. For isolation between ports A and B, the current through the bottom transformer is zero, since with a load connected to B the voltage must be zero. That means $V_2=0$ and thus $V_e=0$ and $V_d=½V_a$ .

For the input impedance at A to be $Z_0$ then the load resistor must be $½Z_0$ . Under those conditions, the current into A goes through the load and out of C. The voltages are thus:

| | | |
|---|---|---|
| At input A | $V_a = Z_0 \bullet I$ | Eqn. 3.8 |
| Across the Load | $½V_a = ½Z_0 \bullet I$ | Eqn. 3.9 |
| At the output C | $½V_a = ½Z_0 \bullet I$ | Eqn. 3.10 |

The equations are thus consistent and the assumption that $V_b=0$ is justified and we have full isolation when $R=½Z_0$ . The circuit works thus as a proper hybrid.

Note: Like the Wilkinson transformer, the impedance at the summing port C has an impedance of $½Z_0$ and a transformer needs to be used to change that to $Z_0$ if required, similar to that for the Wilkinson transformer of figure 3.14.

## Many Way Hybrids

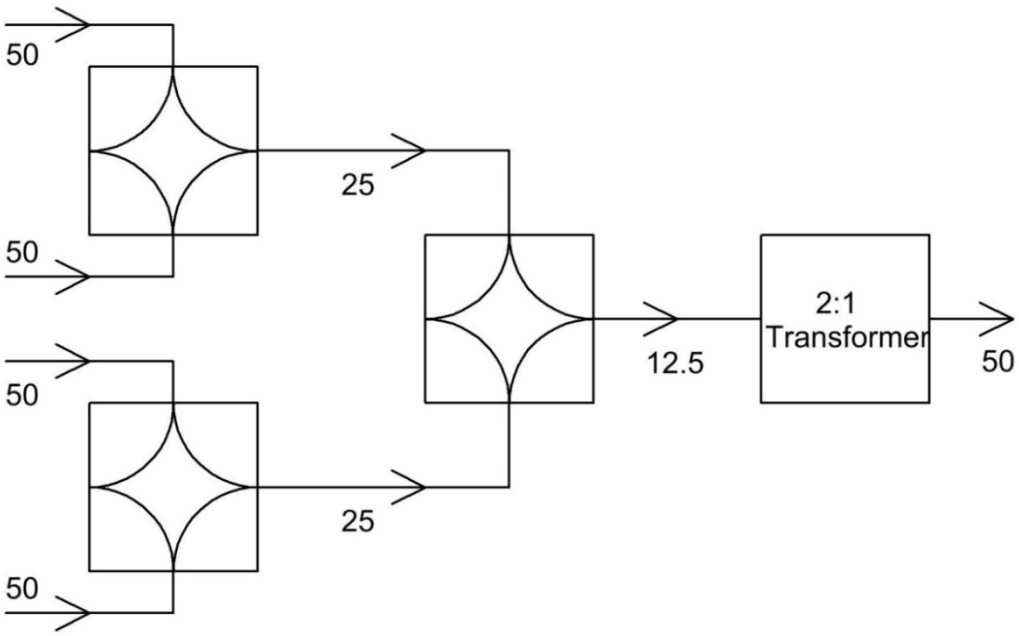



Figure 3.21. A four-way combiner.

In some instances, many signals need to be combined or a signal needs to be split many ways. The hybrids described above can be cascaded to provide a many way splitter/combiner. However, each of those hybrids will include a 25 Ω to 50 Ω impedance transformation transformer. Some savings can be made by using a 4 way hybrid as shown in figure 3.20, where three of two way hybrids are used together to combine 4 input signals and then have a 12.5 Ω output, which can be transformed to 50 Ω by using a 2:1 transformer, as shown in figure 3.20. This saves two transformers, each of which will have some losses associated with it. In addition, the 4:1 impedance transformation is exact, while the 2:1 impedance transformation is actually a 2.25:1 impedance transformation with the 3:2 turns ratio of the transformer. Two of the hybrids below operate at a 50 Ω impedance and one operates at a 25 Ω impedance. The number of turns on the transformer coils needs to be adjusted to allow for this.

## References

1. H. Granberg, “Broadband transformers and power combining techniques for RF”, Mototola Application Note AN749. https://community.nxp.com/t5/Other-NXP-Products /Helge-Granberg-AN749-EB104-and-the-legacy-of-Freescale/m-p/ 261491
2. Minicircuits.Application note AN20-001 “How RF Transformers work” http://www.minicircuits.com/app/AN20-001.pdf
3. Minicircuits.Application note AN20-002 “Application Note on Transformers” http://www.minicircuits.com/app/AN20-002.pdf

# Chapter 4

# Transmission Line Transformers and Hybrids

## Introduction

At RF and microwave frequencies, lines connecting devices can be an appreciable fraction of a wavelength. As a result, transmission lines models should be used, to connect all devices. Those transmission lines can also be used to change impedances, just like the transformers in chapter 3. In addition, by connecting transmission lines in special ways, circuits like hybrids, power splitters, power combiners and couplers can be made. Their design is described in this chapter.

Since this chapter deals with transmission lines and their use in transformers, hybrids and couplers, a brief review of properties of transmission lines will be given.

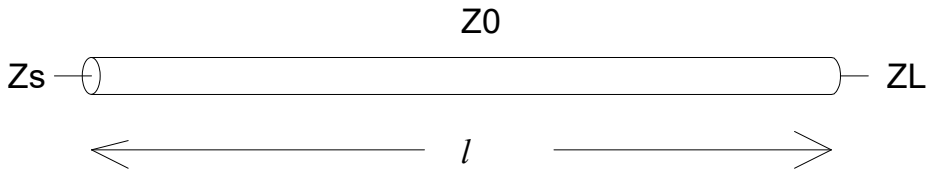



Figure 4.1. Transmission line parameters.

For a transmission line of characteristic impedance $Z_0$ and length $l$, the sending end impedance is given by [1 - 3]:

$$Z_S = Z_0 \frac{Z_L + jZ_0 \tan(\beta l)}{Z_0 + jZ_L \tan(\beta l)} \qquad \text{Eqn. 4.1}$$

If the transmission line is close to one quarter wavelength long then tan(βl) >>1 so that:

$$Z_S = Z_0 \frac{jZ_0 \tan(\beta l)}{jZ_L \tan(\beta l)} = \frac{Z_0^{\,2}}{Z_L} \qquad \text{Eqn. 4.2}$$

so that: $Z_S Z_L = Z_0^2$ or $Z_S = Z_0^2 / Z_L$ Eqn. 4.3

The impedance transformation ratio R is given by:

$$R = \frac{Z_0}{Z_S} = \frac{Z_L}{Z_0} \text{ or } Z_S = \frac{Z_0}{R} \text{ and } Z_L = RZ_0 \qquad \text{Eqn. 4.4}$$

In figure 4.1, if a voltage waveform travels along the transmission line with an impedance $Z_0$, when that arrives at the load $Z_L$, that voltage is reflected and the amplitude of the reflected waveform is changed by a factor of the reflection coefficient Γ, where:

$$\Gamma = \frac{Z_L - Z_0}{Z_L + Z_0} \qquad \text{Eqn. 4.5}$$

If $Z_L = Z_0$, the system is matched. Γ = 0 and there is no reflected wave. If the transmitted wave is a single sinewave, then the reflected wave will reinforce the incident wave at some points and oppose it at other points along the transmission line. The ratio between

the maximum amplitude and the minimum amplitude is the Voltage Standing Wave Ratio (VSWR), and can be related to the reflection coefficient as:

$$VSWR = \frac{1+\Gamma}{1-\Gamma} = \frac{Z_L}{Z_0} \qquad \text{Eqn. 4.6}$$

In general the VSWR is the ratio of the actual impedance of the termination to the desired impedance of the termination. If the allowable (VSWR) is W, the limiting value of the sending end impedance is $WZ_s$, substituting equation 4.4 into equation 4.1 gives:

$$WZ_s = W\frac{Z_0}{R} = Z_0\left\{\frac{RZ_0 + jZ_0\tan(\beta l)}{Z_0 + jRZ_0\tan(\beta l)}\right\} \qquad \text{Eqn. 4.7}$$

Solving for tan(βl) and using the fact that normally $W^2 << R^4$ gives:

$$\tan(\beta l) = \sqrt{\frac{R^4 - W^2}{R^2(W^2-1)}} \cong R\sqrt{\frac{1}{W^2-1}} \qquad \text{Eqn. 4.8}$$

For the desired match the length of the transmission line in figure 4.1 is a quarter wavelength. βl is thus 90 degrees. Equation 4.8 gives the values of βl, where the allowable mismatch limits occur. The higher R, the higher tan(βl) must be and thus the narrower the bandwidth for a given VSWR. This can be illustrated with the following example.

## *Example 4.1: Bandwidth Calculation*

If the allowable VSWR is 1.2, that is for a 50 Ω system the impedance should be between 60 Ω and 41.6 Ω, and if R = 2 (i.e. a 4:1 impedance transformation) then $\beta l = 70.8°$ i.e. $l = 0.197\lambda$. The bandwidth is thus 2(90-70.8)/90 = 43%

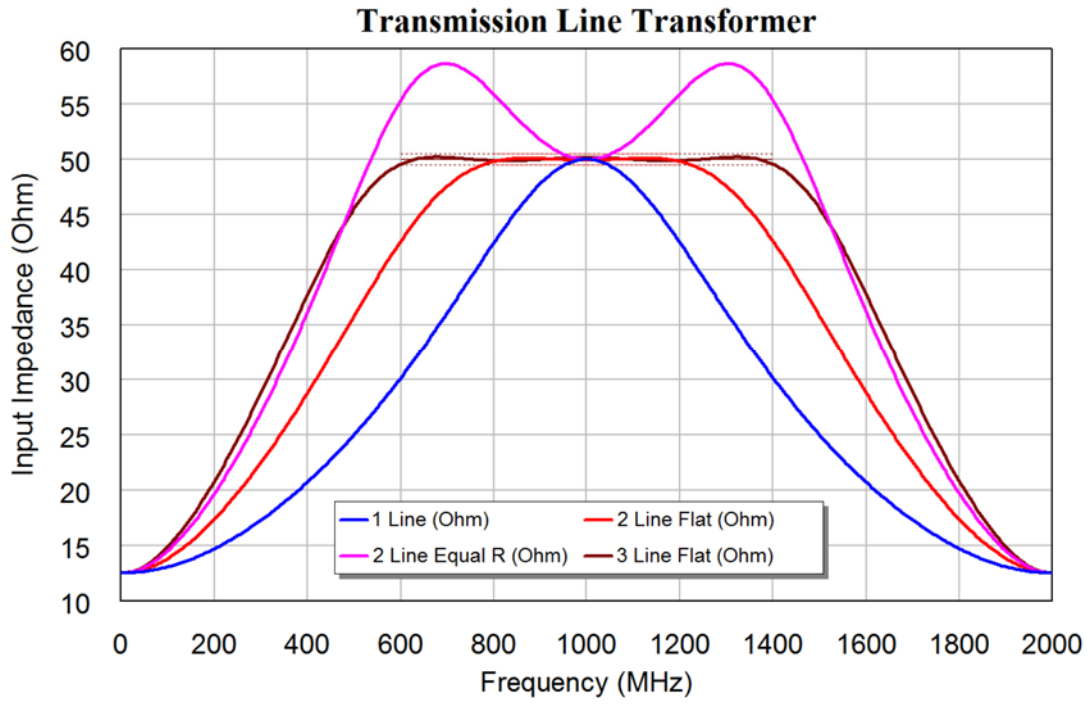



Figure 4.2. Plot of impedance variation versus frequency.

If R is changed to R = √2 (i.e. a 2:1 impedance transformation) then the same total impedance transformation can be achieved by having two quarter wavelength transmission line sections in cascade. If the load impedance is $Z_L$ then the impedance at the end of the first section is $2Z_L$ and the impedance at the end of the second section is

$4Z_L$. The total length of the transformer is thus half a wavelength. Solving for $\beta l$ gives $\beta l$ = 59.6° i.e. $l = 0.166\lambda$. The bandwidth is thus 2(90-59.6)/90 = 67.5%

For very high frequencies, many sections can be cascaded and the line will have an exponential change of impedance for each of the quarter wavelength sections. This can readily be produced using RF PCB technology.

Figure 4.2 shows a plot of the input impedance variation of a transmission line transformer, transforming a 12.5 Ω load into a 50 Ω load. For the one line transformation, the impedance transformation is done in one transmission line section with a characteristic impedance of 25 Ω. The Magenta curve is for a 2-line transformation, with the impedance transformation ratio R = √2 for each line.

If the impedance transformation ratio of the two lines in a two line impedance transformer is changed from the R = √2 for each of the lines, such that the total impedance transformation is still a 4:1 impedance transformation, but that each line has a slightly different transformation ratio, then a very good match can be obtained over a specified bandwidth. For this design, the transformation ratio is made a variable constant, which is optimised to provide the minimum deviation from 50 Ω, over the required frequency range.

For a two-line matching network, a good match can be obtained over the 800 MHz to 1200 MHz frequency range. The result of this optimisation is shown by the red curve in figure 4.2. The first line has $R = Z_{in}/Z_{d1} = 1.638$, where $Z_{d1}$ is the impedance of line 1, corresponding to a characteristic impedance of 30.53 Ω and the second line has R = Zd2/Zout = 1.222 corresponding to a characteristic impedance of 15.28 Ω, instead of the R = √2 for the un-optimised transmission line transformer. (Note: The numerical results obtained from CADENCE AWR DE project files are normally presented in this book with the default 4 digit display accuracy of AWR DE. Results that are more accurate can be obtained by running the corresponding CADENCE AWR DE project files.)

Applying similar principles to a 3-line section gives an even wider bandwidth. The brown curve in figure 4.2 shows the optimisation result of matching 50 Ω to 12.5 Ω, using 3 quarter-wavelength long lines over a 600 MHz to 1400 MHz bandwidth. Instead of all the three transformer ratios being $\sqrt[3]{2} = 1.260$, the ratios are 1.450, 1.357, 1.087 and this corresponds to transmission line impedances are 34.48 Ω, 18.71 Ω and 13.58 Ω as shown in figure 4.3.

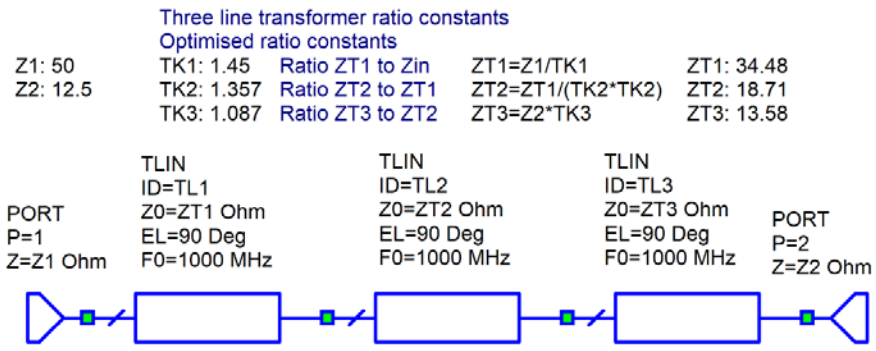



Figure 4.3. Optimised transformation ratios for 3 line flat transformer of figure 4.2

Instead of being as close to 50 Ω as possible over the specified frequency range, it is possible to specify optimisation limits to be say >45 Ω and < 55 Ω, and then making the

bandwidth wider. This then allows very wide bandwidth impedance transformers, with tightly specified VSWR's to be designed.

## Wilkinson Transmission Line Hybrid

The Wilkinson transmission line hybrid [4] consists of two quarter-wavelength long transmission lines forming a combiner, together with a load resistor to provide isolation. The circuit is shown in figure 4.4 and the performance is shown in figure 4.5.

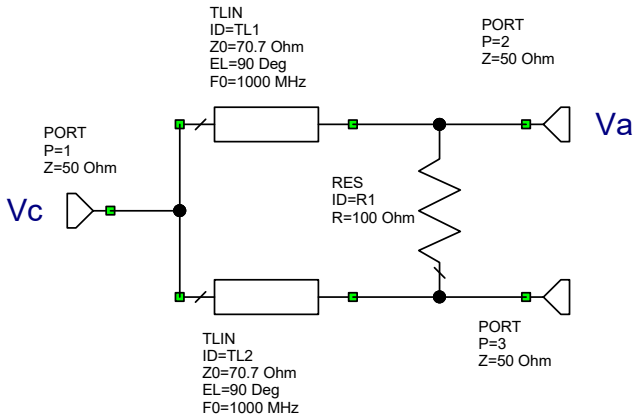



Figure 4.4. Ideal Wilkinson hybrid.

For the analysis, an input is applied to port 2 in figure 4.4. For proper hybrid operation, no voltage should appear at Port 3. Transmission line TL2 has a standing wave on it with 0 Volt at the Port 3 side. Since the line is one-quarter wave long, there will be no current flowing into the line at the Port 1 side, as shown in figure 4.6. For the analysis of the voltage on port 1, we can thus remove TL2, since it is an open circuit at the port 1 end. The voltage at port 1 will thus simply be what we would have if one had the transmission line only, as shown in figure 4.7.

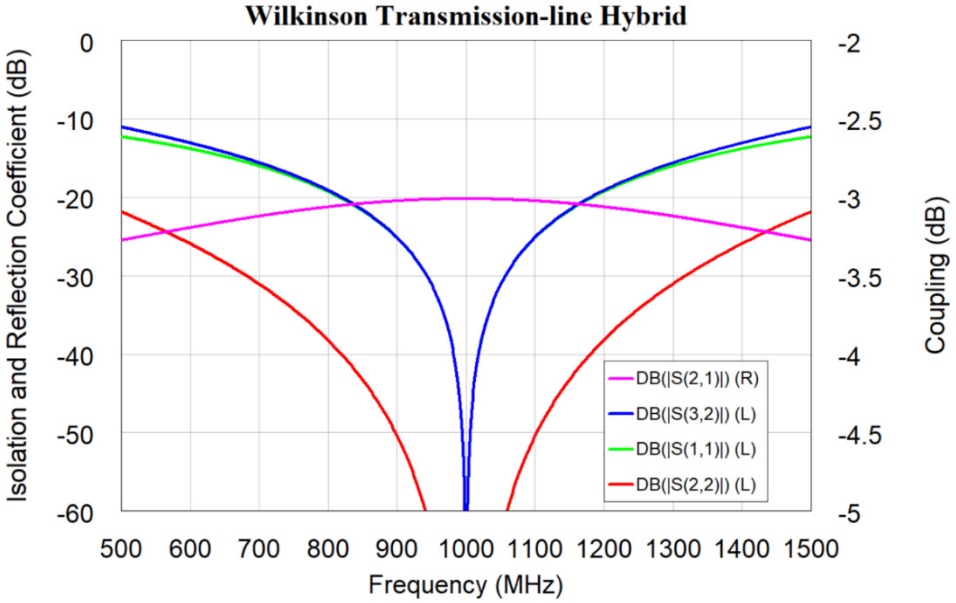



Figure 4.5. Ideal Wilkinson hybrid.

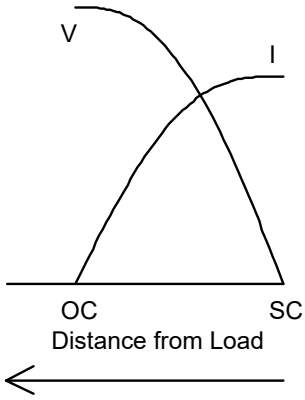



Figure 4.6. Standing wave along TL2.

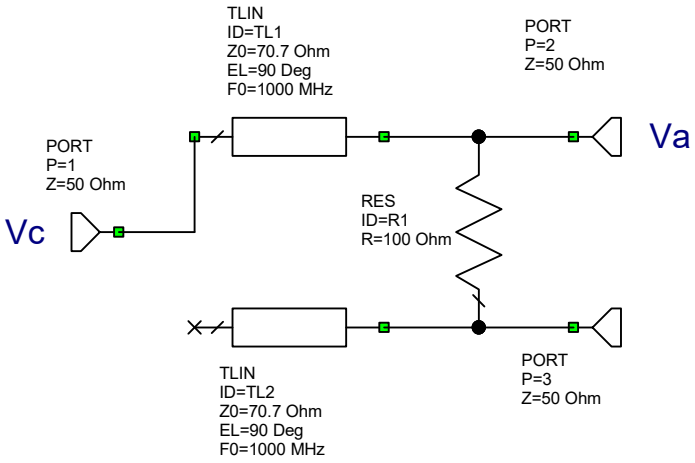



Figure 4.7. Circuit for analysis purposes.

Since the input power is the same as the output power, the voltage $V_c$ at port 1 and the voltage $V_a$ at port 2 relate as $V_a = \sqrt{2}\, V_c$.

The maximum current and maximum voltage on a transmission line relate as:

$$V_{\max} = Z_0 I_{\max} \qquad \text{Eqn. 4.9}$$

In figure 4.4, the current at the port 3 side of TL2 will thus be:

$$I_{\max} = \frac{V_c}{\sqrt{2}Z_0} = \frac{V_a}{\sqrt{2}\sqrt{2}Z_0} = \frac{V_a}{2Z_0} \qquad \text{Eqn. 4.10}$$

Since this current must come through the load resistor R then

$$I_{\max} = \frac{V_a}{R} = \frac{V_a}{2Z_0} \qquad \text{Eqn. 4.11}$$

So that $R = 2Z_0$ for best isolation.

The circuit can be realised using a Microstrip PCB layout. A Rogers 4003 laminate with 1 oz. copper and 0.8128mm thickness are to be used. To calculate the required track widths and lengths, the properties of the PCB to be used are to be selected first. The

parameters of the Rogers RO4003 substrate can be obtained by using the *Libraries* ⇒ *AWR Web Site ⇒ Rogers ⇒ RO ⇒ RO4003 and select *32 mil, 1 oz.* and place that as a component in a circuit. Until recently Rogers only specified an Er= 3.38 for the RO4003 laminate. The latest data sheet from Rogers for RO4003C [5] indicates Er (Process specification) = 3.38 and Er (Design specification) = 3.55. Suggesting that for simulation the value of Er=3.55 gives better results. Those values are used here. The values indicated in MSUB for RO4003 on the CADENCE AWR Web site are ErNom=3.48 and Er=3.55. The value of ErNom is ignored by CADENCE AWR DE and Er=3.55 is used in the simulation. Note some of the earlier designs in this book using the RO4003 substrate still use the 3.38 value.

Determining the required track width and length, as shown in figures 2.21 to 2.23, results in a track width of 1.788 mm for the 50 Ω lines and 0.9519 mm for the 70.71 Ω lines. The layout must allow the isolation resistor to be soldered to the PCB. This requires that a resistor, with a PCB footprint is used. Firstly, determine the size of the surface mount resistor to be used. In our layout, an AVX 1206 resistor was used. AVX resistors are no longer included in the CADENCE AWR web site libraries in CADENCE AWR DE V10 or later, but Panasonic resistors are. Selecting *Libraries ⇒ *AWR web site ⇒ Parts by type ⇒ Lumped element ⇒ Resistor ⇒ Panasonic ⇒ Resistor ⇒ For General Equipment ⇒ S parameter*, allows different size footprint resistors to be selected (0603, 1005, 1608 mm). Simply place the resistor with the required size footprint in the schematic, this will then automatically include the footprint in the layout. If another size footprint, say 1206 is required, then the footprint can be imported by simply placing a suitable size component like a capacitor or inductor. For our circuit, a Coilcraft inductor is used to provide the 1206 footprint. Select *Libraries ⇒ *AWR web site ⇒ Parts by type ⇒ Lumped element ⇒ Inductor ⇒ Coilcraft ⇒ RF Inductors ⇒ Data ⇒ 1206CS series*. Then place any inductor in list in the circuit. Right clicking and selecting the inductor's properties, then selecting *Layout*, shows all the available Coilcraft Footprints, as shown in figure 4.8. The layout properties of the isolation resistor in the Wilkinson Hybrid can now be selected. The library name will be blank. Selecting the Coilcraft Library and the 1206 imperial, (3216 metric) footprint will then link that footprint to the resistor. The inductor can then be removed from the circuit, as the footprint will remain linked to the resistor. With a Modelithics EXEMPLAR Library installed, resistor footprints and their associated simulation files can also be placed. Available footprints are 0402, 0603 and 0805 imperial, which are suitable sizes for microwave layouts.

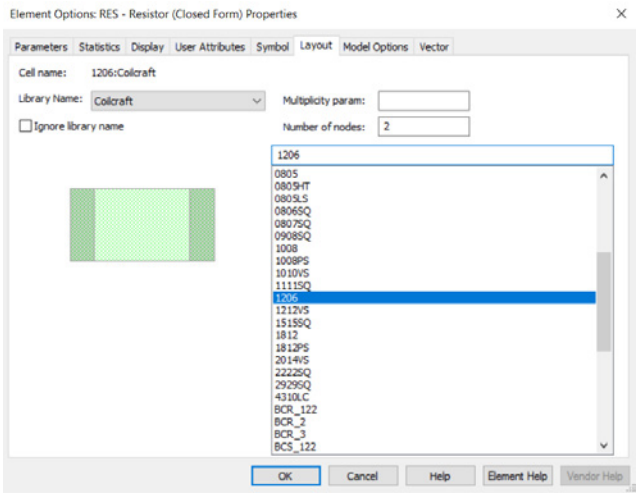



Figure 4.8. Selecting a footprint for resistor R1.

If internet speeds to the AWR DE website are too slow, local vendor libraries need to be installed and used. The Appendix shows how these can be installed. Then simply select the Library parts and footprints from the local libraries instead of the web site.

The rest of the PCB schematic can now be made. The 70.71 Ω Microstrip lines are made using MLIN elements. The two 70.71 Ω lines need to be joined to the 50 Ω line, using a MTEE. There are different versions of this. The most basic one is MTEE, where every connecting line width needs to be specified. MTEE$ is an intelligent version, which automatically uses the line widths of the connecting lines. MTEEX is an EM based model of the junction and is more accurate. MTEEX$ is the corresponding intelligent version of this and this element is used in the circuit. To get the most accurate results, EM based models should be used whenever possible.

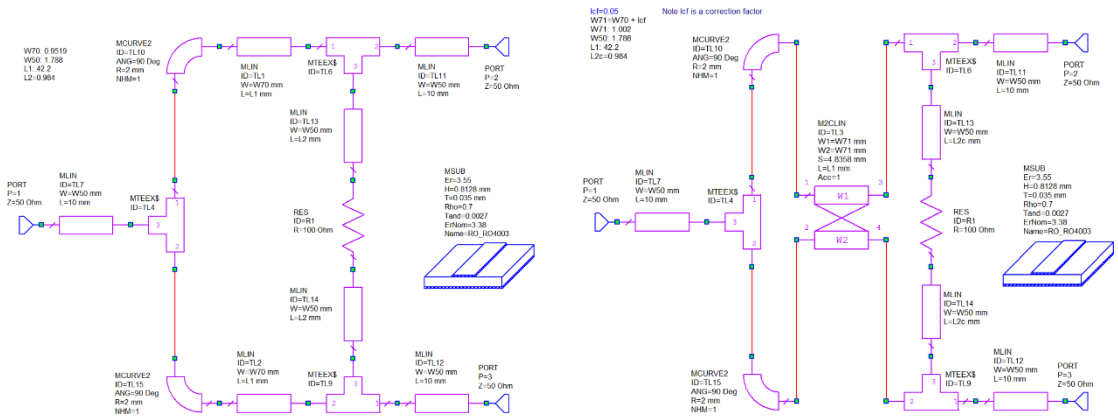


Figure 4.9. Schematics for Wilkinson hybrid PCB layout, using TLIN (Left) and MCLin (Right).

To enable the SMD resistor to be incorporated as shown in figure 4.10, the two 70.71 Ω lines are separated by more than 4 mm. That also keeps the coupling between the lines small. This is achieved by using the two 90 degree bends with 2 mm radius each. In *Circuit Elements* ⇒ *Microstrip* ⇒ *Bends*, there are 4 different versions of curved bends. Since an intelligent MTEEX$ is used, the width of the curved track should be specified. The MCURVE2 element uses EM mode matching and is the most accurate, but will take longer to be evaluated. The length of the 70.71 Ω lines, TL1 and TL2, is made variable, to allow the hybrid to be tuned to the correct centre frequency. Two more MTEEX$ elements are used to allow the resistor to be connected correctly. Two small lines, TL13 and TL14, with a suitable width to allow the isolation resistor R1 to be soldered to it are connected to the MTEEX$ elements. Three 10mm long tracks, TL7, TL11 and TL12 are used, to allow connections to be made to the circuit.



Figure 4.10. PCB layout of a Wilkinson hybrid.

The PCB layout of the circuit can be seen by selecting *View* ⇒ *View Layout*. To connect all the lines together, select *Edit* ⇒ *Select All* (or Ctrl A) and then select *Edit* ⇒ *Snap Together*. That will snap all the elements together. Check that there are no red crosses on the layout, which indicate that the elements are not properly connected together. If that is the case, change line lengths such as L2 for TL13 and TL14 to ensure that the layout fits

exactly. Figure 4.10 shows the resulting layout. The 100 Ωresistor and its connecting lines will have some effect on the performance as shown in figure 4.11, where the notch of $S_{22}$ is shifted in frequency as a result. The performance is however still satisfactory, since a 20 dB isolation or return loss is normally sufficient.

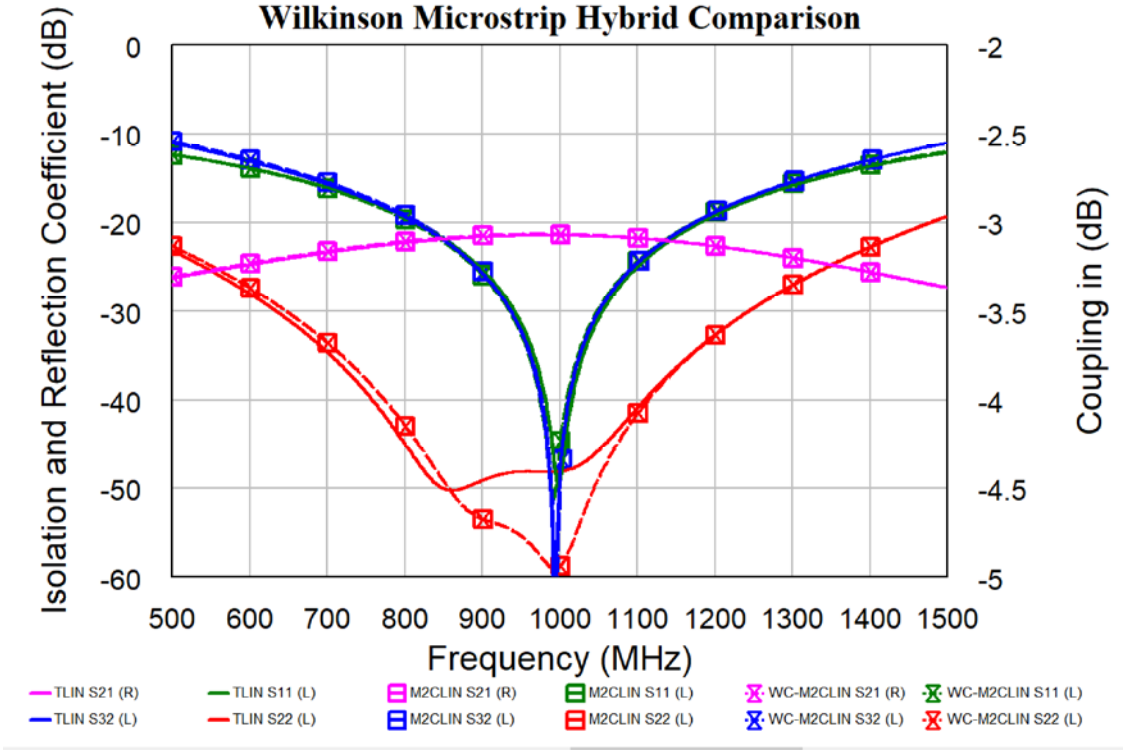



Figure 4.11. Performance of stripline Wilkinson hybrids of figure 4.9.

The line length L1 of TL1 and TL2 can be tuned to ensure that the best isolation occurs at 1.0 GHz. There will be some coupling between TL1 and TL2, since they are in close proximity. The effect of this coupling can be investigated using an EM simulator like AXIEM, which is included with AWR DE. In chapter 7, the section on *EM Simulation*, shows how AXIEM can be used to analyse circuits. A good indication of the coupling between lines TL1 and TL2 can simply be obtained by replacing them with a coupled line element M2CLIN as shown in the right part of figure 4.9. The length of the coupled line is the same as TL1 or TL2. The line width is 0.9519 mm like TL1 or TL2. The spacing is set to 4.836 mm, corresponding to the spacing between TL1 and TL2. The layout is the same as figure 4.10, but now the effect of the coupling between TL1 and TL2 is included.

Figure 4.11 shows a comparison between the performance of the layout of figure 4.10, when TLIN elements are used for TL1 and TL2 of left figure 4.9 are replaced with a coupled line M2CLIN of right figure 4.9, initially with a width correction factor lcf=0. The coupling does not change but the isolation ($S_{32}$) and the return loss of $S_{11}$ and $S_{22}$ are reduced. If needed, the line widths used for M2CLIN can be changed slightly, by varying lcf, to improve these values. Optimising the width of the 70.71 Ω lines, results in a width correction factor, lcf = 0.05 mm, and results in $S_{22}$ = -59 dB at 1 GHz, as shown in the width-corrected WC-M2CLIN curves in figure 4.11. A similar improvement in $S_{22}$ can be made by slightly tuning the width of the lines for the circuit in the left of figure 4.9.

Figure 4.11 does show that unintended coupling between lines can seriously degrade the performance of a circuit, but that steps can easily be taken to overcome any performance degradation.

## *Compensated Wilkinson Hybrid*

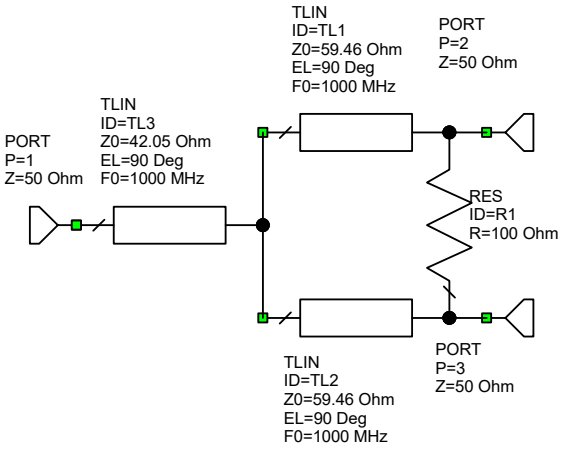



Figure 4.12. Compensated Wilkinson hybrid.

In a compensated Wilkinson hybrid, a two-step impedance transformation is used, like the two line impedance transformation of figures 4.1 and 4.2. The resulting circuit is shown in figure 4.12. The impedance transformation from line TL3 is from 50 Ω at port 1 to 35.36 Ω at the right of TL3. Lines TL1 and TL2 do an impedance transformation from 50 Ω at port 2 and port 3 to 70.71 Ω at the left hand side of transmission lines TL1 and TL2. Those in parallel give a 35.36 Ω, which matches that at the right hand side of line TL3. Each of the three transmission lines will thus have the same impedance transformation ratio of √2.

Figure 4.13 shows a comparison between the conventional (red), and the compensated (blue) Wilkinson hybrid. The compensated Wilkinson hybrid has a wider frequency response for both the isolation and coupling. In addition, the compensated Wilkinson hybrid uses lower impedance transmission lines, resulting in wider track widths for the Microstrip layout, thus lowering the resistive losses in the circuit.

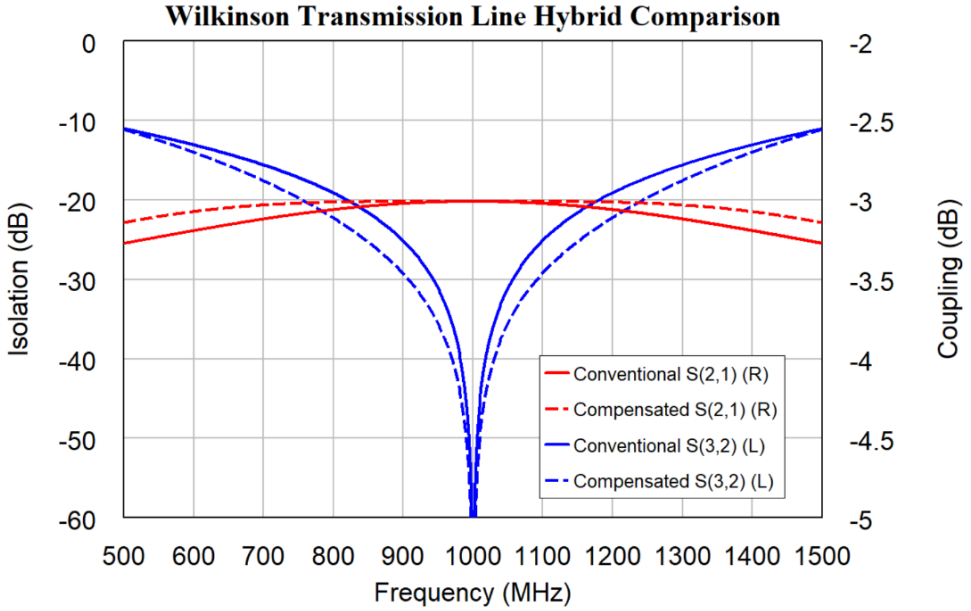



Figure 4.13. Comparison of conventional and compensated Wilkinson hybrid performance.

## Unequal Split Wilkinson Hybrid

Sometimes an unequal power split is required. If a power ratio of P:1 is required, then the impedances seen at the source end of each of the transmission lines must also have a ratio of P:1. Since the total impedance must be $Z_0 = 50\ \Omega$, then the impedances are:

$$\frac{1}{Z_0} = \frac{1}{Z_1} + \frac{1}{Z_2} = \frac{1}{Z_1} + \frac{1}{P * Z_1} = \frac{P+1}{P * Z_1} \qquad \text{Eqn. 4.12}$$

The line impedances are thus:

$$Z_1 = \sqrt{\frac{P+1}{P}} Z_0 \qquad \text{Eqn. 4.13}$$

$$Z_2 = \sqrt{P+1} * Z_0 \qquad \text{Eqn. 4.14}$$

where $Z_1$ and $Z_2$ are the transmission line impedances of the hybrid. As a check when an equal split is used, P=1, so that $Z_1 = Z_2 = \sqrt{2}Z_0$.

Thus for a 10:1 power split in a 50 Ω system, the transmission line impedances are: $Z_1 = \sqrt{1.1}\ Z_0$ and $Z_2 = \sqrt{11}\ Z_0$. For a 50 Ω system, $Z_2$ = 165 Ω. For an RF circuit board substrate, RO4003, which is 0.818 mm thick, at 1 GHz a 50 Ω track is 1.855 mm wide and a 165 Ω track is 0.063 mm wide. As shown in chapter 11, the thinnest recommended track width for PBC manufacture is 0.2 mm. Using laser ablation 0.1 mm tracks are possible. The 165 Ω track is too thin to make accurately, even using laser ablation. In addition, the resistance due to the copper losses of the 165 Ω track is 29 times that of the 50 Ω track. The ability to manufacture and copper losses will thus limit the ratio of the power split. Lowering the impedances of the split lines by reducing the impedance at the junction point just like the compensated Wilkinson hybrid, will reduce the impedances of the transmission lines of the hybrid and may permit it to be constructed. Increasing the substrate thickness will also increase the track width and thus reduce losses as well as easing manufacturing difficulties.

Large differences in power ratios are typically required for sampling signals such as transmitter outputs. Edge coupled lines as described in example 4.2 are very suitable for this, so that the limitation on power ratios for Wilkinson hybrids is not a serious limitation.

## Wideband Wilkinson Hybrid

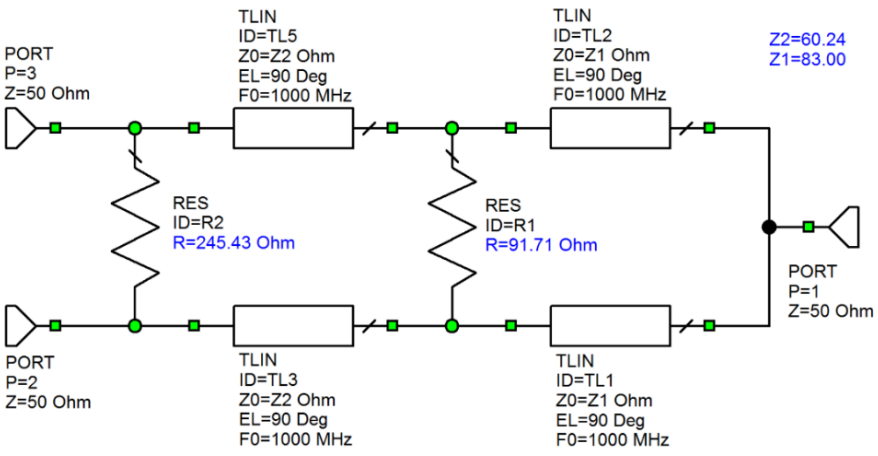



Figure 4.14. Two-stage wideband Wilkinson hybrid.

The bandwidth of the Wilkinson hybrid can be increased by cascading two resistor linked transmission lines as shown in figure 4.14. The characteristic impedances of the lines and the resistor values can be optimised to give the required isolation over the specified bandwidth. There is a compromise between bandwidth and isolation. A wide bandwidth will result in a low isolation and a smaller bandwidth can result in a better isolation. For the hybrid shown in figure 4.14, the isolation was specified as -30 dB. The required values for Z1, Z2, R1 and R2 are then determined by optimisation using AWR DE.

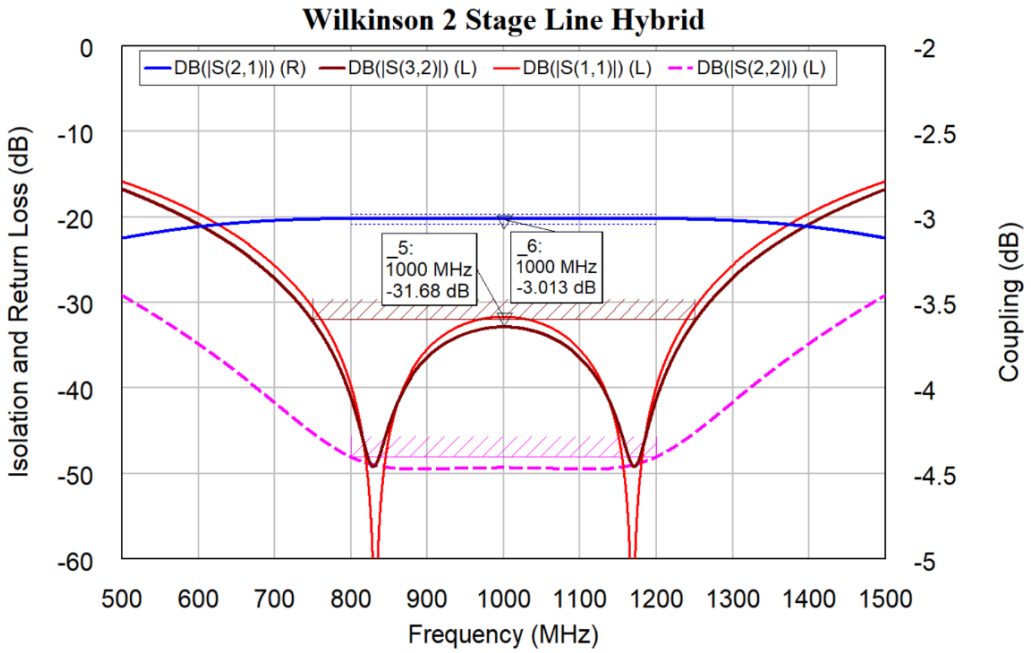



Figure 4.15. Performance of a 2-stage wideband Wilkinson hybrid.

From figure 4.15, it can be seen that a wide bandwidth hybrid results. The impedance for the first section has increased to 83 Ω compared with 70.71 Ω for the conventional hybrid. The higher impedance will result in an increased insertion loss of the hybrid, due to thinner PCB tracks being required. A compensated hybrid configuration will reduce the impedance values and thus reduce the insertion loss of the hybrid as well as having a wider bandwidth still.

## *Example 4.2: 90 MHz to 270 MHz Wilkinson Hybrid*

This process can be extended to produce Wilkinson hybrids with good isolation and return loss on all ports over a 2:1 or even 3:1 frequency range. As an example, a Wilkinson hybrid covering the frequency range from 90 MHz to 270 MHz is to be designed. The target specification is a better than 30 dB isolation over the 90 to 270 MHz frequency range and better than 30 dB return loss for all the ports from 95 MHz to 260 MHz.

The design process requires two steps:
1) The circuit is designed and optimised, using ideal transmission lines for the hybrid.
2) Once the specifications are achieved for this ideal circuit, then the ideal transmission lines are replaced with Microstrip lines, with the same electrical line length and impedance.

Figure 4.16 shows the schematic for a suitable design. The variables for the centre frequency F0, the transmission line impedances Z1 to Z4 and the isolation resistors R1 to R3 are all enabled for optimisation. The initial values for Z1 and Z2 are chosen to be 42 Ω

and 60 Ω respectively, similar to the values of the compensated Wilkinson hybrid shown in figure 4.12. The initial value for Z4 is chosen to be 50 Ω as that should be a close match to the impedance at port 1 and Z3 is chosen to be 55 Ω, being in between the values of Z2 and Z4. The initial value of R1 is chosen to be 100 Ω, being the value of the isolating resistor in figure 4.12. R2 is chosen to be 200 Ω, similar to R2 in figure 4.14 and R3 is chosen as 400 Ω. The initial value of F0 is chosen to be 156 MHz, the geometric mean of 90 MHz and 270 MHz. The optimisation goals are set up to match the specifications. To achieve a better return loss and isolation, the goals are for $S_{11}$ < -32 dB, $S_{22}$ < -32 dB and $S_{32}$ < -33 dB. Setting the circuit to optimise using the Simplex optimiser then yields the circuit values shown in figure 4.16. This circuit achieves the specifications as shown in figure 4.17. Notice that no optimisation goals are set for the through coupling, $S_{21}$, since if the circuit is matched then the coupling loss will be as small as possible.

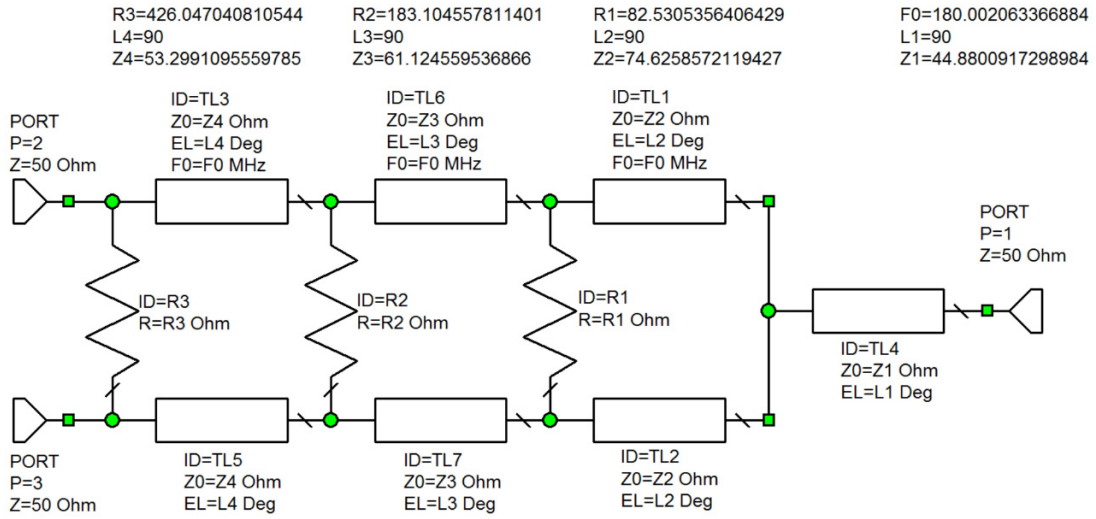



Figure 4.16. Circuit for a 90 MHz to 270 MHz Wilkinson hybrid.

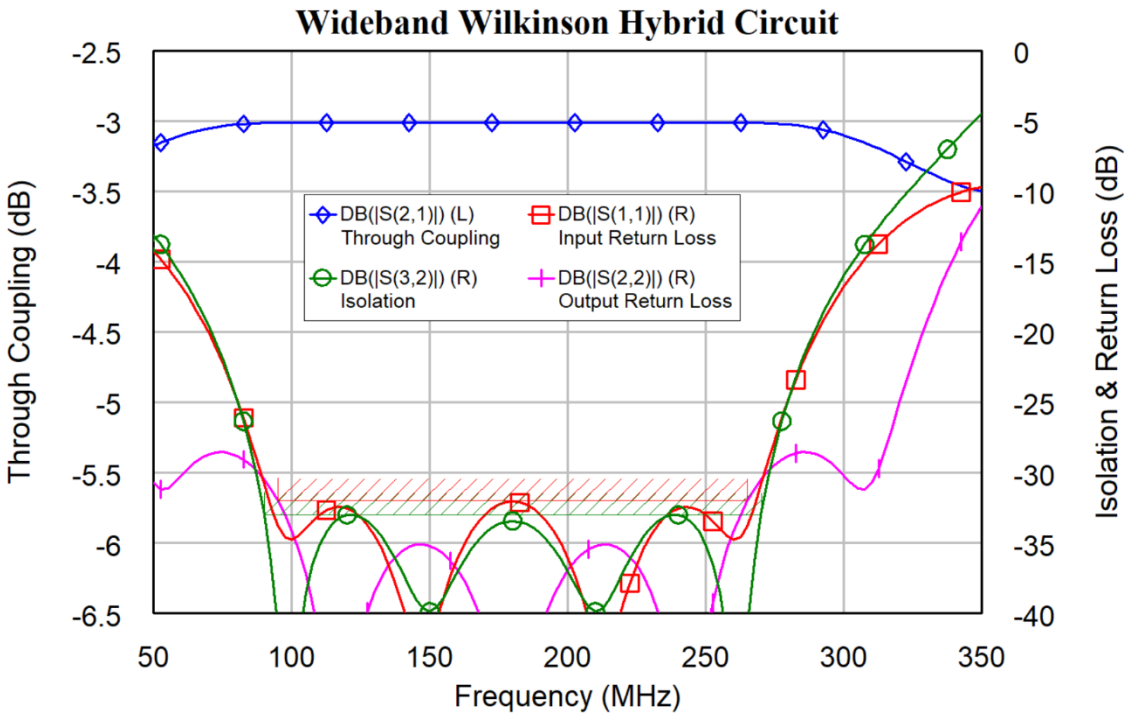



Figure 4.17. Simulated performance of the hybrid of figure 4.16.

Figure 4.16 can now be used as the basis for a PCB layout. Often it is necessary to bend the Microstrip lines to fit the circuit in the available space, as shown in figure 4.17. Each of the transmission lines are a quarter wavelength long. If in figure 4.16, lines TL2 and TL5 are disabled, resistors R1 and R3 are disabled and resistor R2 is made a short circuit (0 Ω), then the circuit becomes a transmission line of various impedances connecting port 1 to port 2 with an open circuited quarter wavelength stub consisting of TL7 connected to it. This line will thus present itself as a short circuit at R2 at the centre frequency. A similar circuit is shown on the right of figure 4.30. The transfer function from ports 1 to 2 will thus have a notch exactly at the centre frequency of the hybrid, where TL7 is a quarter wavelength. The length of the folded sections making up TL7 in figure 4.16, can be adjusted to be exactly a quarter wavelength by changing the lengths of the sections to ensure that the notch in the transfer function from ports 1 to 2 occurs exactly at the centre frequency of the hybrid. This process is repeated for the other three different transmission lines in the hybrid. Variables are used to ensure that the folded transmission lines corresponding to the sets of lines TL1 and TL2, lines TL3 and TL5 and lines TL6 and TL7 are exactly the same length and impedances.

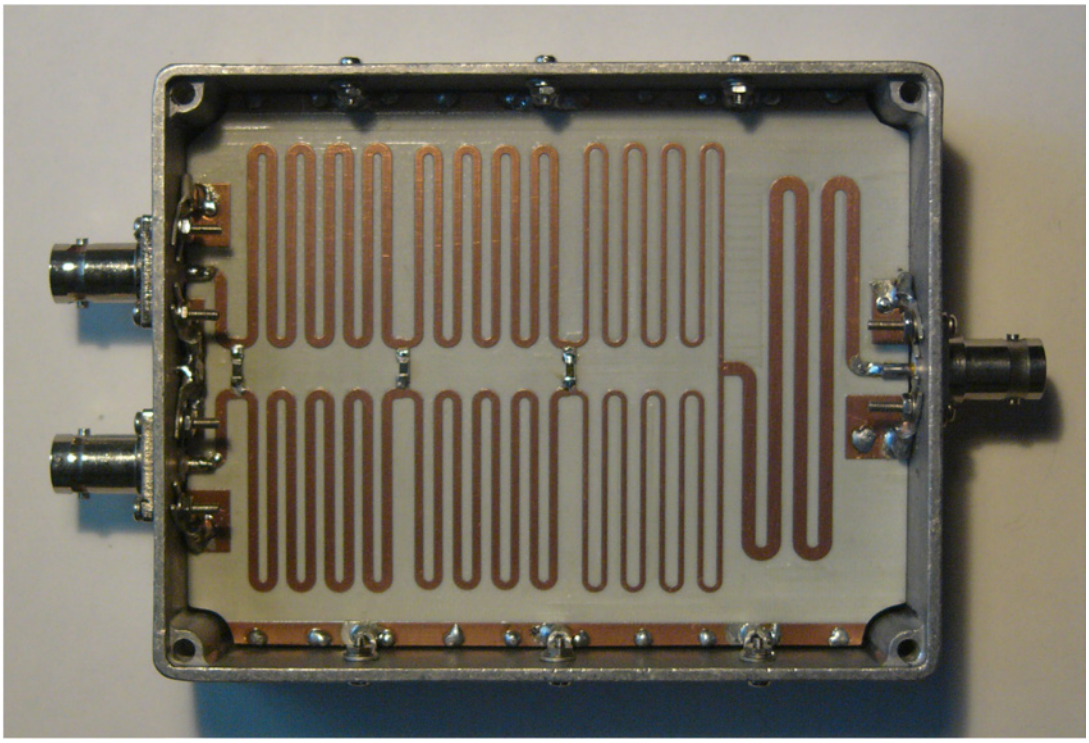


Figure 4.18. Hardware for 90 MHz to 270 MHz Wilkinson Transmission-line hybrid.

Finally, the line lengths and widths are optimised to provide the final layout and meet the required specifications. Figure 4.18 shows the hardware for this layout and figure 4.19 shows the simulated frequency response for the hybrid. The details of the PCB layout are included in the CADENCE AWR DE project file for figures 4.18 and 4.19. The measured performance is shown in figure 4.20. This agrees closely with the calculated values. The hardware has an isolation that is better than 26.9 dB over the entire 90 to 270 MHz frequency range and the return loss is better than 22.0 dB. Figures 4.9 and 4.11 show that just a 50 μm change in track width results in significant changes in the return loss. Manufacturing tolerances on the dielectric constant of the laminate and track width imperfections as part of the PCB milling process resulted in the return loss and isolation not being as good as simulated. The insertion loss of the coupled path is also 0.24 dB

more than obtained by the simulation. Part of this loss could be due to the thin protective coating used to prevent the copper tracks from oxidising. This hybrid has a very satisfactory performance over a 3:1 frequency range and could not have been realised without the computer simulation and optimisation described in this book.

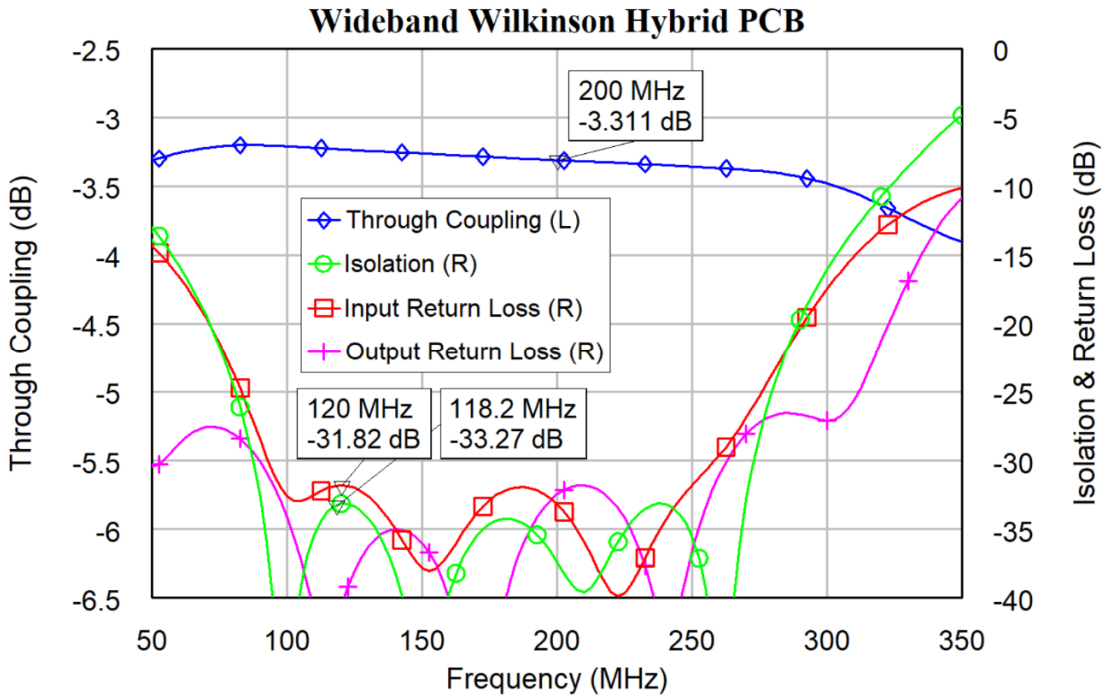



Figure 4.19. Simulated performance of the hybrid of figure 4.18.

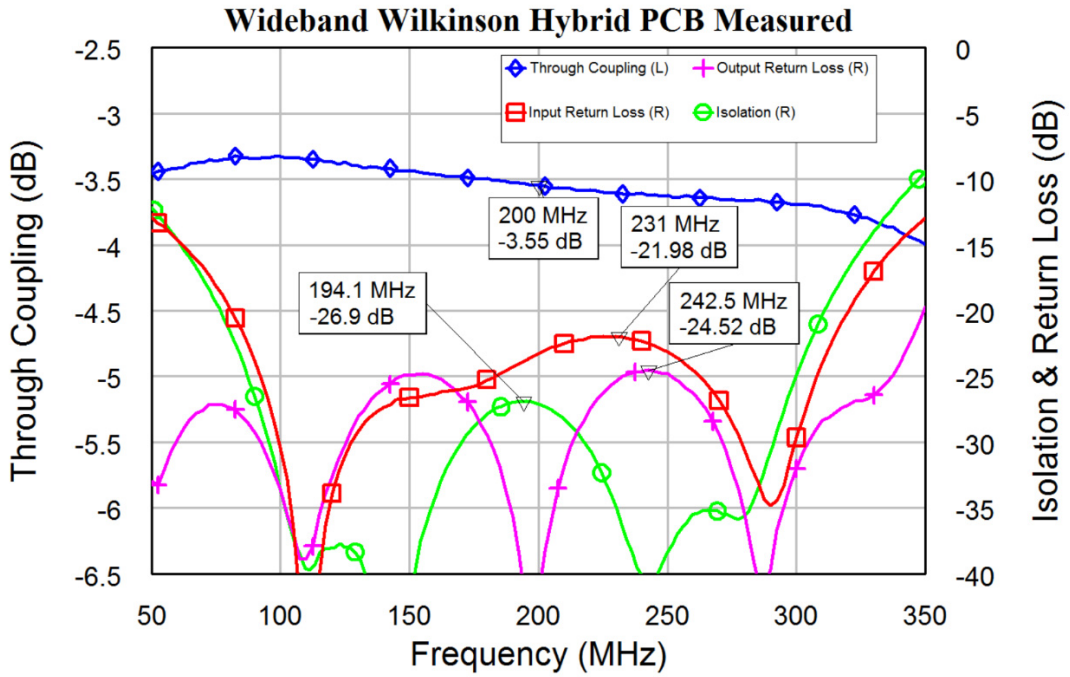



Figure 4.20. Measured performance of the hybrid of figure 4.18.

The losses in the circuit due to the resistance of the tracks, dielectric losses of the substrate and radiation losses of the Microstrip lines, vary with frequency, as can be seen in figures 4.19 and 4.20. Since the difference is only 0.25 dB over a 3:1 frequency range, this is

often ignored in practice. Due to this frequency dependence of the losses, it is better to optimise for input reflection coefficient rather than transfer function since a low input reflection coefficient ensures all the energy passes through the hybrid, thus giving the highest $S_{21}$ possible. Optimising for a value of $S_{21}$ may result in a poor return loss at lower frequencies.

## Quarter Wave Hybrid or 1.5 λ Rat-Race Hybrid

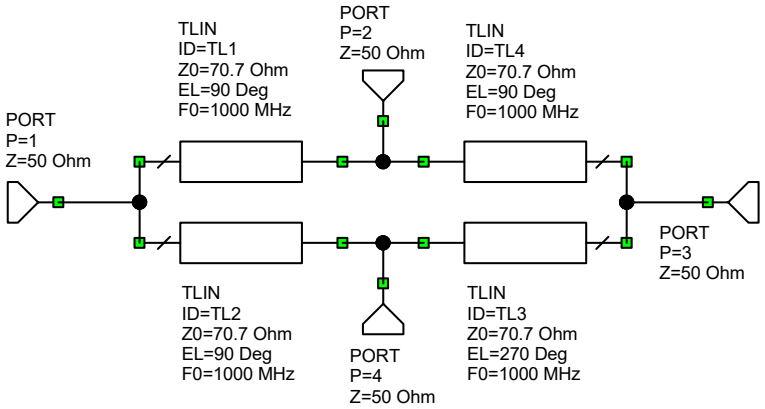



Figure 4.21. 1.5 λ Rat-Race hybrid.

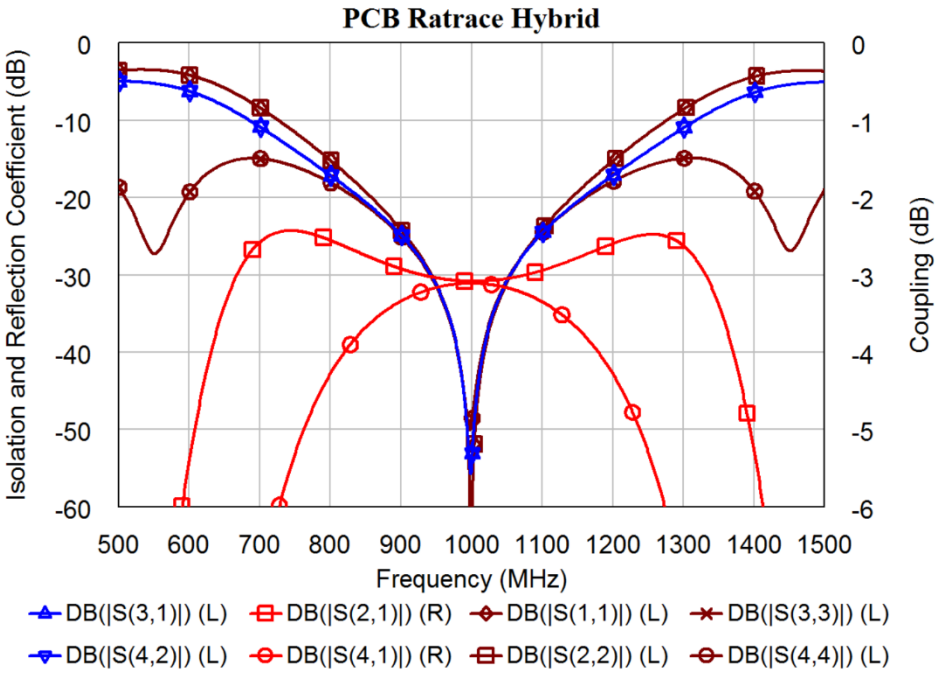



Figure 4.22. Performance of 1.5 λ Rat-Race hybrid.

The circuit diagram of this hybrid is shown in figure 4.21 and its performance is shown in figure 4.22. For the analysis, consider the function of the hybrid. If an input is applied to port 1, then no signal should appear at port 3, resulting at 0 Volt at port 3. Under these conditions, the circuit is similar to the Wilkinson hybrid of figures 4.6 and 4.7 and in figure 4.21, no current flows into TL4 of at port 2 and into TL3 at port 4. The transmission

line TL3 can thus be disconnected at port 4 and line TL4 can be disconnected at port 2, without any effect, as shown in figure 4.23.

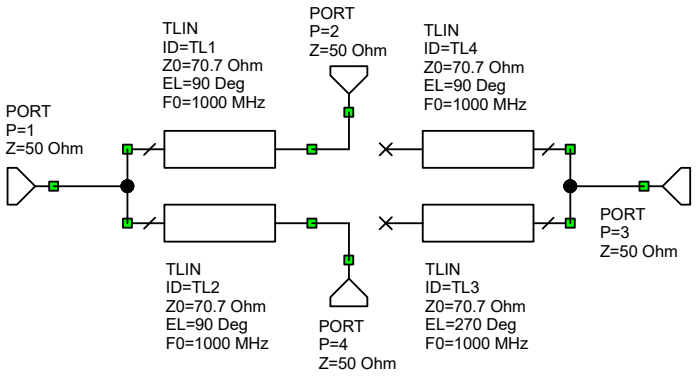



Figure 4.23. 1.5 λ Rat-Race hybrid for analysis.

The resulting circuit is thus just like a Wilkinson hybrid, without the terminating resistor. The line impedances should thus be 70.71 Ω, just like the Wilkinson hybrid. The same analysis can be repeated by looking into each port in turn. A three-quarter wavelength transmission line has exactly the same impedance transformation ratio as a quarter-wavelength line. All the line impedances will thus be $\sqrt{2}Z_0$.

The 1.5 λ Rat-Race hybrid has an advantage over the Wilkinson hybrid that for a 50 Ω system, a 50 Ω load resistor to ground is required for the termination, rather than a 100 Ω load resistor between two active inputs. High power 50 Ω loads are readily available from several manufacturers [6, 7]. 100 Ω floating high power loads are however more difficult to obtain. For TV transmitters, the hybrid is normally made using high power coaxial cables, to combine the outputs from two transmitters into one antenna. If one transmitter fails, the radiated output drops 6 dB and the resistive load then dissipates the same power as is radiated, without any switching being required. If both transmitters are working, no power is dissipated in the resistive load and the sum of the transmitter power is radiated.

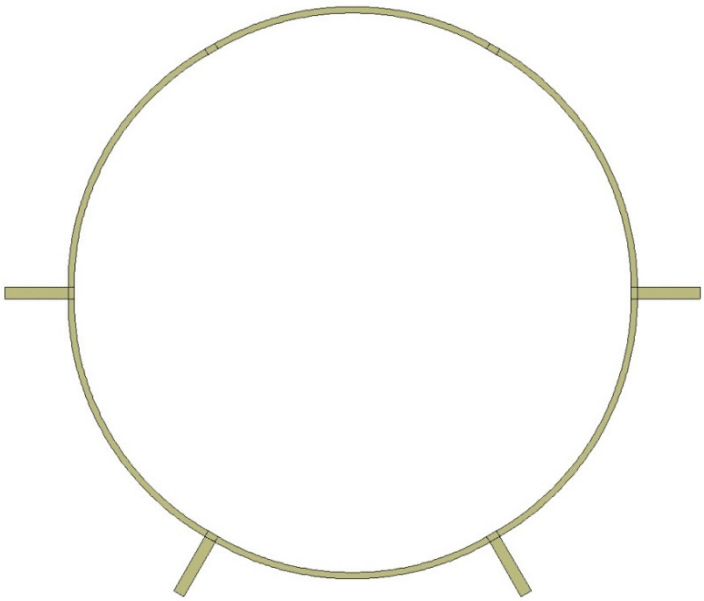


Figure 4.24. PCB layout of a 1.5 λ Rat-race hybrid.

For the 1.5 λ Rat-Race hybrid, a three-quarter wavelength and three one-quarter wavelength transmission lines are required. At microwave frequencies, it is very convenient to arrange these transmission lines in the shape of a circle, as shown in figure 4.24, with the three quarter wavelength line on top and the three quarter wavelength lines at the bottom. One-quarter wavelength will thus occupy a 60-degree arc. The layout can then be made conveniently using six 60-degree arcs, 4 T-junctions and 2 short transmission lines with the same length as the T-junctions are wide, as spacers.

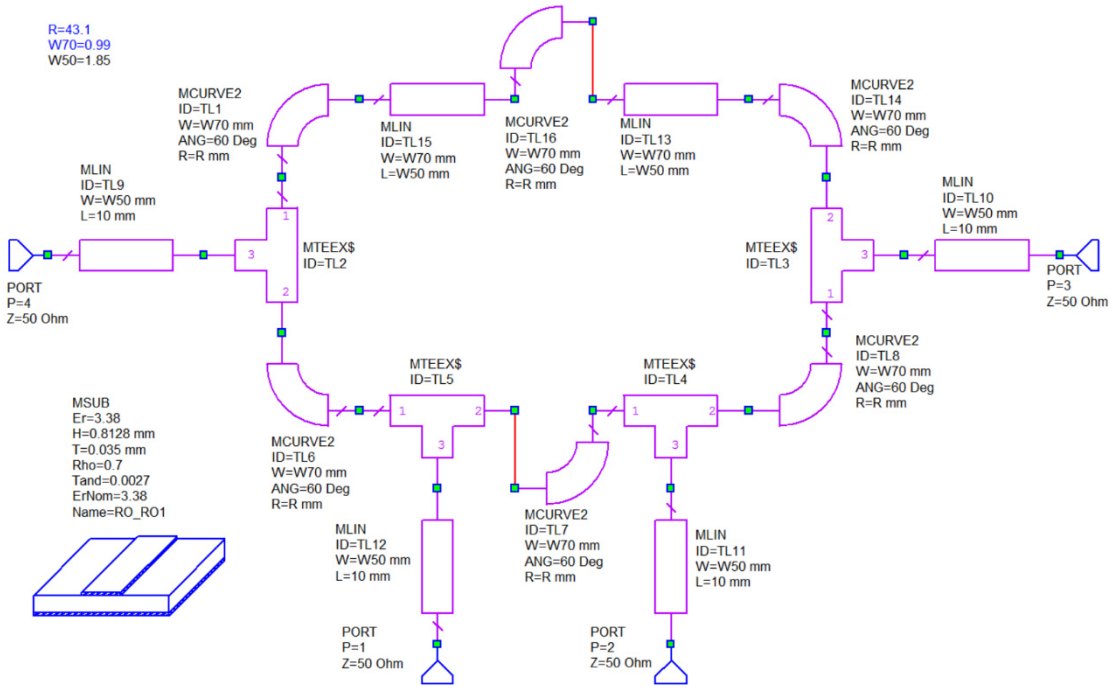



Figure 4.25. 1.5 λ Rat-Race hybrid circuit for PCB layout.

Figure 4.25 shows the circuit schematic, which results in the PCB layout of figure 4.24. The radii of the arcs can be tuned, to obtain the correct centre frequency, without causing any track connection errors. In figure 4.25, MCURVE2 tracks are used to include EM mode matching in the simulation. Intelligent EM based T-junctions, MTEEX$, are used to ensure that the simulation is as accurate as possible, without doing a full EM simulation using AXIEM.

The simulation of the PCB circuit of figures 4.24 and 4.25 shows a near identical performance to the one shown in figure 4.22. The main difference is a 0.07 dB increase in insertion loss of the coupled ports due to the resistive losses in the Microstrip tracks.

Lower line impedances can be obtained with a compensated 1.5 λ Rat-race hybrid, by having 44.5 Ω, quarter wavelength transmission lines at the 4 inputs to the hybrid, for a 50 Ω system. The line impedances of the hybrid then become 56.119 Ω instead of 70.71 Ω. Computer simulation shows that this does not increase the bandwidth of the isolation and it does not reduce the losses for a typical PCB layout, so that compensated 1.5 λ Rat-race hybrids are not used in practice.

## Branchline Coupler

The Branchline coupler consists of 4 transmission lines in a ring, as shown in figures 4.26 and 4.27. If an input is applied at the top left port 1, then part of the output appears at the

coupled port, the bottom right port 3. The remainder appears at the main output port 2 and no power appears at the isolated port 4. For a 3 dB coupler in a 50 Ω system, lines TL1 and TL4 have an impedance of 50/√2 Ω and lines TL2 and TL3 have an impedance of 50 Ω. A Microstrip PCB layout is shown in figure 4.27. The resistive losses of a Branchline coupler are less than that of a 1.5λ Rat-race hybrid.

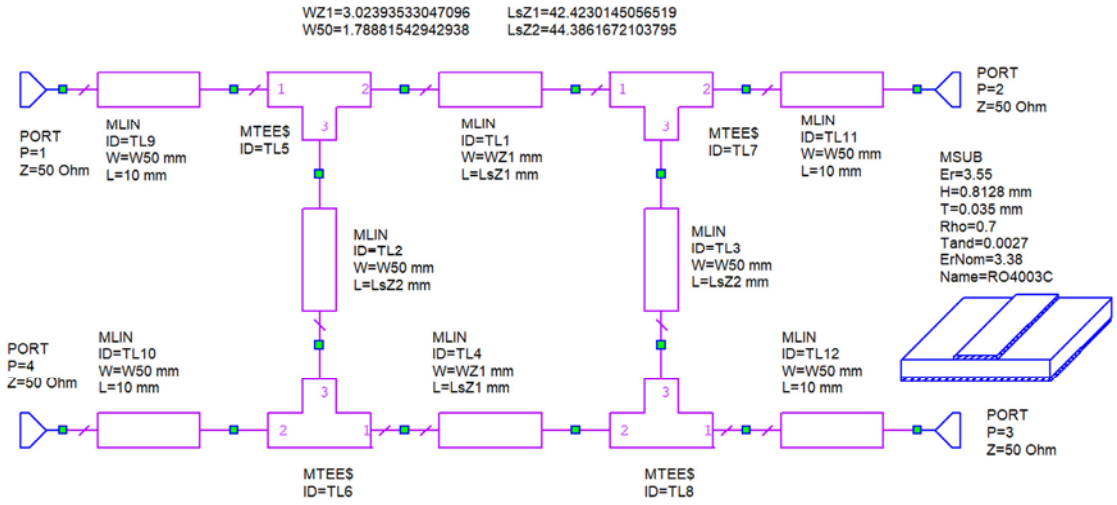



Figure 4.26. Branchline coupler circuit.

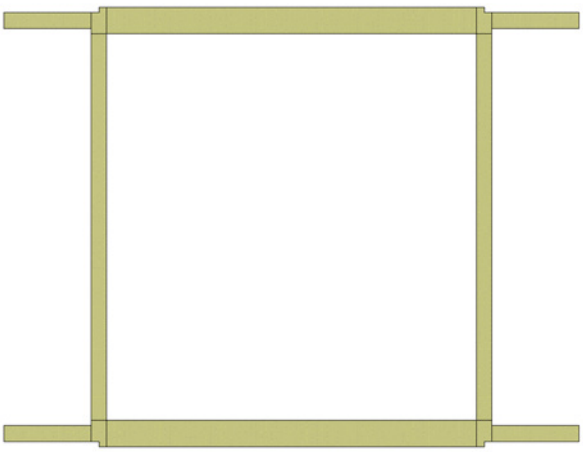


Figure 4.27. Branchline coupler PCB layout.

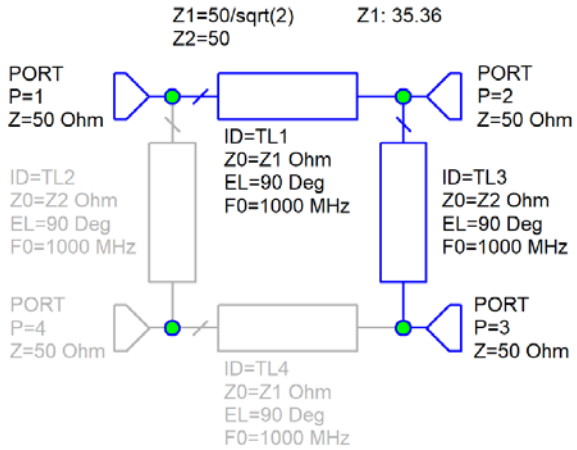



Figure 4.28. Branchline Coupler analysis.

For the analysis, consider figures 4.26 and 4.28. When an input is applied at port 1, port 4 is isolated and has no voltage at that port. Since lines TL3 and TL4 are quarter wavelength long, no current flows in line TL4 at port 3, so that TL4 can be disconnected from the circuit without any effect. Similarly, no current flows in TL3 at port 1, so that TL3 can also be disconnected, resulting in figure 4.28.

If a normalised input power of ***1*** is applied at port 1 and we want an output power of **P** to occur at port 3, then a power of ***(1-P)*** will be available at port 2.

At port 2, the load impedance is $Z_0$, which typically is 50 Ω. If the voltage at port 2 is V2, then the power split at port 2 is given by:

$$V_2^2 = PZ_P = (1-P)Z_0 \qquad \text{so that:} \qquad Z_P = \frac{(1-P)Z_0}{P} \qquad \text{Eqn. 4.15}$$

Where $Z_P$ is the impedance of port 3 transformed through TL3 and seen at port 2 looking into TL1. Since this is obtained by impedance transformation through the quarter wave long transmission line TL1, the impedance required for TL1 is given by:

$$Z_2 = \sqrt{Z_p Z_0} = Z_0\sqrt{\frac{(1-P)}{P}} \qquad \text{Eqn. 4.16}$$

The impedance $Z_e$ seen at the port 2 end of TL1 is $Z_0$ in parallel with $Z_P$ and is thus:

$$\frac{1}{Z_e} = \frac{1}{Z_p} + \frac{1}{Z_0} = \frac{P}{(1-P)Z_0} + \frac{1}{Z_0} = \frac{1}{(1-P)Z_0} \qquad \text{Eqn. 4.17}$$

The line impedance $Z_1$ to transform this to $Z_0$ is thus:

$$Z_1 = Z_0\sqrt{1-P} \qquad \text{Eqn. 4.18}$$

In many cases an equal power split is required, so that P=0.5. Typically $Z_0$ = 50 Ω. Substituting this in equations 4.16 and 4.18 results in $Z_2 = Z_0$ = 50 Ω and $Z_1 = Z_0/\sqrt{2}$ = 35.36 Ω. For a 10 dB coupler P = 0.1, so that $Z_2 = 3Z_0$ = 150 Ω and $Z_1 = 0.949 * Z_0$ = 47.43 Ω. These can just be made using Microstrip circuits, however 150 Ω results in a very thin track and any lower amount of coupling is extremely difficult to make.

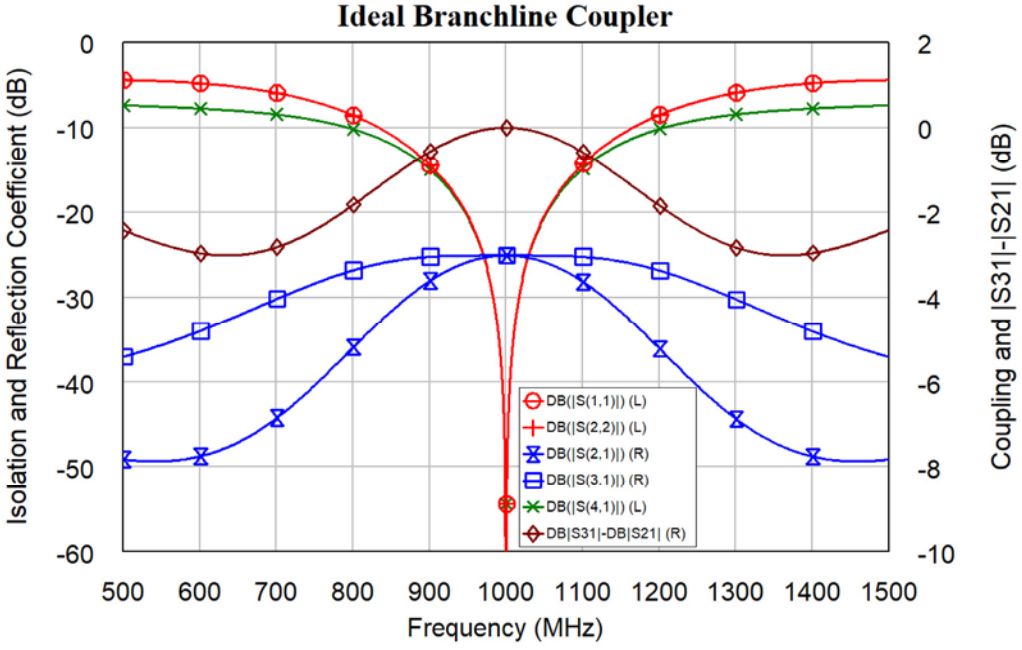



Figure 4.29. Ideal Branchline coupler amplitude response.

Figure 4.29 shows the performance of the Branchline coupler. This coupler is a convenient structure with low impedance values (50 Ω and 35.36 Ω) thus allowing low loss hybrids to be made using Microstrip-line circuits. The output at the coupled port has a 90 ° phase shift compared with the output at the direct port. That is useful for applications such as IQ up or down conversion.

To realise the design as a printed circuit board, the required track widths and lengths need to be calculated. The Roger's RO4003 substrate [5] that was used for the circuits in figures 4.9 and 4.10 is also used in this example. The parameters can be obtained by using the *Libraries* ⇒ *AWR Web Site* ⇒ *Rogers* ⇒ *RO* ⇒ *RO4003* and select *32 mil, 1 oz.* and place that as a component in a circuit. Remember to set Er = 3.55 and ErNom = 3.38 to match Er with the substrate data sheet [5] as described earlier.

To determine the length and width required, TX line from the Tools menu in CADENCE AWR DE can be used or measurements on some simple test circuits can be made. Figure 4.25 shows the resulting test circuit. W50, the width of a 50 Ω track and W35, the width of a 35.36 Ω track are made as variables, so that those values can be used in the rest of the design. The line between port 1 and 2 is very long. W50 is determined by observing $S_{11}$ and tuning S50 to be less than -60 dB over the required frequency band. Similarly, W35 is obtained by tuning it and minimising $S_{33}$. To determine the length of the quarter wavelength long lines, the circuit between ports 5 and 6 is used. The circuit uses a 50 Ω line between ports 5 and 6 and a 35.36 Ω line as a stub. Thus, TL4 and TL6 in figure 4.30 correspond to TL1 and TL2 in figure 4.28 respectively. (For a 3 dB coupler Zy=50 Ω and Zx=35.36 Ω). To obtain accurate results, elements incorporating EM models, such as MTEEX and MLEFX are used in this circuit. The MLEFX element, with the length of half a 50 Ω track-width is used to place the end of the quarter wavelength stub on the middle of the 50 Ω track that is to join as shown in figure 4.30, to produce the complete coupler shown in figures 4.32 and 4.33. The length of the stub (L2) is tuned to place the notch at 1 GHz. A similar circuit is made to determine the required length of the 50 Ω quarter-wavelength lines.

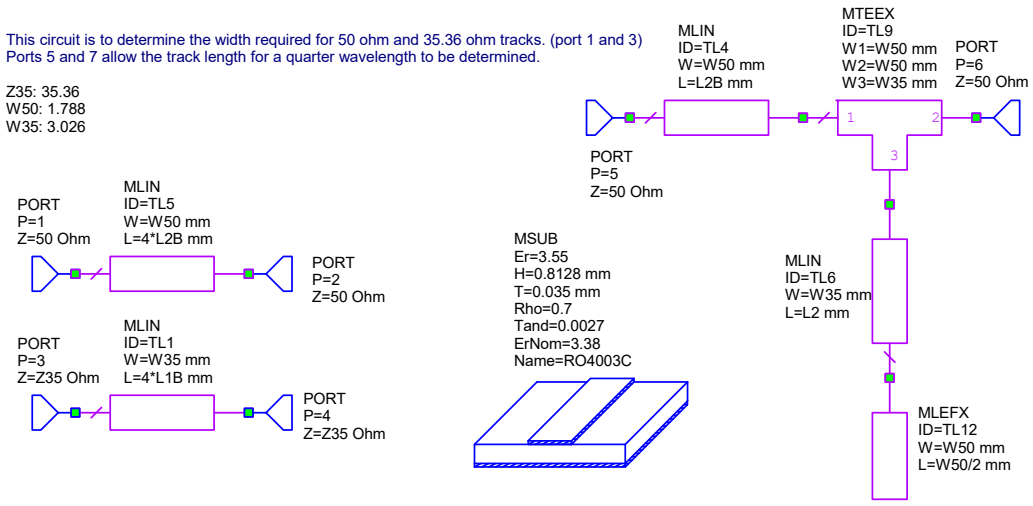



Figure 4.30. Microstrip test circuits for determining length and width of lines.

When the line lengths obtained from figure 4.30 are used in the circuit of figure 4.26, the centre frequency is slightly offset. Fine-tuning is achieved by tuning or optimising the

line lengths LsZ1 and LsZ2, and if needed the line widths WZ1 and W50 to place the isolation notch exactly at 1 GHz and ensure that the attenuation of S21 is the same as that of S31 at 1 GHz, as shown in figure 4.31. Comparing figure 4.29 and 4.31, shows that the frequency dependent losses of the Microstrip lines, result in the isolation and reflection coefficient (S11, S22 and S31) at 1 GHz being slightly worse for the Microstrip circuit than the ideal circuit.

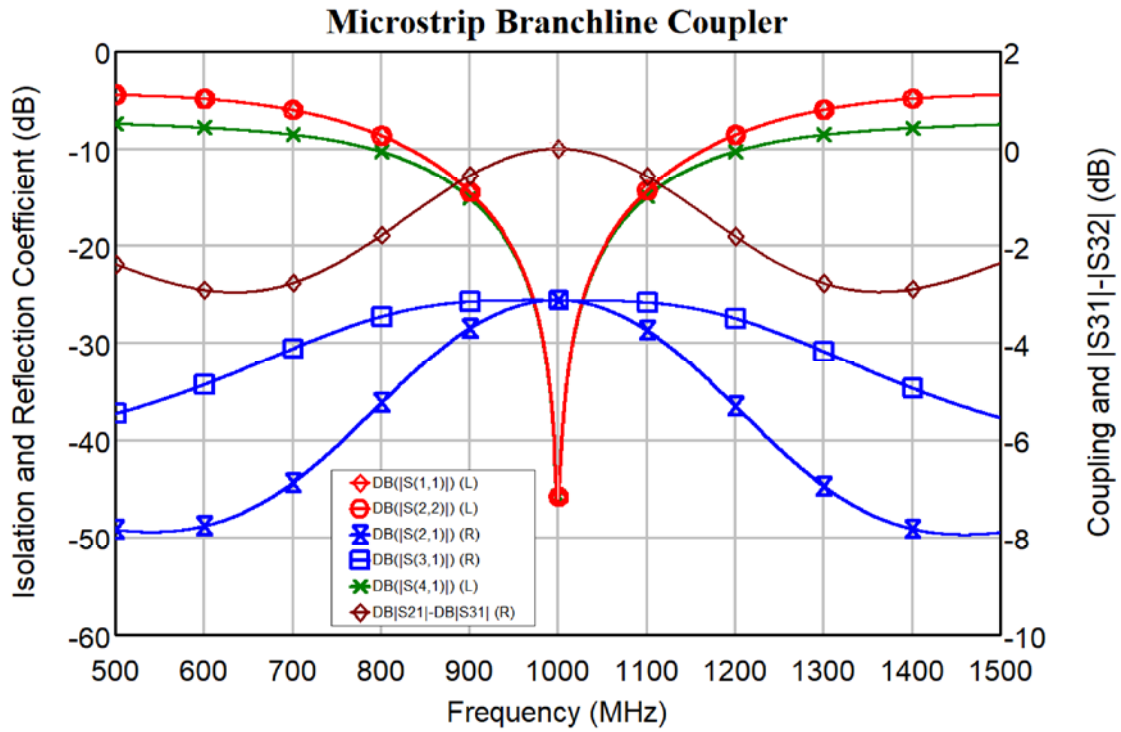



Figure 4.31. Microstrip Branchline coupler amplitude response.

In many cases, the transmission lines are folded in order to reduce the printed circuit board area, as shown in figures 4.32 and 4.33. Like figure 4.9, a M2CLIN coupled line is used, to include the EM coupling between the folded lines. The length of the coupled lines is tuned to place the centre frequency at 1 GHz.

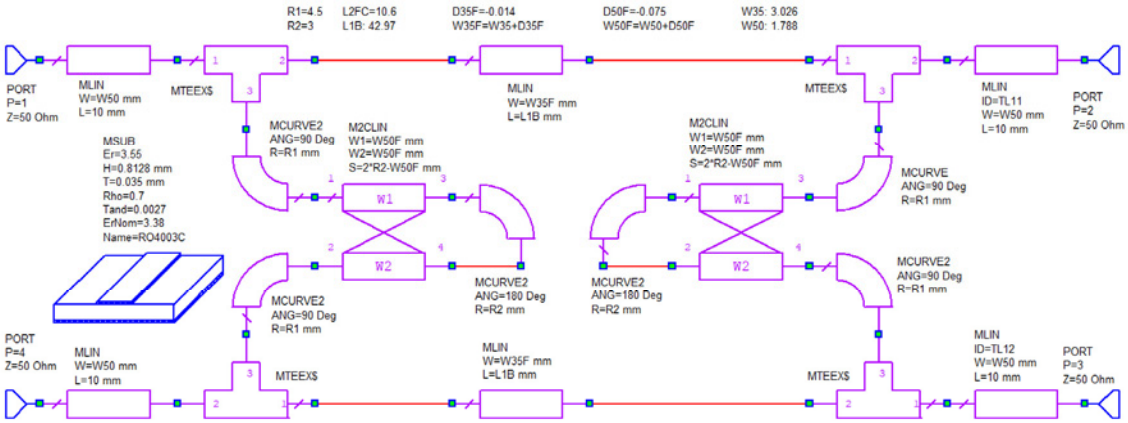



Figure 4.32. Folded Microstrip Branchline coupler schematic.

The power split between port 2 and port 3, is determined by the impedance of this folded line. Ideally, it should be a 50 Ω transmission-line. For an input at port 1, an equal power

split at TL6 results in a slightly smaller output at port 3, due to resistive losses in TL3, TL14, TL18, TL20 and TL7. A slight fine-tuning is included by making the line-width of W50F = W50 +D50F, where D50F is a small correction factor. D50F is then tuned to change the power split to allow for these losses and make the outputs at ports 2 and 3 identical at the centre frequency.

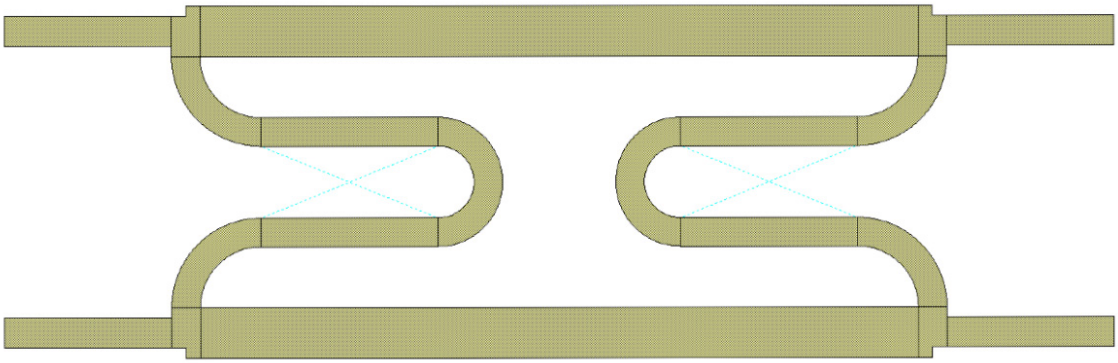


Figure 4.33. Folded Microstrip Branchline coupler PCB layout.

This changes power split causes a change in the impedance seen at terminal 1 of TL6 and will require a slight change in the impedance transformation produced by TL1 and TL4, to present a 50 Ω impedance ($S_{11}$) at port 1. This is achieved by making W35F = W35 + D35F, where D35F is a small correction factor. D35F is tuned to make $S_{11}$ as small as possible at the centre frequency.

Figure 4.34 shows the frequency response of the resulting folded Branchline coupler. There is virtually no difference between figure 4.31 and 4.34. However, the circuit with the bent lines occupies a much smaller area. Constructing the hybrid of figure 4.33 results in a measured performance, that is very close to the calculated performance shown in figure 4.34.

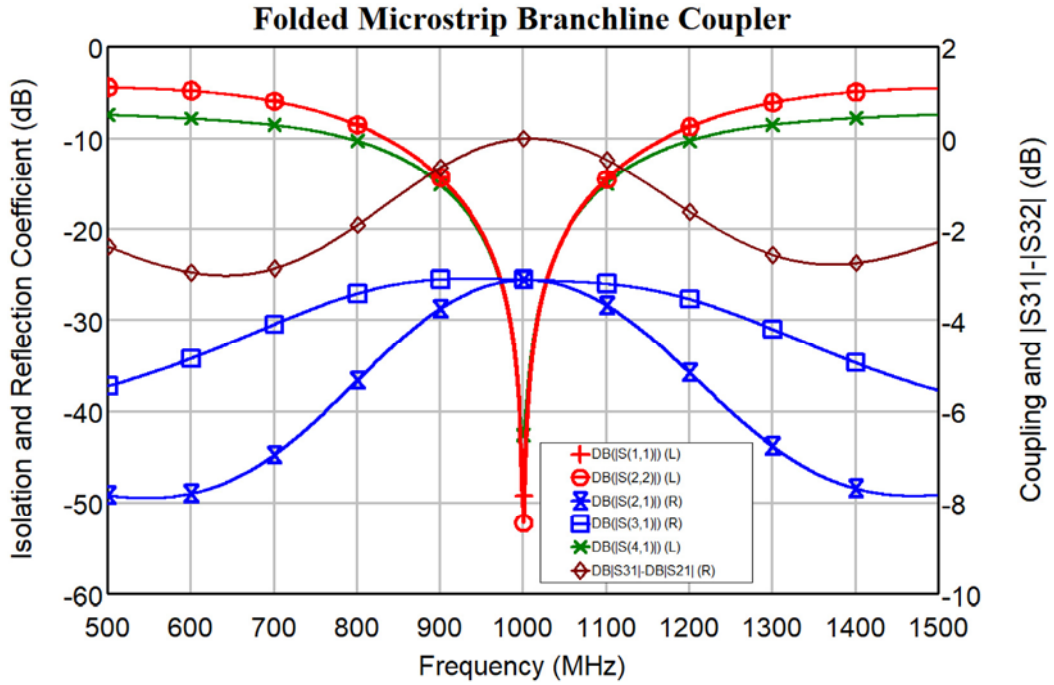



Figure 4.34. Folded Microstrip Branchline coupler amplitude response.

It is possible to produce a wider bandwidth Branchline coupler, by having two loops together as shown in figures 4.35 and 4.36. For a 3 dB double loop Branchline coupler the characteristic impedances of the lines are given by equations 4.19 and 4.20 [8]:

$$Z_3 = Z_0\left(1+\sqrt{2}\right) \qquad \text{Eqn. 4.19}$$

$$Z_2 = \sqrt{2}\, Z_1^2/Z_0 \qquad \text{Eqn. 4.20}$$

Using these equations and optimising the double loop Branchline coupler for the lowest phase difference from 90 degrees results in $Z_1 = Z_3 = 50/\sqrt{2} = 35.35\ \Omega$. The resulting circuit and its layout for a RO4003 RF PCB substrate is shown in figures 4.35 and 4.36.

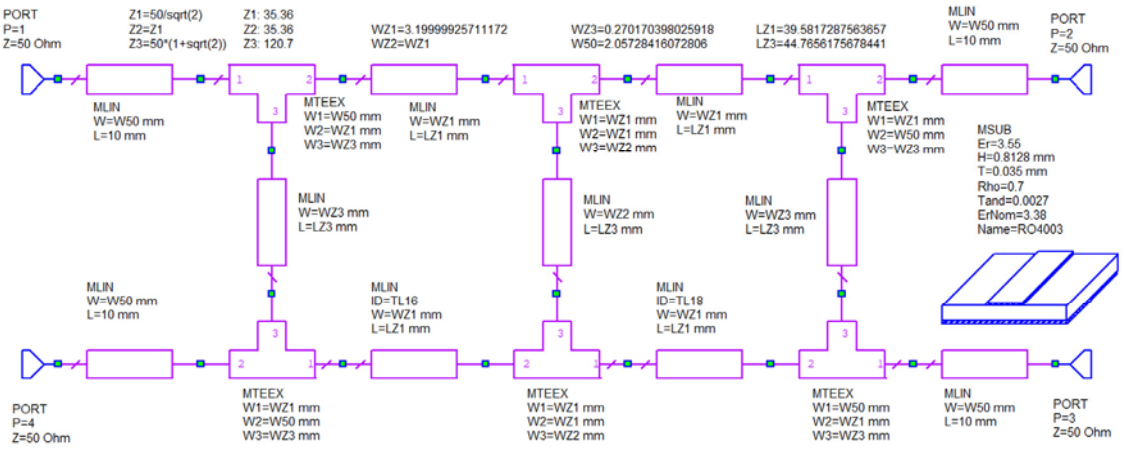



Figure 4.35. Double Branchline coupler schematic.

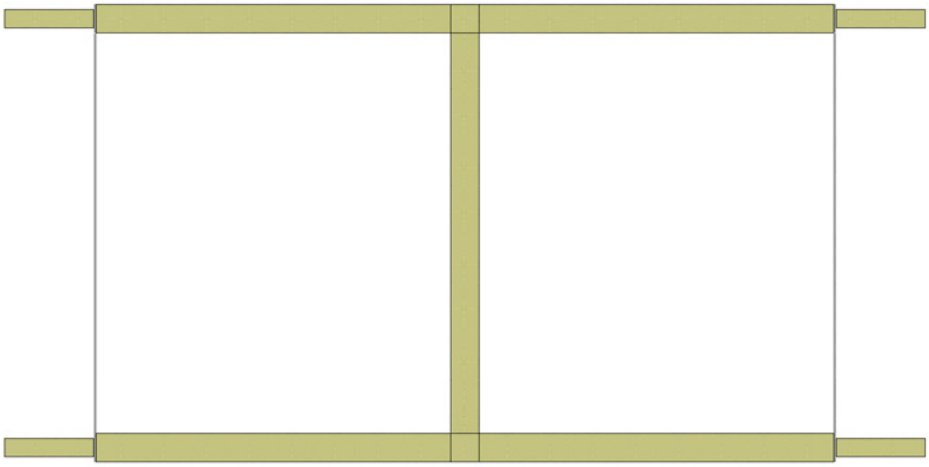


Figure 4.36. Double loop Branchline coupler PCB layout.

Using TXLine, for a RO4003 RF PCB substrate with a 0.8128 mm thickness at 1 GHz, the 120.7 Ω transmission lines require 0.27 mm wide tracks, which is close to the smallest track width that can be realised. The track width are so small that warnings are generated for the MTEEX sections connecting to them, as W3/W2 being too small for the model. The quarter wavelength long track for the Z1=Z3=35.36 Ω impedance is 41.98 mm long, while the corresponding length for the Z3=120.7 Ω track is 45.77 mm long. For straight lines, all three vertical lines should be the same length. This, together with the resistive losses in the 0.27mm wide tracks limits the isolation that can be obtained and the best line length must be obtained by optimisation. The resulting performance of the double loop Microstrip Branchline coupler is shown in figure 4.37.

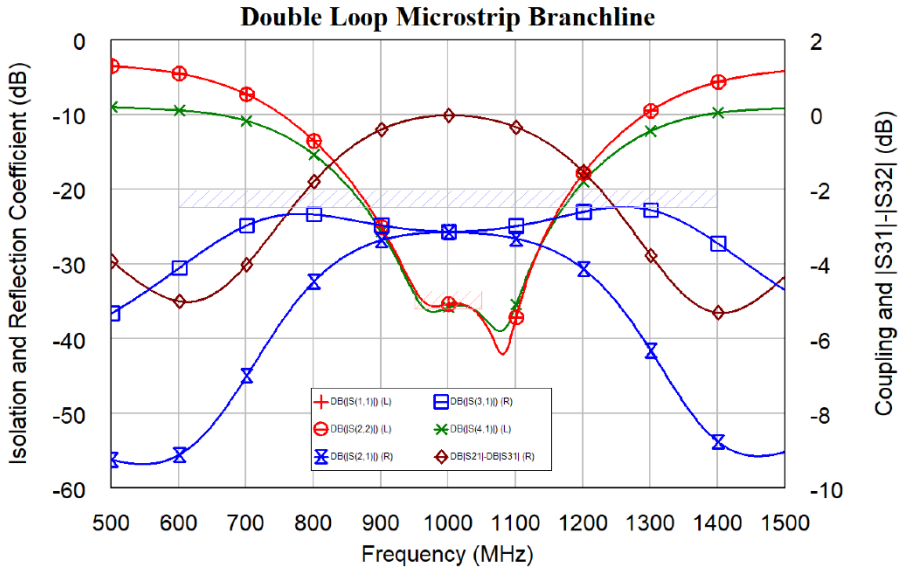



Figure 4.37. Double loop Branchline coupler amplitude response.

It is possible to increase the bandwidth further by using three loops for the coupler. The outer track impedances are then 187 Ω. For this RO4003 substrate, this corresponds to a 0.027 mm wide track, which is not possible to realise. Doubling the substrate thickness doubles the track width for the same impedance. Using thicker substrates may make some of these configurations realisable.

Figure 4.38 and 4.39 show a comparison between the single, double and triple loop Branchline coupler. The red curves are for the single line coupler, the blue curves are for the double line coupler and the green curves are for the triple line coupler. In figure 4.38, the most significant difference is the isolation (between port 1 and 4). The bandwidth over which a good isolation is obtained is increased significantly by using multiple loops. However, figure 4.37 shows that for a Microstrip realisation, increasing the number of loops results in a reduction of the depth of the isolation at the centre frequency of the hybrid.

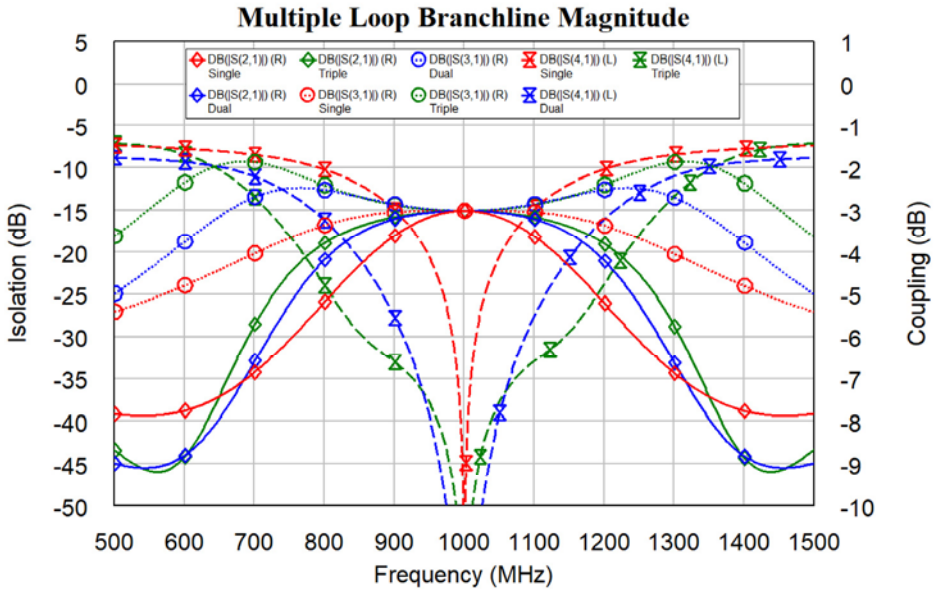



Figure 4.38. Ideal Multi-loop Quadrature hybrid amplitude response.

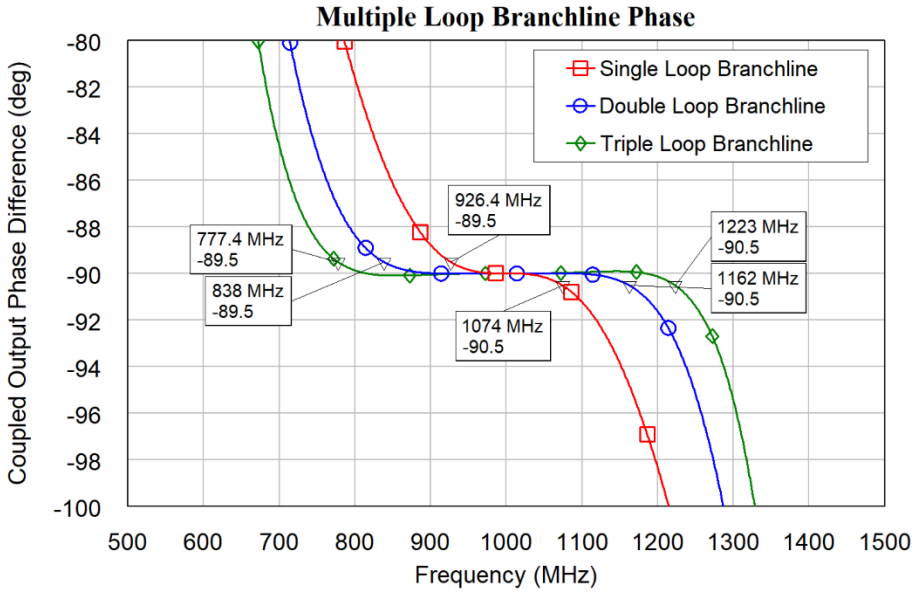



Figure 4.39. Ideal Multi-loop Quadrature hybrid phase response.

Figure 4.38 shows that for less than ±0.5° variation in phase from 90° the single loop Branchline coupler has a bandwidth of 14.76%, the double loop Branchline coupler has a bandwidth of 28.8% and the triple loop Branchline coupler has a bandwidth of 44.56%. For a 1dB difference in S21 and S31 amplitudes, the single loop Branchline coupler has a bandwidth of 27.2% MHz, the double loop Branchline coupler has a bandwidth of 31.8% and the triple loop Branchline coupler has a bandwidth of 34.8%. Branchline couplers can thus be used to provide the I and Q signals, required for image suppressing mixers, with good phase and amplitude accuracy over a >20% bandwidth.

## Backward Travelling Wave Hybrid

If two lines are in close proximity, then there is coupling between the lines. The amount of coupling depends on the spacing between the lines. Consider the two Microstrip coupled lines as shown in figures 4.41 and 4.42. The maximum coupling will occur when the coupled lines are a quarter wavelength long. The resulting coupling is related to the even and odd mode impedances by:

$$Z_{OE} = Z_0\sqrt{\frac{1+C}{1-C}} \qquad \text{Even mode impedance.} \qquad \text{Eqn. 4.21}$$

$$Z_{OO} = Z_0\sqrt{\frac{1-C}{1+C}} \qquad \text{Odd mode impedance.} \qquad \text{Eqn. 4.22}$$

Where C is the voltage at the coupled output relative to the input, $Z_{OO}$ is the odd mode impedance, where the two lines of the transmission line are of opposite polarity, so that most of the field is between the conductors. $Z_{OE}$ is the even mode impedance, where both the lines are at the same potential, so that most of the field is between the conductors and the ground-plane.

### *Edge-Coupled Lines*

Edge-coupled lines are Microstrip lines that are placed in parallel with each other, with a small spacing (S), as shown in the figures 4.41, 4.42, 4.45 and 4.46. The coupled lines are

made using conventional Microstrip lines using double sided PCB with the bottom side a ground-plane. This is easy to manufacture, but places restrictions on the amount of coupling that can be obtained. Typically, the spacing between the lines is very small and this spacing must be accurately controlled along the entire line length to obtain the correct amount of coupling. Edge coupled lines are very suitable for sampling the forward and reverse power from transmitters and for filters. The design process of a backward-coupled hybrid using edge-coupled lines is illustrated as follows:

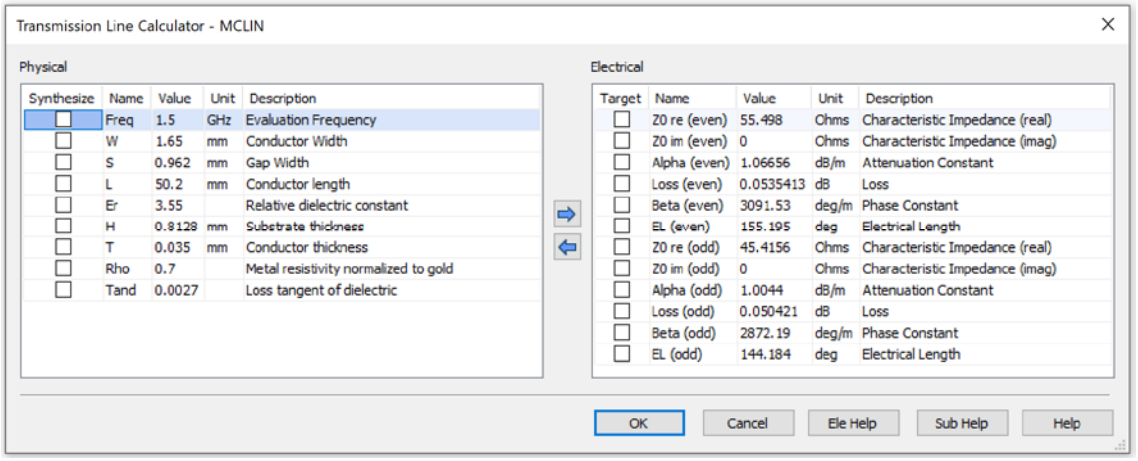



Figure 4.40. Calculated geometry for a λ/4 20 dB coupler.

## *Example 4.3: 20 dB Coupler*

A 20 dB coupler at 900 MHz is required. The coupled output is thus 20 dB below the input. The coupled voltage is one tenth of the input voltage, i.e. C = 0.1. From equations 4.21 and 4.22 one obtains $Z_{OO} = 45.23\ \Omega$ and $Z_{OE} = 55.28\ \Omega$. The required physical spacing can now be determined iteratively using either the old TXLine program, accessible from *Tools* ⇒ *TXLine* or using the Transmission Line Calculator, which can be obtained by right clicking on a MLIN, MCLIN, SLIN, SCLIN, S1LIN, CPW1LINE, RWG_TEmn, COAX, or COAXC element and selecting synthesize. That then opens up the Transmission Line Calculator, as shown in figure 4.40. Entering the above even and odd mode impedances and other physical parameters, then checking the boxes next to the variables that need to be calculated. Clicking on the directional arrows, calculates the target values. Note that for the same line length, the electrical length is different for the even and odd mode, since the propagation velocity of these modes is different.

These calculated values are substituted in the coupled-line circuit diagram shown in figure 4.41. Figure 4.42 shows the corresponding PCB layout including 50 Ω lines needed to connect the input and output ports to the coupler. Figure 4.43 shows the simulated performance. The coupling is 20 dB as expected. Note that the coupled port is in a different location compared with the Branchline coupler.

The coupler was designed for a centre frequency of 1 GHz. Coupled lines have a null in coupling at multiples of a half wavelength length. This was used to tune the length of the coupled line to give a null at 2 GHz, thereby giving maximum coupling at the required 1 GHz. Note that the bandwidth of the coupling and the isolation is very wide compared with the other hybrids described before in these notes. At 1 GHz, the isolation ($S_{31}$) is only 5 dB less than the coupled output ($S_{41}$), so that further design changes are required to improve its performance.

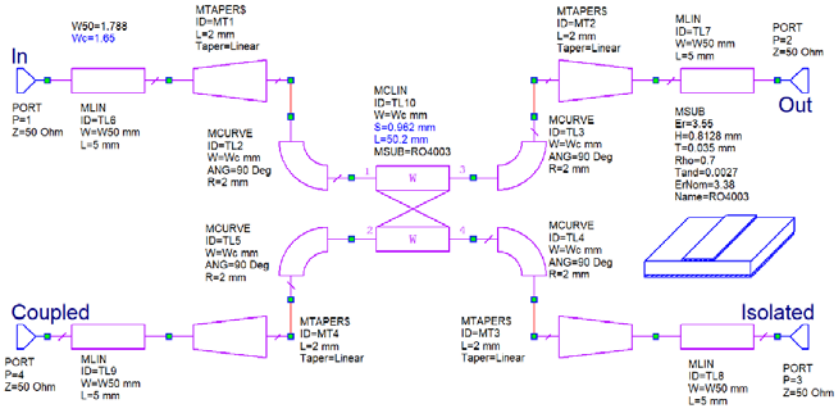



Figure 4.41. λ/4 20 dB coupler schematic and corresponding Microstrip layout.

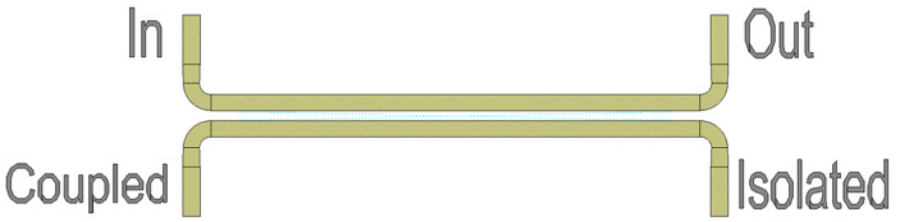



Figure 4.42. λ/4 20 dB coupler schematic and corresponding Microstrip layout.

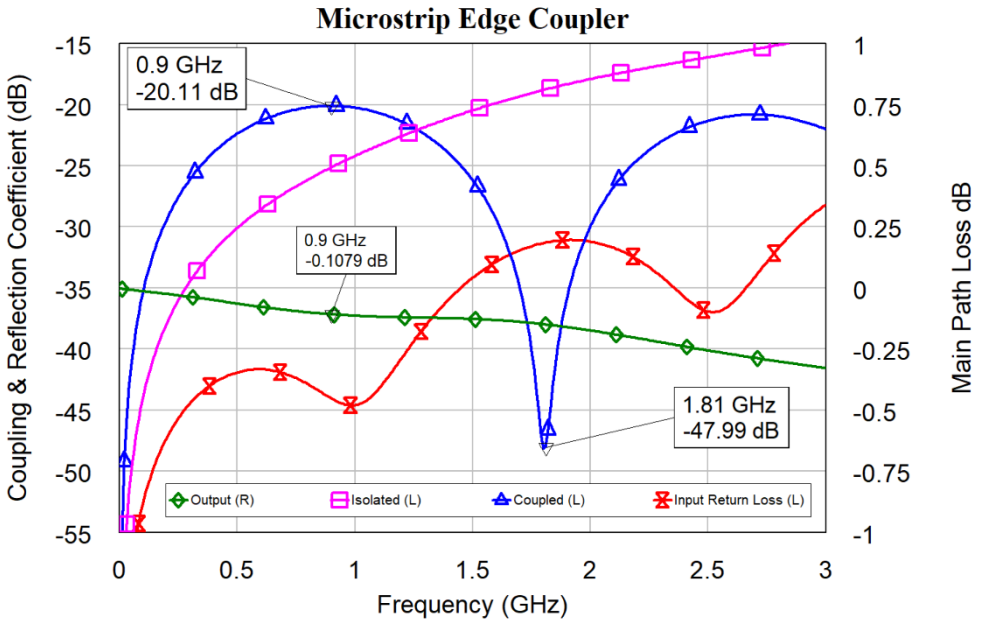



Figure 4.43. λ/4 Microstrip 20 dB coupler performance.

Having a different electrical length for even and odd mode impedances makes it difficult to set the line length to correspond to 90°. The coupling line length and gap can be obtained without using the transmission line calculator of figure 4.40. The coupler line length can be tuned to maximise the output at 900 MHz, while observing figure 4.43. That should result in a coupling null at close to twice the frequency for maximum coupling, (1.8 GHz for figure 4.43). The line spacing can be tuned to give the -20.11 dB attenuation, to produce the coupled output 20 dB below the direct output by tuning those. The line width can be tuned to give a low S11 return loss up to about 1.2 GHz. Double clicking on the MCLIN element after tuning shows the values in figure 4.41. Since there

is an interaction between the maximum coupling, its attenuation and the return loss, the line length, line spacing and line width tuning should be repeated until no further changes occur. These values can also be determined using the optimisation routines included in MWO.

Note that in figure 4.43, the difference between the coupled port $S_{41}$ and the isolated port $S_{31}$ is 5 dB at the centre frequency of 900 MHz. By including some very small, sub-pF, capacitors across the terminals 1 and 4 and terminals 2 and 3 the phase velocity is more equalised over a wide frequency range and a lower input return loss ($S_{11}$) and flatter isolation ($S_{31}$) is obtained. These capacitors can be obtained as pads on the output transmission lines, or they can be realised using small gaps, using the MGAP2 element.

In figures 4.41 and 4.42 the forward signal at the input port 1, passes to the output port 2 with a small loss and couples to port 4 with a desired attenuation. Ideally little power should appear at the isolated port 3. The coupler is symmetrical, so if the output is connected to a load then the reflected signal due to any load mismatch will then appear at the port 2 and couple to port 3. Once can thus also call the coupled port in figure 4.44, the *Forward* port and the Isolated port the *Reverse* port. To accurately measure the reflected power, the power at the *Reverse* port due to the input, must be much smaller than the power from the reflected signal coupled into the *Reverse* port.

One application of the backward travelling wave coupler is in the measurement of power at the output of a device, such as a signal generator or a transmitter. Typically, a coupled signal –20 dB below the forward or reverse power is required. The forward power is the transmitter output power and the reverse power is the reflected signal that occurs if the load for the transmitter is mismatched. At least a 20 dB front to back isolation is required, to accurately measure forward and reflected power. The hybrid will thus require a coupled output of –20 dB and an isolated signal < –40 dB below the input.

As can be seen from figure 4.43, the signal at the isolated port ($S_{31}$) is too large when a quarter wavelength long coupler is used. A suitable coupler with a good forward to reverse ratio can be obtained by making the length of the coupler much smaller than a quarter wavelength and using capacitors shunting the forward and reverse coupled outputs to produce a constant frequency response over the required frequency band.

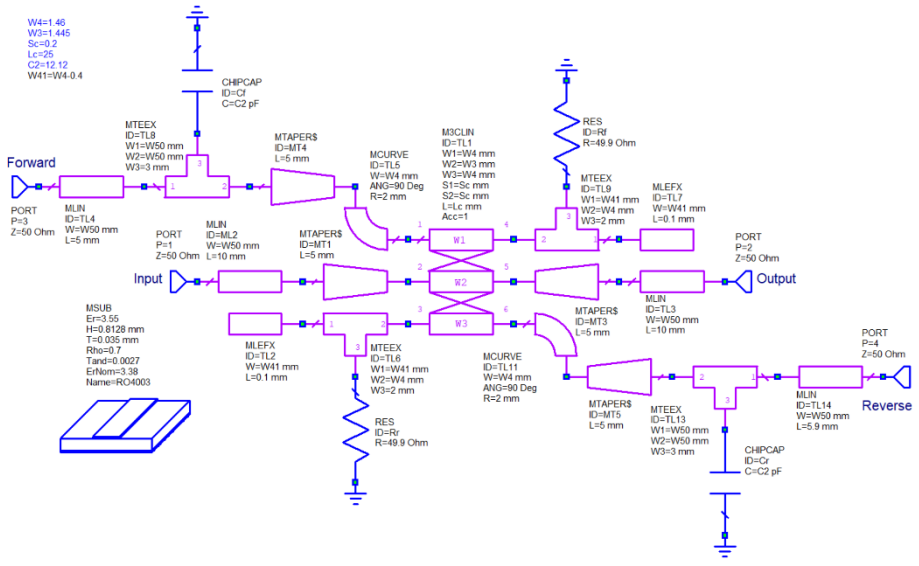



Figure 4.44. Circuit diagram of Microstrip coupler.

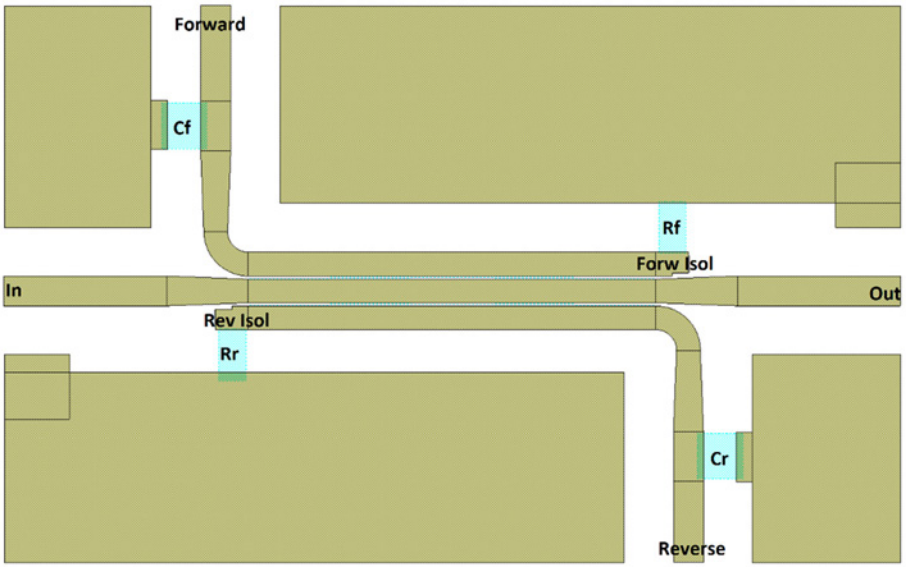



Figure 4.45. Layout of the Microstrip coupler.

To enhance the forward and reverse port isolation, two coupled lines are used and each coupled line is terminated in a resistor, as shown in figures 4.44, 4.45 and 4.47. In figure 4.44, the blue variables for widths, length, coupling gap and capacitor values are the parameters that are optimised to obtain the specified performance.

The resulting PCB layout is shown in figure 4.45. For a λ/4 long coupler and –20 dB coupling, a 0.95 mm gap is required. For the shorter length coupler of figure 4.45, the coupling gap is 0.2 mm, which is easy to achieve using current technology.

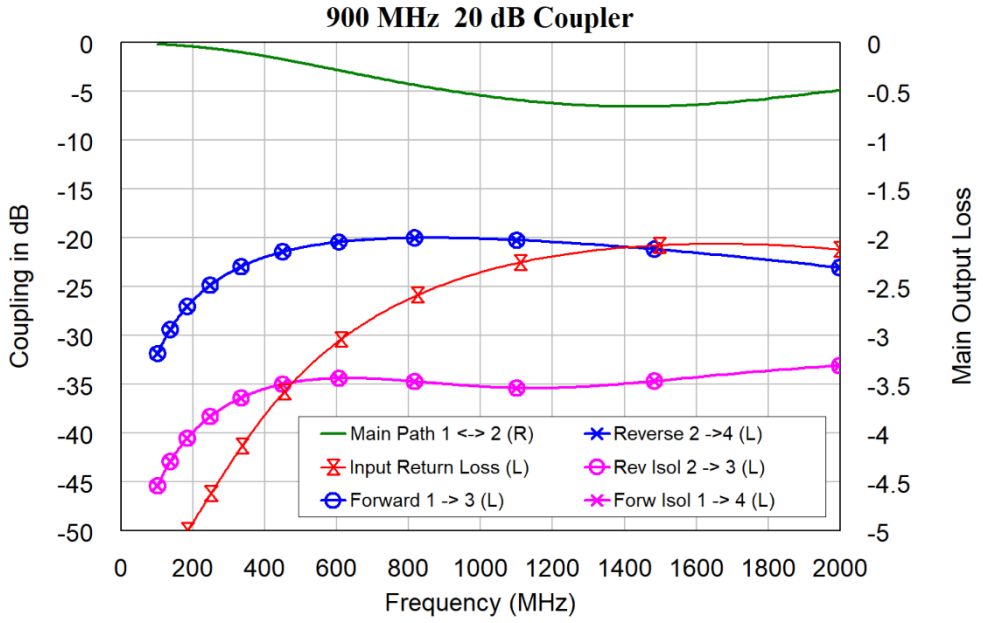



Figure 4.46. Simulated performance of the Microstrip coupler.

Figure 4.46 shows the simulated performance of such a 20 dB coupler. Comparing this with figure 4.43 shows that the isolated port has a much better isolation and the coupled port has a flatter and wider frequency response. This performance is obtained by using the optimiser in AWR DE to vary the coupling gap, line widths, lengths and capacitance values until a suitable performance is obtained.

Figure 4.46 shows a photograph of the Microstrip coupler. To provide suitable shielding and allow for the resistors, capacitors and BNC connectors to be soldered to the PCB, large earth pads are incorporated. Such an earth-plane also allows the circuit to be mounted in a metal box, without affecting the performance. That top ground-plane needs to be solidly connected to the bottom ground-plane, using lots of vias or pins. This is commonly done in commercial designs and figure 7.67 shows a commercial design from Codan [9], using many vias, connecting the top and bottom ground planes. The measured performance closely matches the simulated performance of figure 4.47. The spacing between the vias or pins needs to be a small fraction of a quarter wavelength at the highest operating frequency of the circuit.

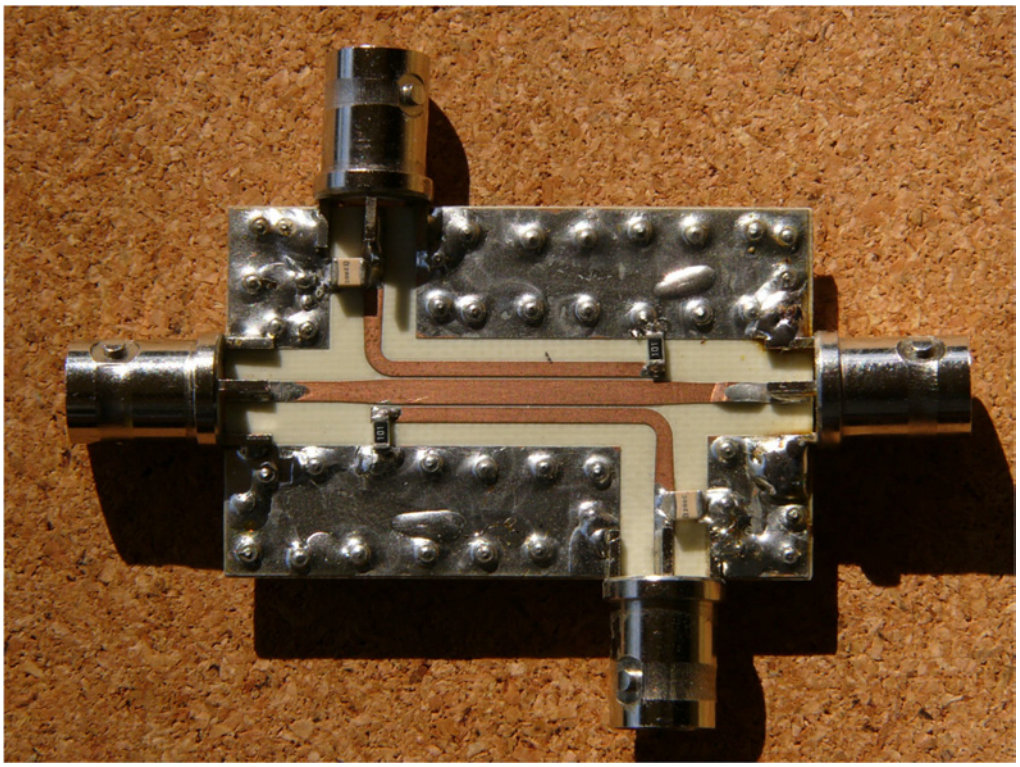


Figure 4.47. Photograph of the Microstrip coupler.

Edge-coupled Backward travelling wave hybrids as shown in figure 4.46, are the best choice if a wide bandwidth and low coupled outputs (-20 dB) and good front to back ratios are required.

## *Lange Coupler*

For a 3 dB coupler, C = 0.707 and $Z_{OE}$ = 120.7 Ω and $Z_{OO}$ = 20.7 Ω. For edge coupled Microstrip lines, this requires a coupling gap far smaller than 0.1 mm, which is impossible to make. To increase the coupling, many lines can be used in parallel. This is called a Lange Coupler. Figure 4.48 shows a layout of a Lange coupler. At the middle, a bonding-wire is used to connect the upper track end to the middle track and the lower other track end, thus keeping those transmission lines in parallel. Similarly, the track ends at the edges of the coupler are connected to the other appropriate lines. One will thus have the top left port connected by a set of parallel lines to the bottom right port. The top right port is connected by a set of parallel lines to the bottom left port. Typically, the spacing between the tracks and the track widths are of the order of 0.25 mm, which is close to the smallest widths that can conveniently be made using conventional processes.

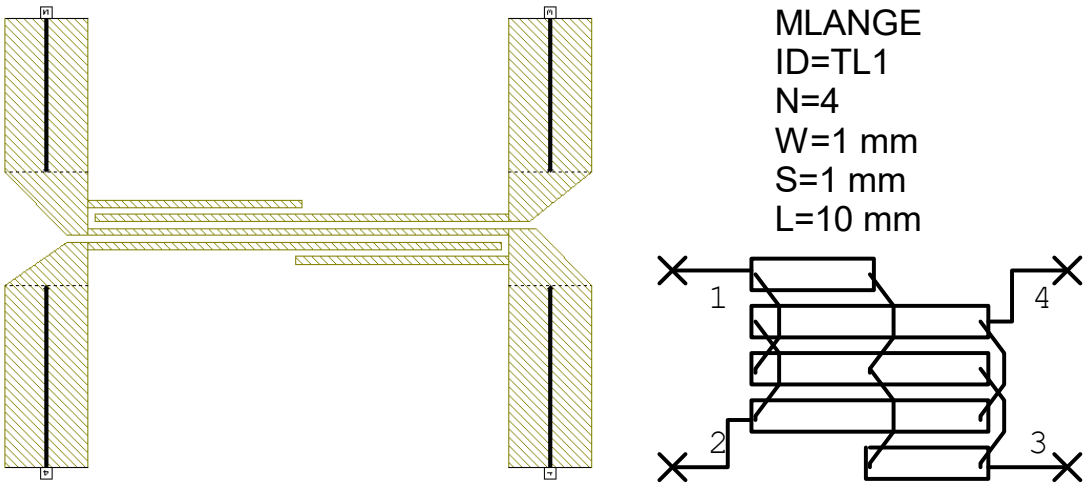



Figure 4.48. Lange coupler layout from MLANGE and schematic.

Even having these parallel lines result in very fine track widths and coupling gaps, making the Lange Coupler expensive to make. The Lange coupler [10] is however, the only planar hybrid that offers better than an octave (2:1) of useable bandwidth. With the high cost of manufacturing the Lange Coupler, due to the small track and gap widths and the high cost of attaching the bond wires, Lange Couplers are not often used. The required coupling can be obtained at a lower cost and can be better controlled, using broadside coupled lines and multilayer RF printed Circuit Boards. They can also be implemented using Low Temperature Co-fired Ceramic (LTCC) substrates, which are discussed in chapter 11. Since CADENCE AWR DE V10, the Lange coupler circuit element MLANGE and the associated layout as shown in the left of figure 4.48 is no longer available since it was not accurate enough. The replacement circuit elements MLANG and the more accurate M2LANGE, which includes an EM model, only shows the thin coupled lines of the schematic in the layout.

## Broadside Coupled Lines

It is possible to have multilayer printed circuit boards with RF substrates. These can be used to design coupling structures with higher coupling and 3 dB couplers are quite practical. The typical configuration is shown in figure 4.49.

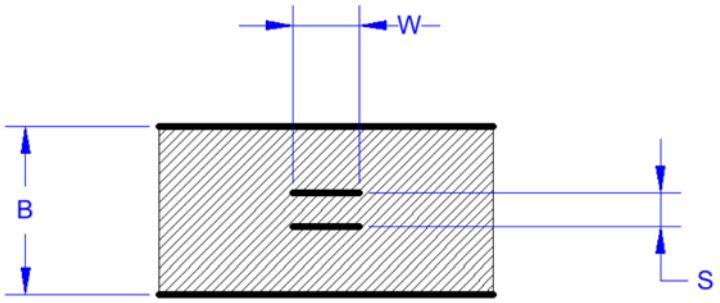
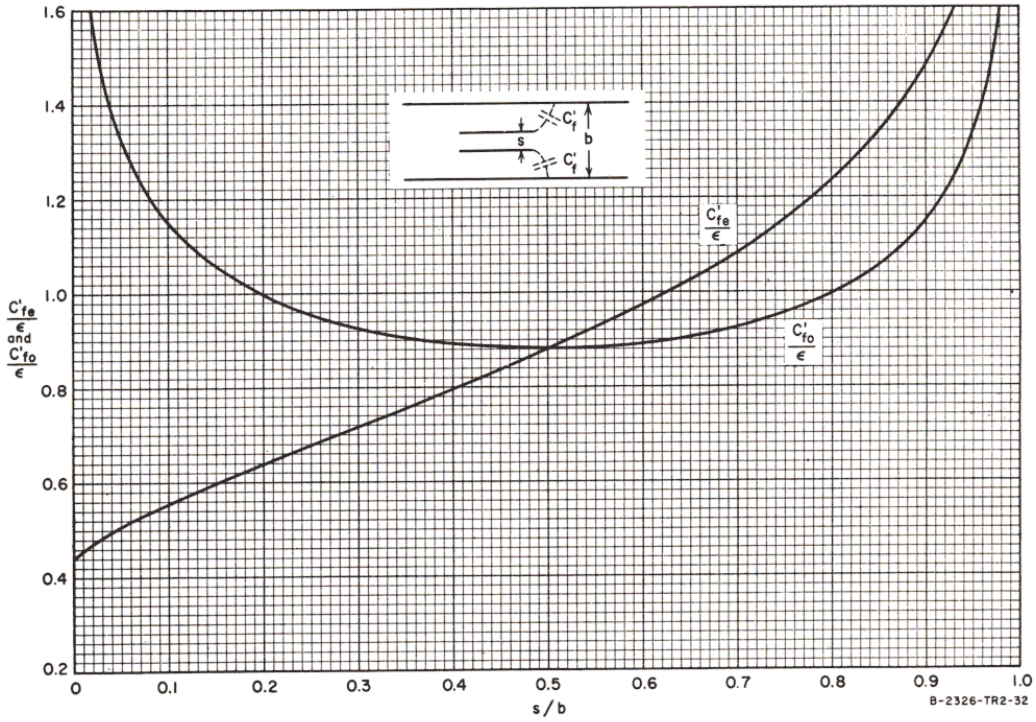



Figure 4.49. Stripline broadside coupled lines

The advantages of this structure are firstly that bigger coupling between the transmission-lines can be obtained with a good control over impedance values. Secondly, the Stripline

structure has no radiation losses. The disadvantage is that a non-planar structure is required.

TXLine is not capable of calculation the broadside-coupled transmission-line coupling gap (s) and line width (W), shown in figure 4.49. Books like Matthei, Young and Jones [11]. Microwave Filters, Impedance Matching Networks and Coupling Structures. Artech House 1980. (McGraw Hill 1964) pages 180 and 181 give empirical equations for $Z_{oo}$ and $Z_{oe}$ are given in equations 4.23 and 4.24. The capacitance $C_{fe}$ and $C_{fo}$ are fringing capacitances between the coupled lines and the ground plane and these can be determined from figure 4.50.




SOURCE: Final Report, Contract DA-36-039 SC-74862, SRI; reprinted in *IRE Trans., PGMTT* (see Ref. 5, by S. B. Cohn).

Figure 4.50. Values for $C_{fe}$ and $C_{fo}$ from Matthei, Young and Jones, pp181.

$$Z_{OE} = \frac{188.3/\sqrt{\varepsilon_r}}{\frac{w/b}{1-(s/b)}+\frac{C_{fe}}{\varepsilon}} \qquad \text{Eqn. 4.23}$$

$$Z_{OO} = \frac{188.3/\sqrt{\varepsilon_r}}{\frac{w/b}{1-(s/b)}+\frac{w}{s}+\frac{C_{fo}}{\varepsilon}} \qquad \text{Eqn. 4.24}$$

Using the two-line broadside coupled line element, SBCPL, and the schematic circuit simulation, allows an easier and more accurate determination of the broadside coupler parameters, than using equations 4.23, 4.24 and figure 4.50. The SBCPL element is a two-line broadside-coupled line element. The cross-section is similar to that of figure 4.49.

In addition, the width of each of the lines can be specified independently, the lines can be offset and the dielectric constants between the lines can be different from that above and below the line. None of these advanced features can be determined using the alternative techniques. The use of the SBCPL element to determine the required coupling gap and line width for a coupler is illustrated in the following example.

## *Example 4.4: 100 Watt 3 dB Broadside Coupler*

A 3 dB coupler was required to operate at a power level of about 100 Watt at a frequency of 100 MHz. At the time of the design, MWO did not yet exist and the equations 4.23 and 4.24 and Figure 4.50 were required to complete the design.

Two 12.6 mm thick pieces of Polyethylene, which has a dielectric constant of $\varepsilon_r = 2.26$, were used for the top and bottom dielectric sheets for this coupler. Polyethylene sheets of this thickness can conveniently be purchased as a cutting board for bread from most local supermarkets. For a 3dB coupler, C = 0.707 and $Z_{OE} = 120.7\ \Omega$ and $Z_{OO} = 20.7\ \Omega$. Since these impedances must be evaluated iteratively, it is the easiest to enter the above equations for $Z_{OE}$ and $Z_{OO}$ into an Excel or other spreadsheet. Using the values B = 29 mm, s = 2.9 mm, w = 12.7 mm, gives $\frac{s}{B} = 0.1$ and thus from the table gives $\frac{C_{fe}}{\varepsilon} = 0.56$ and $\frac{C_{fo}}{\varepsilon} = 1.15$. This then results in $Z_{OE} = 119.7\ \Omega$ and $Z_{OO} = 20.8\ \Omega$, which is close enough. At 100 MHz the length of a quarter wavelength line is given by:

$$\frac{\lambda}{4} = \frac{c}{\sqrt{\varepsilon}F} = 50cm \qquad \text{Eqn. 4.25}$$

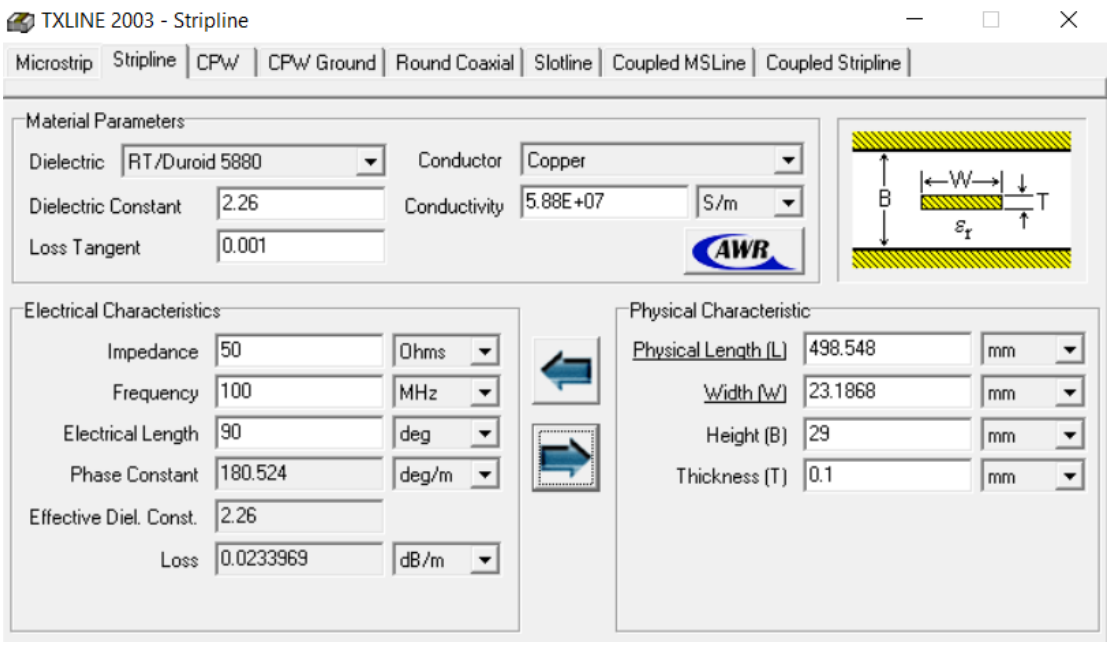



Figure 4.51. Terminating line-width calculation.

As shown in figure 4.51, the width of 50 Ω terminating lines can be calculated using TXLine or equivalent programmes as 23.2 mm. A 2.9 mm thickness of Polyethylene is not readily available. However, a 3.17 mm thickness of Perspex, with a dielectric constant of approximately 3.42 was available and was used. The effect of this substitution cannot readily be calculated using the above techniques. This coupler was constructed and performed as expected, even though the line spacing was not ideal.

The use of SBCPL in CADENCE AWR DE gives much more flexibility and allows a more accurate determination of the performance. The actual cutting boards used are 12.6 mm (0.5 inch) thick, pieces of Polyethylene. They are used for the top and bottom dielectric and a 3.17 mm (0.125 inch) thick Perspex sheet is used to separate the tracks.

Entering these values in the SBCPL element and then fine-tuning the track width, track length and offset, allows the required performance to be obtained. Polyethylene has a dielectric constant of $\varepsilon_r = 2.26$ and Perspex has a dielectric constant of 3.42 ±0.3.

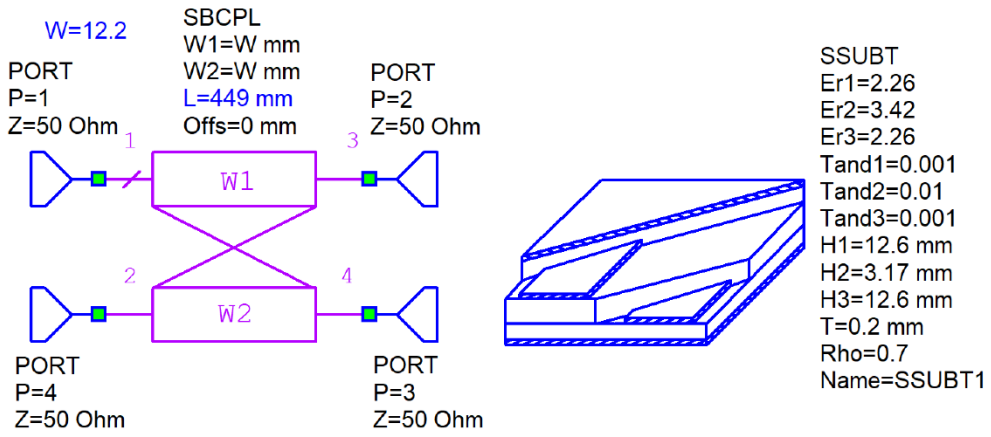



Figure 4.52. MWO broadside coupled-line circuit using SBCPL.

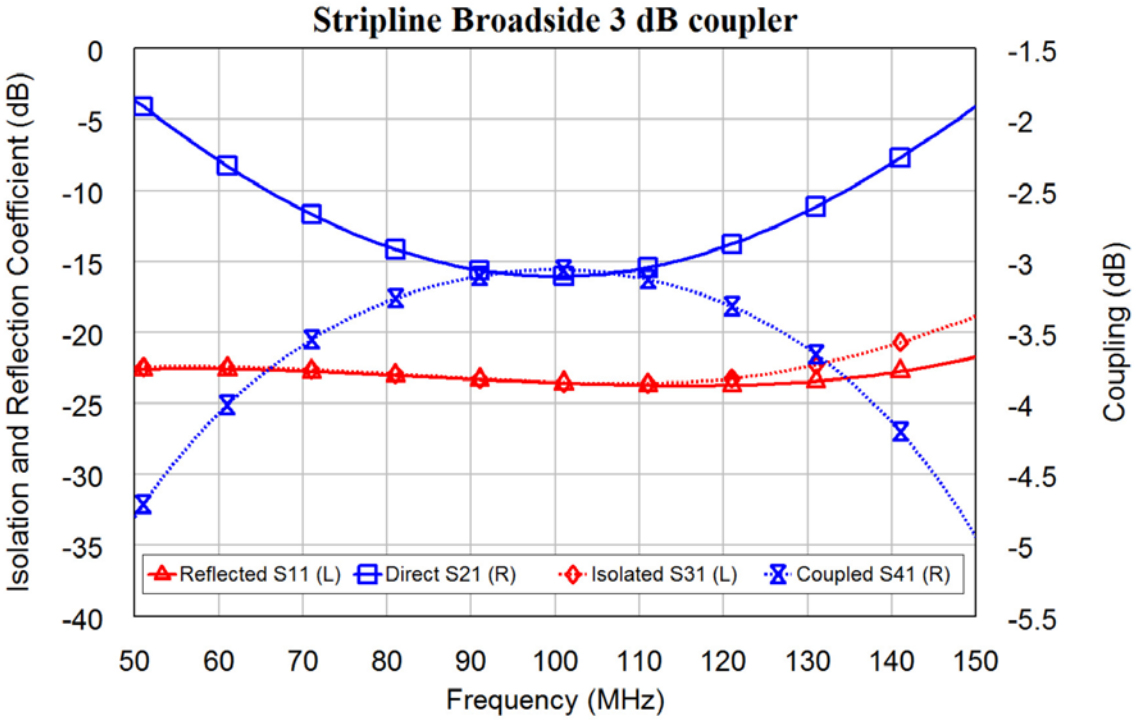



Figure 4.53. Performance of broadside coupled-line circuit using SBCPL element.

Tuning the coupler length (L = 449) sets the centre frequency of the coupler to 100 MHz and tuning the line width (W = 12.2) adjusts the coupling to have close to 3 dB coupling over the 85 MHz to 115 MHz frequency range and achieve a return loss on the ports of less than -20 dB. The resulting MWO circuit diagram is shown in figure 4.52 and its performance is shown in figure 4.53. The track width of 12.2 mm and length of 440 mm obtained from MWO agrees closely with the 12.7 mm and 500 mm obtained for the earlier design, which used equations 4.23 and 4.24 together with figure 4.50. The MWO design is far more accurate since it allows for losses in the dielectric and the Perspex sheet for separating the tracks, having a different dielectric constant and loss tangents compared with the Polyethylene. The constructed coupler has a measured isolation and coupling

very similar to the performance shown in figure 4.53 and is able to handle 100W of output power.

Prepreg sheets are available [12], which can be used to convert single layer PCB's to multilayer PCB's, so that broadside couplers can be constructed. The Roger's RO4403 Prepreg sheets have a dielectric constant of 3.17 and are 0.1 mm thick and can be used to bond two single layer PCB's to form a multilayer PCB. The sandwich is pressed together with a pressure of 2.8 MPa (400 psi) and a temperature controlled profile up to 180 °C (350 °F) for a cycle time of 2 hours to form the correct bond. For further details, see the RO4403/4450 data sheet. Other manufacturers have similar materials.

# Coaxial Couplers

## *Transmitter Power Meters*

For transmitters both the amplifier output and the return loss from the antenna is normally monitored. This can be done using a coupler like shown in figure 4.44 to 4.47. High power amplifiers have coaxial outputs, and the forward and reverse power sensors are normally small coupling loops placed close to the centre conductor of the coax. When power levels are required, a diode rectifier and a capacitor are used to provide a DC voltage or current proportional to the power level. A typical schematic of such a power meter is shown in figure 4.54. In that power meter the coupling loop can be reversed, so that both forward and reverse power can be measured. The plugins, shown on the right of figure 4.54, can provide an RF output, or they cover a specified frequency range and power level. For high power transmitters forward and reverse power sensors are normally incorporated [13].

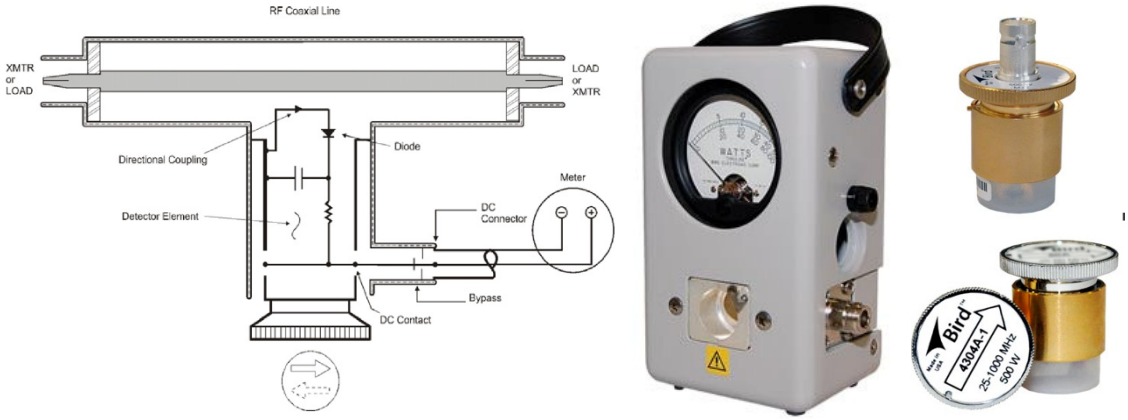



Figure 4.54. Bird Wattmeter schematic, instrument and plugins [14,15].

# Transmission Line Baluns

A 180-degree Hybrid or Balun (balanced to un-balanced) is used for microwave balanced-mixers and for converting connect dipole antennae to coaxial cables. At lower power levels and below 1 GHz, ferrites can be used as shown in the TV Balun of figures 3.7 and 3.8. The use of ferrite cores is not desirable for Microstrip or Stripline circuits or for a high power transmitter output. Removing the ferrite core from figure 3.7 results in the Parallel coaxial line Balun of figure 4.55. A Balun can also be made by connecting the outer of a coaxial cable and the centre to two load of half the impedance, as shown in figure 4.56. The floating length of coax is normally 90 degrees in length. A ferrite core around the coaxial cable can be used to enhance the isolation between port 3 and ground.

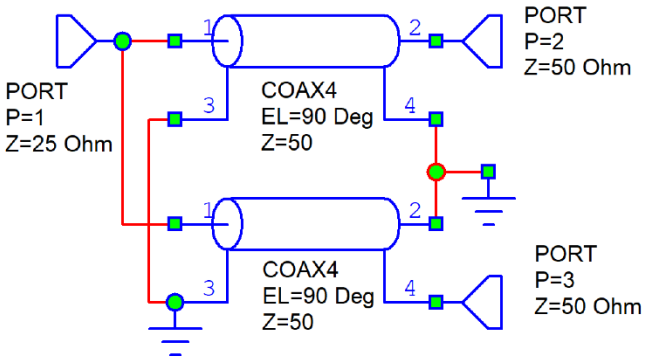



Figure 4.55 Parallel coaxial line Balun.

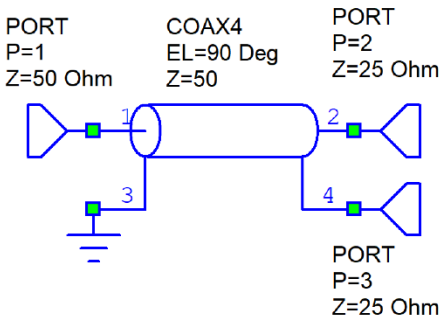



Figure 4.56 Floating coaxial line Balun.

## *Marchand Balun*

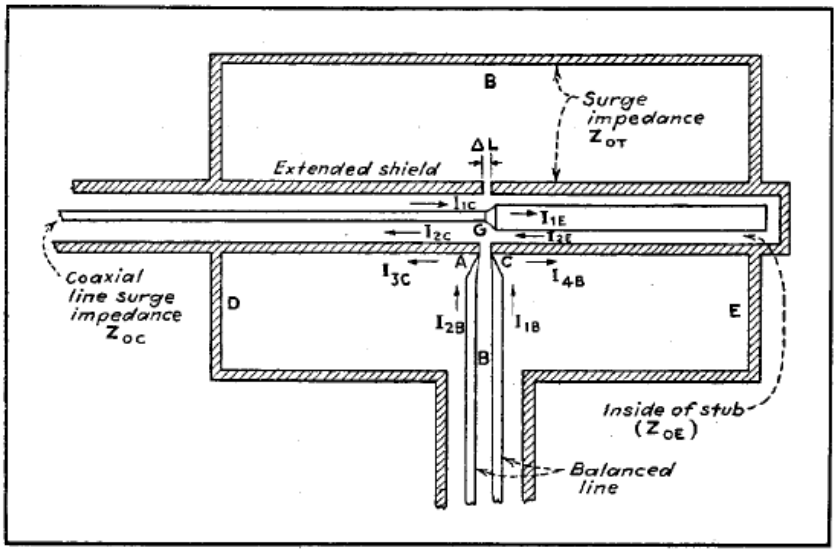



Figure 4.57 Original Marchand Balun [16,17].

The Marchand Balun [16-18] as shown in figure 4.57 was developed to allow a transmitter with a coaxial output to drive dipole antennae. The two balanced signals to the antenna must have the same amplitude and be 180° out of phase over as wide a bandwidth as possible. The Marchand Balun includes a basic Balun consisting of coaxial lines $Z_{oc}$ and $Z_{oe}$. The short-circuited transmission line with an impedance $Z_{ot}$ improves the phase difference between the balanced output voltages.

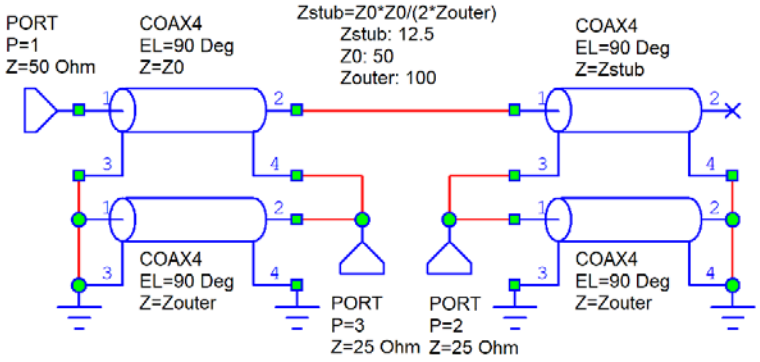



Figure 4.58 Full Marchand Balun.

Canning [19] described how the inherent coupling between the outer connector of the floating coaxial line Balun, can be represented by a transmission line with and impedance of Zouter to ground. Figure 4.58 shows the corresponding coaxial line representation of this Full-Marchand Balun.

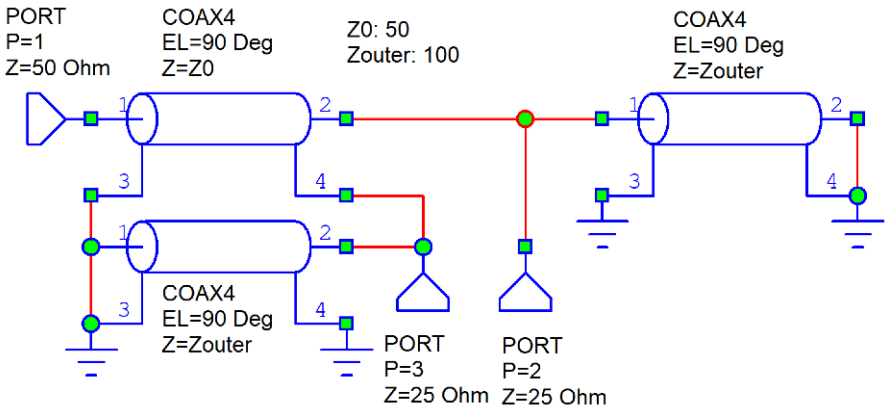



Figure 4.59 Lite Marchand Balun.

The Marchand Balun can be simplified by connecting the centre conductor of $Z_{oc}$ to the outer conductor of $Z_{oe}$ at the balanced line output and removing the centre conductor of Zoe. Canning called that the 'Lite Marchand Balun' as shown in figure 4.59. This Lite Marchand Balun is easier to realise in stripline or Microstrip technology.

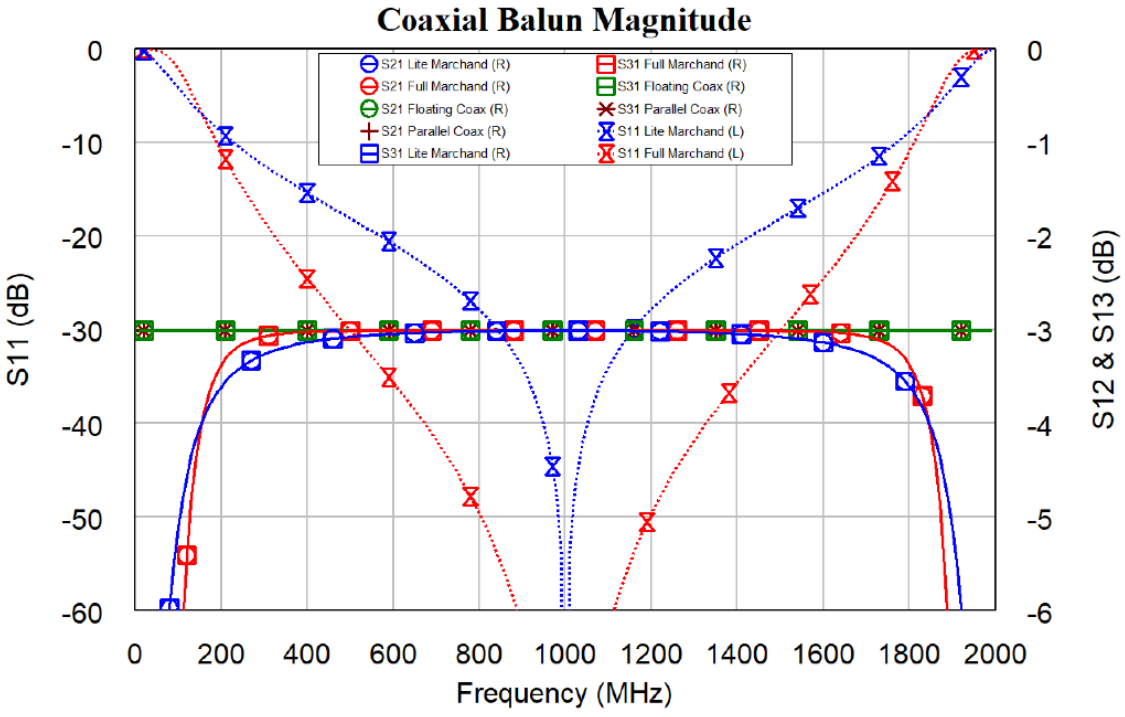



Figure 4.60 Floating, Parallel and 2 Marchand Balun amplitude responses.

Figure 4.60 shows the magnitude and figure 4.61 shows the phase responses of these three Baluns. For the Full and Lite Marchand Baluns, the output magnitudes at the coupled ports S12 and S13 are exactly, the same and their phase difference is exactly 180°. Both these Marchand Baluns are thus ideal for producing the out of phase signals for driving dipole antennae or balanced mixers.

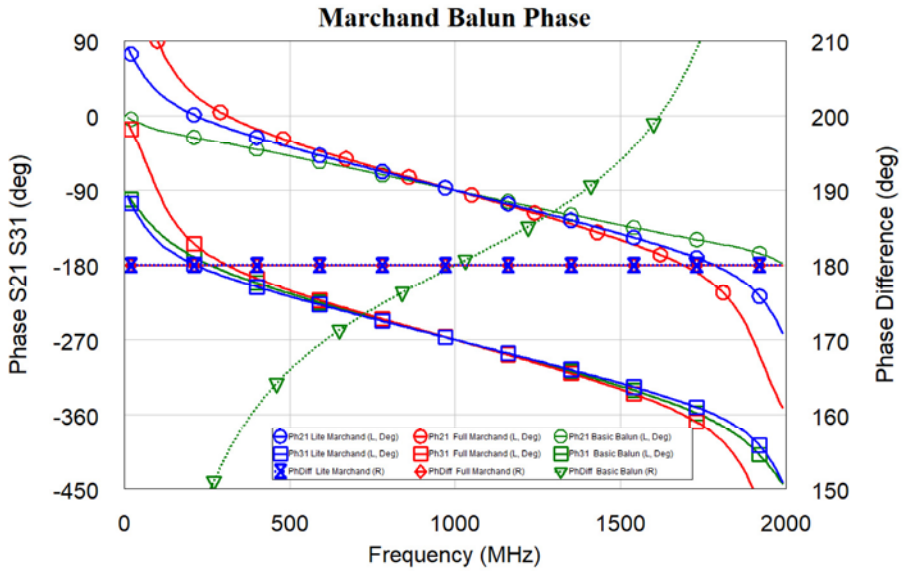



Figure 4.61 Basic and Marchand Balun phase response.

## *Marchand Balun Realisation*

The original Marchand Balun was designed using coaxial lines, and for convenience, coaxial lines are used to explain their operation in figures 4.58 to 4.61. For low power applications, Stripline, Microstrip, LTCC or MMIC configurations are preferred. A Microstrip circuit would give the lowest cost realisation. Because a large amount of coupling is required between the tracks, Lange type couplers will need to be used.

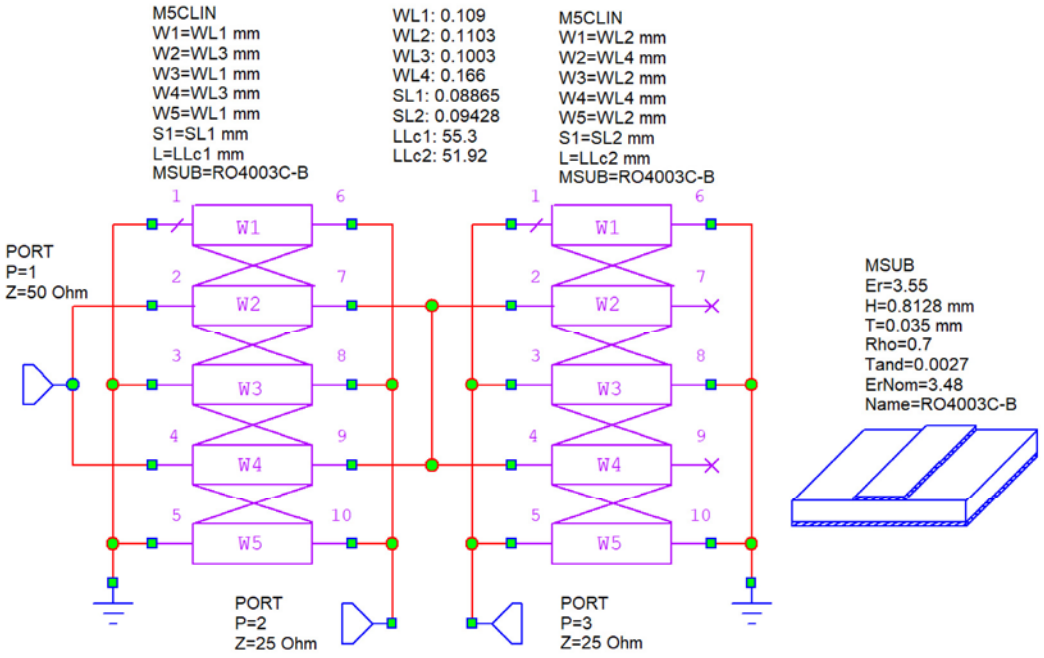



Figure 4.62 Lange Marchand Circuit (5 track).

The Lange coupler in figure 4.48 has half-length tracks at the edges and the same number of fingers for both lines to be coupled. For this Balun, three fingers (W1, W3 and W5) are used for the lines that are grounded at one end and two fingers (W2 and W4) are used for the other lines. Their widths (WL1 to WL4) can be made different. Those couplers can be realised using M5CLIN elements as shown in Figure 4.62. To compare the

difference in performance of the different realisations, no tracks connecting the couplers together or connecting the couplers to ports are included in these realisations.

The number of tracks in the Lange coupler can be varied and the performance optimized by varying the width, length and spacing of the fingers. This optimization shows that a five track Lange coupler has less difference between S21 and S31 than three track or seven track Lange couplers. Figure 4.63 shows the resulting magnitude response and figure 4.64 shows the corresponding phase response.

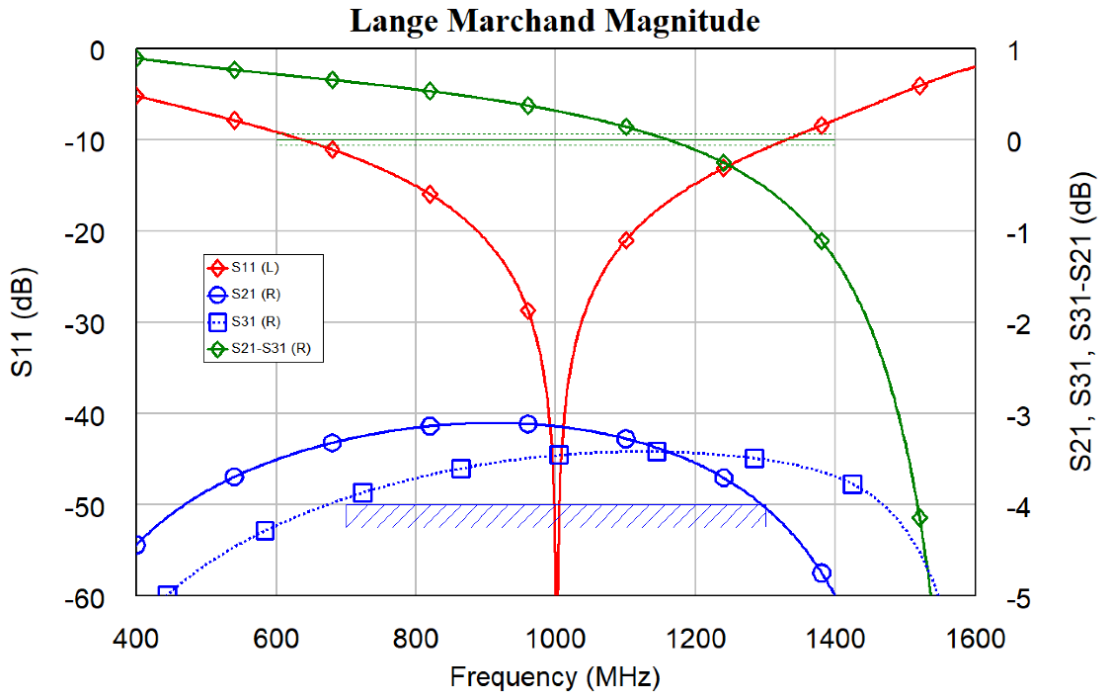



Figure 4.32. Lange Marchand Magnitude Response (5 track).

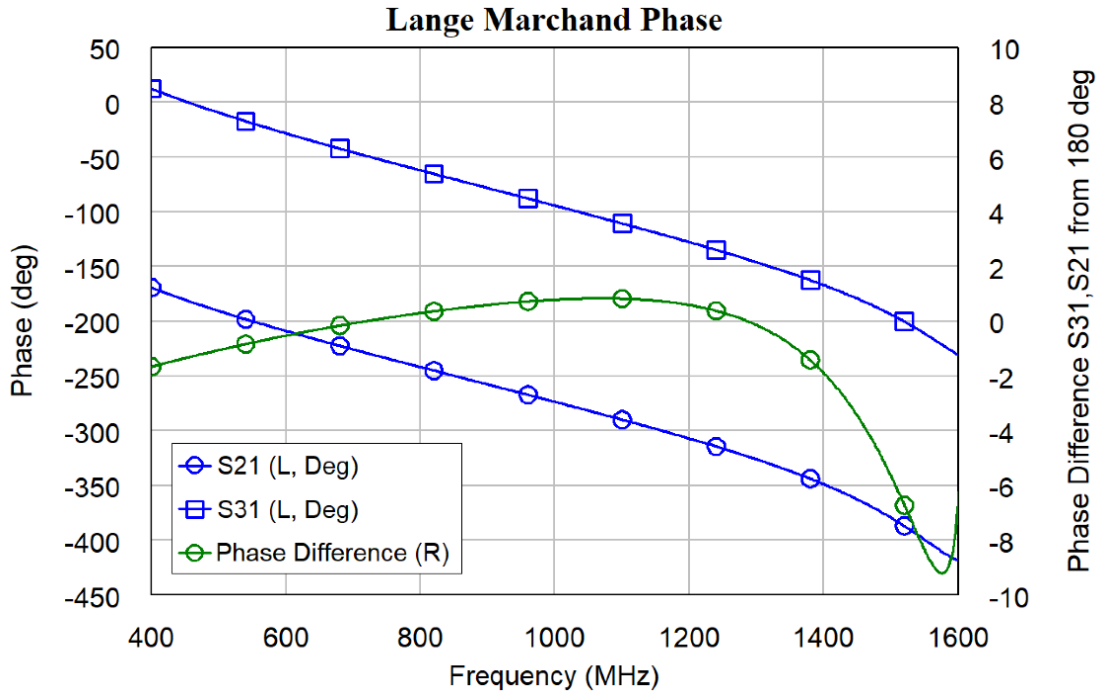



Figure 4.64. Lange Marchand Phase Response (5 track).

Lin [20] used a 7 track Lange coupler for a Marchand Balun operating at 21-41 GHz and shown in figure 4.65. The chip size is approximately 200 µm x 420 µm.

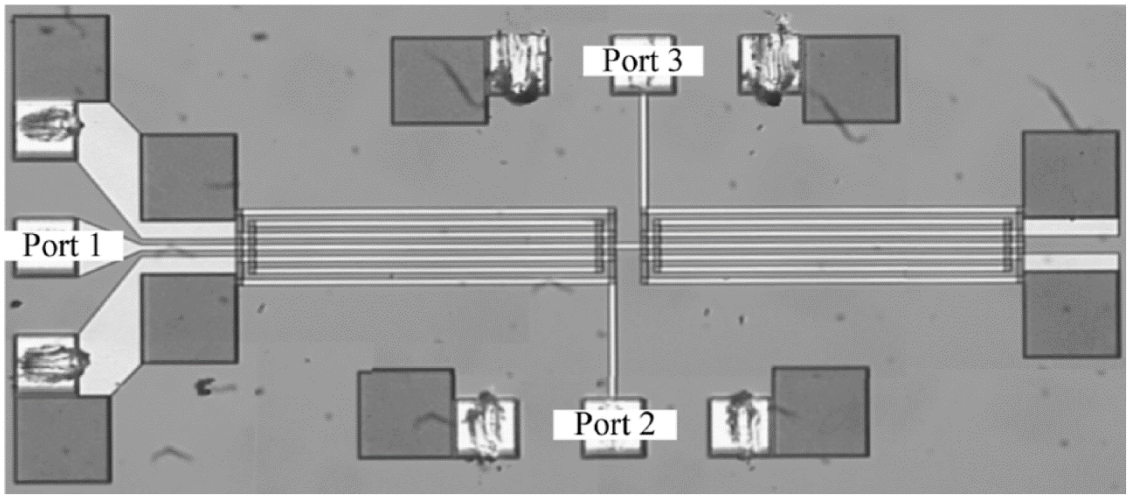



Figure 4.65 Chip photograph of 21-41 GHz MMIC Marchand Balun [20].

By isolating the ground-plane layer under the coupled lines, Zhang [21] was able to increase the even mode impedance of the coupling lines, to obtain a Marchand Balun using Microstrip coupled lines. For such a circuit, care needs to be taken with the coupling between the isolated ground-plane layer tracks and the ground of the mounting structure.

Stripline techniques can be used to obtain a practical Marchand Balun by putting coupled tracks on both sides of a 0.2033mm thick RO4003 [5] substrate and make this into a 3 layer SSUBT substrate by mounting single sided 1.525mm substrates on both sides, using Prepreg sheets [12], as described in chapter 11 under heading *Multilayer Boards*. Figure 4.66 shows the resulting schematic diagram. Since the impedance of the right stub (Zstub) in figure 4.58, is different from Z0 of the left input coupling line, the widths of the coupling lines is W1 for the input and W2 for the stub coupling structures. In addition, the amount of coupling can be varied by varying the offset between the coupling lines. It can be seen that after optimisation, there is little difference between TL1 and TL2 of figure 4.66

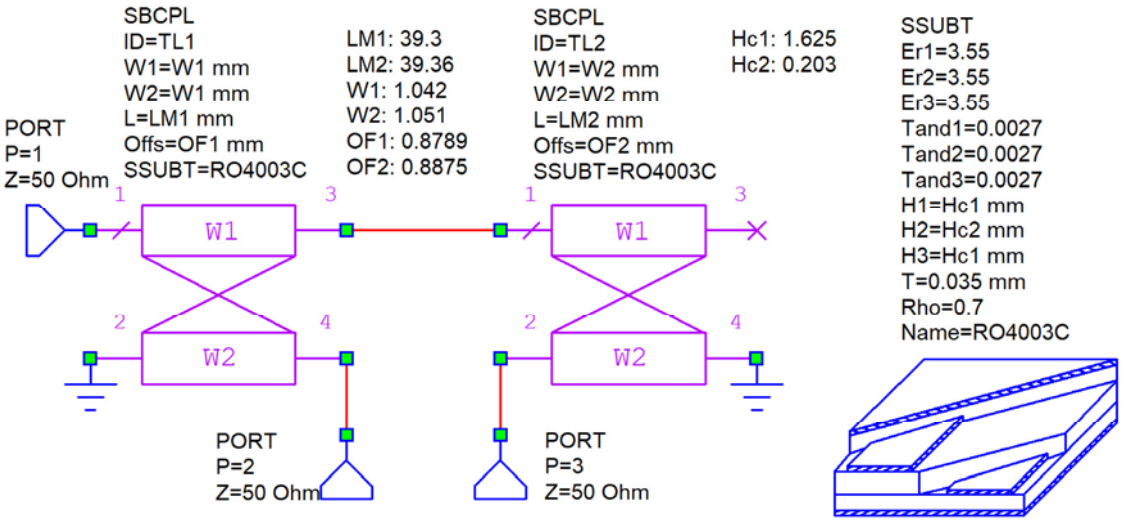



Figure 4.66 Stripline Marchand Balun Circuit.

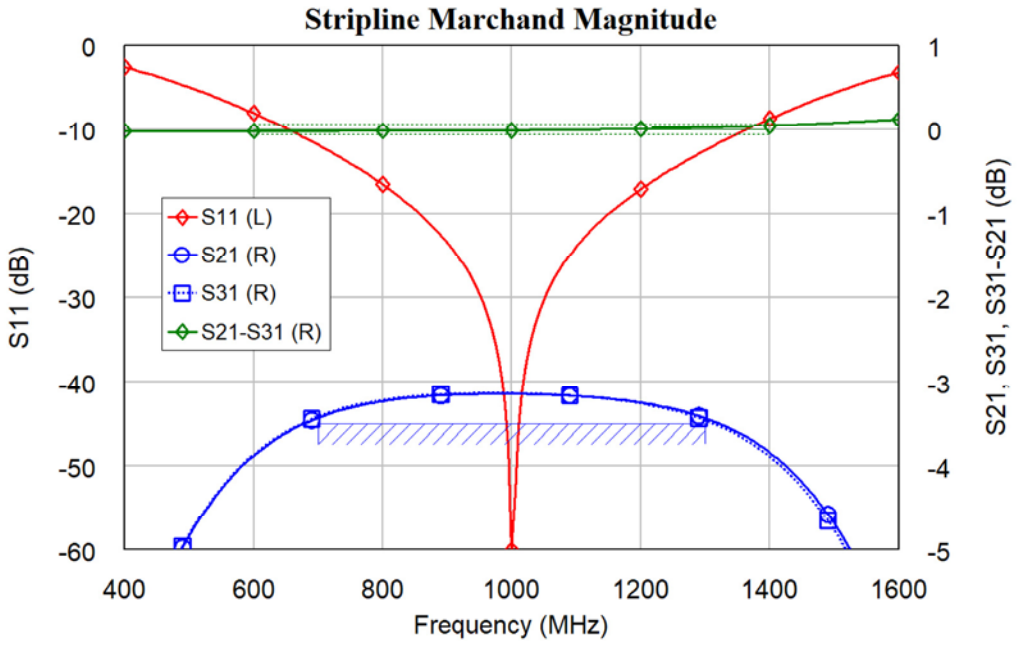



Figure 4.67 Stripline Marchand Balun magnitude response.

Figure 4.67 shows the magnitude frequency response of the Stripline Marchand Balun and figure 4.68 shows the phase response. Comparing figures 4.67 and 4.68 with figures 4.63 and 4.64, show that the Stripline Marchand Balun has a much better performance than the Microstrip Lange Marchand Balun.

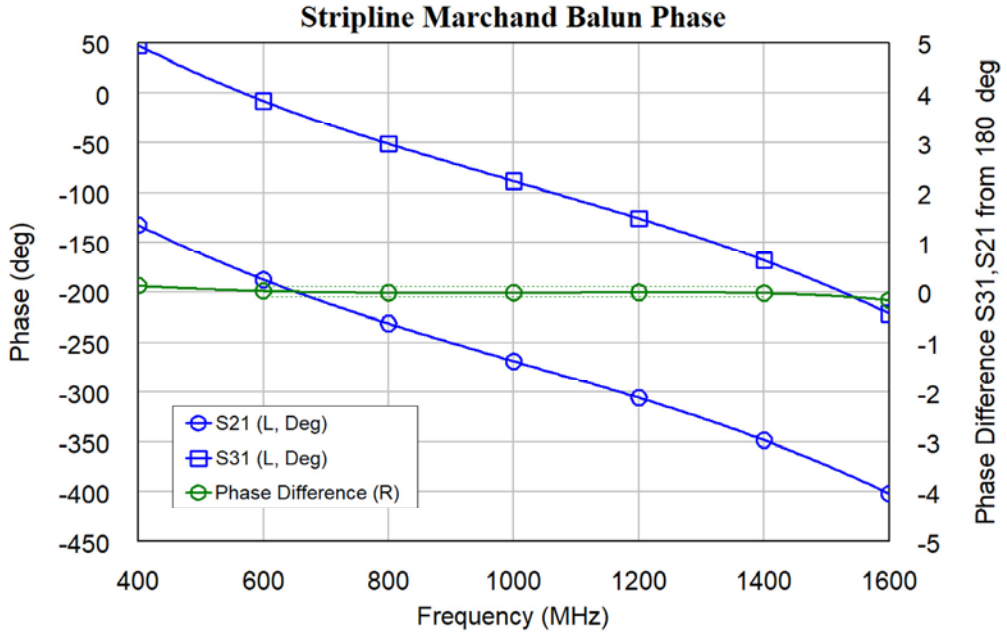



Figure 4.68 Stripline Marchand Balun phase response.

## *Parallel Line Balun Realisation*

As a further comparison, the Parallel Line Balun of figure 4.55 is realised using Stripline couplers. Figure 4.69 shows the resulting circuit diagram. For a good phase balance, the shorted line SL1 needs to be added. For this Balun, the width of the lines was also fixed at 1 mm. The substrate configuration is the same as for the Stripline Marchand Balun.

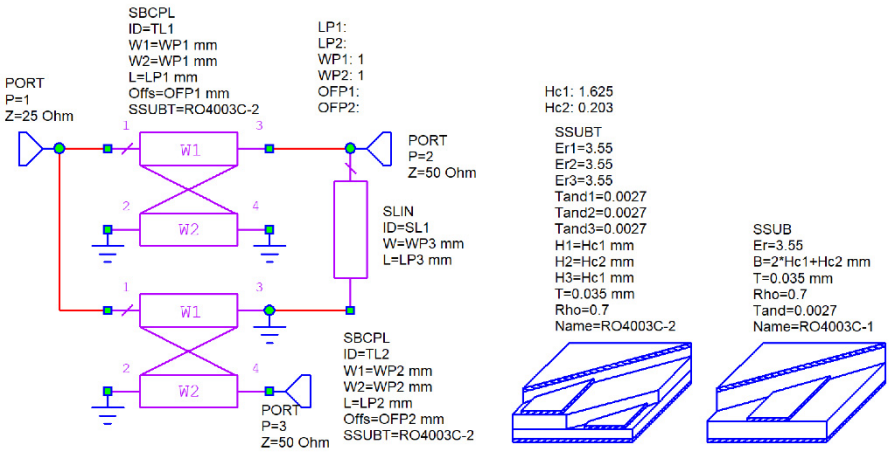



Figure 4.69 Stripline Parallel Line Balun Circuit.

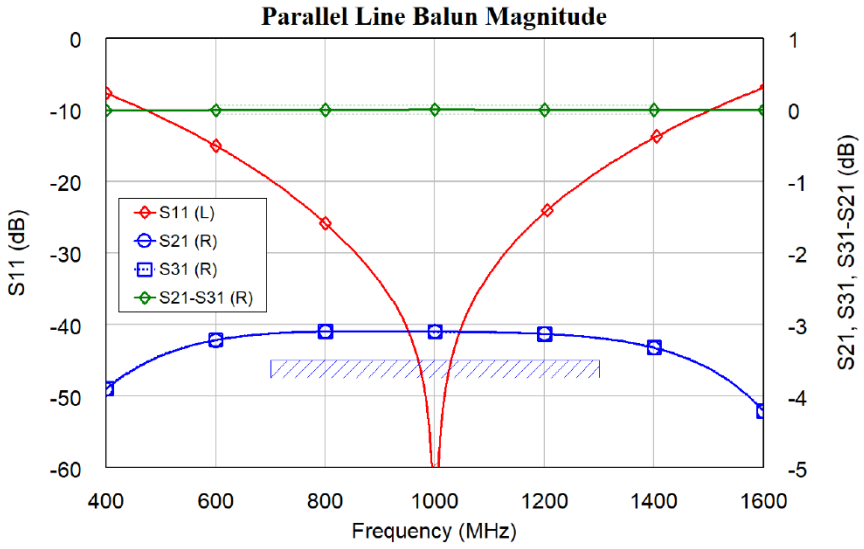



Figure 4.70 Stripline Parallel Line magnitude response.

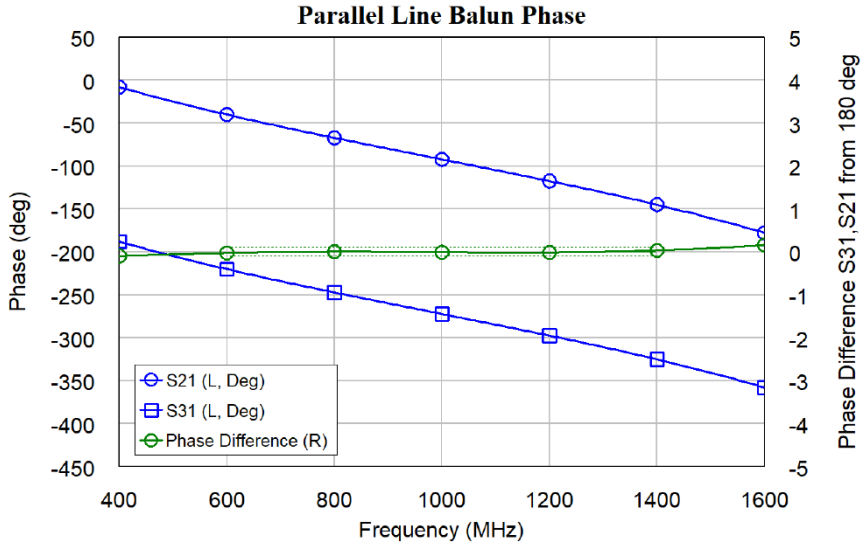



Figure 4.71 Stripline Parallel Line phase response.

Figure 4.70 shows the magnitude frequency response of the Stripline Parallel Line Balun and figure 4.71 shows the phase response. Comparing this with figures 4.63, 4.64, 4.67 and 4.68, show that the Stripline Parallel Line Balun has a better magnitude performance and a similar phase performance than Stripline Marchand Balun of figure 4.66, and a much better performance than the Microstrip Lange Marchand Balun of figure 4.62.

## *Wireline and Wirepac Couplers*

Sage Laboratories, now part of API Technologies Corp, filed a patent for Wireline [22,23] couplers in 1983. These couplers consist of a coaxial cable like structure, except for the inner conductor, two conductors with a controlled spacing is used as shown in figure 4.72.



Figure 4.72 Wireline (left) and Wirepac (right) couplers.

Wireline uses a smaller diameter cables, can be bent to put a long line in a small space and can handle 100 W or 200 W continuously, Wirepac [23] cannot be bent and can handle up to 500 W continuously. The operating frequency range is from about 50 MHz (940 mm long wireline) to more than 5 GHz (9.4 mm long wireline). The upper frequency limit is simply determined by the ability to connect to the coupled conductors.

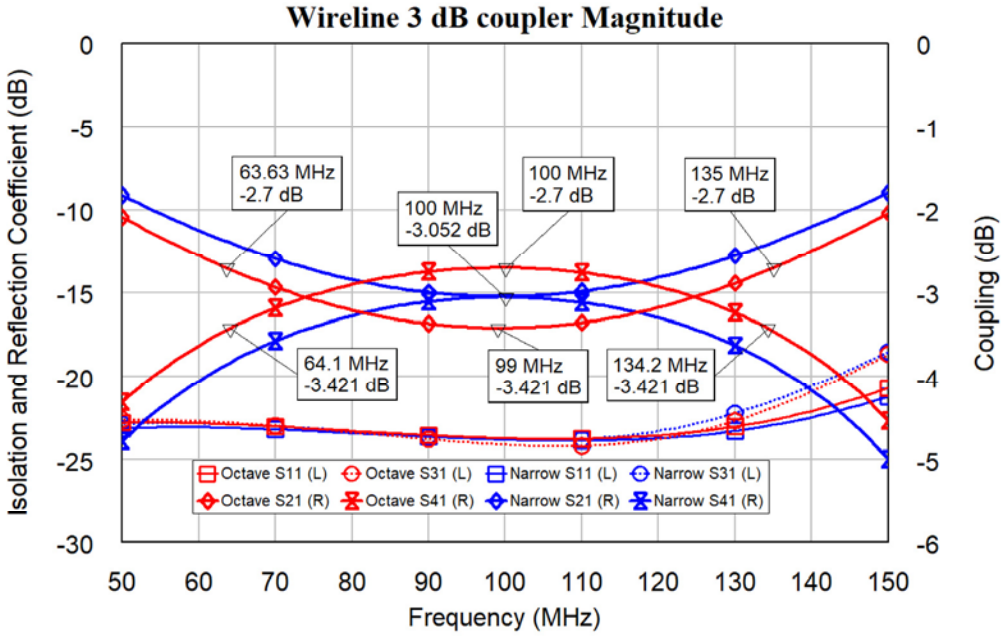



Figure 4.73 Wireline amplitude response.

These couplers behave exactly like the broadside couplers shown in figures 4.52 and 4.53, When the line length is one quarter of a wavelength long, figure 4.73 shows that these couplers typically have a 3 dB coupling to both the direct port (S21) and coupled port (S31) and more than 20 dB isolation (S41) and return loss (S11). This is called a Narrow wireline coupler. By increasing the coupling slightly, the bandwidth over which a -3 ± 0.5 dB direct output and coupling outputs can be maintained is more than one octave. That is called an Octave wireline coupler. Figure 4.74 shows that the phase difference between the direct and the coupled output is close to 90 degrees over an octave bandwidth.

Couplers with -10 dB or -20 dB, coupled outputs, like the one shown in figures 4.44 to 4.47 can easily be obtained by using much shorter than a quarter wavelength long coupler. Having a capacitor between the coupler output to ground, like C2 and C3 in figure 4.47, results in a reasonably flat frequency response over a wide frequency range.

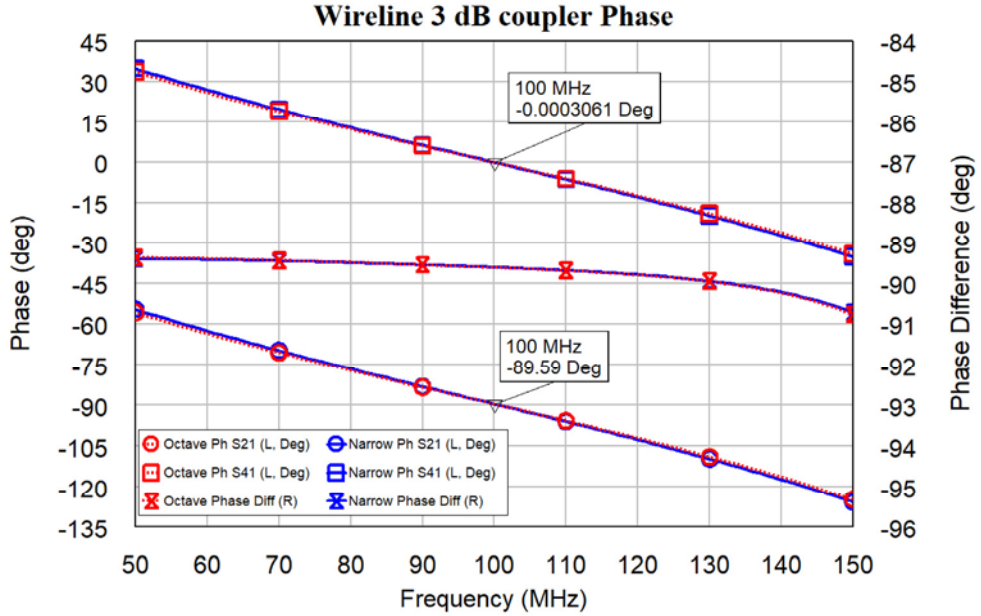



Figure 4.74 Wireline phase response.

By varying the spacing between the coupled conductors, the coupling ratio for a quarter wavelength long cable can be varied. Wirepac cables with -10 dB coupling at a quarter wavelength are available. Ham radio operators use this principle to make detectors for antenna matching by sliding an insulated wire underneath the shield of a short length of standard coaxial cable. Then connecting a diode detector and a meter, results in a circuit similar to the Bird Wattmeter shown in figure 4.54, and with suitable calibration allows forward and reverse power of their transmitter and antenna to be measured.

## References

1. W. C. Johnson, Transmission Lines and Networks, Mc Graw Hill June 1950.
2. Wikipedia, Transmission lines: http://en.wikipedia.org/wiki/Transmission_line
3. D. M. Pozar, “Microwave Engineering”, 3rd Ed, Wiley, 2005.
4. E Wilkinson, “An N way Hybrid Power Divider,” IRE Trans. Trans Microwave Theory and Techniques, vol. MTT-8, pp. 116-118, Jan. 1960.
5. Rogers R04000 Series High Frequency Circuit materials. https://rogerscorp.com/advanced-electronics-solutions/ro4000-series-laminates
6. Bird RF https://birdrf.com/Products/Test%20and%20Measurement/

7. RF-Lambda https://rflambda.com/search_loadtermination.jsp
8. Double-Box Branchlines https://www.microwaves101.com/encyclopedias/double-box-branchlines
9. Codan, http://www.codan.com.au/.
10. J. Lange, “Interdigitated Stripline Quadrature Hybrid”, *IEEE Trans Microw. Theory Tech.*, vol. 17, pp1150-1151, Dec 1969.
11. Matthaei, George L.; Young, Leo and Jones, E. M. T. “Microwave Filters, Impedance-Matching Networks, and Coupling Structures”, McGraw-Hill, 1964.
12. Rogers Corporation, “RO4400 Series Prepreg Data Sheet”, https://www.rogerscorp.com/ advanced-electronics-solutions//prepregs-and-bondplys
13. Bird Broadcast Power Monitors. https://birdrf.com/Products/Test and Measurement/RF-Power-Monitors/BPME-Series-Broadcast-Power-Monitors.aspx.
14. Bird RF Power Meters. https://birdrf.com/Products/Test and Measurement/RF-Power-Meters/Wattmeters-Line-Sections.aspx
15. Bird Plug in elements https://birdrf.com/Products/Test and Measurement/RF-Power-Meters/Plug-In-Elements.aspx.
16. N. Marchand, "Transmission Line conversion transformers", Electronics, Vol 17, pp. 142-145, Dec 1944.
17. Marchand Balun https://www.microwaves101.com/encyclopedias/marchand-balun
18. Ahn H., Nam S.; New Design Formulas for Impedance-Transforming 3-dB Marchand Baluns. *IEEE Trans Microw. Theory Tech.*, vol. 59, no. 11, pp 2816-2823, Nov 2011.
19. Canning, T., J. R. Powell, and Steve C. Cripps, Optimal Design of Broadband Microwave Baluns Using Single-Layer Planar Circuit Technology *IEEE Trans Microw. Theory Tech.*, vol. 62, no. 5, pp 1183-1191, May 2014.
20. C-S Lin, et. al., Analysis of Multiconductor Coupled-Line Marchand Baluns for Miniature MMIC Design, *IEEE Trans Microw. Theory Tech.*, vol. 55, no. 6, pp 1190-1199, Jun 2007.
21. Z-Y Zhang, Y-X Guo, L.C. Ong and M.Y.W. Chia. “A New Planar Marchand Balun” , 2005 IEEE MTT-S Microwave Symposium Digest, DOI: 10.1109/MWSYM.2005.1516893.
22. Sage Wireline Coupler, https://patents.google.com/patent/US4547753, filed 14 Nov 1983.
23. Wireline and Wirepac https://www.apitech.com/products/rf-solutions/power-dividers-couplers-splitters/wireline-wirepac/.

# Chapter 5

# Frequency Mixers

## Introduction

Figure 5.1 shows the typical block diagram of a transmitter and a receiver. It can be seen that in both cases frequency translation is achieved by the use of a frequency mixer. A frequency mixer can be a passive mixer using diodes or it can be an active mixer using transistors or FETs. In many receivers and transmitters, a succession of frequency mixing and filtering stages are used, to ensure that the filtering requirements can be satisfied.

A frequency mixer is used as an up-converter when the output frequency is higher than the input frequency. This is typical in a transmitter. A frequency mixer is used as a down-converter when the output frequency is lower than the input frequency. This is typical for a receiver. In this chapter, the term *mixer* denotes a frequency mixer.

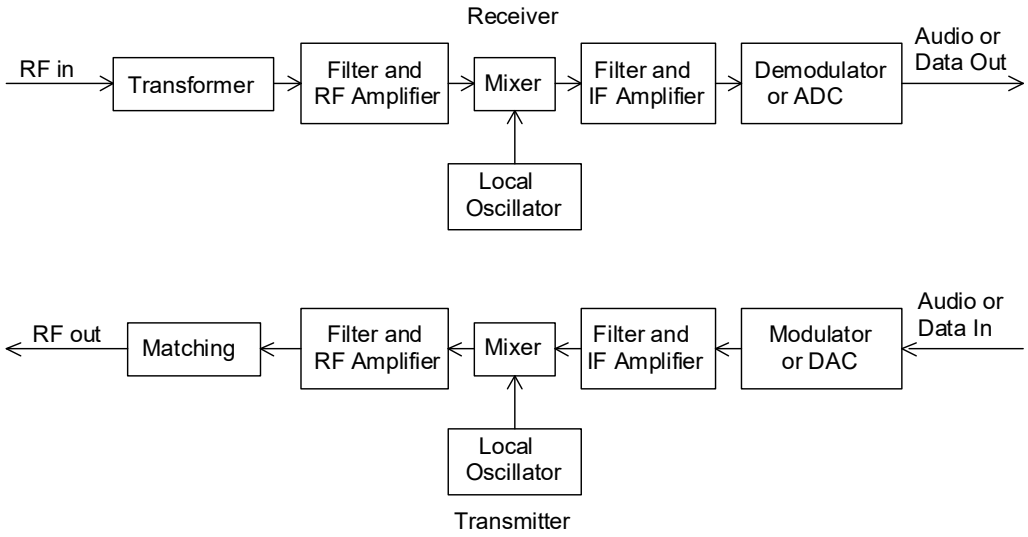



Figure 5.1. Typical transmitter and receiver block diagram.

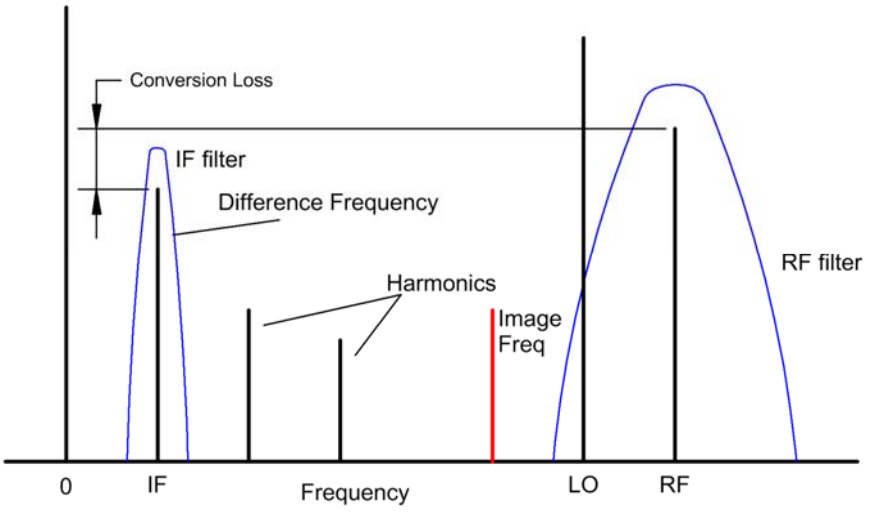



Figure 5.2. Frequencies of a mixer.

A mixer produces sum and difference frequencies. An ideal multiplier is a perfect mixer since mathematically it produces sum and difference frequencies. The aim in frequency mixer design is thus to make the frequency mixer behave as close to an ideal multiplier as possible. This chapter describes different circuits to achieve this.

For a receiver the RF signal is down-converted. A receiver has a Local Oscillator (LO), the frequency of which is determined by the radio frequency (RF) of the TV, WiFi, GPS or Cellular Phone signal that is to be received. Figure 5.2 shows the frequencies for a receiver or down-converter. $F_{LO}$ is the frequency of the LO and $F_{RF}$ is the frequency of the RF signal. The RF signal is mixed with a LO signal to produce sum and difference frequencies. The sum frequency $F_{LO} + F_{RF}$ is outside the operating frequency range of the system and the difference frequency $F_{LO} - F_{RF}$ is the required Intermediate Frequency (IF) signal, which is filtered and amplified using an IF filter and its associated amplifiers. The IF frequency is $F_{IF} = F_{LO} - F_{RF}$. It should be noted that a signal at the image frequency results in a signal at the same IF frequency since for the image frequency $F_{IF} = F_{IM} - F_{LO}$, where $F_{IM}$ is the image frequency. The RF filter should be sufficiently narrow so that the image frequency, shown in figure 5.2, is not passed through the RF filter, since the difference frequency of the image frequency and the local oscillator is at exactly the same frequency as the required IF signal.

For an up-converter, the LO signal is multiplied by an IF signal and a double sideband suppressed carrier RF signal results. The resulting RF frequencies are $F_{RF} = F_{LO} \pm F_{IF}$. Generally only one of these RF signals are required, so that an RF filter, like the one shown in figure 5.2 is required to remove the unwanted signal.

There are two types of frequency mixers: 1) Passive mixers, using diodes, FETs or other nonlinear devices. In passive mixers the power in the LO signal provides the power for producing the sum and difference frequencies. 2) Active mixers, where transistors or FETs supplied with DC power provide the frequency mixing action.

# Definition of Terms

## *Conversion Loss*

For a down-converter, the conversion loss [1] is the ratio of the RF input signal to the wanted IF output signal. Most frequency mixers are used in receivers, for which this definition is applicable. For up-conversion, the conversion loss is the ratio of one of the wanted RF output signal spectral components to the IF input signal. For an ideal frequency mixer, half the input power is frequency shifted to the difference frequency and half the power is shifted to the sum frequency. The conversion loss is the ratio of the input signal to either the sum or the difference component. An ideal passive mixer will thus have a conversion loss of 3 dB. Practical balanced or double balanced mixers typically have a conversion loss of less than 6 dB. The conversion loss does depend on the amount of LO signal power applied to the LO port as can be seen in figures 5.17, 5.26 and 5.34. The frequency mixer is normally operated at a LO power close to that giving the lowest conversion loss. Active mixers can have a conversion gain.

The conversion loss must be taken into account in noise figure calculations of a receiver. A frequency mixer with a 6 dB conversion loss typically has a 6.5 dB noise figure. For high quality receivers, an amplifier with a gain much greater than the conversion loss is normally used before the mixer, to ensure that the mixer does not dominate the noise performance of the receiver.

Note Cadence AWR DE calculates the conversion gain. As a result, it is more appropriate to use a consistent term conversion gain in the plots and have negative dB values to indicate the loss. The term conversion loss is however used more frequently in literature. To use "*Conversion Loss*" would require the minus signs to be removed from the Cadence AWR DE generated plots, which is not easy to do. Similarly the term Insertion Gain and Return Gain are used in plots, with negative dB values indicating when the plotted variables have a loss.

## Isolation

In practice it is desirable to have isolation between the LO, RF and IF ports of the mixer. Typical double balanced mixers have more than 30 dB isolation [1, 2] between all ports. Single diode mixers have virtually no isolation between ports. Since single diode mixers are used in TV receivers, the LO signal is coupled to the antenna, which radiates the LO signal. In countries where TV licences are required, the "detector vans" look for the LO radiation and match the radiation coming from a house with any licence fee payment. One can also do a good survey to find out what TV channel people are watching by simply driving around a street with a spectrum analyser and noting the LO frequencies. For a balanced mixer, the isolation is directly related to the match between the diodes used. As a result, many manufacturers sell matched sets of diodes, especially for use in mixers. In many cases two or 4 diodes come as one package.

## Compression Point

For an ideal down-conversion mixer the IF output produced should be directly proportional to the RF input signal. However as the RF input approaches about 10 dB below the LO power. The IF output starts to saturate and the conversion loss starts to increase, as is shown in figure 5.3. Most manufacturers of frequency mixers specify the 1 dB compression point for their mixers [1, 2]. The 1 dB compression point is typically 6 dB below the LO level for mixers up to +23 dBm LO power.

Since the 1 dB compression point is related to the LO drive, a higher LO level results in a higher 1 dB compression point and as a result a bigger dynamic range of the mixer.

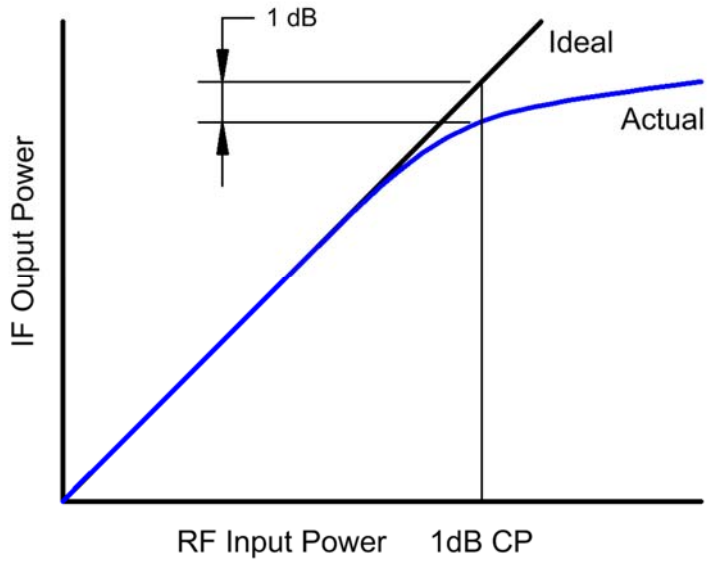



Figure 5.3. 1 dB Compression Point of a mixer.

## Dynamic Range

Dynamic range is the range over which a frequency mixer provides useful operation. The 1 dB compression point determines the upper limit of the dynamic range. The noise figure of the mixer determines the lower limit of the dynamic range. Since the mixer noise figure is only about 0.5 dB higher than its conversion loss, the lowest conversion loss is desirable to obtain the largest dynamic range. High and Extra High level mixers have a higher 1 dB compression point and thus a bigger dynamic range. Higher-level mixers are significantly more expensive and require more LO power, so that a compromise between cost, power consumption and dynamic range exists.

## Two-tone Third Order Intermodulation Distortion

In this section one considers the frequency mixer as a "linear" device, since for a down-converter, the IF mixer output amplitude is directly related to the RF input amplitude. The output Y(t) of a frequency mixer or amplifier will depend on the input X(t). The gain of the device, relating the output to the input is $a_1$. In addition, a DC component and harmonics of the input may be created due to the distortion of the device. The output is thus:

$$Y(t) = a_0 + a_1 X(t) + a_2 X(t)^2 + a_3 X(t)^3 + a_4 X(t)^4 + a_5 X(t)^5 + .... \quad \text{Eqn. 5.1}$$

For the devices we are considering, the terms above the 5th harmonic are so small they can be ignored.

When two signals, $X_1$ and $X_2$ are used as input. The output will then be:

$$Y(t) = a_0 + a_1\left[X_1(t) + X_2(t)\right] + a_2\left[X_1(t) + X_2(t)\right]^2 + a_3\left[X_1(t) + X_2(t)\right]^3 + a_4\left[X_1(t) + X_2(t)\right]^4 + a_5\left[X_1(t) + X_2(t)\right]^5 + .... \quad \text{Eqn. 5.2}$$

When $X_1(t)$ is a sine wave of frequency $F_1$ and $X_2(t)$ is a sine wave of frequency $F_2$, ($F_2 > F_1$) the frequency components at the fundamental and different intermodulation frequencies can be collected as follows:

The fundamental frequency component, i.e. at $F_1$ due to $X_1(t)$ and at $F_2$ due to $X_2(t)$ is:

$$Y_F = a_1 + (\frac{3}{4} + 3\frac{1}{2})a_3 + (\frac{5}{8} + 10\frac{3}{8} + 5\frac{3}{8})a_5 = a_1 + \frac{9}{4}a_3 + \frac{25}{4}a_5 \quad \text{Eqn. 5.3}$$

The Third Order Intermodulation (3IM) frequencies are 3IM (upper) due to $\pm F_1 \pm 2F_2$ and 3IM(lower) due to $\pm 2F_1 \pm F_2$ , and are given by:

$$Y_{3IM} = \frac{3}{4}a_3 + \frac{1}{2}(5\frac{1}{2} + 10\frac{3}{8})a_5 = \frac{3}{4}a_3 + \frac{25}{8}a_5 \quad \text{Eqn. 5.4}$$

The Fifth Order Intermodulation (5 IM) frequencies are 5IM (upper) due to $\pm 2F_1 \pm 3F_2$ and 5IM(lower) due to $\pm 3F_1 \pm 2F_2$ , and are given by:

$$Y_{5IM} = \frac{1}{2}10\frac{1}{8}a_5 = \frac{5}{8}a_5 \quad \text{Eqn. 5.5}$$

The frequencies of these spectral-components are shown in figure 5.4. The second order intermodulation (2IM) and the fourth order intermodulation (4IM) distortion produced by the amplifier or mixer do not create any components near the desired frequency components. As a result, the 2IM and 4IM performance is less important for an amplifier.

The second order intermodulation produces the required mixing action in a mixer and is thus of utmost importance.

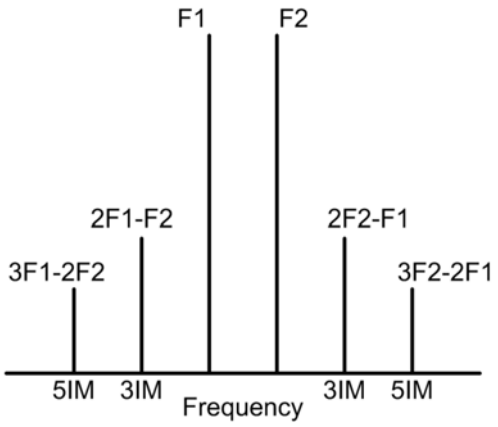



Figure 5.4. IM distortion of an amplifier or frequency mixer.

The third order IM (3IM) and fifth order IM performance is very important in linear amplifiers since when two tones are used as an input to the amplifier, the 3IM and 5IM distortion results in additional frequency components, which again cannot be filtered out, as can be seen in figure 5.4. The 5IM components are often too small to be observed in a spectrum like figure 5.4. For mobile phone base-stations, these IM signals are likely to create interference in adjacent mobile phone channels, as a result the IM performance of amplifiers and mixers are a critical part of their specification.

## *Third Order Intercept Point*

In practice $a_1 >> a_3 >> a_5$, so that the fundamental frequency components are proportional to $a_1$, the 3IM components are proportional to $a_3$ and the 5IM components are proportional to $a_5$. If the input signals are increased by 1 dB, then the 3IM components will increase by 3 dB since they are caused by $a_3\left[X_1(t)+X_2(t)\right]^3$ in equation 5.2 and the 5IM components will increase by 5 dB since they are caused by $a_5\left[X_1(t)+X_2(t)\right]^5$ in equation 5.2.

A popular method of determining the “linearity” of a frequency mixer is the "third-order intercept" approach [1]. The Third-Order Intercept Point is a theoretical point on the RF input versus IF output curve where the desired output signal and third order products become equal in amplitude as RF input is raised.

For a down-converter, the RF power is the input and as the RF signal increases by 1 dB, the 3IM distortion component increases 3 dB. The Third Order Intercept Point is determined by increasing the RF level and noting both the desired and the 3IM levels. The third order intercept point is the point where the extension of the plotted desired output and 3IM output level versus RF input meet, as shown in figure 5.5. The corresponding level on the horizontal, input, axis (RF) is the third order input intercept point (IIP3) and the corresponding level on the vertical, output, axis (IF) is the third order output intercept point (OIP3). Sometimes the input, output or both is implied and just IP3 is used. The difference is the conversion loss. It is not possible to drive the mixer to those RF levels. As a rule of thumb the third order intercept point is about 8 to 10 dB above the LO level for a typical diode based double balanced mixer and up to 15 dB above the LO

level for passive FET mixers. Passive FET mixers however have a much narrower bandwidth.

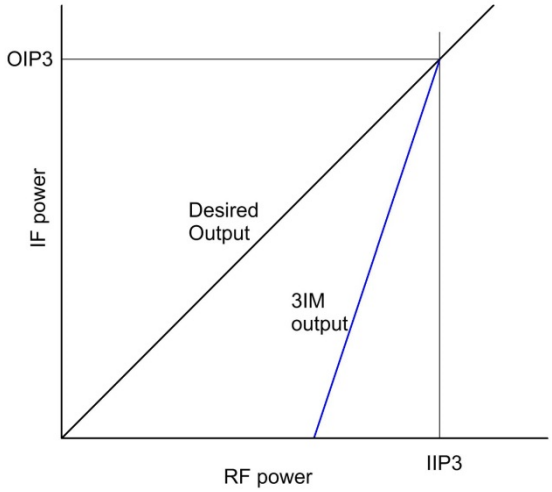



Figure 5.5. Third order input and output intercept points.

The third order intercept point is useful in determining the RF level required for a specified 3IM distortion performance. If for example, the 3IM signal is to be 40 dB below the required signal, then the RF level must be 20 dB below the Third Order Intercept Point, since then the desired signal will be 20 dB below the intercept point and the 3IM signals will be 3*20 = 60 dB below the intercept point.

## *LO Level*

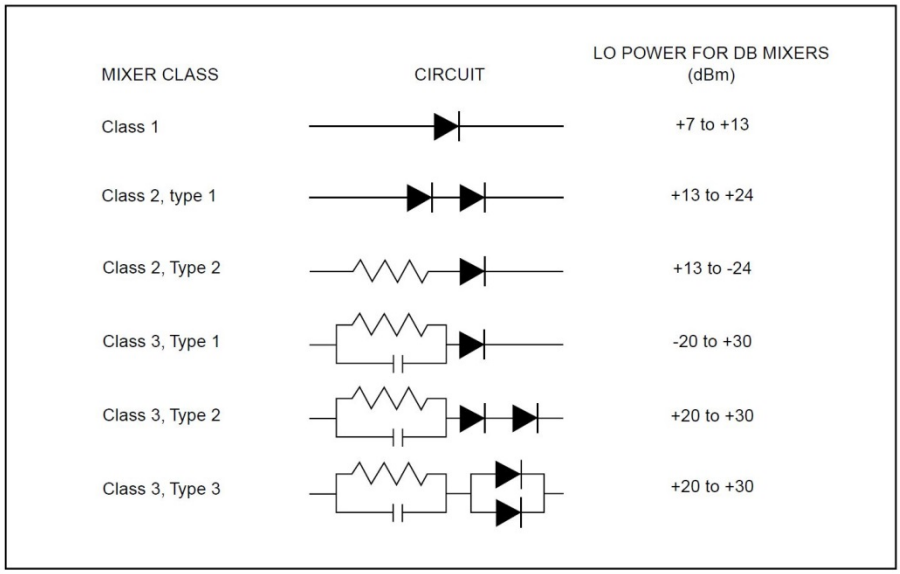



Figure 5.6. Different diode configurations for different mixer levels [3].

Frequency mixer manufacturers make mixers to operate at different LO power levels. For standard level mixers, the LO power required is +7 dBm. Other mixer power levels are +10, +13, +17, +23, +27 dBm. Mini-Circuits [1, 2] denote their mixer according to the LO power required, so a Level 7 mixer requires a LO power of +7 dBm. For a good Double Balanced Mixer, the third order IIP3 is 10 dB above the LO level. By having a higher power level available, the manufacturers are able to control the diode I-V

characteristics more to ensure that the $a_2$ coefficient in the binomial expansion of the diode I-V characteristic shown as equations 5.1, 5.2, 5.7 and 5.8 is maximized in relation to the other terms, thus minimizing the unwanted components. Figure 5.6 by Bert Henderson shows how diodes can be arranged in different ways [3], to obtain these different mixer LO levels. These diode models can be implemented in AWDE to investigate the different mixer LO levels.

### *Example 5.1: Mixer LO Level Calculation*

A maximum RF input signal of -10 dBm and a level of third order intermodulation products (3IM) of 60 dB below the desired signals is required for a specific application. For a typical 7 level mixer, the IIP3 point is +17 dBm. The RF signal at -10 dBm is thus 27 dB below the IIP3 point. This will result in the 3IM signals being (3-1)*27= 54 dB below the wanted signal.

Similarly, a level 10 mixer will result in the 3IM signals being (3-1)*30 = 60 dB below the wanted signals, a level 13 mixer will result in the 3IM signals being (3-1)*33 = 66 dB below the wanted signals. A level 17 mixer will result in the 3IM signals being (3-1)*37 = 74 dB below the wanted signals. A level 23 mixer will result in the 3IM signals being (3-1)*43 = 86 dB below the wanted signals and a level 27 mixer will result in the 3IM signals being (3-1)*47 = 94 dB below the wanted signals. The higher the LO level, the higher the cost of the mixer. A level 10 mixer with thus be the lowest cost device, which will satisfy the specifications.

## Ideal Multiplier

An ideal multiplier is a perfect mixer and its performance is a good measure for the evaluation of the different mixers in the following sections. To enable the comparison to be made, the same input conditions are used for the multipliers and all the mixers in the following sections. Figure 5.7 show the circuit schematics for ideal multipliers for down-conversion (left) and up-conversion (right).

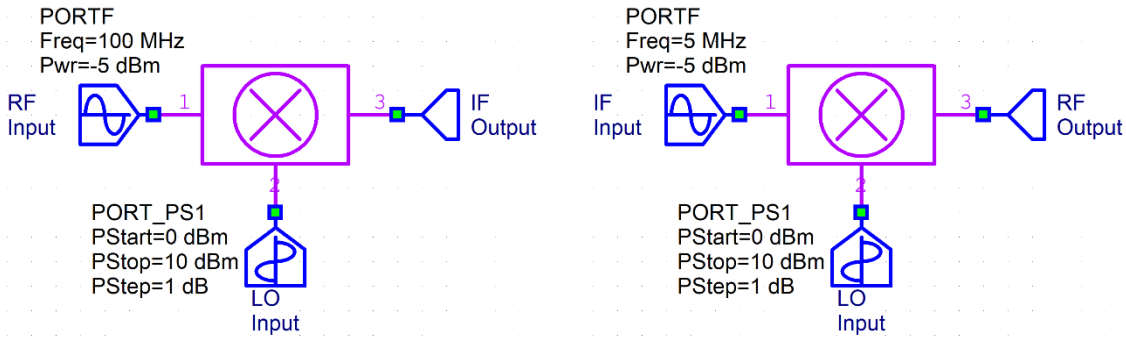



Figure 5.7. Schematics for Multipliers as mixers.

If $V_A$ is the LO voltage, A is ($\omega_{LO}t$) , $V_B$ is the IF voltage and B is ($\omega_{IF}t$), the multiplication process will generate sum and difference frequencies, as shown in equation 5.6.

$$V_A Cos(A) \times V_B Cos(B) = \frac{1}{2} V_A V_B \{Cos(A-B) + Cos((A+B)\} \quad \text{Eqn. 5.6}$$

From equation 5.6 the conversion loss is proportional to the LO power level, resulting in LO AM noise appearing in the IF or RF output signals. That is not desirable. A conversion loss that is not dependent on the LO power level will produce cleaner IF or RF signals.

The output spectra for the multipliers of figure 5.7 are shown in figures 5.8. Only the sum and difference frequency components are visible in the output spectra. The corresponding waveforms are shown in figures 5.9 and 5.10.

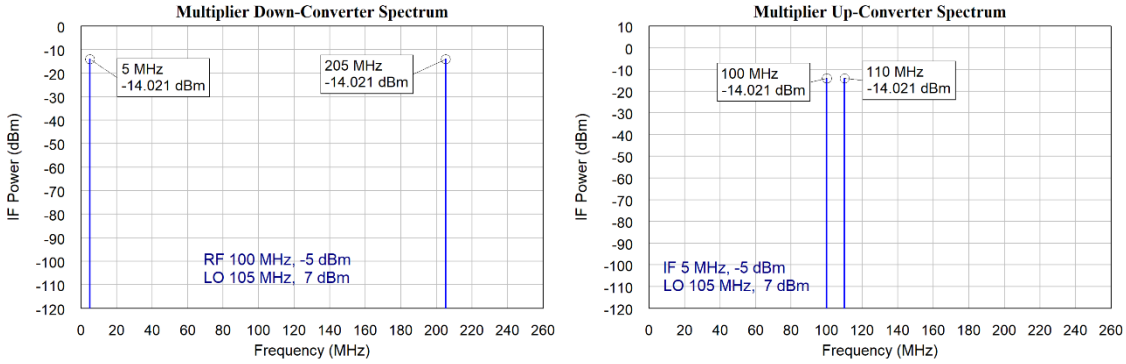



Figure 5.8. Output spectrum of a multiplier, down-converter (left) up-converter (right).

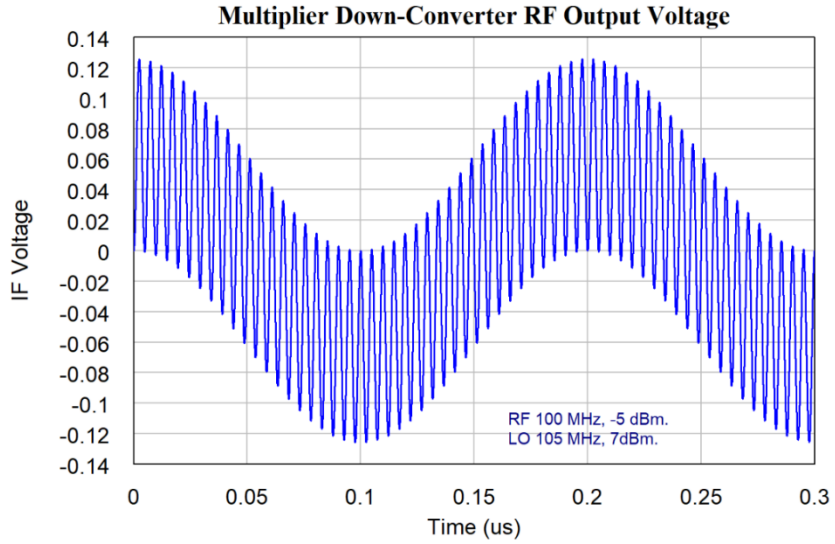



Figure 5.9. Down-converter voltage of a multiplier

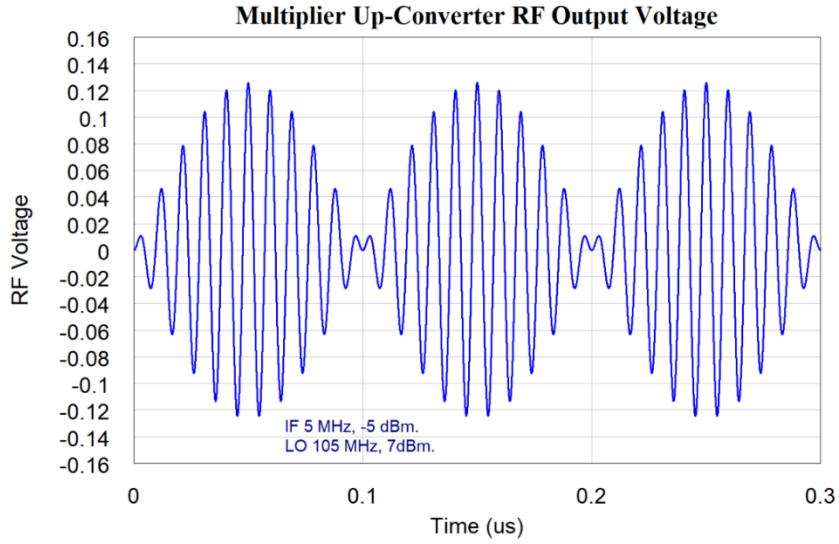



Figure 5.10. Up-converter voltage of a multiplier

## Single Diode Mixer

Single diode mixers use a single diode to produce the required frequency components.

Single diode mixers are often used in cost critical applications, such as Radio or TV receivers, where the low cost is more important than good performance. With the advent of low cost active mixer IC's, single diode mixers are progressively being used less. Single diode mixers are very suitable for microwave applications like speed guns and shopping centre door openers, where the transmitted signal is used as the LO for the received signal, and the receiver diode is simply mounted in the antenna horn. The resulting IF signal is the difference frequency, which is due to the speed of the car being detected or the speed of the person moving towards the door.

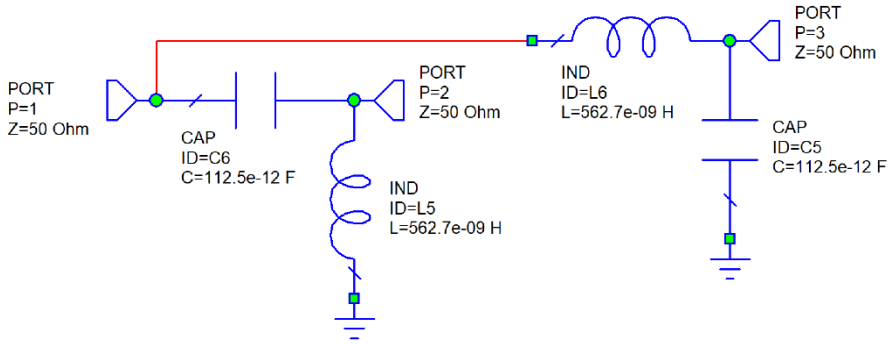



Figure 5.11. Low return loss diplexer circuit.

A single diode mixer requires a diplexer to separate the high frequency RF and LO signal from the low frequency IF signal. Since the single diode mixer is normally a lower cost consumer type application, the diplexer is normally kept simple with either a first or second order high pass and low pass filters.

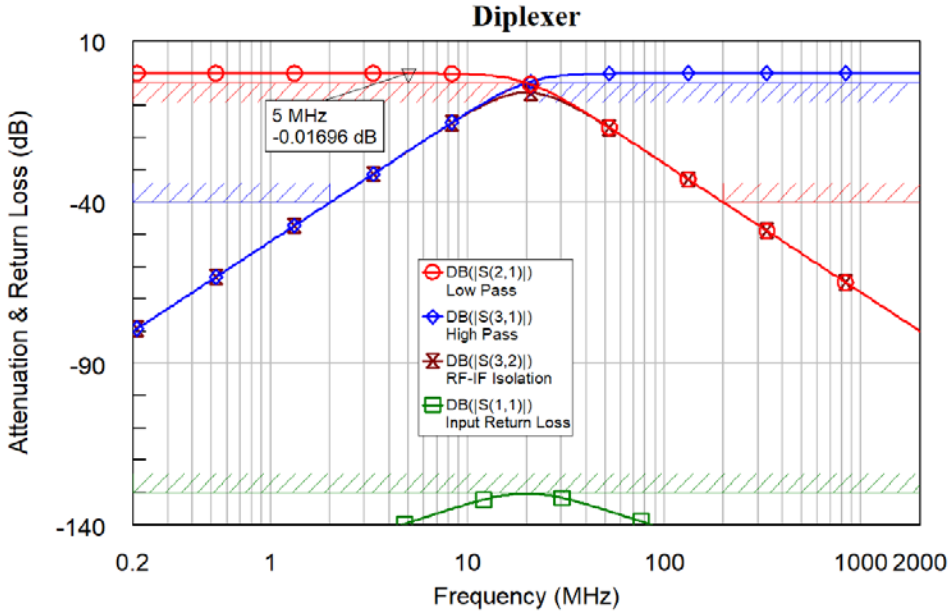



Figure 5.12. Frequency response of low return loss diplexer after optimisation.

Figure 5.11 shows a simple diplexer consisting of second order high pass and low pass filters. The crossover frequency is a compromise with a lower corner frequency of the low pass filter removing more LO and RF signals from the IF signal but causing an loss

at the IF frequency and thus increasing the conversion loss. In the following designs a 20 MHz corner frequency is chosen, allowing baseband signals up to 5 MHz to be used, with <0.02 dB loss. To obtain the best impedance looking into port 1, series elements are required to connect to port 1. A Butterworth high pass and low pass filter design is a good starting point and optimisation to provide a low S11 return loss, as is done in example 2.2 and figures 2.8 to 2.15 can be used to improve the impedance match for the mixer diodes. This S11 optimisation results in a 0.575 dB improvement in conversion loss for the single diode mixer and 0.2365dB improvement in conversion loss for the balanced mixer, compared with the Butterworth filters. These optimised values are used in the single diode and balanced mixer circuits of figures 5.13, 5.22 and 5.25.

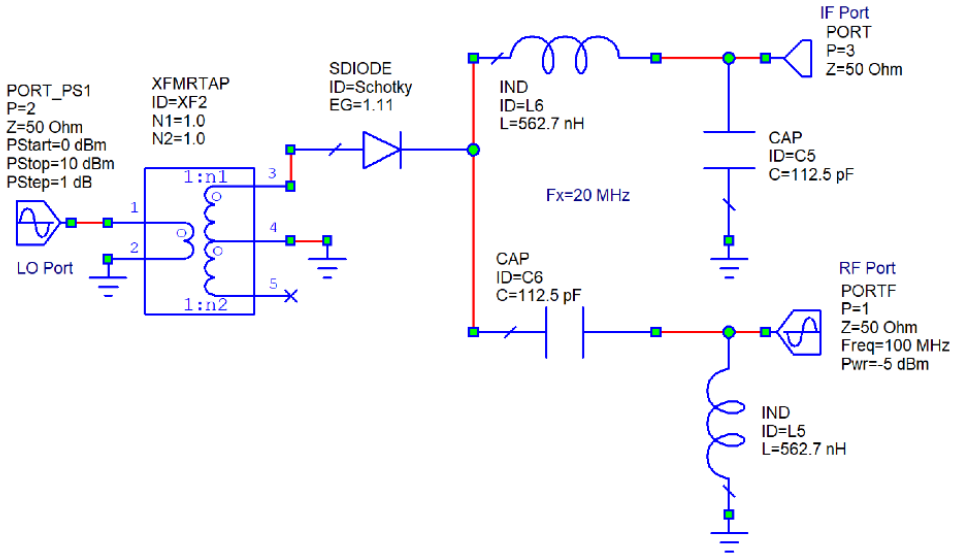



Figure 5.13. Circuit diagram of a single diode mixer as a down-converter.

Figure 5.13 shows the circuit diagram of a single diode mixer. The transformer is normally not included in the circuit, since in this case it is simply a non-inverting transformer. It is included here to illustrate the differences between the single diode mixer of figure 5.13 and the balanced mixer of figure 5.25.

The mixing behaviour of a single diode mixer can be demonstrated by considering the current flowing through the diode of figure 5.13. The current can be expressed as:

$$I_a = a_0 + a_1 V_a + a_2 V_a^2 + a_3 V_a^3 + a_4 V_a^4 + a_5 V_a^5 + \mathrm{K} \qquad \text{Eqn. 5.7}$$

If two voltages $V_a$ and $V_b$ are now applied to the diode, due to the LO and the RF signals, then the current will be

$$I_a = a_0 + a_1(V_a + V_b) + a_2(V_a + V_b)^2 + a_3(V_a + V_b)^3 + a_4(V_a + V_b)^4 + a_5(V_a + V_b)^5 + \mathrm{K} \qquad \text{Eqn. 5.8}$$

The term $a_2(V_a + V_b)^2 = a_2(V_a^2 + 2V_aV_b + V_b^2)$ contains the required $2a_2V_aV_b$, which results in the sum and difference frequencies. All the other terms cause unwanted frequency components. It is thus desirable to use diodes with an I-V characteristic where $a_2$ is large in comparison with the other terms in the binomial expansion of the I-V characteristic. Some of the additional frequency components due to the $a_3$, $a_4$ and higher order diode nonlinearities, can fall close to the desired frequency thus causing an interference.

# Computer Simulation of Mixers

The advanced RF Computer simulation programs like MWO and ADS allow frequency mixers to be simulated accurately. A frequency mixer requires two inputs, both at different frequencies and the output is normally at a frequency that is different from both the inputs to the mixer. The simulation is thus very different from that of a linear device, like a transformer, hybrid or filter.

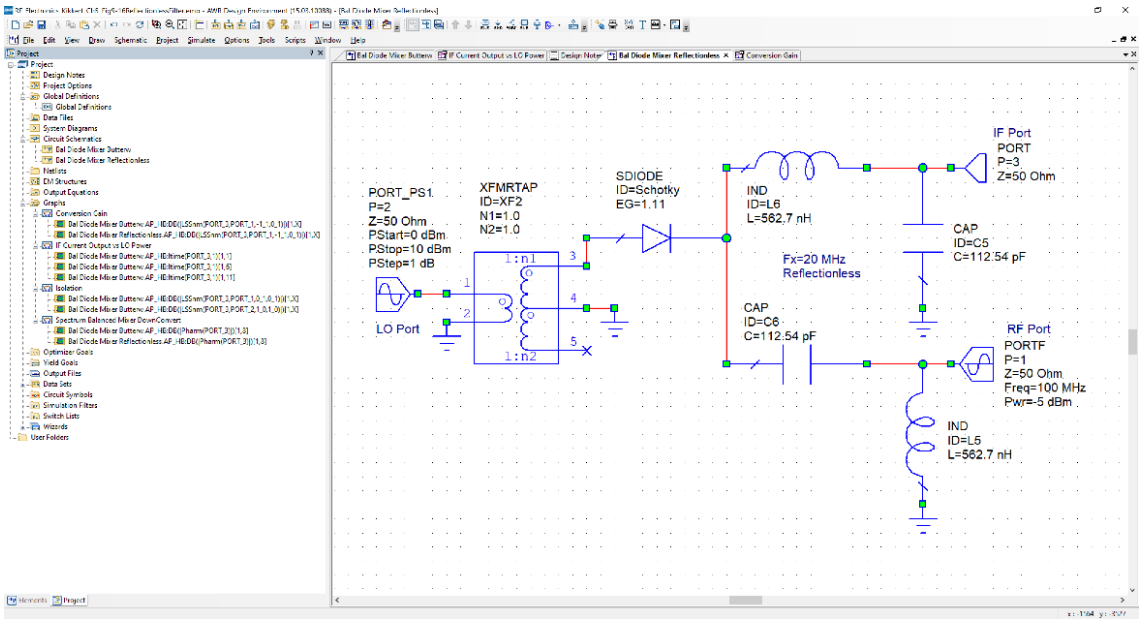



Figure 5.14. Typical Measurements for a mixer.

The Project Options menu sets the frequencies used for the simulation. For the single diode mixer of figure 5.13 and 5.14, these frequencies are used by the PORT_PS1 port element, which is applied to the LO port (Port 2). The PORT_PS1 element allows the signal power to be varied as specified by the parameters for the PORT_PS1 element. A PORTF element produces a single tone signal with frequency and power level set by the parameters for that element. For a down-conversion mixer, the PORTF element is applied to the RF port. The RF simulation will then use these frequency and power levels to determine the time waveforms at the IF port, using a SPICE modelling of the diode and the circuit. Figure 5.15 shows the project frequency and typical measurements settings used for the mixer measurements to figure 5.41.

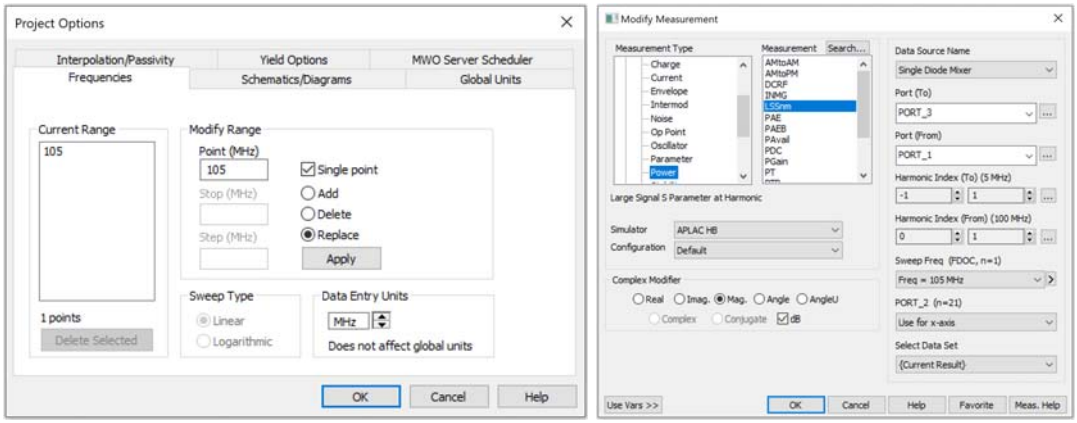



Figure 5.15. Project frequency and parameters for conversion loss measurements.

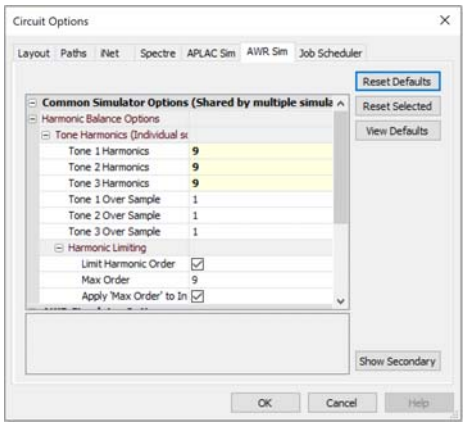



Figure 5.16. Setting the number of harmonics used in Harmonic Balance analysis.

The conversion gain or loss is the most important mixer parameter. When determining the conversion loss of a mixer, it is important to include many harmonics and IM products, say up to the 7th or 9th order in the Harmonic Balance (HB) analysis, as shown in figure 5.15. The number of harmonics can be set using *Tools →Circuit Options*. Even though most of these IM products will fall outside the frequency range of interest, there will still be some falling inside the required bandwidth and will this affect the accuracy of the results produced by the simulation. If in doubt, simply increase the order of the harmonics and IM to be analysed and note any changes in the simulated results. As the speed of computers and the efficiency of the Harmonic Balance calculations increases, there is less cost in erring on the side of calculating an excess of harmonic and IM components. For the figures in this chapter, the Harmonic Balance settings use 9 harmonics for tone 1, tone 2 and tone 3 are used for the HB analysis. Different spectra result, when these values or the default values are used and when APLAC HB or Harmonic Balance (legacy) are used and when the harmonic order is limited to 9 orders or is not limited. Those changes can easily be observed and only effect small IM amplitudes. The current edition of this book uses the APLAC HB simulator, since the Harmonic Balance simulator that was used in the 2013 edition is now a legacy product.

The conversion loss of the mixer can be determined as the LO power level is varied, by setting the relevant parameters of the PORT_PS1 element to provide a power level sweep at the LO port. The sum or difference frequency that is analysed for determining the conversion loss is set by the parameters for the Large Signal S parameter (LSSnm) measurement shown in figure 5.15. The conversion loss is determined as the ratio of the power levels at the specified frequencies of port 1 as input and port 3 as output.

For a realistic determination of performance of the frequency mixer, a LO frequency of 105 MHz (as set by the project frequency setting in figure 5.15 and an RF frequency of 100 MHz with a level of -5 dBm (as set by PORTF) is chosen. The project frequency is set as a single frequency for speed of simulation. If a range of frequencies is specified, then one or all of these can be used for the conversion loss or spectral output calculations. It is thus possible to determine the conversion loss for a range of LO frequencies as well. For a LO input at 105 MHz and an RF input at 100 MHz, the desired IF output is at 5 MHz. The appropriate harmonic index combinations are selected such that the input is at 100 MHz and the output is at 5 MHz, as indicated in figure 5.15. MWO automatically calculates the relevant frequency as the harmonic indices are changed.

Figure 5.17 shows the resulting conversion loss as a function of LO power level for the single diode mixer of figure 5.13. Note that the conversion loss decreases with an

increasing LO drive level. A higher LO power level increases the power consumption of the mixer, requires a higher power LO source and dissipates more heat. By comparing figures 5.17, 5.26 and 5.34, it can be seen that the conversion loss of the single diode mixer is very poor.

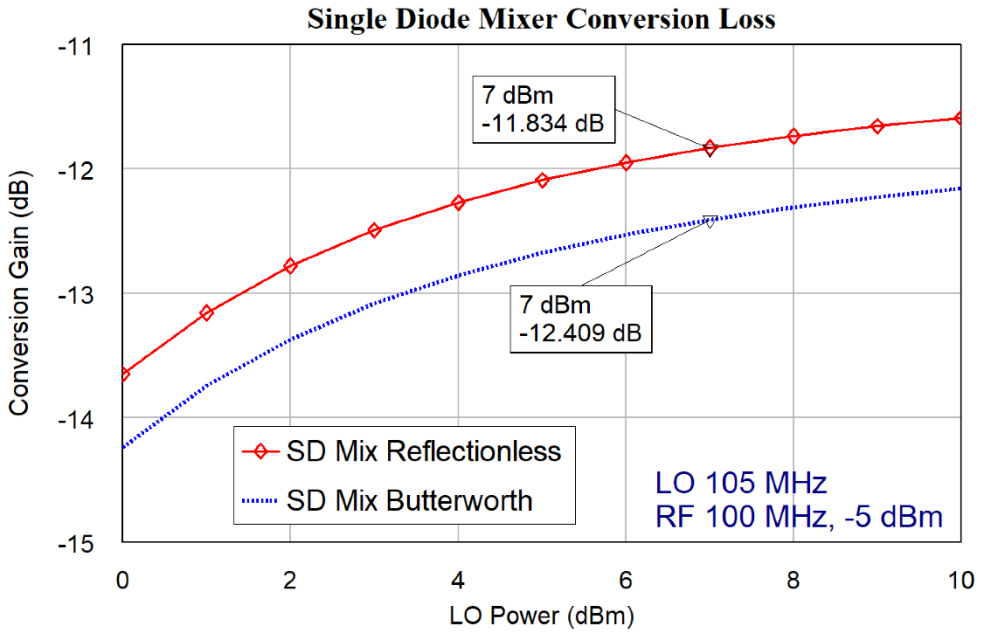



Figure 5.17. Conversion loss of a single diode down-conversion mixer.

The IF spectrum can be determined using the Frequency Domain Power Measurement shown in figure 5.18. The waveform at the IF port is determined using the harmonic balance simulator. The spectral components are determined from that waveform. Figure 5.19 shows the resulting IF spectrum for an input power at the LO port of +6 dBm. It is possible to select other values or to plot the spectra for a sweep of power values.

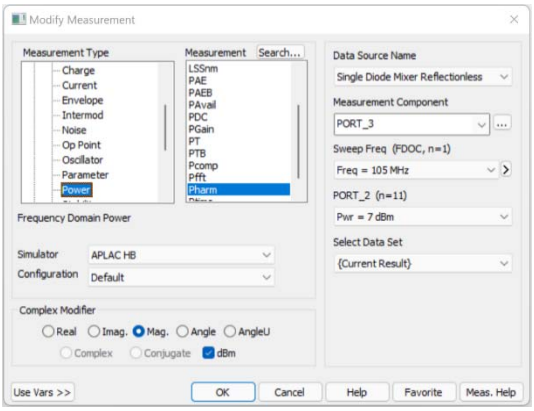



Figure 5.18. Frequency domain power measurement.

In figure 5.19, the desired 5 MHz component is -16.6 dBm. Since the RF signal is -5 dBm, the conversion loss is 11.6 dB. The LO signal at 105 MHz is 7 dBm and the LO signal at the IF port is -30.26 dB. The LO to IF isolation is thus 37.26 dB. The RF signal at 100 MHz signal is -5 dBm and the RF signal appearing at the IF port is -28.66 dBm. The RF to IF isolation is thus 23.66 dB. Comparing this with figure 5.8(left) for the multiplier, shows that the single diode mixer produces a large number of unwanted components. Since the IF bandwidth is 20 MHz, it is not possible to filter out the unwanted 10 MHz,

15 MHz and 20 MHz components. Comparing figure 5.19 with figure 5.22 for the balanced mixer, and figure 5.30 for the double balanced mixer, shows that the conversion loss, the levels of the harmonics and the isolation produced by the single diode mixer are significantly worse than those of balanced mixers.

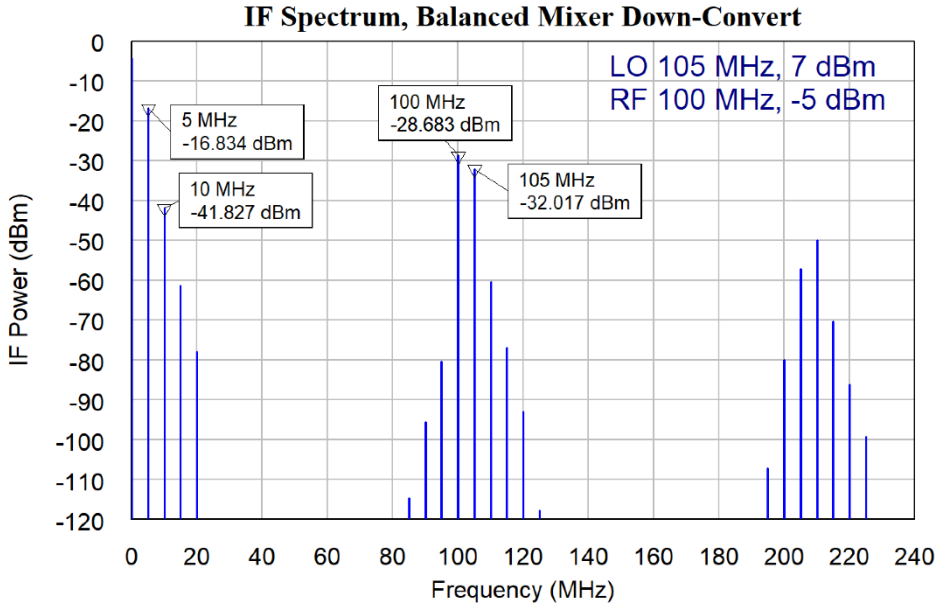



Figure 5.19. IF spectrum of a single diode mixer as a down-converter.

If a two-tone RF input signal is used, the single diode mixer has a high level of IM components. As a result, the single diode mixer requires more stringent RF filtering to avoid those IM signals being generated by the mixer and appearing in the IF output. The single diode mixer also requires more stringent IF filtering to remove those unwanted IF components from the IF signal, to prevent the unwanted signals from affecting the demodulated output from the receiver. Most AM radios use single diode mixers and this is one reason why their performance is poor compared to FM radios.

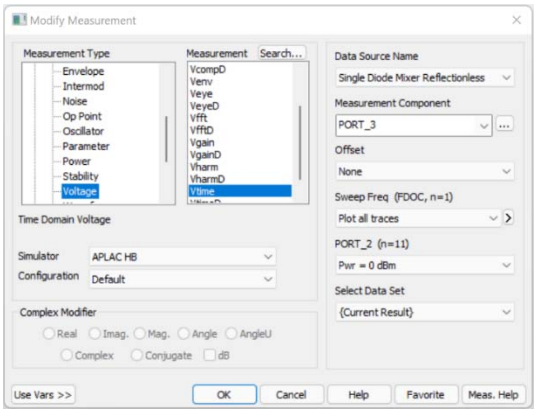



Figure 5.20. Vtime measurement setting.

The voltage and current time waveforms can also be determined, using the Vtime and Itime measurements. The measurements can be done at a single LO power level or at a range of levels as is done by selecting plot all traces instead of the 0 dBm level in the Port_2 entry of the Vtime measurement window shown in figure 5.20. Alternately, as has been done in this project, a limited power sweep can be obtained by performing multiple single level measurements as shown in figure 5.21.

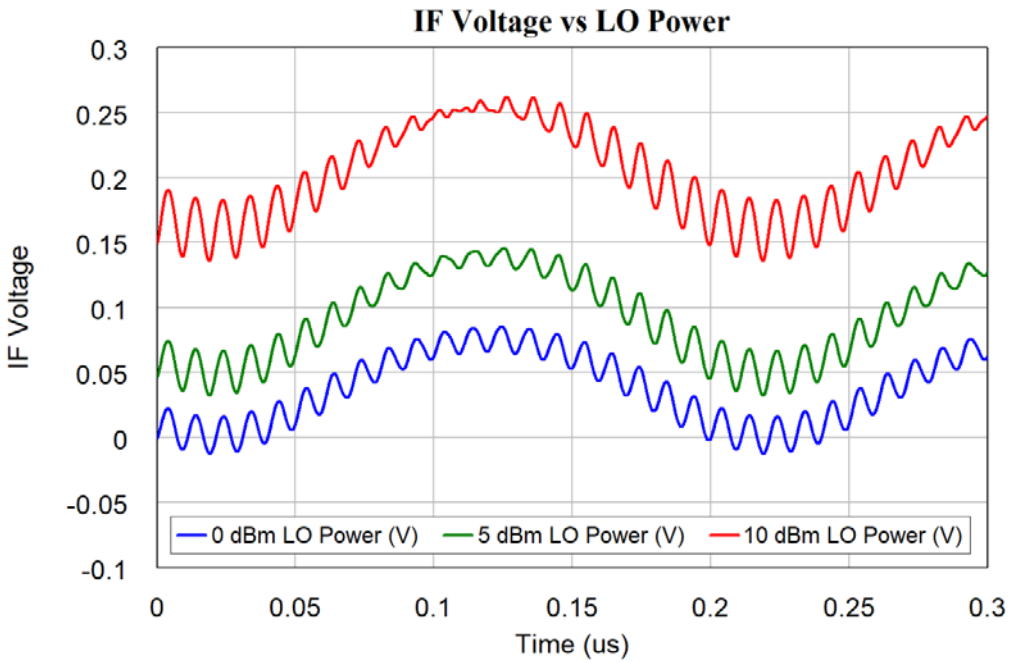



Figure 5.21. IF voltage for a single diode mixer as a down-converter.

Figure 5.21 shows the resulting IF voltage of a single diode mixer, notice with the 2nd order filters used in the diplexer, there is still significant RF voltaget components present in the IF signal. A higher order filter will improve the isolation, but will not improve the performance sufficiently to justify the additional cost. For the frequencies used, the output spectra and conversion loss will be the same if higher order diplexer filters are used. As can be seen from figure 5.21, the single diode mixer has a significant DC voltaget component, which changes with LO drive level.

To operate the frequency mixer as an up-converter, the PORTF element is applied to the IF port and the signal generated by that port is set to 5 MHz and a power of -5 dBm. The mixer output is then at the RF port. Figure 5.22 shows the resulting circuit diagram for the single diode mixer as an up-converter. The same measurements can be performed for the down-converter.

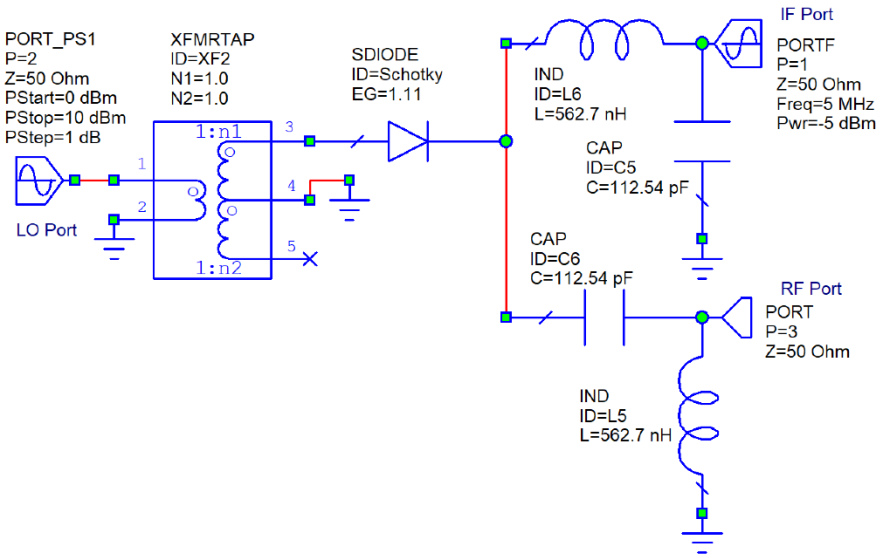



Figure 5.22. Circuit diagram of a single diode mixer as an up-converter.

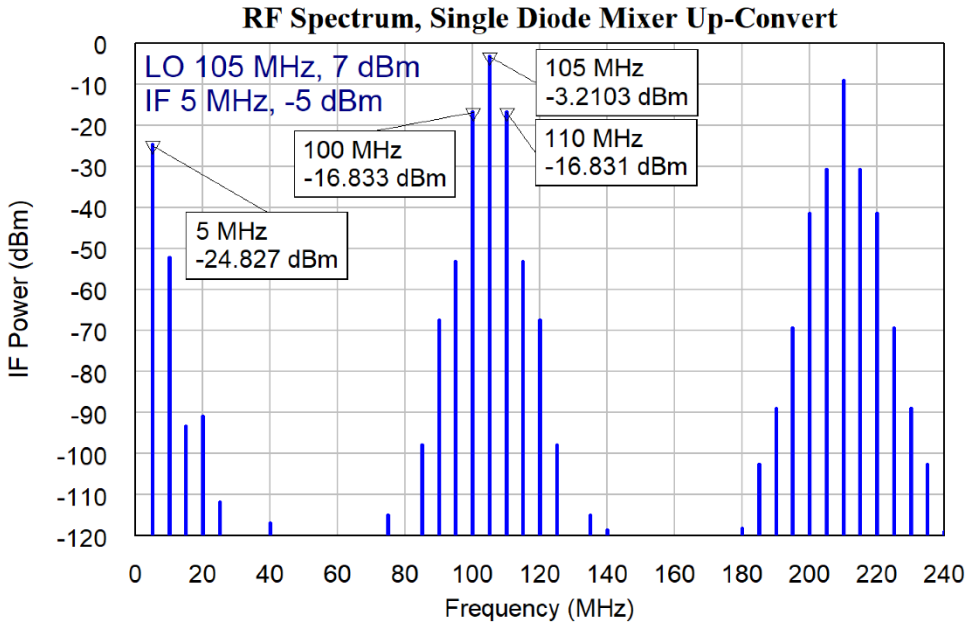



Figure 5.23. RF spectrum of a single diode mixer as an up-converter.

The RF output spectrum is shown in figure 5.23. From this spectrum, it can be seen that the conversion loss, being the amplitude of the 100 MHz RF component due to the 5 MHz IF signal is the same as for the down-converter. The components around 100 MHz show a large 105 MHz LO component in the RF output, indicating only a 7+3.2 = 10.21 dB LO-RF isolation. The LO spectral component at the RF port is larger than any of the wanted components. The second harmonic components at 90 MHz and 110 MHz are slightly asymmetrical. There are significant components at harmonics of the LO frequency, which must be filtered out in most practical applications.

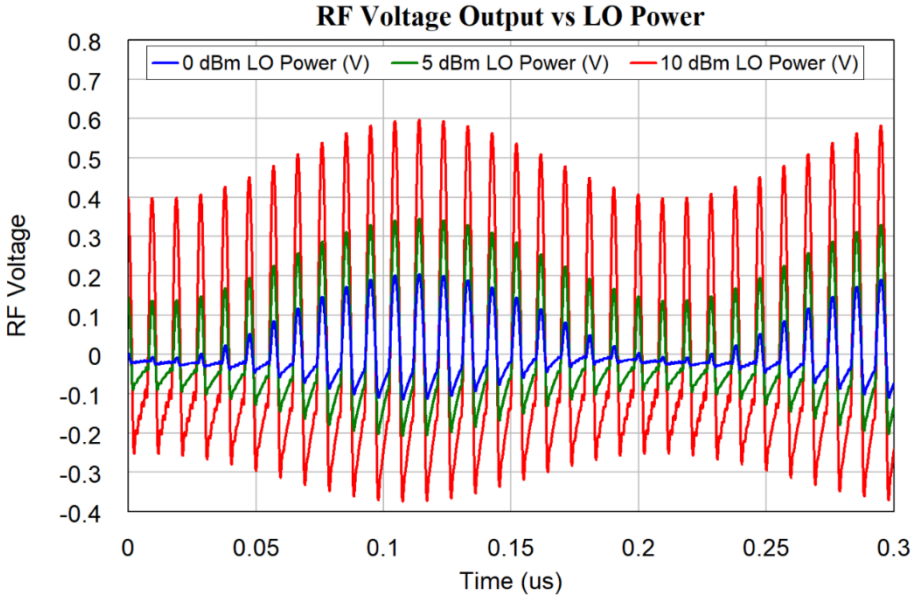



Figure 5.24. RF voltage for a single diode mixer as an up-converter.

The RF voltage waveforms can be determined using the Vtime measurement in a similar manner as for the down-converter shown in figure 5.21. The results for the up-converter are shown in figure 5.24 and are highly asymmetrical. The waveform is rich in harmonics as can be seen from the spectrum of figure 5.23.

**Advantages of single diode mixers:**

1. They can be used at very high (microwave) frequencies.
2. They have a low cost, using only one diode.

**Disadvantages of single diode mixers:**

3. They have a high conversion loss.
4. A high level of unwanted components are generated. These must be filtered out using additional circuitry.
5. There is no RF to LO isolation, IF to LO and IF to RF isolation only due to diplexer.

## Balanced Mixer

Adding a second diode to the circuit shown in figure 5.25 results in a balanced mixer. The first diode has $V_a$+$V_b$ across it and the second diode has $V_a$-$V_b$ where voltage $V_a$ is the LO and $V_b$ is the RF voltage. The currents through the diodes are thus:

$$I_{D1} = a_0 + a_1(V_a + V_b) + a_2(V_a + V_b)^2 + a_3(V_a + V_b)^3 + a_4(V_a + V_b)^4 + a_5(V_a + V_b)^5 + \mathrm{K} \quad \text{Eqn. 5.9}$$

$$I_{D2} = a_0 + a_1(V_a - V_b) + a_2(V_a - V_b)^2 - a_3(V_a - V_b)^3 + a_4(V_a - V_b)^4 + a_5(V_a - V_b)^5 + \mathrm{K} \quad \text{Eqn. 5.10}$$

The difference between the diode currents flows into the IF port and RF port, so that the current flowing through the IF and RF port is:

$$I_{IF-RF} = I_{D1} - I_{D2} = +2a_1V_b + 4a_2V_aV_b + 6a_3V_a^2V_b + 2V_b^3 + 8a_4(V_a^3V_b + V_aV_b^3) + 10a_5V_a^4V_b + 20a_5V_a^2V_b^3 + 2a_5V_b^5 + \mathrm{K} \quad \text{Eqn. 5.11}$$

For a single diode mixer the current through the IF and RF port is the same as is shown in equation 5.9. Comparing equation 5.11 with equation 5.9, shows that most of the unwanted components cancel. The only components that are in the IF band are:

$$I_{IF} = 4a_2V_aV_b + 8a_4(V_a^3V_b + V_aV_b^3) + \mathrm{K} \quad \text{Eqn. 5.12}$$

Which is close to ideal multiplication as the $a_4$ term is normally very small.

Since the LO voltage, $V_a$ >> the RF voltage, $V_b$ , the $V_aV_b$ and the $V_a^3V_b$ terms dominate. The $V_b$ and the $V_a^2V_b$ terms do not produce any frequency components in the region of interest. For an ideal frequency mixer one wants the a, c, d and e components to be as small as possible, the manufacturers of mixers ensure their diodes satisfy this as much as possible. The balanced mixer will thus have a much better performance than the single diode mixer.

The circuit diagram of the balanced mixer is shown in figure 5.25. The only difference between that and the circuit for the single diode mixer of figure 5.13 is the use of the second diode, having the second diode results in a significant performance improvement.

The conversion loss of the frequency mixer is shown in figure 5.26. This shows that the reflectionless configuration of the RF/IF diplexer improves the conversion loss. The conversion loss is far less than that of a single diode mixer. For LO levels of around 7 dBm, any variation in LO power does not cause any change in conversion loss, so that

the mixer is then very insensitive to AM noise of the LO. This is an important advantage of the balanced mixer over the single diode mixer, or even the ideal multiplier of figure 5.7 or the Frater-Gilbert Cell mixer shown in figure 5.76 – 5.87 later in this chapter.

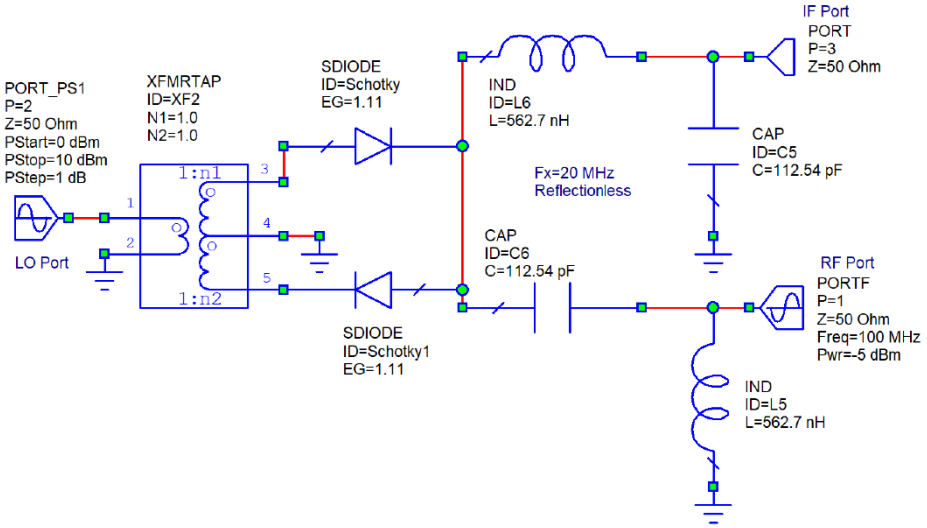



Figure 5.25. Circuit diagram of a balanced mixer.

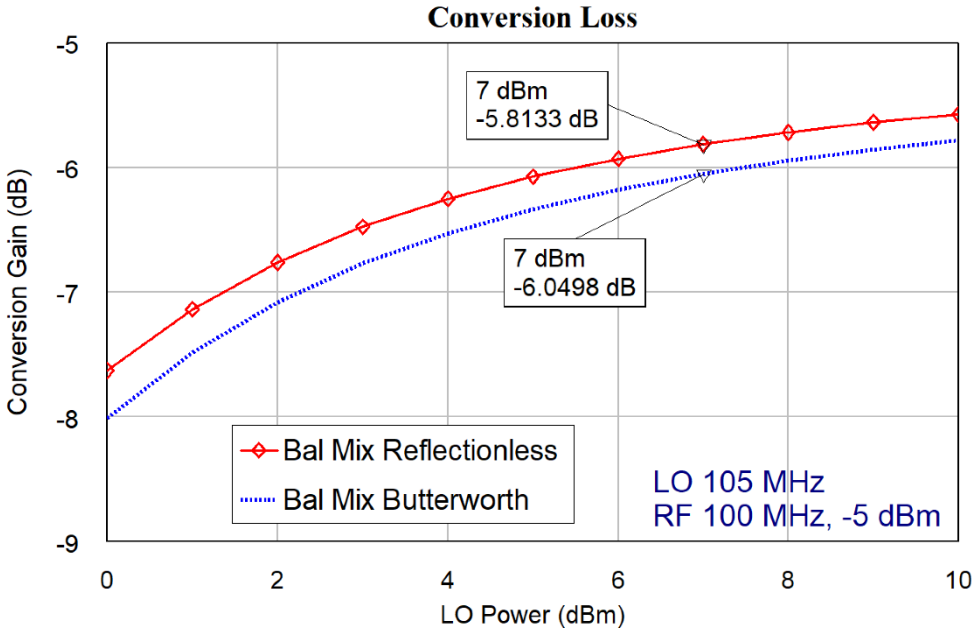



Figure 5.26. Conversion gain of a balanced diode mixer.

Figure 5.27 shows the IF spectrum of the balanced mixer. As expected from the equation 5.11, many of the unwanted spectral components have significantly reduced amplitudes compared with the single diode mixer. The difference in amplitude of the 5 MHz and 205 MHz components is due to the low pass filter at the IF port in figure 5.25. A higher order filter will attenuate the components above 20 MHz more. Figure 5.27 shows that the level of unwanted components above 80 MHz for the reflectionless filter are slightly higher, since the Butterworth Low pass filter has a higher attenuation at those frequencies than the reflectionless filter. Table 5.1 shows how each component in figure 5.27, relates to the 105 MHz LO and the 100 MHz RF frequencies. The third harmonic of the desired IF signal, at 15 MHz, is caused by the mixing process and is about 45 dB below the desired

5 MHz signal. The LO signal appearing in the IF spectrum is extremely small (-304.8 dB in the figure 5.27 data). Bert Henderson shows that these harmonic levels depend on the diodes class [3], which determines the mixer LO level required. The isolation depends on how well the diodes are matched. In the computer simulation, the diodes are identical. In hardware, this is not the case.

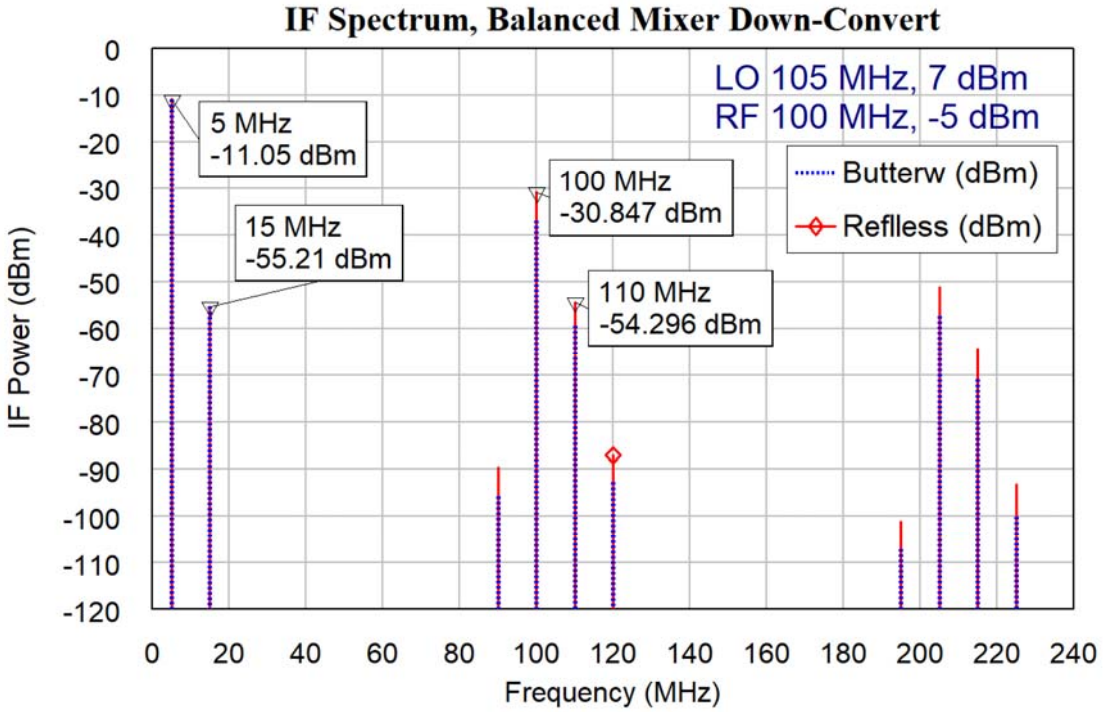



Figure 5.27. IF spectrum of a balanced diode mixer as a down-converter.

Table 5.1 Frequency components of figure 5.27

| Frequency MHz | Down Convert Due to | Up Convert Due to |
|---|---|---|
| 5 | LO-RF | IF |
| 15 | 3*(LO-RF) | 3IF |
| 25 | 5*(LO-RF) | 5IF |
| | | |
| 80 | | LO-5IF |
| 90 | 2RF-LO | LO-3IF |
| 100 | RF | LO-IF |
| 110 | 2LO-RF | LO+IF |
| 120 | 4LO-3RF | LO+3IF |
| 130 | | LO+5IF |
| | | |
| 185 | | 2LO-5IF |
| 195 | 3RF-LO | 2LO-3IF |
| 205 | RF+LO | 2LO-IF |
| 215 | 3LO-RF | 2LO+IF |
| 225 | 5LO-3RF | 2LO+3IF |
| 235 | | 2LO+5IF |

The RF signal appearing at the IF port is -30.847 dBm. Since the RF signal is -5 dBm, the RF to IF is isolation is 25.847 dB. This can only be improved by using a higher order diplexer as part of the mixer, or by using another mixer configuration like the double balanced mixer.

Figure 5.28 shows the IF voltage for the balanced mixer and it can be seen that the waveforms are much more like a pure sine wave than the corresponding waveforms for the single diode mixer. With the second order filters used in the diplexer, there are still some RF signals present at the IF output but they are small enough not to cause any problems. As expected from equations 5.11 and 5.12, the balanced diodes mixer has no DC signal at the IF port, in contrast to the single diode mixer.

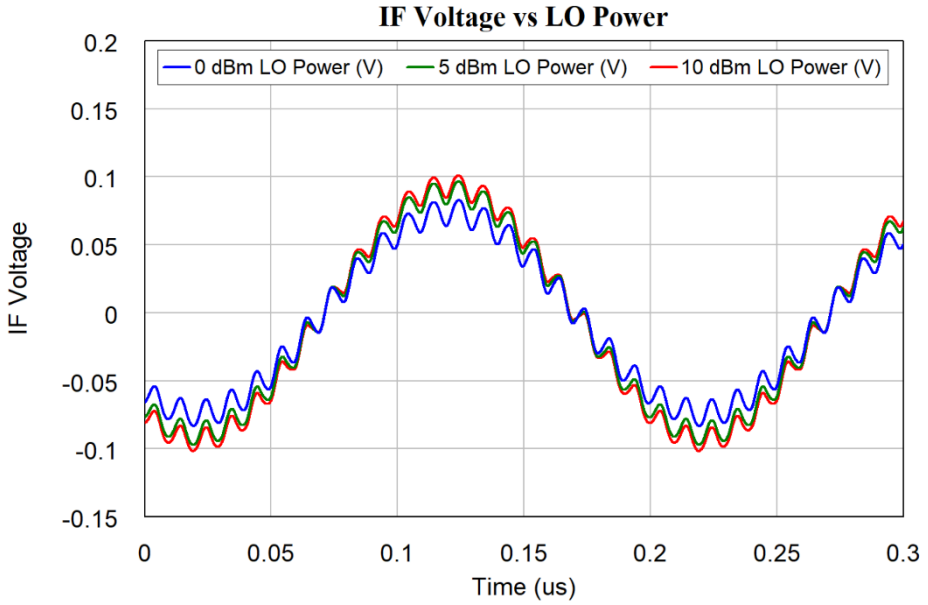



Figure 5.28. IF voltage for a balanced diode mixer as a down-converter.

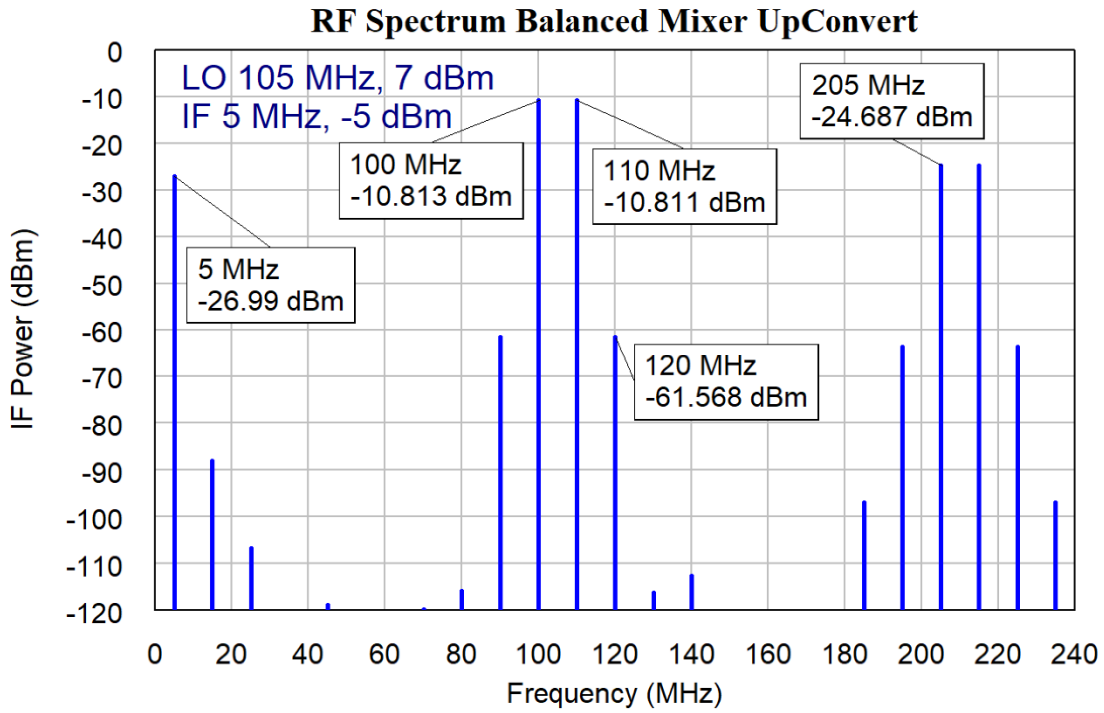



Figure 5.29. RF spectrum of a balanced diode mixer as an up-converter.

Figure 5.29 shows the performance of the balanced mixer as an up-converter. The relationship between the spectral components and LO and IF frequencies are shown in table 5.1. It can be seen that a near ideal frequency mixer performance is obtained, with all the unwanted components more than 40 dB below the wanted components. This is good enough for practical applications. The 3IM components increase 3 dB for every 1 dB increase in the RF and IF levels. The RF level can thus be varied to obtain the specified 3IM performance, thereby maximising IF signal and the dynamic range. The LO feed-through at the RF port can be minimised by adding a very small DC signal to the IF port and adjusting that DC signal to cancel the LO signal at the RF port. This cancellation is temperature dependent, since the diode characteristics change slightly with temperature.

Figure 5.30 shows the RF voltage for the balanced mixer. These waveforms resemble the ideal multiplier waveforms shown in figure 5.10. The results from the simulation closely agree with those obtained in practice. There are however still some IF components present, which are due to the limited RF-IF isolation caused by the diplexer. The Double Balanced mixer overcomes those limitations.

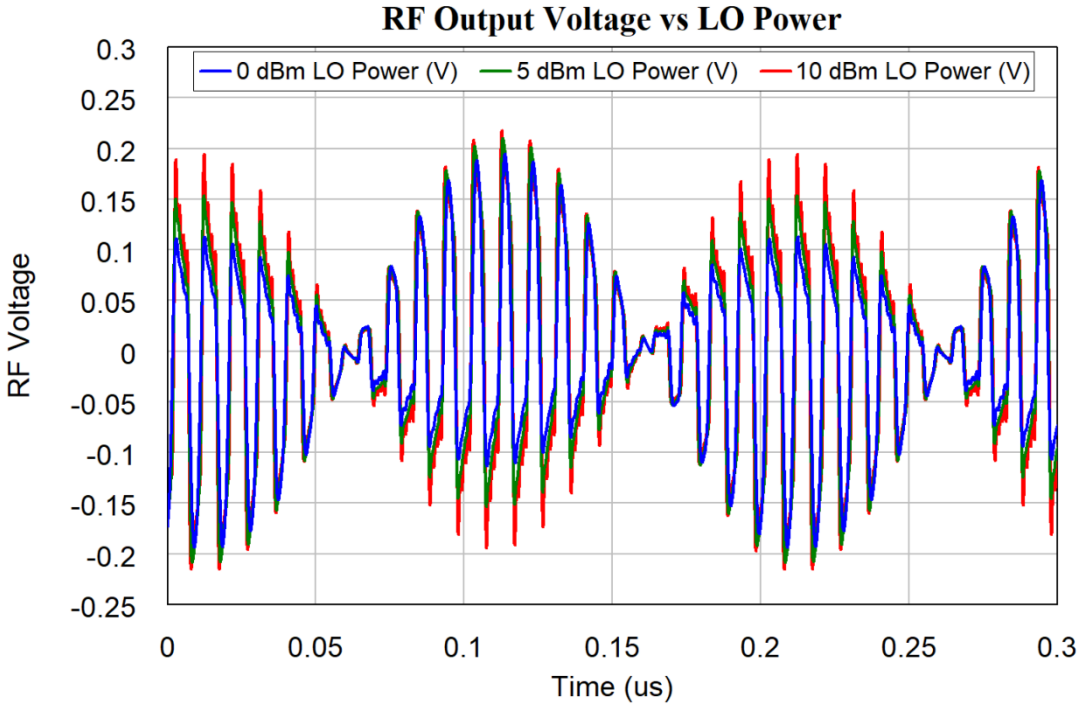



Figure 5.30. RF voltage for a balanced diode mixer as an up-converter.

## Double Balanced Mixer

The Double balanced mixer (DBM), together with the active mixers are the dominant frequency mixers used in non-consumer oriented transmitters and receivers. There are several companies making DBMs, Mini-Circuits is one of the largest of these. Mini-Circuits produce more than 350 different DBMs. Table 5.2 shows a small selection of those. To allow the table to fit, the some parameters have been omitted. Typically the LO frequency range is the same as the RF frequency range, the maximum IF frequency is the same as the RF maximum frequency and the minimum IF frequency is DC.

There are many different packages styles available as can be seen from table 5.2. Surface mount packages are now more popular and cheaper. The packages with BNC or SMA connectors are much more expensive. Most of the available DBMs use Core and Wire

technology and have a schematic diagram as shown in figure 5.31. It is interesting to see the change in price over time for different packaging styles. As an example, the SRA-1, a through-hole (plugin) mounted mixer was released in 1972, and for many years cost $1.95, the SRA-1+ now costs $20.95. A similar performance surface mount mixer, ADE-1, was more expensive initially and now costs $3.75. (All these prices are in $USA and per mixer for 100 units). Because surface-mount packages are used in the vast majority of new designs, the cost of plugin packages is increasing and the cost of surface-mount packages is decreasing. Those costs should be considered in a design.

Table 5.2. Selection of Mini-Circuit DBMs [2].

| model | interface | RF MHz low | RF MHz high | LO lvl typ | conv loss typ | LO-RF isol | LO-IF isol | technology |
|---|---|---|---|---|---|---|---|---|
| ADE-1+ | SMT | 0.5 | 500 | 7 | 5 | 55 | 40 | Core & Wire |
| ADE-1H+ | SMT | 0.5 | 500 | 17 | 5.3 | 52 | 42 | Core & Wire |
| ADE-1L+ | SMT | 2 | 500 | 3 | 5.2 | 55 | 45 | Core & Wire |
| ADE-1LH+ | SMT | 0.5 | 500 | 10 | 5 | 55 | 45 | Core & Wire |
| ADE-1MHW+ | SMT | 0.5 | 600 | 13 | 5.2 | 53 | 44 | Core & Wire |
| ADE-3G+ | SMT | 2300 | 2700 | 7 | 5.6 | 36 | 26 | Core & Wire |
| ADE-3GL+ | SMT | 2100 | 2600 | 7 | 6 | 34 | 20 | Core & Wire |
| ADE-18W+ | SMT | 1750 | 3500 | 7 | 5.4 | 33 | 12 | Core & Wire |
| ADE-30W+ | SMT | 300 | 4000 | 7 | 6.8 | 35 | 16 | Core & Wire |
| SRA-1+ | Plug-In | 0.5 | 500 | 7 | 5.11 | 45 | 40 | Core & Wire |
| SRA-1H+ | Plug-In | 0.5 | 500 | 17 | 6.01 | 45 | 40 | Core & Wire |
| SRA-1MH+ | Plug-In | 0.5 | 500 | 13 | 5.65 | 45 | 40 | Core & Wire |
| SRA-2+ | Plug-In | 1 | 1000 | 7 | 5.66 | 35 | 30 | Core & Wire |
| SRA-3+ | Plug-In | 0.025 | 200 | 7 | 4.61 | 45 | 40 | Core & Wire |
| SRA-3H+ | Plug-In | 0.05 | 200 | 17 | 5.18 | 40 | 40 | Core & Wire |
| SRA-6+ | Plug-In | 0.003 | 100 | 7 | 4.58 | 45 | 40 | Core & Wire |
| SRA-8+ | Plug-In | 0.0005 | 10 | 7 | 5.69 | 50 | 50 | Core & Wire |
| MBA-15L+ | SMT | 1200 | 2400 | 4 | 6.5 | 27 | 14 | LTCC |
| MBA-15LH+ | SMT | 1200 | 2400 | 10 | 5.6 | 26 | 22 | LTCC |
| MBA-15MH+ | SMT | 1400 | 2400 | 13 | 5.5 | 28 | 16 | LTCC |
| MCA1-12G+ | SMT | 3800 | 12000 | 7 | 6.2 | 36 | 40 | LTCC |
| MCA1-12GL+ | SMT | 3800 | 12000 | 4 | 6.5 | 38 | 40 | LTCC |
| SIM-153+ | SMT | 3400 | 15000 | 7 | 8 | 36 | 30 | LTCC |
| SIM-153LH+ | SMT | 3200 | 15000 | 10 | 7.5 | 36 | 20 | LTCC |
| SIM-153MH+ | SMT | 3200 | 15000 | 13 | 7.5 | 35 | 19 | LTCC |
| SIM-24MH+ | SMT | 7300 | 20000 | 13 | 8 | 35 | 20 | LTCC |
| MDB-24H+ | SMT | 5000 | 21500 | 15 | 7.9 | 35 | 44 | MMIC |
| MDB-24H-D+ | Die | 5000 | 21500 | 15 | 7.9 | 35 | 44 | MMIC |
| MDB-44H+ | SMT | 10000 | 40000 | 15 | 8.4 | 37 | 37 | MMIC |
| MDB-44H-D+ | Die | 10000 | 40000 | 15 | 8.4 | 37 | 37 | MMIC |
| MDB-73H+ | SMT | 2200 | 7000 | 15 | 8.2 | 39 | 46 | MMIC |
| MDB-73H-DG+ | Die | 2200 | 7000 | 15 | 8.5 | 40 | 51.6 | MMIC |
| ZAD-1+ | Connector | 0.5 | 500 | 7 | 5.24 | 45 | 40 | Core & Wire |
| ZAD-1-1+ | Connector | 0.1 | 500 | 7 | 4.83 | 45 | 40 | Core & Wire |
| ZAD-1H+ | Connector | 0.5 | 500 | 17 | 6.16 | 45 | 40 | Core & Wire |
| ZAD-2+ | Connector | 1 | 1000 | 7 | 5.66 | 35 | 35 | Core & Wire |
| ZAD-3+ | Connector | 0.025 | 200 | 7 | 4.61 | 45 | 40 | Core & Wire |
| ZAD-3H+ | Connector | 0.05 | 200 | 17 | 4.89 | 45 | 40 | Core & Wire |
| ZAD-6+ | Connector | 0.003 | 100 | 7 | 4.65 | 45 | 40 | Core & Wire |
| ZAD-8+ | Connector | 0.0005 | 10 | 7 | 5.79 | 50 | 50 | Core & Wire |

DBMs can be used as analogue multipliers in applications like a phase detector or a true RMS power meter. For phase detection, the IF port of a DBM provides the phase output. For multiplier operation, the DBM is operated in an unsaturated mode. For phase detection, the mixer is operated in a saturated mode, where large signals are applied to both the LO and RF ports. In addition the IF port must be DC coupled. Mini-Circuits make *Phase Detectors*, which are optimised for phase detection.

The circuit diagram of a DBM is shown in figure 5.31. The two transformers provide isolation for all ports. Four diodes are now required.

For the analysis of the mixer, consider a +ve input signal being applied to the IF port in figure 5.31. Under those conditions, the diodes shown in figure 5.32 conduct and the others are an open circuit. The resulting connection of the transformers cause a positive signal at the LO port, to cause a negative signal at the RF port. Thus, for a +ve IF signal, the mixer inverts the LO signal to the RF port.

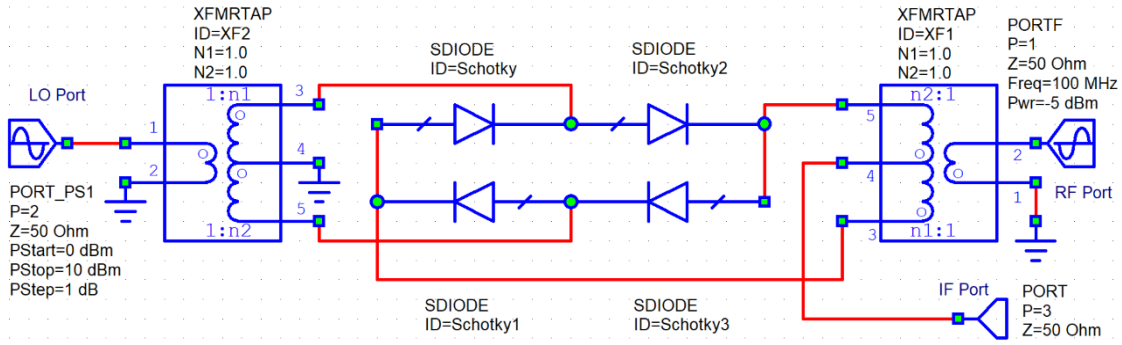



Figure 5.31. Circuit diagram of a DBM.

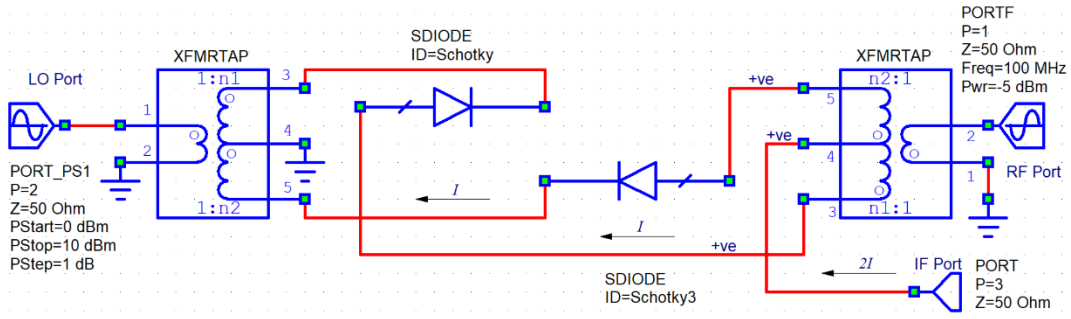



Figure 5.32 Mixer with +ve voltage applied at the IF port.

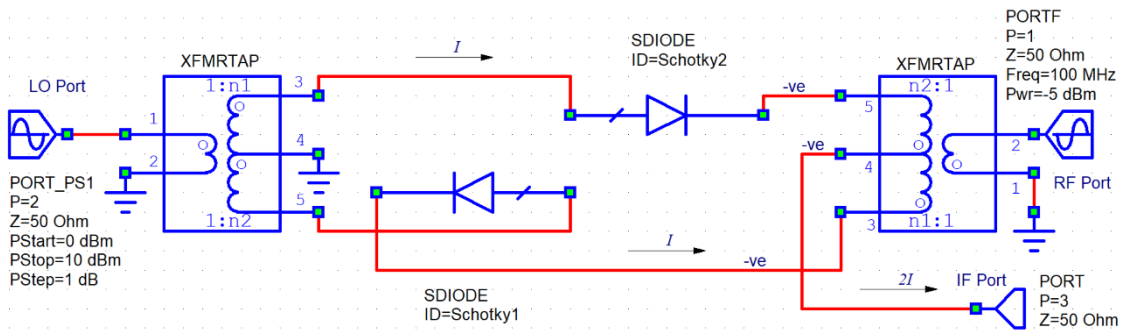



Figure 5.33. Mixer with –ve voltage applied at the IF port.

If a -ve input signal is applied to the IF port, the diodes shown in figure 5.28 conduct and the others are an open circuit. The resulting connection of the transformers cause a

positive signal at the LO port, to cause a positive signal at the RF port. Thus, for a -ve IF signal, the mixer does not inverts the LO signal to the RF port.

If a zero voltage signal is applied at the IF port all the diodes are equal resistances and the LO signal is cancelled at the RF port. Having a smaller IF voltage, results in a smaller RF voltage. The voltage at the RF port is thus a multiplication of the LO signal and the IF signal. Similarly the signal at the IF port is a multiplication of the LO signal and the RF signal. Comparing figures 5.34 with figures 5.10, 5.24 and 5.30, shows that the DBM is a near ideal multiplier. At a high LO power some clipping of the RF signal occurs, but that does not affect the desired signals at frequencies of LO ± IF (100 MHz and 110 MHz in figure 5.38). Figures 5.35 and 5.38 show that the DBM is a near ideal device for producing sum and difference frequency signals. Unwanted components that cannot easily be filtered out are more than 50 dB below the desired signals. A practical DBM is operated at a LO power such that the diodes are turned on hard and the resistive losses are minimised.

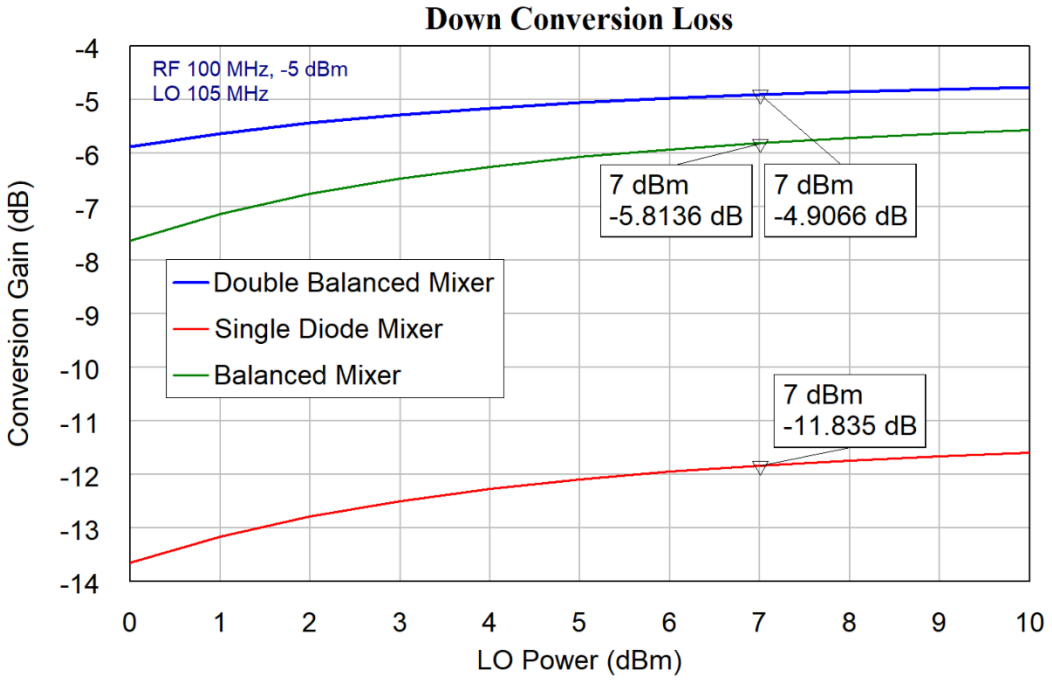



Figure 5.34. Down-conversion loss of a DBM compared with other mixers.

Figure 5.34 shows that the conversion loss of a DBM and compares it with the conversion loss of the single diode and balanced mixers from figures 5.17 and 5.26. The conversion loss is approximately 0.9 dB less than that of a balanced mixer and more than 6.9 dB less than that of a single diode mixer. At an LO power of 7 dBm, the slope of the conversion gain is 0.06 dB/dB for the DBM. The DBM will this have an excellent LO AM noise immunity. Figure 5.35 shows the IF spectrum of a down-converting DBM. The relationship between these components and LO and RF frequencies are shown in table 5.1. Comparing this with figures 5.8(Left), 5.19 and 5.27 for the ideal multiplier and single and balanced diode mixers, shows that this mixer performs nearly as an ideal own converter. There are no unwanted signals in the 20 to 180 MHz frequency range. The difference signal at 5 MHz and the sum signal at 205 MHz are the same amplitude. The signal at 215 MHz is due to the third harmonic of the input signal mixing with the local oscillator. In a receiver, these harmonic signals must be evaluated, to ensure that they do not cause signals in the IF frequency band.

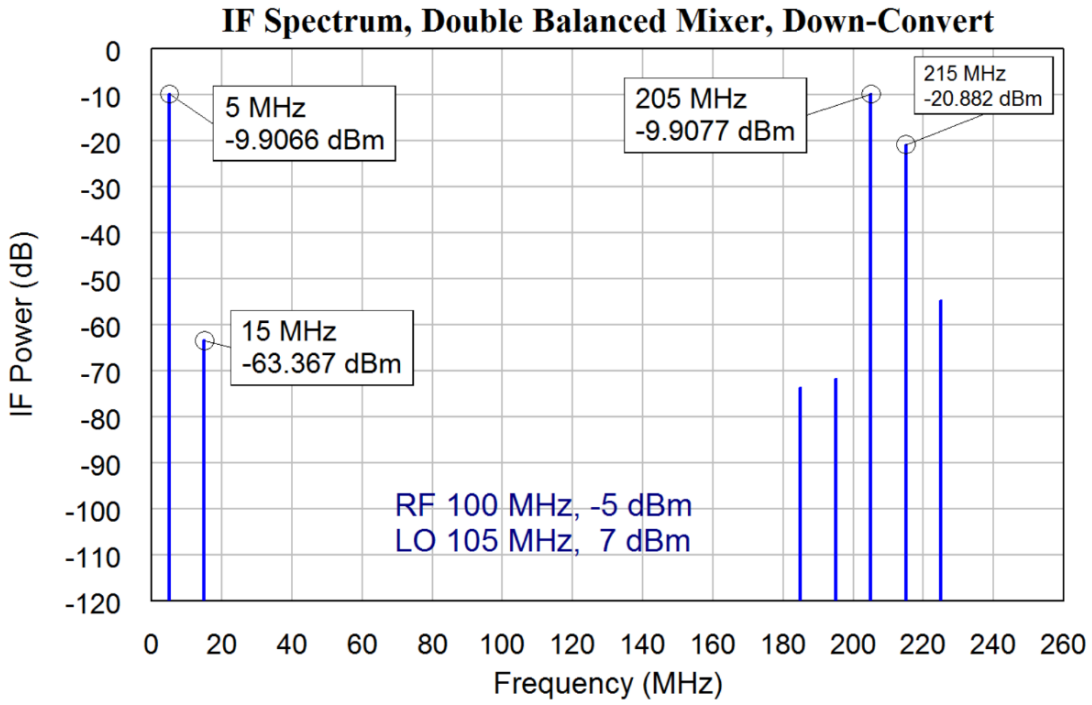



Figure 5.35. IF spectrum of a double balanced diode mixer as a down-converter.

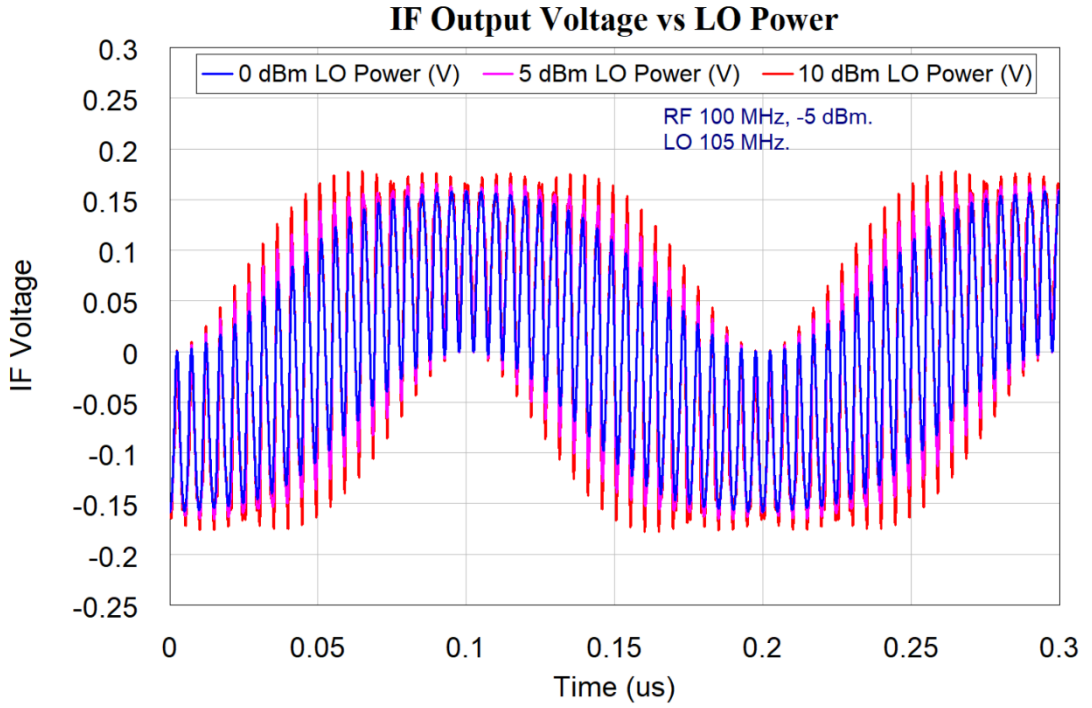



Figure 5.36. IF voltage for a balanced diode mixer as a down-converter.

Figure 5.36 shows the IF voltage. There is a significant high frequency content. Figure 5.37 shows the same IF voltage with the IF signal passed through a 25 MHz low pass filter to remove the high frequency components. The waveform looks like an ideal Sine wave and there is little change in the output as the LO power is changed between 0 dBm and 10 dBm. The LO AM noise will thus have little effect on the IF output. Applying the low pass filter at the IF output reduces the conversion loss by 0.47 dB, due to a short circuit being presented at >25 MHz at the IF port of the mixer.

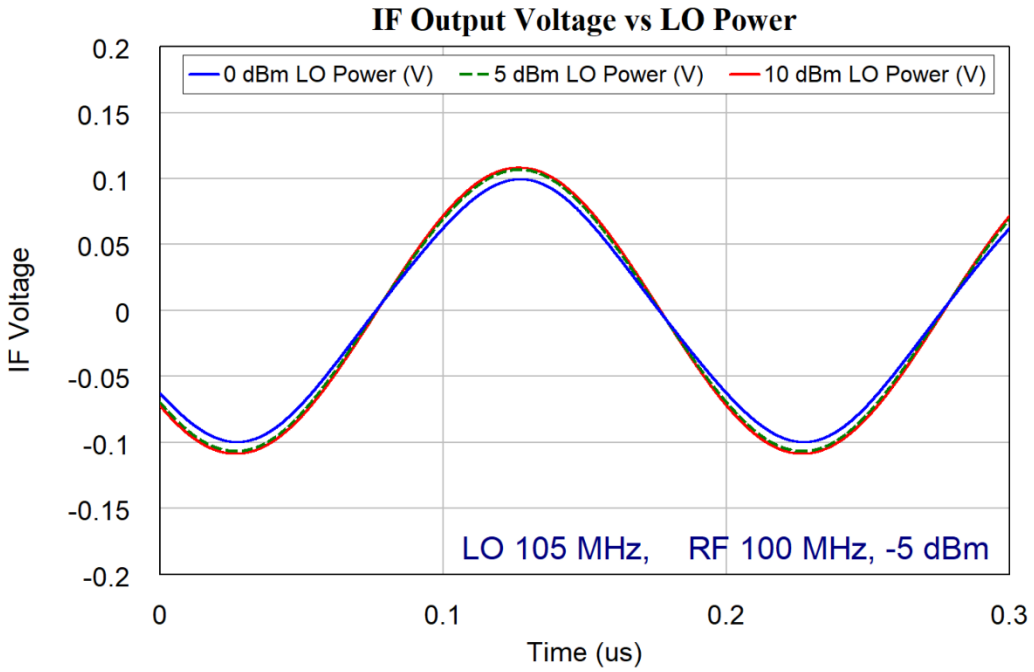



Figure 5.37. IF voltage of figure 5.36 with frequency components >25 MHz removed.

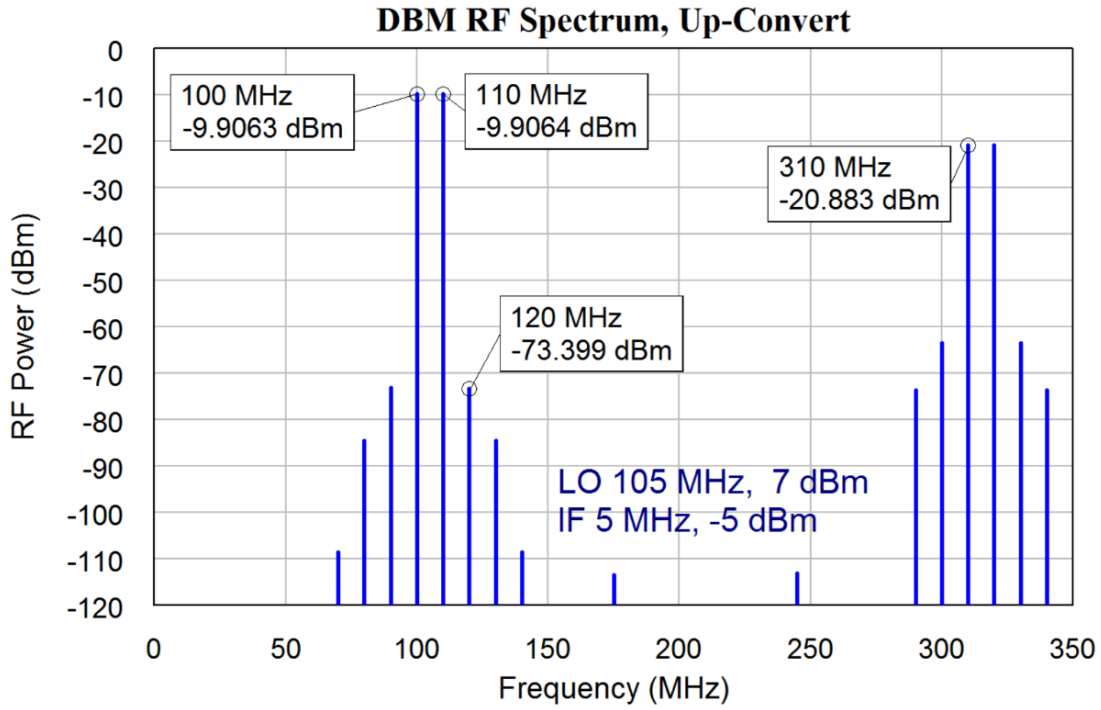



Figure 5.38. RF spectrum of a double balanced diode mixer as an up-converter.

Figure 5.38 shows the RF spectrum of a DBM as an up-converter. The relationship between the spectral components and LO and IF frequencies are shown in table 5.1.The desired spectrum around the 105 MHz LO is near ideal and shows no unwanted spectral components above -65 dBm. Figure 5.39 shows the corresponding RF voltage. The spectrum and the waveform are very similar to that for an ideal multiplier, shown in figures 5.8 and 5.10. Note the 180º phase change in the waveforms at times t=0.05 and 0.15 µs and the near constant amplitude of the RF voltage as the LO level is changed. This shows the mixer has a very low sensitivity to LO AM noise.

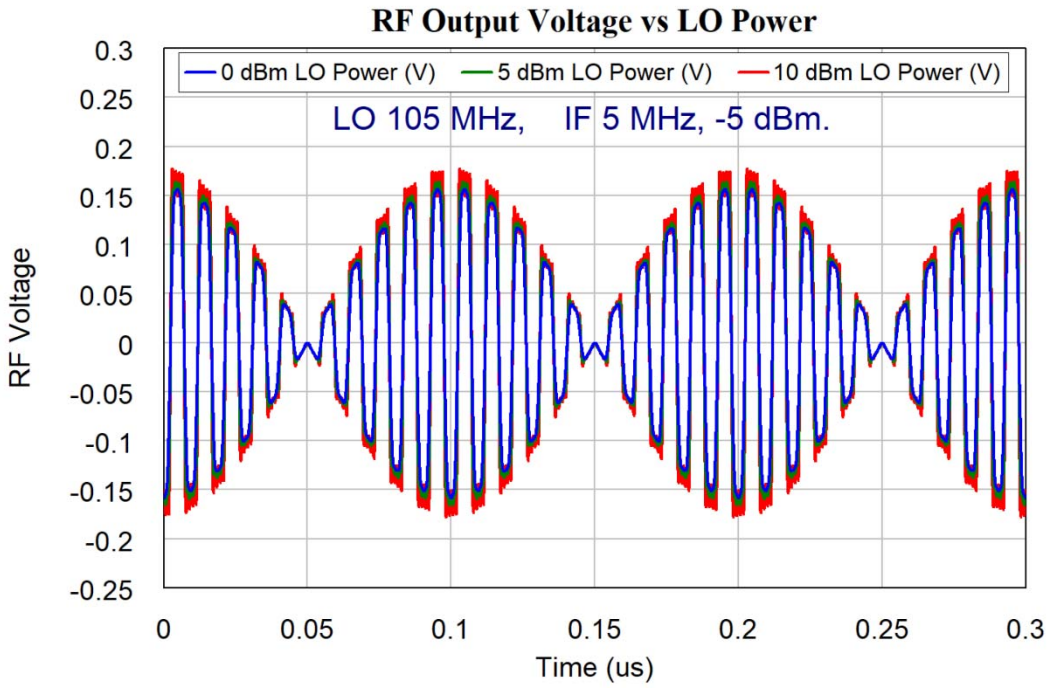



Figure 5.39. RF voltage for a double Balanced Diode Mixer as an up-converter.

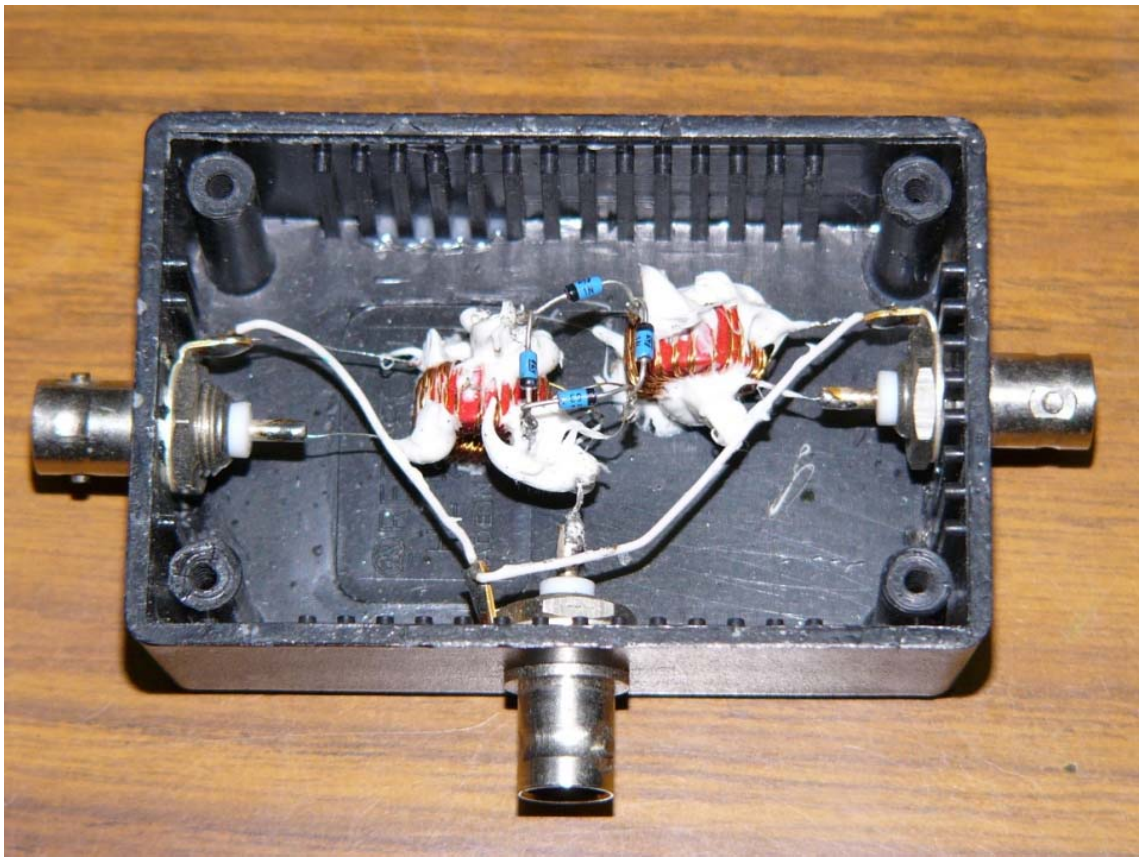


Figure 5.40. Construction of a DBM for use in Practical Sessions.

Figure 5.40 shows the construction of a simple home-made DBM, the transformers are held in-place with Silicone Sealant. The diodes are conventional Schotky-Barrier diodes that have been matched for their V-I characteristic in order to obtain the best LO ⇨ RF isolation.

The measured performance of this mixer is shown in Figure 5.41. The transformers for this mixer were designed for operation at 1 MHz. The mixer was found to perform well as a mixer for LO and RF frequencies between 20 kHz and 50 MHz. Above 50 MHz the mixer performance was good, but for up-conversion the LO carrier isolation became less. The mixer was still useful as a mixer to 100 MHz.

As a result an IF frequency of 250 kHz and an LO of 10 MHz was used for the spectrum in figure 5.41. For this figure, the LO signal had a level of +7 dBm. The IF signal was at a frequency of 250 kHz and a level of -10 dBm. The measured conversion loss is 6 dB and the LO ⇨ RF isolation is -60 dB. This mixer performs well for RF and LO signals in the range of 30 kHz to 30 MHz and IF signals up to 30 MHz.

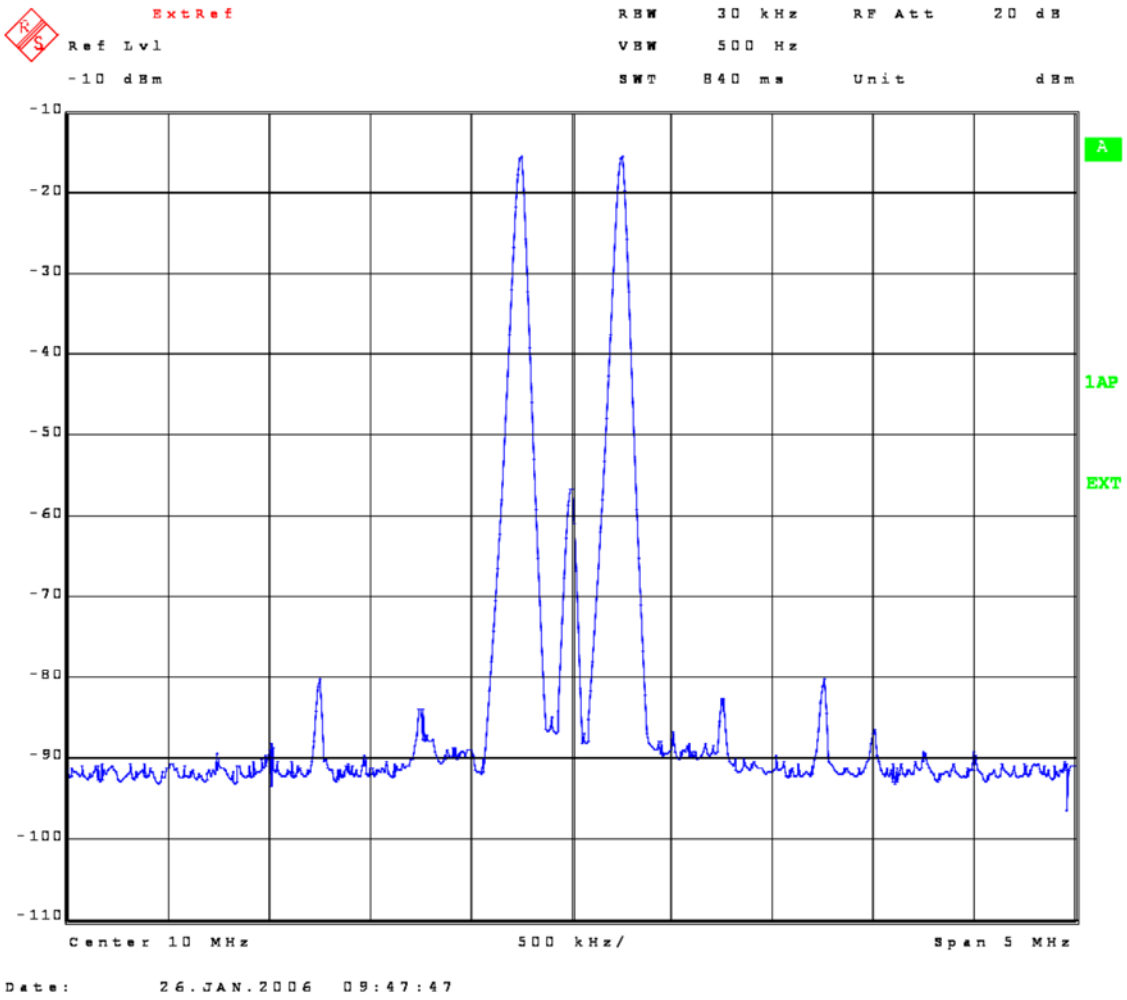



Figure 5.41. Measured performance of the mixer of figure 5.40. (Hor: Centre 10 MHz, 500 kHz/div, Vert: Max -10dBm, 10 dB/div.)

Comparing the spectrum around the LO in figure 5.40 with the corresponding spectrum around the LO in figure 5.38, shows that in practice there will be some LO ⇨ RF carrier feed-through due to a slight mismatch of the diodes or a slight mismatch in the signal path lengths. Such path lengths are particularly difficult to match exactly at microwave frequencies. Figure 5.41 shows that the 5IM distortion components, which are 1.250 MHz from the LO frequency at the centre of the plot, are bigger than the 3IM components, which are 750 kHz from the LO frequency.

## Mixer terminations

As shown in figure 5.37, for down conversion, it is normal to remove the RF and LO frequency components at the IF port, as they can cause intermodulation distortion in the subsequent IF circuits. Mini-Circuits application note AN-75-007 [4] shows that mixer improvement can be obtained by using reflectionless filters at all ports of a mixer and thus provide a near ideal termination to the mixer. Figures 5.17 and 5.26 show that using reflectionless filters instead of Butterworth High pass and Low pass filters for the IF/RF diplexer improved the conversion loss of the mixer. To illustrate this for a DBM, different types of filters are added to the basic DBM of figure 5.31, as shown in figure 5.42. The reflectionless filters used are the same as shown in figure 5.7 and provide a better than 120 dB return loss for the mixer ports. Like figures 5.11, 5.13 and 5.22, the corner frequency of the filter was 20 MHz, so that LO and RF signals are severely attenuated at the IF port. A comparison was made between the performances of the different DBM terminations.

DBM1: Basic DBM of figure 5.31, no filters at the ports.
DBM2: A DBM with reflectionless filters added to all ports, as shown in figure 5.42.
DBM3: A DBM with a reflectionless filter only added to the IF port.
DBM4: A DBM with a second order low pass filter at the IF port, resulting in a high impedance at the mixer transformer at high frequencies as shown in the left of figure 5.43.
DBM5: A similar configuration but resulting in a low impedance at high frequencies as shown in the right of figure 5.43.

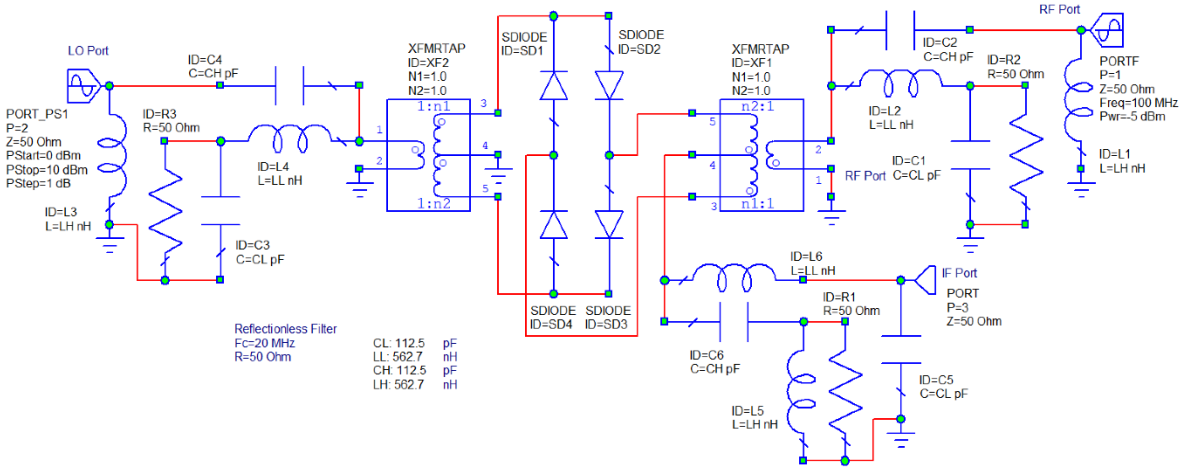



Figure 5.42. Circuit diagram of a DBM with reflectionless filters (DMB2).

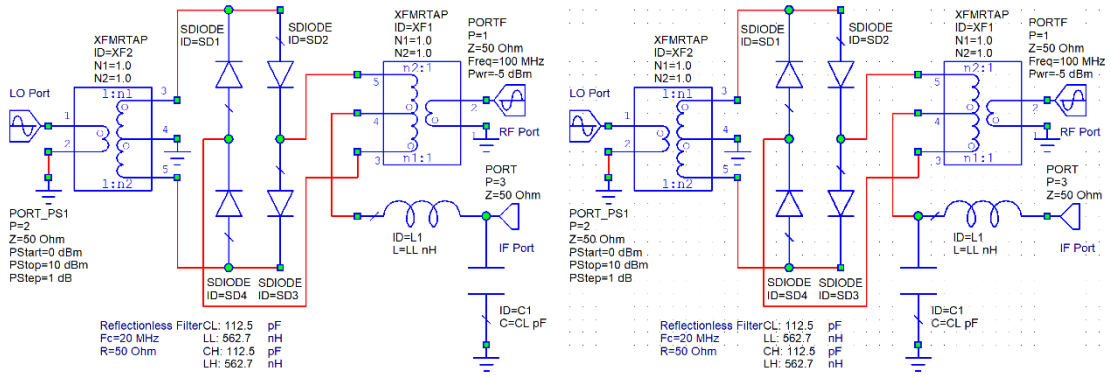



Figure 5.43. DBM4 with Inductor First (L) and DDM5 with Capacitor First (R).

The basic DBM1 and DBM2 with reflectionless filters have all ports terminated into 50 Ω. As a result, there is not much difference in performance like conversion loss and IF spectral components below 100 MHz. Figure 5.44 shows the conversion loss of the different mixer configurations. There is no discernible difference in conversion loss between the basic DBM1, DBM2 with all ports terminated in a reflectionless filter or DBM3 only the IF port terminated in a reflectionless filter. DBM4 of figure 5.43(L), presents a high impedance at the centre point of the transformer and reduces the RF and LO currents flowing into the IF port. Figure 5.44 shows that this increases the conversion loss. DBM5 of figure 5.43(R), presents a low impedance at the centre point of the transformer and increases the RF and LO currents flowing into the IF port. Figure 5.44 shows that this reduces the conversion loss.

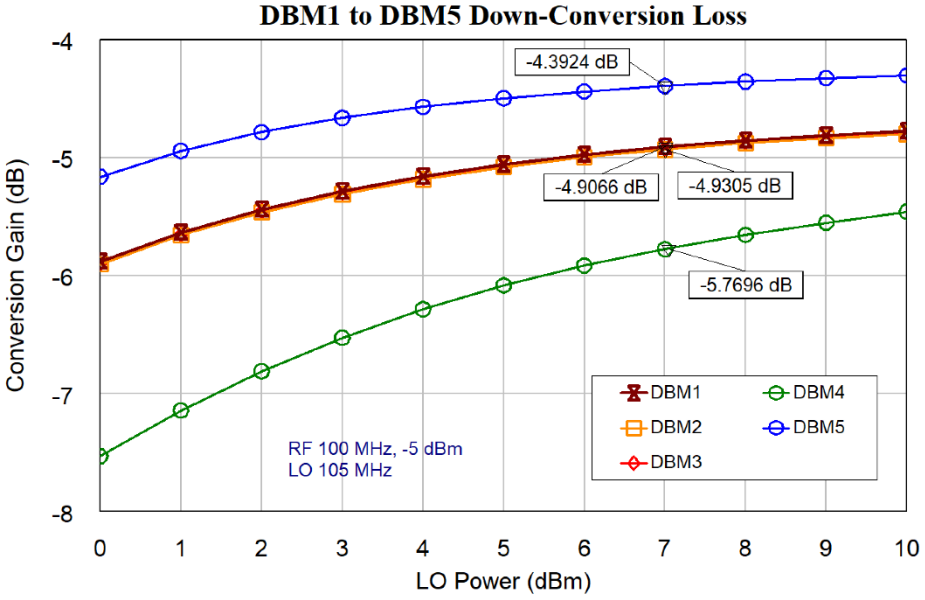



Figure 5.44. Down-conversion loss of DBM configurations.

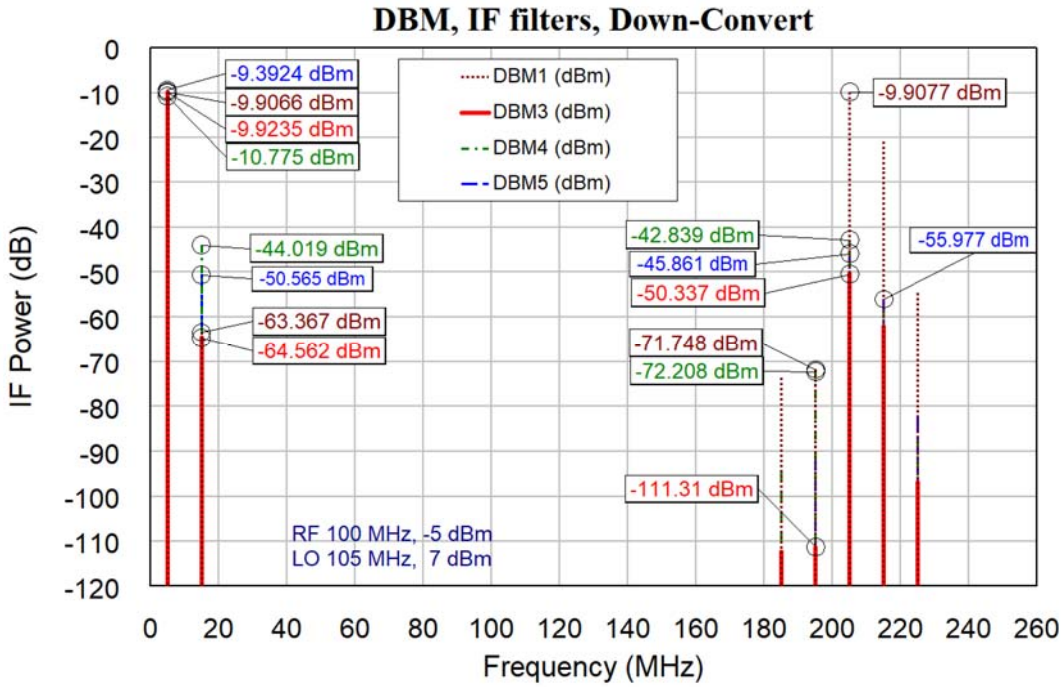



Figure 5.45. IF Spectra of different DBM configurations.

Figure 5.45 shows the down conversion spectra for DBM1, DBM3, DBM4 and DBM5. The conversion loss and IF spectra produced by DBM 2 and DBM3 are near identical. That is expected, since the LO and RF ports are terminated in 50 Ω, which is a reflectionless termination and for a down converter we do not consider the spectra at the RF and LO ports. As a result, DBM2 is not plotted in figure 5.45.

The relationship between the spectral components and LO and RF frequencies are shown in table 5.1. DBM1 and DBM3, have similar performance below 100 MHz. At 200 MHz, the low pass section of the IF filter reduces those signal amplitudes by 40 dB. The 3rd harmonic component at 15 MHz for DBM 1 and DBM3 is much lower than those of DBM4 and DBM5. At the sum frequency of 205 MHz, DBM3 gives the best performance. However if low cost and low conversion loss are critical, then DBM 5, which provides a low impedance at the RF and LO frequencies is the best option.

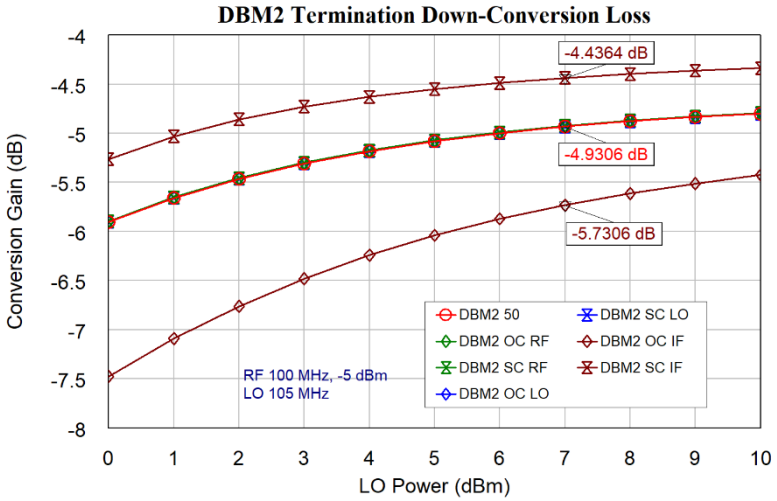



Figure 5.46. Down-conversion loss DBM2 with different reflectionless filter terminations.

Since the DBM2 circuit has each port connected to a reflectionless filter, it is worthwhile to see how terminating the out of band ports changes the performance, by leaving R1 to R3 as 50 Ω, or changing them to an open or short circuit. Figure 5.46 shows that the conversion loss is not affected by changing the resistors R2 and R3 at the RF and LO ports. The conversion loss is reduced by replacing the IF termination, R1, by a short circuit and it is increased by replacing R1 by an open circuit. The effect is similar to what is shown in figure 5.44 for DBM3 and DBM4. For the corresponding spectra, the lowest level of unwanted signals are obtained when the IF filter is terminated into 50 Ω, just like figure 5.45.

For Up-conversion, the conversion loss is similar to figure 5.46, with the RF and LO terminations not affecting the conversion loss, but an open circuit R1 also resulting in a higher conversion loss and a short circuited R1 resulting in a lower conversion loss than R1= 50 Ω. The corresponding spectrum is shown in figure 5.47. Similar to figure 5.45, the lowest level of unwanted signals are obtained by having a 50 Ω termination at the IF port. There is little change in the IF spectrum when the out of band termination of the RF and LO ports are changed by changing resistors R2 and R3.

In summary, the lowest level of unwanted spectral components are obtained when the IF port of a mixer is terminated into 50 Ω. If a low conversion loss is more critical than low unwanted signals, then providing a low impedance for RF/LO frequencies at the IF port can reduce the conversion loss by 1 dB.

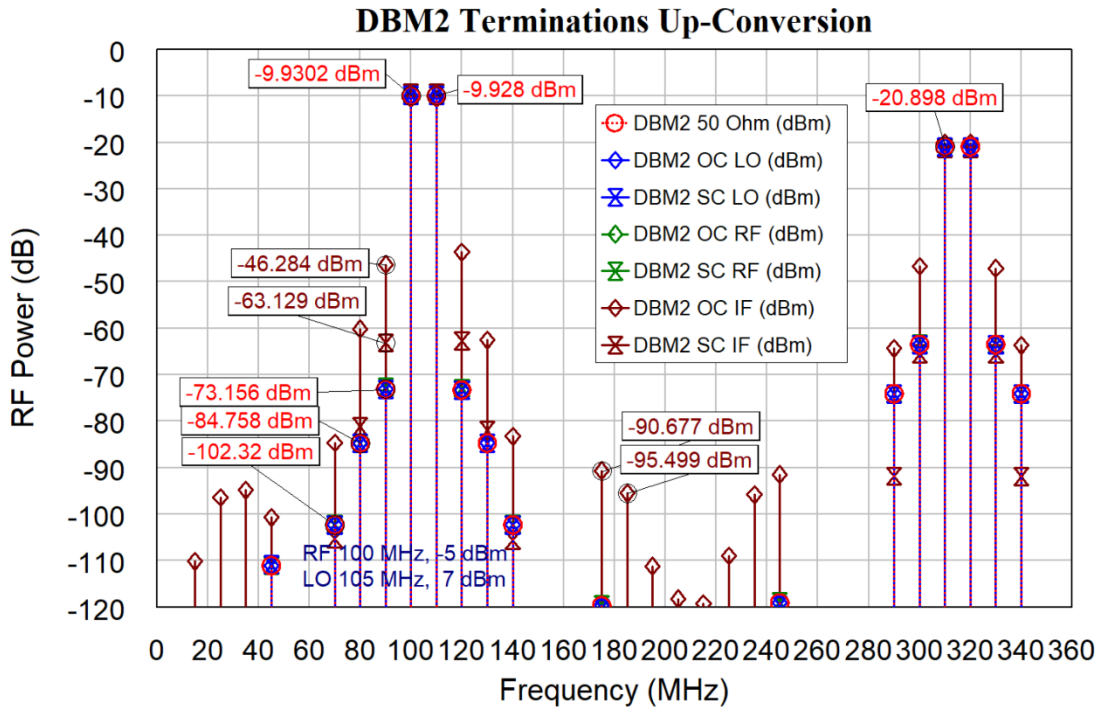



Figure 5.47. RF spectra of DBM2 with different reflectionless filter terminations.

## Triple Balanced Mixer and High Level DBM

Triple balanced mixers (TBM) use two diode quads and three separate baluns. That results in a mixer which has a wider bandwidth, a better L-R, L-I and R-I isolation, a better return loss, a higher 1-dB compression and IP3 power than a DBM. The TBM has to drive twice as many diodes than a DBM and thus requires 3 dB more LO power to drive the diodes at the same level. Figure 5.48 shows the circuit diagram of a TBM.

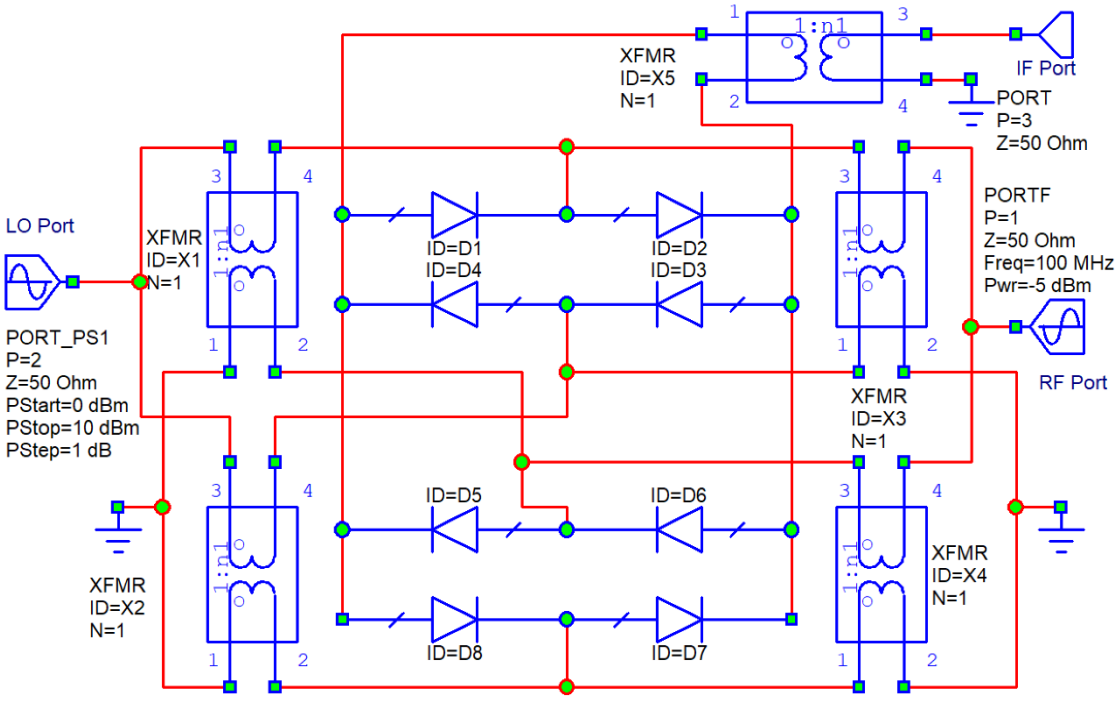



Figure 5.48. Circuit diagram of a triple balanced mixer.

The TBM requires 8 diodes, and extra baluns results in additional costs for the mixer. With the 8 diodes, additional LO power is required to achieve the same currents in the diodes. The transformers used can be achieved as floating coaxial line baluns of figure 4.70 and using LTTC technology [5] as shown in figures 5.98 and 11.11.

As indicated in figure 5.6, mixer performance can be improved by putting two diodes in series to produce a high-level double balanced mixer (HL-DBM), as shown in figure 5.49. The HL-DBM circuit has 8 diodes identical to those used in the simulation for the DBM and the TBM. When operating that at a 10 dBm LO and performing the same simulations as for the TBM, results in a near identical performance for the HL-DBM to the TBM shown in figure 5.50 to 5.52.

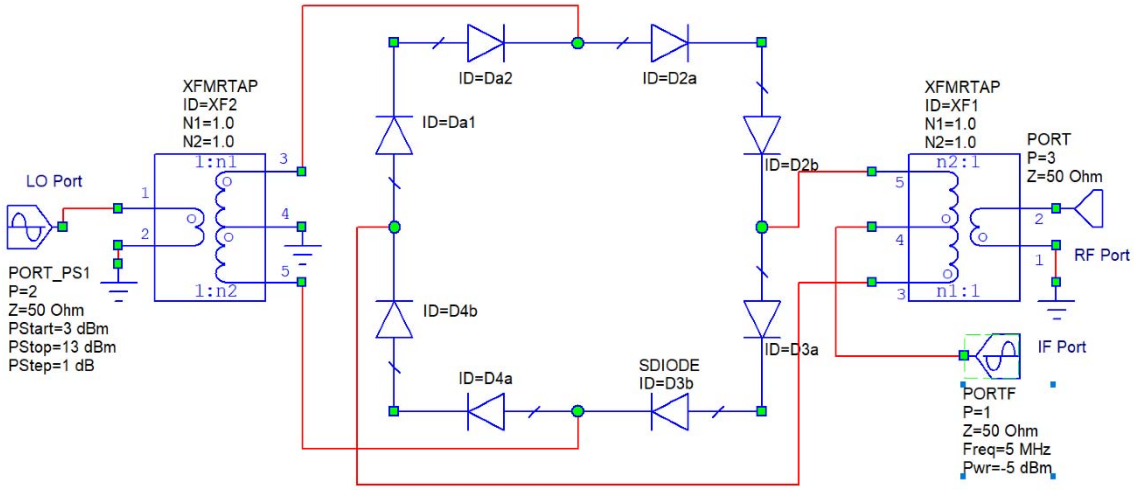



Figure 5.49. Circuit diagram of a high-level double balanced mixer as an up-converter.

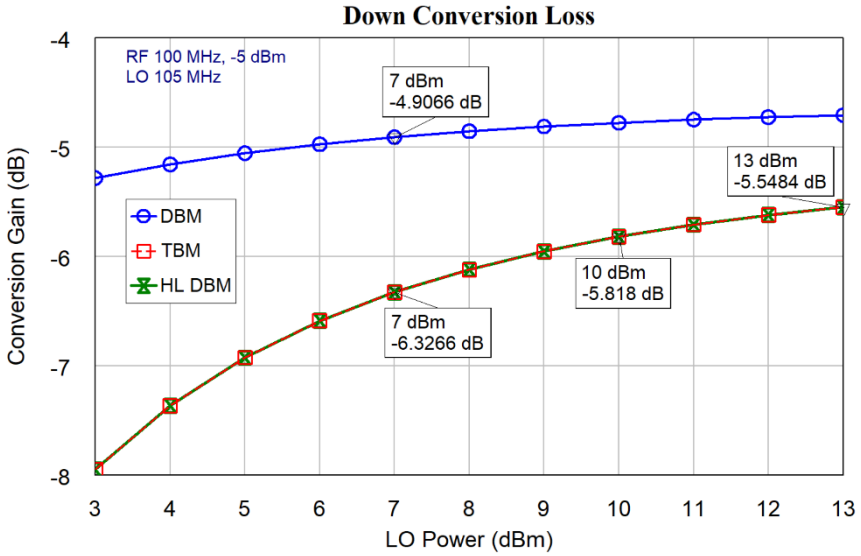



Figure 5.50. Conversion loss of a TBM and DBM.

Figure 5.50 shows a comparison of the down conversion loss of a HBM, TBM and a HL DBM. The DBM has a lower conversion loss. The TBM and HL DBM have the same conversion loss and an actual mixer will have a slightly worse conversion loss than simulated. For example a Mini Circuits ADE-201FMH+ covering the same RF/LO frequencies as the mixers in this section, has a typical 6.4 dB conversion loss at an LO level of 13 dBm. That is 1 dB worse than the results shown in figure 5.50.

Figure 5.51 shows the IF spectra of a DBM operating at a LO of 7 dBm and a TBM and HL DBM operating at a LO of 10dBm. The relationship between the spectral components and LO and RF frequencies are shown in table 5.1.The third harmonic signal at 15 MHz is 20 dB lower for the TBM and HL DBM, which is a significant improvement in performance.

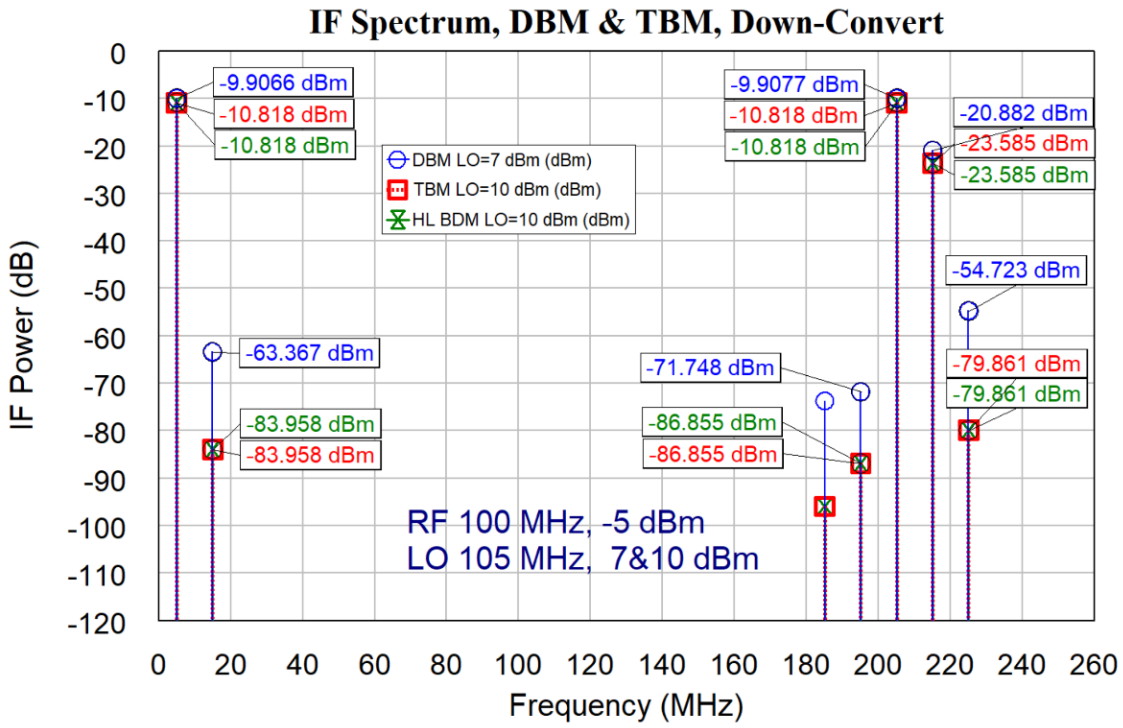



Figure 5.51. Down conversion spectra of a DBM, TBM and HL-DBM.

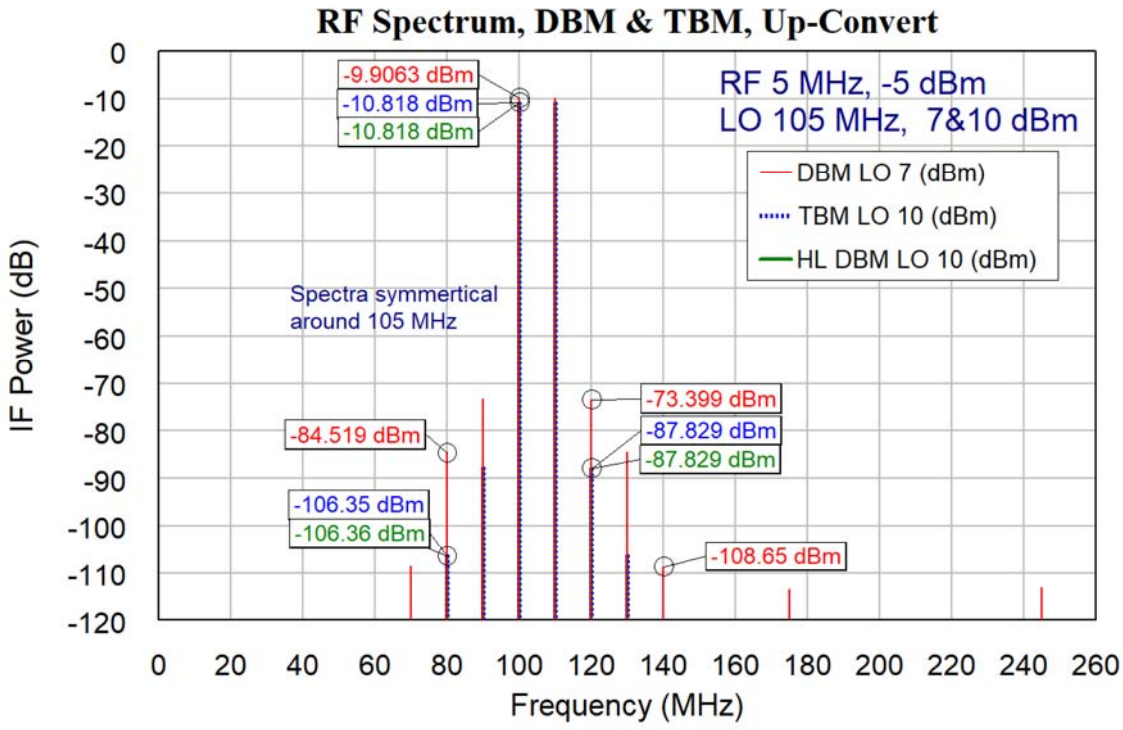



Figure 5.52. Up conversion spectra of a DBM, TBM and HL-DBM.

Figure 5.52 shows a comparison between the spectra of the DBM, TBM and HL-DBM used as up-converters. The relationship between the spectral components and LO and RF frequencies are shown in table 5.1. For the TBM and HL-DBM the spectra are near ideal, with the largest unwanted components being 76.9 dB below the wanted components. For the DBM the largest unwanted components are 63.3 dB below the wanted components. Comparing the TBM or HL-DBM performance in figure 5.52 with the DBM performance in figures 5.52 and 5.38 and with the Balanced Mixer performance in figure 5.29, shows that the TBM or HL-DBM should be used in applications where superior performance is required.

During computer simulation the LO-RF and the RF-LO isolation is ideal. In practice that is not the case, since firstly the diodes will not be matched exactly and secondly there will be slight differences in capacitive coupling between the different windings in the transformers. As a result, the typical isolation and conversion loss of practical mixers is worse than the computer simulations. Table 5.3 compares 3 different types of mixers, from the same manufacturer, all made using core and wire technology. The performance data is taken from the data sheets for an RF signal at or close to 2.5 GHz. Computer simulation result in the same performance for TBM and HL-DBM devices. Table 5.3 shows that a better performance is achieved from TBM hardware.

Table 5.3 Typical Mixer performance for a 2.5 GHz RF input [6-8].

| | MCA-35MH+ | ADE-30W+ | ADE-R30WLH+ |
|---|---|---|---|
| Type | TBM | DBM | High Rel DBM |
| LO/RF | 500-3500 MHz | 300-4000 MHz | 300-4000 MHz |
| LO | 13 dBm | 7 dBm | 10 dBm |
| Conversion loss | 5.95 dB | 6.79 dB | 8.21 dB |
| LO-IF isolation | 26.01 dB | 12.0 dB | 13.46 dB |
| LO-RF isolation | 30.44 dB | 33.67 dB | 40.68 dB |
| IIP3 | 20 dBm | 12 dBm | 15 dBm |

## Microwave Mixers

At microwave frequencies (>1 GHz) transformers become progressively more difficult to make. In addition, the capacitance associated with the diodes used in the mixer cause the diodes to become less efficient as a mixer, any PCB's have larger skin depth and dielectric losses and ferrites have larger magnetic material losses. As a result, mixers at microwave frequencies have higher conversion losses than mixers used at lower frequencies. Conversion losses of 6 to 10 dB are typical. The frequency dependence of the conversion loss on the RF frequency can easily be seen from [2], selecting surface mount and level 7 devices and then sorting the devices according to frequency. The ADE-6+, core & wire based mixer with a 250 MHz upper frequency has a conversion loss of 4.6 dB, the 15 GHz upper frequency SIM-153+, LTCC based mixer has a conversion loss of 8 dB and the ZX05153-S+ core & wire based mixer has a conversion loss of 7.5 dB. Surface Mount Double balanced mixers are available to 40 GHz [9]. Balanced based mixers are available for frequencies up to 90 GHz [10].

## *Transmission Line Balanced Mixer*

At microwave frequencies, transmission lines are often used to produce two outputs with a 180° phase shift, instead of the transformers used in the balanced mixer of figure 5.25. The circuit for the corresponding microwave mixer is shown in figure 5.53. In this design, the mixer is used for a down-converter for a weather satellite receiver and uses a 1565 MHz Local Oscillator to shift a 1700 MHz RF signal to a 135 MHz IF frequency. The transformer in figure 5.25 provides balanced voltages to drive the diodes. For a 50 Ω impedance at the LO port, the diodes should be 100 Ω each. For an accurate comparison with the balanced mixer of figure 5.25, a 100 Ω impedance is also assumed for the diodes in figure 5.53. The half-wavelength long transmission line TL2 should thus have a 100 Ω impedance for the best impedance match bandwidth. The quarter-wavelength transmission lines TL3 and TL4 provide a DC path for the diodes and a high impedance at 1565 MHz for good mixer operation. Changing the line lengths or impedances of the transmission lines TL2 to TL4 does not have a significant impact on the mixer performance, as can be demonstrated by tuning those parameters in the simulation.

For the RF port high pass and the IF port low pass filter, a reflectionless filter similar to the one shown in figures 5.11 and 5.12 is used. A lower crossover frequency gives smaller spectral components at the IF output but a slightly higher conversion loss. For the mixer of figure 5.53, a 480 MHz crossover frequency, being close to the geometric mean of the RF and IF frequency is used.

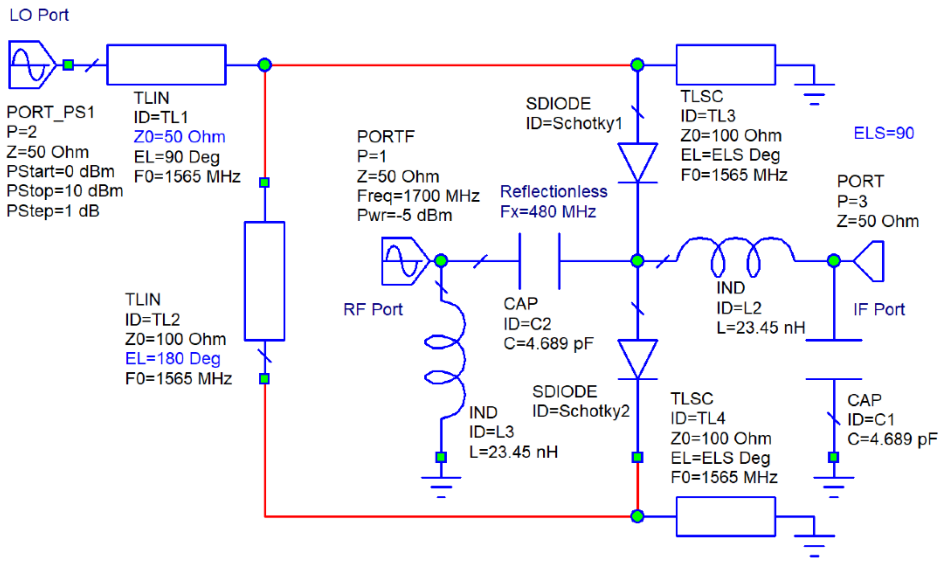



Figure 5.53 Circuit diagram of a transmission line balanced mixer.

The conversion loss for this mixer and for the mixer of figure 5.25 both operating at the same RF and LO frequency and with the same RF and IF crossover filter is shown in figure 5.54. The simulation for the transmission line balanced mixer of figure 5.53 shows 0.224 dB less conversion loss than for the corresponding transformer-based mixer. In practice, the transmission lines can be made with very little loss while a transformer operating at 1.5 GHz will have an appreciable loss. Figure 5.55 shows the spectrum for the mixer as a down-converter. The mixer performs well. The RF frequency components in the IF spectrum can be attenuated more by changing the 2$^{nd}$ order RF-IF diplexer to a 4$^{th}$ order diplexer similar to the one in figures 2.13 to 2.15.

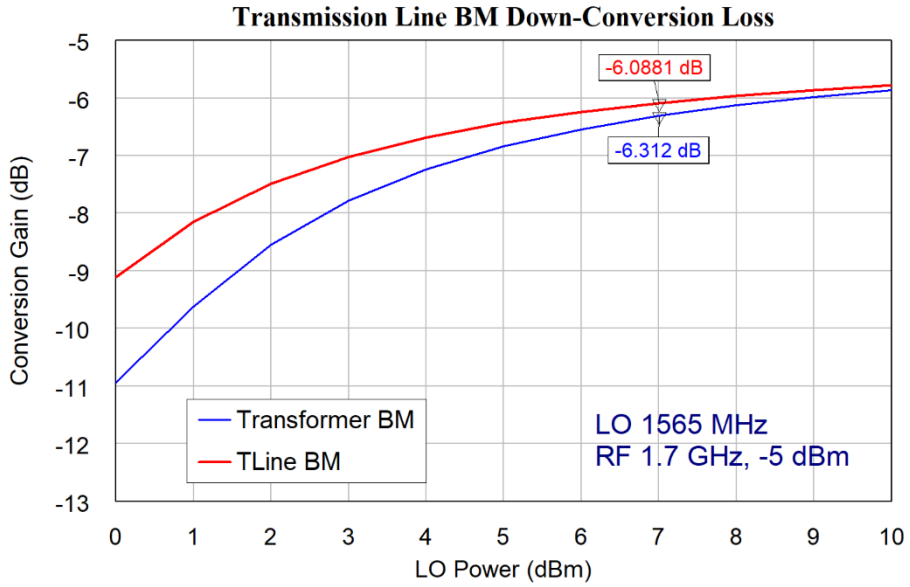



Figure 5.54. Conversion loss of the transmission line balanced mixer.

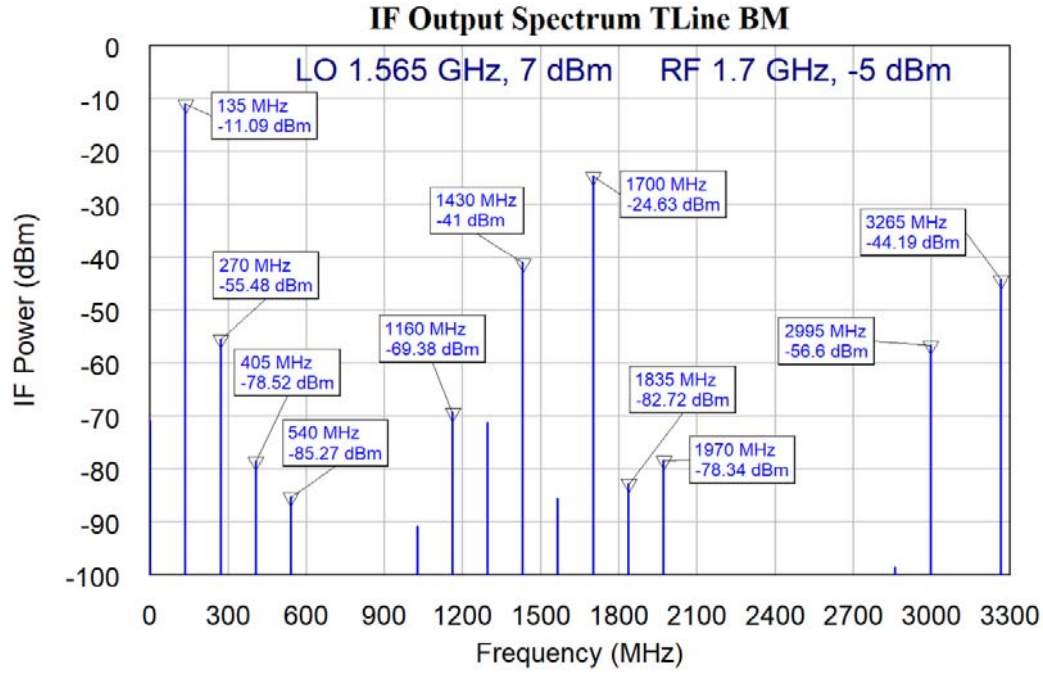



Figure 5.55. IF Spectrum of the transmission line balanced mixer as a down-converter.

Changing the transformer to a transmission line will thus not change the performance of the mixer very much apart from a reduction of the bandwidth, since the transmission line only produces a 180° phase shift at a single frequency. However, in many microwave applications the resulting bandwidth is sufficient. The mixer can also be used as an up-converter.

## *Branchline Coupler Balanced Mixer*

A transmission line, used to produce the 180° phase shift in figure 5.53 produces a linear phase shift with frequency. As shown in figure 4.39, the Branchline coupler has less than 2° variation of phase from a 90° phase shift between ports 2 and 3 over a 20% bandwidth.

The Branchline coupler can be used to produce the required phase shifts for efficient mixing. If the LO signal is applied at port 2 of the Branchline coupler in figure 5.56 and the RF signal is applied to port 1. The frequency of the Branchline coupler is chosen such that full isolation is obtained at the RF port for the LO signal, since the LO signal is much bigger in power than the RF signal. For a practical down-converting mixer, the LO and RF signals are within 10% of each other, so that reasonable isolation will be obtained for the RF signal at the LO port.

The signal at the junction of TL2 and TL3 will then be LO∠90° + RF∠180°, giving a phase difference between the LO and RF signals of -∠90°. The signal at the junction of TL4 and TL3 will be LO ∠180° + RF∠90° giving a phase difference +∠90°. These are the correct conditions for obtaining balanced mixing in a down-converter.

## Basic Operation

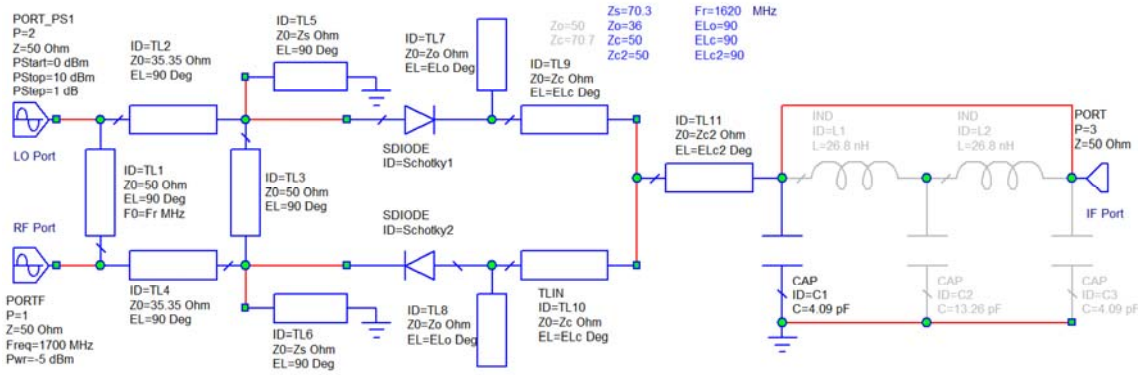



Figure 5.56. Basic circuit diagram of a Branchline coupler balanced mixer.

To illustrate the principles of operation, a basic Branchline balanced mixer is shown in figure 5.56. The Branchline hybrid consists transmission lines of TL1 to TL4. In figure 5.56, all electrical lengths are in degrees at the reference frequency Fr. Initially the frequency of Fr is the same as the LO frequency. Fr can be tuned to optimise the performance of the mixer. All the lines are of the Branchline coupler are one-quarter wavelength long at Fr.

Correct biasing for the diodes must be provided, such that all the RF and LO energy is dissipated in the diodes and all the resulting low frequency energy is passed to the IF port and is not reflected back into the RF or LO ports. TL5 and TL6 are short circuited transmission lines, providing no load to the RF and IF signals, but providing a low impedance to ground so that DC and IF currents can flow easily. Transmission lines TL7 and TL8 are open circuited lines, one quarter wavelength long at the Fr frequency, and will this provide a low impedance to ground at the LO and RF frequencies and a high impedance at IF frequencies. All the RF and LO energy coming from the Branchline coupler is thus dissipated in the diodes.

The size of capacitor C1 is chosen to act as a short circuit to the RF and LO signals but have little effect at the IF frequency. Line TL11 is a quarter wavelength long at Fr, so that C1 causes a high impedance at the LO/RF frequencies and little RF energy goes to the IF port. Lines TL9 and TL10, with the high impedance at the junction with TL11, are half a wavelength long. The short circuit at the Fr frequency due to TL7 will reflect as a short circuit and reinforce the short circuit due to TL8 at diode 2 and vice versa. TL9 to TL11 will this ensure that the IF energy from the diodes is passed to the IF port as much as

possible, while impeding the higher frequency signals. To make the removal of the LO and RF signals at the IF port as effective as possible, the size of capacitor C1 is chosen to act as a short circuit to the RF and LO signals but have little effect at the IF frequency. If needed, a low pass LC filter can be used at the IF port. A filter with a 480 MHz cut off frequency will reduce the RF/LO signals significantly and also reduce the conversion loss. The low pass filter is disabled (greyed out) in figure 5.56. That results in the *Branchline BM* plots shown in figure 5.57 and 5.58. Enabling that filter and removing the bypass wire, results in the *Branchline BM + IF Filter* plots shown in figure 5.57 and 5.58.

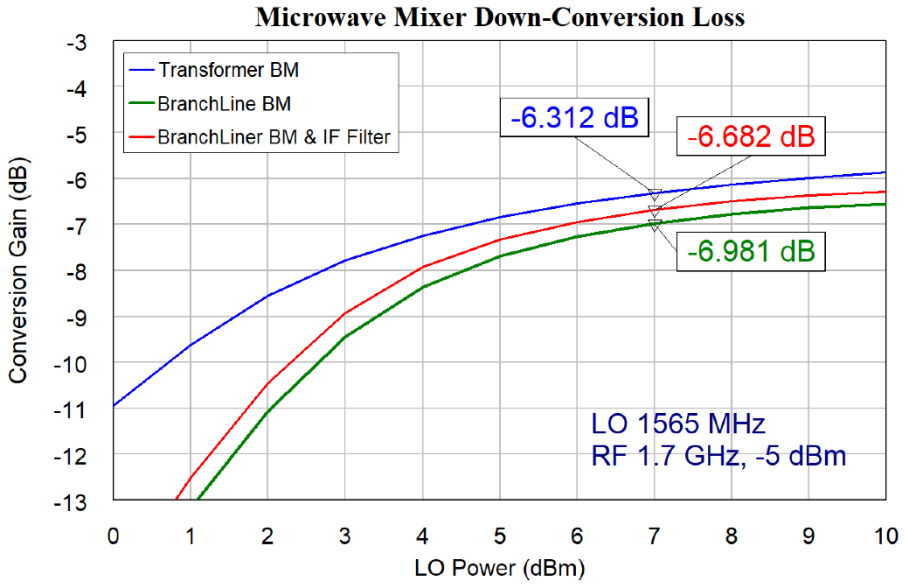



Figure 5.57. Conversion loss of a Branchline coupler balanced mixer.

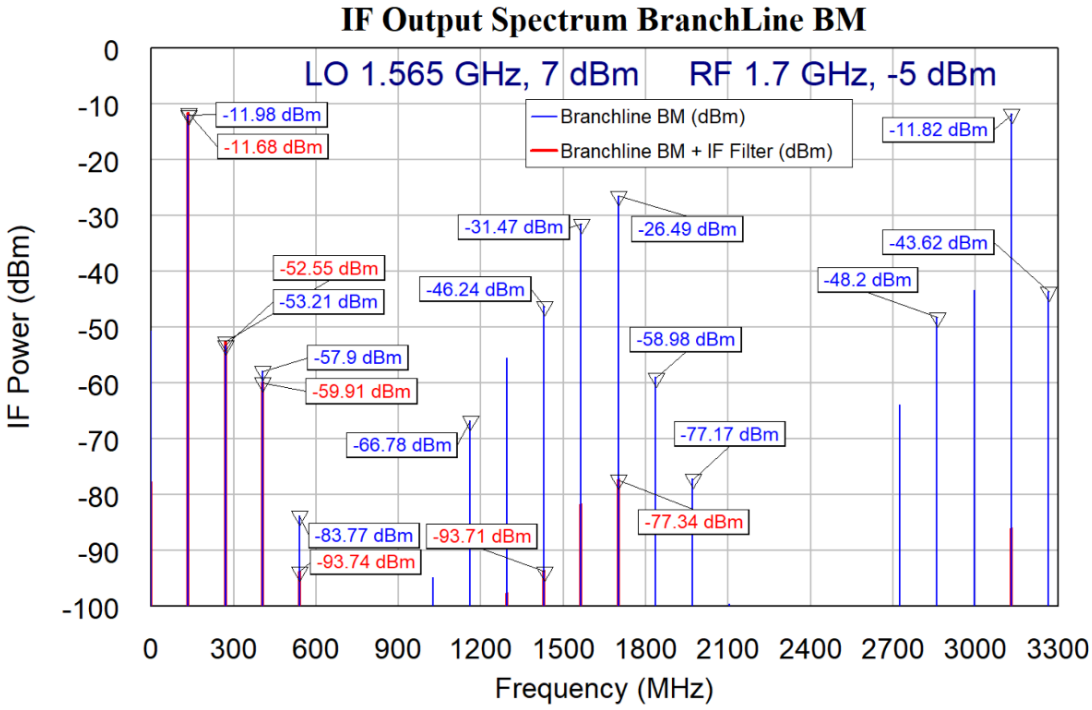



Figure 5.58 IF spectrum of the Branchline coupler balanced mixer.

A balanced mixer should not produce a DC component, since the signals across the diodes are balanced. The RF frequency is 1700 MHz and the LO frequency is 1565 MHz. Tuning

Fr to 1611 MHz results in the lowest DC signal in the IF spectrum and gives a good conversion loss. For all the transmission lines, except TL1, the reference frequency label *F0=Fr* has been hidden to simplify the schematic. The impedance and length of the transmission lines can be tuned to optimise the design and gain a good understanding of their effect on the performance. For example, the Impedance of TL9 and TL10 have a significant effect on the conversion loss. The hardware shown in figure 5.60 was built, based on a design where Zc = 50 Ω and Zo = 36 Ω therefore that is shown in figure 5.56 and used in figure 5.57 and 5.58. However, changing Zc to 70.7 Ω and Zo to 50 Ω, reduces the conversion loss from 6.981 dB to 6.642 dB.

Figure 5.58 shows the IF spectrum of the Branchline coupler balanced mixer. The spectral frequencies are shown in figure 5.55. The IF spectral components for the *Branchline BM* circuit are comparable to those of figure 5.55 for the transmission line balanced mixer. It is easy to optimise the circuit parameters of the circuit in figure 5.56, before a Microstrip realisation is produced.

Figures 4.38 and 4.39 show that the amplitude and phase shift between the two output ports of the Branchline coupler is nearly constant over a 20% bandwidth. As a result, the bandwidth of the Branchline coupler mixer of figure 5.56 is wider than the bandwidth or the transmission line mixer of figure 5.53.

## Hardware Realisation

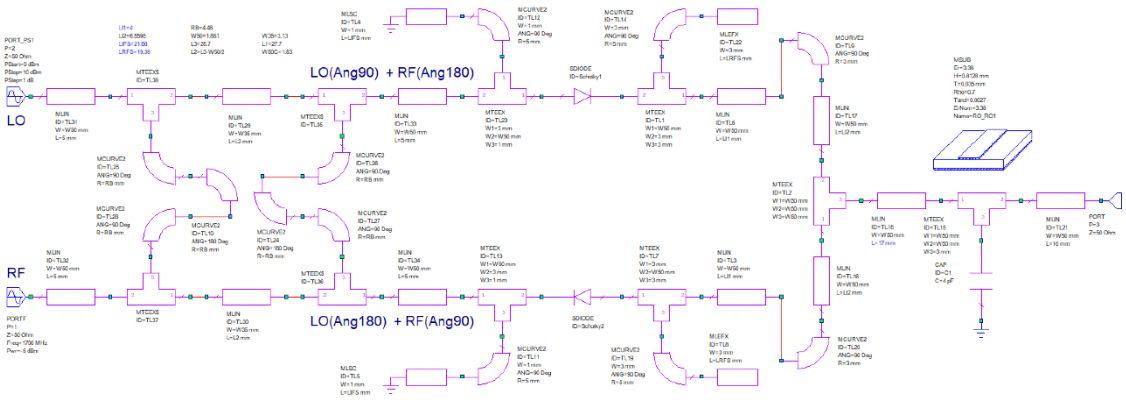



Figure 5.59. Microstrip realization of a Branchline coupler balanced mixer.

The basic block diagram of figure 5.56 is realised as a Microstrip circuit, as shown in figure 5.59. This circuit was based on a long-standing mixer design and produced by the author before AWRDE was available, and as a result, the impedance of lines TL7 to TL19 of this layout, do not result in the optimum conversion loss, that can be obtained by tuning the basic circuit of figure 5.56. Figure 5.60 shows the corresponding layout.

Figure 5.60 shows the PCB layout corresponding to the circuit diagram of figure 5.59. The vertical transmission lines of the Branchline coupler are folded using bends, to reduce the size of the PCB. The green pads are the locations for the diodes and the capacitor. The short circuited quarter wave stubs are thin, corresponding to a high characteristic impedance to ensure as high an impedance over as wide a bandwidth around the LO and RF frequencies. The open circuited quarter wavelength stubs are wide transmission lines, providing a low shunt impedance for as wide a bandwidth as possible corresponding to as wide a bandwidth around the LO and RF frequencies, so that as much of the RF energy is converted to IF signals as possible. The layout is designed so that the position of C1 can be moved closer to or further away from the IF port, to optimise the performance.

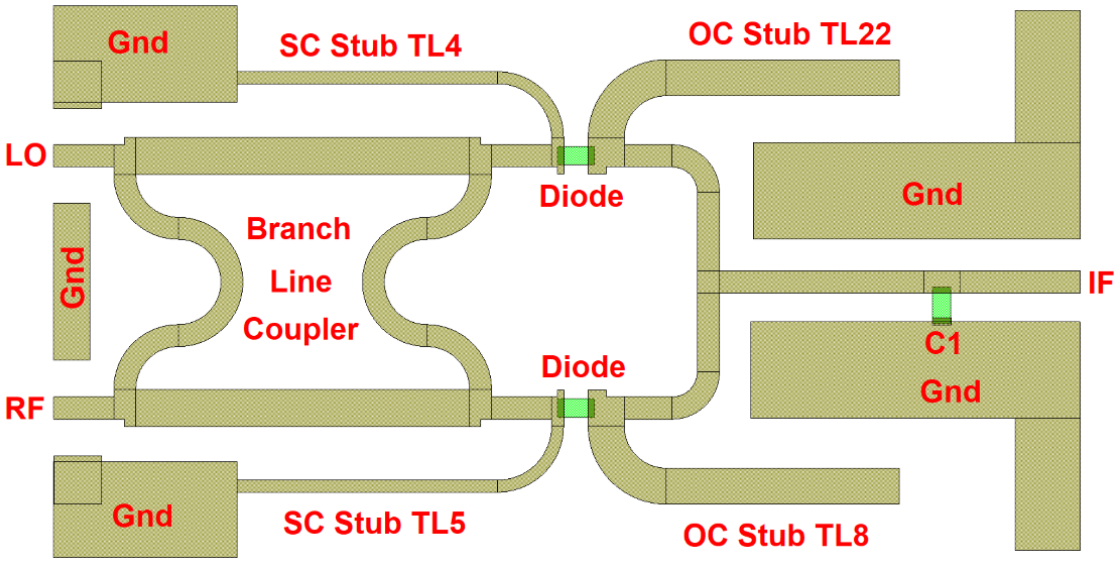



Figure 5.60. Branchline coupler balanced mixer layout.

Figure 5.61 shows the conversion loss of the microwave mixer of figure 5.59. The conversion loss is 1.23 dB worse than that of the basic Branchline coupler balanced mixer shown as the red curve in figure 5.57. The conversion loss includes approximately 0.5 dB losses in the PCB tracks.

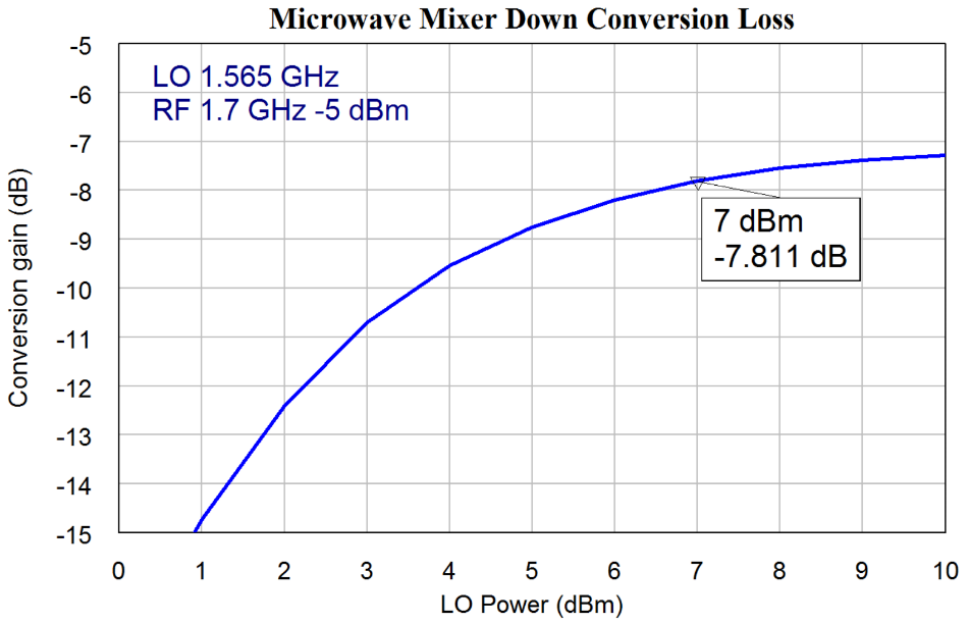



Figure 5.61. Conversion loss of a balanced mixer with a Branchline coupler.

Figure 5.62 shows the simulated IF spectrum of the mixer and it can be seen that the mixer performs well. The components above 1 GHz can easily be filtered out using a simple low pass filter at the IF output, as shown in figures 5.56 and 5.58.

Figure 5.63 shows the hardware for the PCB layout of figure 5.60. Notice the many vias connecting the top ground-plane to the bottom ground-plane, to ensure that a good earth is obtained at the end of the quarter wavelength long lines TL4 and TL5 in figure 5.59, which are needed to provide a DC path for the diode currents.

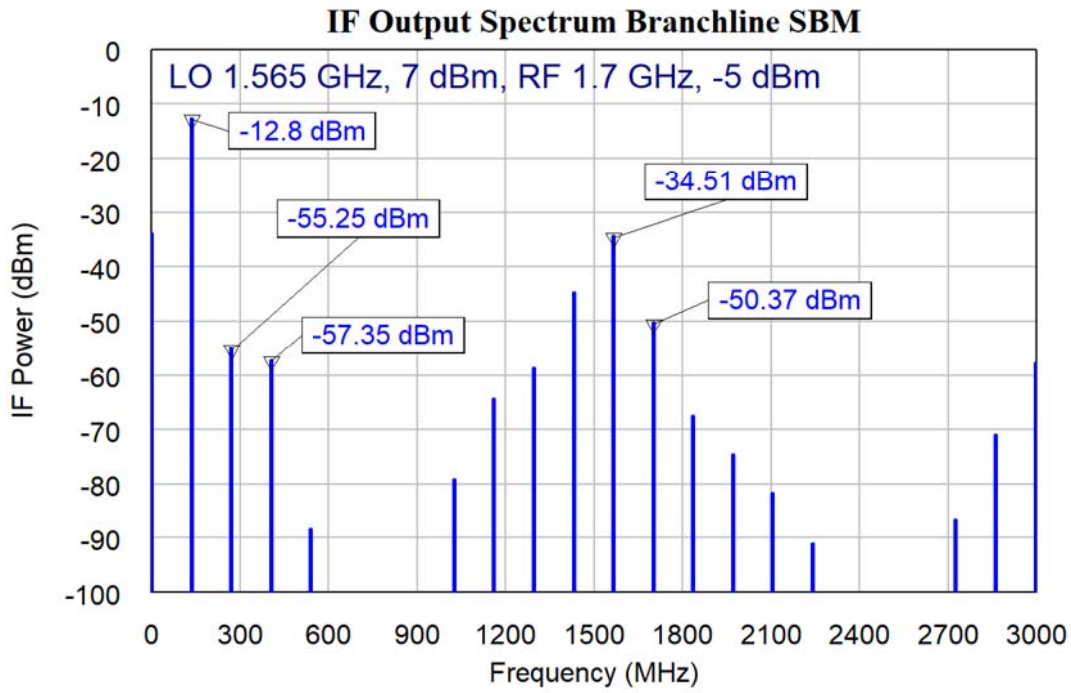



Figure 5.62. IF spectrum of a Branchline coupler balanced mixer.

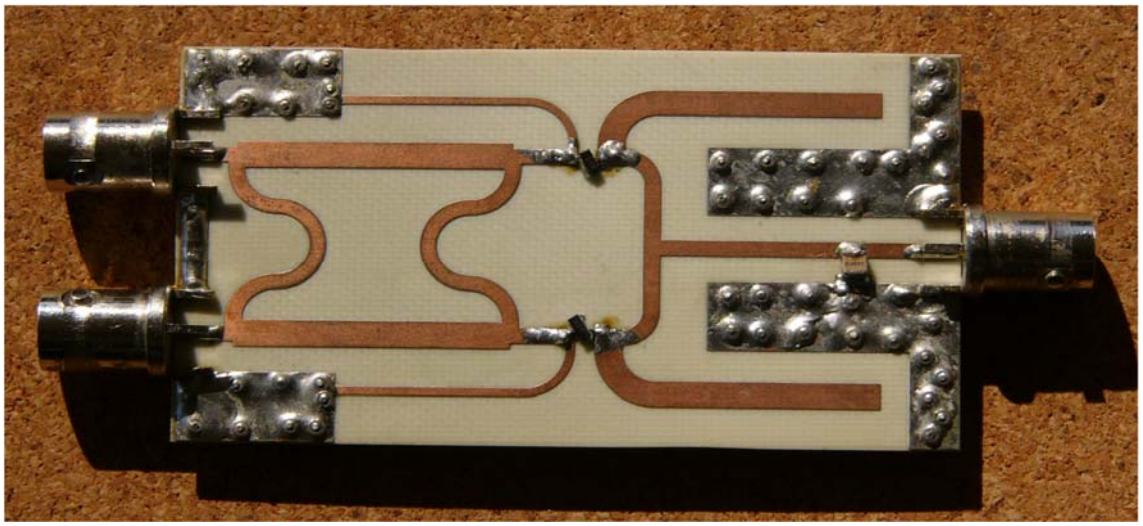


Figure 5.63. Hardware realisation of the balanced mixer using a Branchline coupler.

Figure 5.64 shows the measured performance of the hardware of figures 5.59, 5.60 and 5.63. This IF spectrum closely resembles the simulation results shown in figure 5.62. For an LO level of 7 dBm at 1.565 GHz and an RF signal of –5 dBm at 1.7 GHz, the IF signal was –12.25 dBm, being within 0.6 dB of the performance shown in figure 5.62, and corresponding to a conversion loss of 7.25 dB. The second harmonic distortion at 270 MHz, at -55 dBm, is nearly the same as the computer simulation. The LO feed-through is 10 dB larger, but two microwave diodes were selected for the mixer, without being matched. Third harmonic distortion is 10 dB larger in figure 5.62, than it is in figure 5.64. In figure 5.64, the signal components in the region 88 to 108 MHz at -80 dBm are the local 100 kW EIRP FM transmitters, located Mt. Stewart, 2.7 km from James Cook University. The 170 MHz TV transmitter and a block of five 200 kW DVB-T transmitters covering the spectrum from 545 to 625 MHz all located at Mt Stewart (Townsville Qld, Australia) can also be seen on the spectrum.

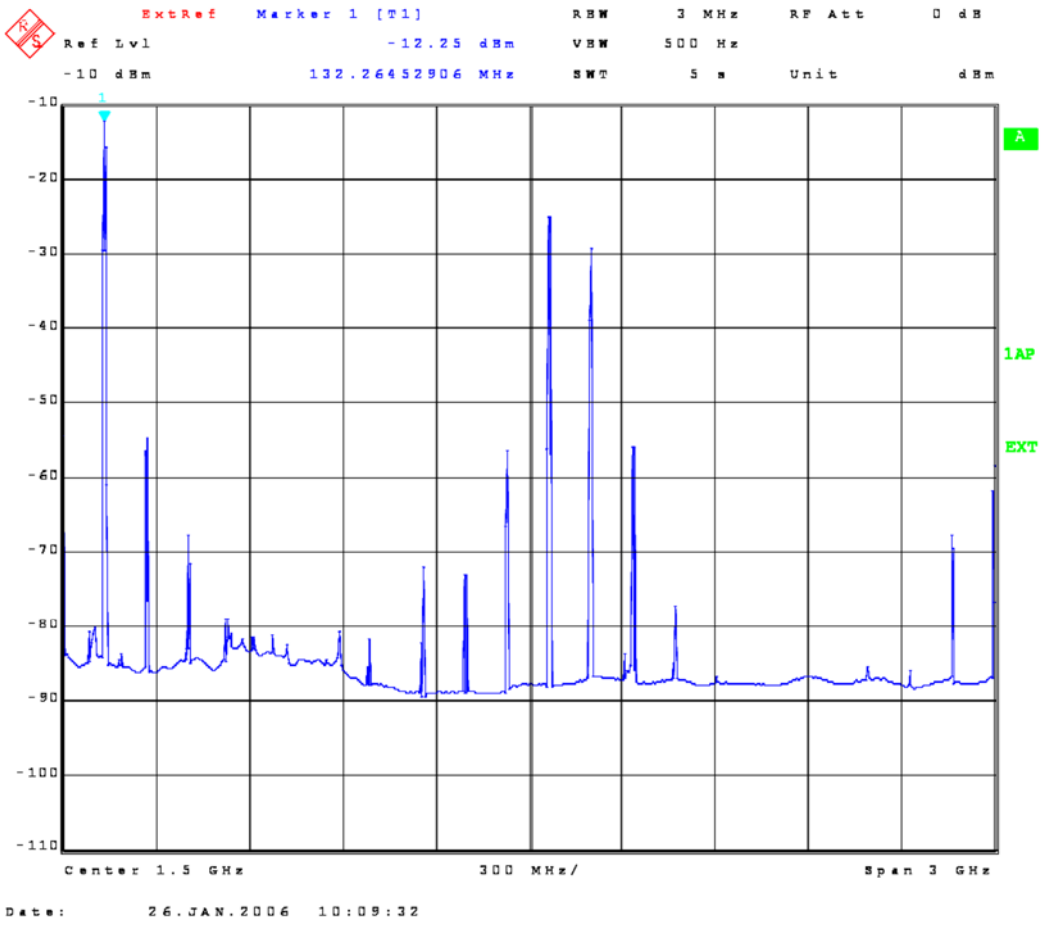



Figure. 5.64, Measured spectrum of Branchline coupler balanced mixer of figure 5.63. (Hor: Centre Frequency 1.5 GHz, 300 MHz/div. Vert: Max -10 dBm, 10 dB/div.)

It is possible to use a multi-loop Branchline hybrid, as shown in figures 4.35 to 4.39, for the mixer. That extends the operating bandwidth of the mixer. M. Y. Algumaei [11] used a triple loop Branchline hybrid to produce a mixer for RF inputs bandwidth of 3 GHz to 12 GHz.

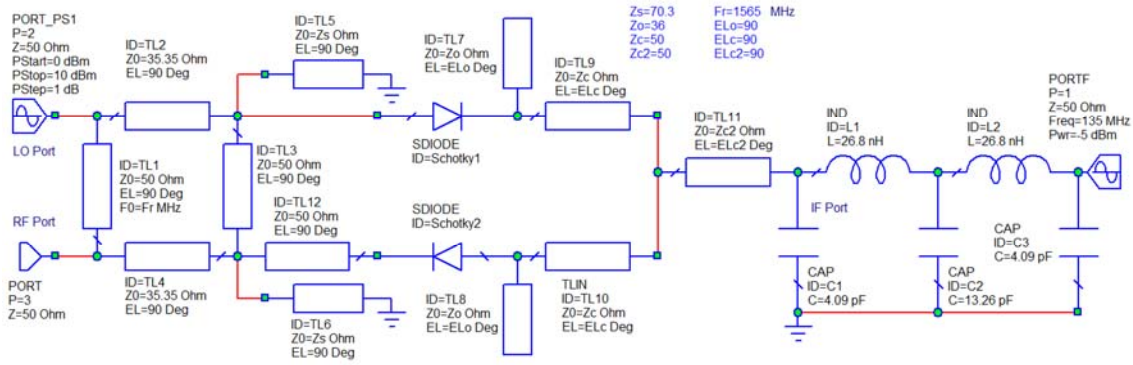



Figure 5.65. Branchline coupler balanced mixer for up-conversion.

The mixer of figure 5.56 can also be used for up-conversion. However, since now the inputs are LO and IF, the circuit of figure 5.56 will no longer result in the correct phase angles for efficient mixing in the diodes. As a result, line TL12 in figure 5.65, needs to be added to produce a 180 ° LO and a 0 ° IF phase difference across the diodes, to ensure efficient mixing in the diodes. Figure 5.65 shows the resulting circuit schematic.

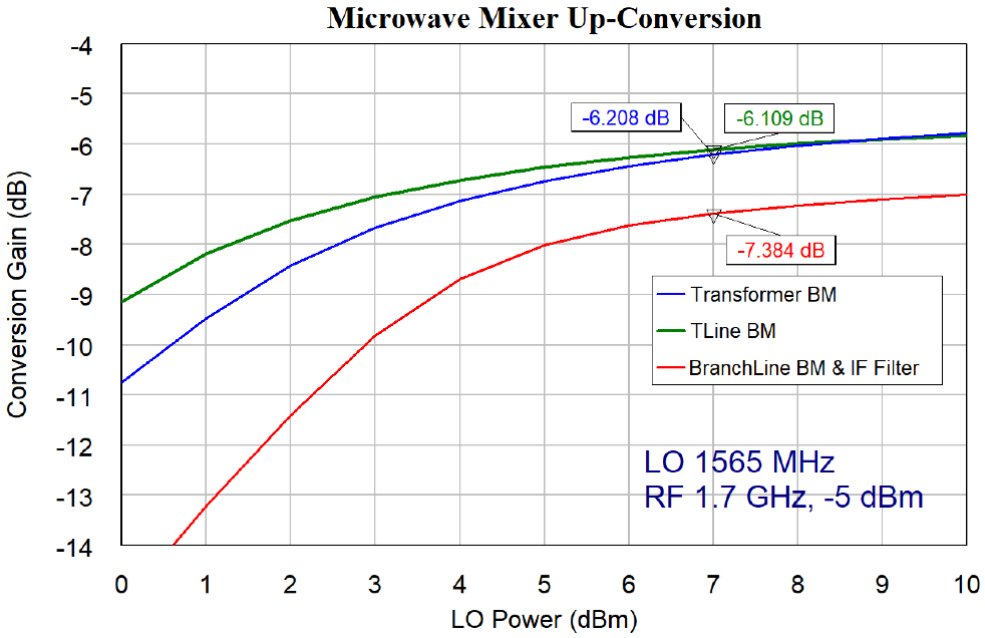



Figure 5.66. Conversion gain of microwave balanced mixer up-converters.

Figure 5.66 shows the conversion loss of the mixer and compares that with the transformer based balanced mixer of figure 5.25 and the transmission line balanced mixer of figure 5.53, used for up-conversion at the fame frequencies. The Branchline balanced mixer has 1 dB more conversion loss. Requiring the extra transmission line (TL12 in figure 5.65), makes the Branchline balanced mixer uncompetitive for up-conversion.

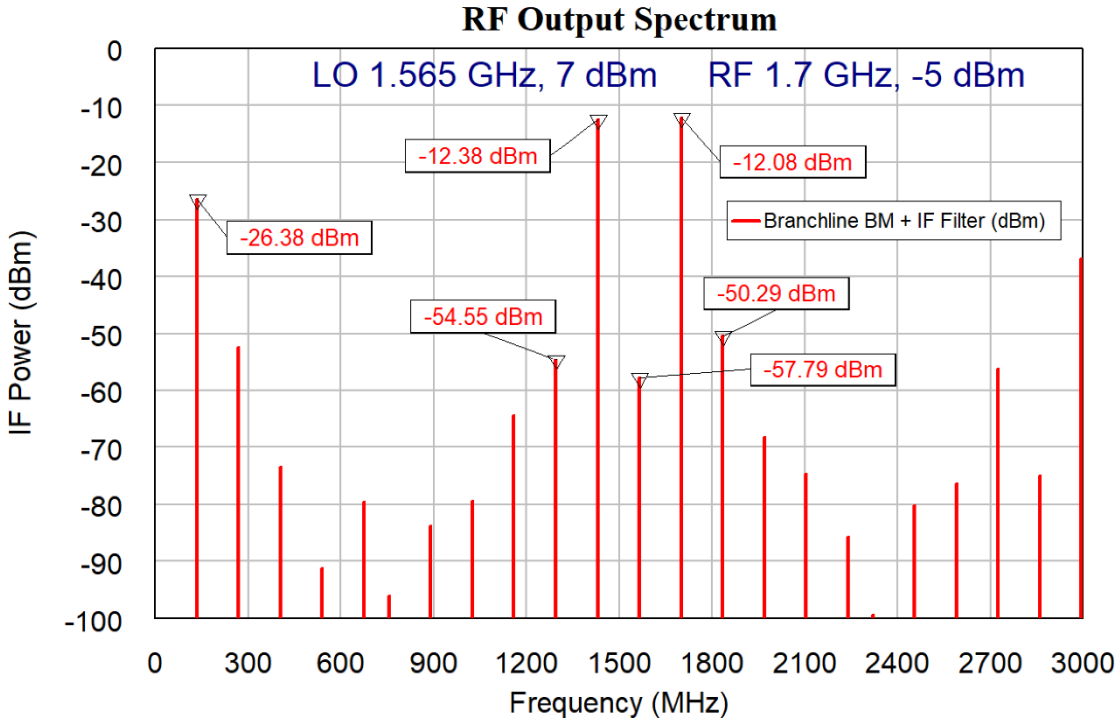



Figure 5.67. RF spectrum of a Branchline coupler balanced mixer up-converter.

Figure 5.67 shows the RF spectrum of a Branchline coupler balanced mixer up-converter. The spectrum of the transmission line balanced mixer of figure 5.53, when used as an up-converter is similar.

# 180° Hybrid Microwave DBM

A 180°hybrid consisting of the Parallel Coaxial Balun of figure 4.55 or the Marchand Balun of figure 4.58 can also be used to produce microwave double balanced mixers, as shown in figure 5.68.

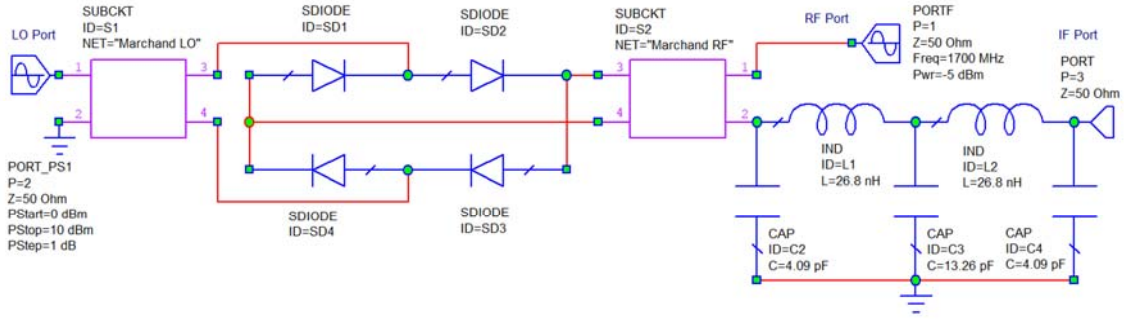



Figure 5.68. 180°Hybrid DBM used for down-conversion.

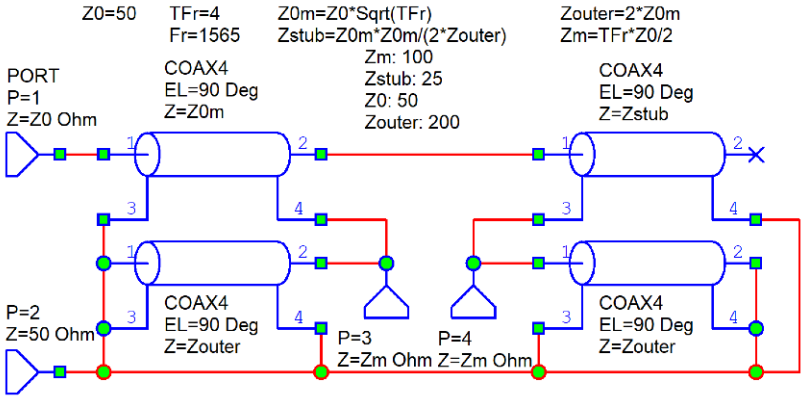



Figure 5.69. Marchand Balun for use in figure 5.68.

The baluns need to be modified to enable the replace the ground with port 2 as shown in figures 5.69 and 5.70. For the Balun at the LO port in figure 5.68, port 2 is grounded and at the RF port, port 2 of the Balun is connected to the IF port. In figure 5.68 a low pass filter is included at the IF port, to slightly reduce the conversion loss and remove most of the RF and LO signals from the IF port. These baluns can be used as subcircuits for the mixer of figure 5.68. A transformer balun, like the centre-tapped transformer, XFMRTAP shown in figure 5.31 can also be used as subcircuits for the mixer of figure 5.68.

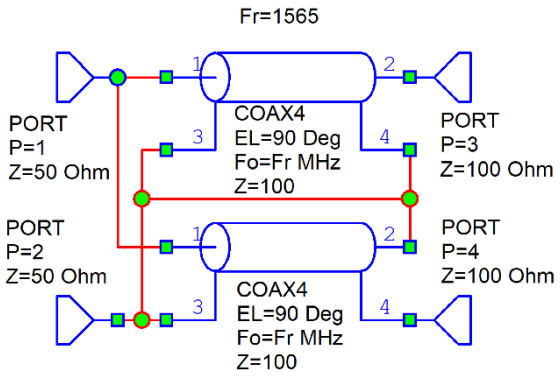



Figure 5.70. Parallel line Balun for use in figure 5.68.

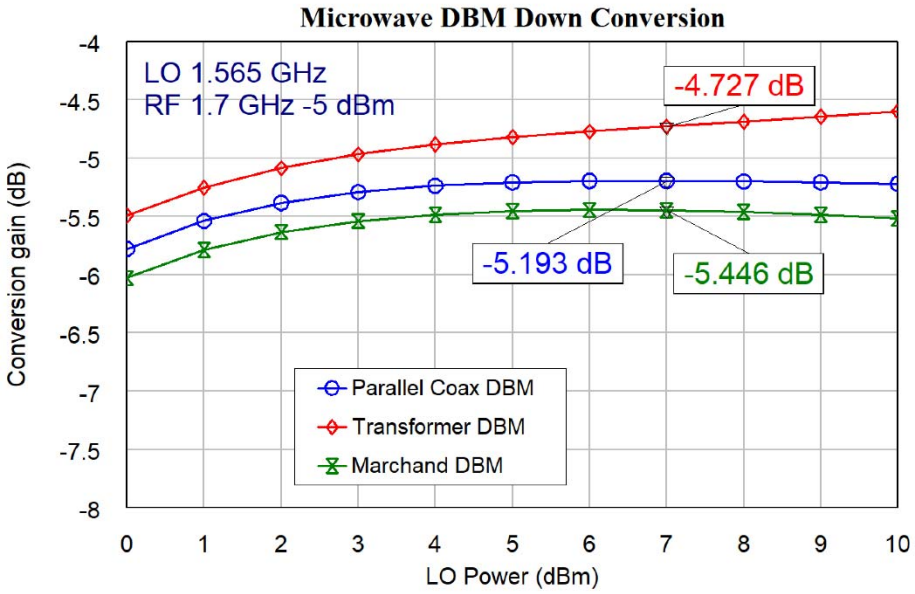



Figure 5.71. Comparison of Conversion gains for the 180° Hybrid mixers.

Figure 5.71 shows the conversion loss of the DBM using the Parallel line and Marchand Balun and compares that with the conventional transformer based DBM of figure 5.31.

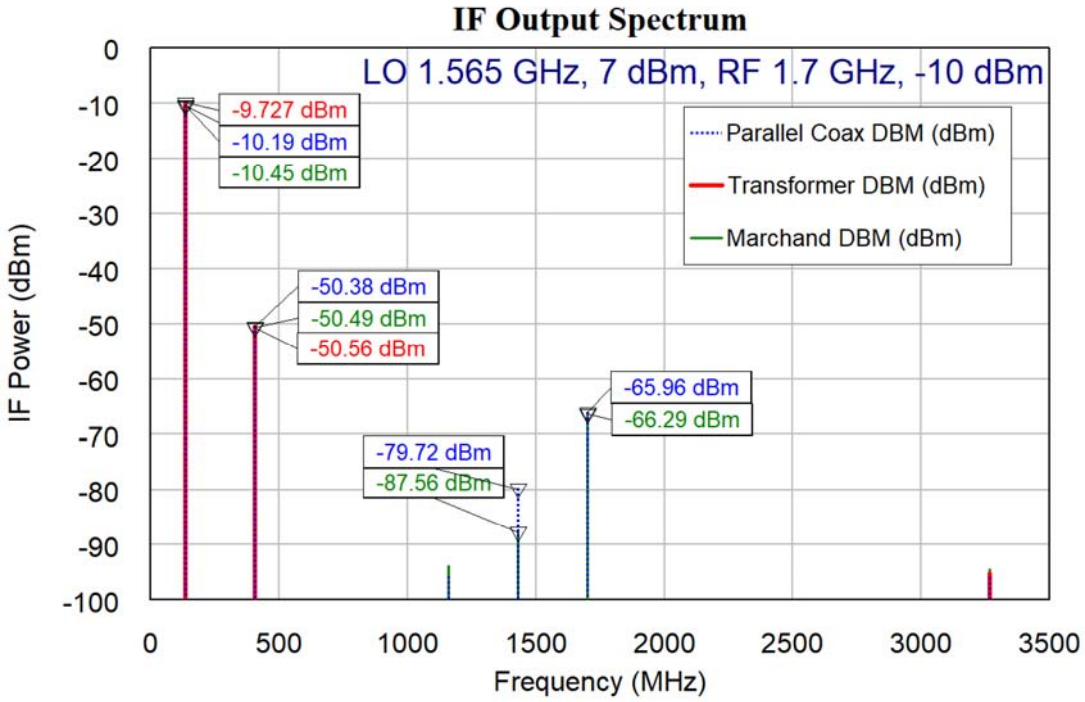



Figure 5.72. Microwave DBM down-conversion spectrum.

Figure 5.73 shows a comparison of the IF spectra, when using these mixers for down-conversion. The signals below 1 GHz are nearly the same. The transformer based DBM does not have any unwanted signals in the 1 – 3 GHz band. These mixers can also be used for up-conversion. Figure 5.73 shows the mixer of figure 5.68 as an up-converter. The resulting up-conversion loss is very similar to the conversion loss as down-converters for the 3 mixers shown in figure 5.71. Figure 5.74 shows the RF spectrum of the Marchand DBM used as an up-converter.

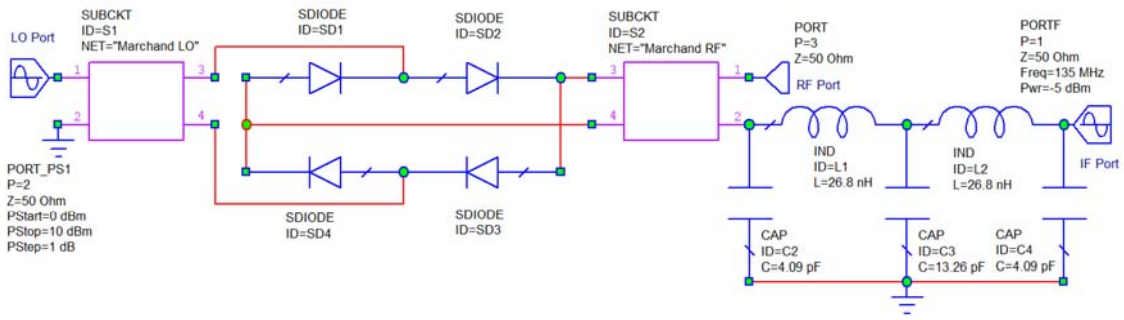



Figure 5.73 180° Hybrid DBM used for up-conversion.

At present companies like Analog Devices, produce commercial core and wire mixers for RF frequencies up to 20 GHz. For designs up to 20 GHz, commercial transformer based DBMs are smaller and cheaper than the designs shown in figures 5.53 to 5.73. Transmission line based, balanced and double balanced mixer designs can operate above 20 GHz and show that as long as the RF, LO and IF signals are combined correctly, a frequency mixer with a low conversion loss and a clean spectrum will result. The design techniques shown in figures 5.53 to 5.73 can be implemented in LTCC, silicon or gallium arsenide. They can form the basis for MMIC DBM designs, described near the end of this chapter.

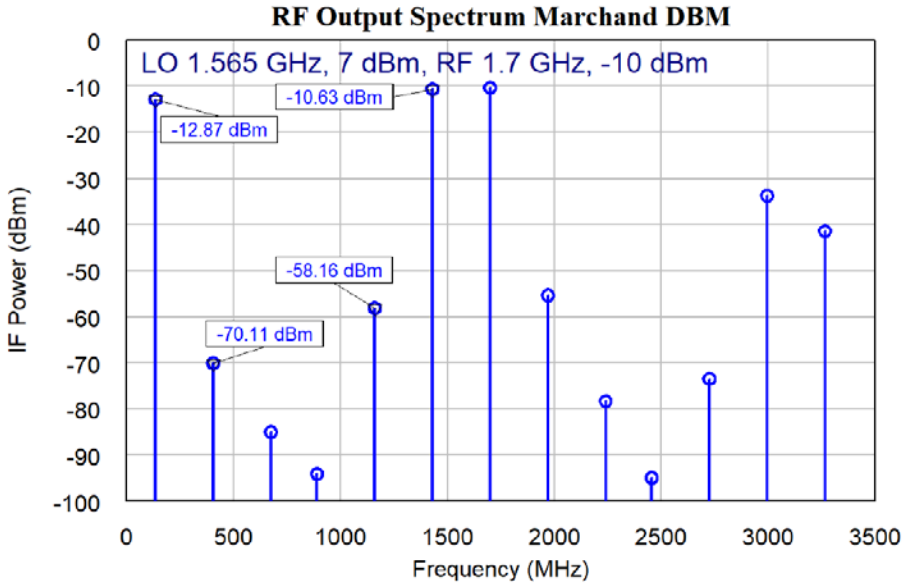



Figure 5.74. Marchand Hybrid DBM used for up-conversion.

## Active Single Transistor Mixer

Figure 5.75 shows the *Low_Power_Mixer* [12], which is an active single diode mixer from the Cadence AWR DE mixer examples. This example also shows how Conversion Loss or Gain, Gain Compression and other mixer parameters can be determined using MWO. An active single transistor mixer has a similar spectral performance to a passive single diode mixer, but has a conversion gain. The mixer of figure 5.75 has a conversion gain of more than 10 dB. Active single transistor mixers are used in many consumer devices like radio and TV receivers. It is possible to improve the mixing performance by using two transistors in a push-push amplifier configuration and thus produce an active balanced mixer.

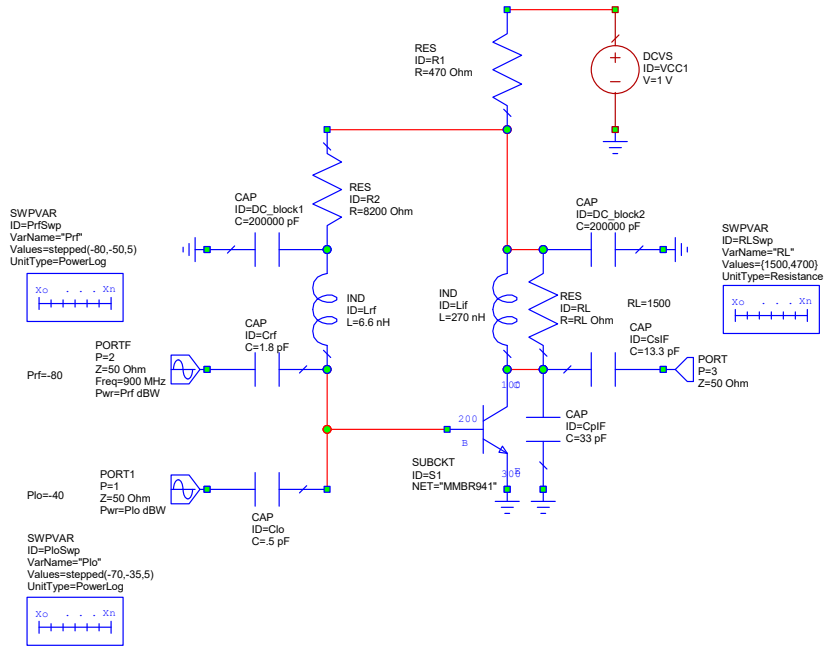



Figure 5.75. Active single diode mixer (Cadence AWR DE example, Low_Power_Mixer).

# Frater-Gilbert Cell Active Mixer

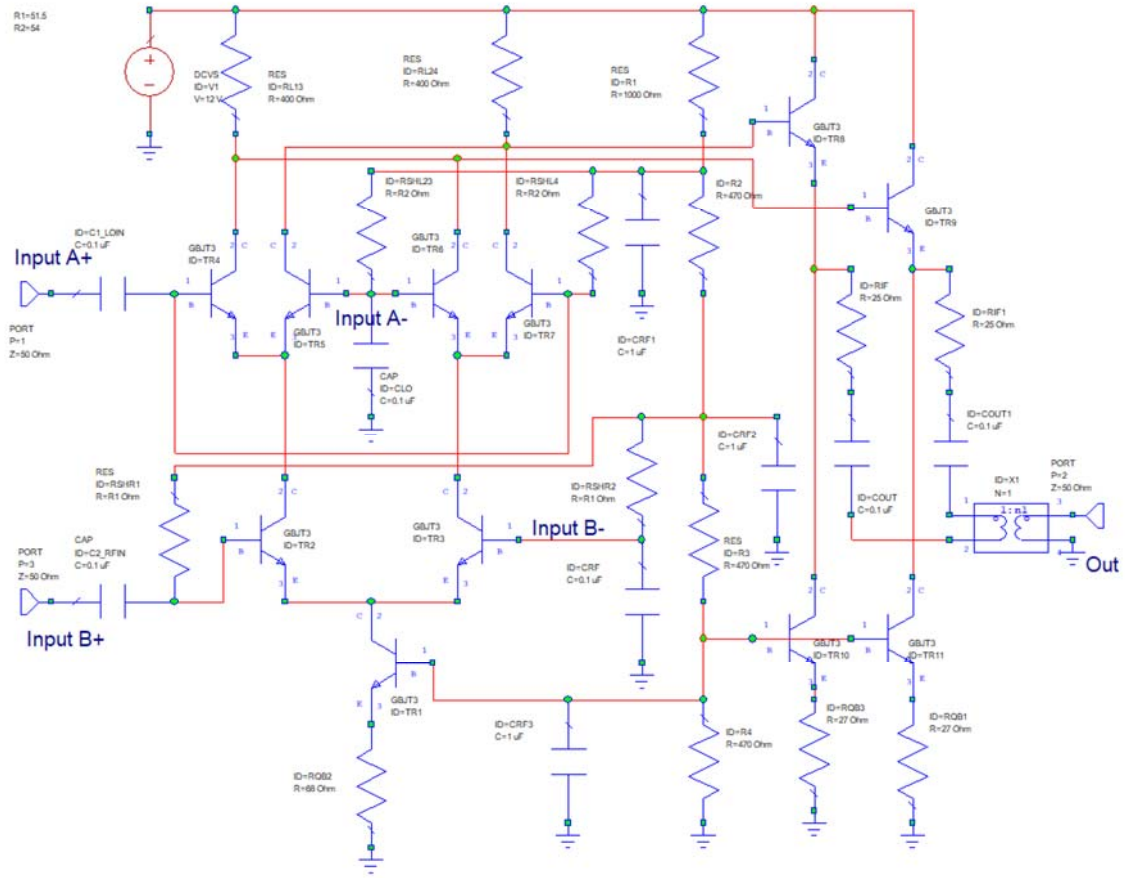



Figure 5.76. Basic Frater-Gilbert Cell active multiplier.

The long tail multiplier, developed by Frater [13] and now more commonly known as the Gilbert Cell [14] provides close to ideal multiplier performance. As a result, it is used as an active mixer in many IC's. There is a *Gilbert-Cell* mixer in the examples provided by MWO. That Frater-Gilbert cell example has been simplified to illustrate its principle of operation as shown in figure 5.76. Commercial Frater- Gilbert Cell mixers with very good IM performances and a frequency range from DC to 5 GHz are available. The circuit consists of 3 parts, the left part of figure 5.76 consisting of transistors TR2 to TR7 is the Frater-Gilbert Cell, long tail multiplier. Transistor TR1 is a constant current source for this multiplier. Transistors TR8 and 9 are voltage followers for the output of the long tail multiplier. Transistors TR10 and TR11 are constant current sources for those voltage followers. Resistors R1 to R4 form a biasing chain to provide the correct biasing for the transistors. All the capacitors are for AC bypassing. The output is a differential signal and for convenience, an ideal transformer is used to convert this to a single ended output. For best performance, the inputs are differential, however to minimise the circuit complexity, Input A- and Input B- are connected to an AC ground. Either input can be used for the LO input, however for the circuit in figure 5.76, using input B for the LO results in a lower level of unwanted sidebands at the expense of a slightly lower conversion gain and a higher level of LO feed-through to the output. For the best input-match, resistor values R1 and R2 are tuned, to result in values slightly above 50 Ω. Normally all these components in figure 5.76 would be included in an IC.

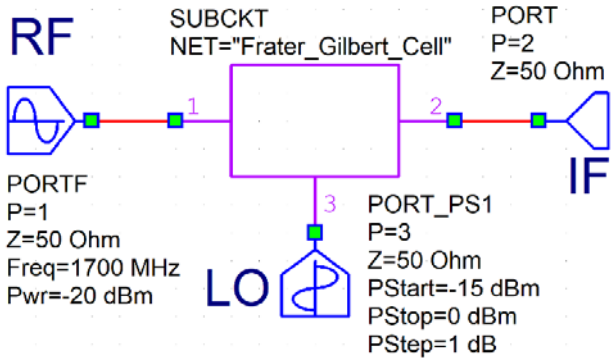



Figure 5.77. Frater-Gilbert Cell down-conversion mixer

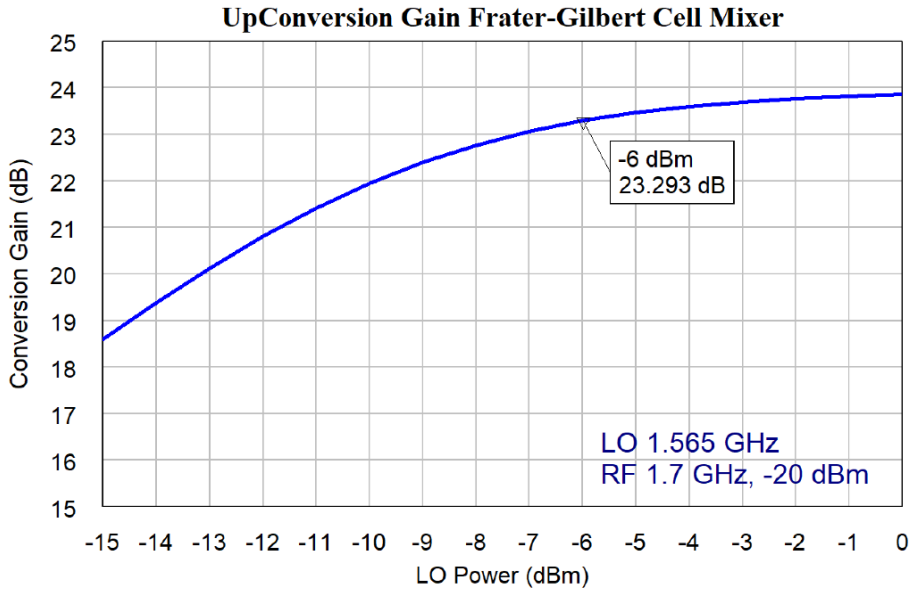



Figure 5.78. Conversion gain of the Frater-Gilbert Cell mixer of figure 5.76.

Figure 5.77 shows the Frater Gilbert Cell connected as a down-conversion mixer, with a stepped LO input power to determine the conversion gain. Figure 5.78 shows the resulting conversion gain. The LO and RF frequencies are chosen to be the same as that for the microwave mixers of figure 5.53 and 5.56.

The Frater-Gilbert Cell mixer is different from the diode mixers in that the best performance is obtained when the LO signal does not cause saturation in the transistors of the Frater-Gilbert Cell. Comparing figure 5.78 with figure 5.34, shows that the slope of conversion gain versus LO power is much larger for the Frater-Gilbert Cell mixer in figure 5.73 than for the DBM in figure 5.26. As a result, variations in AM noise on the LO will cause more of this AM noise to appear on the IF signal in the Frater-Gilbert Cell mixer than in the DBM. Figure 5.78 shows that the largest signal that can be used without the mixer saturating too much is about -6 dBm and that level of LO power has been used for the subsequent measurements. Using a lower LO power gives more ideal mixer action but reduces the conversion gain.

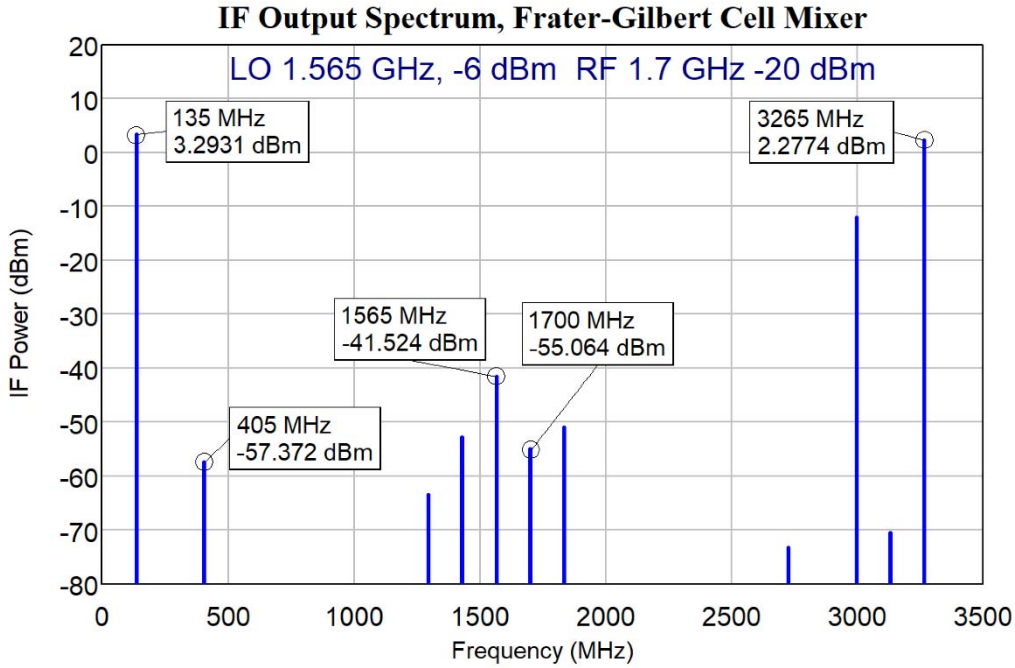



Figure 5.79. IF spectrum of the Frater-Gilbert Cell mixer of figure 5.77 as a down-converter.

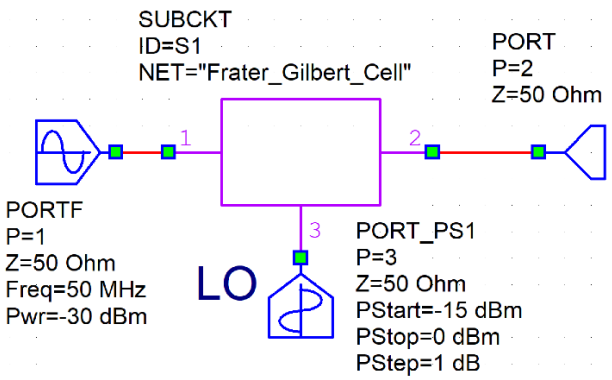



Figure 5.80. Frater-Gilbert Cell up-conversion mixer for RF=-30 dBm.

Figure 5.79 shows the IF output spectrum of the mixer as a down-converter. The LO power is -6 dBm and the RF level is -20 dBm. To enable a comparison to be made, the

same frequencies are used as for figures 5.50 and 5.57. Using a lower RF power level gives a better performance with a better LO and RF isolation at the IF output. The RF signal is at 1.7 GHz and the LO signal is at 1.585 GHz resulting in a difference signal at 135 MHz and a sum signal at 3.265 GHz. Figure 5.79 shows that these nearly the same power level and are the largest signals. The Frater-Gilbert cell acts thus as a near ideal mixer.

Figure 5.81 shows a plot of the conversion gain for Frater-Gilbert Cell up-converter as both the LO and the IF level are varied. The IF level of -18.13dBm corresponds to a 1 dB reduction of the conversion gain of the mixer and thus corresponds to the 1 dB compression point.

Figures 5.82 to 5.86 show the RF spectra of the Frater-Gilbert Cell mixer used as an up-converter, when the IF signal level is varied. The LO signal is -6 dBm and IF signal level is -35 dBm, -30 dBm, -25 dBm and -20 dBm and -15 dBm. For an IF signal of -35 dBm, apart from the LO feedthrough, the unwanted components are more than 58 dB below the wanted components, so that the Frater-Gilbert Cell is near ideal mixer. In precision applications, calibrated biasing can be used to minimise any LO feedthrough.

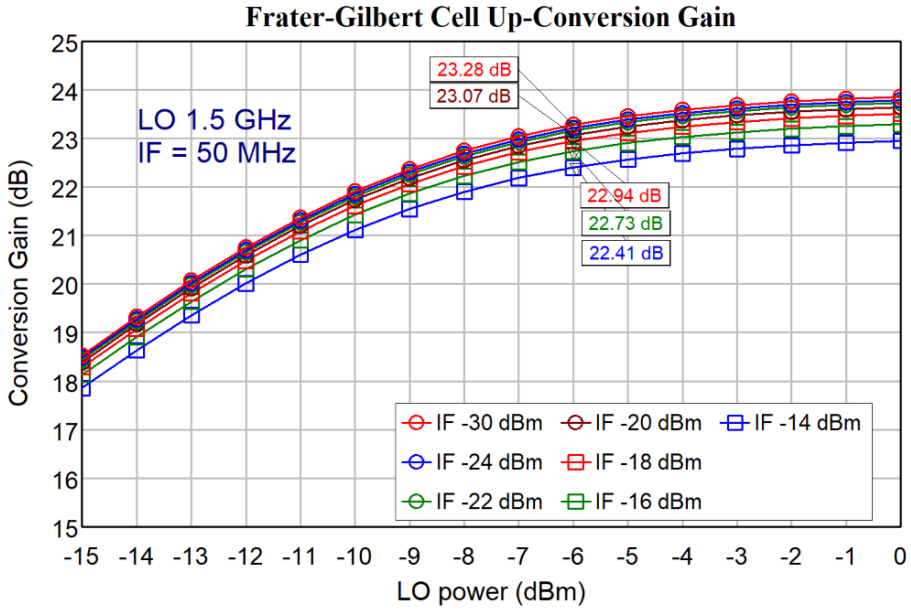



Figure 5.81. Up-conversion gain of the Frater-Gilbert Cell mixer of figure 5.80.

Changing the IF level by 10 dB, from -35 dBm to -25 dBm, causes a 10 dB change in level of the 1.45 GHz and 1.55 GHz components and a 30 dB change in the 3IM component at 1.35 GHz. The mixer is thus operating in a linear range and the expected third order output intercept point (OIIP3) from figures 5.5 and 5.77 is at (0.5*(-11.708 - (-83.162)) + (-11.708)) = 24.019 dBm. Figure 5.76 shows that the conversion gain at a LO of -6 dBm and an IF of -35 dBm is 23.28 dB, the IIP3 point occurs at an IF input level of 24.019 -23.28 = 0.789 dBm. Figure 5.76, shows that at a LO of -6 dBm, an IF signal of -13.5 dBm has 1 dB less conversion gain than an IF of -30 dBm. The 1 dB compression point is thus at an IF level of -13.5 dBm. The IIP3 point is thus 14.3 dB above the 1 dB compression point. That is similar to the corresponding 14 to 16 dB for a typical DBM. These computer simulations or similar measurements on the actual devices can thus easily determine the critical mixer parameters. Passive DBMs, can operate at higher input levels, but produce lower output levels than Frater-Gilbert Cell mixers, because Frater-Gilbert Cell mixers have a conversion gain.

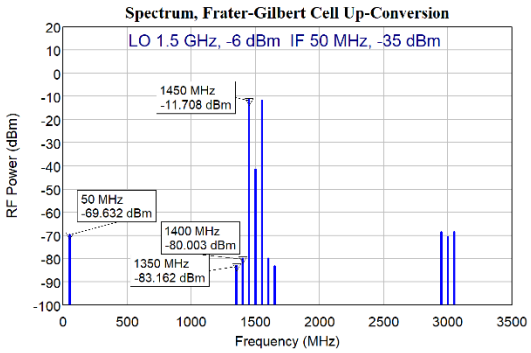



Figure 5.82. RF spectra for IF = -35 dBm

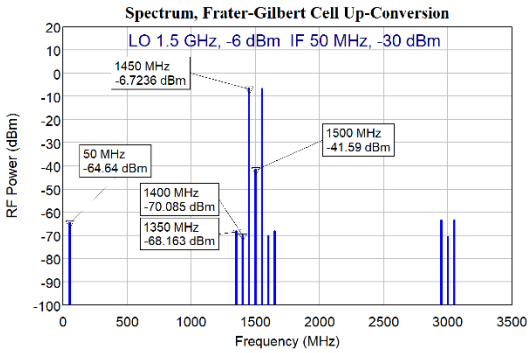



Figure 5.83. RF spectra for IF = -30 dBm

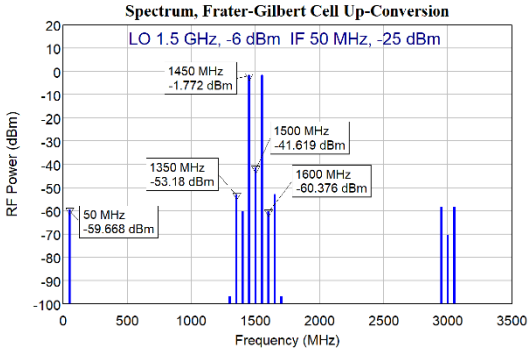



Figure 5.84. RF spectra for IF = -25 dBm

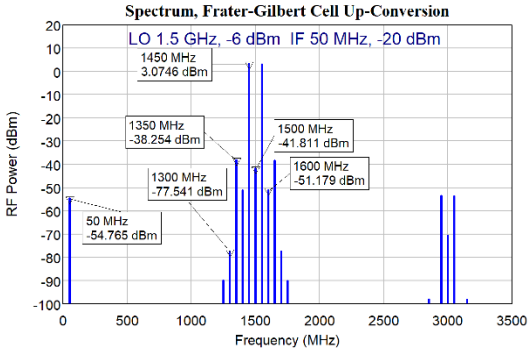



Figure 5.85. RF spectra for IF = -20 dBm

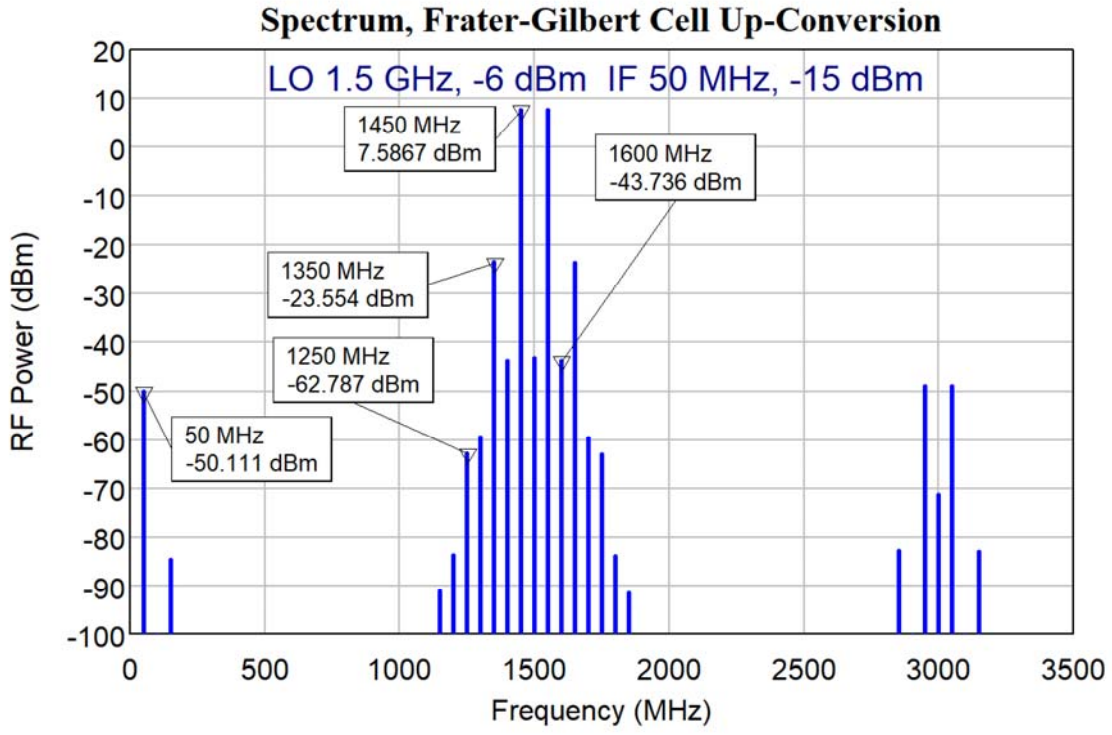



Figure 5.86. RF spectra for the mixer of figure 5.80 as an up-converter, IF = -15 dBm.

Figure 5.87 shows the corresponding RF waveform. This waveform is similar to figure 5.10 for the multiplier and corresponds to an ideal Double Sideband Suppressed Carrier waveform. Any unwanted signals cannot be observed in the time waveform, but can be detected in the spectrum of figure 5.85.

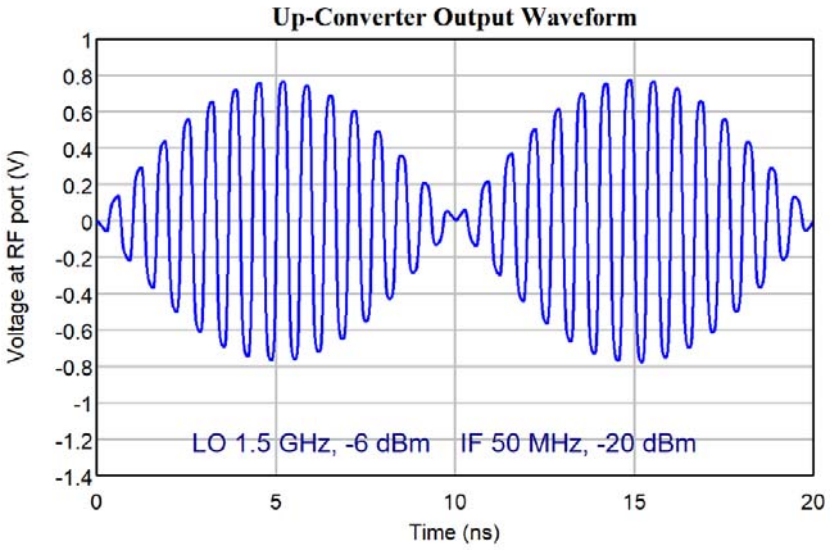



Figure 5.87. RF Waveform for the mixer of figure 5.80.

## Quadrature (IQ) Mixers

Most modern modulation methods, such as QAM, CDMA, OFDM and LTE, use vector modulation and require IQ modulators. The vector modulator typically uses DSP techniques to calculate a complex baseband signal with Real ⇒ I and Imaginary ⇒ Q components corresponding to the desired signal. Those digital signals are then converted to analogue signals using two Digital to Analogue converters, one for the baseband I (BB-I) signal and one for the baseband Q (BB-Q) signal. Since for quadrature mixers, a zero frequency IF is normally used, the term Baseband (BB) is a more accurate description and as a result is used here.

In quadrature mixers a quadrature or 90 degree hybrid, like a Branchline coupler is used to produce two LO signals, corresponding to Cosine (LO-I) and Sine (LO-Q) of the LO frequency. In an up-converter, BB-I signal is multiplied with the LO-I signal using a DBM and the BB-Q signal is multiplied with the LO-Q signal using a DBM, as shown in figure 5.88. The resulting signals are then added, using a combiner like a Wilkinson hybrid to produce the RF signal. The result is the baseband spectrum shifted to the LO frequency. This can be demonstrated mathematically by considering the baseband signal to be a vector of magnitude $A_b$ and a phase angle $\Phi_b$, then:

$$BB = A_b Cos(\emptyset_b) + jA_b Sin(\emptyset_b) = BB\text{-}I + jBB\text{-}Q \quad \text{Eqn. 5.13}$$

$$LO\text{-}I = Cos(\omega_c t) \quad \text{Eqn. 5.14}$$

$$LO\text{-Q} = -Sin(\omega_c t) \quad \text{Eqn. 5.15}$$

$$RF\text{-}I = BB\text{-}I * LO\text{-}I = \frac{A_b}{2}\{Cos(\omega_c t + \emptyset_b) + Cos(\omega_c t - \emptyset_b)\} \quad \text{Eqn. 5.16}$$

$$RF\text{-}Q = BB\text{-}Q * LO\text{-}Q = \frac{A_b}{2}\{Cos(\omega_c t + \emptyset_b) - Cos(\omega_c t - \emptyset_b)\} \quad \text{Eqn. 5.17}$$

$$RF = RF\text{-}I + RF\text{-}Q = A_b Cos(\omega_c t + \emptyset_b) \quad \text{Eqn. 5.18}$$

The RF signal is thus the baseband vector with an amplitude and phase of the baseband signal. If needed, the phase angle $+\Phi_b$ in equation 5.18 can be changed to $-\Phi_b$ by either generating a – (BB-Q) signal, or swapping LO-I and LO-Q. When $\Phi_b = \omega_b$ then a single sideband RF signal results.

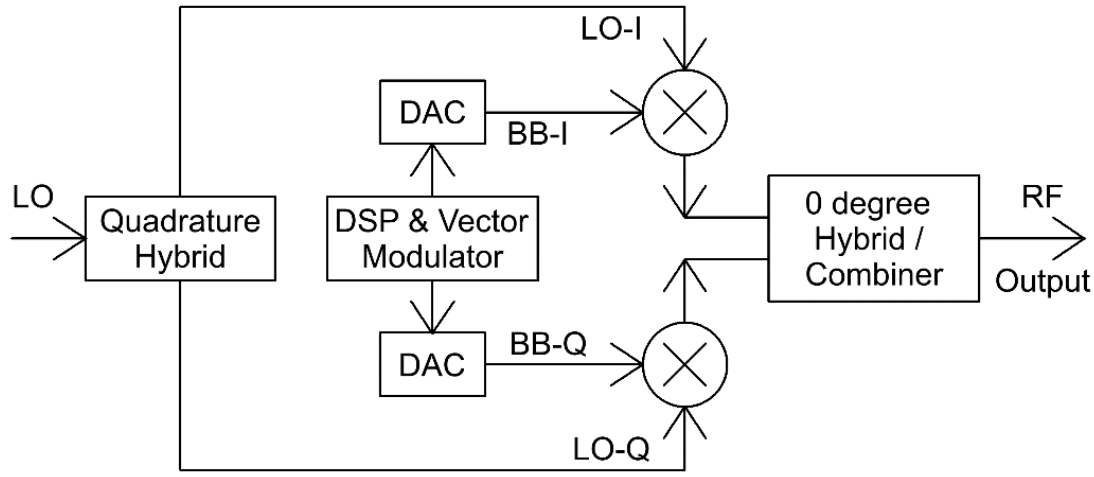



Figure 5.88. Block diagram of a quadrature mixer in up-conversion.

From figure 5.88, for a down-converter, the directions of the RF and BB signals are reversed, the Digital to Analogue converters are replaced by Analogue to Digital converters and the vector modulator is replaced with a vector demodulator. To prevent LO signals from overloading the ADC, low pass anti-aliasing are normally used before the ADC. The resulting block diagram is shown in figure 5.89. When the LO frequency and the RF frequency are not the same, then the IQ down-converter is called an Image reject mixer. These are described in more detail later on.

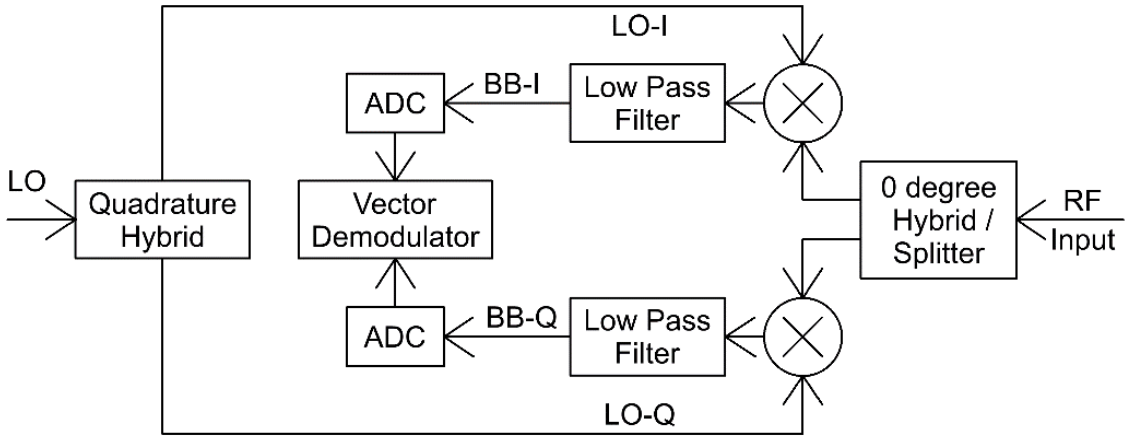



Figure 5.89. Block diagram of a quadrature mixer in down-conversion.

The 90-degree hybrids required for quadrature mixers can also be produced using LC networks, so that quadrature hybrids at frequencies below 500 MHz are possible. As an example, Mini-Circuits make quadrature mixers, for IQ modulators and IQ demodulators, up to 176 MHz as shown in figure 5.90. Analogue devices make IQ and Image-Reject Mixers for up and down conversion with RF/LO frequencies from 2.5 GHz to 64 GHz. Because of limitations in the bandwidth over which an accurate 90° phase shift can be produced, the bandwidth of these mixers is typically limited to a 2:1 frequency range.

Local oscillators produced using phase locked loops or using Direct Digital Synthesis, can have two outputs, which have an exact 90° phase difference over a wide range of frequencies, as is required for the quadrature mixers. A simple twisted ring divide by 2 flip-flop circuit can produce two signals, which are exactly 90° apart. Some commercial IQ mixers include such divide by 2 circuits.

**I & Q Modulators, Surface Mount, 52 MHz to 2000 MHz**

| Model Number | Case Style | RF/LO Freq. Low (MHz) | RF/LO Freq. Hi (MHz) | I&Q Freq. (MHz) Min., DC to _ | I&Q Freq. (MHz) Max., DC to _ | Conv. Loss (dB), Typ. | Conv. Loss (dB), (σ) | Conv. Loss (dB), Max. | Carrier Rejection (dBc), Typ. | Carrier Rejection (dBc), Max. | Sideband Rejection (dBc) Typ. | Sideband Rejection (dBc) Min. | Harmonic Suppression (dBc), 3XI/Q Typ. | Harmonic Suppression (dBc), 3XI/Q Max. | Harmonic Suppression (dBc), 5XI/Q Typ. | Harmonic Suppression (dBc), 5XI/Q Max. | LTCC Construction |
|---|---|---|---|---|---|---|---|---|---|---|---|---|---|---|---|---|---|
| JCIQ-88M+ | BG291 | 52 | 88 | DC | 5 | 5.6 | 0.10 | 7.0 | 40 | 32 | 35 | 30 | 45 | 35 | 65 | 50 | - |
| JCIQ-176M+ | BG291 | 104 | 176 | DC | 5 | 5.6 | 0.10 | 7.0 | 35 | 30 | 35 | 30 | 45 | 35 | 65 | 50 | - |

**I & Q Demodulators, Surface Mount, 104 MHz to 1880 MHz**

| Model Number | Case Style | RF/LO Freq. Low (MHz) | RF/LO Freq. Hi (MHz) | I&Q Freq. (MHz) Min., DC to _ | I&Q Freq. (MHz) Max., DC to _ | Conv. Loss (dB), Typ. | Conv. Loss (dB), (σ) | Conv. Loss (dB), Max. | Amplitude Unbalance (dB) Typ. | Amplitude Unbalance (dB) Max. | Phase Unbalance (deg.) Typ. | Phase Unbalance (deg.) Max. | Harmonic Suppression (dBc), 3XI/Q Typ. | Harmonic Suppression (dBc), 3XI/Q Max. | Harmonic Suppression (dBc), 5XI/Q Typ. | Harmonic Suppression (dBc), 5XI/Q Max. |
|---|---|---|---|---|---|---|---|---|---|---|---|---|---|---|---|---|
| JCIQ-176D+ | BG291 | 104 | 176 | DC | 5 | 5.5 | 0.10 | 7.0 | 0.15 | 0.60 | 2 | 5 | 52 | 40 | 65 | 50 |

Figure 5.90. Mini-Circuits IQ mixers. [15]

### *Active IQ Mixers*

For cellular base stations, radio and TV transmitters, and their test equipment, IQ modulation is used to produce the complex modulated waveforms used in modern communication systems. The mixers used in such signal generators are often active (Frater-Gilbert cell) IQ mixers. Computer controlled DC bias (control and calibration) signals are used to ensure that the carrier feed-through, quadrature phase shifts and I and Q gains are correct. The design of such IC's can cost more than one million dollars. For large-scale applications, such as cellular base stations or automotive distance and collision detection radars, commercial IQ modulator and demodulator IC's are available.

IQ demodulators allow a zero IF frequency to be used, by placing the LO at the centre of the RF band, and producing I and Q baseband outputs, which are passed through simple low pass filters before being digitised. This avoids the need for bulky IF filters. The required filtering is then done digitally, allowing very frequency selective filtering to be achieved.

## Image Reject Mixers

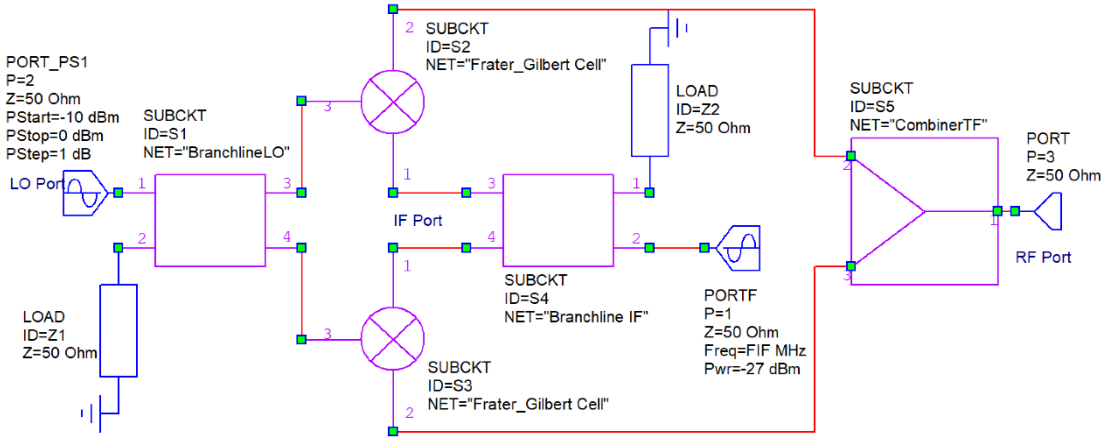



Figure 5.91. Image reject mixer (up converter).

A mixer operating as a down-converter will shift RF signals that are the IF frequency above and below the LO frequency to the IF frequency. The unwanted signal is called the "image signal" in figure 5.2. Normally a filter is used at the RF front-end to filter out any signals inside this image frequency band. Any thermal noise inside this image frequency band will contribute to the noise at the IF frequency band. An image reject mixer will only shift the required signals to the IF frequency and will not shift the signals or noise of the image band to the IF frequency. Image reject mixers can thus provide an improved noise performance. By simply using a non-zero IF frequency, IQ mixers can be used as image reject mixers, for both up-conversion, by applying an input signal at the IF port 1, as shown in figure 5.91, or for down-conversion, by applying an input signal to the RF port 3.

For Up-conversion, a Single Sideband signal is generated. For details of the mathematics involved, see articles on using the Hilbert Transform for generating Single Sideband [16]. In this design, Branchline couplers are used to produce the required 90-degree phase shifted signals. Figure 4.39 shows that Branchline couplers maintain a 90 ±1.22º phase shift over a ±10% bandwidth, which is sufficient for many communication systems. To simplify the design, ideal transmission lines of 90º electrical length are used, without regard of the physical length of those lines. In figure 5.91, at port 1, a Branchline coupler (Branchline IF) is used at the IF frequency of FIF=50 MHz, clearly those lines would be too long to realise and normally LC networks or Digital Signal Processing (DSP) techniques are used to produce the required phase shifts or the required IQ signals at those frequencies. The block diagram is the same as that for the IQ mixer in figure 5.88, with the IF-Q signal being constrained to be the Hilbert transform (90-degree phase shift) of the IF-I signal. In figure 5.88, the in-phase combiner uses a transformer Wilkinson hybrid, however this can also be realised using a Wilkinson transmission line hybrid.

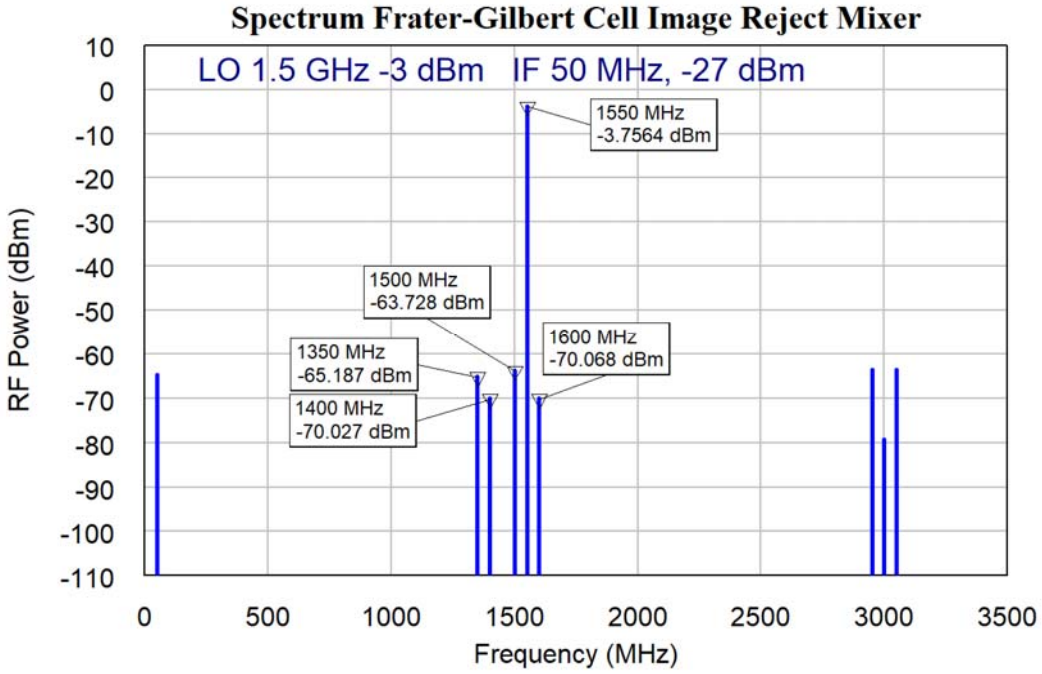



Figure 5.92. Image reject mixer spectrum for Frater-Gilbert Cell upper sideband up-converter.

For active IQ mixers, the Frater-Gilbert cell mixers in figure 5.91 are the same as the one shown in figure 5.76. For figure 5.83, a LO level of -6 dBm and an IF signal of -30 dBm were used. Since the LO signal is split to drive the 2 mixers, a LO of -3 dBm and an IF

signal of -27 dBm is required. Figure 5.92 shows the resulting spectrum for the image reject mixer, when used as an upper sideband up-converter. Comparing this with figure 5.83, the signal at 1550 MHz has increased by 3 dB, due to the signals from both mixers being added. The 1450 MHz signal is removed due to the signals from both mixers being subtracted. The signals at 1400 MHz (LO-2*IF) and 1600 MHz (LO+2xIF) are second harmonics of the IF and thus will have 180 degree phase shift at the output of the IF Branchline coupler, so that these signals do not have image rejection and should have the same amplitude. The signal at 1350 MHz (LO-3*IF) due to the third harmonic of the IF signal and has a 270 degree phase shift at the output of the IF Branchline coupler. That causes a single sideband signal at 1350 MHz, with no signal at 1650 MHz. These harmonic relationships can be verified by tuning FIF.

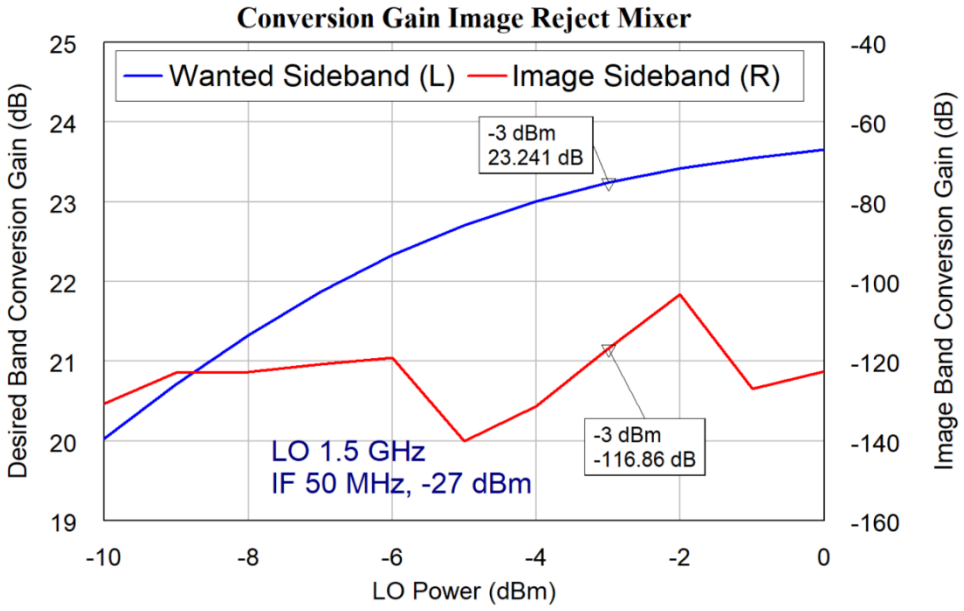



Figure 5.93. Conversion gains of the image reject up-conversion mixer of figure 5.91.

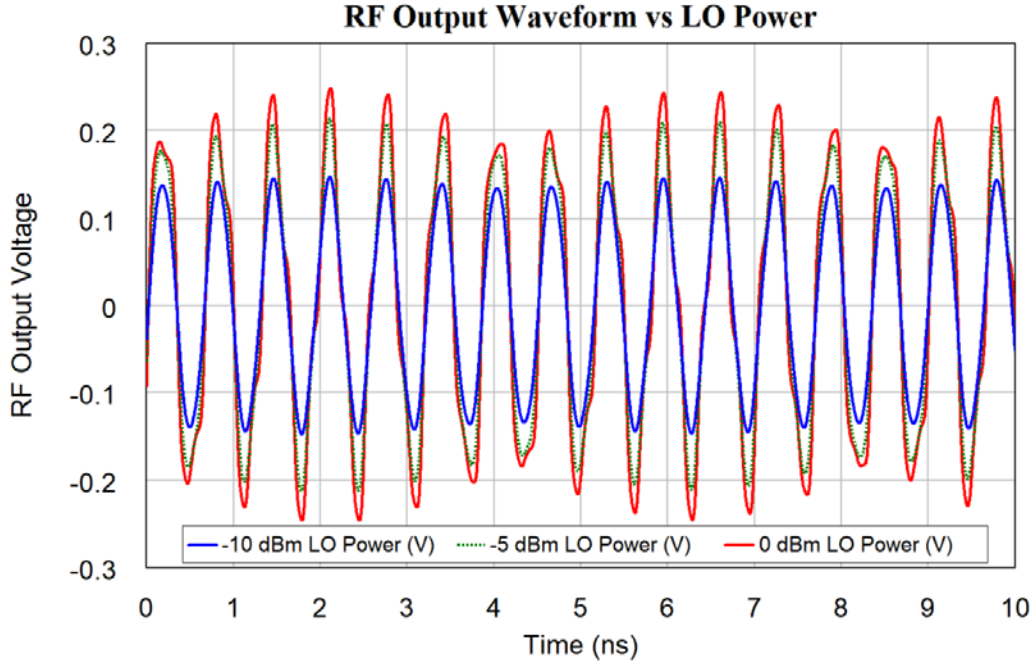



Figure 5.94. RF output current of image reject mixer.

Figure 5.93 shows the up-conversion gains for this mixer. Figure 5.81 shows the conversion gain of the same Frater-Gilbert Cell mixer when used as an up-converter operating at a similar LO frequency. The LO power of -3 dBm and IF power of -27 dBm in figure 5.87 correspond to a LO power of -6 dBm and IF power of -30 dBm in figure 5.78. The wanted sideband conversion gain in figure 5.93 of 23.241 dB is very similar to the 23.293 dB in figure 5.78. Figures 5.92 and 5.93 show that the image rejection, the difference between the wanted and unwanted sideband, is 23.241 -116.86 dB = 140.1 dB, so that this mixer works perfectly as an image reject mixer. In practice a perfect match between the conversion gain and phase shifts produced by 2 separate mixers is unlikely to be achieved, in addition, the hybrids used will not produce perfect 90 degree phase shifts, so that a 25 dB image rejection is more common [17-18]. Figure 5.89 shows the output current at the RF port of the mixer. For a -10 dBm LO, the output waveform is nearly a pure sine wave at 1.55 GHz. As the LO level is increased, the increase in the amplitude variation of the RF output due to the LO can be seen.

## *Passive IQ Mixers*

The Frater-Gilbert Cell in figure 5.86 can be replaced by a DBM and the LO level and IF levels changed to match. Figure 5.90 shows the RF spectrum when the LO is +10 dBm and the IF level is -8 dBm. The conversion loss is -4.9 dB and the image rejection is more than 70 dB. In practice, the image /sideband rejection will be more like 22 dB [19] due to differences in diodes and the hybrids not producing perfect 90-degree phase shifts.

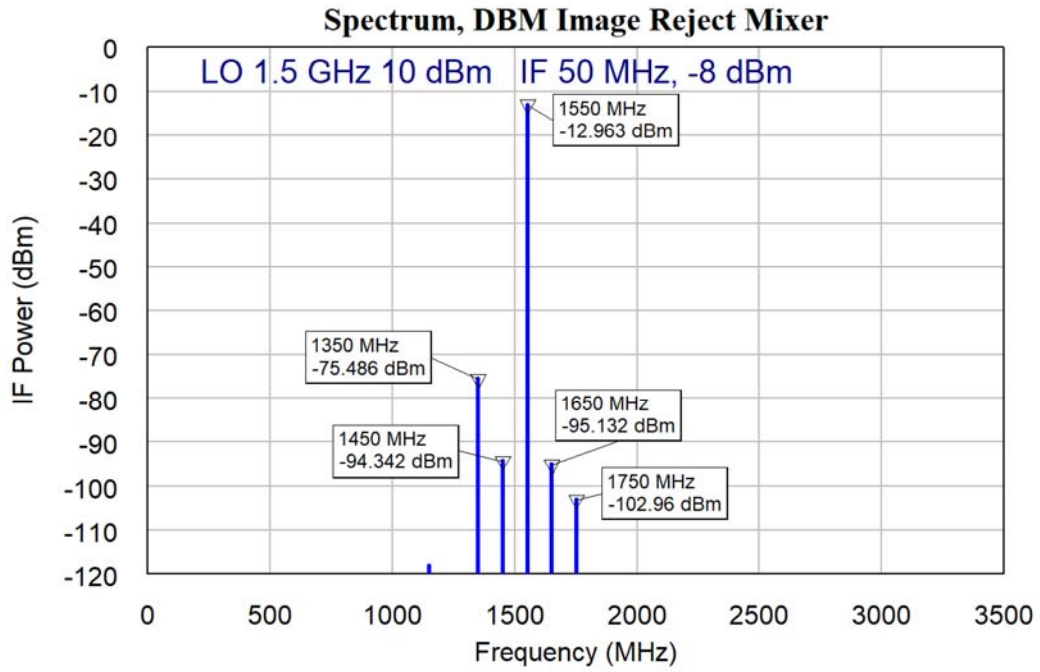



Figure 5.95. Spectrum for DBM upper sideband up-converter.

For an image reject down-conversion mixer, the same block diagram of figure 5.91 is used. At port1, the IF input, the IF frequency and the IF Branchline coupler of the up-conversion circuit, is changed to the RF input, the RF frequency and the RF Branchline coupler, for down-conversion. Also, the RF output port and the RF in-phase combiner of the up-conversion circuit is changed to the IF frequency and an IF in-phase combiner to achieve down-conversion. If a DBM is used, then the mixers low frequency ports should be used for the IF, as an input for up-conversion and as an output for the down-conversion.

If Frater-Gilbert Cells are used then the mixers inputs need to be connected to the LO and RF signals for down conversion and to the LO and IF signals for up conversion.

## Examples of Commercial Active Mixers

Many manufacturers produce active mixers for use in commercial equipment. In particular, mixers for use in mobile and cordless phones, wireless LANs and similar consumer devices are readily available.

The LTC5588-1 IQ mixer shown in figure 5.96 is used as an up-converter for mobile radio applications. This mixer uses Frater-Gilbert cells for the mixers. An IQ mixer allows the required RF output signal to be produced, without the need to filter out unwanted sidebands. The LTC5588-1 has a minimum image rejection of -27 dBc. An I and Q signal, up to 430 MHz can be used, to produce a quadrature modulated RF signal from 200MHz to 6GHz, with an output power up to -1.9 dBm. In the 900 MHz mobile/cellular phone band, the typical image rejection is -45 dBc and in the 1.8 and 2.1 GHz bands, the typical image rejection is -55 dBc. The mixer performance satisfies all the G2 to G4 mobile radio standards. These devices are aimed at base-stations, point-to point microwave links, Digital TV and DAB modulators and military radios. GaAs Microwave Monolithic IC's (MMIC) are used for most commercial mixer applications.

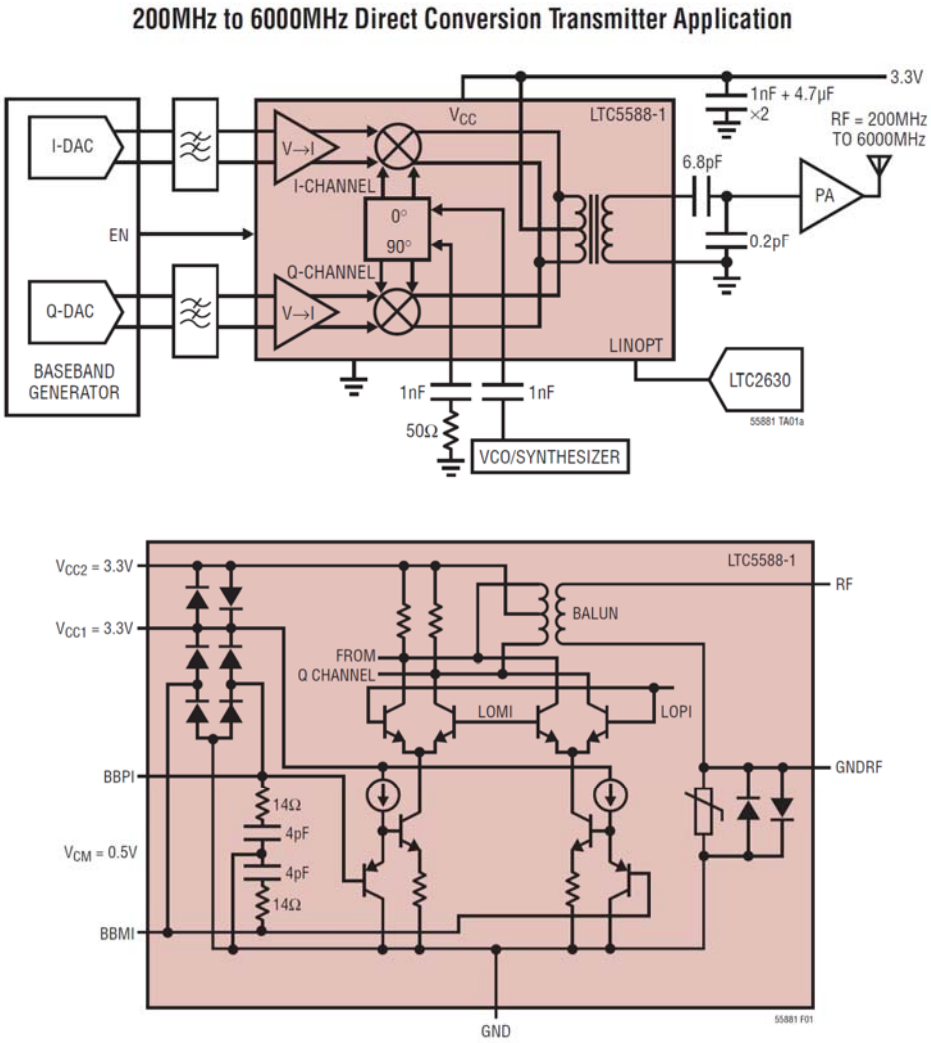



Figure 5.96. LTC5588-1 typical application (top) and simplified schematic for one channel [20].

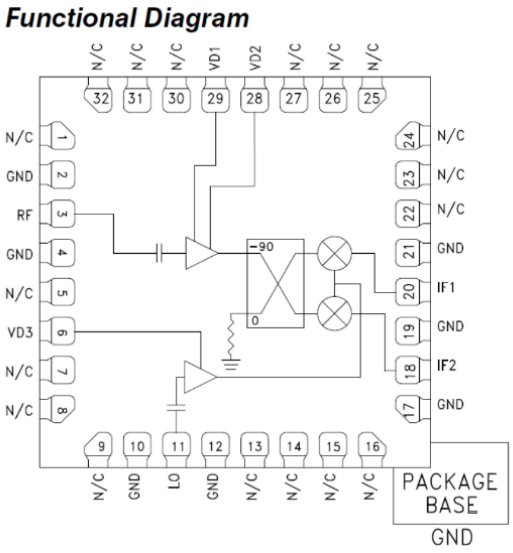



Figure 5.97. Analog Devices HMC1113LP5E [22].

For Satellite receivers, a low noise amplifier (LNA) and an IQ mixer are often combined in one IC [21]. Figure 5.97 shows this in the block diagram of a HMC1113LP5E MMIC IQ Mixer down-converter [22]. It has a typical noise figure of 1.8 dB an image rejection of 25 dB and a conversion gain of 12 dB over the 10 to 16 GHz RF input frequency range. Having RF image/sideband rejection minimises the noise due to the image band. For higher RF frequencies, a frequency multiplier is included to ease the LO requirements. MMIC's are also available for up-converters [19].

## LTCC Mixers

At higher frequencies, the magnetic losses of ferrites increase and it becomes more difficult to wind the transformers required for the mixers. Low Temperature Cofired Ceramic (LTCC) thick film technology, allows a circuit to be made up from multiple layers of ceramic materials. By depositing conductive or magnetic inks, on a set of thin ceramic layers and then fusing those layers, coupled transmission lines can be produced [23]. Typically [24], the schematic for these transformers looks and performs like the Marchand Balun of figure 5.69, but without the $Z_{outer}$ transmission line. These transformers can then be used to result in a DBM as shown in figure 5.68. Since transmission lines are used to produce a transformer/Balun, this technique is most suited to microwave LO and RF frequencies. The diodes can be attached externally, as shown in left and centre images in figure 5.98, or they can be hermetically sealed as shown in the right image of figure 5.98. Because high dielectric constant materials are used, the resulting package can be made small. Since the process can be automated, lower production costs result.

Typical examples of LTCC mixers are:

1) MBA-18LH+ DBM [25]. This DBM requires a +10 dBm LO signal and has a LO/RF frequency range of 1.6 GHz to 3.2 GHz with a conversion loss of 5.8 dB. The device package is 6.35x7.62 mm and is shown on the left of figure 5.98.

2) SIM-43+ DBM [26]. This DBM requires a +7 dBm LO signal and has a LO/RF frequency range of 750 MHz to 4.2 GHz with a conversion loss of less than 6.3 dB. The

device package is much smaller at 5.08x4.57 mm and is shown in the middle of figure 5.98.

3) MAC-24+ High Reliability DBM [27]. This DBM requires a +7 dBm LO signal and has a LO/RF frequency range of 300 MHz to 2.4 GHz with a conversion loss of 6.5 dB. The device package is a hermetically sealed package 7.62x6.35 mm shown on the right of figure 5.98. This mixer is about 3 times the price of the other two mixers. The schematic diagram for all these mixers is the same as figure 5.31.

The performance of the LTCC mixers is similar that of the Core & Wire mixers for the same frequency range and LO level, but the LTCC mixers tend to cost less. More details on LTCC circuits are given in chapter 11: Circuit Manufacture.




Figure 5.98. Mini-Circuits LTCC DBM packages 1) SM2 [25], 2) HV1195 [26], 3) DZ1650 [27].

## MMIC Mixers

At microwave frequencies, the DBM can also be produced on silicon. Silicon has a dielectric constant of 11.7 and the same techniques that can be used to make LTCC DBMs, can also be used with silicon. MMIC transformers are typically made by precision printing parallel lines as spiral inductors on a substrate. Including the diodes then result in an MMIC mixer. Several manufacturers make MMIC mixers [2, 28-31]. These can be either active mixers or passive mixers. As a typical example, the CMD251C3 [32] is a passive 4 - 8.5 GHz fundamental mixer, that has a performance similar to high-level core and wire DBMs, but uses a 3x3 mm SMT package.

## Other Mixers

Mixer manufacturers make other types of mixers, such as DBMs using FETs in a passive mode (no DC supplied to the FET) in order to obtain an improved IP3 performance. The description of such devices are beyond the scope of these notes, but some further details can be found at the Mini-Circuits web site (www.minicircuits.com).

## Additional Resources

1 Mini-Circuits, Application notes on Frequency mixers AN00-001 to AN00-015 available from: https://www.minicircuits.com/applications/application_notes.html or https://blog.minicircuits.com/engineering-resources/ and then selecting Frequency Mixers or Modulators/ Demodulators

2 Mini-Circuits, “RF Frequency Mixers”, available from: https://www.minicircuits.com/WebStore/Mixers.html

3 Stephen A Maas, “Microwave Mixers”, Artech House, 2nd Ed, 1993.

# References


1 Mini-Circuits, “Understanding Mixers- Terms Defined, and Measuring Performance”. Application note AN-00-009, available from: https://www.minicircuits.com/app/AN00-009.pdf

2 Mini-Circuits “Frequency Mixer Selection Guide”, available from: https://www.minicircuits.com/WebStore/Mixers.html

3 Bert Johnson, Watkins & Johnson Tech Note “Mixers in Microwave Systems (Part 1)” https://www.scribd.com/document/231853839/Mixers-in-Microwave-Sstems-WJ

4 Mini-Circuits “Pairing Mixers with Reflectionless Filters to Improve System Performance”, Application note AN-75-007. https://www.minicircuits.com/appdoc/AN75-007.html

5 Mini-Circuits “Low Cost Triple Balanced, LTCC Mixer”, Application note AN00-002. https://www.minicircuits.com/appdoc/AN00-002.html

6 Mini-Circuits “MCA-35MH+ Level 13, Triple Balanced Mixer”, https://www.minicircuits.com/WebStore/dashboard.html?model=MCA-35MH%2B

7 Mini-Circuits “ADE-30W+ Level 7, Double Balanced Mixer”, https://www.minicircuits.com/WebStore/dashboard.html?model=ADE-30W%2B

8 Mini Circuits “ADE-R30WLH+ Level 10, High Reliability”, https://www.minicircuits.com/WebStore/dashboard.html?model=ADE-R30WLH%2B

9 Mini-Circuits “MDB-44H+ Level 15 SMT Double Balanced Mixer”, https://www.minicircuits.com/WebStore/dashboard.html?model=MDB-44H%2B

10 Analog Devices, “HMC-MDB277 GaAs MMIC fundamental mixer, 70 - 90 GHz”, http://www.analog.com/media/en/technical-documentation/data-sheets/hmc-mdb277.pdf

11 Algumaei, M. Y., N. A. Shairi, Z. Zakaria and B.H. Ahmad, “A Single Balanced Mixer Using Compact Branch Line Balun for Ultra-Wideband Applications”, 2018 IEEE International Workshop on Electromagnetics: Applications and Student Innovation Competition (iWEM), 29-31 Aug. 2018, Nagoya, Japan, DOI:10.1109/iWEM.2018.8536650

12 Cadence AWR DE, V15, Examples: *“Low_Power_Mixer.emp”*. (Part of the Cadence AWR DE software installation).

13 R. H. Frater, “Accurate Wideband Multiplier-Square Law Detector,” Review of Scientific Instruments, Vol. 35, No 7, July 1964, pp 810-813

14 B. Gilbert, A precise four quadrant multiplier with subnanosecond response. IEEE Journal of Solid State Circuits Vol. 3 No 4. Dec. 1968, pp 365-373.

15 Mini-Circuits “I&Q Modulators, Surface Mount”, https://www.minicircuits.com/WebStore/ModulatorsDemodulators.html

16 Hilbert Transform for Single Sideband Modulation, Mathematical Formulation, Wikipedia, https://en.wikipedia.org/wiki/Hilbert_transform

17 Analog Devices, IQ and Image Reject Mixers https://www.analog.com/en/product-category/iq-and-image-reject-mixers.html

18 Mini-Circuits, Application notes, I&Q and QPSK Modulators/ Demodulators MOD11-2 and Mod11-8. https://www.minicircuits.com/applications/application_notes.html or https://blog.minicircuits.com/engineering-resources/ and then selecting Modulators/ Demodulators.

19 Analog Devices GaAs MMIC I/Q Upconverter HMC7912. http://www.analog.com/media/en/technical-documentation/data-sheets/HMC7912.pdf.

20 Linear Technology Corporation, “LTC5588-1 data sheet”, available from: http://cds.linear.com/docs/en/datasheet/55881fb.pdf
21 Analog Devices, “Need more bandwidth for the Ka Band? Here are three options” https://www.analog.com/en/technical-articles/need-more-bandwidth-for-the-ka-band.html
22 Analog Devices, HMC1113LP5E data sheet, http://www.analog.com/media/en/technical-documentation/data-sheets/HMC1113.pdf
23 MCDI, “Demystifying RF transformers”, https://www.mcdi-ltd.com/2020/06/17/demystifying-rf-transformers-a-primer-on-the-theory-technologies-and-applications/
24 Mini-Circuits, “NCSI-23+ 1:1 LTCC transformer 1300-2000 MHz, 50 Ω, https://www.minicircuits.com/WebStore/dashboard.html?model=NCS1-23+
25 Mini-Circuits “MBA-18LH+ Level 10 SMT DBM, RF/LO Freq 1600-3200 MHz”, https://www.minicircuits.com/WebStore/dashboard.html?model=MBA-18LH+
26 Mini-Circuits “SIM-43+ Level 7, SMT DBM, RF/LO Freq 750-4200 MHz”, https://www.minicircuits.com/WebStore/dashboard.html?model=SIM-43+
27 Mini-Circuits “MAC-24+ Level 7, SMT H-Rel, RF/LO Freq 300-2400 MHz”, https://www.minicircuits.com/WebStore/dashboard.html?model=MAC-24+
28 Maxim Integrated, RF Mixers and Vector Multipliers, https://www.maximintegrated.com/en/products/comms/wireless-rf/rf-mixers-vector-multipliers.html
29 Qorvo Mixers, https://www.qorvo.com/products/frequency-converters
30 Analog Devices, Single, Double and Triple Balanced Mixers, https://www.analog.com/en/product-category/single-double-triple-balanced-mixers.html
31 Marki Microwave, MMIC/Monolithic Surface Mounts, https://www.markimicrowave.com/mixers/mixers-products.aspx#mmic-microlithic-surface-mounts
32 Qorvo, “CMD251C3 4-8.5 GHz Fundamental Mixer”, https://www.qorvo.com/products/p/CMD251C3#documents

## Abbreviations

2IM Second Order Intermodulation
3IM Third Order Intermodulation
4IM Fourth Order Intermodulation
5IM Fifth Order Intermodulation
BM Balanced Mixer
BB-I In-Phase component of baseband signal.
BB-Q Quadrature component of baseband signal.
dBm dB with respect to 1 mW.
DBM Double Balanced Mixer.
DSP Digital Signal Processing.
HB Harmonic Balance.
HL-DBM High-Level Double Balanced Mixer.
IF Intermediate Frequency.
IIP3 Third order Input Intercept Point (power level).

IQ In-Phase and Quadrature.
LO Local Oscillator (Frequency)

| | |
|---|---|
| LO-I | In-Phase component of Local Oscillator. |
| LO-Q | Quadrature component of Local Oscillator. |
| LNA | Low Noise Amplifier. |
| LTCC | Low Temperature Cofired Ceramic. |
| LSSnm | Large Signal S parameter for ports n and m. |
| MMIC | Microwave Monolithic Integrated Circuit. |
| OIP3 | Third order Output Intercept Point (power level). |
| RF R | Radio Frequency. |
| TBM | Triple Balanced Mixers. |

# Chapter 6

# Oscillators

## Principles of Oscillators

Requirements

1 The LO must be able to supply required output power specified. For example +7 dBm to drive a level 7 mixer.

2 The LO must have a sufficient low Phase and amplitude noise for the application. For example, FM radio has a 75 kHz deviation. For 60 dB SNR at the receiver output, a LO with < 75 Hz phase noise when measured in the 50Hz to 15 KHz band is needed.

3 The harmonics of the LO must be sufficiently small not to cause interference to other users or other parts of the receiver. In particular, harmonic mixing products must be very small and not cause any unwanted spurious components (spurii).

## Oscillator Types

There are two basic oscillator types:

**Oscillator using positive feedback**: This is the most common oscillator design technique for common lower frequencies and can be used at any frequency with a variety of different topologies (see below).

**Oscillator using negative Resistance:** This relies on S11 of an amplifier in a circuit being >1 at some frequencies, resulting in oscillation. The amplifier is unstable at those frequencies where S11 >1, causing the amplifier to oscillate. This design technique is predominantly used for microwave operating frequencies. The design of oscillators using negative resistance is outside the scope of this book.

### *Positive Feedback Oscillators*

The oscillator consists of an amplifier and a Frequency Selective Network. The amplifier output is applied to the frequency selective network, the output of which is applied to the amplifier input. For the analysis, a switch can be imagined to open the closed loop signal path, as shown in figure 6.1. If V2 is exactly the same as V1, both in amplitude and in phase then steady state oscillations result. If the magnitude of V2 > V1 and the phase is the same then the oscillations will grow. If V2 < V1, then the oscillations will decay.

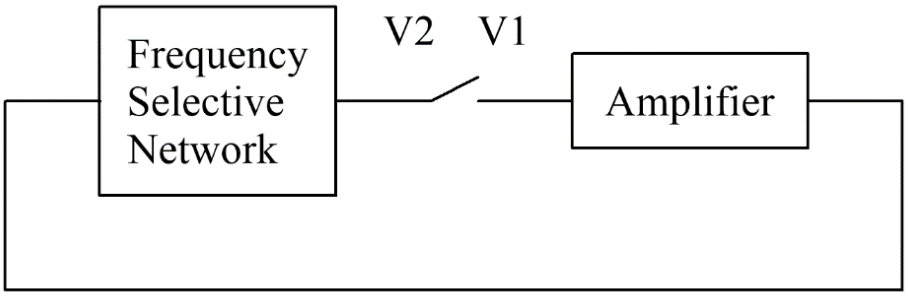



Figure. 6.1. Feedback oscillator block diagram.

# Oscillator Design Process

1: Design the Feedback network to have the correct frequency selective behaviour at the required operating frequency. A high Q network will have a rapid change of phase with frequency resulting in a lower phase noise of the resulting oscillator.

2: Select or design the amplifier to have the required gain at the operating frequency. The input and output impedances should match the expected loads to be seen by the frequency selective network.

3: Simulate the amplifier and ensure the biasing is correct to provide the required gain and phase shift at the operating frequency.

4: Connect the frequency selective network and amplifier as shown in figure 6.2, and do a linear analysis to ensure that the required gain (>1) and phase (V2 in-phase with V1) conditions are satisfied. In MWO the OSCTEST element is specially designed to perform this function and is used in place of the switch shown in the above diagram. It is important that the secondary parameter FC of OSCTEST be set to be above the expected fundamental frequency and below the second harmonic frequency.

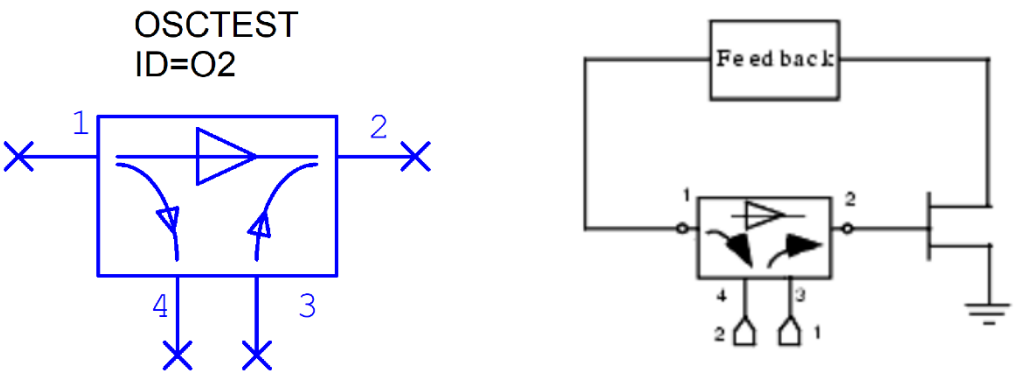



Figure 6.2. The use of OSCTEST for linear analysis of oscillators.

5: Once the circuit has been adjusted to have the correct gain and phase for oscillation, modify the linear circuit by replacing the OSCTEST probe with the OSCAPROBE. The OSCAPROBE is connected to ground at the point where the switch was, as shown in figure 6.3.

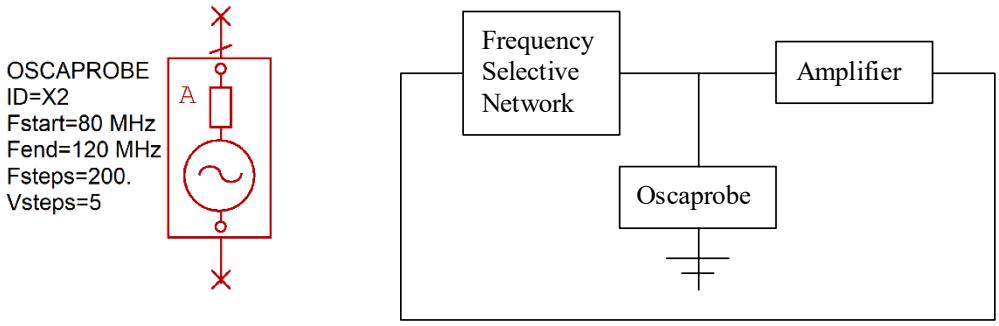



Figure 6.3. The use of OSCPROBE for nonlinear analysis of oscillators.

The OSCAPROBE is a network that is a short circuit at the specified frequency of oscillation and an open circuit at all other frequencies, the voltage amplitude and phase is adjusted, until no current flows through the probe, under which conditions the correct

oscillating amplitude is determined. This amplitude is then used in a non-linear Harmonic Balance simulation of the oscillator circuit. This allows the output waveforms, harmonics and the phase noise of the oscillator to be determined. The accompanying NI AWR DE project files for the oscillator designs presented in this chapter are very useful to investigate changes in phase noise performance, output power and harmonic levels that can be obtained by varying different parameters in the oscillators. It is important that the secondary parameter F0 be set to the expected oscillating frequency and that VPMax be set to be slightly larger than the saturated voltage at that node in the circuit.

## Frequency Selective Networks

For typical RF and Microwave oscillators, the following oscillator types are commonly used:

**Wien Bridge Oscillator**; This uses an RC network with a Q of 1/3. This is a low Q resulting in a high phase noise for the oscillator. The oscillator is however easy to construct and tune and as a result this oscillator is often used for audio frequencies, where the inductors required by other configurations would be too large to be used in oscillators.

**Colpitts Oscillator**; This uses a tapped capacitor LC network, and the similarly related.

**Hartley Oscillator**; This also uses a tapped Inductor LC network. Both the Colpitts and Hartley oscillators are similar, in their frequency range of operation, output voltage and phase noise. The LC resonators used in both the Colpitts and Hartley oscillators will have a typical maximum Q of 250. In practice, unloaded Q values of 100 are more common.

**Voltage Controlled Oscillator;** One of the capacitors in the LC network for a Colpitts of Hartley oscillator is replaced with a varactor diode, allowing the capacitance of the LC network to be varied by applying a DC bias. Voltage controlled oscillators are used in many applications.

**Crystal Oscillator**; A quartz crystal is used as part of the frequency selective network, resulting in a very high Q resonator. Fundamental mode crystal oscillators are available for frequencies between 32 kHz and 100MHz. Crystal oscillators have very low phase noise. Quartz Crystal resonators will be discussed in more details later.

**Stripline or Microstrip Transmission-Line Resonator**; At VHF and microwave frequencies, these resonators are a reasonable size and have typical unloaded Q values of 200.

**Coaxial Cavity Oscillator**; The resonators can be made from coaxial resonators with a centre length of one-quarter wavelength. These resonators can cave unloaded Q values of several thousand. The resonators are large, restricting the applications.

**Dielectric Resonator Oscillator**; By filling the coaxial resonator with a material with a high dielectric constant, the linear dimension is reduced by the square root of the dielectric constant. Having a dielectric constant of 25 will thus reduce the volume of the resonator to 1/125 of the air filled resonator volume. Dielectric resonators are used frequently at microwave frequencies. The resonators can be based on the coaxial resonator and have a centre conductive resonator and conductive walls, or they can simply be a high dielectric material, relying on the dielectric-air interface to keep the electric fields inside the resonator.

A plot of the Q values of different resonators and their corresponding volume is shown in figure 6.4. The phase noise of an oscillator is primarily determined by the Q of the

resonator used in the oscillator, and the way that the amplifier loads the resonator. The higher the Q of the resonator, the lower the phase noise and in general, the lower the frequency variation that can be obtained by tuning the resonator. The choice of the resonator and its Q is thus the primary factor affecting the oscillator properties [1].

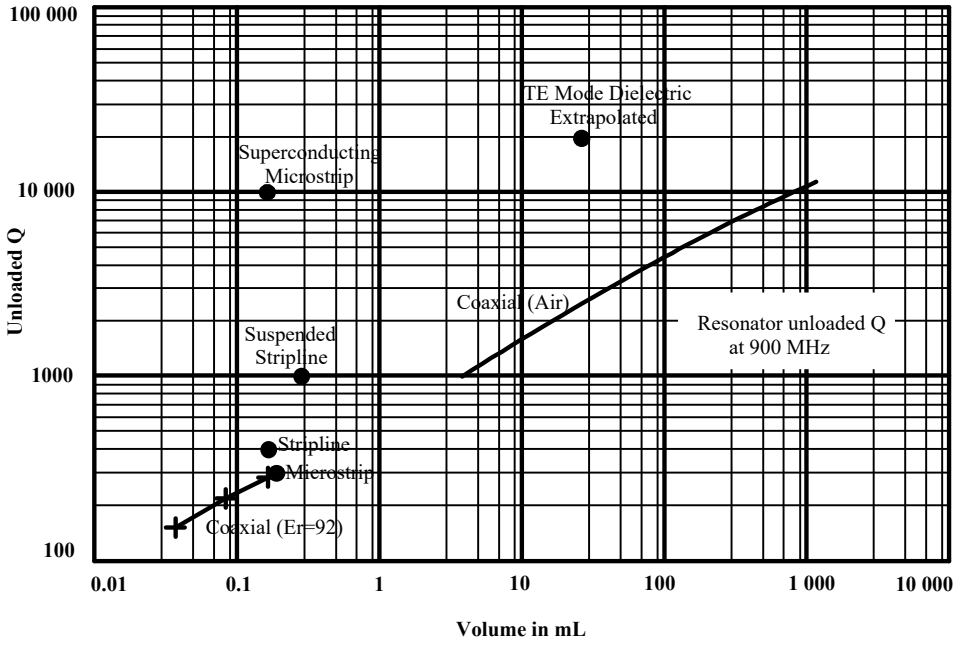



Figure 6.4. Q values and volume of different resonators at 900 MHz.

# Colpitts Oscillator Design Procedure

A 100 MHz oscillator is required, to operate from a 10V supply. The oscillator in this chapter can easily operate at > 100 MHz. Simply change Fo in the Global Definitions of the project file for figures 6.5 to 6.22, to select the desired operating frequency. The design procedure is illustrated by designing a Colpitts oscillator.

## *Step 1: Select an Amplifier Type*

The active device used in an oscillator is very important, factors for consideration are; Output power, oscillating frequency, supply voltage and cost. The low frequency phase noise of the oscillator does depend on the flicker noise of the amplifier, so that the noise figure of the amplifier is important for low noise oscillators. When designing a circuit, it is important to ensure that the devices used will be available for a reasonable time. Infineon's [2] BFR193W is a High Linearity low noise transistor that is "active and preferred" for VHF and UHF applications. The transistor has a maximum Vceo of 12V and a collector current of 80 mA. The Spice model for that transistor is available from Libraries *X Libraries* → **AWR web site* → *Parts By Type* → *Nonlinear* → *Infineon* → *RF Bipolar Transistors* → *High Linearity Si- and SiGe:C- Transistors up to 6 GHz* → *BFR193W*. That transistor has a typical noise figure of 1 dB @ Vce=8V, Ic = 10 mA and 900 MHz. The design procedures outlined in this chapter apply to any active device. The only requirements are that a Spice model is available to allow non-linear simulations to be carried out and that the device can operate at the voltage and current used in the simulations.

The most important design parameter is the biasing of the transistor. The IV curve is very useful in determining the correct biasing conditions. It should be realised that some of the critical transistor parameters like β can vary over a 5:1 ratio between transistors. The transistor parameters used in the models of the computer simulation software, include typical values. The design must be such that the oscillator will work under all permissible variations of transistor parameters. The I-V curve can easily be obtained in MWO as shown in figure 6.5. For linear biasing, a 10V supply and quiescent collector current of between 40 and 5 mA is required. 15 mA is a good compromise to minimise the power dissipation in the transistor and still have sufficient output power.

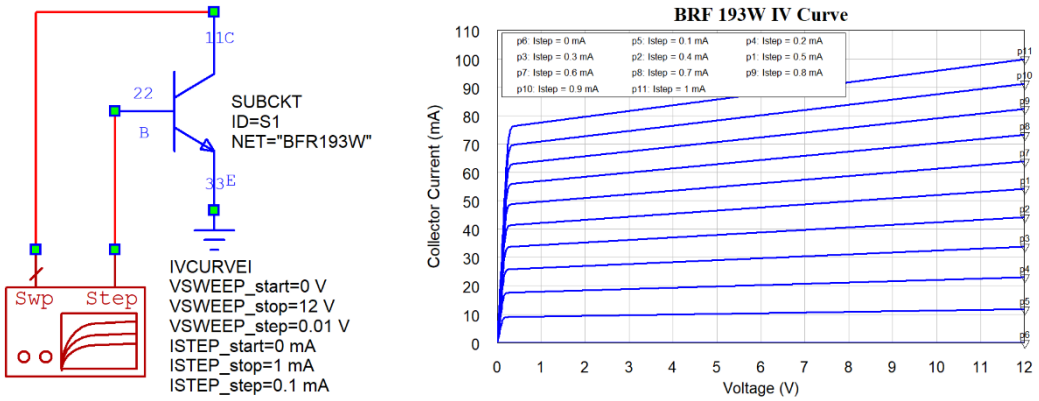



Figure 6.5. Circuit for determining the I-V characteristic of a transistor.

## *Step 2: Design an Amplifier*

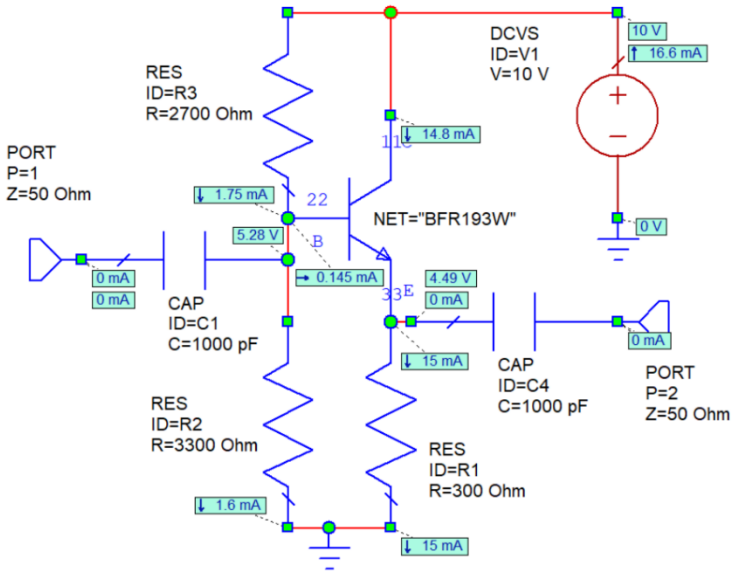



Figure 6.6. Amplifier for the Colpitts oscillator.

A typical amplifier configuration and one that is used for this design is shown figure 6.6. The first step is to select the bias voltages. For a 10 Volt supply, and having an emitter follower configuration for the amplifier, the emitter voltage should be close to half of the supply voltage, minus one volt. An emitter voltage of 4.5 Volt and a resistor R1 = 300 Ω, for a quiescent current of 15 mA is thus suitable. This results in a large swing without the transistor saturating. The current through the biasing chain should be about one tenth of the quiescent current, i.e. 1.5 mA, for good quiescent stability with temperature. For an

emitter voltage of 4.5 Volt, a base voltage of 5.3 Volt is desired, so that a biasing resistor, of about 5.3V/1.5 mA = 3.53 kΩ is required for R2. The nearest E12 value is R2=3.3 kΩ. A 2.7 kΩ resistor is then required for R3 to then obtain close to 4.5 V at the emitter of the transistor. The annotation setting allows the circuit voltages to be indicated on the circuit diagram in Microwave Office, and allow the biasing and voltages to be checked.

Figure 6.7 shows the performance of the amplifier from 50 MHz to 150 MHz. The gain of 5.24 dB is the magnitude of S(2,1), assuming 50 Ω source and load impedances. The input impedance is 982 Ω and the output impedance is 19 Ω, with a significant reactive component that will affect the resonance of the Colpitts oscillator if it is not allowed for in the design process.

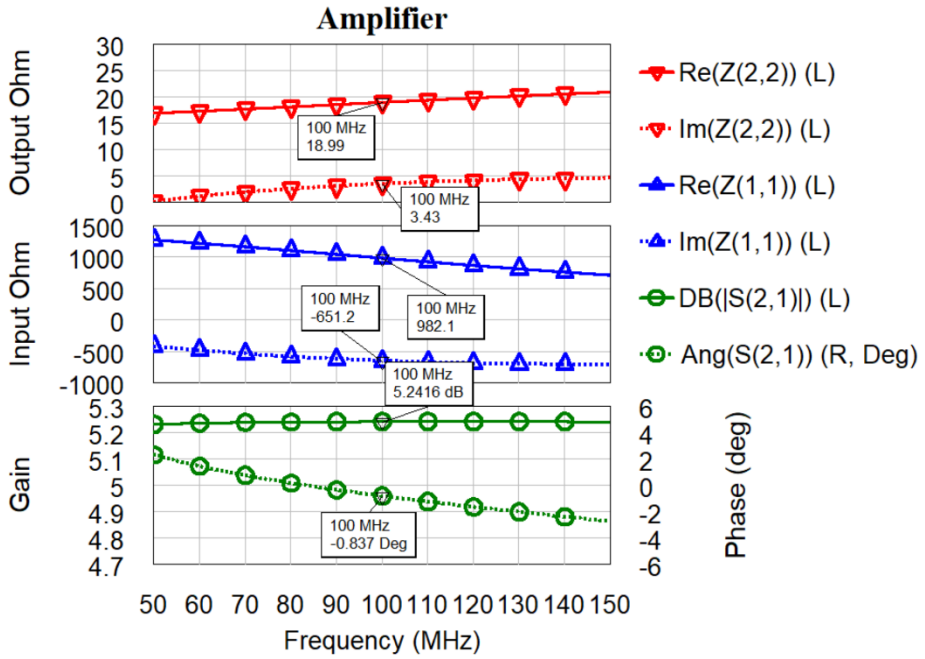



Figure 6.7. Amplifier Performance.

## *Step 3: Design a Resonator*

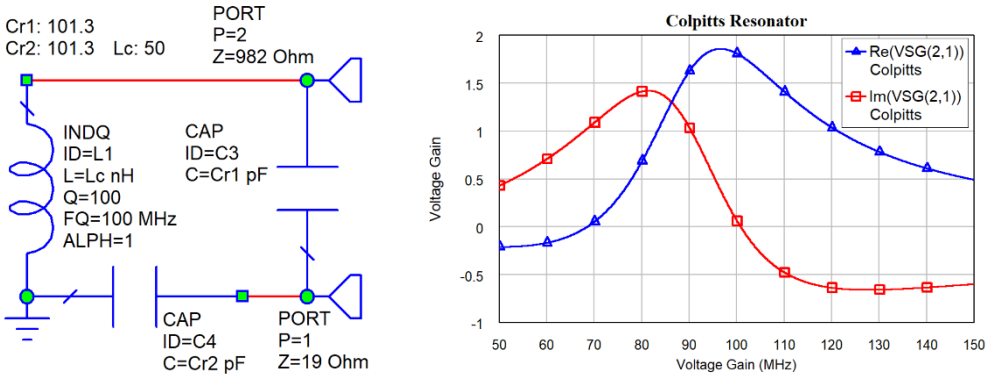



Figure 6.8. Colpitts resonator network.

The resonator must be a frequency selective network, to ensure that the conditions for oscillation only apply at one frequency. In addition, the network must be matched to the input impedance and output impedance of the amplifier and have a high Q. Figure 6.7 shows the amplifier real input impedance is 982 Ω. That is the impedance used for Port 2

of the resonator. Figure 6.7 shows the amplifier real output impedance is 19 Ω. That is the impedance used for Port 1 of the resonator. The reactive impedances are chosen to make Lc = 50 nH at 100 MHz, resulting in Cr1 = Cr2 = 101.3 pF as shown in figure 6.8. Those are practical values. The components can be tuned to ensure a 0° (or 180° if needed) phase shift at the required operating frequency. In figure 6.8, the imaginary part of the transfer function is not exactly zero, since the network shown corresponds to the one actually used in the oscillator and allows for phase changes produced by the amplifier.

## Step 4: Linear Oscillator Analysis

The resonator and amplifier are now combined into the one circuit. The element OSCTEST is used to determine the loop gain and phase shift. Set the secondary parameter FC to 160 MHz, which is just above the largest frequency of figure 6.9 and is below the expected 200 MHz second harmonic frequency. The resonator network is now tuned to give a phase shift of zero degrees between port 1 and 2, at the required operating frequency. If needed, the loop gain is changed to ensure that it is just slightly above one at the operating frequency. That then corresponds to the correct conditions for oscillations. To minimise the loading on the amplifier, and that load affecting the Q of the resonator circuit, port 3 is terminated in a 1 kΩ load. If needed, the resonator network centre frequency can be tuned to make the imaginary part of VTG(2,1) = 0.

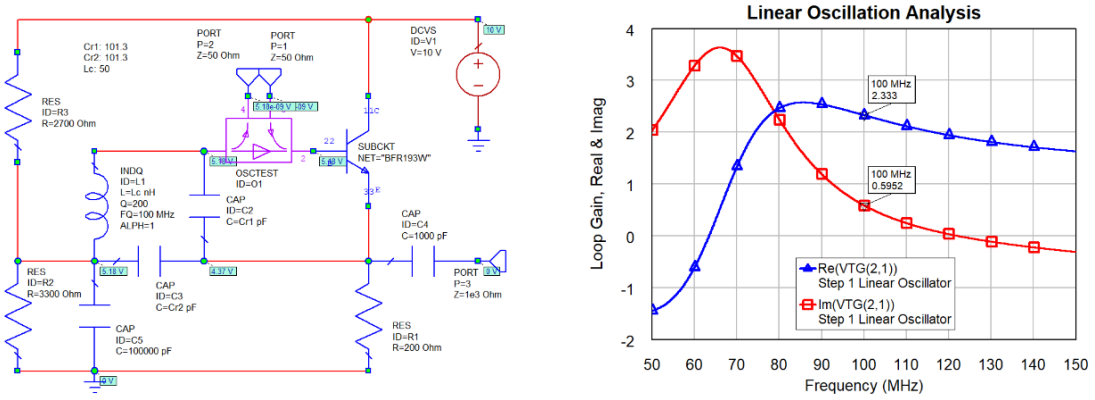
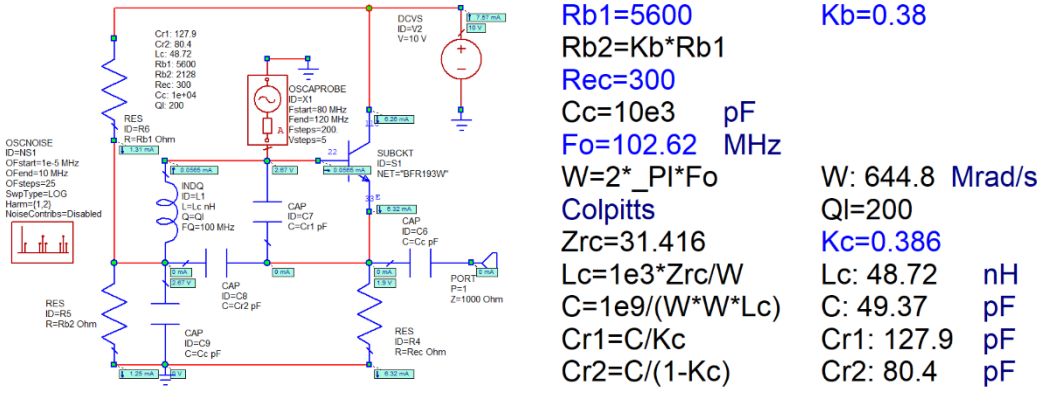



Figure 6.9. Linear analysis using OCSTEST

## Step 5: Nonlinear Oscillator Analysis




```
Rb1=5600          Kb=0.38
Rb2=Kb*Rb1
Rec=300
Cc=10e3     pF
Fo=102.62   MHz
W=2*_PI*Fo        W: 644.8  Mrad/s
Colpitts          Ql=200
Zrc=31.416        Kc=0.386
Lc=1e3*Zrc/W      Lc: 48.72     nH
C=1e9/(W*W*Lc)    C: 49.37      pF
Cr1=C/Kc          Cr1: 127.9    pF
Cr2=C/(1-Kc)      Cr2: 80.4     pF
```

Figure 6.10. Circuit for non-linear analysis and corresponding circuit elements.

Replace OSCTEST with OSCPROBE as shown in figure 6.10, to do a harmonic balance analysis. Set the secondary parameter F0, to 100 MHz, to make that the initial guess for

the oscillation frequency and set the secondary parameter VpMax to 8V, since the oscillating waveform at the base of the transistor will be less than 8Vp. The APLAC HB (Harmonic Balance) simulator, allows the oscillation frequency, output power, output waveforms, and output spectrum to be determined. The frequency Fo can now be tuned, to ensure the circuit oscillates at the 100 MHz. This requires changing Fo to 102.62 MHz in the equations shown in figure 6.10, and also gives minor changes to Cr and Lc.

If desired, Zrc, the impedance of the inductor at the resonating frequency, and Kc, which is related to the ratio of Cr1 and Cr2, or the biasing resistors Rb1, Rb2 and the emitter resistor Rec, can be tuned to provide lower harmonics, a larger output voltage or a lower phase noise. Equations are used in the Global Definitions block, to ensure that both the linear and non-linear circuit keep identical circuit elements. For figures 6.10, the blue (tuneable) variables have been tuned to achieve the phase noise shown in figure 6.13. That results in a close to 10Vpp output voltage and noticeable harmonic components. At this stage the characteristic impedance of the resonator, Zrc is kept constant. Figure 6.11 shows the resulting output spectrum of the oscillator and figure 6.12 shows the resulting output waveform.

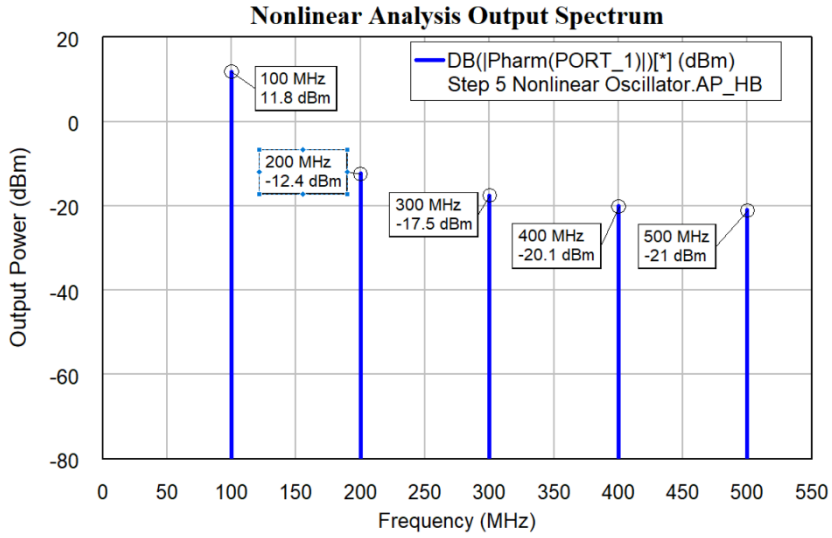



Figure 6.11. Output spectrum determined by non-linear analysis.

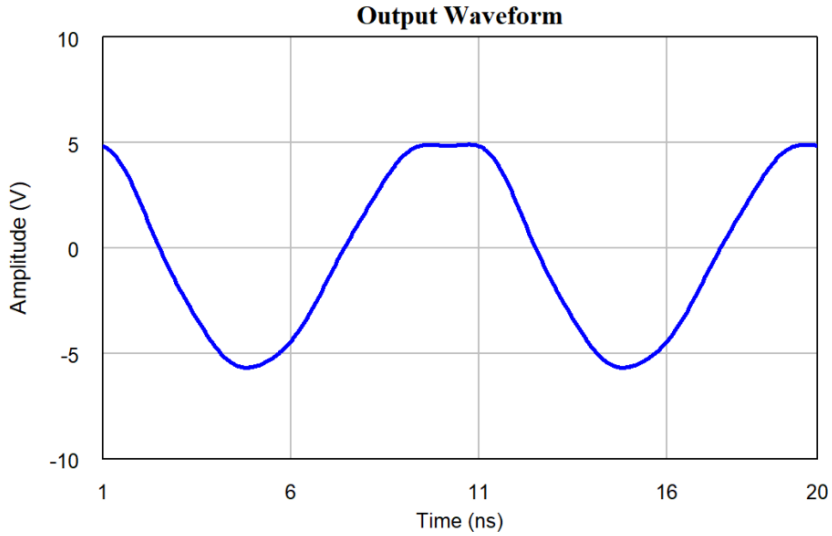



Figure 6.12. Output waveform determined by non-linear analysis.

The non-linear analysis can also be used to determine the Phase Noise of the oscillator [3]. The OSCNOISE measurement (Element ⇒ MeasDevice ⇒ Controls ⇒ OSCNOISE) allows the phase noise of the oscillator to be measured as shown in figure 6.13. The phase noise will depend on the Q of the resonant network as well as other parameters, such as the noise figure of the amplifier and the amplifier power level and the loading that the amplifier places on the resonant network. Being able to change the circuit elements in figure 6.10 and observe the effect of that change on the phase noise is a great advantage in designing good oscillators. For AWRDE V15 and V16 FREQ=1000 MHz is indicated in the markers, even though the phase noise is evaluated at 100 MHz.

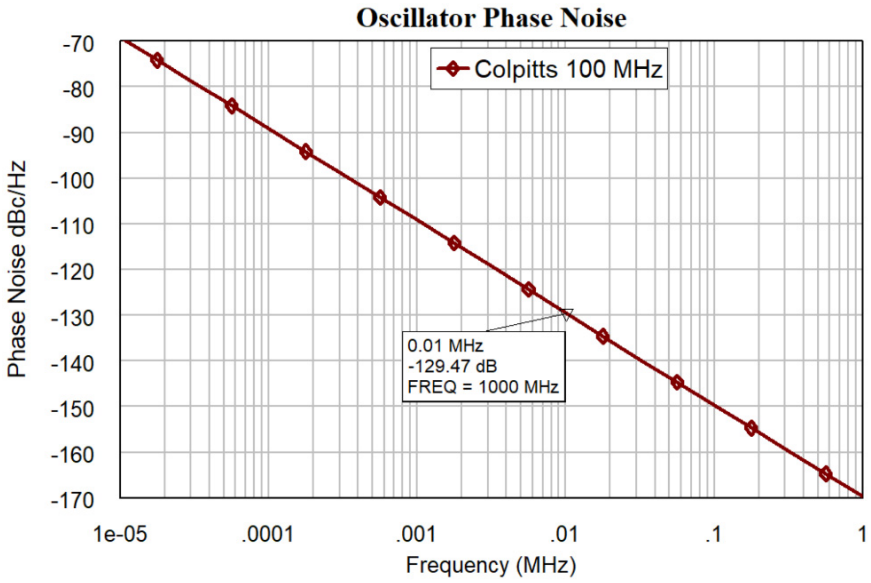



Figure 6.13. Phase noise of the oscillator using non-linear (harmonic balance) analysis.

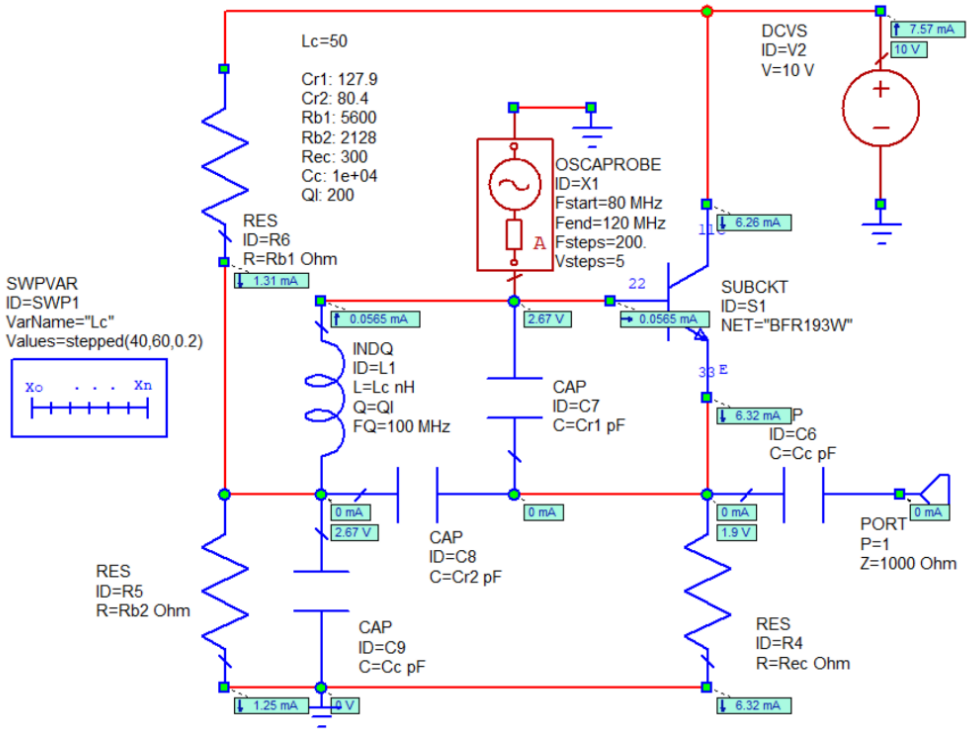



Figure 6.14. Schematic for determining the oscillator frequency versus the resonating inductor.

By including a SWPVAR simulation control (Element ⇒ Simulation Control ⇒ SWPVAR) in the schematic of figure 6.10, as shown in figure 6.14, the effect of variations of inductor values on the oscillating frequency can be investigated. For this to work, the value Lc must be included as a fixed variable, as shown in figure 6.14 rather than Lc being calculated as shown in figure 6.10. The resulting plot is shown in figure 6.15.

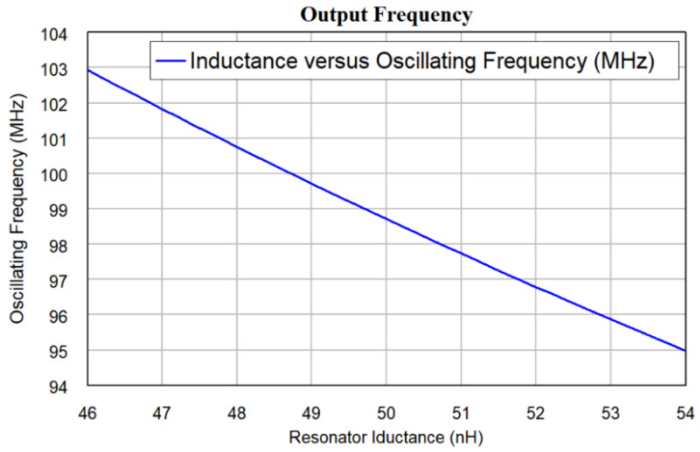



Figure 6.15. Change in oscillating frequency as the resonator inductor varies.

The oscillating frequency can be set by winding the inductor L1 on a coil former and using a ferrite tuning-slug to change the inductance of the coil. A varactor diode allows electronic control of the frequency or frequency modulation of the oscillator. By placing a varactor diode either in parallel with Cr2 or in parallel with inductor L1, in figure 6.8, together with suitable biasing allows the frequency of the oscillator of figure 6.10 to be controlled by varying the reverse bias voltage across the varactor diode.

The above design procedure allows the performance of an oscillator to be accurately determined prior to the hardware being produced. This greatly reduced the cost of designing oscillators. The non-linear analysis can only be produced when a full Spice model of the active device is available. Many transistor manufacturers provide the required models for their transistors. Unfortunately, the SPICE models are not available for many commercially available Microwave Monolithic Integrated Circuits (MMIC). The same design process can be used for oscillators using the Operational Amplifiers described in chapter 10.

## Hartley Oscillator

A Hartley oscillator uses a tapped inductor, while the Colpitts oscillator uses a tapped capacitor. There are different ways that the resonator can be connected to the transistor. The transistor can be arranged as a common emitter, a common collector or a common base amplifier. A Hartley oscillator is typically [4] made using a common emitter transistor as shown in figures 6.17 and 6.18. The resonators are arranged to minimise their loading. The input is connected to the collector, which is close to a constant current source, and the output connected to the base of the transistor, which presents a high impedance. In addition, the biasing of the transistor in figures 6.17 and 6.18 are arranged so that it does not load the resonator. To be able to optimise the designs and keep the same circuit values for both the linear and nonlinear circuit simulations, the tuneable parameters and equations shown in Figure 6.16 are used.

The tapped inductor for the Hartley oscillator is often made by winding both coils on a former and using a ferrite slug to tune the oscillator to the correct frequency. As a result, there will be some mutual coupling between those coils. The MUC2 coupled inductor element represents this configuration and for figure 6.17, a coupling coefficient of 0.3 is used. The supply voltage of the common emitter Hartley oscillators is 6V, to ensure that Vce is less than 12V. Figure 6.18 shows the corresponding Hartley common emitter oscillator with resonator inductors that are not coupled.

General Constants
Zr=31.416 Ohm Cc=10e3 pF Qh=200

Hartley Common Emitter
Kbe=1 Rbe1=4700 Ohm
Rbe2=Kbe*Rbe1
Kg=1 Rg=Zr/Kg Rg: 31.42 Ohm
Re=470 Ohm
Reh=Re-Rg

Hartley Common Emitter with non-coupled coils Q 200
Fe=107.14 MHz We=2*_PI*Fe We: 673.2 Mrad/s
Leh=1e3*Zr/We Leh: 46.67 nH
Ceh=1e9/(We*We*Leh) Ceh: 47.28 pF
Kel=1.39 Khe=Kel*Kg/(1+Kg) Khe: 0.695
Leh1=Leh*(1-Khe) Leh1: 14.23 nH
Leh2=Leh*Khe Leh2: 32.43 nH
Re1=We*Leh1/(1000*Qh) Re1: 0.04791 Ohm
Re2=We*Leh2/(1000*Qh) Re2: 0.1092 Ohm

Hartley Common Collector with non-coupled coils Q 200
Fc=102.78 MHz Wc=2*_PI*Fc Wc: 645.8 Mrad/s
Lch=1e3*Zr/Wc Lch: 48.65 nH
Cch=1e9/(Wc*Wc*Lch) Cch: 49.29 pF
Kcl=0.584 Lch1=Lch*Kcl Lch1: 28.41 nH
Lch2=Lch*(1-Kcl) Lch2: 20.24 nH
Rbc1=5600 Ohm
Kbc=0.413 Rbc2=Kbc*Rbc1 Rbc2: 2313 Ohm
Rec=288 Ohm

Hartley Common Emitter with coupled coils Q 200
Ft=88.66 MHz Wt=2*_PI*Ft Wt: 557.1 Mrad/s
Lth=1e3*Zr/Wt Lth: 56.4 nH
Cth=1e9/(Wt*Wt*Lth) Cth: 57.14 pF
Ktl=1.202 Kht=Ktl*Kg/(1+Kg) Kht: 0.601
Lth1=Lth*(1-Kht) Lth1: 22.5 nH
Lth2=Lth*Kht Lth2: 33.89 nH
Rt1=Wt*Lth1/(1000*Qh) Rt1: 0.06267 Ohm
Rt2=Wt*Lth2/(1000*Qh) Rt2: 0.09441 Ohm

Figure 6.16. Hartley oscillator tuneable constants and equations.

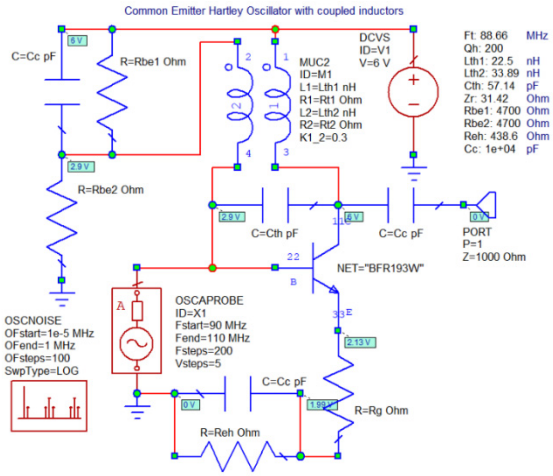



Figure 6.17. Hartley CET (Common Emitter Transformer coupled inductors) oscillator.

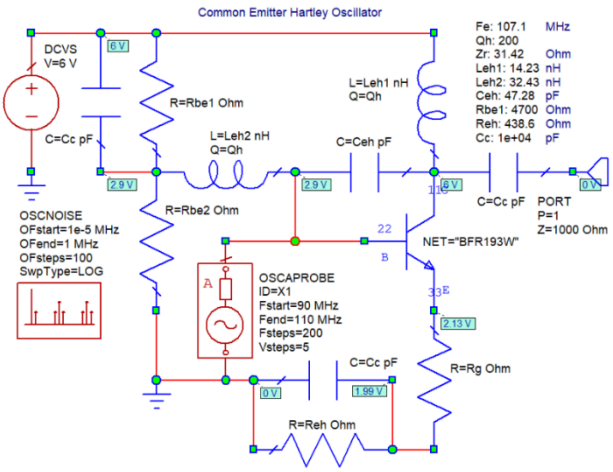



Figure 6.18. Hartley CE (Common Emitter) oscillator with non-coupled inductors.

The gain of the common emitter amplifiers of figures 6.17 and 6.18 are stabilised by using a tuneable gain constant Kg and including a resistor Rg = Zr/Kg in the circuits. The amplifier gain is then close to -Kg at resonance. The resonators themselves can have gain, depending on the tapping ratio. The tapping constants Khe and Kht include the gain constant Kg as shown in the equations in figure 6.16. Changing the amplifier gain by changing Kg, will then also change the resonator tapping-ratio, to keep the step 4 linear oscillator gain, shown in figure 6.9, nearly constant. Figure 6.16 shows that to obtain an oscillating frequency of 100 MHz, the designed resonator frequency for the non-coupled coils is 107.14 MHz and for the coupled coils is 88.66 MHz. The coupling will thus cause a significant frequency shift that must be corrected.

A common collector transistor configuration can be used, similar to figure 6.10 with the resonating inductor Lc replaced by a capacitor and the capacitors Cr1 and Cr2 replaced by inductors. The resulting Hartley oscillator circuit is shown in figure 6.19. To facilitate a comparison between the common collector Colpitts and the Hartley oscillators, the bias voltages for the Hartley oscillator in figures 6.19, is similar to those for the Colpitts oscillator in figure 6.10.

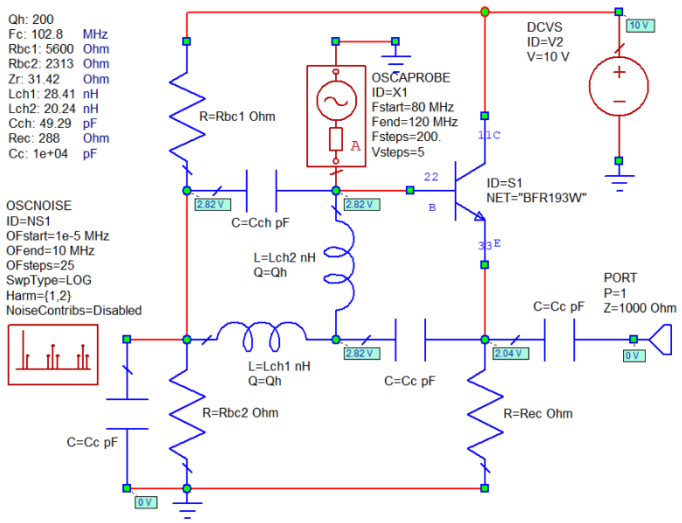



Figure 6.19. Hartley CC (Common Collector) oscillator with non-coupled inductors.

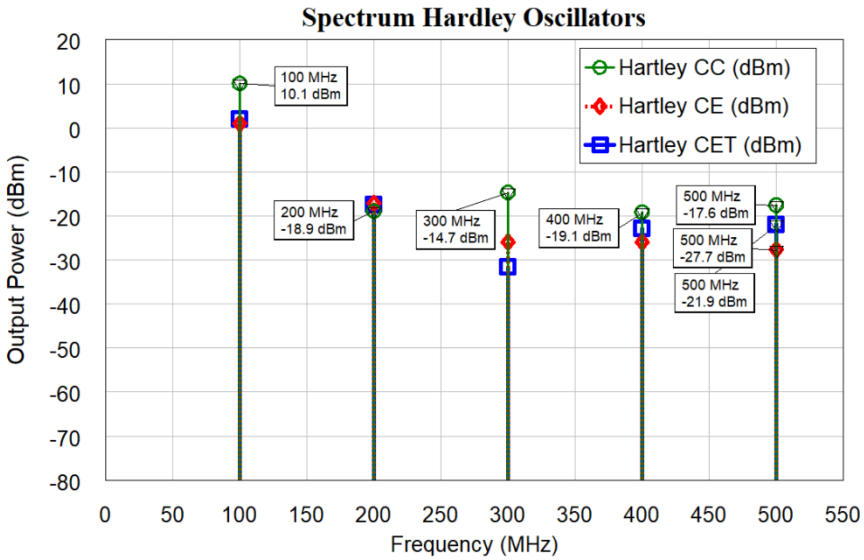



Figure 6.20. Output spectrum of Hartley oscillators.

Figure 6.20 shows the spectra of all three Hartley oscillators. Comparing the spectrum of the common collector (CC) oscillator with figure 6.11 shows that the Hartley oscillator has a similar output, a lower second harmonic, but higher high frequency harmonics than the Colpitts oscillator. This is to be expected, since Colpitts resonator with a ground placed at the capacitor tapping point is like a low pass filter and the Hartley resonator with the inductor tapping point is like a high pass filter. The Colpitts resonator will thus attenuate harmonics more than the Hartley resonator. The common emitter (CE and CET) oscillators have an 8 dB lower output voltage and a similar level of harmonic components.

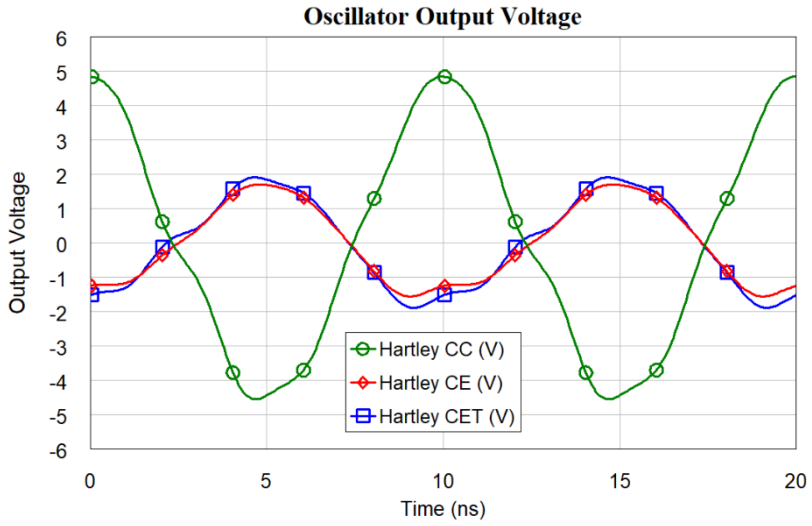



Figure 6.21. Output waveforms of Hartley oscillators.

Figure 6.21 shows the waveforms from the 3 different Hartley oscillators. The output voltage of the common emitter oscillators is smaller than that of the common collector oscillator. Higher power oscillators should have a lower phase noise as is demonstrated by this graph.

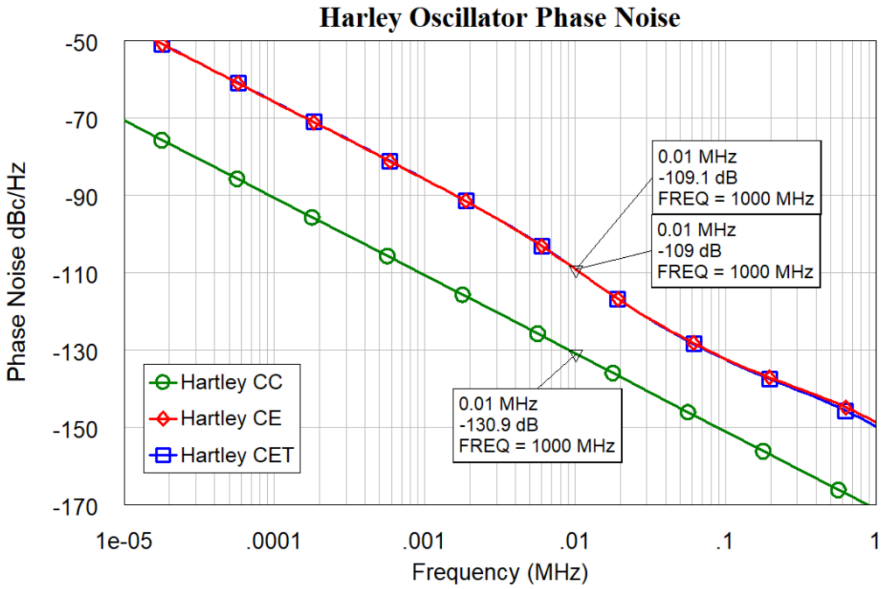



Figure 6.22. Phase Noise of Hartley oscillators.

The component values of the three Hartley oscillators of figures 6.17 to 6.19 have been tuned to obtain a low phase noise. Figure 6.22 shows the resulting phase noise from the

oscillators. The phase noise of the Hartley common collector (CC) oscillator is within 1 dB to that of the Colpitts oscillator shown in figure 6.14. The common emitter (CE) Hartley oscillators have a similar phase noise, and their phase noise is 10 dB worse than that of the common collector oscillator.

To ensure that a fair comparison can be made between the performance of the oscillators in figures 6.10 and figures 6.17 to 6.19, the same transistor and the same resonator total inductance and capacitance values are used. Normally the Q of the capacitors used in the resonator is much higher than the Q of the inductors, so that the Q of the resonator is determined by the Q of the inductor. A Q of 200 can be achieved by careful construction of the inductor used for the resonator.

The designs presented above are for a 100 MHz oscillator. The resonator elements are calculated using equations in AWR DE, so that the oscillation frequency can simply be changed by changing one variable. Since the amplitude of the waveform across the OSCAPROBE element may be larger than the secondary parameter VpMax, that value should be increased to 8V. It is also important to set the value of FC in the OSCTEST element to 160MHz, which is greater than the frequency sweep used for the linear gain test and less than the expected 200 MHz second harmonic of the oscillating frequency.

## Practical Inductors

Making the resonator impedance (Zrc) small will reduce the phase noise. However, that may result in unrealistic component values. Wheeler's [5] empirical formula for the inductance of a single layer air core is given as:

$$L = \frac{N^2 r^2}{9r+10l} \qquad (r, l \text{ in inch and } L \text{ in } \mu H) \text{ Eqn. 6.1}$$

The inductance; $L$ is in μH, the radius r and coil length $l$, are in inches and N is number of turns on the coil. Using the coil diameter d, and converting this to metric units gives the approximate metric version, which has the inductance in nH as:

$$L = \frac{N^2 d^2}{(0.45d+l)} \qquad (d, l \text{ in mm and } L \text{ in nH}) \text{ Eqn. 6.2}$$

For RF coils, the highest Q is obtained when the spacing between the turns is about the same as the wire diameter. A closer spacing increases the capacitance between the turns and lowers the self-resonance of the inductor. A larger spacing reduces the inductance. Often the insulation covering the wire provides close to the required spacing for the optimum Q. AWG 26 gauge solid wire has a 0.405mm diameter, covered with 0.38mm insulation, giving a total diameter of 1.165 mm. A d = 2.641 mm coil diameter, 3 turns will result in a coil length of $2x1.165 + 0.405 = 2.735$ mm and from equation 6.2, that coil will have an inductance of 16.00 nH, That is a reactive impedance of 10.053 Ω at 100 MHz. AWR DE implement more advanced calculations of this using the element COIL. Those equations, instead of the diameter to the centre of the conductor coil, require the inner coil radius, the radius of a former if the coil has no insulation. The above 2.641 mm coil diameter corresponds to a $(2.641 - 0.405)/2 = 1.118$ mm inner radius. That results in a reactive impedance of 9.946 10 Ω at 100 MHz. Wheeler's formula and the AWR DE Coil element agree closely. The coil dimensions are about as small as one may wish to use for this design. As a result, we limit the impedance of the inductor's Zr to be 10 Ω or greater in this example. The inductance can be changed slightly by stretching or compressing the length of the coil. Figure 6.23 shows the Real and Imaginary part of

the Impedance for the three different coil configurations. The Q of the Coil element is 189 at 100 MHz. A near value Q = 200 is used for convenience in the following designs.

Any vibration will slightly change the inductances, that will frequency modulate the oscillating frequency with the vibration. That is called microphony. Putting the coils on a solid former reduces this microphony. The element MCINDN is uses a spiral Microstrip inductor without a bridge for the connector at the centre of the spiral. Using MCINDN on an RO4003 substrate, with 1.5 turns, a track width of 1.5 mm, a spacing of 0.2 mm and centre wire radius of 3.016 mm results in the same 16 nH inductance as the coil above. However, figure 6.23 shows that a lower Q of 93.8 is obtained for the MCINDN coil. One can also use a length of Microstrip transmission line as an inductor, that allows smaller "inductors" to be made, but they need to be simulated as transmission lines to obtain the correct circuit performance.

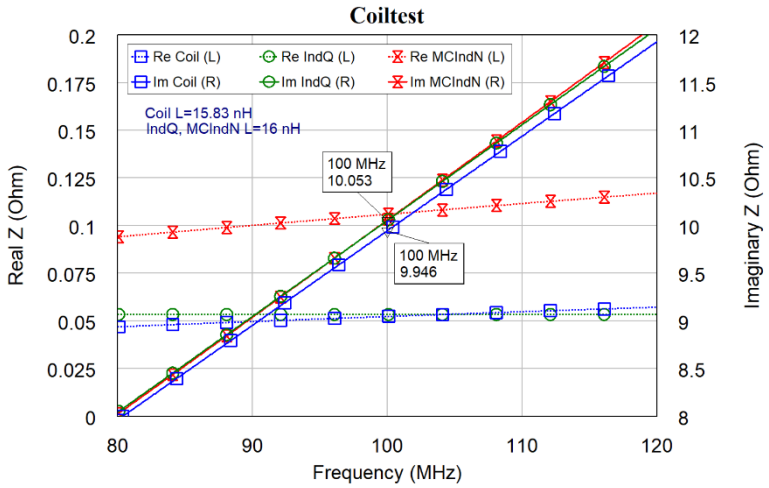



Figure 6.23. Element COIL, INDQ and MCINDN impedances.

# Example 6.1: Low Phase Noise Oscillator Design

## *Low Phase Noise Colpitts Oscillator*

The Q of the resonator is a prime factor in the phase noise of the oscillator. With practical limits of Zr = 10 Ω and Q =200, the effective Q of the resonator can be maximised by minimising the loading on the resonant network. The output impedance of the emitter in figures 6.10 and 6.19 is a low impedance that reduces the effective Q of the resonator. By placing a resistor Rsc in series with the resonator, the effective loading of the resonator can be reduced, resulting in a reduction of the phase noise. In addition, the performance of the active devices will affect the phase noise of the oscillator. Tuning the different components of the circuit allows the phase noise to be minimised. Whether this also results in a minimum phase noise of the hardware, depends on how good the simulation model of the transistor matches the hardware.

For the low noise Colpitts Oscillator, the circuit of figure 6.10, is used as a starting point. Lowering Zr to 10 Ω reduces the resonator loading of the base and emitter of the transistor and thus reduces the phase noise. Reducing Zr further, will reduce the phase noise, but then require inductors that are very difficult to realise. Adding a voltage follower to buffer the output prevents the load connected to the oscillator from changing (pulling) the oscillation frequency. Tuning Kc, the ratio of Cr1 and Cr2, so that the total capacitance

remains constant, reduces the phase noise further. Other parameters, like the biasing resistors (Rbc1, Rbc2), the supply voltage and collector current all affect the phase noise and can be tuned to minimise the phase noise.

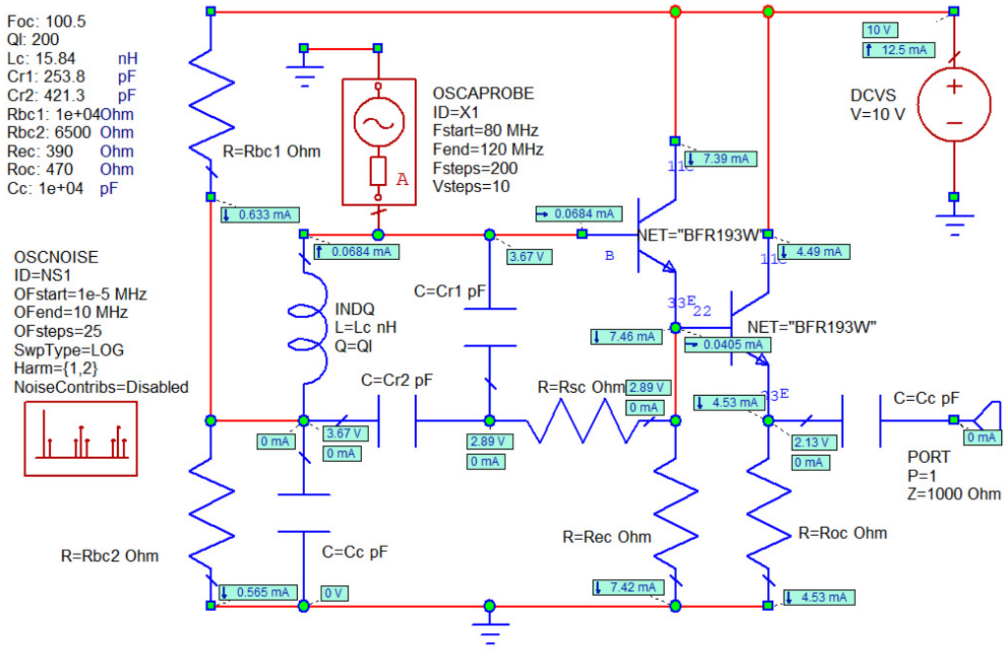



Figure 6.24 Low Noise Colpitts oscillator.

If needed compromises can be made to provide more output at the expense of phase noise. A simple low pass filter can be included at the output to reduce any harmonics. Figure 6.24 shows the resulting circuit. Figure 6.26 shows that the phase noise of 143.2 dB is 13.7 dB lower than that of figure 6.13.

## *Low Phase Noise Hartley Oscillator*

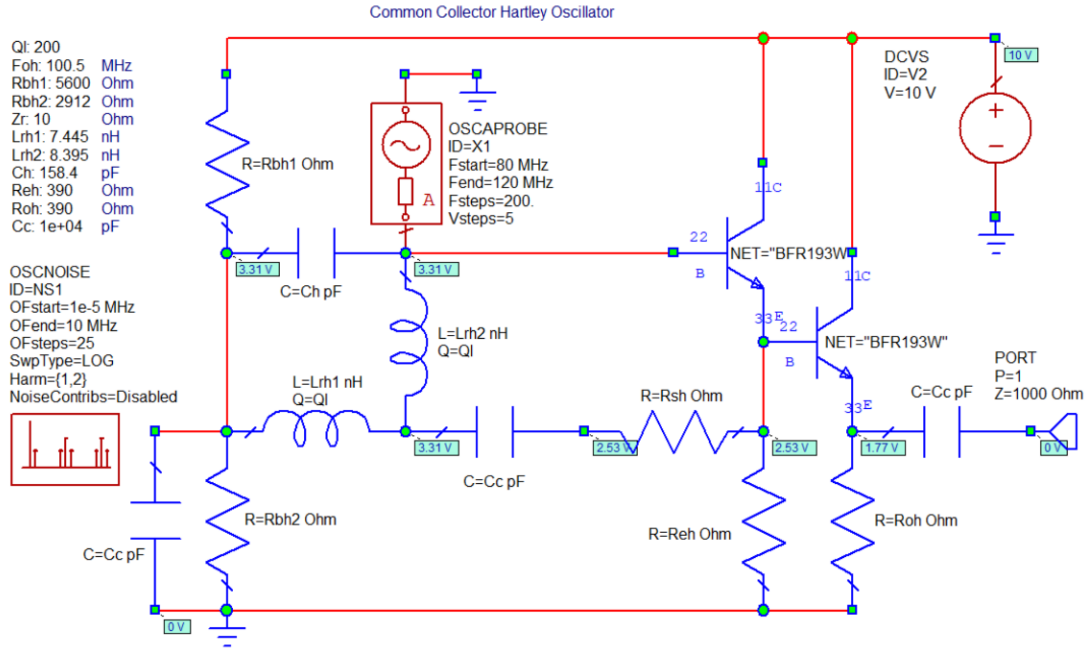



Figure 6.25 Low noise Hartley oscillator.

For a low noise Hartley oscillator, the circuit of figure 6.19 is used as a starting point. The resonator impedance is the same as that of the Colpitts resonator, Zrh = 10 Ω. Just like the Colpitts oscillator, the resonator loading is minimised by adding a series resistor Rsh and a buffer amplifier is added. Similar to the Colpitts oscillator, the circuit parameters are tuned to achieve the lowest phase noise. Figure 6.25 shows the resulting oscillator schematic.

Figure 6.26 shows that the phase noise of 143 dB is 12.9 dB lower than that of figure 6.22. The phase noise for both the Hartley and the Colpitts oscillator are nearly the same. Changing the Q to 20000, does not reduce the phase noise, indicating that the transistor parameters are the dominant limitation on the phase noise.

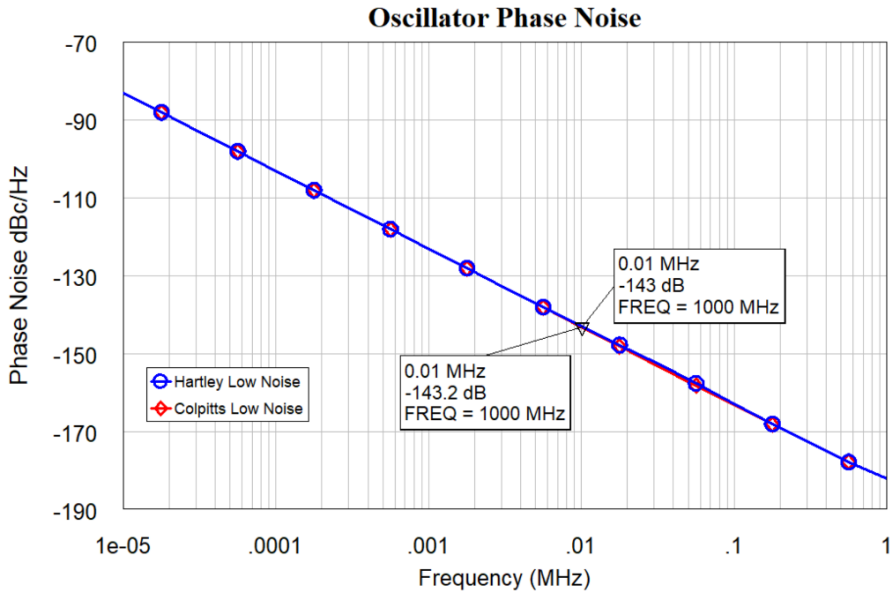



Figure 6.26 Phase noise of Colpitts and Hartley low noise oscillators.

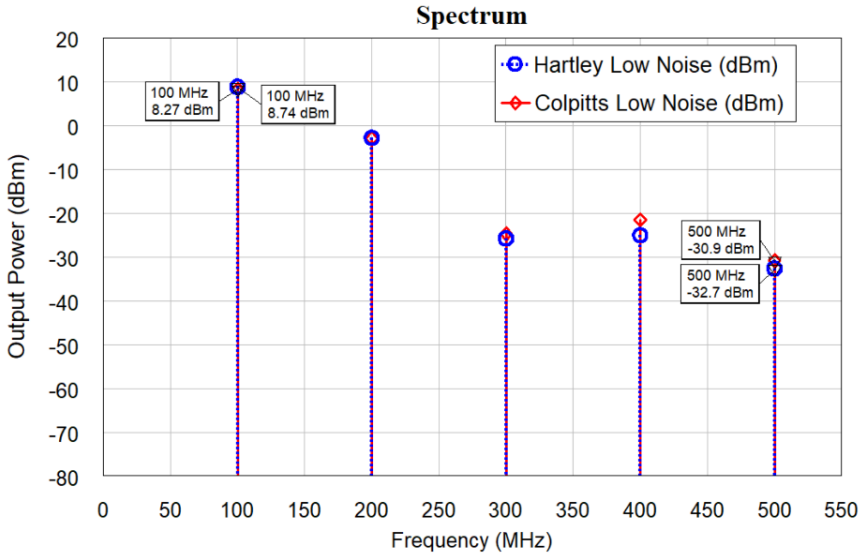



Figure 6.27 Spectra of Colpitts and Hartley low noise oscillators.

Figure 6.27 show the spectra of the output signals. The predominant distortion is due to even harmonics. Figure 6.28 shows the output waveforms from the oscillators. The output voltages are close to 8V peak to peak, which is 80% of the supply voltage.

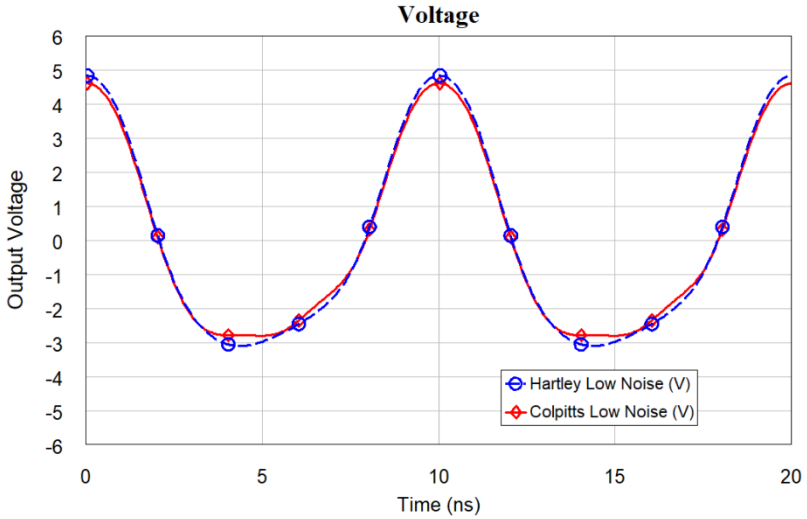



Figure 6.28 Output waveforms of Colpitts and Hartley low noise oscillators.

# Crystal Oscillators

Crystal have very high Q values, so that crystal oscillators have much lower phase noise than oscillators with LC resonators. For details of Quartz Crystals see "Quartz Crystal Resonators and Oscillators for Frequency Control and Timing Applications - A Tutorial" [6] by the 2009 IEEE president John Vig. He has graciously given permission for his slides to be used as a resource for this book.

## *Example 6.2: Crystal Oscillator Design*

The design of a crystal oscillator is similar to that of any other oscillator. For most fundamental mode crystal oscillators, the crystal is inductive at the operating frequency and the inductor in any LC oscillator is replaced with the crystal. In figure 6.29, the inductance of a phase shift oscillator is replaced with a quartz crystal. The inductance is calculated from the crystal's frequency Fs and capacitance C1. A minor frequency change for Fs is made for the resonance shown in figure 6.34 to be exactly at 25 MHz.

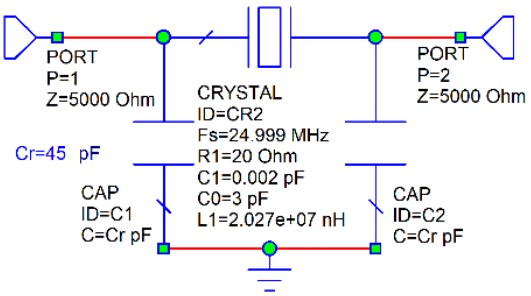



Figure 6.29. Phase shift network using a quartz crystal.

The amplifier shown in figure 6.30 has a gain of 25 dB from the input port 1 to the output port 3. The gain from the input to port 2 is enough to cause oscillations. The gain of the amplifier can be controlled by changing R4, the resistor connected to the emitter, without affecting many other parameters. The resonant network and the amplifier are connected together to form a Crystal oscillator as shown in figure 6.31. Using OSCTEST, the gain around the amplifier and resonator loop is now determined using a linear oscillator analysis as shown in figures 6.31 and 6.33.

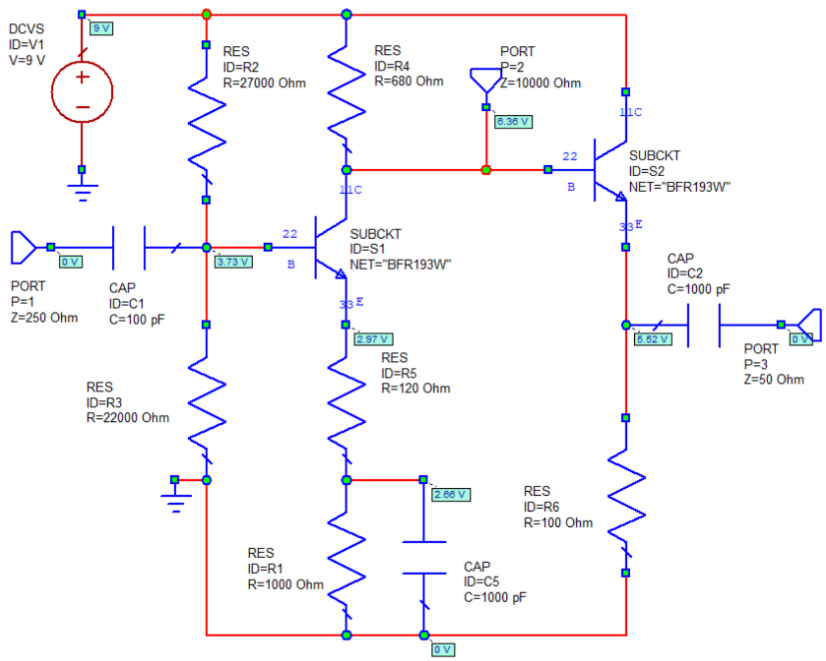



Figure 6.30. Amplifier for a 25 MHz crystal oscillator.

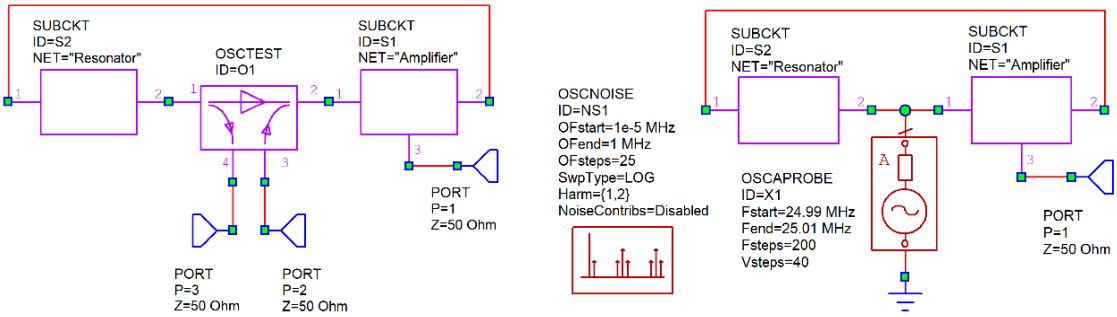



Figure 6.31. Linear and non-linear oscillator circuits

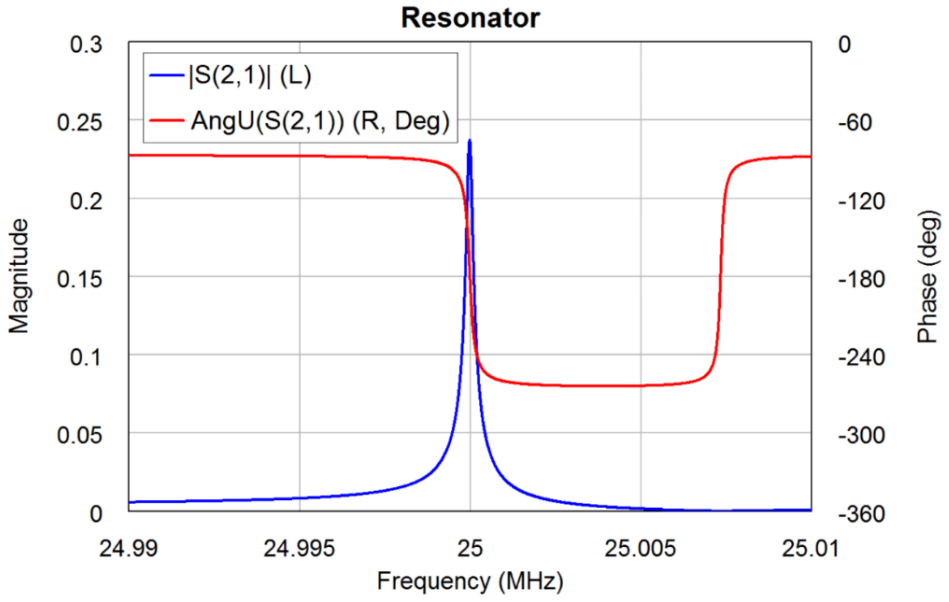



Figure 6.32. Frequency response of the resonator of figure 6.29.

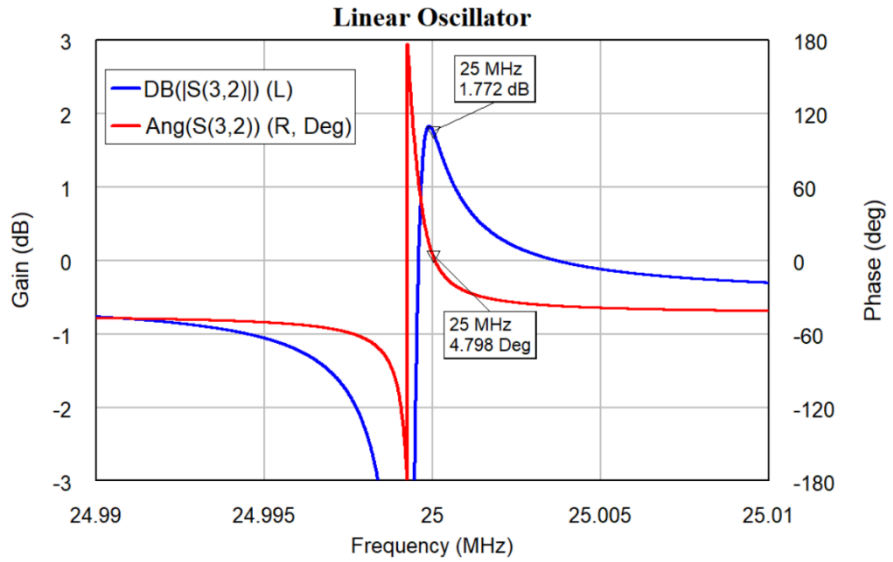



Figure 6.33. Frequency response for the oscillator using linear oscillator analysis (OSCTEST).

Replacing the OSCTEST element with the OSCAPROBE element as shown in figure 6.31, allows a harmonic balance analysis to be performed. Figure 6.34 shows the output spectrum, figure 6.35 shows the corresponding waveforms, and the phase noise is shown in figure 6.36

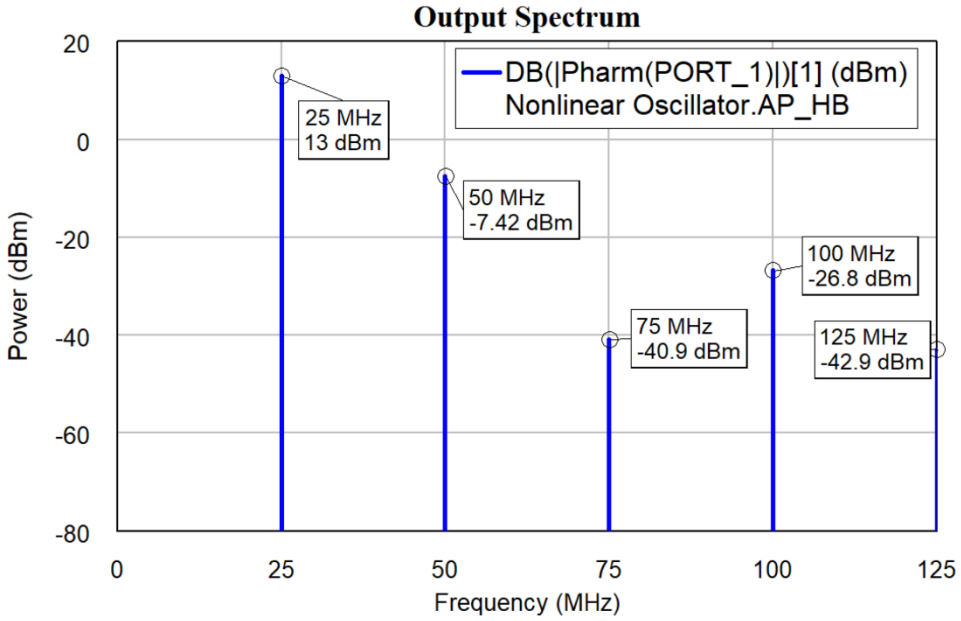



Figure 6.34. Output spectrum obtained using harmonic balance analysis. (OSCAPROBE)

The oscillating frequency can be varied by typically tens of parts per million, by placing a varactor diode either in parallel with C1 or C2 in figure 6.29 and controlled the frequency by varying the reverse bias voltage across the varactor diode. The oscillator then is a VCXO (Voltage Controlled Crystal Oscillator). Such control is used to obtain the precise frequency setting required for radio transmitters.

By comparing figures 6.13, 6.22 and 6.26 with figure 6.36, it can be seen that the crystal oscillator has a much lower phase noise, due to the Q of the resonator being much higher. The phase noise at 25 kHz in figure 6.36 is determined by the resistor and transistor noise

rather than the resonator. For low noise crystal oscillators, the output amplifier should impose a negligible load on the resonator and should use low noise transistors and low resistor values. For best comparison the same transistors and the same APLAC-HB simulator is used in all the simulations of figures 6.13 to 6.36.

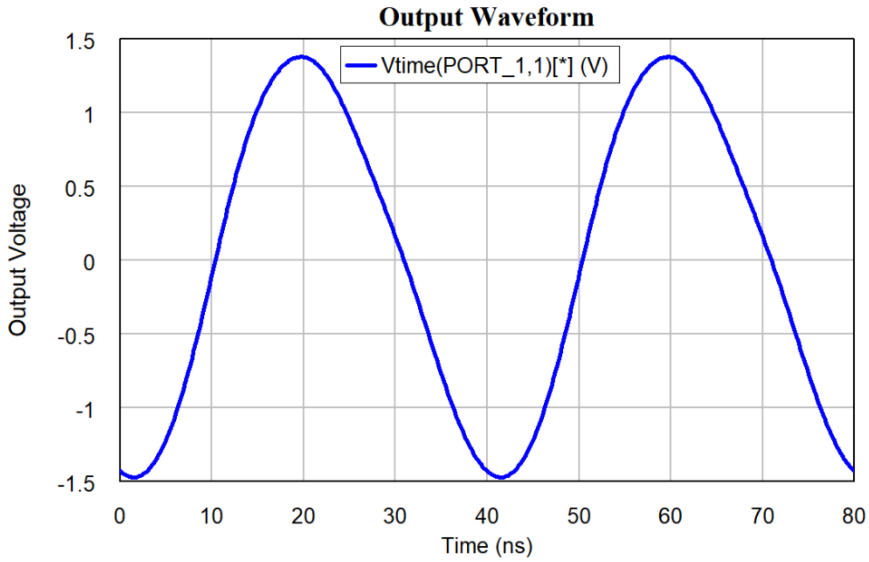



Figure 6.35. Output waveform obtained using nonlinear (harmonic balance) analysis.

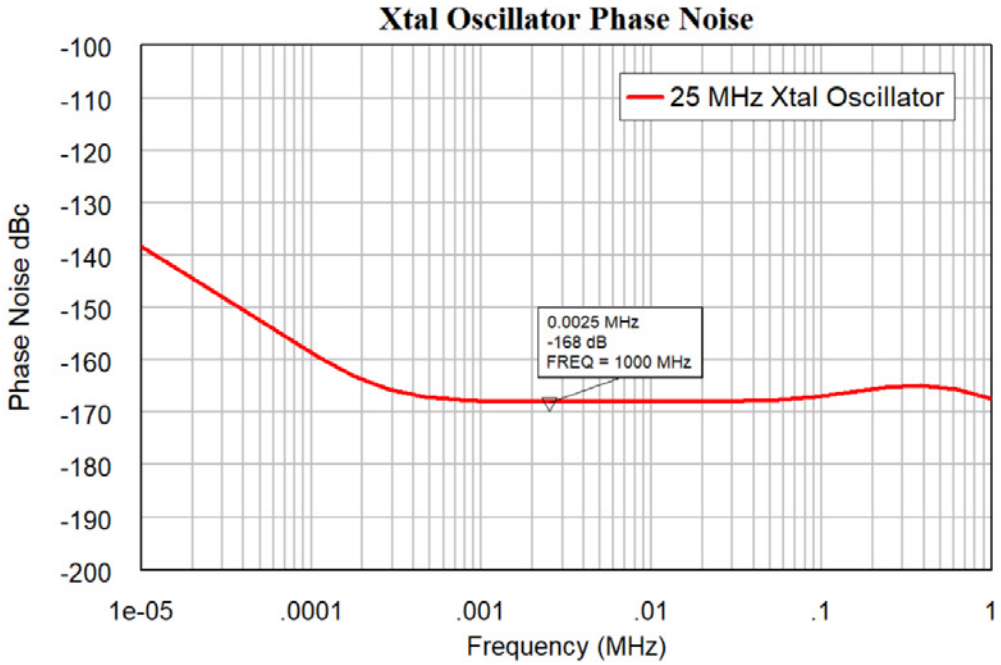



Figure 6.36. Phase noise of the oscillator.

## RF and Microwave Oscillators

At RF and Microwave frequencies (above 1GHz), transmission lines are often used as circuit elements. The MAR6 amplifier, used here, is a typical MMIC costing less than $10. These devices are very simple to use, are convenient, and can be used as low power amplifier blocks in many applications. The S parameters for these devices can be obtained from the Mini-Circuits web site as follows:

Table 6.1. S parameter file from Mini-Circuits with added line in blue.

| | | | | | | | | |
|---|---|---|---|---|---|---|---|---|
| !MAR-6 (TA = 25°C, Id = 16mA) | | | | | | | | |
| !FREQ. | S11 | | S21 | | S12 | | S22 | |
| !MHz | dB | Ang | dB | Ang | dB | Ang | dB | Ang |
| # MHZ S DB R 50 | | | | | | | | |
| 100 | -27.96 | 171 | 20.1 | 171 | -22.50 | 5 | -27.96 | -30 |
| 500 | -26.02 | -105 | 18.7 | 138 | -21.30 | 21 | -20.00 | -104 |
| 1000 | -17.72 | -118 | 16.4 | 107 | -18.80 | 28 | -17.08 | -150 |
| 1500 | -13.56 | -140 | 14.1 | 84 | -17.10 | 28 | -16.48 | 180 |
| 2000 | -10.75 | -163 | 12.0 | 65 | -15.80 | 26 | -15.92 | 157 |
| 2500 | -9.37 | -176 | 10.3 | 55 | -15.20 | 28 | -15.92 | 150 |
| 3000 | -7.74 | 169 | 8.7 | 42 | -14.80 | 25 | -16.48 | 143 |
| 3500 | -6.74 | 157 | 7.2 | 30 | -14.20 | 22 | -17.72 | 144 |
| 4000 | -6.20 | 146 | 6.1 | 18 | -13.80 | 20 | -20.00 | 156 |

This file can be imported into Microwave Office so that those S parameters for the device can be used in a simulation. To import the s parameter file, it needs to be in the "Touchstone" file format [7]. The only change that needs to be made to the S parameter file as obtained from Mini-Circuits, is the addition of the line shown in blue:

# MHZ S DB R 50

That line indicates to Microwave Office that the file has frequencies in MHz, contains S parameters, which must be in the order S11(Real, Imag), S21(Real, Imag), S12(Real, Imag) and S22(Real, Imag), The real part is in DB and the reference impedance is 50 ohm. Any line beginning with "!" is a comment line and is ignored in the data file import.

For other formats for data-files see the Microwave Office help files on "Adding Data Files to a project", which includes details on the Touchstone Import files format. That data file is then used as a sub-circuit in the circuit diagram.

## *Example 6.3: 1 GHz Microstrip Oscillator Design*

This data file is now used to design a 1 GHz oscillator using this MAR6 amplifier and using Microstrip circuits on a Rogers RO4003 substrate. The oscillator consists of three parts: The MAR6 amplifier, A Microstrip resonator (TL1) with tap coupling in order to obtain the correct impedance levels for the coupling into and out of the resonator and thirdly transmission lines TL2 to TL11, which are required to connect the output back to the input and thus provide feedback. The path length around the loop must have the appropriate phase shift to ensure that oscillations will result. In addition, two coupling capacitors are used to provide the correct DC levels at the input to the MAR6 and prevent the output from being shorted at DC.

The impedance of the resonator should be as low as possible to provide a reasonable Q, with low radiation losses and a good frequency stability. This is achieved by making the width of the resonator 5 mm. As shown in figure 2.27, for the current version of AWRDE, the *Transmission line Calculator* can be opened by right clicking on a MLIN element in the project and selecting *Synthesize*. The resonator (TL5) shown in figure 6.39 uses an MLEF circuit element for which the *Synthesize* function is not implemented. The MLEF element must thus be temporarily changed to MLIN, or the older program TXLine, which is part of MWO can be used for the calculations of the resulting resonator impedance and the required length of the resonator. For the RO4003 substrate with Er = 3.38, using the *Transmission line Calculator,* results in a characteristic impedance of 24.8 Ω and 44.0 mm length for a quarter wavelength. The same values are obtained from TXLine as shown in figure 6.37.

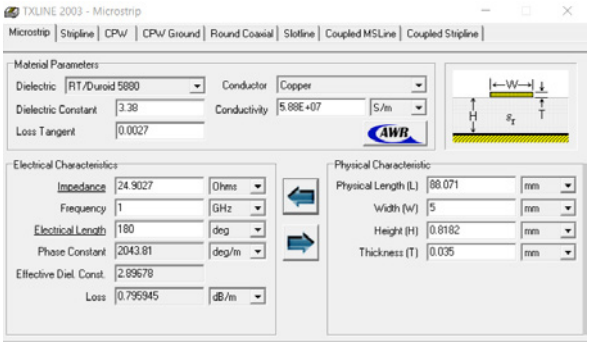



Figure 6.37. Resonator Width and Length Calculation

Since a full SPICE model is not available for the MAR6, only a linear analysis of the oscillator can be carried out. The circuit schematic for the oscillator is shown in figure 6.38. This design was produced in early 2005 and presented at [8]. At that time the more advanced X models were just becoming available and as a result MTEE, MCROSS and MLEF elements were used. For current designs, the more advanced EM based MTEEX, MCROSSX and MLEFX elements should be used. In addition Rogers had not yet suggested that Er = 3.55 should be used for simulation of RO4003 substrates, so the value Er = 3.38 was used in this design. To enable a comparison between the simulations and measurements to be made, the results in figures 6.41 to 6.45 are obtained from the original design.

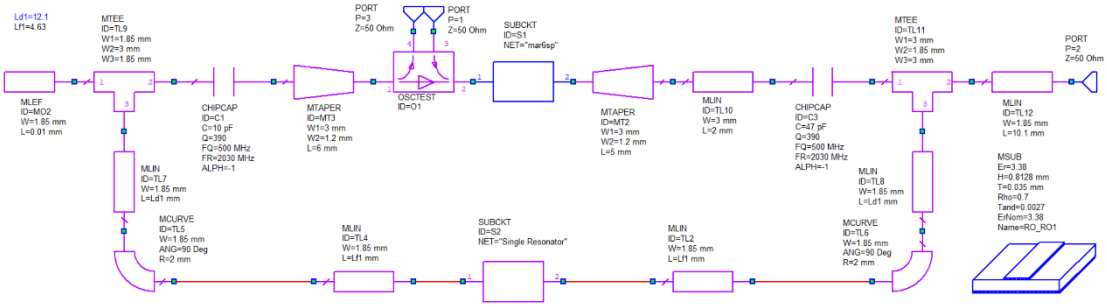



Figure 6.38. Circuit schematic for 1GHz oscillator.

Figures 6.39 and 6.40 show the circuit diagram and layout of the resonator. A capacitor is incorporated. That capacitor can be replaced with a variable capacitor in the hardware, to allow the oscillator to be fine-tuned to the correct frequency. With a minor modification, this can be replaced with a varactor diode, to enable the oscillator to be phase locked or frequency modulated.

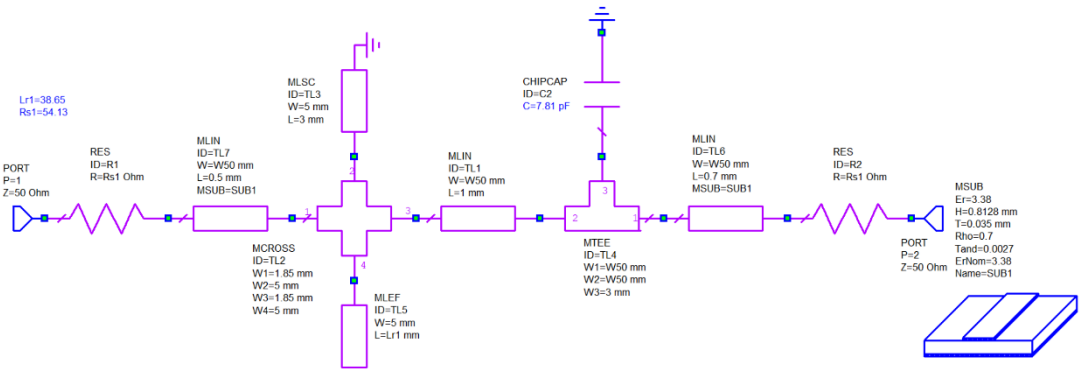



Figure 6.39. Circuit Schematic for 1GHz Microstrip resonator.

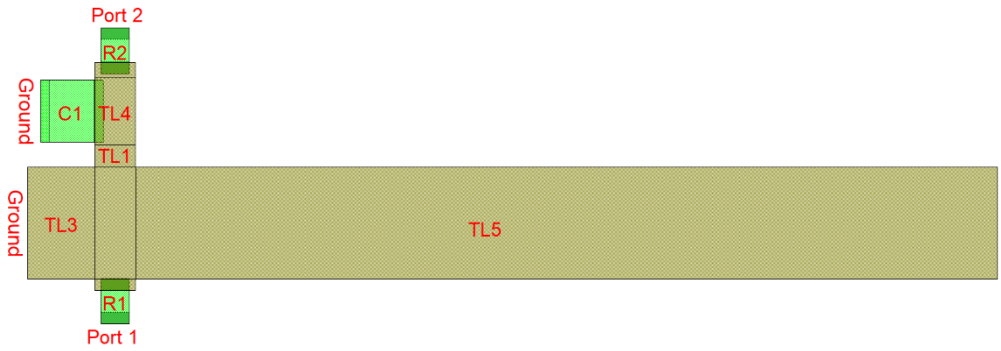



Figure 6.40. Layout for 1GHz Microstrip resonator.

The length of TL3 is made small as is practicable to minimise the loading of the resonator due to the rest of the circuit. The length of TL3 should be several times larger than the width of the connecting tracks, to ensure a uniform current distribution on the input and output connectors. The 50 Ω track width of TL1 is 1.84 mm. As a result, the smallest length of TL3 is about 3 mm. Resistors R1 and R2 are placed at the input and output, to firstly provide a reasonable termination impedance to the amplifier at frequencies other than the resonant frequency and secondly to provide some fine tuning for the resonator loading, and thus the loop-gain of the oscillator. Figure 6.40 shows the layout for the resonator and the coupling capacitors. The left end of the circuit is grounded.

Figure 6.41 shows the amplitude and phase of the resonator of figure 6.40, as a function of frequency.

**Tuning Step 1:** Tune the length of the resonator Lr1, to ensure that the resonator has a maximum gain from port 1 to port 2 at the desired oscillating frequency in figure 6.41. The gain at other frequencies should be low, to ensure that the oscillator does not oscillate at another frequency.

The resonator has a well-behaved response at 1 GHz, but if the amplifier gain is too high, there is a possibility of oscillation at the secondary response of 1.34 GHz. The loop gain of the amplifier and resonator must thus be carefully controlled to ensure that only oscillation at 1 GHz is possible.

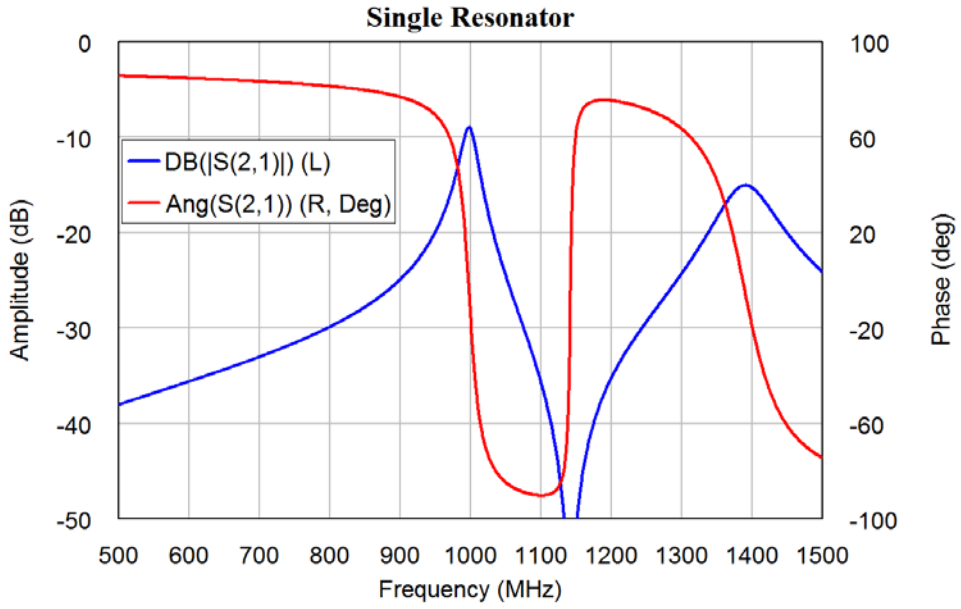



Figure 6.41. Resonator transfer function, amplitude and phase.

The element OSCTEST is used to check if the oscillator has the correct gain and phase in the feedback path. The phase shift around the loop should be exactly 0 degrees and the gain should be greater than one. An excess gain of 3 dB ensures that the loop gain is greater than one, even when different MAR 6 devices are used.

**Tuning Step 2:** The length of TL7 and TL8, which form part of the feedback signal path, are both adjusted in order to obtain the correct phase shift of 0 º at 1 GHz. Having a loop gain greater than 1 and a 0 º phase shift is a sufficient condition for oscillation.

Note that tuning capacitor C1 of figure 6.39 shows that this resonance at 1.3 GHz is due to that capacitor, so that it is desirable to keep this capacitor as small as possible.

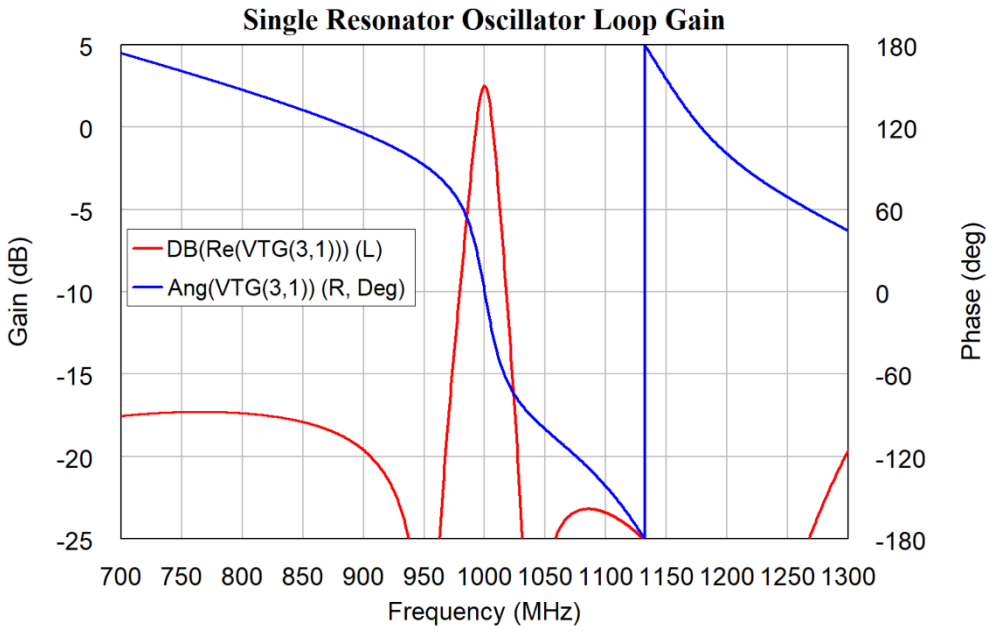



Figure 6.42. Single resonator oscillator open loop gain (OSCTEST) output.

**Tuning Step 3:** The design must now be arranged so that it fits on a PCB with all the track ends joining in the correct manner. The lengths of all the tracks and the phase shift produced by the MMIC must be kept exactly the correct length to satisfy the zero degree open loop phase shift from OSCTEST and a gain slightly greater than one as shown in figure 6.42.

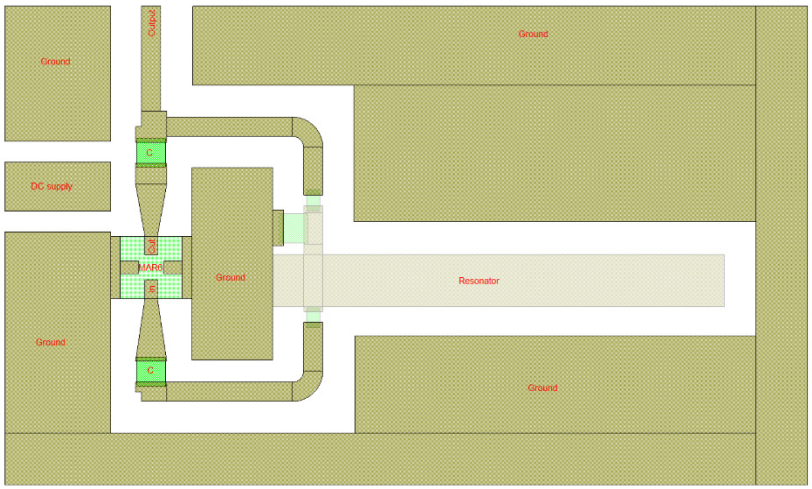



Figure 6.43. PCB layout for the 1GHz oscillator.

The resulting Microstrip layout is shown in figure 6.43, with the oscillator output at the top, the supply voltage pad at the left and the largest element being the resonator. The resonator is shown slightly lighter, since that is a separate element in the layout. The only elements not shown on this layout are the power supply biasing and vias connecting the ground pins of the MAR to the ground-plane. Figure 6.44 shows the corresponding hardware.

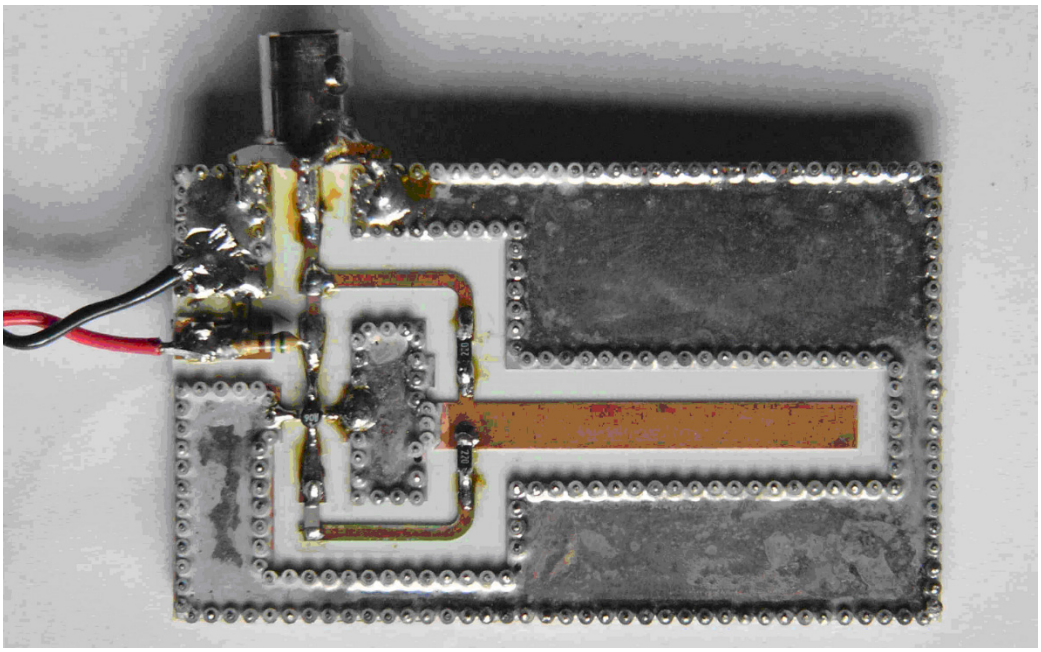


Figure 6.44. Photograph of the 1 GHz oscillator.

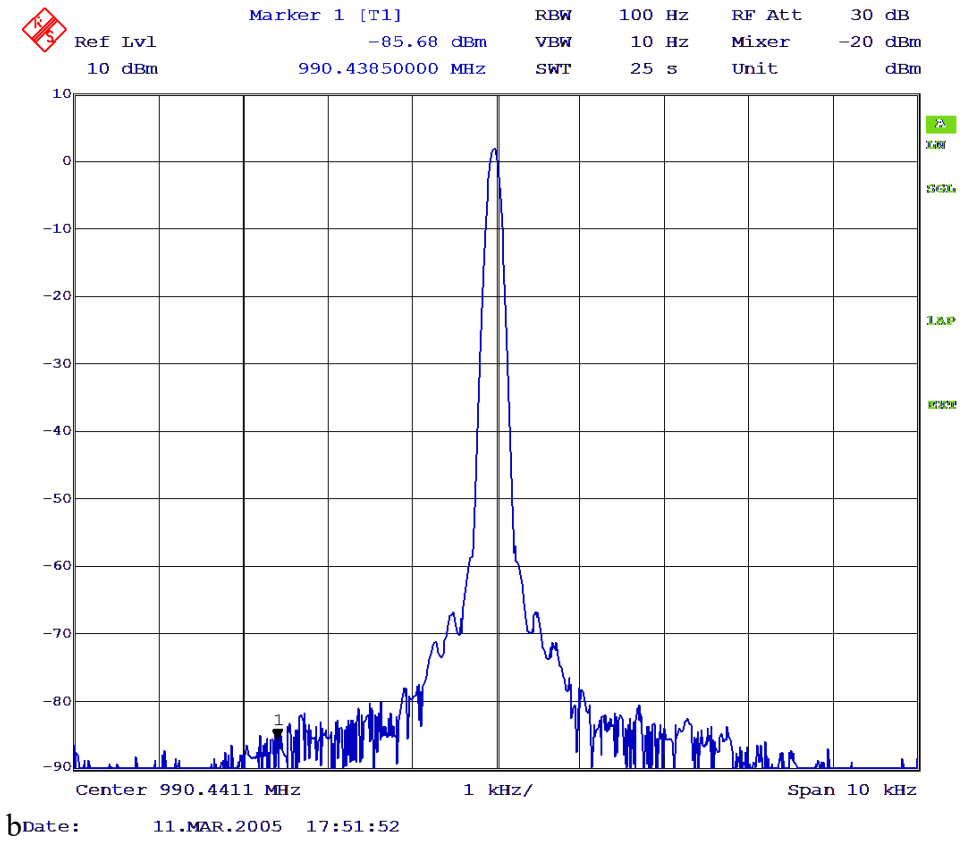



Figure 6.45. Measured output spectrum for the 1 GHz oscillator.

Figure 6.45 shows the spectrum obtained from the oscillator. The oscillator has a clean output signal and an acceptable phase noise performance. The output frequency is 990 MHz, which is within 1% of the design value. The output power is +5 dBm.

# Dual Resonator Oscillator

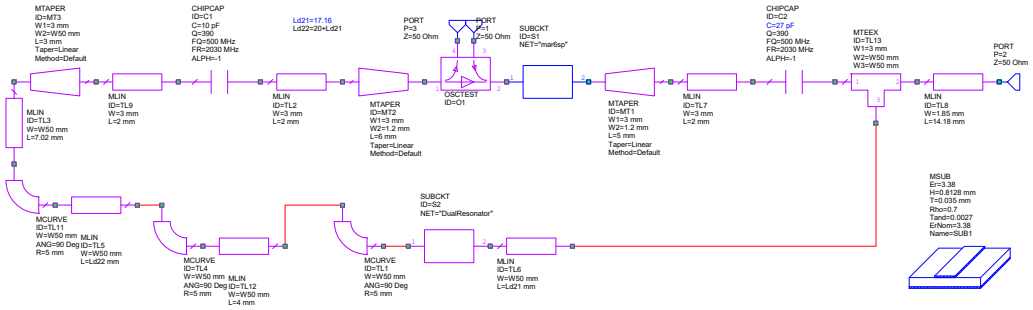



Figure 6.46. Circuit schematic for 1GHz dual resonator oscillator.

It is desirable to design oscillators, which produce the least amount of phase noise for a given frequency and tuning range. The primary factors determining the phase noise of the oscillator are the Q of the resonant network, the noise figure of the amplifier and its output power. Leeson's [3] simplified model for phase noise shows the phase noise is inversely proportional to the square of the Q of the resonator. The higher the Q, the more rapid the resonator's change of phase with frequency at the resonance.

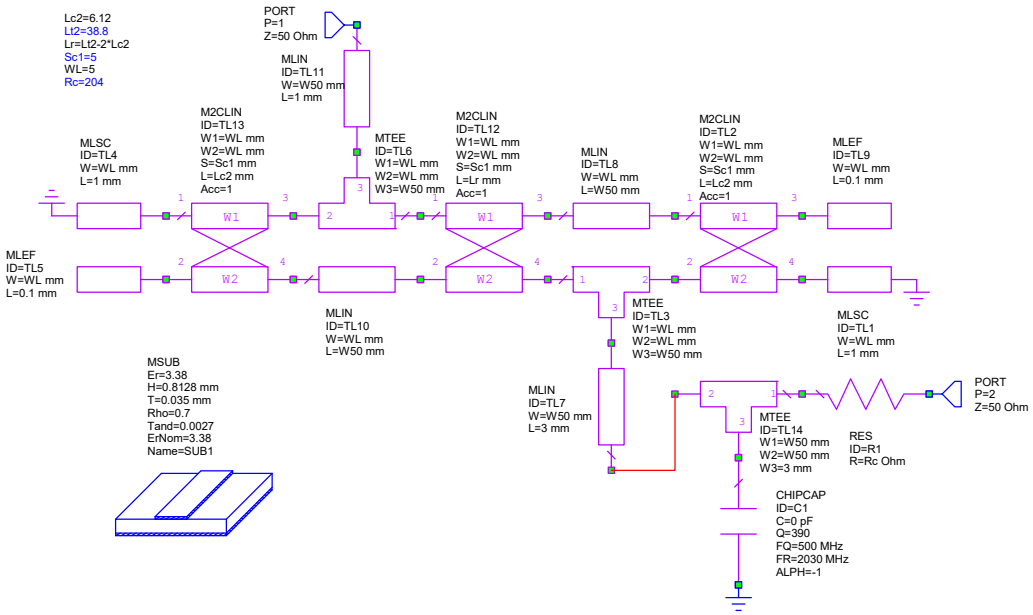



Figure 6.47. Simplified Circuit Schematic for 1GHz Microstrip coupled dual resonator.

By using two resonators that are coupled, a faster change of phase at the resonance can be obtained, thus reducing the phase noise. Figures 6.39 and 6.40 show a single resonator.

Figures 6.47 and 6.48 show the corresponding coupled dual resonator. As described above, this design was done early in 2005 [8] and the more advanced EM based Microstrip elements were not used. Like the tuning carried out on the single resonator shown in figure 6.39, the lengths of TL2 and TL13 of the double resonator are adjusted to minimise the loading on the resonator by the amplifier, while still giving the correct open loop gain, corresponding to the switch in figure 6.1 being open. Thus producing a result similar to figure 6.42 for the single resonator design using OSCTEST.

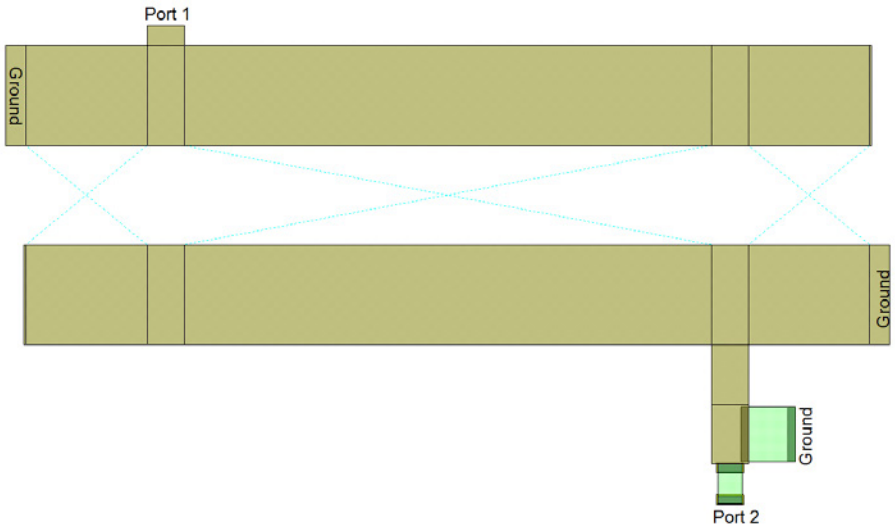



Figure 6.48. PCB layout of for the dual resonator of figure 6.47.

An oscillator using a MAR6 amplifier, similar to figure 6.43 and 6.44, is designed and the lengths of TL2 and TL13 and the value of Rc are adjusted to ensure an open loop gain slightly greater than 0 dB and the length of the transmission lines making up the feedback loop are adjusted to give a 0° phase shift.

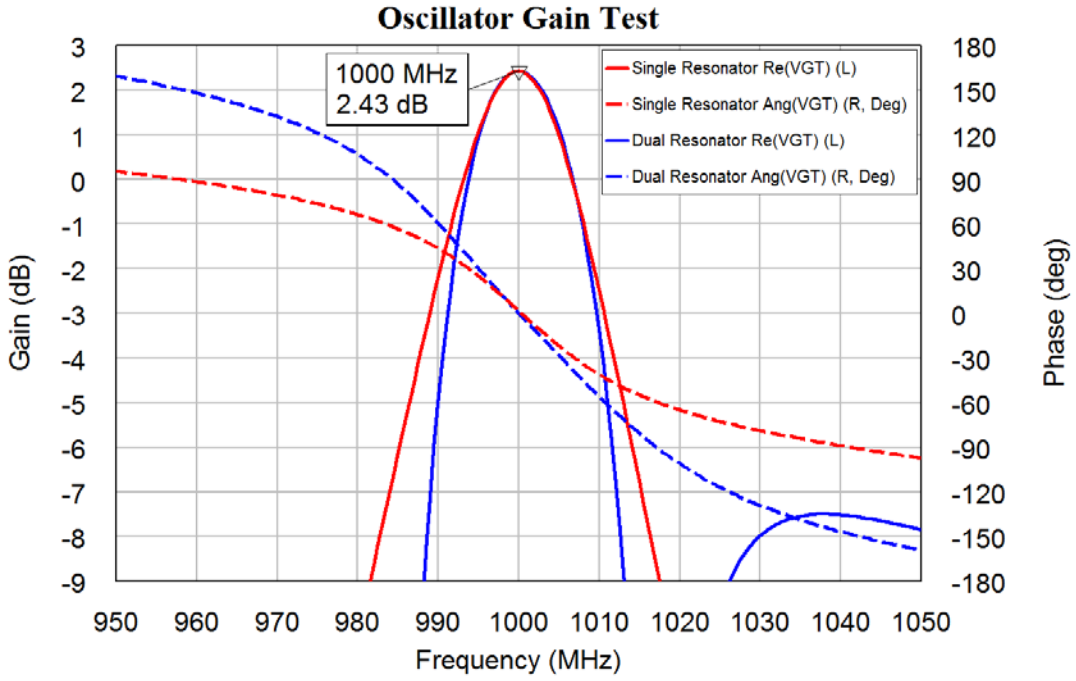



Figure 6.49. Comparison of single and dual resonator open loop gain and phase.

Figure 6.49 shows a comparison of the oscillator open loop gain for the single and dual resonator oscillator open loop gain. The rate of change of phase for the dual resonator is greater and since the same amplifier is used, the phase noise of the dual resonator oscillator should be less. The open loop gain has been adjusted to be the same for both circuits. Both circuits were also designed to have a 0° phase shift at 1 GHz. Both circuits should thus have the same oscillating frequency.

Figure 6.50 shows the resulting hardware and figure 6.51 shows the corresponding measured output spectrum. The oscillators of figures 6.44 and 6.50 use the same PCB material, the same amplifier and supply voltage and the same measurement technique. The only difference is the type of resonator used. Comparing figures 6.45 and 6.51 clearly shows the improved phase noise of the dual resonator design.

Since the non-linear models of the MAR amplifier are not available, it was not possible to do a phase noise measurement using NI AWR DE as was done for in figures 6.13, 6.22, 6.26 and 6.36. A paper by the author [8] includes the design of a transistor amplifier, which is used with both the single resonator of figure 6.39 and the dual resonator of figure 6.47, and thus allows the phase noise for single and dual resonator designs to be compared. For those designs, the dual resonator oscillator gives a 3 dB phase noise improvement.

It is possible to extend this technique to more resonators, however an N resonator design can produce N x 180 degree phase shift, making it progressively more difficult to ensure that only one oscillating frequency is possible.

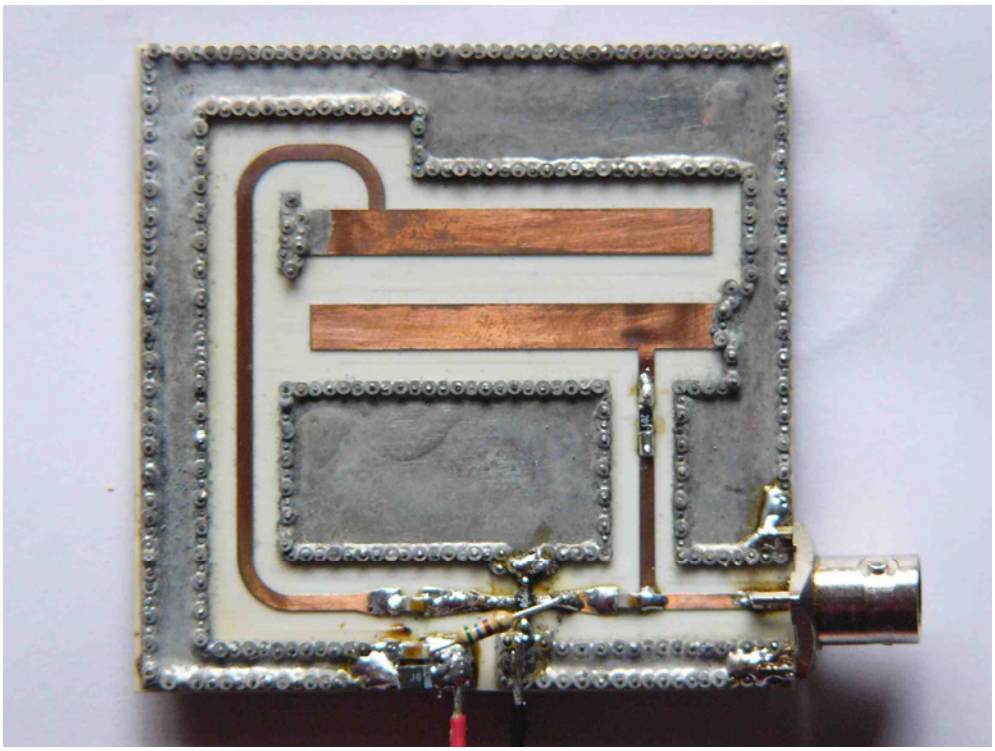


Figure 6.50. Photograph of the 1GHz dual resonator oscillator.

## *Design Improvements*

The group delay of the open loop circuit gain as obtained from OSCTEST is directly related to the Q of a single resonator network. For a dual resonator, Q is not defined, so that the group delay is a good measure of the expected phase noise of the oscillator. For

the single resonator design of figures 6.38 and 6.44, the group delay is 13.6 ns at 1 GHz. For the dual resonator design of figures 6.46 and 6.50, it is 16.17 ns at 1 GHz.

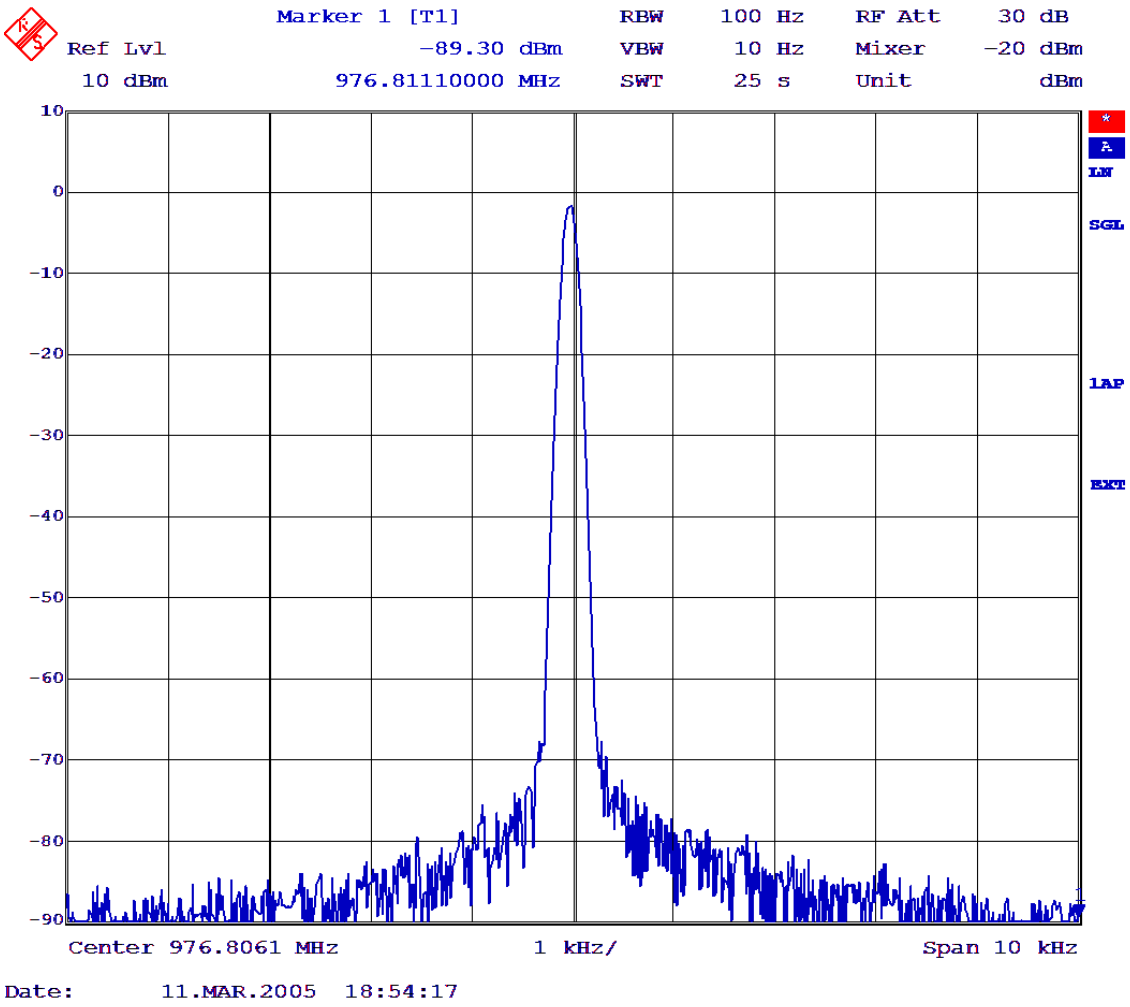



Figure 6.51. Measured output spectrum for the 1 GHz oscillator.

It is possible to improve the designs of figures 6.38-6.44 and 6.46-6.50, by reducing the loading on the resonators. To achieve the best accuracy for the simulation, the EM based MTEEX, MCROSSX and MLEFX elements are used and the Rogers recommended Er =3.55 is used for the simulation of the RO4003 substrate.

For the single resonator oscillator, capacitor C1 in figure 6.39, significantly reduces the loop gain as it is increased from 0 to 10 pF. Tuning without resonator gain variations can however be achieved by having a very small capacitor coupled at the top of the resonator, like the tuning screws in the interdigital filters as shown in figure 7.57 and 7.58. For the PCB layout, this can simply be done by soldering a nut to the ground-plane at the top of the resonator and using a screw parallel and above the top of the resonator to provide an adjustable small capacitance. That significantly increases the Q of the resonator and results in an OSCTEST loop-gain group delay of 23.09 ns.

For the dual resonator, resistors are included at the input and output of the resonator, similar to those for the single resonator. For the dual resonator, the resonator cannot be tuned effectively by tuning one of the resonators as can be done for the single resonator. However, since the line lengths of the required tracks need to be much longer, as can be seen by comparing figures 6.44 and 6.50, it is possible to obtain good tuning control by

placing a small capacitor at a strategic location along the feedback path. Then the lengths of TL13 and TL2, the resonator spacing Sc1 and the values of the terminating resistors R1 and R2 in figure 6.46 are tuned, to obtain the correct resonator frequency, the correct phase for OSCTEST and a high group delay.

For both the oscillators, the effect of external loads was reduced by inserting a 150 Ω resistor in series with the oscillator output. The resulting reduction in output signal can easily be made up using an additional MMIC.

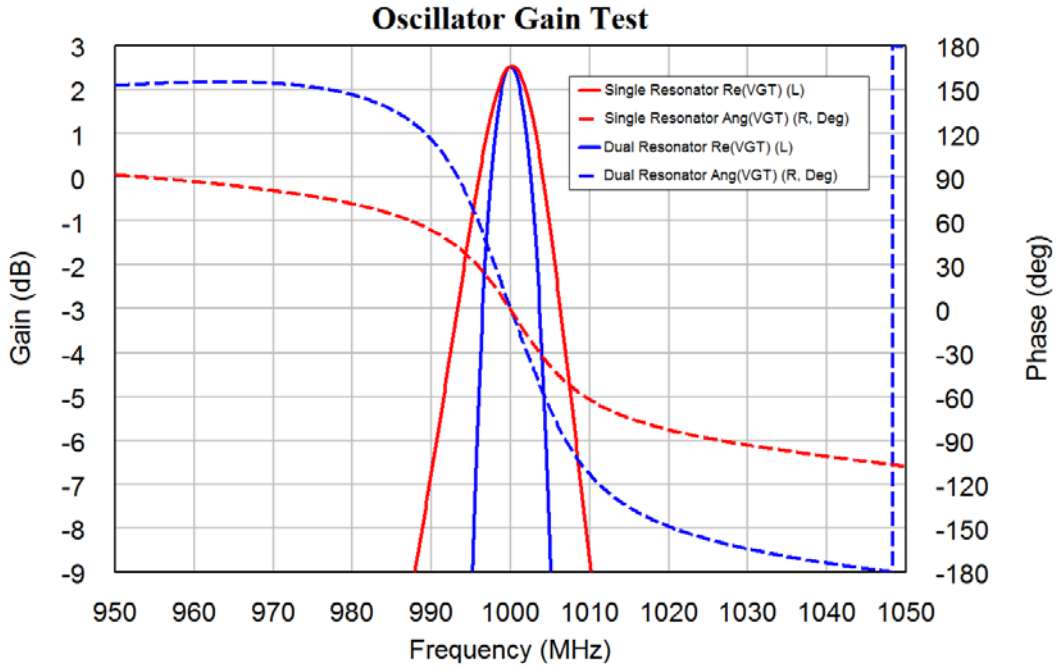



Figure 6.52. Comparison of improved single and dual resonator oscillator OSCTEST results.

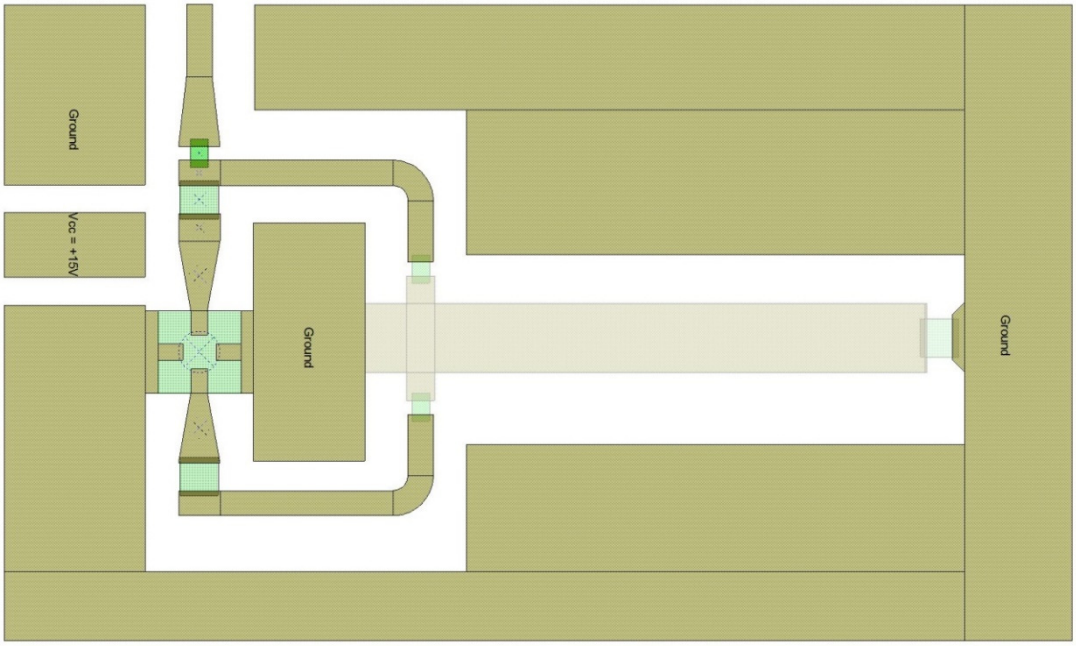



Figure 6.53. PCB layout for the improved 1GHz single resonator oscillator.

Figures 6.52 shows the OSCTEST loop gain and phase for both the improved single and dual resonator oscillators. Comparing this with figure 6.49 shows a narrower bandwidth,

corresponding to a higher effective Q and a lower expected phase noise. The group delay of the single resonator oscillator is now 23.09 ns at 1 GHz and that of the dual resonator is 40.69 ns, a ratio of 1.76. This should give a 4.9 dB better phase noise [8] for the dual resonator oscillator compared with the single resonator oscillator.

Figures 6.53 and 6.54 show the corresponding layouts of the oscillators. Comparing figure 6.43 with 6.53 shows only minor differences in the layout. The capacitor at the top of the resonator in figure 6.53 is the 0-1 pF tuning capacitance used for setting the centre frequency. Comparing figure 6.50 with figure 6.54 shows significant differences. The spacing between the coupled resonators has increased significantly. To be able to produce the correct length of the feedback path, the feedback track had to be run in-between the resonators. It is not possible to obtain the correct length if the feedback was run outside the resonator, as was done in figure 6.50. The frequency tuning capacitor is the capacitor to ground at the top middle-right of the layout. Isolating that part of the ground-plane allows a varactor diode to be used for electronic frequency tuning.

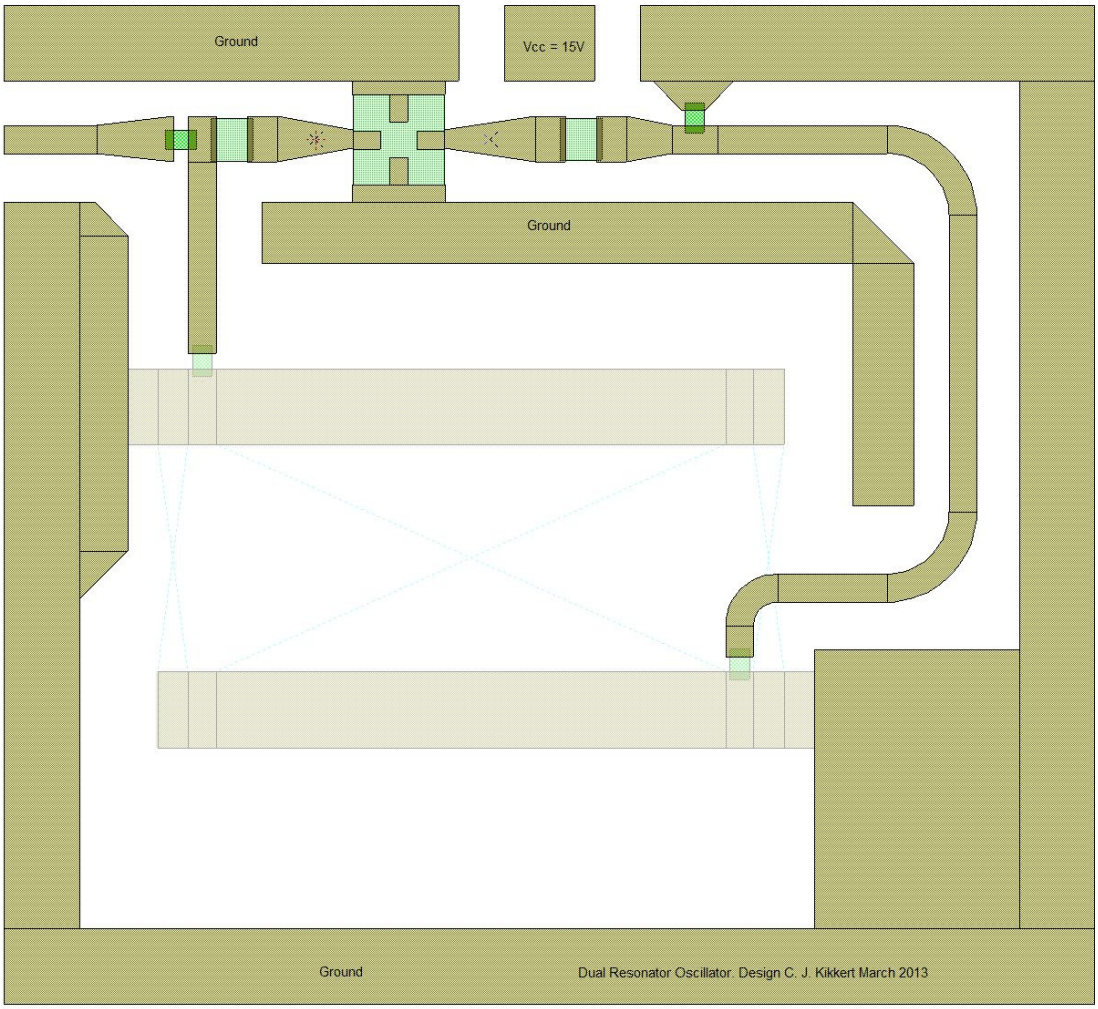



Figure 6.54. PCB layout for the improved 1GHz dual resonator oscillator.

The distance between the resonators is larger than the distance between a resonator and the ground-plane. As a result, the ground-plane should have some effect on the oscillator performance. That should be evaluated using an EM simulator like AXIEM prior to construction of the circuit. The EM simulation process is described in the section “EM

Simulation" in chapter 7 of this book and will not be dealt with here. The design techniques presented in this chapter will allow low noise RF and microwave oscillators to be designed. For a low phase noise, it is important to minimise the external loading on the resonator. Measuring the group delay as part of the OSCTEST gain and phase adjustment gives a good indication of the phase noise performance.

## Phase Locked Loops

In practice RF oscillators are used in transmitters and receivers. As a result, the oscillation frequency must be precisely controlled to satisfy the relevant communication system regulations. To enable the frequency of an oscillator like the one in figure 6.9 or 6.24 to be electronically controlled, a varactor diode is used as an electronically variable capacitor and placed in parallel with either Cr2 or in parallel with Lc. Then changing the reverse voltage across the varactor changes the frequency of the oscillator, so that the oscillator is a voltage-controlled oscillator (VCO).

The block diagram of a phase-locked loop is shown in Figure 6.55. It consists of VCO, and a loop filter which primarily determines the transient behaviour of the phase locked loop, but which must also attenuate any high frequency components produced by the phase detector. The reference input can be the output from a Crystal oscillator, like the one of figure 6.31. When the PLL is locked, the output frequency is N times the input frequency. The type of Phase Detector used, as well as the loop filter and VCO determines the behaviour of the phase locked loop.

$$\frac{\emptyset out}{\emptyset in} = \frac{N\,K\,H(s)}{Ns+K\,H(s)} \qquad \text{Eqn. 6.3}$$

N is the divider ratio, K is a gain = KpKv, where Kp is the phase detector transfer function and Kv is the VCO Hz/V constant. H(s) is the loop filter transfer function and s is the complex frequency variable.

The PLL transfer function is a low pass function, so that at low frequency, the phase noise is dominated by the crystal oscillator noise, multiplied to the VCO frequency [9, 10]. At frequencies above the natural frequency (loop filter band-with) of transfer function of equation 6.3, the VCO noise dominates. Typical phase detectors are multipliers or mixers described in chapter 5, exclusive OR gates or phase-frequency detectors [11]. Phase frequency detectors provide a feedback signal when the VCO is not locked, and will thus provide more reliable phase locking of the VCO. All these phase detectors produce unwanted signals at harmonics of the Reference Input frequency. Those must be filtered out to produce a clean output spectrum. The natural frequency must thus be much lower than the reference frequency input.

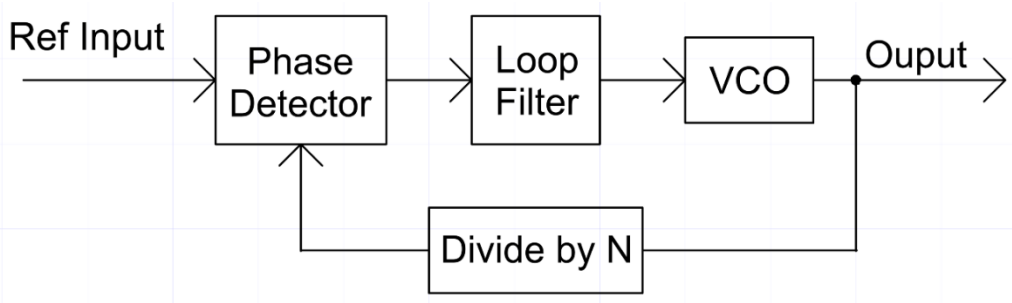



Figure 6.55. PLL Block Diagram.

When an oscillator is phase locked, the noise below the natural frequency of the transfer function of equation 6.3 is a little bit more than N times the crystal oscillator noise. The extra phase noise is due to noise produced by the frequency divider and the phase detector. It is possible to simulate that [10] but that is outside the scope of this book. Figure 6.56 shows the phase noise of the 100 MHz oscillator of figure 6.24 and the 25 MHz crystal oscillator of figures 6.29 to 6.36. The green dotted curve is the phase noise of the crystal oscillator multiplied by 4 to go from 25 MHz to 100 MHz. The red curve is the typical phase noise of the phase locked 100 MHz oscillator. (Note figure 6.56 is for illustration only, and is not based on measurements or detailed simulations).

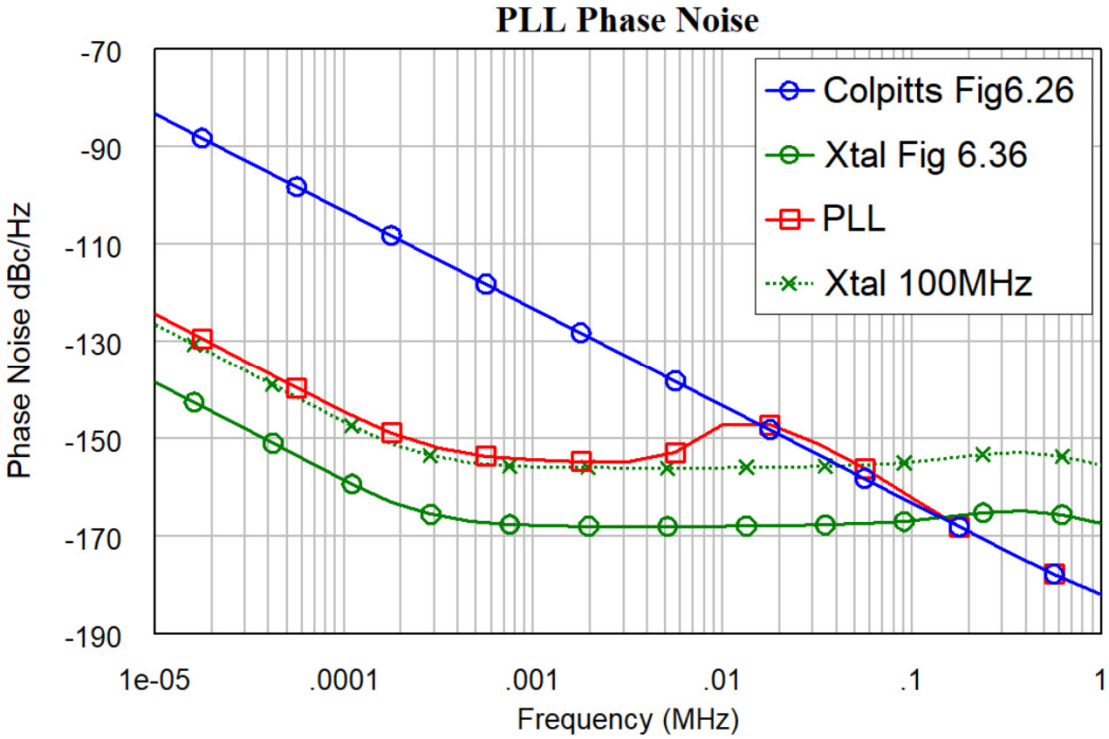



Figure 6.56. Noise from a phase locked oscillator.

### *Frequency Locked Loop*

There are some applications where phase locking is impossible, but where a frequency detector (or phase frequency detector) is used instead of a phase detector. In that application, the frequency of the divided VCO signal, is made to lock to the frequency of the reference input, resulting in a frequency locked loop. Typical examples of this are: 1) Frequency locking a crystal oscillator to the 1 pulse per second output from a GPS receiver. 2) Frequency locking an oscillator that is used for FM broadcasting to a reference crystal. The combination of these will allow an FM transmitter to have a carrier frequency accuracy better than 1 part per million. Under those conditions, the phase noise of the locked VCO is the same as the phase noise of the unlocked VCO.

## References

1. J P Silver “Oscillator Resonator Design Tutorial”, Oscillator Resonators, https://fdocuments.net/document/oscillator-resonator-design-resonator-design-tutorial-j-p-silver-varactor-in.html?page=1

2. Infineon, High Linearity Transistors, https://www.infineon.com/cms/en/product/rf-wireless-control/rf-transistor/high-linearity-si-and-sigec-transistors-for-use-up-to-6-ghz/
3. D. B Leeson, "A Simplified Model of Feedback Oscillator Noise Spectrum", Proceedings of the IEEE, Vol. 42, February 1965, pp. 329-330.
4. Electronics Tutorials, Hartley Oscillator, https://www.electronics-tutorials.ws/oscillator/hartley.html
5. H. A. Wheeler, "Simple Inductance Formulas for Radio Coils," Proceedings of the Institute of Radio Engineers, vol. 16, no. 10, pp. 1398-1400, Oct. 1928, doi: 10.1109/JRPROC.1928.221309.
6. John Vig "Quartz Crystal Resonators and Oscillators for Frequency Control and Timing Applications - A Tutorial", tf.nist.gov/sim/2010_Seminar/vig3.ppt. Nov 2008.
7. Touchstone File format, NI AWR DE Help: AWRDE User Guide, Chapter 3: Data Files (section 3.2.10).
8. Kikkert, C. J. “Dual Coupled Resonator Local Oscillator”, IEEE Tencon ’05, Melbourne, Australia, 21-24 November 2005, paper 1568965076.
9. A Mehrotra, Noise Analysis of Phase Locked Loops, IEEE Trans Circuits and Systems I, Vol. 49, No. 9, Sep 2002, pp1309-1316.
10. P. Delos, Phase Locked Loop Noise Transfer Functions, High Frequency Electronics, January 2016, https://www.highfrequencyelectronics.com/index.php?option=com_content&view=article&id=1354:phase-locked-loop-noise-transfer-functions& catid=134:2016-01-january-articles&Itemid=189
11. Kikkert C. J. "Two novel phase-frequency detectors." 2006 IEEE Asia Pacific Conference on Circuits and Systems (APCCAS2006), Singapore, 4-7 Dec 2006, Proceedings pp 713 - 716, publisher IEEE.

# Chapter 7

# RF Filters

## Introduction

Filters used for RF signals are nearly always Bandpass filters using coupled resonator design techniques. The basic properties of the most common types of filters are:

### *Electrical Filters*

**LC Bandpass Filters**. Typical unloaded Q valued are 60-150, resulting in a large % Bandwidth filter with a high insertion loss. Frequency range 455 kHz to 2 GHz.

**Helical Filters.** Typical unloaded Q values > 1000. The Q value can be increased, by increasing the size of the resonator cavity. Frequency range 30 MHz – 1 GHz.

**Coaxial Filters.** Typical unloaded Q value > 5000. Frequency range 80 MHz – 2 GHz. Using a Ceramic dielectric results in a small size, for mobile radio use. Air dielectric coaxial filters are used for high power diplexers in Radio and TV transmitters.

**Microstrip and Stripline filters**. Made using lines on PCB. Typical unloaded Q value 250. Wide % bandwidth.

**Transmission Line Filters.** Designs based on Short or open circuited stubs. Wide Bandwidth.

**Interdigital Filters.** High Q and < 10% bandwidth.

### *Acoustic filters*

**Ceramic filters.** Commonly used frequencies only. 455 kHz, 10.7 MHz IF filters, 800 MHz and 1.9 GHz diplexers for cellular phones.

**Crystal Filters.** Very High Q values and very low bandwidths. Typical 6 kHz Bandwidth at 10.7 MHz. Used for SSB filters. High cost compared to other filters.

**SAW filters.** Frequencies from 40MHz to 3 GHz. Relatively high insertion loss. The amplitude response and group delay can be controlled independently.

Several of the above filter types are discussed in detail in these notes.

## Filter Design Revision

For this chapter, it is assumed that the reader knows about basic filter requirements and the resulting specifications of filtering characteristics if required, please refer to filter design texts, such as Zverev[1]. Most RF filter designs start with a normalised lowpass filter design and that filter has the required specifications in terms of filter order required, amplitude and group delay performance. This normalised lowpass filter is then transformed into the appropriate bandpass filter. There are two starting points:

1 Normalised LC filter tables or equations
2 K and Q filter tables.

These two are related and one can be derived from the other. For some filter types, like Butterworth filters, simple equations can be used for the normalised lowpass filter prototype.

## *Filter Tables*

For RF designs K and Q tables are better than the LC filter tables or equations, since they include the effect of finite Q values in the resonators used. A good book for filter tables is "Handbook of Filter Synthesis" by A. I. Zverev, Wiley, 1967 [1] and more recently from Artech House. This together with Matthaei, Young, and Jones, "Microwave Filters, Impedance-Matching Networks, and Coupling Structures" [2] these are RF filter design classics and are still in print. Chapter 8 of Pozar [3] also describes microwave filters.

Table 7.1a. Butterworth Response, K And Q Value filter table, From Zverev[1], pp 341.

| n | q0 | I. L. | q 1 | q n | k 12 | k 23 | k 34 | k 45 |
|---|---|---|---|---|---|---|---|---|
| 2 | INF. | 0.000 | 1.4142 | 1.4142 | 0.7071 | | | |
| | 14.142 | 0.915 | 1.4142 | 1.4142 | 0.7071 | | | |
| | 7.071 | 1.938 | 1.4142 | 1.4142 | 0.7071 | | | |
| | 4.714 | 3.098 | 1.4142 | 1.4142 | 0.7071 | | | |
| | 3.536 | 4.437 | 1.4142 | 1.4142 | 0.7071 | | | |
| | 2.829 | 6.021 | 1.4142 | 1.4142 | 0.7071 | | | |
| | 2.357 | 7.959 | 1.4142 | 1.4142 | 0.7071 | | | |
| | 2.020 | 10.459 | 1.4142 | 1.4142 | 0.7071 | | | |
| | | | | | | | | |
| 3 | INF. | 0.000 | 1.0000 | 1.0000 | 0.7071 | 0.7071 | | |
| | 20.000 | 0.958 | 0.8041 | 1.4156 | 0.7687 | 0.6582 | | |
| | 10.000 | 2.052 | 0.8007 | 1.5359 | 0.7388 | 0.6716 | | |
| | 6.667 | 3.300 | 0.9097 | 1.6301 | 0.7005 | 0.6879 | | |
| | 5.000 | 4.742 | 0.8226 | 1.7115 | 0.6567 | 0.7060 | | |
| | 4.000 | 6.443 | 0.8406 | 1.7844 | 0.6077 | 0.7256 | | |
| | 3.333 | 8.512 | 0.8625 | 1.8497 | 0.5524 | 0.7470 | | |
| | 2.857 | 11.157 | 0.8884 | 1.9068 | 0.4883 | 0.7706 | | |
| | | | | | | | | |
| 4 | INF. | 0.000 | 0.7654 | 0.7654 | 0.8409 | 0.5412 | 0.8409 | |
| | 26.131 | 1.002 | 0.5376 | 1.4782 | 1.0927 | 0.5668 | 0.6670 | |
| | 13.066 | 2.162 | 0.5355 | 1.6875 | 1.0745 | 0.5546 | 0.6805 | |
| | 8.710 | 3.489 | 0.5417 | 1.8605 | 1.0411 | 0.5373 | 0.6992 | |
| | 6.533 | 5.020 | 0.5521 | 2.0170 | 1.0004 | 0.5161 | 0.7207 | |
| | 5.226 | 6.822 | 0.5656 | 2.1621 | 0.9547 | 0.4906 | 0.7444 | |
| | 4.355 | 9.003 | 0.5819 | 2.2961 | 0.9051 | 0.4592 | 0.7706 | |
| | 3.733 | 11.772 | 0.6012 | 2.4159 | 0.8518 | 0.4192 | 0.7998 | |

Table 7.1b. Butterworth Response, K And Q Value filter table, From Zverev[1], pp 341.

| n | q0 | I. L. | q 1 | q n | k 12 | k 23 | k 34 | k 45 |
|---|---|---|---|---|---|---|---|---|
| 5 | INF. | 0.000 | 0.6180 | 0.6180 | 1.0000 | 0.5559 | 0.5559 | 1.0000 |
| | 32.361 | 1.045 | 0.4001 | 1.5527 | 1.4542 | 0.6946 | 0.5285 | 0.6750 |
| | 32.361 | 1.045 | 0.5662 | 0.7261 | 1.0947 | 0.5636 | 0.5800 | 0.8106 |
| | 16.180 | 2.263 | 0.3990 | 1.8372 | 1.4414 | 0.6886 | 0.5200 | 0.6874 |
| | 16.180 | 2.263 | 0.5777 | 0.7577 | 1.0711 | 0.5408 | 0.6160 | 0.7452 |
| | 10.787 | 3.657 | 0.4036 | 2.0825 | 1.4088 | 0.6750 | 0.5080 | 0.7066 |
| | 10.787 | 3.657 | 0.5927 | 0.7869 | 1.0408 | 0.5144 | 0.6520 | 0.6860 |
| | 8.090 | 5.265 | 0.4111 | 2.3118 | 1.3670 | 0.6576 | 0.4927 | 0.7290 |
| | 8.090 | 5.265 | 0.6100 | 0.8157 | 1.0075 | 0.4844 | 0.6887 | 0.6278 |
| | 6.472 | 7.151 | 0.4206 | 2.5307 | 1.3195 | 0.6374 | 0.4732 | 0.7542 |
| | 6.472 | 7.151 | 0.6293 | 0.8449 | 0.9722 | 0.4501 | 0.7267 | 0.5681 |
| | 5.393 | 9.425 | 0.4321 | 2.7375 | 1.2675 | 0.6149 | 0.4479 | 0.7821 |
| | 5.393 | 9.425 | 0.6508 | 0.8748 | 0.9355 | 0.4103 | 0.7663 | 0.5048 |

## *Butterworth Filters*

Butterworth filters have a maximally flat amplitude response. That means all the derivatives of the amplitude with respect to frequency are zero at DC. The Butterworth response is a good compromise between attenuation characteristic and group delay. The characteristics of the other filter types described in this chapter will be compared with the Butterworth filter to highlight the advantages and disadvantages of each filter type.

For a Butterworth Lowpass filter of $n^{th}$ order, with a cut off frequency of $f_c$ and a source and load resistance of R, the filter component values are given by:

$$C_i = \frac{1}{\pi f_c R} Sin \frac{(2i-1)\pi}{2n} \qquad i=1,3,5.... \qquad \text{Eqn. 7.1}$$

$$L_i = \frac{R}{\pi f_c} Sin \frac{(2i-1)\pi}{2n} \qquad i=2,4,6.... \qquad \text{Eqn. 7.2}$$

The first component (i=1) is a shunt capacitor, the second (i=2) component is a series inductor etc. The normalised q values and coupling coefficients are related to the normalised lowpass impedances for a filter, using the following equations:

$$q_0 = Z_1 \qquad q_n = Z_n \qquad k_{ij} = \frac{1}{\sqrt{Z_i Z_j}} \qquad \text{Eqn. 7.3}$$

Where $Z_i$ is the normalised impedance as obtained from LC filter tables or from equations 7.1 and 7.2. Applying equation 7.3 to equations 7.1 and 7.2 gives:

$$q_0 = q_n = 2Sin \frac{(2-1)\pi}{2n} = 2Sin \frac{\pi}{2n} \qquad \text{Eqn. 7.4}$$

These equations will then allow the k and q values for IL = 0 and $q_0 = \infty$ as shown in table 7.1 to be calculated.

Figure 7.1 shows the resulting circuit for a 7th order Lowpass filter with a 500 MHz cut-off frequency. For the Butterworth filter, equations 7.1 and 7.2 are used to calculate the required component values in the schematic. For the other filters, the component values are calculated using a spreadsheet and the filter tables in Zverev.

Seventh order Butterworth Low Pass Filter
For the Butterworth filter, the component values are calculated using the following equations:

| | | |
|---|---|---|
| Fc=500 | Fc in MHz | pi=3.142 |
| R=50 | Terminating Impedance in ohm | |
| C1=1e6*Sin(pi/14)/(pi*Fc*R) | C1: 2.833 | C in pf |
| C3=1e6*Sin(5*pi/14)/(pi*Fc*R) | C3: 11.47 | |
| C5=1e6*Sin(9*pi/14)/(pi*Fc*R) | C5: 11.47 | |
| C7=1e6*Sin(13*pi/14)/(pi*Fc*R) | C7: 2.833 | |
| L2=1e3*R*Sin(3*pi/14)/(pi*Fc) | L2: 19.85 | L in nH |
| L4=1e3*R*Sin(7*pi/14)/(pi*Fc) | L4: 31.83 | |
| L6=1e3*R*Sin(11*pi/14)/(pi*Fc) | L6: 19.85 | |

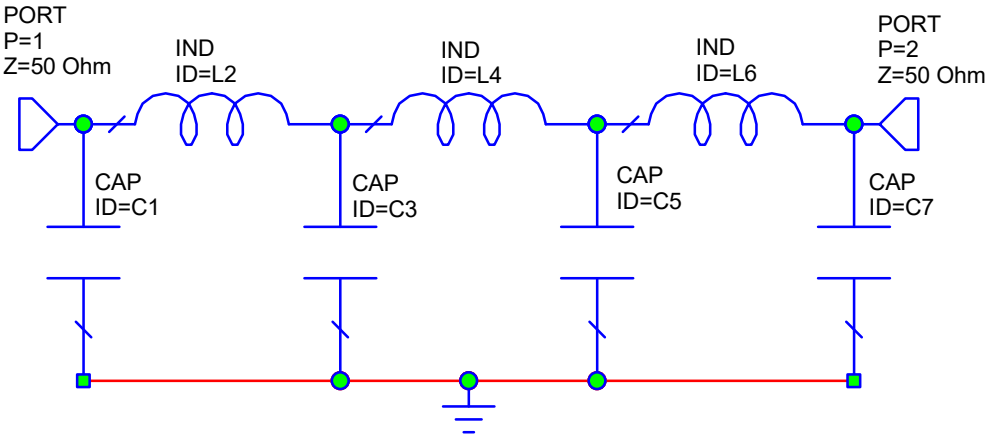



Figure 7.1. Butterworth Lowpass Filter.

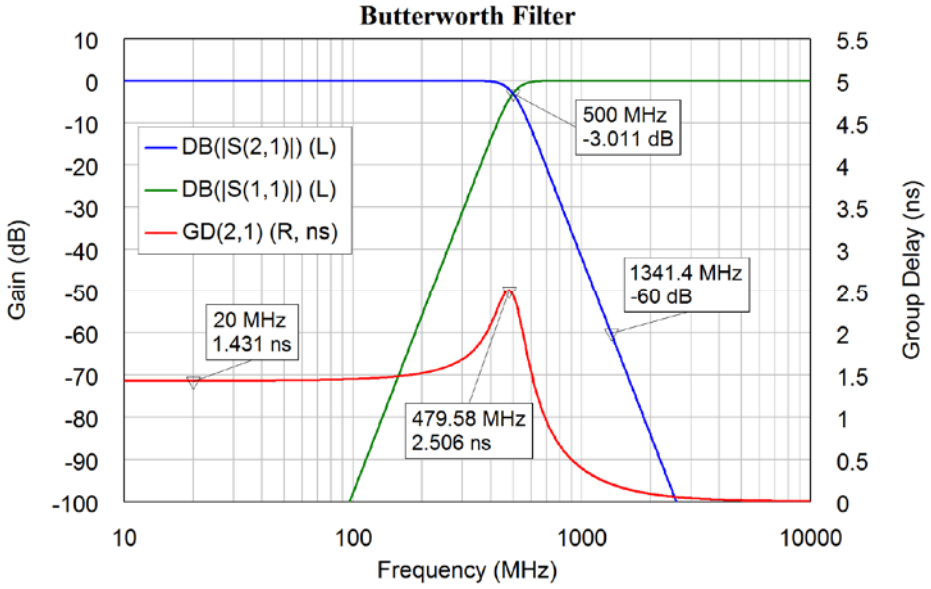



Figure 7.2. Butterworth Frequency Response.

The frequency response for the Butterworth filter is shown in figure 7.2. The group delay of Butterworth filters is reasonably flat but has a rise near the cut off frequency. The step response of these filters exhibits some ringing, which degrades its use for data communications.

## *Bessel Filters*

The bigger the difference between the group delay at low frequency and the maximum group delay, normally occurring near the filter cut-off frequency of the filter, the bigger the ringing and overshoot in the step response. The Bessel filter has a maximally flat group delay and does not have any ringing or overshoot in its step response. As a result, the Bessel filter type is very suitable for data communication systems. Simple equations like equations 7.1 and 7.2 do not exist for Bessel filters, so that normalised filter element values have to be obtained from filter tables. Many filter tables for Bessel filters are normalised for a group delay of one second, rather than a 3 dB cut-off frequency. The Bessel filter in figure 7.3 has a cut-off frequency of 500 MHz so that accurate comparisons between the filter types can be made.

The Bessel filter has a less sharp roll-off of the attenuation characteristic but a flatter group delay than the Butterworth filter, as can be seen by comparing figure 7.2 and 7.4. For the Butterworth filter, the 60 dB attenuation level occurs at 1.3 GHz while for the Bessel filter it occurs at 2.4 GHz.

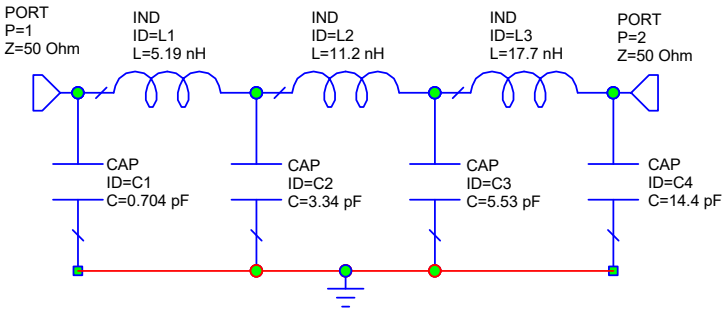



Figure 7.3. Bessel Lowpass Filter.

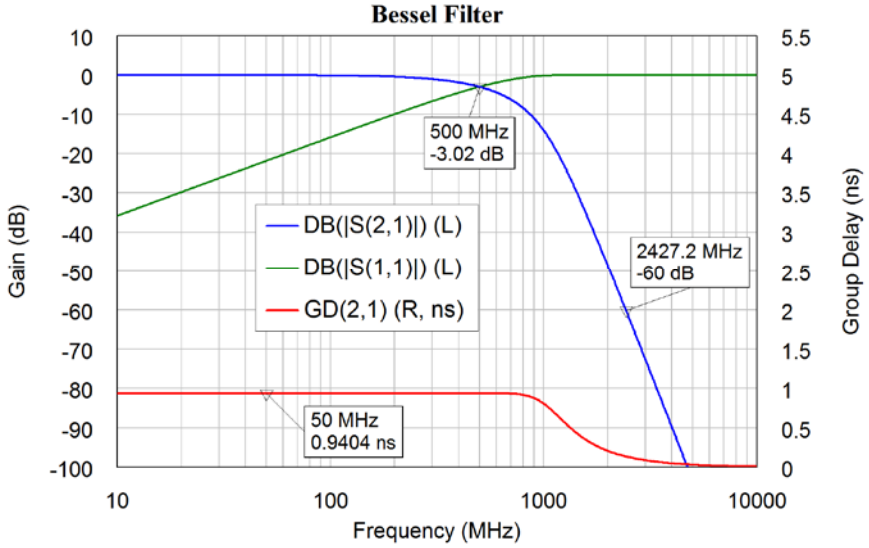



Figure 7.4. Bessel Lowpass Filter Frequency Response.

## Chebyshev Filters

The Chebyshev filter has ripples in the passband and the value of the ripples is a parameter that is selected as part of the filter design. The filter of figure 7.5 has a 0.1 dB passband ripple as shown on figure 7.6. The inductors and capacitors for the Chebyshev filter are larger than those used in Bessel or Butterworth filters. The Chebyshev filter has a very sharp attenuation response in the stop band, with a -60 dB attenuation at 967 MHz, compared with 1.3 GHz for the same attenuation for the Butterworth filter. Increasing the passband ripple will increase the passband attenuation. The group delay for the Chebyshev filter is larger than that of the Bessel and Butterworth filters. As a result, the Scale on figure 7.6 is different from figure 7.2 and 7.4.

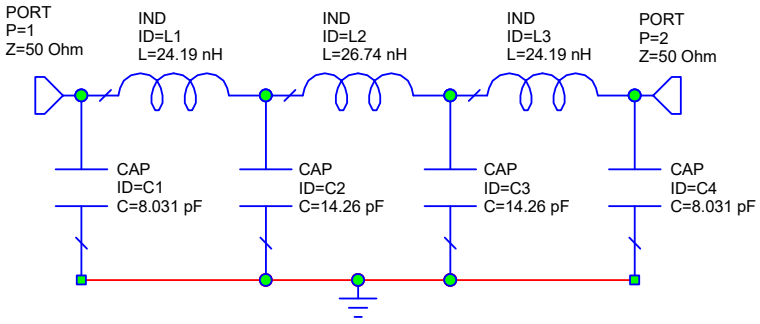



Figure 7.5. Chebyshev Lowpass Filter.

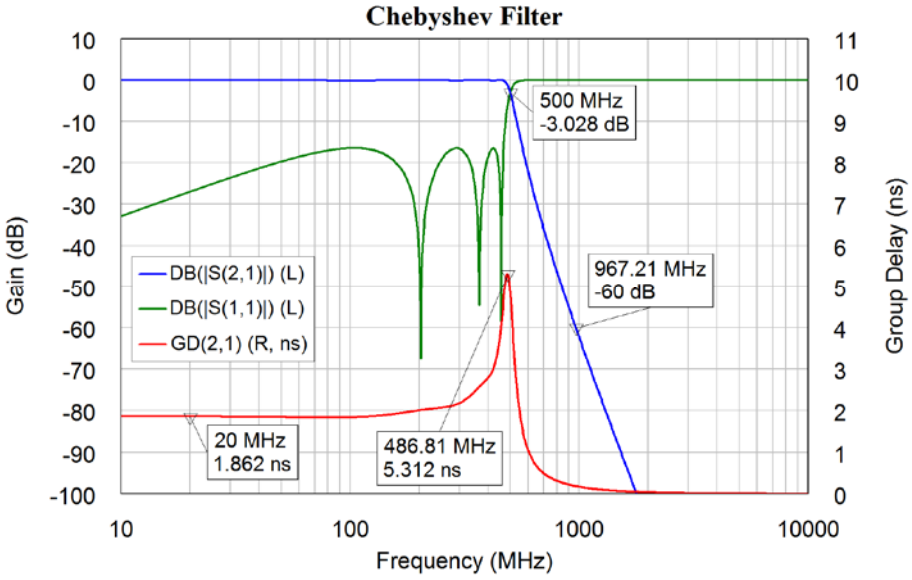



Figure 7.6. Chebyshev Lowpass Filter Frequency Response.

## Cauer-Chebyshev Filters

A Cauer-Chebyshev filter is a derivative of the Chebyshev filter and has capacitors in parallel with the inductors to cause zeros in the stopband as shown in figure 7.7. The zeros are placed, such that the minimum stopband attenuation values are the same as shown in figure 7.8. This gives an even higher stopband attenuation, with a 60 dB attenuation at 628 MHz compared with 1.3 GHz for the Butterworth filter. The Cauer-Chebyshev filter has an even bigger variation in the group delay than the Chebyshev filter and will thus have very poor transient response. The group delay of the Chebyshev and Cauer-

Chebyshev filters are poor and these filters should not be used for data communications or applications where the group delay is important.

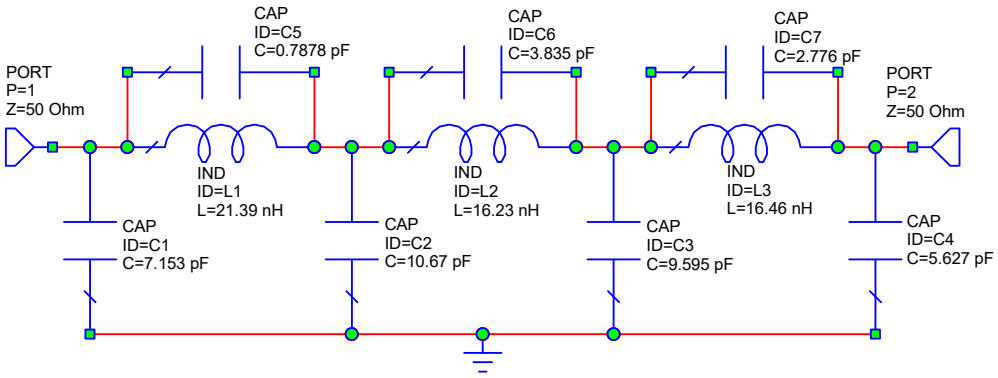



Figure 7.7. Cauer-Chebyshev Lowpass Filter.

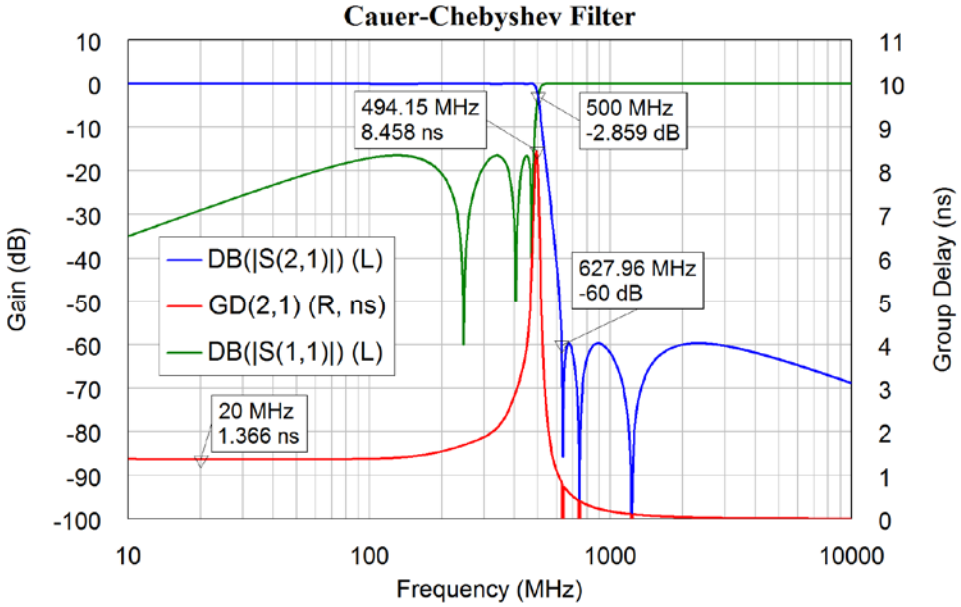



Figure 7.8. Cauer-Chebyshev Lowpass Filter Frequency Response.

Figure 7.9 shows the passband response of the four different filter types. The 0.1 dB passband ripple of the Cauer-Chebyshev and Chebyshev filters can clearly be seen. The Bessel filter has a significant attenuation for frequencies above 100 MHz.

Both the Chebyshev and Cauer-Chebyshev filters have poles on an ellipse and are elliptical filters. As a result, it is better not to specify a filter as an elliptic filter since it does not fully specify the filter type.

From filter tables, which include losses due to the finite Q values of the filter elements, it can be determined that for a given Q value for the components, the Chebyshev filter has a higher passband insertion loss than a Butterworth filter and a Bessel filter has a lower insertion loss than a Butterworth filter. The same applies for Bandpass filters, so that for the same unloaded Q of the resonators used in coupled resonator RF filters, the Bessel filter will have the lowest insertion loss and the Chebyshev filter will have the highest insertion loss.

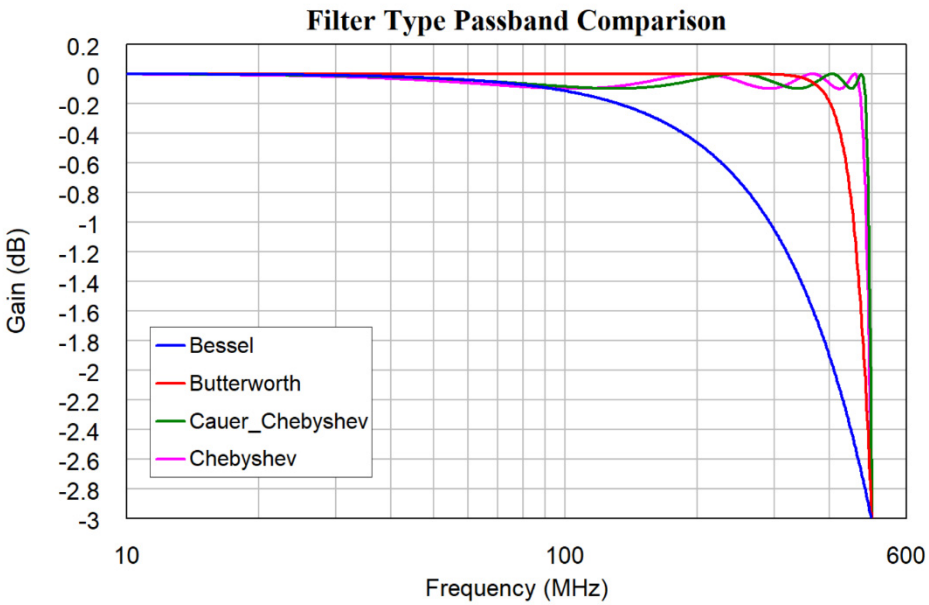



Figure 7.9. Passband Frequency Response of the filters of Figures 7.2, 7.4, 7.6 and 7.8.

The selection of the correct filter type is critical to ensure that the filter used satisfies both the transient response requirements and the passband insertion loss and stopband attenuation requirements for the filter. In digital communication applications, the Bit Error Rate (BER) after demodulating is the critical parameter. To reject signals in an adjacent channel intuition suggests the use of a Chebyshev filter. However, computer simulations carried out by the author [4] for a 3rd Generation Mobile Radio system, have shown that when there is a large unwanted signal in an adjacent channel, the lowest demodulated BER is obtained with a Bessel type filter response for the Channel filters.

## Reflectionless Filters

The filters shown above have a low return loss in the pass band, but attenuate the signal by reflecting the signal and having a high return loss in the stop band. The hybrids discussed in chapters 3 and 4 all require a resistive termination at all ports, to provide the required performance. In some applications, such as RF amplifiers, as discussed in chapters 8 and 9, the high return loss can lead to instability of amplifiers. It is possible to design filters to have a low return loss, so that the filter absorbs rather than reflects the signals to be filtered out. These filters are called reflectionless filters. Mini-Ccircuits [5] now make a range of reflectionless low pass and bandpass filters. Having the IF port of a mixer terminated in a reflectionless low pass filter, results in a much cleaner output spectrum as described in [6].

The diplexer shown in figure 2.9 and 2.13 is in fact a reflectionless filter for the combined port (port 1), having a very low reflection coefficient at all frequencies. When used as a high pass filter, the below cut-off frequency signals appear at port 2. When used as a low pass filter, the above cut-off frequency signals appear at port 3. Port 1 will thus have a low reflection coefficient, but ports 2 and 3 do not. The frequency dependent signal steering principle of the diplexer can be used to design a filter to have low reflections at both input and output terminals. Since the design principles are different from the reflectionless filter of [5-8] and figure 7.14, these filters are called “low reflection filters” here. A low reflection low pass filter must thus include two high pass filters, one to absorb all the unwanted signals at the input and another to absorb them at the output. Similarly,

a low reflection high pass filter must include two low pass filters and a low reflection bandpass filters must include two bandstop filters.

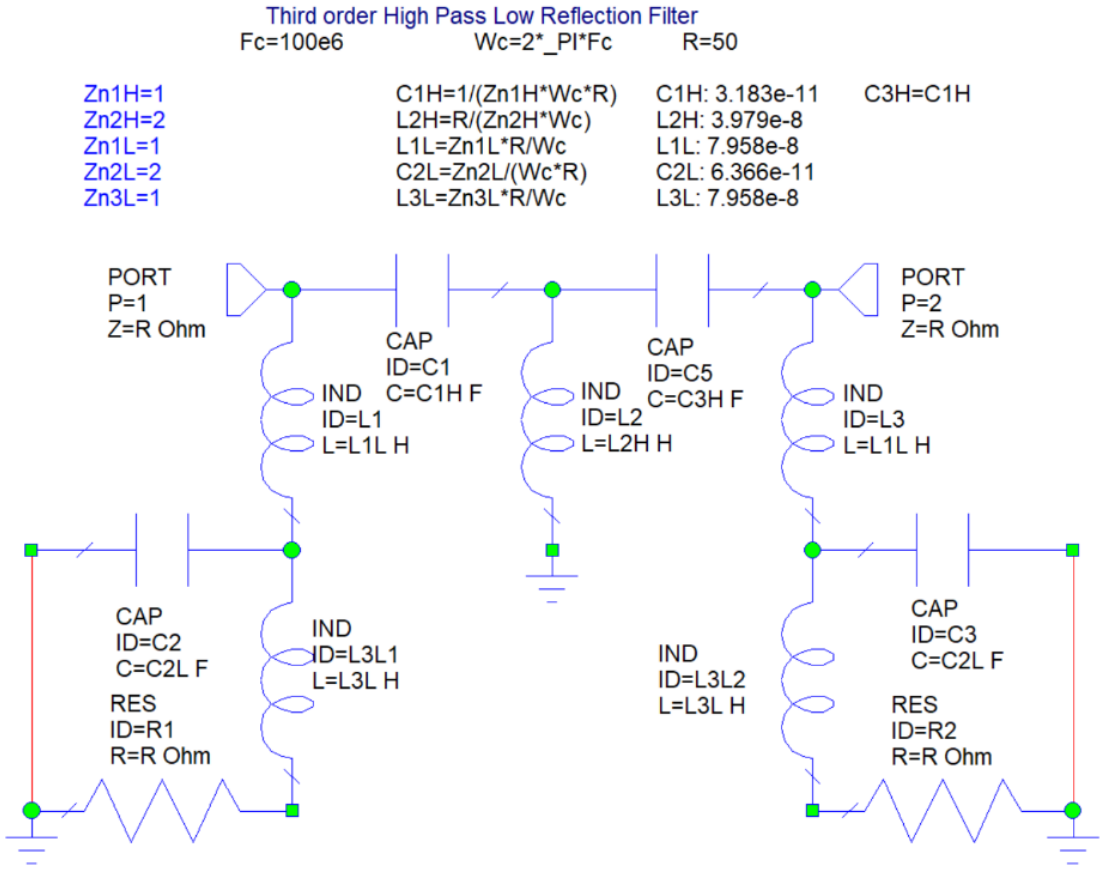



Figure 7.10. Low reflection 3rd order high pass filter, starting circuit.

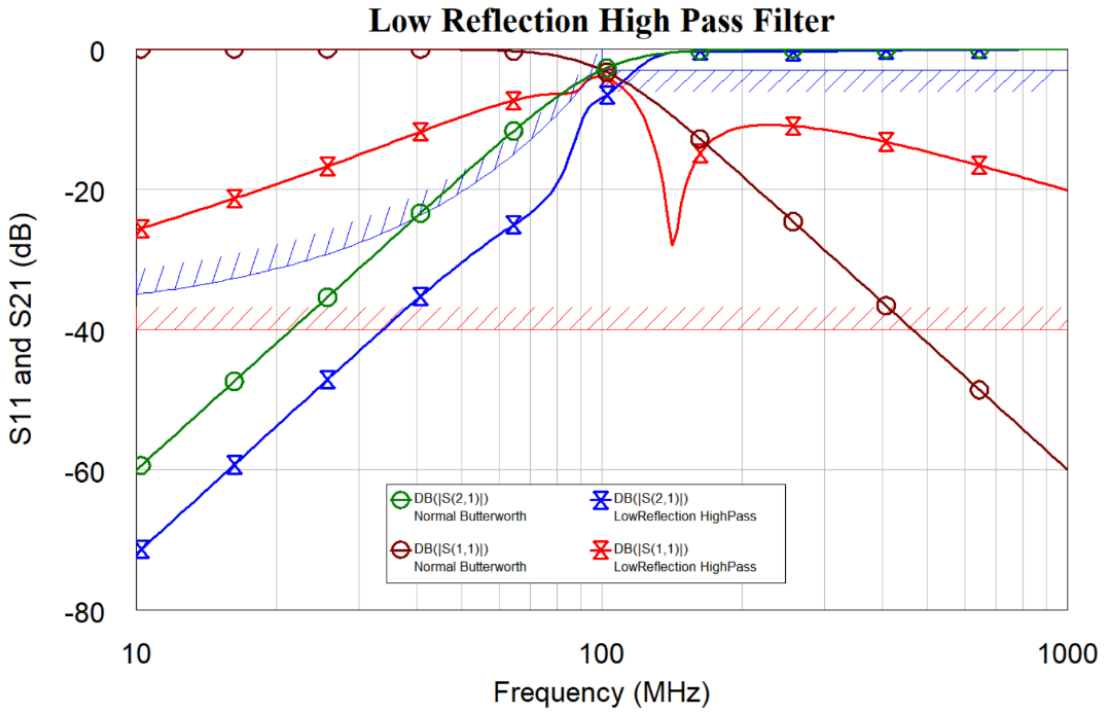



Figure 7.11. Low reflection 3rd order high pass filter, starting frequency response.

The design principles are outlined by designing a 3th order low reflection high pass filter with a cut-off frequency of 100 MHz and a 50 Ω impedance. Similar to figures 2.7 and 2.8, the input terminal of both the highpass and lowpass filters making up the low reflection filter must have a high impedance for the unwanted frequencies. Figure 7.10 shows the starting schematic. The *ZnXX* values are optimised, with the starting values being the normalised Butterworth filter impedance values obtained from equations 7.1 and 7.2 with $R = 1$ and $\omega_c = 1$. As a result, the highpass filter is symmetrical, with *C3H = C1H*. To obtain the best return loss, the symmetry restriction on the lowpass filters is removed, to allow *L1L* and *L3L* to become different during the optimisation.

Third order High Pass Low Reflection Filter
Fc=100e6 Wc=2*_PI*Fc R=50

| | | | |
|---|---|---|---|
| Zn1H=1.44040790172559 | C1H=1/(Zn1H*Wc*R) | C1H: 2.21e-11 | C3H=C1H |
| Zn2H=1.7393807396616 | L2H=R/(Zn2H*Wc) | L2H: 4.575e-8 | |
| Zn1L=1.6400227606175 | L1L=Zn1L*R/Wc | L1L: 1.305e-7 | |
| Zn2L=1.66758429969081 | C2L=Zn2L/(Wc*R) | C2L: 5.308e-11 | |
| Zn3L=0.818190540664024 | L3L=Zn3L*R/Wc | L3L: 6.511e-8 | |

Figure 7.12. Low reflection 3rd order high pass filter, optimised values.

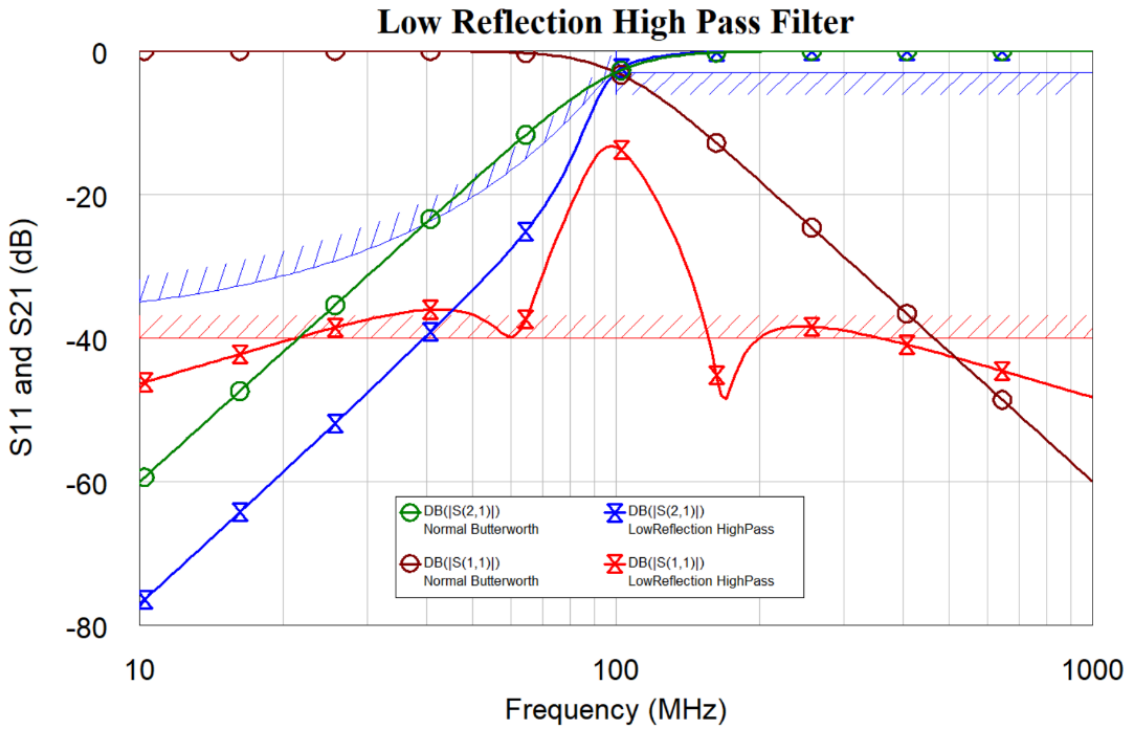



Figure 7.13. Optimised low reflection 3rd order high pass filter, frequency response.

The optimisation constraints are the passband and stopband attenuation, specified so that the corner frequency does not change during the optimisation, and the return loss. Figure 7.12, shows the component values after optimisation and figure 7.13 shows the resulting transfer function and return loss. The blue curve in figure 7.13 shows that this circuit has more attenuation in the stop band than the basic 3rd order Butterworth filter, corresponding to the green curve. At the cut off frequency, the red curve shows it has 10 dB more return loss than the return loss of the 3rd order Butterworth filter shown as the brown curve. Below 70 MHz, the low reflection filter has a return loss more than 30 dB, compared to close to 0 dB, for the conventional filter. That is thus a big improvement, but the low reflection filter requires 3 times the reactive components of a conventional low pass filter in addition to the two resistors to absorb the unwanted signals.

The design of the low reflection filter above has been based on a diplexer design. Microwaves101 [8] and Mini-Circuits [5] use a reflectionless filter design technique based on even and odd mode impedances [7]. This includes some cross-coupling between the output and the input. Figure 7.14 shows the circuit diagram similar to that used by [5] and figure 7.15 shows the frequency response and return loss after optimisation. The return loss of figure 7.15 is much better that that shown in [8] and shows the advantages of being able to optimise circuits using Cadence AWRDE. Figure 7.15 shows that the return loss is ideal (<-300 dB), but the stopband attenuation is poorer than that of figure 7.13.

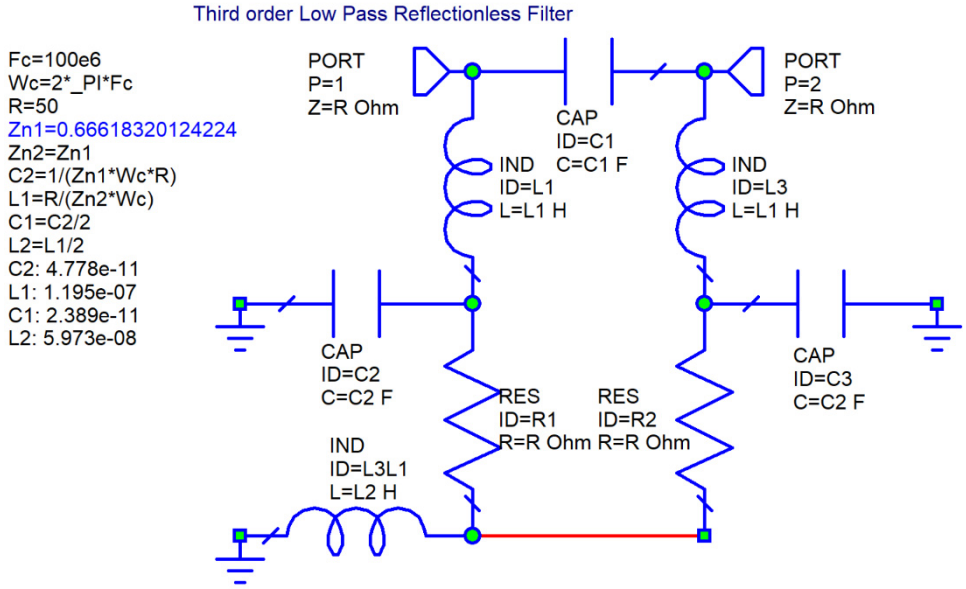



Figure 7.14. Even & Odd mode, impedance reflectionless filter circuit.

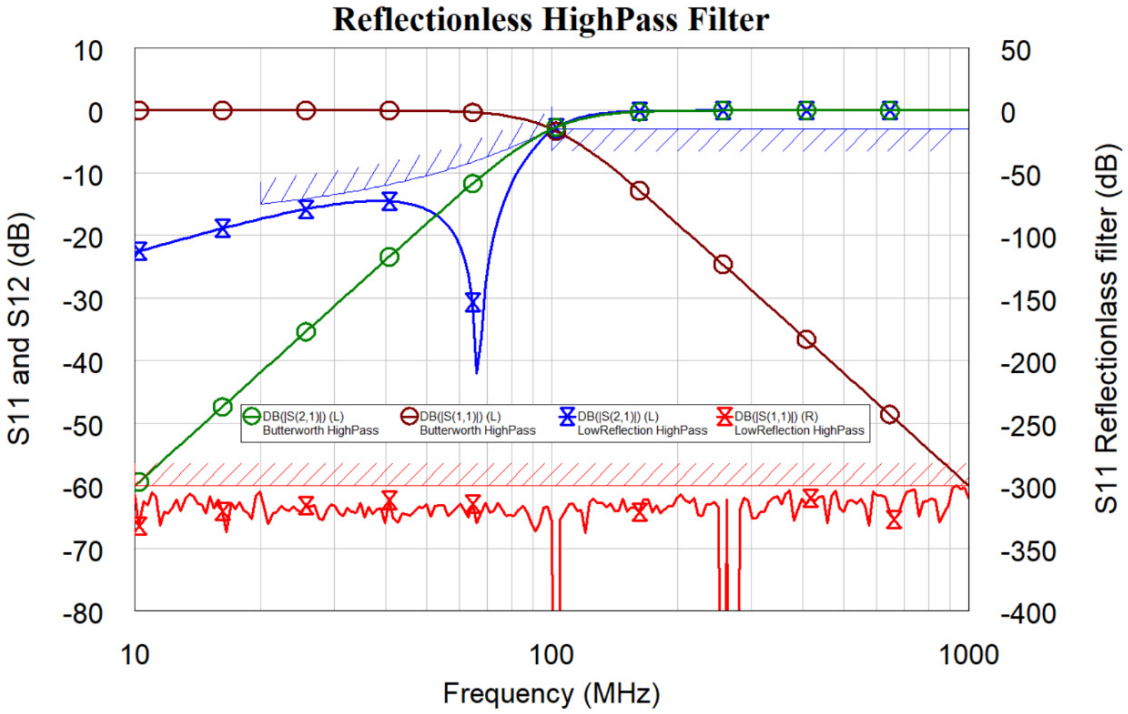



Figure 7.15. Even & Odd mode, impedance reflectionless filter frequency response.

Cascading these filters preserves the low return loss and increases the stopband attenuation. However, including a conventional high pass filter as part of such a cascaded filter, results in a passband return loss similar to that of the conventional high pass filter.

Low reflection and reflectionless lowpass, bandpass and bandstop filters can be made by using the relevant low-pass to highpass, low-pass to band-pass, low-pass to band-stop transformations described later in this chapter. These filters require close to twice the number of reactive components, compared to conventional filters.

Reflectionless filters are also very useful for ensuring stability of amplifiers described in chapter 8, by reducing the gain to signals outside the required bandwidth, whilst maintaining near ideal termination for the amplifier.

Higher order low reflection and reflectionless filters can be designed using the principles outlined in [7] for reflectionless filters and using the optimisation outlined in figures 7.10 to 7.14 for low reflection filters. In practice, both designs techniques will result in reflections less than -20 dB.

## RF Lowpass Filter design

Lowpass filters at RF and microwave frequencies, can be designed and constructed using conventional LC filter design principles. However, care should be taken to ensure that:

1 The impedance of the leads is kept as small as possible. In particular, the impedance of the leads on capacitors connecting the capacitors to ground, or the length of any PCB layout track connecting the components to the ground-plane must be kept as small as possible, since its inductance will affect the frequency response of the filter.

2 Components must be used that have self-resonant frequencies well above the cut off frequency of the filter if a lowpass filter is used and well above any useable frequency if a high pass filter is used. Most commonly used capacitors have self-resonant frequencies well below 1 GHz.

It is feasible to design conventional LC lowpass filters with cut off frequencies in excess of 1 GHz. Surface-mount components generally have a higher cut-off frequency than leaded components. When the frequency becomes too high for either of them to be used, inductors can be replaced with thin transmission lines of the length required to give the desired inductance and capacitors can be replaced by wide transmission lines.

As an example, consider the design of a $7^{th}$ order Butterworth lowpass filter with a cut off frequency of 2 GHz. From the equations 7.1 and 7.2 for Butterworth filters or from tables, by de-normalising and using a cut off of 2 GHz and input impedance of 50 Ω, the component values shown in table 7.2 are obtained for the filter.

Table 7.2. LC filter values and corresponding Microstrip line size.

| L C | Value Required | Line Length | Line Width |
|---|---|---|---|
| L1 | 1.771 nH | 3.54 mm | 0.5 mm |
| C2 | 1.985 pF | 4.2 mm | 10 mm |
| L3 | 7.170 nH | 13.5 mm | 0.5 mm |
| C4 | 3.183 pF | 6.6 mm | 10 mm |
| L5 | 7.170 nH | 13.5 mm | 0.5 mm |
| C6 | 1.985 pF | 4.2 mm | 10 mm |
| L7 | 1.771 nH | 3.54 mm | 0.5 mm |

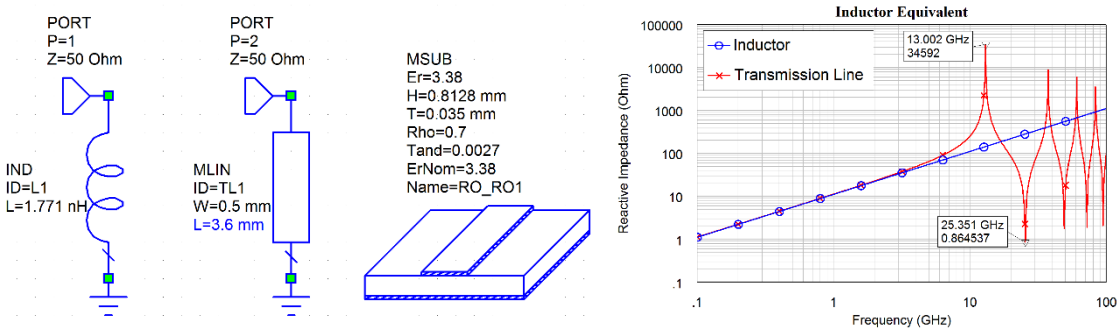



Figure 7.16. Replacement of inductors using Microstrip transmission lines

For Rogers RO4003 substrate with $H$ = 0.83 mm and $T$ = 35 µm, the width for a 50 Ω transmission line is 1.843 mm. the thinnest line that is desirable is 0.5 mm and the thickest is 10 mm. That corresponds to impedances of 96.5 Ω and 14.3 Ω respectively. One needs to find out what length of transmission lines corresponds to the inductance required for the filter. In Cadence AWR DE it is easy to compare the impedance of an inductor with one of a transmission line, as shown in figure 7.16. The circuit of figure 7.16, together with the line width restrictions results in the line widths and line lengths shown in table 7.2. The length of the transmission line is tuned to ensure that at low frequency both have the same impedance. It can be seen that the short section of transmission line accurately represents the inductor for frequencies up to 10 GHz. This process is repeated for all the inductances. Note for larger inductances, at higher frequencies the transmission line will be a quarter wavelength resulting in an infinite impedance or half a wavelength, resulting in a very small impedance. For lowpass filters, the length of the transmission line should be less than one-quarter wavelength for all frequencies or interest.

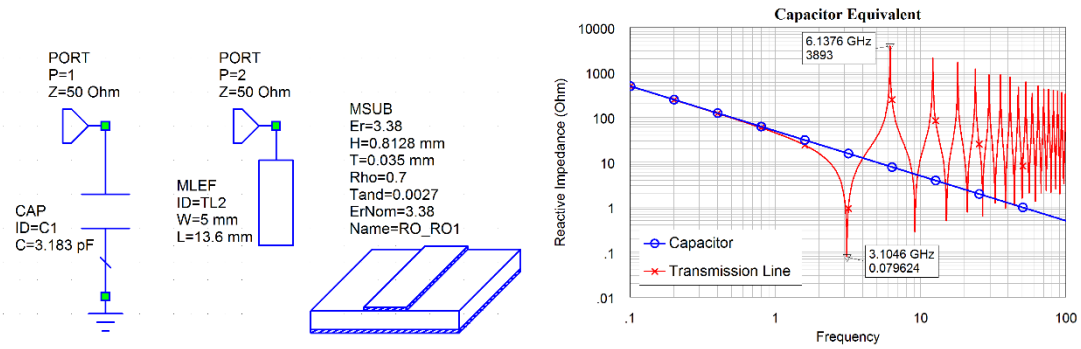



Figure 7.17. Replacement of capacitors using series Microstrip transmission lines.

The Capacitors can be replaced with open circuited transmission lines as shown in figure 7.17. The resulting line sections have been placed in table 7.2 and it can be seen that some line sections are wider than they are long, which will cause some errors in the simulation as the actual fields will be different from what is assumed in the simulation of the transmission lines.

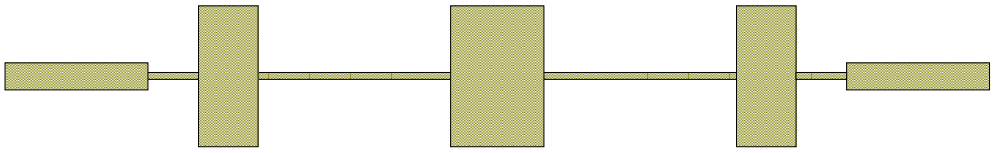


Figure 7.18. PCB Layout of the 2 GHz Lowpass filter.

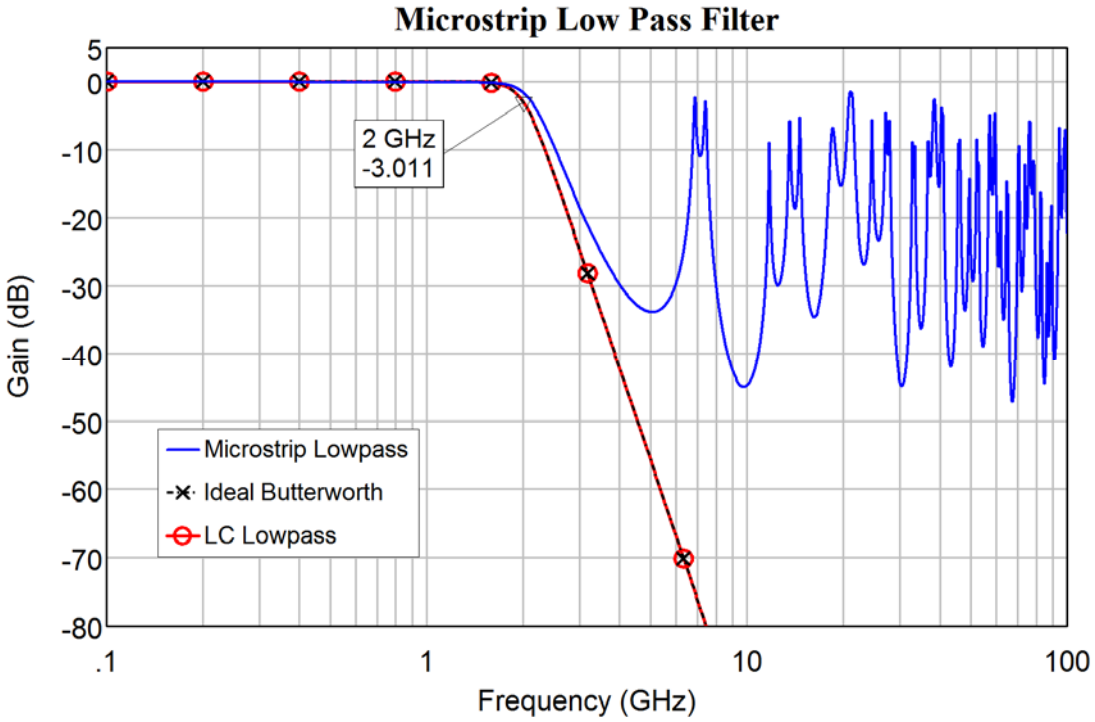



Figure 7.19. Frequency response of the LC filter and the corresponding Microstrip design.

Figure 7.19 compares the frequency response of the ideal LC filter (red) with the PCB filter of figure 7.19 (blue) and it shows that the PCB filter behaves well in the passband, but that the stopband performance is not very good. That is due to the elements becoming comparable to a quarter or half wavelength long at certain frequencies.

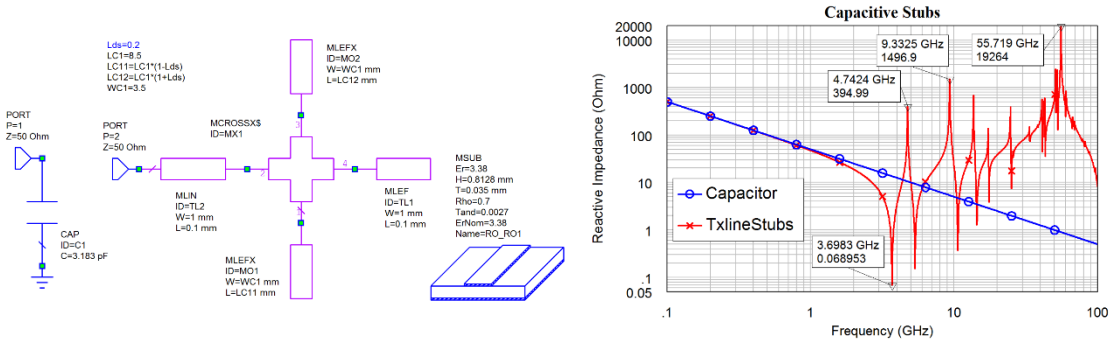



Figure 7.20. Replacement of capacitors using shunt Microstrip transmission lines.

By replacing the capacitors with open circuited shunt transmission lines as shown in figure 7.20, it is possible to obtain a better stopband performance. By making the lengths of the stubs connected at each cross-point slightly different, the effect of the transmission lines being one quarter or one-half wavelength is minimised. In figure 7.20, the transmission line has a high impedance of 2.48 kΩ at 2.48 GHz. For figure 7.20, by using stubs, the impedance is 1.82 kΩ at 9.2 GHz. By using radial stubs as shown in figure 7.21, the resonance can be extended even further to give a peak impedance of 1.59 kΩ at a frequency of 12.5 GHz. The shape of the radial stub is shown in figure 7.21. The angle for that stub is set to 60 degrees. A wider-angle stub will push the high impedance frequency even further. It is possible in a filter to vary the radii and angles to ensure that the resonances do not coincide.

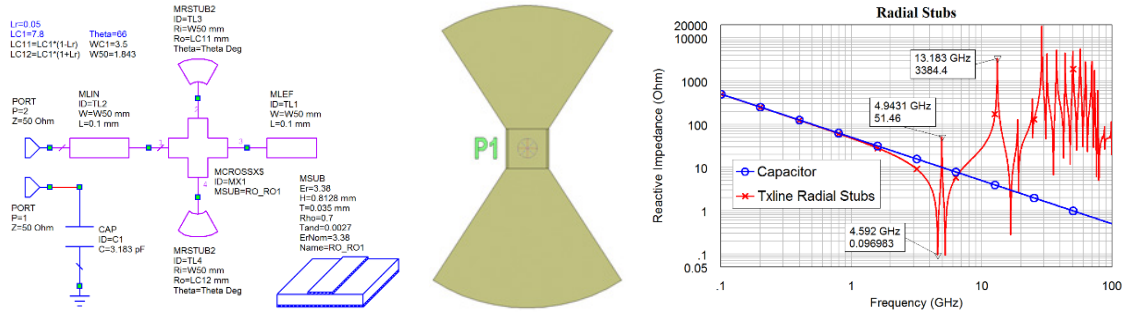



Figure 7.21. Replacement of capacitors using shunt radial stub Microstrip transmission lines.

Once the circuit schematic for the whole filter is complete, the lengths and width of the stubs and the lengths of the inductive sections are optimised, to ensure the filter meets the passband and the stopband specifications. As part of this, the width to length ratio of the stubs can be changed, to increase the attenuation at particular frequencies in the stopband. Starting with the line elements shown in table 7.1, the resulting circuit diagram of the filter, obtained after this optimisation, is shown in figure 7.22.

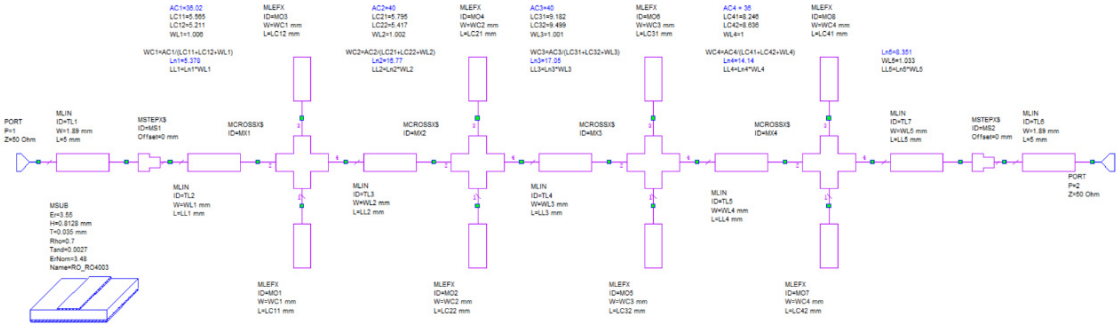


Figure 7.22. Circuit schematic for the 2 GHz lowpass filter.

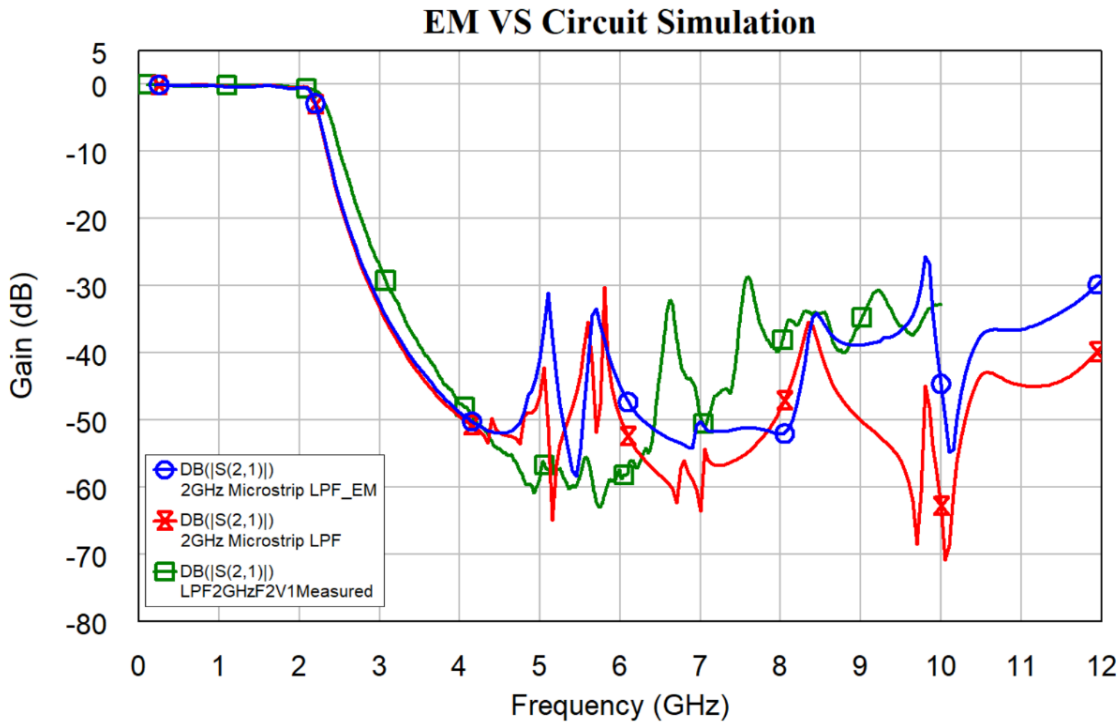



Figure 7.23. Frequency response of the 2 GHz lowpass filter.

The behaviour of the resulting filter is also calculated using a full electromagnetic (EM) simulation of the capacitive stub lines. The process of EM simulation using AXIEM is described in the section *EM simulation* in this chapter. The frequency response obtained from the circuit simulation, the EM simulation and the measured performance is shown in figure 7.23. It can be seen that there is a good agreement for frequencies below 4 GHz but that the stopband behaviour is still not adequate. The filter hardware realisation is shown in figure 7.24.

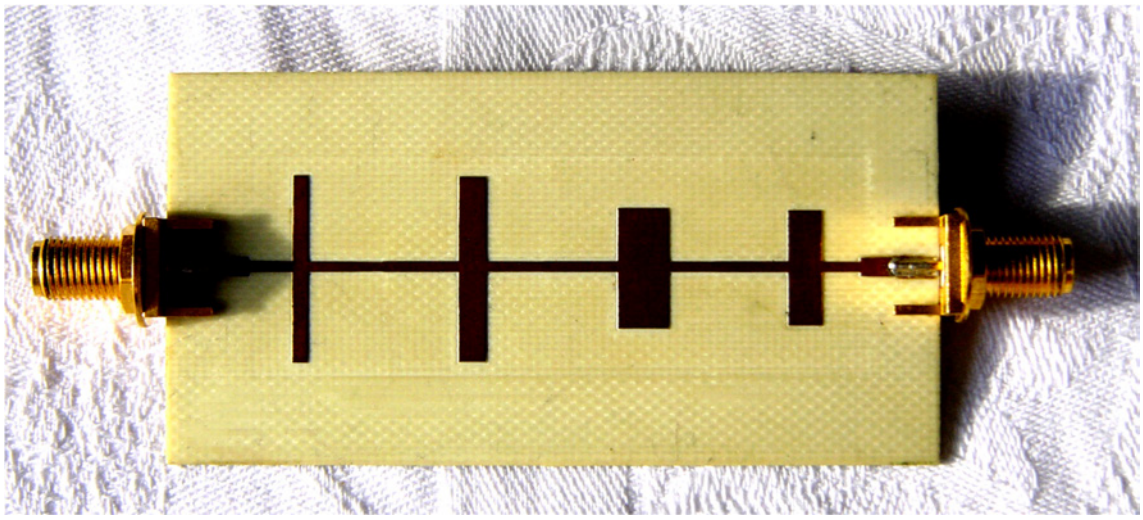


Figure 7.24. 2 GHz Lowpass filter hardware.

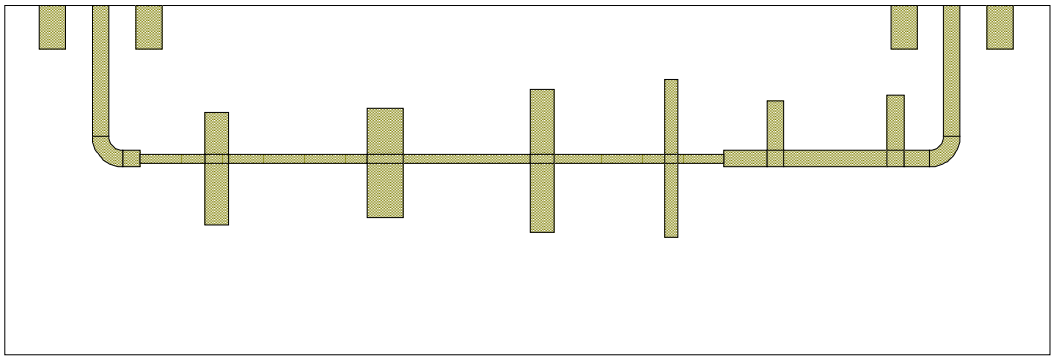


Figure 7.25. 2 GHz lowpass filter with stubs added.

The attenuation in the stopband can be improved by adding open circuited stubs, which create a transmission zero in the stopband at the frequencies where the filter without the stubs has an inadequate attenuation. In this application, a good stopband performance to up to 6 GHz was required. The stubs will affect the passband performance and the circuit elements need to be re-tuned and optimised to restore the passband performance to match that of figure 7.23. The resulting PCB layout is shown in figure 7.25. The end of each stub should be a minimum of 3 substrate thicknesses and preferably 5 substrate thicknesses (4 mm) away from the nearest metal structure to minimise coupling. This design satisfies that requirement. If needed the right most stub can be placed on the other side of the transmission line to reduce the distances to other structures.

This filter was constructed and figure 7.26 shows the simulated and measured performance. The simulated performance has a very good stopband performance. The

measured performance has a significant amount of coupling between the input and output, which is due to electromagnetic coupling between the input and output tracks and leads connecting the filter. The stopband performance was improved by enclosing the filter and placing microwave absorber on the ground-plane on the back of the filter and on the inside lid of the enclosure. The EM simulation in the stopband is sensitive to cell size. Figure 7.26 uses a cell size of 0.1 mm, using a cell size of 0.25 mm does not show a peak of -44 dB at 5.5 GHz and shows a larger peak at 6.5 GHz.

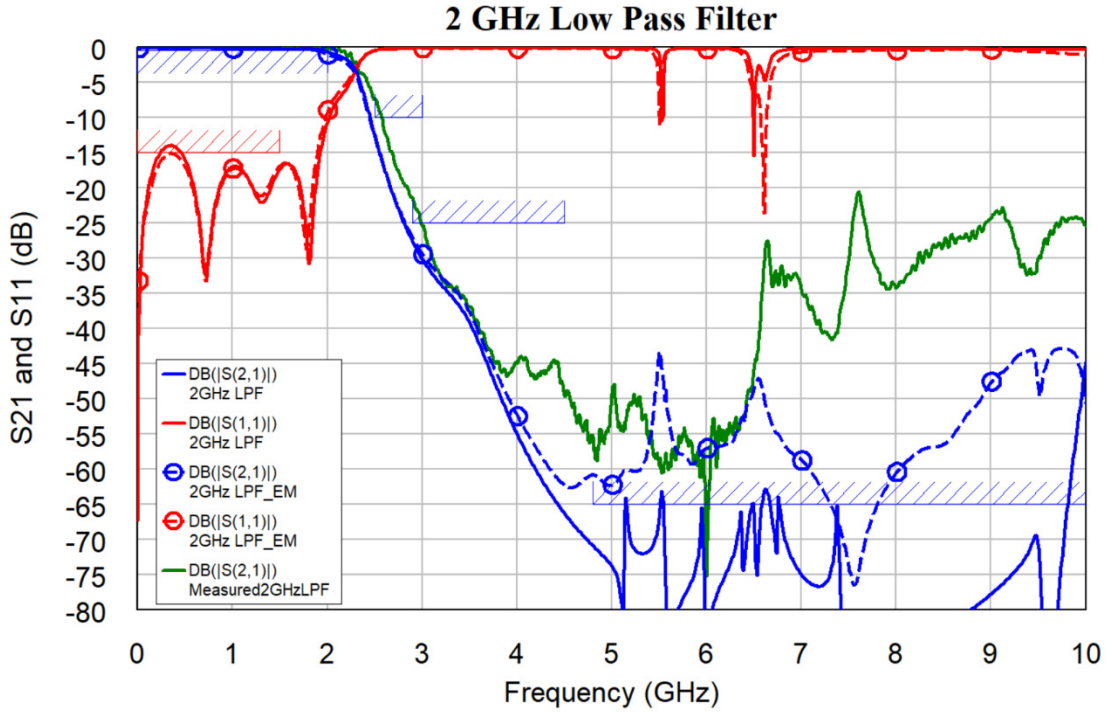



Figure 7.26. Simulated and measured performance of 2 GHz lowpass filter with stubs.

# Bandpass Filter Design

## *LC Bandpass Filters*

To illustrate the design principles, a filter with a centre frequency of 18.48 MHz and a bandwidth of 2 MHz is designed, using different techniques. This particular filter was required for a weather satellite data receiver, designed at JCU, to filter the IF data signal prior to demodulation. Since the transmitted signal is a Binary Phase Shift Keyed (BPSK) modulated RF signal containing digital data, a Bessel filter results in the lowest BER after demodulation.

## *Low-Pass to Band-Pass Transformation*

A simple way of designing bandpass LC filters is to use the low-pass to band-pass transformation, described in most filter books. The low-pass to band-pass transformation will often give impractical component values for the bandwidths required for most RF filters. As a result, the low-pass to band-pass transformation is not suitable for most bandpass filter designs.

More practical component values are obtained using coupled resonator designs. The filter resulting from the low-pass to band-pass transformation is shown in figure 7.27. A

2.0 mH and a 4.4 mH inductor is required. These are very large inductors and will be difficult to make with acceptable Q values. Figure 7.28 shows the frequency response of this filter. The low-pass to band-pass transformation has transformed the amplitude response correctly, but the group delay is no longer flat.

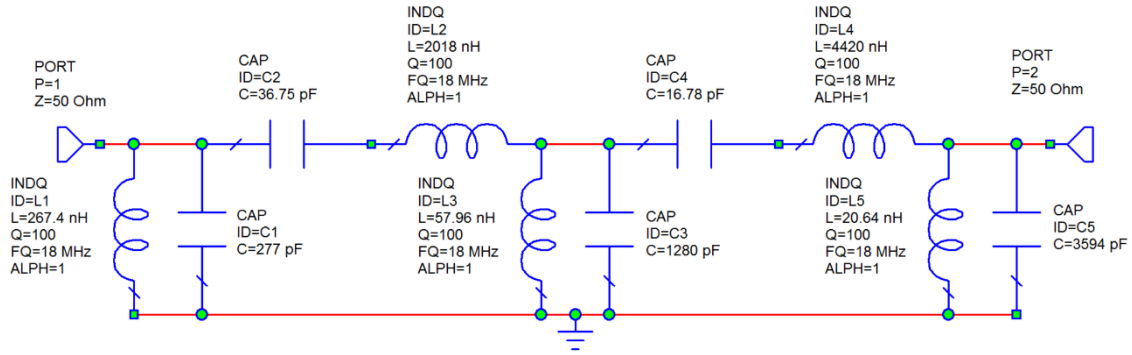



Figure 7.27. Filter from lowpass to bandpass transformation.

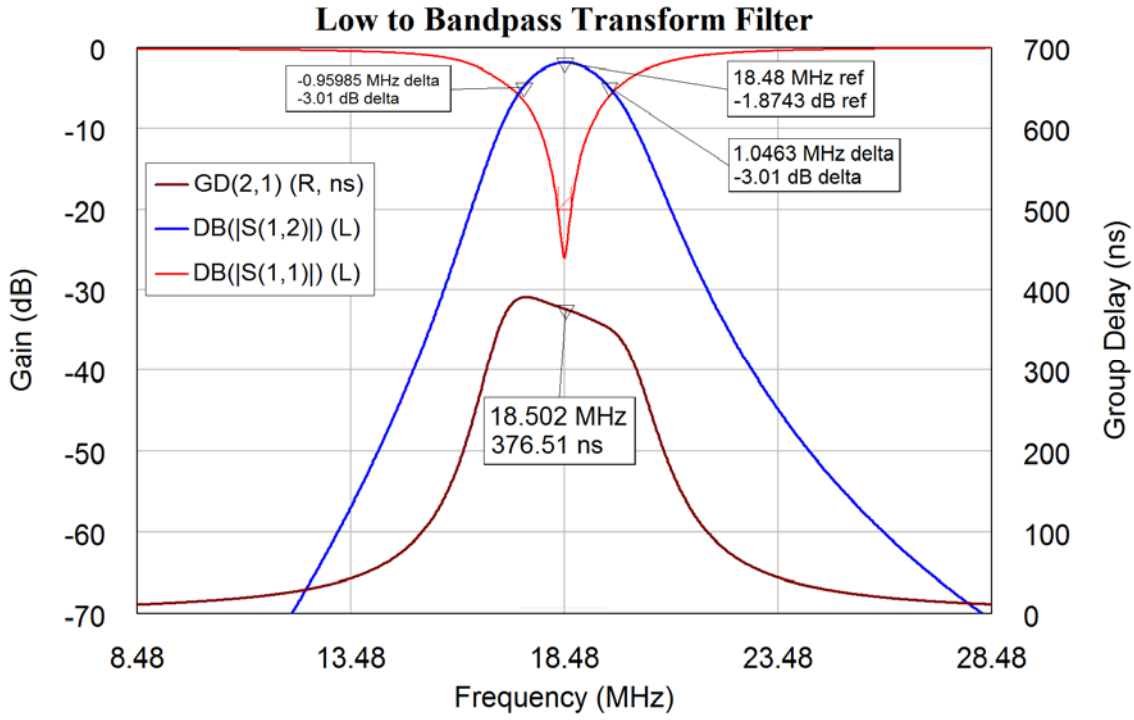



Figure 7.28. Frequency response of filter of figure 7.25.

## *LC Coupled Resonator Filter*

In coupled resonator filters, the filter consists of a series of resonators, which are coupled using capacitive or inductive impedances, coupling loops, as shown connected to the BNC connectors in figure 7.58, or coupling apertures, as shown by the gap between the resonators in figures 7.57 and the slots cut between the resonators in figure 7.101. For many Microstrip filters like the one shown in example 7.1, the coupling between the resonators are achieved by varying the spacing between the MCFIL lines making up the filter. Example 7.3 shows how the correct coupling between resonators can be determined.

The centre frequency of the filter is determined by the frequency of the resonator and the bandwidth of the filter is determined by the coupling between the resonators. The input impedance of the filter is determined by the coupling into the first resonator and

conversely the output impedance is determined by the coupling out of the last resonator. For LC coupled resonator filters, the resonators consist of parallel LC circuits. The coupling between LC resonators can be done by connecting capacitors between the resonators, this is called capacitive coupling. The coupling can also be done by connecting inductors between the resonators, this is called inductive coupling. Capacitive coupling is the cheapest as standard capacitors can be used, while the inductors often need to be wound individually. Equation 7.3 together with normalised impedance values from Filter tables, or equations 7.5 for Butterworth filters, give the required coupling factors (K) for the desired filter.

The loading required to achieve the desired first and last resonator Q values, can be obtained from the Q values of the filter tables, from equation 7.3 or for Butterworth filters, equation 7.4. In many cases, filters with 50 Ω input and output impedances are required, while the desired loaded Q values of the resonators require very different impedances. A capacitive impedance transformer can be used to obtain the required impedance transformations.

Equations 7.3 and 7.4 only apply for lossless resonators. The K and Q filter tables in Zverev allow the filter to be designed to accommodate the finite Q values of the LC resonators, which result in the filter having an insertion loss. Table 1 shows the K and Q value table from Zverev for Butterworth filters. De-normalising the filter coefficients:

$$K_{ij} = k_{ij}\frac{BW}{F_c} \qquad Q_n = q_n\frac{F_c}{BW} \qquad \text{Eqn. 7.6}$$

Zverev shows that the coupling capacitor is given by:

$$C_{ij} = K_{ij}\sqrt{C_i C_j} = k_{ij}\frac{BW}{F_c}\sqrt{C_i C_j} \qquad \text{Eqn. 7.7}$$

where $C_i$ and $C_j$ are the resonator capacitors for the i$^{th}$ and j$^{th}$ resonator and $K_{ij}$ is the de-normalised coupling coefficient, $k_{ij}$ is the normalised coupling coefficient from the tables, $F_c$ is the centre frequency and BW is the filter bandwidth. Note the coupling capacitors are to be included in the total capacitance of the resonator so that for the resonator $j$ the resonating capacitance is given by:

$$C_j = C_{res} - C_{ij} - C_{jk} \qquad \text{Eqn. 7.8}$$

where $C_{res}$ is the total resonating capacitance as determined from the resonant frequency and inductance for the resonator. Using coupling inductors results in:

$$L_{ij} = \frac{\sqrt{L_i L_j}}{K_{ij}} = \frac{F_c}{k_{ij}\times BW}\sqrt{L_i L_j} \qquad \text{Eqn. 7.9}$$

Where $L_i$ and $L_j$ are the resonator inductors. In a similar manner, the coupling inductors must be considered part of the inductance of the resonator, so that the total resonator inductance is made up the inductance of the resonator in parallel with the coupling inductors on either side.

$$\frac{1}{L_j} = \frac{1}{L_{res}} - \frac{1}{L_{ij}} - \frac{1}{L_{jk}} \qquad \text{Eqn. 7.10}$$

where $L_{res}$ is the total resonating inductance as determined from the resonant frequency and capacitance for the resonator. To facilitate the design of these filters, Figure 7.29 shows the equations, which can be incorporated into a Cadence AWR DE project, to allow the component values for the filter shown in figure 7.30 to be calculated.

The design process is illustrated using the Bessel filter with an 18.48 MHz centre frequency and 2 MHz bandwidth filter, in the previous design. The filter design requires 4 resonators. Inductors with an inductance of 200 nH and an unloaded $Q_0$ of 100 are available. In LC resonators, the Q of the capacitors used is generally much higher than the Q of the inductors, so that by using equation 7.6, the resonator has a normalised q of: $q_0 = \frac{BW}{F_c} Q_0 = \frac{2}{18.48} 100 = 10.8$. From the Bessel filter tables in Zverev, the nearest value corresponds to a $q_0$ of 10.048 and results in an insertion loss of 1.85 dB. Since the actual Q is slightly higher, one should obtain an actual insertion loss that is slightly less as is evident from figures 31, 32 and 35. The corresponding K and Q values from this filter table for this value of $q_0$ are: $q_1$ = 0.3891, $q_4$ = 0.5098, $k_{12}$ = 1.7120, $k_{23}$ = 0.6794 and $k_{34}$ = 0.8512. Entering those values in the LC Bandpass Filter design equations on the global definitions page of the accompanying Cadence AWR DE project file for figures 7.29 - 7.31 program gives the filter values as shown in figure 7.29.

AWRDE Global Definition folder. Design equations for any 4th order bandpass filter using LC components and capacitive coupling
Author C. J. Kikkert, James Cook University, 2015

| | | | |
|---|---|---|---|
| pi=2*acos(0) | pi: 3.142 | | |
| Fc=18.48 | Centre Frequency in MHz | Wc=2*pi*Fc | |
| BW=2 | Bandwidth in MHz | | |
| n=4 | n - number of resonators | twon=2*n | twon: 8 |
| Zin=50 | Zout=50 | | |
| q1=2*sin(pi/twon) | | q1: 0.7654 | Equations for Q and K for Butterworth filters with no loss |
| qn=q1 | | qn: 0.7654 | Included here for ease of use when desinging Butterworth filters. |
| k12=1/(2*sqrt(sin(pi/twon)*sin(3*pi/twon))) | | k12: 0.8409 | |
| k23=1/(2*sqrt(sin(3*pi/twon)*sin(5*pi/twon))) | | k23: 0.5412 | |
| k34=1/(2*sqrt(sin(5*pi/twon)*sin(7*pi/twon))) | | k34: 0.8409 | |
| NBW=BW/Fc | | NBW: 0.1082 | |
| Lr=200 | Lr -Resonator Inductnace in nH | Lra=Lr/1e9 | Lra: 2e-7 |
| Qcoil=100 | Qcoil - Q value of Lr | | |
| Cr=1e9/(Wc*Wc*Lr) | Cr -Resonator Capacitance in pF | Cr: 370.9 | |

In this example values from tables (Zverev) for inductor Q value of 100 are used.

| | |
|---|---|
| q1a=0.3891 | q1a - actual q1, from tables if allow for losses or from eqnations if ideal |
| qna=0.5098 | qna - actual qn, from tables if allow for losses or from eqnations if ideal |
| k12a=1.7120 | k12a - actual k12, from tables if allow for losses or from eqnations if ideal |
| k23a=0.6794 | k23a - actual k23, from tables if allow for losses or from eqnations if ideal |
| k34a=0.8512 | k34a - actual k34, from tables if allow for losses or from eqnations if ideal |

Now calculate the component values

| | | |
|---|---|---|
| C12=k12a*NBW*Cr | C12: 68.71 | Coupling Capacitances |
| C23=k23a*NBW*Cr | C23: 27.27 | |
| C34=k34a*NBW*Cr | C34: 34.16 | |
| Cr1=Cr-C12 | Cr1: 302.1 | Resonator Capacitances |
| Cr2=Cr-C12-C23 | Cr2: 274.9 | |
| Cr3=Cr-C23-C34 | Cr3: 309.4 | |
| Cr4=Cr-C34 | Cr4: 336.7 | |
| Rt1=1e6*Wc*Lra*q1a/NBW | Rt1: 83.49 | Input total resistance, Load and Coil |
| Rtn=1e6*Wc*Lra*qna/NBW | Rtn: 109.4 | Output total resistance, Load and Coil |
| Rcoil=1e6*Wc*Lra*Qcoil | Rcoil: 2322 | |
| Rl1=Rt1*Rcoil/(Rcoil-Rt1) | Rl1: 86.61 | Load resistance required at input |
| Rln=Rtn*Rcoil/(Rcoil-Rtn) | Rln: 114.8 | Load resistance required at output |

Now do a capacitive impedance transformation to obtain the required load and source impedances

| | | | |
|---|---|---|---|
| C1s=Cr1*sqrt(Rl1/Zin) | Input | C1s: 397.7 | Input shunt capacitance after load impedance transformation |
| C1t=C1s/(sqrt(Rl1/Zin)-1) | | C1t: 1258 | Input top capacitance after load impedance transformation |
| Cns=Cr4*sqrt(Rln/Zout) | Output | Cns: 510.2 | Output shunt capacitance after load impedance transformation |
| Cnt=Cns/(sqrt(Rln/Zout)-1) | | Cnt: 990.1 | Output top capacitance after load impedance transformation |

Figure 7.29. Global definitions LC bandpass filter design equations for a Bessel filter.

As can be seen, using equations in Cadence AWR DE in this way is very powerful. Just changing some input variables in these equations will calculate and simulate any 4 resonator bandpass filter. The equations can easily be modified for different numbers of resonators. The equations in figure 7.29 also include capacitive impedance transformation equations, to allow any desired input and output impedances to be obtained. In addition, the K and Q equations for Butterworth filters have been included

in these equations, so that if a Butterworth filter is required, those values can easily be linked to the actual K and Q values used for the filter ($q_{1a}$, $q_{na}$, $k_{12a}$, $k_{23a}$, $k_{34a}$).

Using those variables in the filter schematic gives the filter shown in figure 7.30. Since the values are calculated in the Global Definitions folder, the resulting variables have been displayed in figure 7.30 for convenience.

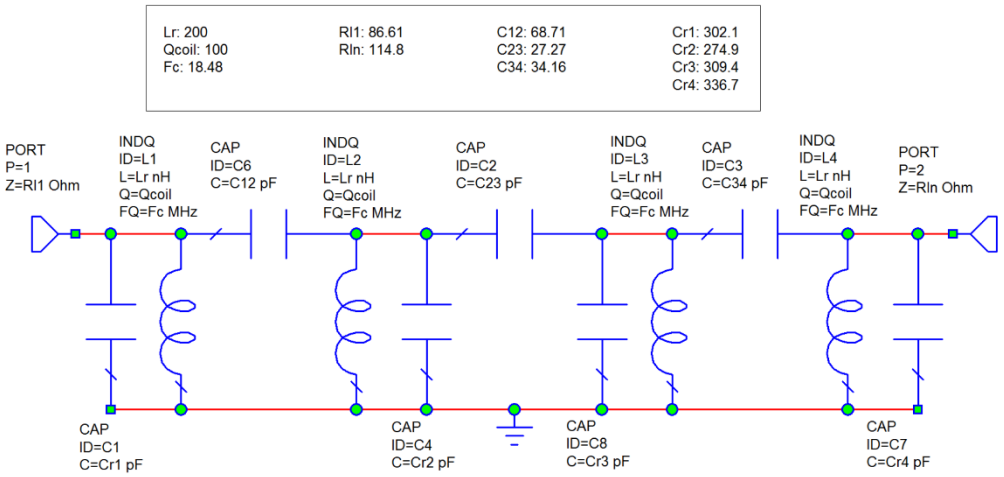



Figure 7.30. Capacitive coupled Bessel LC coupled resonator filter.

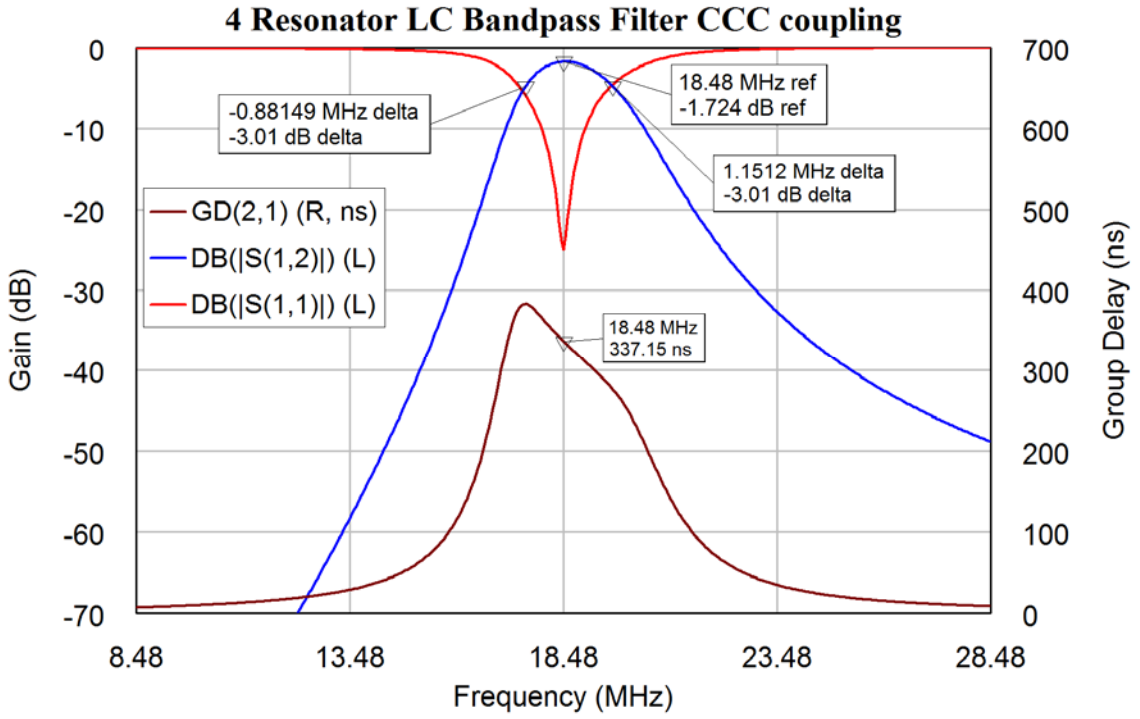



Figure 7.31. Frequency response of the filter of figure 7.30.

By comparing figure 7.28 and figure 7.31, it can be seen that capacitive coupling reduces the attenuation at high frequencies and increases the attenuation at low frequencies. In addition, the group delay is less flat than for the lowpass to bandpass transformation.

Instead of using capacitive coupling, inductive coupling can be used. For capacitive coupling, the total resonating capacitance is made up of the capacitor of a resonator plus the adjacent coupling capacitors according to equation 7.8, which is incorporated in the LC Bandpass filter design program of figure 7.29. For inductive coupling the capacitance

of the resonators are simply the resonant capacitance (371 pF in the design example) and the inductance of the resonator is adjusted to account for the coupling inductors. For this, the equations for the coupling capacitors in figure 7.29 are replaced with the equations shown in figure 7.32, which also shows the circuit of the filter. Figure 7.33 shows the frequency response of the filter. The group delay for inductive coupling has an opposite slope to the one for capacitive coupling.

Now calculate the component values required

| | | |
|---|---|---|
| L12=Lr/(k12a*NBW) | L12: 1079 | Coupling Inductances |
| L23=Lr/(k23a*NBW) | L23: 2720 | |
| L34=Lr/(k34a*NBW) | L34: 2171 | |
| Lr1=1/(1/Lr-1/L12) | Lr1: 245.5 | Resonator Inductances |
| Lr2=1/(1/Lr-1/L12-1/L23) | Lr2: 269.8 | |
| Lr3=1/(1/Lr-1/L23-1/L34) | Lr3: 239.7 | |
| Lr4=1/(1/Lr-1/L34) | Lr4: 220.3 | |

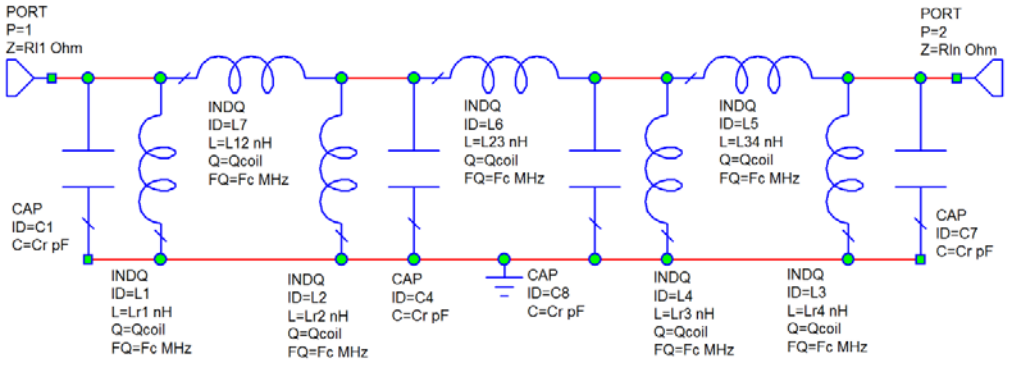



Figure 7.32. Inductively coupled LC resonator filter.

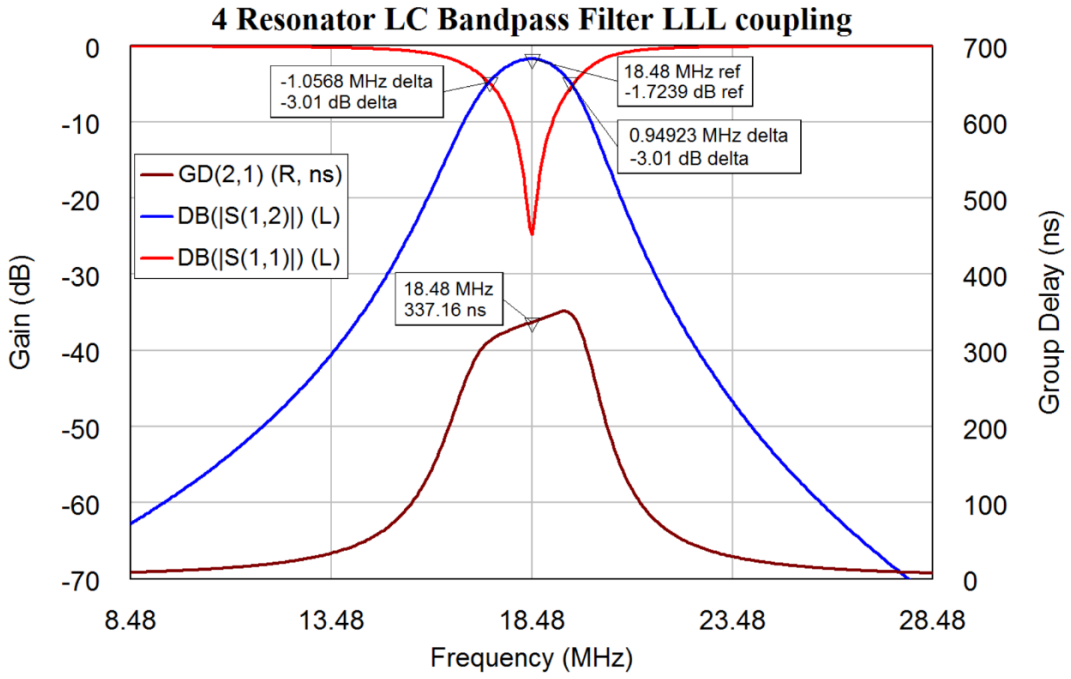



Figure 7.33. Frequency response of the filter of figure 7.32.

By using a combination of capacitive and inductive coupling, as shown in figure 7.34, a flatter group delay is obtained, as shown in figure 7.35. The equations from the Global Definitions folder of the Cadence AWR DE project for figures 7.34 and 7.35 are shown in figure 7.34. If a filter with a flat group delay is to be designed and the extra cost of

inductors over capacitors is a serious problem, then a filter with two coupling capacitors and one inductor can easily be obtained using these equations. The group delay of such a filter can still be made sufficiently flat over the passband using optimisation.

Now calculate the component values required

| | | |
|---|---|---|
| L12=Lr/(k12a*NBW) | L12: 1079 | Coupling Inductance |
| C23=k23a*NBW*Cr | C23: 27.27 | Coupling Capacitance |
| L34=Lr/(k34a*NBW) | L34: 2171 | Coupling Inductance |
| Lr1=1/(1/Lr-1/L12) | Lr1: 245.5 | Resonator 1 Inductance |
| Cr1=Cr | Cr1: 370.9 | Resonator 1 Capacitance |
| Lr2=1/(1/Lr-1/L12) | Lr2: 245.5 | Resonator 2 Inductance |
| Cr2=Cr-C23 | Cr2: 343.6 | Resonator 2 Capacitance |
| Lr3=1/(1/Lr-1/L34) | Lr3: 220.3 | Resonator 3 Inductance |
| Cr3=Cr-C23 | Cr3: 343.6 | Resonator 3 Capacitance |
| Lr4=1/(1/Lr-1/L34) | Lr4: 220.3 | Resonator 4 Inductance |
| Cr4=Cr | Cr4: 370.9 | Resonator 4 Capacitance |

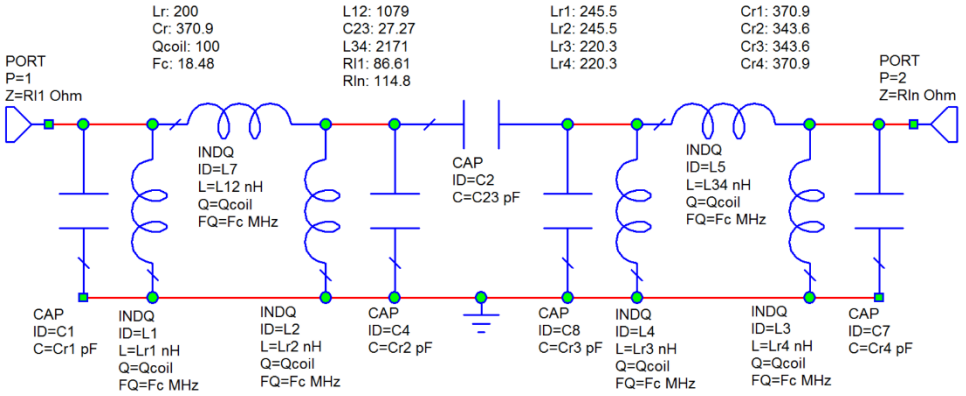



Figure 7.34. Filter with both capacitive and inductive coupling.

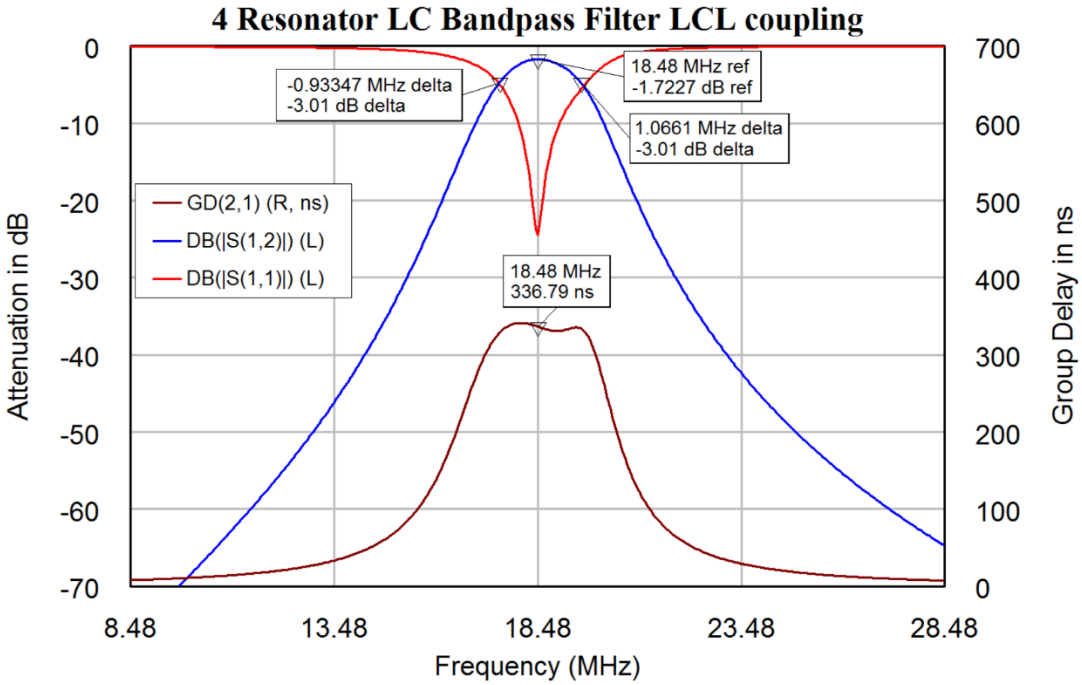



Figure 7.35. Frequency response of the filter of figure 7.34.

The input and output impedances of the filter can be changed to 50 Ω, by replacing *C1* and *C7* with capacitive transformers as shown in figure 7.36. The equations for the value of *C1* is calculated by the equation for *C1s* (C1shunt) and *C3* is calculated as *C1t* (C1top). The impedance transformation for the output is done in a similar manner. This will

slightly change the frequency response and the group delay. To achieve the best input and output match and a flat group delay, the component values linked to variables, calculated using the equations in the Global Definitions folder on the *Project* palette are replaced with the fixed values, which can be optimised. The filter is optimised to provide a flat group delay and meet the bandwidth specification. To achieve the lowest insertion loss at the centre frequency, $S_{11}$ and $S_{22}$ are optimised to be better than -30 dB at 18.48 MHz. The group delay is optimised to be as close to 325 nS as possible. Having a constant group delay results in a Bessel type filter and the filter bandwidth is determined by the group delay. The 325 nS group delay results in a 2 MHz bandwidth. The component values after optimisation are shown in figure 7.36. Figure 7.37 shows the corresponding frequency response. The resulting filter has a very flat group delay.

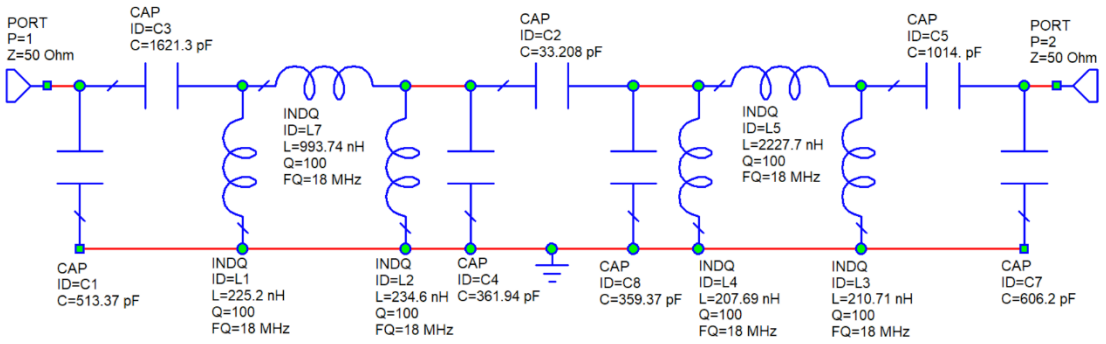



Figure 7.36. Optimised coupled resonator LC filter.

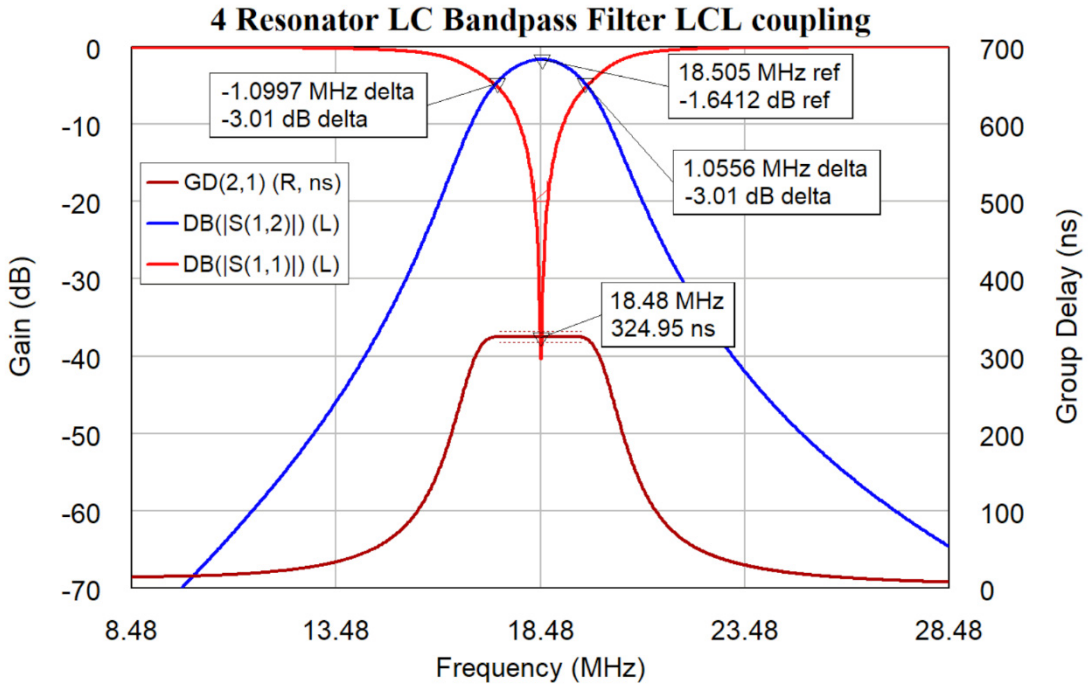



Figure 7.37. Frequency response of the filter of figure 7.36.

## *HF Filters*

At higher frequencies, tuneable inductors become difficult to make and the inductors can be replaced by Microstrip inductors as shown in figure 7.38. This is a capacitive coupled LC resonator filter with a 160 MHz centre frequency and a 27 MHz bandwidth. The

vertical transmission lines form the inductors. The parallel plates at the end of the transmission lines are pads for capacitors. Sufficient space is allowed to fit 2 capacitors in parallel to permit the capacitors to be realised with a high precision. The first and last inductors are tapped transmission lines, to allow the input and output to be coupled to the filter at the correct impedances.

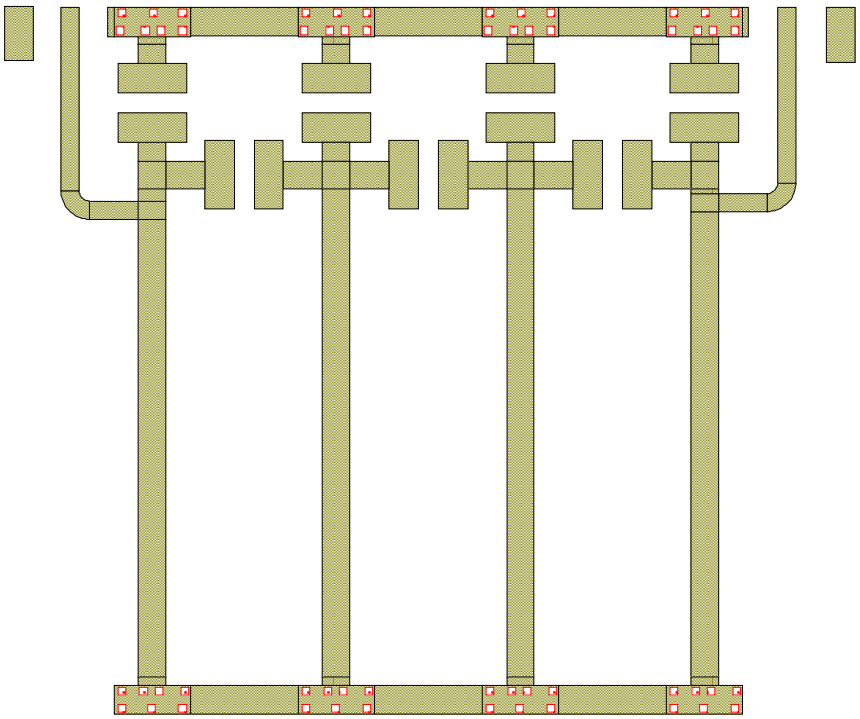


Figure 7.38. Coupled resonator filter using Microstrip inductors.

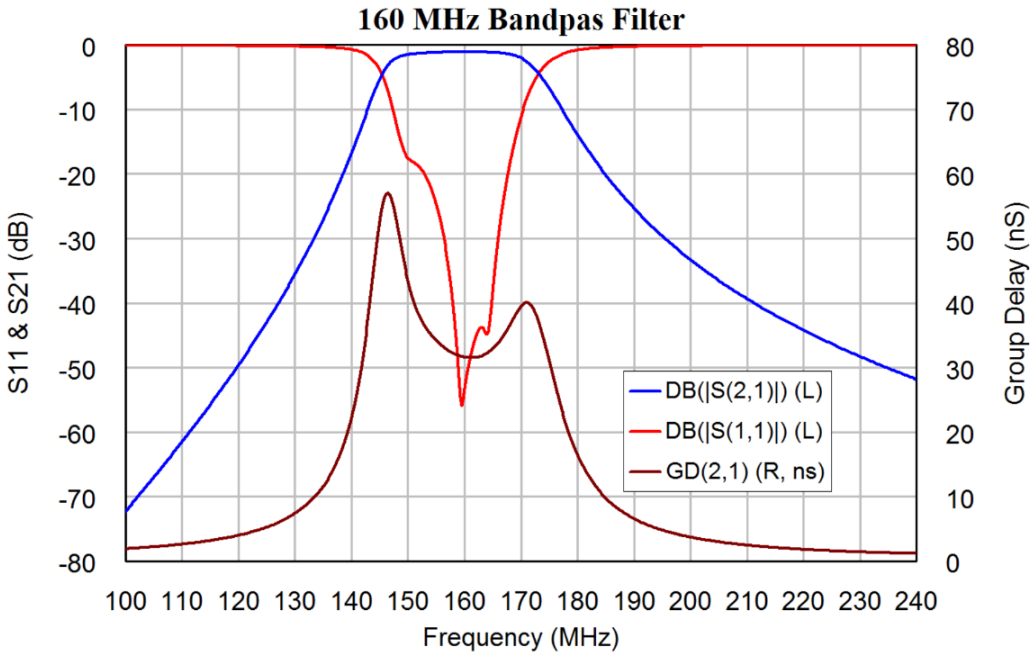



Figure 7.39. Frequency response of the filter of figure 7.38.

Figure 7.39 shows the frequency response of the filter. This filter had to satisfy passband insertion-loss constraints and as a result it corresponds to a Butterworth type frequency

response and the group delay has peaks at the passband edges, similar to figure 7.2. Like the Bessel type filter of figure 7.31, the group delay is bigger at the lower corner frequency than the upper corner frequency. Like the other capacitive coupled filters, the attenuation at higher frequencies (220 MHz) is far less than the attenuation at lower frequencies (100 MHz). The measured frequency response of the filter is close to the calculated response shown in figure 7.39.

### *Cauer-Chebyshev Bandpass filters*

Cauer-Chebyshev filters have zeros in the stopband resulting in equal ripples in the stopband as well as having ripples in the passband. It is more difficult to include zeros in the stopband of coupled resonator RF filters, as this requires coupling between adjacent resonators. It is also possible to include zeros of transmission by including open circuited stubs of one-quarter wavelength at the appropriate frequency. Such stubs are normally used to suppress the unwanted passbands occurring at the second and third harmonic of the passband frequency. In other RF filters, transmission zeros are placed at frequencies that must be rejected, such as the transmission frequency in the receive input of a diplexer. In these cases an equal stopband ripple design as specified by the Cauer-Chebyshev filters is not implemented.

## Parallel Coupled-Line Filters

This filter type is also known as a Stripline filter. For this filter, the design equations 7.11 to 7.14 can be used. However, one can also use the generalised coupled resonator filter equations shown in equations 29 and 30 and applied to the interdigital filter design example on page 170.

The filter parameters a(i) and the resulting even and odd mode Characteristic impedances are given as:

$$a(0) = \sqrt{\frac{\pi BW}{2q_1 F_c}} \qquad \text{Eqn. 7.11}$$

$$a(i) = \frac{\pi BW}{2F_c} k_{i,i+1} \qquad \text{Eqn. 7.12}$$

$$Z_{oo} = Z_{in}(1 - a(i) + a(i)^2) \qquad \text{Eqn. 7.13}$$

$$Z_{oe} = Z_{in}(1 + a(i) + a(i)^2) \qquad \text{Eqn. 7.14}$$

In these expressions BW is the bandwidth of the filter, $F_c$ is the centre frequency, $q_1$, $q_n$ are the normalised input and output loaded Q values and $k_{i,i+1}$ is the coupling coefficient between the $i^{th}$ and the $(i+1)^{th}$ resonator as obtained from filter tables.

### *Example 7.1: 1 GHz, 70 MHz Bandwidth Filter*

Design a 4-resonator filter with a bandwidth of 70 MHz and a centre frequency of 1 GHz. The attenuation should be as low as possible in the passband. The input and output impedances should be 50 Ω. The filter is made using 0.82 mm thick RO4003 substrate with 35 micron copper. A Butterworth filter type is selected for the initial design. Equations 7.4 and 7.5 can thus be used for obtaining the K and Q values, or they can be taken from table 7.1 to give:

| Normalised | De-normalised |
|---|---|
| $q_1 = q_n = 0.7654$ | $Q_1 = Q_n = 0.7654*1000/70 = 10.93$ |
| $k_{12} = k_{34} = 0.8409$ | $K_{12} = K_{34} = 0.8409*70/1000 = 0.05886$ |
| $k_{23} = 0.5412$ | $K_{23} = 0.5412*70/1000 = 0.03788$ |

Substituting this into equations 7.13 and 7.14 and substituting the resulting a(0) and a(i) into equations 7.11 and 7.12 gives the values for $Z_{oe}$ and $Z_{oo}$ shown below. Those values are then entered into the TxLine program as shown in figure 7.40.

Table 7.3 Parallel coupled-line filter parameters.

| Line | a | $Z_{oe}$ | $Z_{oo}$ | Width | Space | Length |
|---|---|---|---|---|---|---|
| 0 | 0.3902 | 76.13 | 38.23 | 1.26 mm | 0.12 mm | 47.3 mm |
| 1 | 0.09246 | 55.05 | 45.80 | 1.71 mm | 1.08 mm | 46.2 mm |
| 2 | 0.05951 | 53.15 | 47.20 | 1.74 mm | 1.57 mm | 46.0 mm |
| 3 | 0.09246 | 55.05 | 45.80 | 1.73 mm | 1.2 mm | 46.2 mm |
| 4 | 0.3902 | 76.13 | 38.23 | 1.26 mm | 0.12 mm | 47.3 mm |

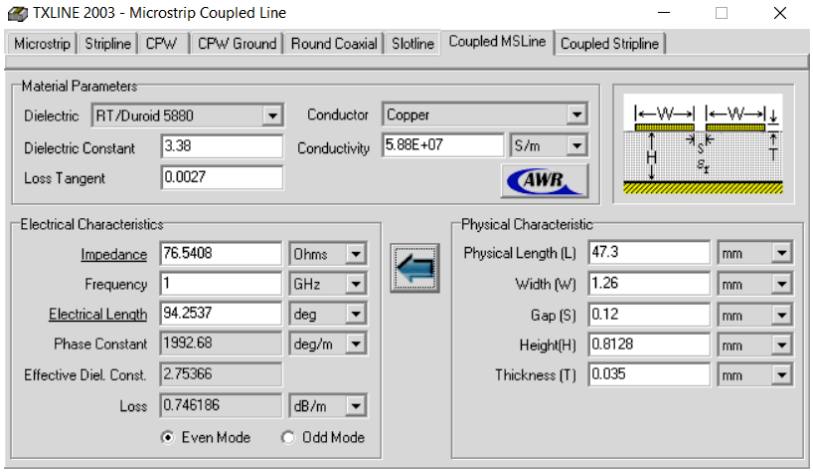



Figure 7.40. Calculating line widths and coupling gaps.

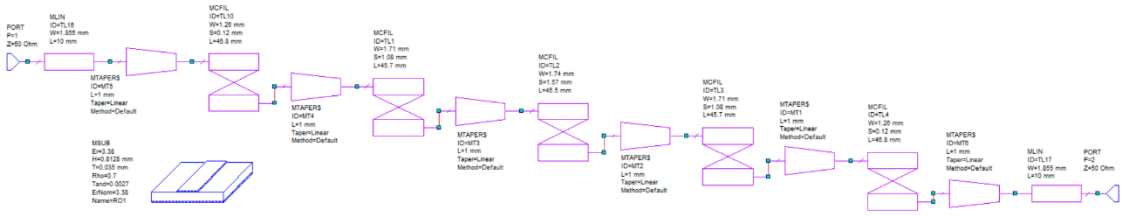


Figure 7.41. Cadence AWR DE schematic for the 1 GHz filter

Those line geometries are then entered in a circuit schematic to give the circuit shown in figure 7.41. End effects have been included by using the Microstrip filter element "MCFIL". A 1 mm long taper has been added between each coupled section to ensure that the coupled lines do not produce a short circuit at the transition in width. As a result, all resonators are shortened by 0.5mm to keep the total resonator length the same. The computer simulation software will produce a layout from the schematic as shown in figure 7.42. This layout can be plotted and produced as a PCB.

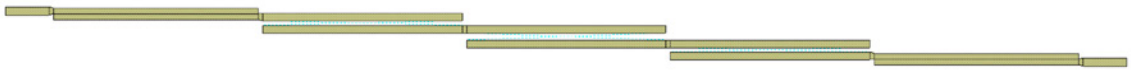


Figure 7.42. PCB layout for this filter produced by Cadence AWR DE.

Figure 7.43 shows a close-up of the centre of the first resonator, and shows *TL10*, *MT4* and *TL1* of figure 7.41. It can be seen that without the tapered transition a short circuit would be produced. The filter from figure 7.41 as designed using the above procedure has a centre frequency of 981 MHz, and is 1.9% low. The bandwidth is 62 MHz and is 12 % low. The resonator lengths and coupling gaps are optimised, using the optimisation routines in Cadence AWR DE, to achieve the correct centre frequency and bandwidth. Since the design procedure gives a result very close to the specifications, the optimisation procedure is quick. The resulting frequency response is shown in figure 7.44. The insertion loss of the filter is 1.9 dB. The return loss can be improved if needed by setting optimisation goals on $S_{11}$ and using the optimiser to automatically fine tune the elements.

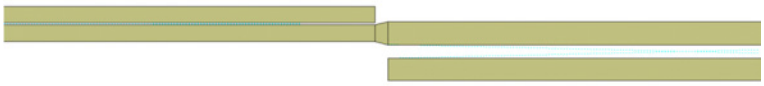


Figure 7.43. Close-up of part of figure 7.42, showing TL10, MT4 and TL1.

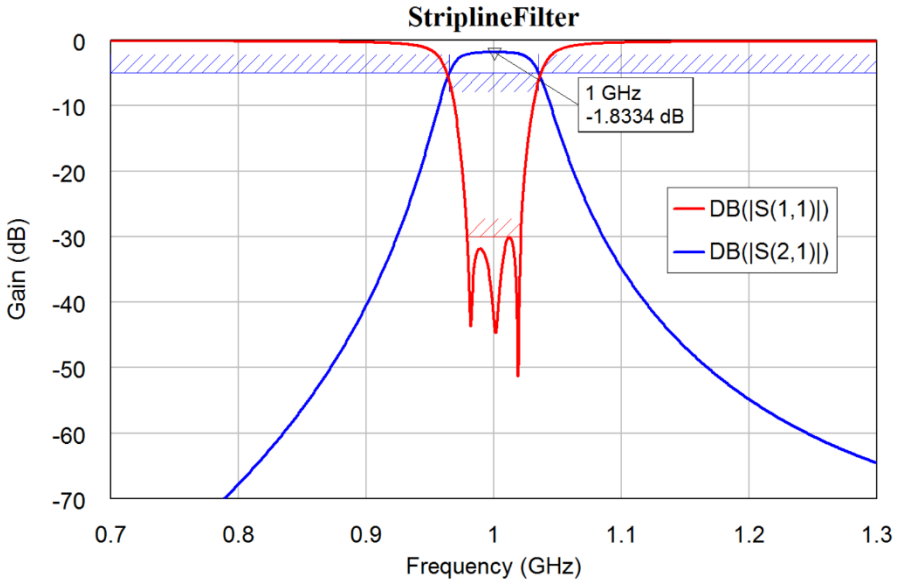



Figure 7.44. Frequency response of the filter from figure 7.41 after optimisation.

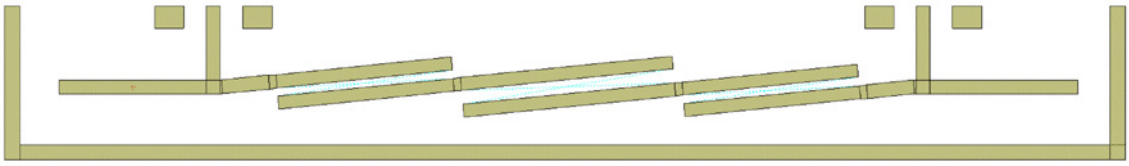


Figure 7.45. PCB layout for coupled-line filter with tap coupling into and out of the filter.

For the filter in figures 7.41 to 7.43, the input coupling gap is 0.14 mm. This gap is close to the limit of reliable manufacturing capability. To avoid this limitation, tap coupling is used to connect to the input and output resonators, as shown for the 100 MHz bandwidth at a 1.7 GHz centre frequency filter shown in figure 7.45. For wider bandwidth filters, the input and output coupling gaps are very small and tap coupling is best. For very narrow bandwidth filters, the connection point for tap coupling becomes too close to the effective ground point of the first resonator, so that line coupling as shown in figure 7.41 is more practical.

The actual filter, when produced, will have a centre frequency and bandwidth that will be slightly different from the simulated results. These differences are due to; the computer simulation not being completely accurate, variations in PCB substrate materials, etching, or milling errors in producing the PCB and so on. In many instances, the filter performance will be good enough. When the filter specifications are critical, a second iteration of the filter can be produced, where the simulation is biased to correct for the discrepancy between the measured and simulated results.

## *Hairpin Filters*

The filters of figure 7.42 and 7.45 are long and skinny and are difficult to mount securely. To obtain a better form factor for the filter, the resonators can be folded as shown in figure 7.46. Coupled resonator filters where the resonators are made up from quarter wavelength transmission lines will have additional passbands when the wavelength of the resonators are three quarter of a wavelength long, five quarter of a wavelength long and so on. These harmonic resonances are normally undesirable. To avoid these harmonic stubs can be added.

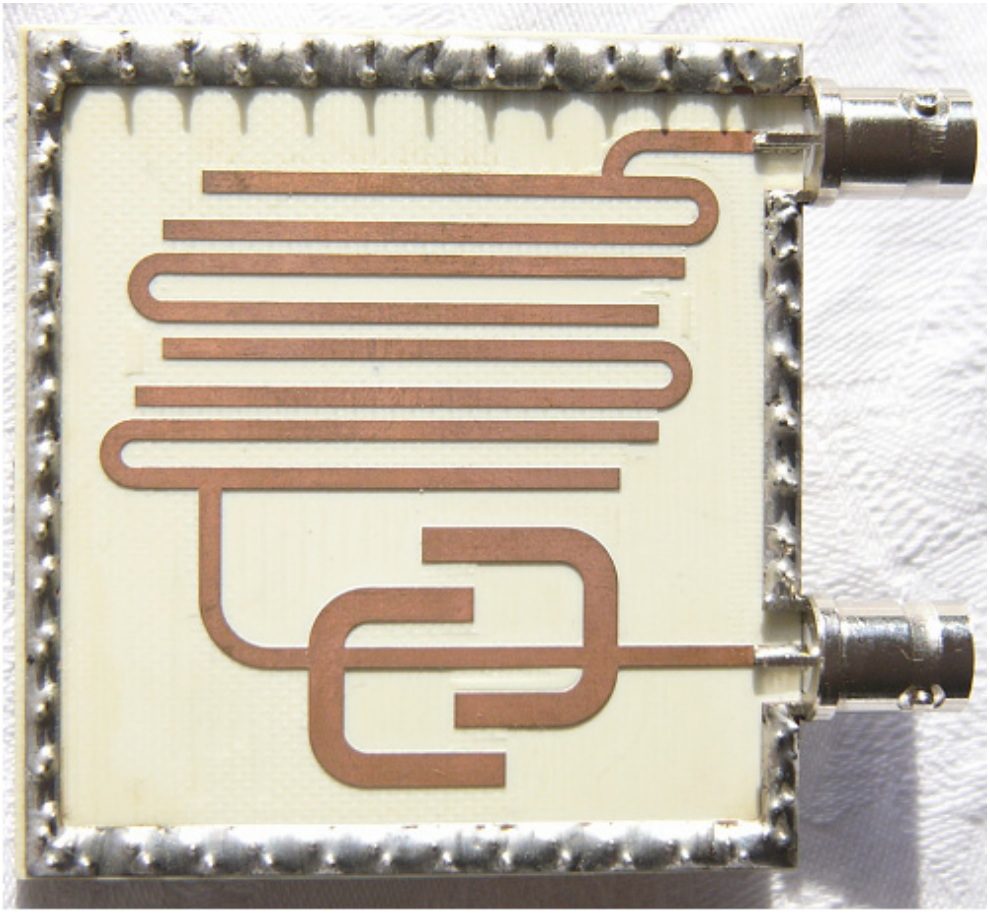


Figure 7.46. Hairpin filter with harmonic stubs.

The hairpin filter in figure 7.46 has two second and third harmonic suppression stubs incorporated as part of the design. The design procedure consists of firstly designing and optimising a basic hairpin filter as outlined in the previous example. Second and Third harmonic suppression stubs are then designed as a separate circuit, as shown in figure 7.47. The second harmonic stubs are one-quarter wavelength long at the second harmonic and the third harmonic stubs are one-quarter wavelength long at the third harmonic. The

spacing between the stubs is then adjusted such that the return loss of the circuit is large at the centre frequency of the filter, so that the harmonic stub circuit has the least effect on the filter performance. The stubs are folded to minimise the space used by the whole filter. Note this filter was designed and build before EM based X models were readily available. At present one would use MTEEX, MCROSSX$ and MLEFX elements for better accuracy.

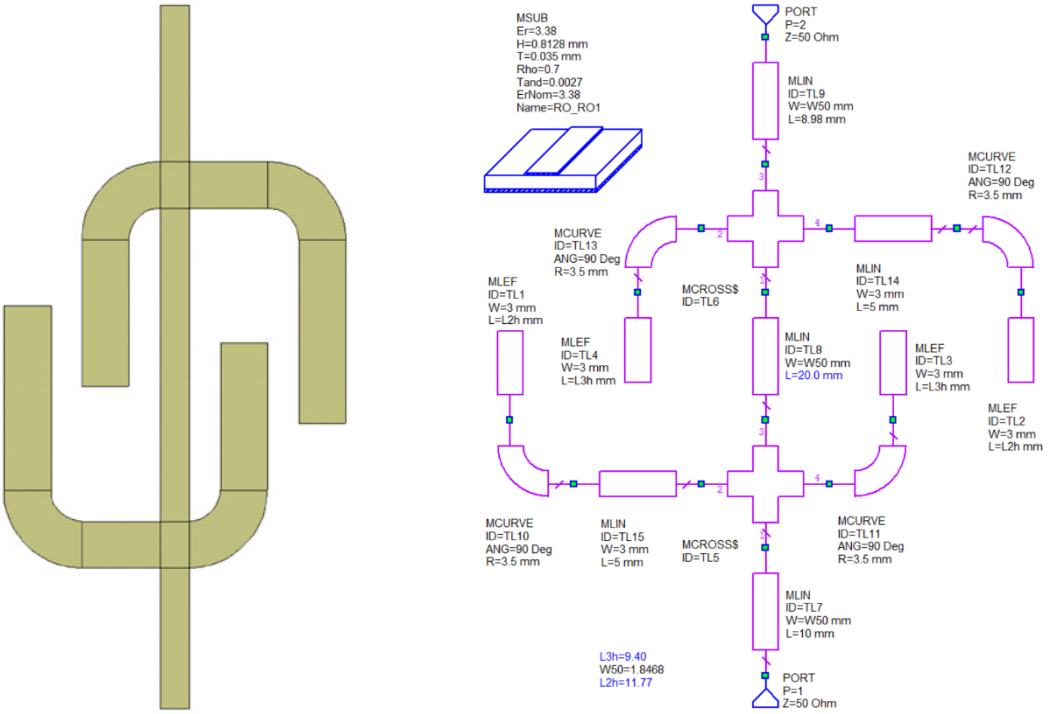



Figure 7.47. Folded harmonic stubs.

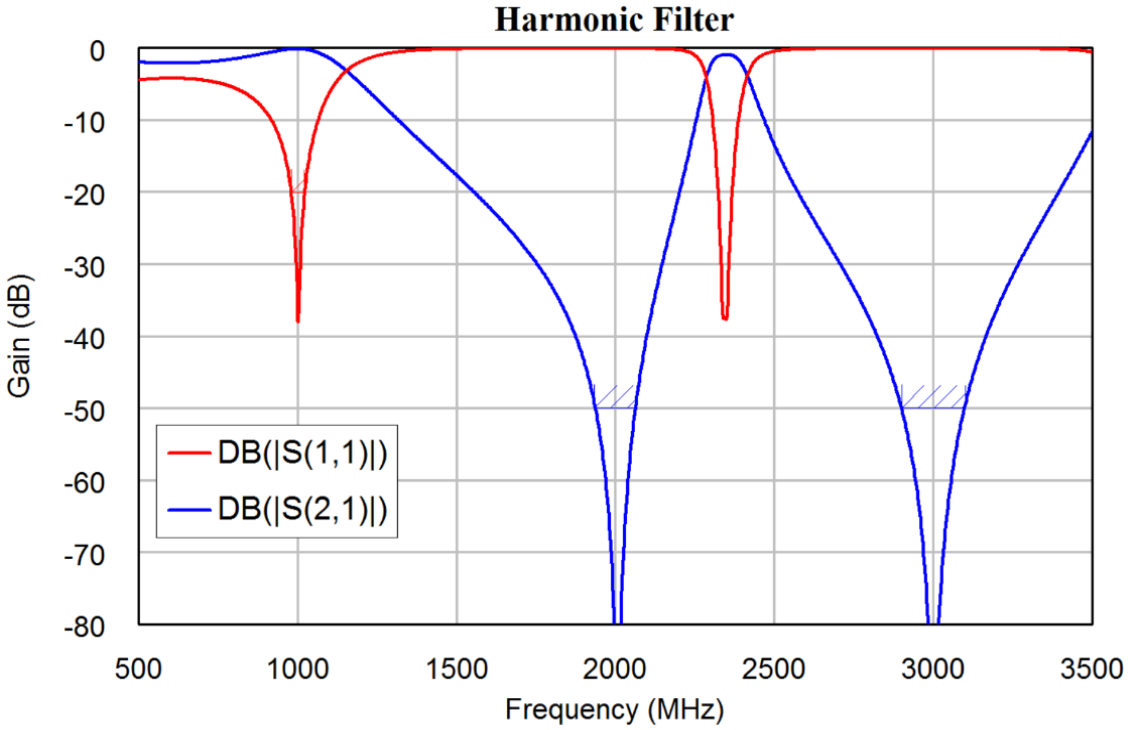



Figure 7.48. Frequency response of harmonic stubs.

Figure 7.48 shows the frequency response of the harmonic stub circuit. It can be seen that there is some effect on the passband of the filter, so that further optimisation to the design of the hairpin filter must be carried out in order to ensure that the combination of the hairpin filter and the harmonic stubs have the required passband response. Figures 7.51 and 7.52 show the frequency response of the actual filter of figure 7.46 and compares this with the frequency response of the simulation.

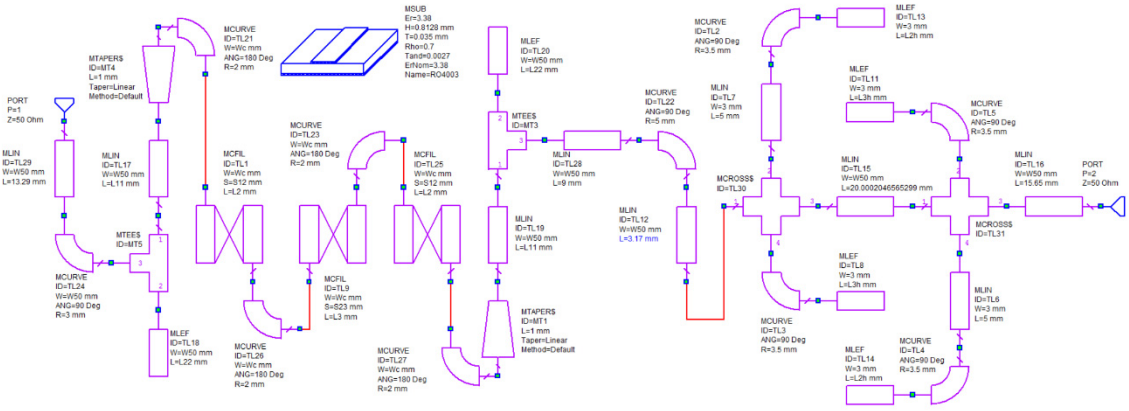


Figure 7.49. Circuit schematic of hairpin filter as built.

The filter hardware was realised from the circuit schematic using the "MCFIL" elements as shown in figure 7.49. To compare the different ways this circuit can be simulated, The MCFIL elements can be replaced with the coupled line element "MCLIN" with "MLEF" elements compensating for the end effect of the open circuited ends of the coupled line elements, as shown in figure 7.50. An AXIEM EM simulation is carried out on the circuit of figure 7.49, as described in the *EM Simulation* section later in this chapter. Finally the MTEE$, MCROSS$ and MLEF elements in 7.49 are replaced with the EM based elements MTEEX$, MCROSSX$ and MLEFX.

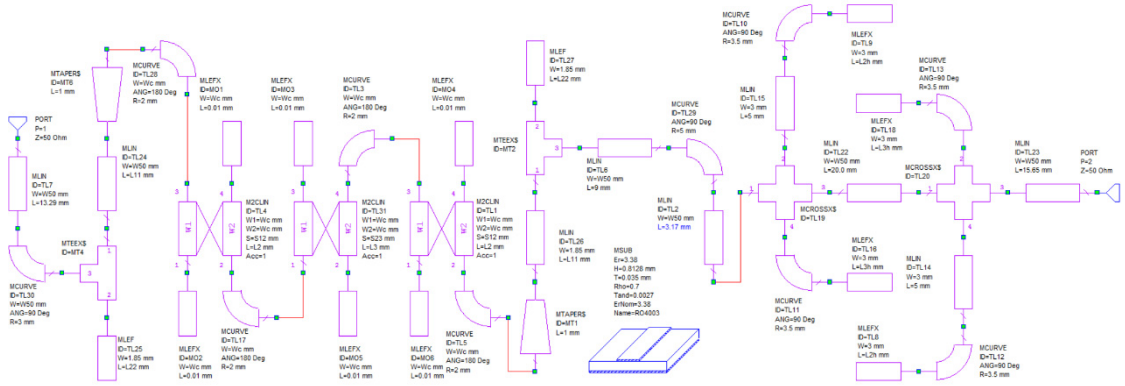


Figure 7.50. Circuit schematic of hairpin filter using MCLIN elements.

The value of $E_r$ = 3.38 was specified by the manufacturer and is used for the simulation and optimisation of this filter prior to its manufacture. Figures 7.51 and 7.52 show a comparison between the simulated and measured performance. The EM simulation, using AXIEM and EM EXTRACTION, gives a better agreement for the passband centre frequency and bandwidth, than the circuit simulations. Using EM based elements MTEEX$, MCROSSX$ and MLEFX makes no noticeable difference below 2 GHz.

Figure 7.52 shows the stopband performance of the filter for both the measured performance and the computer simulation. The most significant difference is the reduction in attenuation in the stopband. This is due to EM coupling between parts of the

circuit and the input and output leads. The stopband attenuation can be optimised by mounting the filter in a conductive (aluminium) enclosure and applying microwave-absorbing material in the appropriate places, to be determined experimentally. In many cases, applying the absorber to the back ground-plane of the filter improves the stopband performance sufficiently. Both EM simulations give a good agreement between the measured and simulated results at 2 GHz, but the circuit simulations give a poor agreement there.

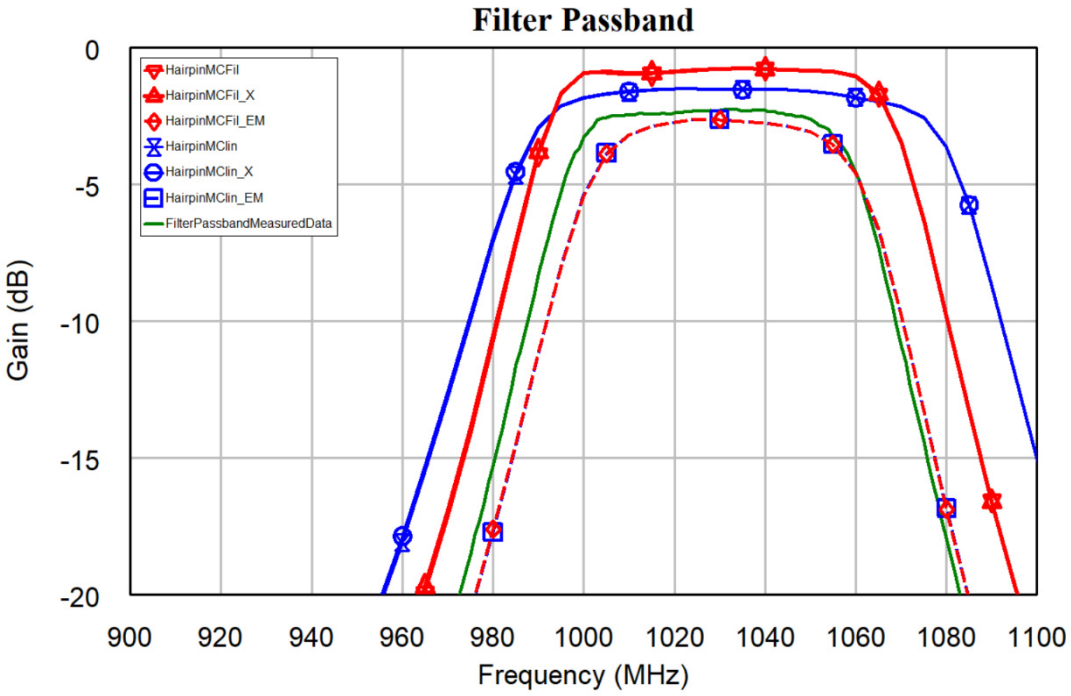



Figure 7.51. Passband response of hairpin filter of figures 7.46 and 7.49.

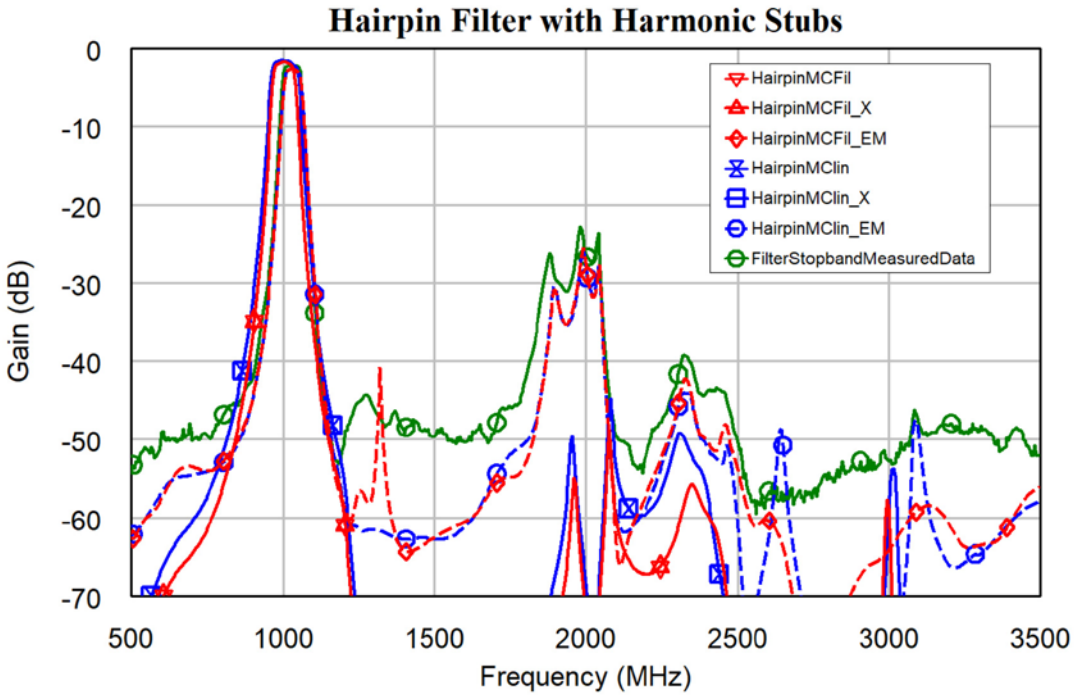



Figure 7.52. Frequency response of hairpin filter of figures 7.46 and 7.49.

# Helical Filters

For high Q value resonators at UHF frequencies, a cylindrical rod of one-quarter wavelength long is placed inside a cavity. This cavity can be cylindrical but in many cases, the cavity is rectangular for ease of construction. Such cylindrical structures are called coaxial filters, as the cross-section of the filter is a coaxial transmission line.

At VHF frequencies, the size of the coaxial filter becomes too large for many applications. To reduce the length of the resonator, the centre quarter-wave resonator is wound as a helix. Often the helix is wound on a former or bobbin, as shown in figure 9.29 of Zverev [1]. One has to ensure that the material for the former is not lossy at the operating frequency. Polyethylene is suitable for low loss formers.

The resonators have shields between them to confine the fields for the resonators. The resonators are coupled by having the appropriate shield height, so that some of the field of a resonator couples to the next resonator. The coupling is controlled by adjusting the difference between the height of the shield and the top of the helix as shown by dimension *"h"* in figure 7.53. Alternately, the coupling can be achieved by having a coupling hole in the centre of a full-height shield or by having a slot at the bottom of the shield. The choice of coupling aperture depends on the construction of the cavity.

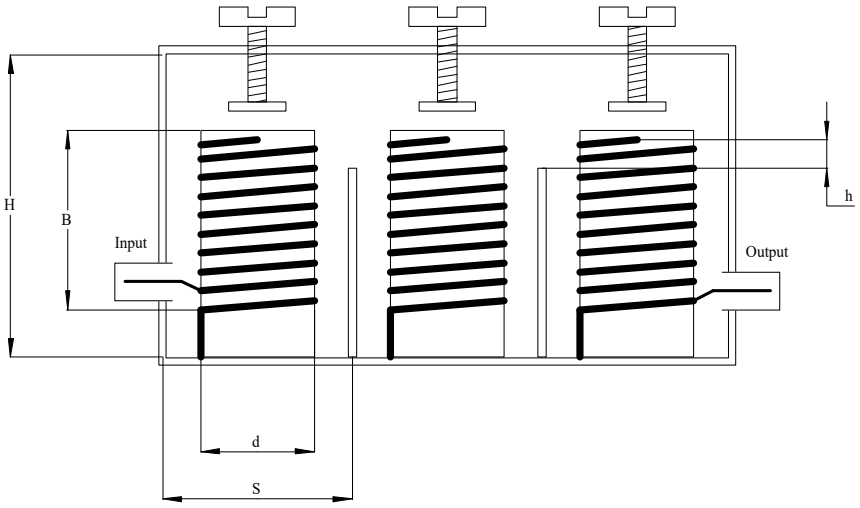



Figure 7.53. Drawing of a helical filter showing the sizes used in the formulae.

Formula for Helical Filters (from Zverev [1])

f is the centre frequency of the helical resonator in MHz

S is the width of the rectangular resonator cavity. (units m)
H is the height of the resonator cavity (units m)
B is the height of the helix (units m)
d is the diameter of the helix (units m)
N is the number of turns of the helix
$Z_0$ is the characteristic impedance of the helical transmission line in the cavity.
$\delta$ is the skin depth. The wire diameter should be > 5 times the skin depth.
$Q_0$ is the unloaded Q of the resonator cavity.

If instead of a rectangular cavity, a cylindrical cavity is used, the diameter D of the cavity is D = 1.2 S.

For the cavity:

$$d = 0.66S \quad \text{Eqn. 7.15}$$

$$B = S \quad \text{Eqn. 7.16}$$

$$H = 1.6S \quad \text{Eqn. 7.17}$$

$$Q_0 = 2363 \times S\sqrt{f} \quad \text{Eqn. 7.18}$$

For the highest Q value, the wire diameter of the helix is selected to be half the pitch of the helix. The gap between the wires is thus the same as the wire diameter.

For the helix:

$$N = \frac{40.6}{S \times f} \quad \text{Eqn. 7.19}$$

$$\delta = \frac{6.6 \times 10^{-5}}{\sqrt{f}} \quad \text{Eqn. 7.20}$$

$$Z_0 = \frac{2070}{S \times f} \quad \text{Eqn. 7.21}$$

$$\frac{R_b}{Z_0} = \frac{\pi}{4}\left(\frac{1}{Q_d} - \frac{1}{Q_0}\right) \quad \text{Eqn. 7.22}$$

The doubly loaded input $Q_d$, is defined as ½ $Q_1$ for the input tapping point calculation and ½$Q_n$ for the output tapping point calculation, and represents the total load seen by the resonator if there is a very small insertion loss as is normally the case. The electrical length $\theta$ from the bottom of the helix to the point where the input or output connects to the helix is given by:

$$Sin(\theta) = \sqrt{\frac{R_b R_{tap}}{2Z_0^2}} \quad \text{Eqn. 7.23}$$

The gap between the shield and the top of the helix is given by:

$$K = 0.071\left(\frac{h}{d}\right)^{1.91} \quad \text{Eqn. 7.24}$$

When the bandwidth increases, the gap between the top of the shield and the top of the coil increases. For wideband filters, no shield is required, thus reducing the cost of construction. In that instance, it is also possible to vary the coupling by varying the spacing between the resonators.

## Example 7.2: 100 MHz, 1 MHz Bandwidth Filter

Design a helical filter to have a 1 MHz bandwidth at 100 MHz. A diecast box of 112 mm width and 50 mm depth and 90 mm height is available. This can be split into two cavities 56 x 50 x 90 mm. The average side S is 53 mm. The H/S ratio is 90/53 = 1.7, which is close enough to the h = 1.6S value from equation 7.17.

The K and Q values required can be obtained from table 7.1. Since for two resonators and Butterworth filters the K and Q values are independent of the insertion loss, equations 7.4 and 7.5 can be used to calculate the required K and Q values.

For Butterworth filters, equation 7. 4 and 7.5 are:

$$q_0 = q_n = 2Sin\frac{(2-1)\pi}{2n} = 2Sin\frac{\pi}{2n} \qquad \text{Eqn. 7.4}$$

$$k_{ij} = \frac{1}{2\sqrt{Sin\frac{(2i-1)\pi}{2n}\,Sin\frac{(2i+1)\pi}{2n}}} \qquad \text{Eqn. 7.5}$$

For a two-resonator filter n = 2, this gives q = 1.4142 and k = 0.7071

The reader is reminded that the small letters k and q denote the normalised values as would be obtained from table 7.1 and the capital letters K and Q are the de-normalised values, which relate to the normalised values by equations 7.6 and 7.7.

Since S = 53 mm and f = 100, equation 7.18 gives the unloaded Q of the cavity as: $Q_0$ = 2363*0.053*10.0 = 1252. The normalised unloaded Q is q = 1259*1/100 = 12.52. From the filter table 7.1, the resulting filter will thus have close to 1 dB insertion loss.

Since S = 53 mm, applying equation 7.15 gives the coil diameter as: d = 35 mm. From equation 7.17, the coil height is 53 mm and equation 7.19 indicates it requires 7.6 turns. The optimum wire diameter is thus 53/(2*7.6) = 3.49 mm. A one-eighth of an inch copper tube is 3.2 mm and is used for winding the coil. The minimum wire diameter of five times the skin depth (equation 7.20) is 0.033 mm. For practical windings, the minimum skin depth requirement is normally satisfied.

From the filter tables the normalised values for Q and K are: $q_1 = q_n$ = 1.4142 and $k_{12}$ = 0.7071. De-normalising this gives $Q_1 = Q_n$ = 1.4142*100/1 = 141.42 and $K_{12}$ = 0.7071*1/100 = 0.007071. $Q_1$ and $Q_n$ are the loaded Q values, which are due to the input and output load impedance being coupled into the resonators and thus appearing as a load to the resonators. The doubly loaded input Q is defined as ½ $Q_1$. This represents the total load seen by the resonator, if there is a very small insertion loss, as is the case here. The doubly loaded output Q is defined as ½ $Q_n$. $Q_d$ is thus 70.71 for both the input and output. Putting this in the expression for $R_b/Z_0$ gives: $R_b/Z_0$ = 0.0105. Since we want the filter to be have 50 Ω input and output impedance, $R_{tap}$ = 50 Ω resulting in θ = 1.48 degrees. Since the coil wire length is 7.6*35*π = 842 mm and corresponds to a quarter wavelength at the centre frequency, or 90 degrees, the tapping point should be 1.48*842/90 = 13.9 mm from the bottom of the helix. In practice, the tapping point needs to be fine-tuned, to match the actual conditions after construction and include losses of the former used for winding the helix on.

For this Butterworth filter, the tapping points for the input and output are the same. For Chebyshev or Bessel filters, or for lossy higher order Butterworth filters, the input and output tapping points will be different, and the above calculation needs to be performed for $Q_1$ and for $Q_n$.

The filter was constructed and performed exactly as expected. The measured bandwidth for the helical filter was 1 MHz and the insertion loss was 0.8 dB. A photograph of the filter is shown in figure 7.54 and the measured response is shown on figure 7.55.

The tuning procedure for adjusting the tapping point for the input and output, and for verifying and if needed adjusting the coupling, is described on page 518 and figure 7.9.23 in Zverev [1]. This same procedure is used, to determine the coupling factors for interdigital filters as shown in figures 7.57, 7.58 and equations 7.29 and 7.30.

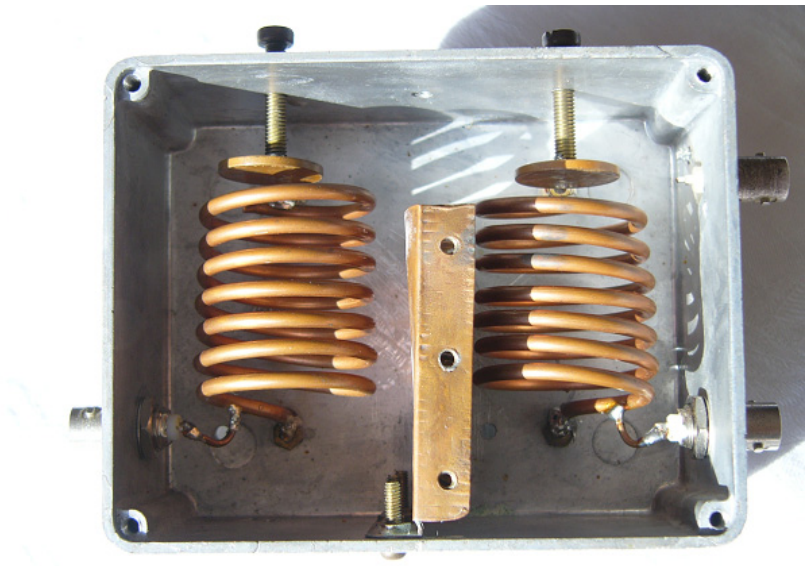


Figure 7.54. 101 MHz helical filter 1 MHz bandwidth

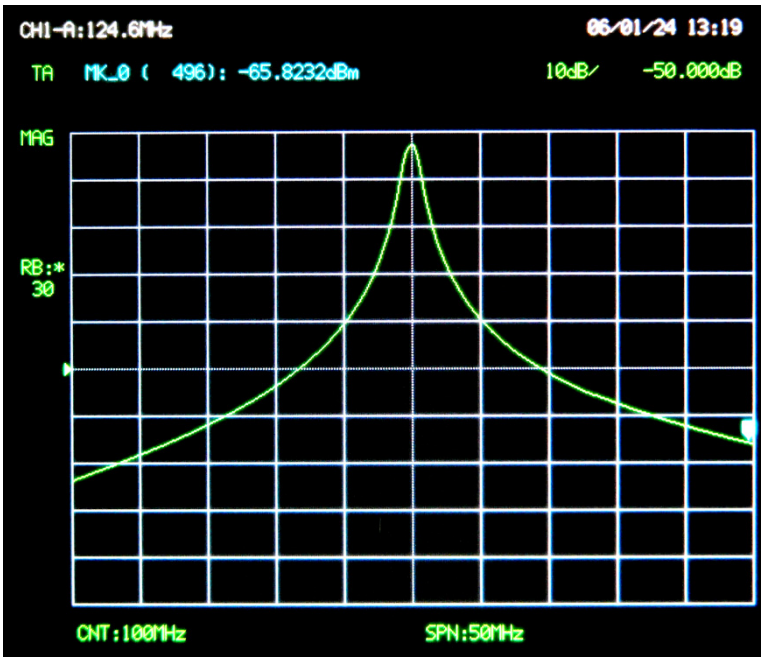



Figure 7.55. Frequency response of 101 MHz helical filter, vertical 10 dB/div.

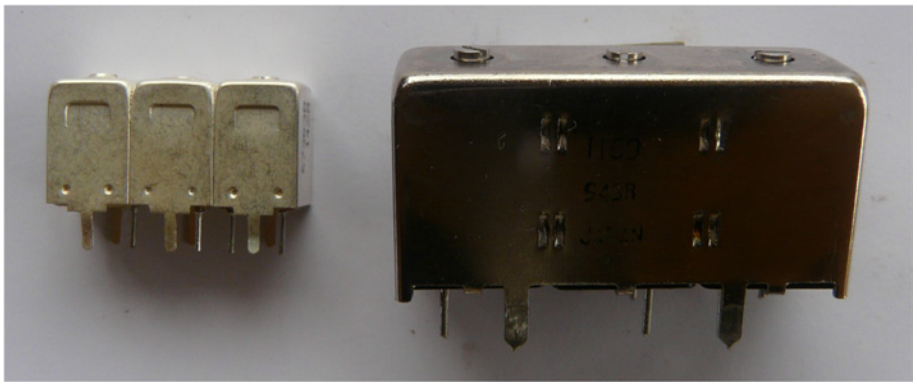


Figure 7.56. Commercial Helical Filters. Temwell [9] Left, Toko 7HT [10] Right.

The left filter in figure 7.54 shows a 3-resonator 142 MHz helical filter with a bandwidth of 6 MHz from Temwell [9]. Each resonator is 8mm wide and 12mm high. Temwell specialise in helical filters and make commercial filters from 45 MHz to 2.6 GHz. The right filter in figure 7.54 is an older, 3-resonator, 137 MHz helical filter with a bandwidth of 2 MHz originally made by Toko in Japan. The resonators are 12mm wide and 18mm high. Temwell [9] now supply both filters in figure 7.56. The measured dimensions of these filters are the outside dimensions of the cavities. The ratio of the internal dimensions thus satisfies equation 7.17.

## Interdigital Filters

With interdigital filters, the resonators are grounded at alternate ends. This reduces the coupling between the resonators and as a result, a compact filter can be constructed that has no walls between the individual resonators. A drawing of an interdigital filter is shown in figure 7.57a.

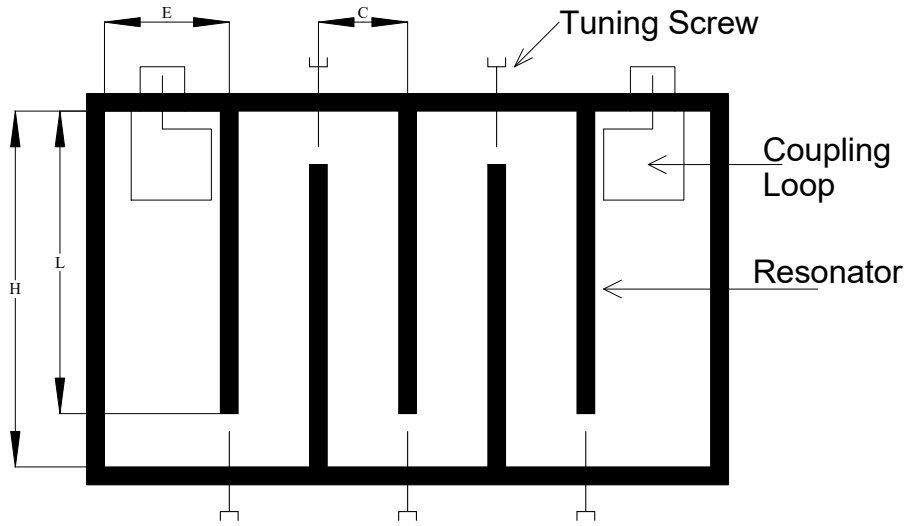



Figure 7.57a. Interdigital filter dimensions, top view.

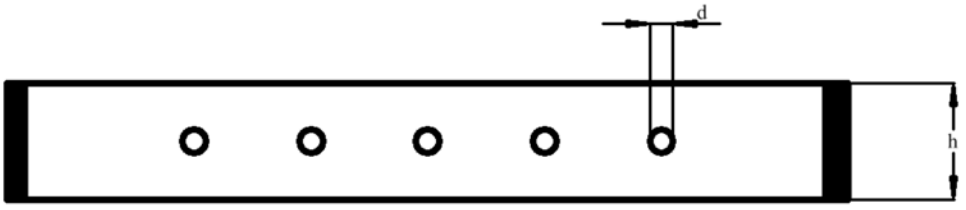



Figure 7.57b. Interdigital filter dimensions, side view.

For a small bandwidth (<10%) M. Dishal [11] provided the following equations for designing interdigital filters:

$$\frac{E}{h} = 0.6 \qquad \text{Eqn. 7.25}$$

$$LogK = \left[ -1.37\frac{C}{h} + 0.91\frac{d}{h} - 0.048 \right] \qquad \text{Eqn. 7.26}$$

Where *h* (figure 7.57b) is the spacing between the walls and d is the rod diameter. Knowing K from the filter tables and *d* and *h* from the design specifications, allows the spacing C between the resonators to be calculated.

In addition, the impedance of the resonator is given by:

$$Z_0 = 138 Log\left[\frac{4h}{\pi d}\right] \tanh\left(\frac{\pi E}{h}\right) \qquad \text{Eqn. 7.27}$$

The singly loaded Q for the input ($Q_1$) and output ($Q_n$) resonators are:

$$Q_1 = \frac{\pi R}{4Z_0} \frac{1}{Sin^2\left(\frac{\pi \lambda_1}{2L}\right)} \qquad \text{Eqn. 7.28a}$$

$$Q_n = \frac{\pi R}{4Z_0} \frac{1}{Sin^2\left(\frac{\pi \lambda_n}{2L}\right)} \qquad \text{Eqn. 7.28b}$$

Since $Q_1$ and $Q_n$ can be obtained by de-normalising $q_1$ and $q_n$ from filter tables, R is the desired termination impedance, (usually 50 Ω) and $Z_0$ is the characteristic impedance of the resonator as obtained from equation 7.27, that the tapping points $l_1$ and $l_n$ can be determined using equation 7.28.

Several companies produce commercial interdigital filters, K&L Microwave [12] is one of them. Interdigital filters have two forms:

## Round Rod Interdigital Filters

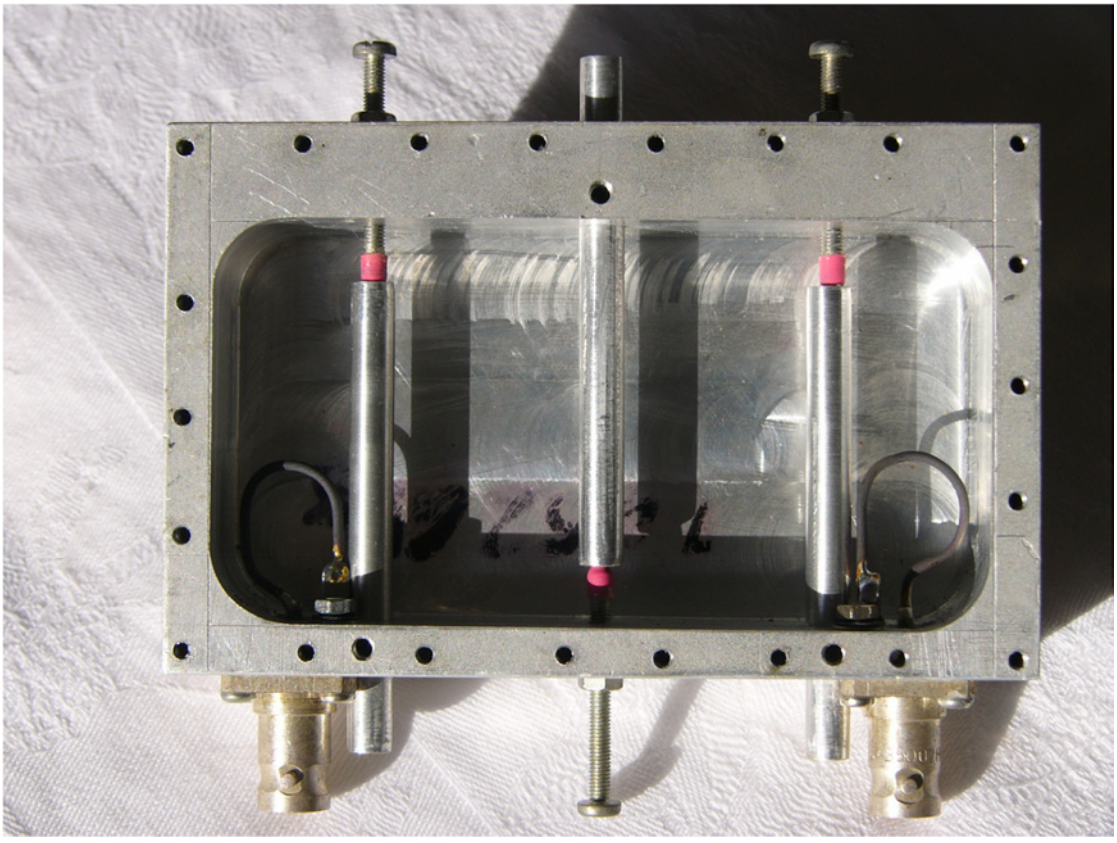


Figure 7.58. Interdigital filter for operation at 940 MHz, with top plate removed (Kikkert).

Similar to the Helical filter, the larger the filter cavity, the lower the insertion loss of the filter and the bigger the power handling capability of the filter. The Round Rod Interdigital filters are reasonably large and as a result have a low insertion loss and a high power handling capability, permitting them to be used at the output of transmitters. These filters normally have bandwidths less than 10%. The filters become very large for frequencies below 300 MHz. The coupling into the filter can be achieved by coupling loops as shown in figure 7.58, or by direct tapping to the resonator rod. In most instances the resonator rods length can be adjusted. This provides a coarse tuning adjustment. In the figure 7.58, the Allen key locking screws for the resonator rods can be seen at the base of each of the resonators allow the course adjustment to be performed. A small variable capacitor, in the form of an insulated screw that slides inside the hollow resonator rod, as shown in figure 7.58, result in filters that can easily be fine-tuned to the correct frequency.

The filter in figure 7.58 was designed using equations 25 to 28. Applying the course-tuning and fine-tuning and adjusting the coupling loops enabled a filter to be obtained, which satisfied the design specifications exactly.

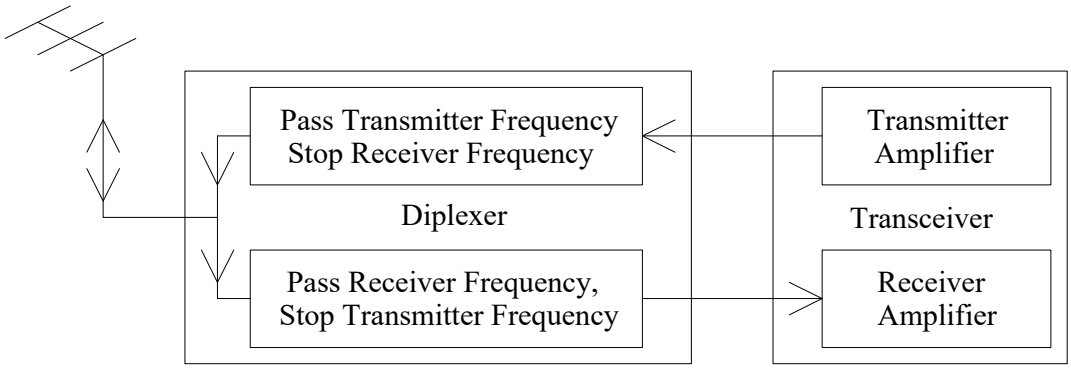



Figure 7.59. The use of a diplexer to provide full duplex operation.

Round rod interdigital filters are often used as a diplexer in mobile radio transceivers, as shown in figure 7.59. The filter connected to the receiver has a very high, typically greater than 60 dB, attenuation at the transmitter frequency. This ensures that the transmitter output, which is typically 25 W, does not damage the receiver input, which is typically designed to accurately demodulate signals of 1 nW. The use of the diplexer will thus permit full duplex operation, simultaneous transmission and reception, of the transceiver.

Mobile phones have similar diplexers. Some older phones use diplexers made using a ceramic material with a typical dielectric constant of 30, allowing a $\sqrt{30}$ reduction in each dimension of the filter as shown on the left of figure 10.2. The resulting filter will thus have 0.6% of the volume of the air-filled filter and have a fraction of the weight. More recent phones, use surface acoustic wave (SAW) or bulk acoustic wave (BAW) filters to obtain an even smaller size and weight, whilst keeping the same functionality shown in figure 7.59.

## *PCB Interdigital Filters*

With circuit miniaturisation, and improved Microstrip simulation tools, interdigital filters are often designed using Stripline or Microstrip circuits for the resonating elements. The power handling capacity of these filters is small, so that they can only be used as filters in receivers or low power parts of communication equipment. The design procedure is illustrated with the following example.

## *Example 7.3: 1 GHz, 70 MHz Bandpass Filter*

Design a 5-resonator filter with a 70 MHz bandwidth centred at 1 GHz, using a RO4003 substrate for the PCB. The required *k* and *q* values can be obtained from table 7.1, the relevant part of which is shown in table 7.4. The design procedure used here is also described in [13, 14].

Table 7.4. Butterworth response, K and Q value filter table, from Zverev [1], pp 341.

| n | q0 | I. L. | q 1 | q n | k 12 | k 23 | k 34 | k 45 |
|---|---|---|---|---|---|---|---|---|
| 5 | INF. | 0.000 | 0.6180 | 0.6180 | 1.0000 | 0.5559 | 0.5559 | 1.0000 |
| | 32.361 | 1.045 | 0.4001 | 1.5527 | 1.4542 | 0.6946 | 0.5285 | 0.6750 |
| | 32.361 | 1.045 | 0.5662 | 0.7261 | 1.0947 | 0.5636 | 0.5800 | 0.8106 |
| | 16.180 | 2.263 | 0.3990 | 1.8372 | 1.4414 | 0.6886 | 0.5200 | 0.6874 |
| | 16.180 | 2.263 | 0.5777 | 0.7577 | 1.0711 | 0.5408 | 0.6160 | 0.7452 |
| | 10.787 | 3.657 | 0.4036 | 2.0825 | 1.4088 | 0.6750 | 0.5080 | 0.7066 |
| | 10.787 | 3.657 | 0.5927 | 0.7869 | 1.0408 | 0.5144 | 0.6520 | 0.6860 |
| | 8.090 | 5.265 | 0.4111 | 2.3118 | 1.3670 | 0.6576 | 0.4927 | 0.7290 |
| | 8.090 | 5.265 | 0.6100 | 0.8157 | 1.0075 | 0.4844 | 0.6887 | 0.6278 |

Notice that the *k* and *q* values vary depending on the losses. One could guess the losses to be about 2 dB and use the corresponding *k* and *q* values. Note that for each value of insertion loss, there are two sets of *k* and *q* values. Since the tap coupling is normally used and the tapping points only cover a limited range, it is desirable to select the table values where the difference between the q values is small.

Alternately, the design is done assuming no losses, so that equations 4 and 5 can be used. After the design is completed, any variations in k and q values required to accommodate the losses can be achieved by optimisation. That process is implemented here. The lossless q values are thus $q_1 = q_n = 0.6180$, resulting in $Q_1 = Q_n = 0.6180*1e9/70e6 = 8.828$.

The bandwidth, without loading due to adjacent resonators is given by equation 9.4.1 in Zverev [1] for the first and last resonator respectively as:

$$\text{Resonator 1 } \Delta_{3dB} = \frac{FilterBW_{3dB}}{q_1} \qquad \text{Eqn. 7.29a}$$

$$\text{Resonator } n \ \Delta_{3dB} = \frac{FilterBW_{3dB}}{q_n} \qquad \text{Eqn. 7.29b}$$

In our design the filter $BW_{3dB}$ is 70 MHz, $\Delta_{3dB}$ is thus 70/0.618 MHz = 113.2 MHz. For this filter, $q_1 = q_n$ and the input and output tapping points are the same.

The tapping point can be determined using Cadence AWR DE and the two-resonator circuit of figure 7.60. To prevent the second resonator from influencing the tuning of the tapping point, a very large coupling gap is used and the resonance of the coupled resonator is placed far away from the centre frequency by disabling all the possible elements as shown in figure 7.60. To measure the voltage of the input resonator, a high impedance (1 MΩ) port (port 2) is connected to the resonator. The signal at port 2 is then the voltage at the top of resonator and has the correct frequency response for determining the loading

of the resonator, as shown in the graph of figure 7.60. After tuning the tapping point for the correct bandwidth, the correct $q_1$ and $q_n$ for the filter has been determined.

The tapping point in the circuit of figure 7.60 of 3.125 mm (+5 mm for TL7) results in the required 113.2 MHz bandwidth. The total resonator length of *Ltot* = 46.46 mm places the maximum response of the loaded resonator at 1 GHz.

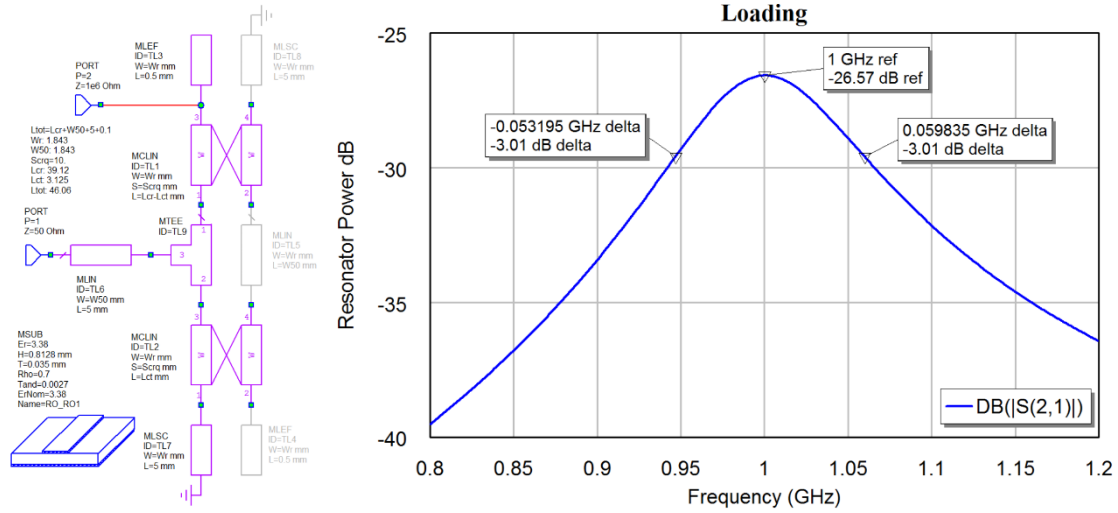



Figure 7.60. Left: circuit for input tap determination, right: frequency response.

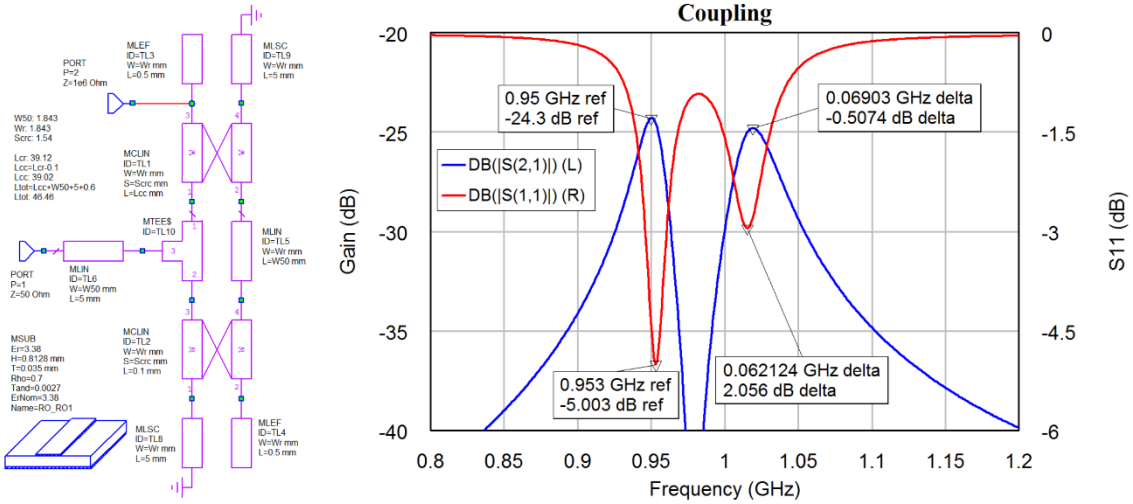



Figure 7.61. Left: circuit for coupling determination, right: frequency response.

The coupling gap is tuned to obtain the correct coupling between resonators. To reduce the effect of loading, the tapping length *Lct* is made as small as possible, while keeping the total resonator length the same as before, resulting in the test circuit shown in figure 7.61. When the second resonator is tuned and brought close to the first resonator, a double peak response will result as shown in figure 7.61. The frequency difference between the peaks is given by equation 9.4.3 in Zverev [1] as:

$$\Delta_{fp} = k_{12} BW_{3dB} \qquad \text{Eqn. 7.30}$$

For this filter $k_{12} = 1$, so that $\Delta_{fp}$ =70 MHz for the peaks in frequency response of the test circuit, coupling between the first and second resonator as shown in figure 7.61. This corresponds to a coupling gap of 1.54 mm. The same test circuit is used to determine the coupling gaps for the other resonators. For the coupling between the second and the third

resonator $\Delta_{fp}$ = 0.5559*70 MHz = 38.9 MHz. The coupling gap is re-tuned to obtain a difference of 38.9 MHz between the peaks. This corresponds to a coupling gap of 2.5 mm. This procedure is then repeated for all the remaining coupling gaps for the filter using the respective coupling coefficients from tables or equations 4 and 5.

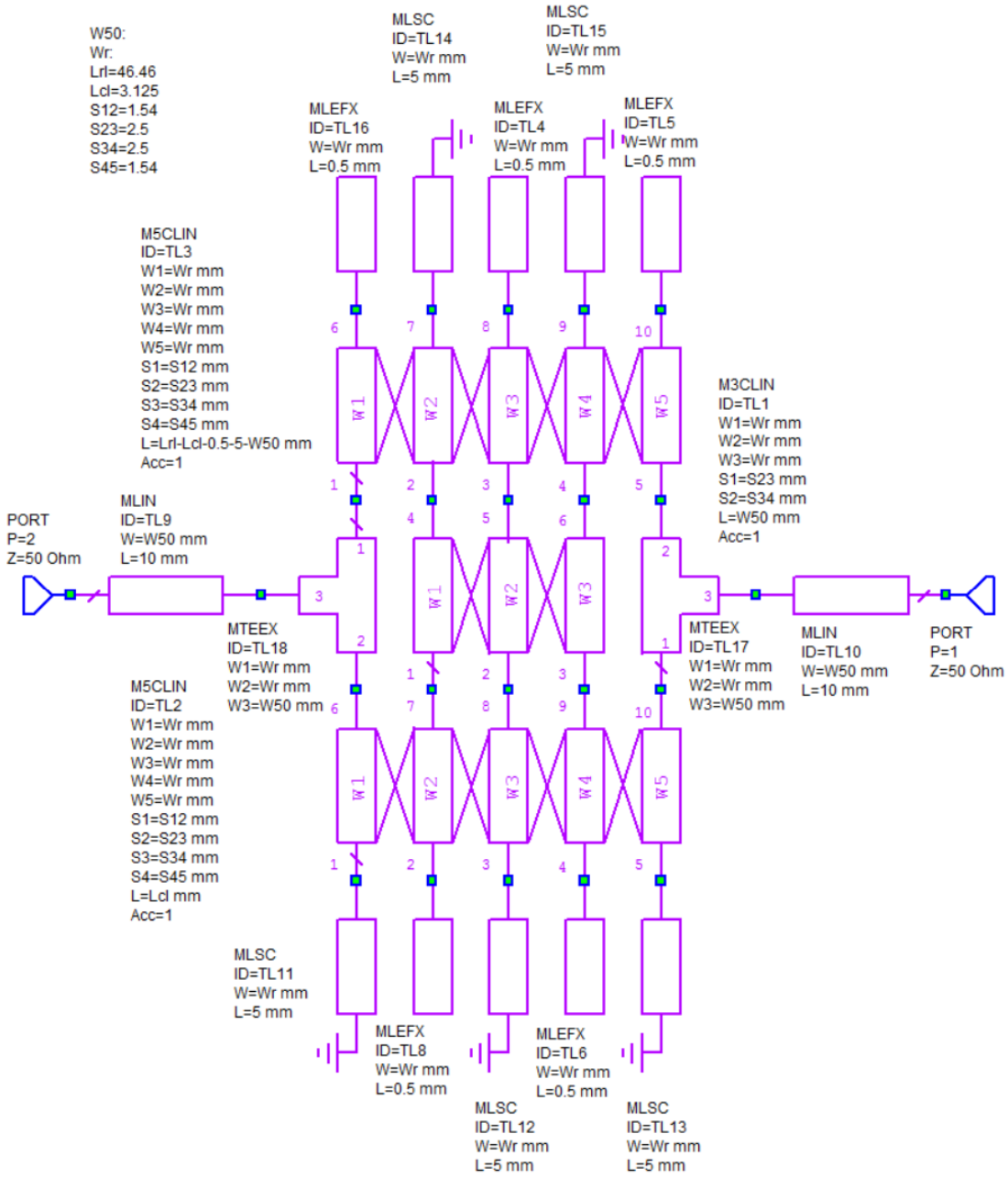



Figure 7.62. Circuit for the interdigital filter using calculated loading and coupling values.

Simulating this circuit of figure 7.62 gives a filter with a response close to the desired value, as shown in figure 7.63. To obtain the precise desired specification, the filter needs to be optimised. For a lossless Butterworth filter, the coupling gaps are symmetrical. However, for lossy filters or different filter types, asymmetrical coupling gaps result. For a practical Butterworth Bandpass filter, the design procedure can assume a lossless filter. Subsequent optimisation for the desired filter performance, accommodates the losses by; allowing changes in resonator lengths, coupling points and coupling gaps. Note that after optimisation, the resonators in this design are not of equal length and the filter is no longer

symmetrical from the input and output. This asymmetry is expected from *k* and *q* filter table for the1.5 dB insertion loss that this filter has, as shown in table 7.4.

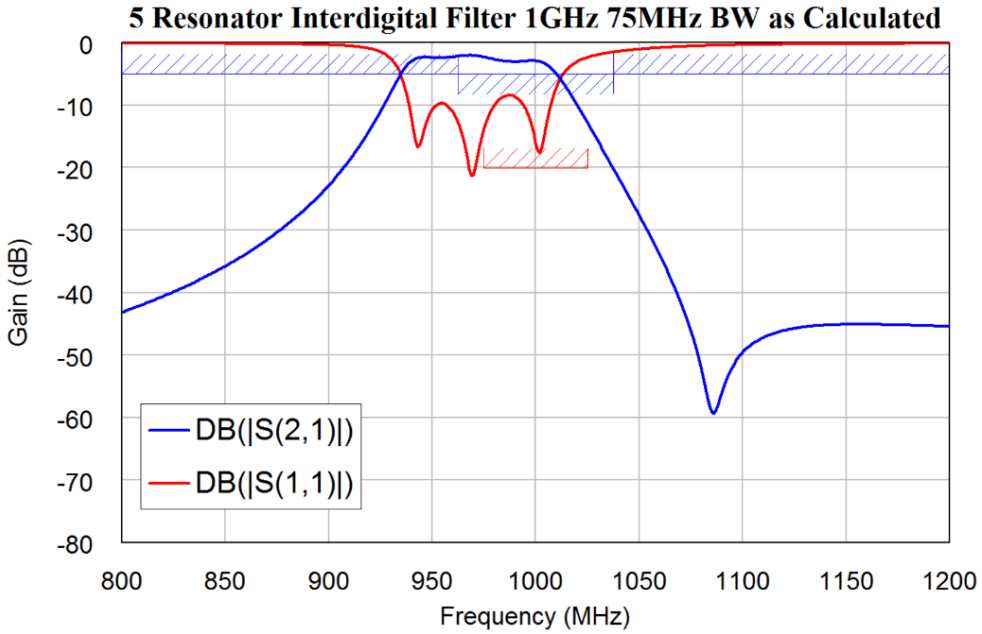



Figure 7.63. Frequency response of the filter of figure 7.62, as calculated.

The filter of figures 7.62 and 63 was optimised to give a 70 MHz bandwidth at a 1 GHz centre frequency, as shown in figure 7.64.

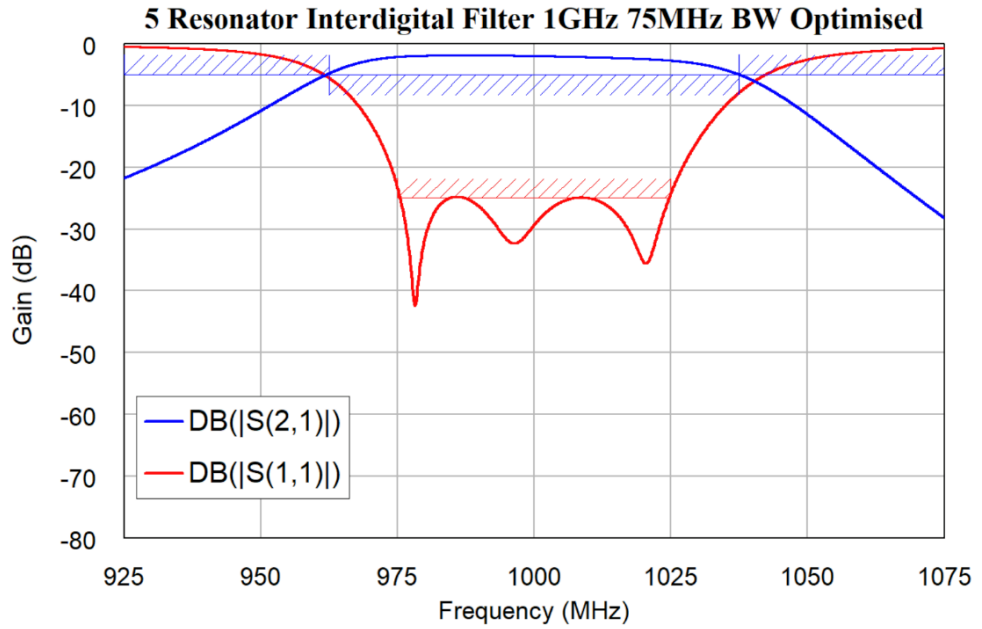



Figure 7.64. Frequency response of the filter of figure 7.62, after optimisation.

When the prototype filter was produced, it was found to be 20 MHz (2%) low in centre frequency, have a passband amplitude response that is slightly sloping and a bandwidth that was too small. To compensate the centre frequency of the designed filter, was shifted to 1.02 GHz and the bandwidth was increased. By optimising for a low return loss in the passband one can ensure that the insertion loss is minimised. The passband attenuation slope is thus due to the changing transmission line losses of the resonators with frequency.

It is possible to specify a sloping passband attenuation to compensate for this, but this will result in a higher insertion loss and a worse return loss. The measured performance of the second filter is shown in blue in figure 7.65 and it has a centre frequency of 984 MHz compared to the 1 GHz specification. The measured bandwidth is 92 MHz compared to the 70 MHz specification. This may be sufficiently close to satisfy the required specifications. If this is inadequate, then another filter needs to be designed.

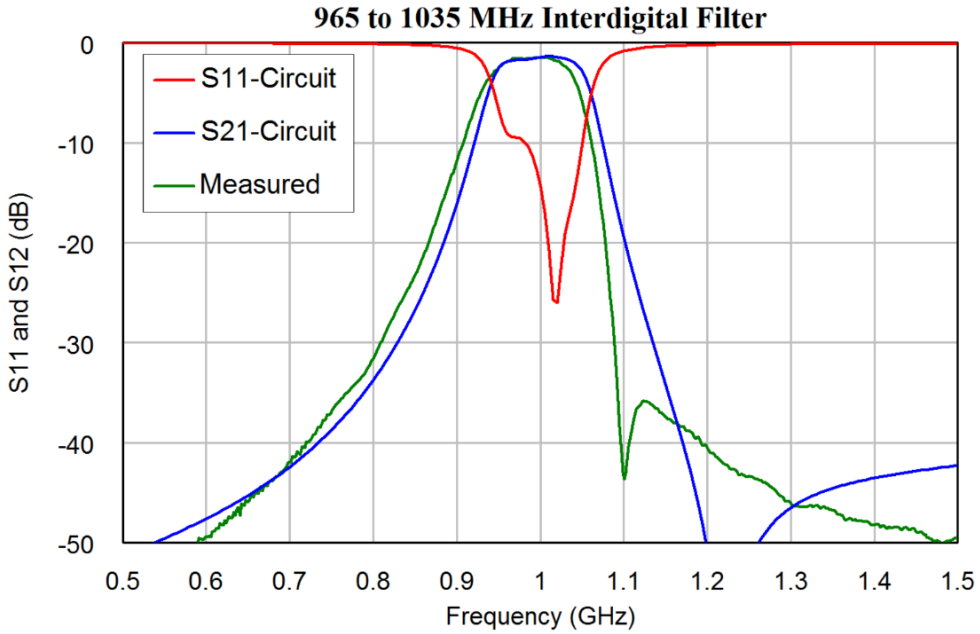



Figure 7.65. Measured and designed frequency response of the interdigital filter.

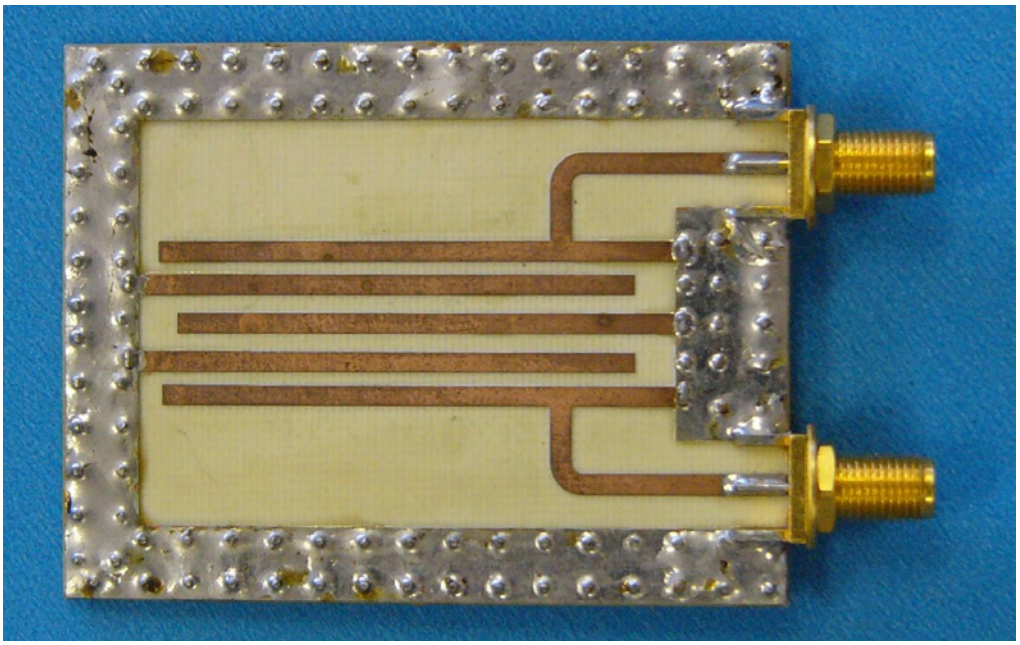


Figure 7.66. Microstrip interdigital filter, 70 MHz bandwidth at 1 GHz.

Figure 7.66 shows the resulting filter realisation. For this realisation, bends are incorporated in the input and output transmission lines, so that the input and output connectors can be mounted on the same panel. Interdigital filters are often used in commercial designs as can be seen in figure 7.67, which is part of a microwave layout produced by Codan in Adelaide, South Australia. Comparing figures 7.66 and 7.67,

shows that the procedure for earthing the grounded end of the resonator to the bottom layer ground-plane is slightly different. The positioning of the vias in figure 7.66 is the most likely cause of the centre frequency being 2% low.

As the number of resonators increases, the stopband attenuation does not significantly increase. As a result, hairpin or direct-coupled filters are a better choice when a very high close-in stopband attenuation is required. Interdigital filters are however smaller than hairpin of direct-coupled filters and they are thus the best filter to use when PCB space is at a premium.

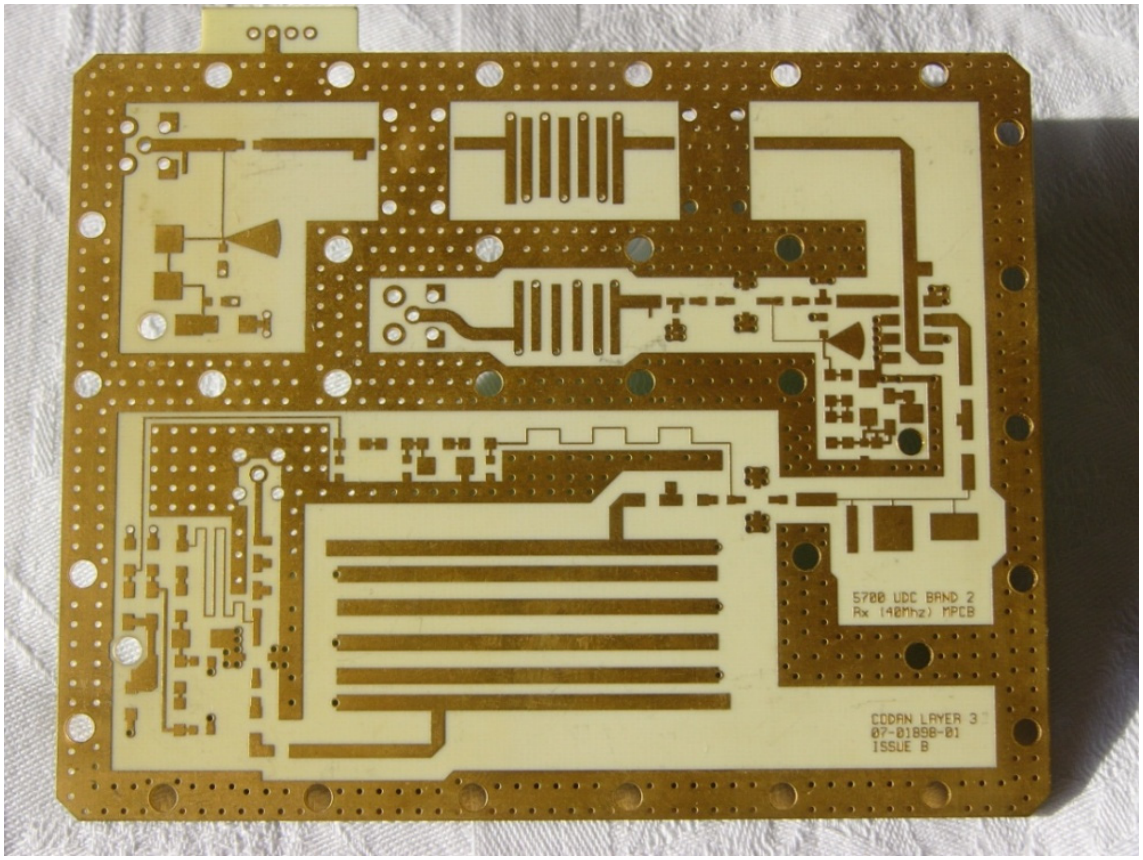



Figure 7.67. PCB showing three interdigital filters. (Codan [15]).

## Direct-Coupled Resonator Filters

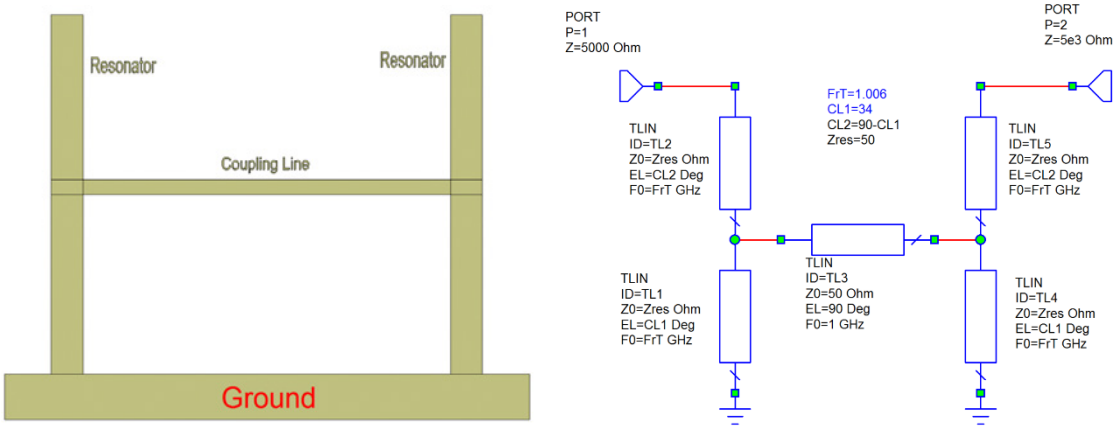



Figure 7.68. Transmission line coupled resonators.

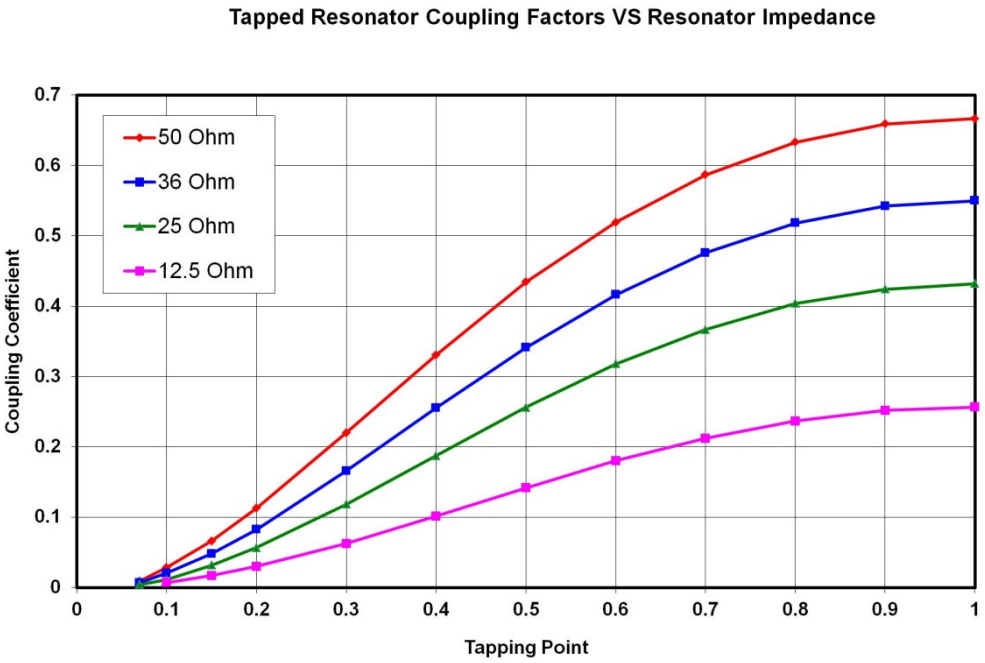



Figure 7.69. Coupling coefficient versus tapping point for different line impedances.

This design technique is also described by the author in [13]. When the percentage bandwidth of the filter becomes greater than 20%, the coupling gaps for interdigital filters become too small to be produced using readily available technology. As a result, a different coupling technique is required. It is possible to couple two resonators using a quarter-wavelength long transmission line as shown in figure 7.70. The coupling can be varied by changing the tapping point. When this is done, graphs similar to figure 7.61 are produced by the circuit of figure 7.68 and from equation 7.30 the coupling coefficient can be determined as a function of tapping point as shown in figure 7.69, since the spacing between the peaks and the bandwidth are known.

## *Example 7.4: 1 GHz, 500 MHz Bandwidth Filter*

The coupling coefficients shown in figure 7.69 can now be applied to the design of a wideband filter. As an example, the design of a 5-resonator Butterworth bandpass filter with a lower 3 dB cut-off frequency of 750 MHz and an upper cut off frequency of 1250 MHz is chosen the filter will thus have a 50% bandwidth.

Equations 4 and 5 give the normalized Q values and coupling coefficients as:

| Normalised | De-normalised for 50% Bandwidth |
|---|---|
| $q_1 = q_n = 0.618$ | $Q_1 = Q_n = 1.236$ |
| $k_{12} = k_{45} = 1$ | $K_{12} = K_{45} = 0.5$ |
| $k_{23} = k_{34} = 0.5559$ | $K_{23} = K_{34} = 0.278$ |

Figure 7.69 shows that different transmission line impedances should be used for different coupling coefficients in order to obtain realistic tapping points. For the filter, 50 Ω transmission lines are used for the input and output resonators, which require the highest coupling coefficients of 0.5. For the other resonators, 36 Ω transmission lines, which have lower losses, are used. Interpolating the tapping points from figure. 7.69, results in the following normalised tapping points, TXLine results in the following resonator line lengths:

| | | | |
|---|---|---|---|
| Resonator 1 | 50Ω | Tap = 0.487 | Lr = 46.96 mm |
| Resonator 2 | 36Ω | Tap = 0.614 | Lr = 44.99 mm |
| Resonator 3 | 36Ω | Tap = 0.426 | Lr = 44.99 mm |
| Resonator 4 | 36Ω | Tap = 0.614 | Lr = 44.99 mm |
| Resonator 5 | 50Ω | Tap = 0.487 | Lr = 46.96 mm |

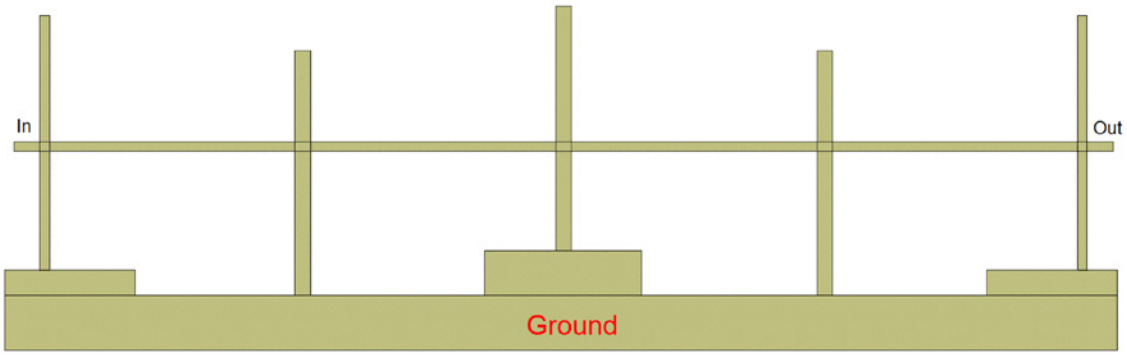



Figure 7.70. Filter layout for initial tap values.

Entering those values in the Cadence AWR DE circuit schematic of the filter, results in the initial filter layout shown in figure 7.70, with the corresponding frequency response shown in figure 7.71. To highlight differences between the 750 MHz and 1250 MHz, corner frequency specifications and frequency-response obtained from the computer simulation, an optimisation mask is superimposed on figure. 7.71. In addition, an optimisation mask for a –1 dB attenuation from 780 MHz to 1220 MHz is shown. It can be seen that the design procedure results in a filter that has a bandwidth that closely matches the design specifications, but whose centre frequency is 3.5% low. This difference is due to the end effect of the open circuit resonators not being taken into account in the above calculations.

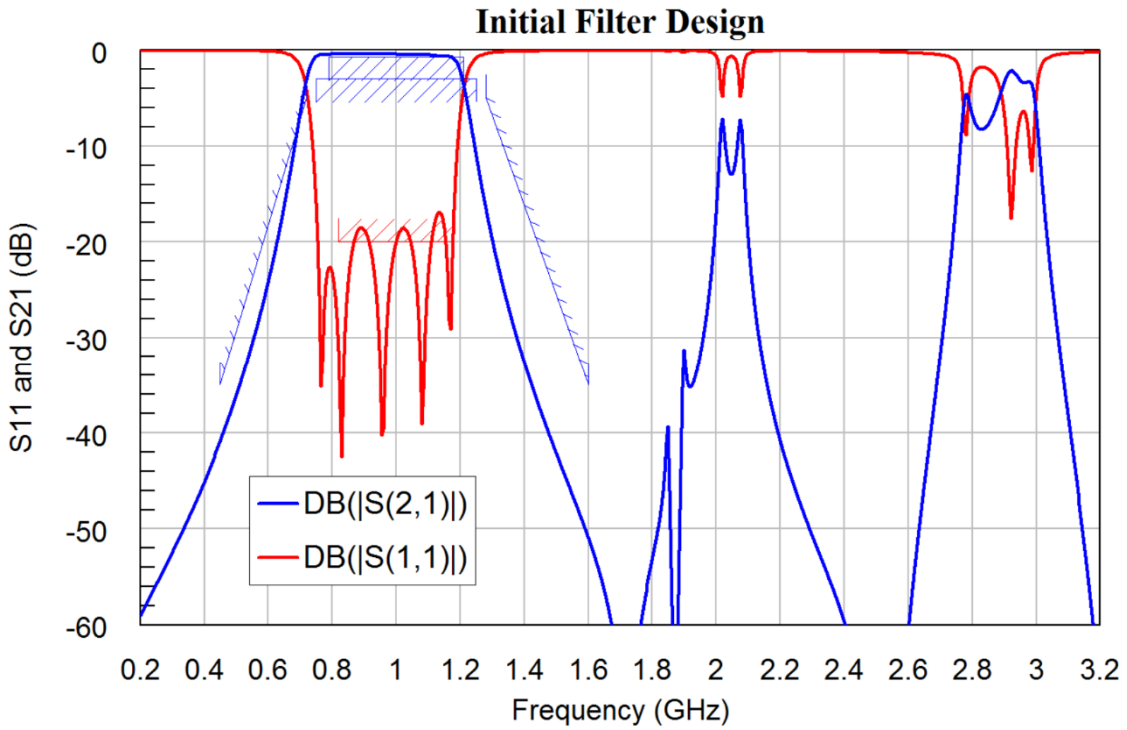



Figure 7.71. Frequency response for initial wideband filter.

## Fine Tuning the Filter

To shift the centre frequency, the length of all the resonators is changed slightly using the 'tuning simulation' capability of Cadence AWR DE. In addition, it is desirable to fine-tune the filter to obtain the lowest insertion loss. This is best achieved by ensuring that the filter has a low return loss. Setting the optimiser constraints on $S_{11}$ to be less than -20 dB and carrying out the first stage of the optimisation process of the filter to meet this return loss as well as the passband specifications results in the following tapping points:

| | | |
|---|---|---|
| Resonator 1 | 50Ω | Tap = 0.5147 |
| Resonator 2 | 36Ω | Tap = 0.5969 |
| Resonator 3 | 36Ω | Tap = 0.4304 |
| Resonator 4 | 36Ω | Tap = 0.5969 |
| Resonator 5 | 50Ω | Tap = 0.5147 |

Figure 7.72 shows the resulting frequency response of the filter after this first stage of optimisation. For a wideband filter implementation like this, the spurious response at the harmonics, particularly that at 2 GHz is unacceptable. To provide better attenuation at those frequencies, stubs need to be added to the filter. Those stubs will distort the frequency response of the filter. In order to minimise the effect of the stubs on the centre frequency of the filter, it is desirable to use two sets of stubs and vary the spacing between the two sets of stubs to provide a low return loss at the centre frequency of the filter. In addition, it is desirable to make the harmonic stubs slightly different lengths, to widen the bandwidth over which good harmonic attenuation is obtained.

In addition, some change in the harmonic response is obtained by changing the length of the coupling lines. Comparing figures 7.71 and 72, for a filter with a quarter wavelength coupling line, with that of figures 7.82 and 85, for a filter with a one-eight wavelength transmission line for the coupling illustrates this effect.

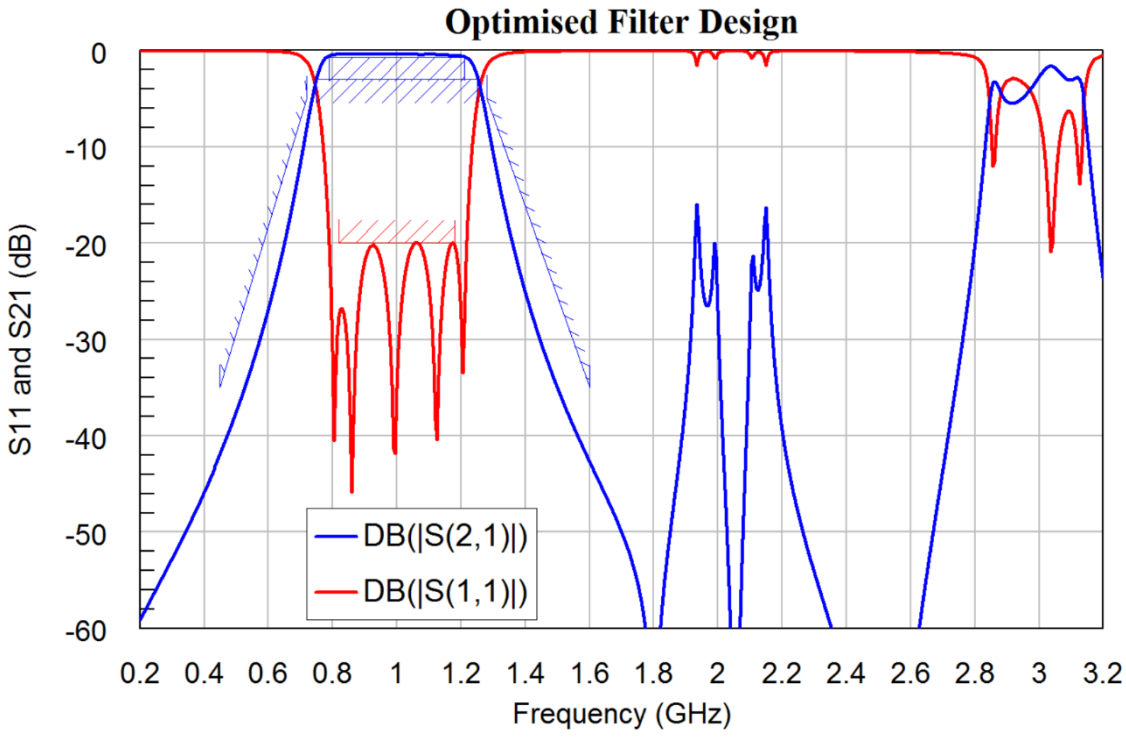



Figure 7.72. Frequency response of the filter after stage 1 optimisation.

The final step in the filter design is to change the layout from a simple design as shown in figure 7.70, to a more compact and easier to manufacture design. To achieve this, the three tiered ground level shown in figure 7.70 is made one level and the coupling transmission lines are folded and bent in order to take up as little space as possible, while connecting to the resonators at the correct tapping points. The harmonic stubs may be folded, as shown in figures 7.46 and 47. The final layout should also ensure that the input and output connectors are in the correct location for mounting the filter. Figure 7.73 is a photograph of the final filter.

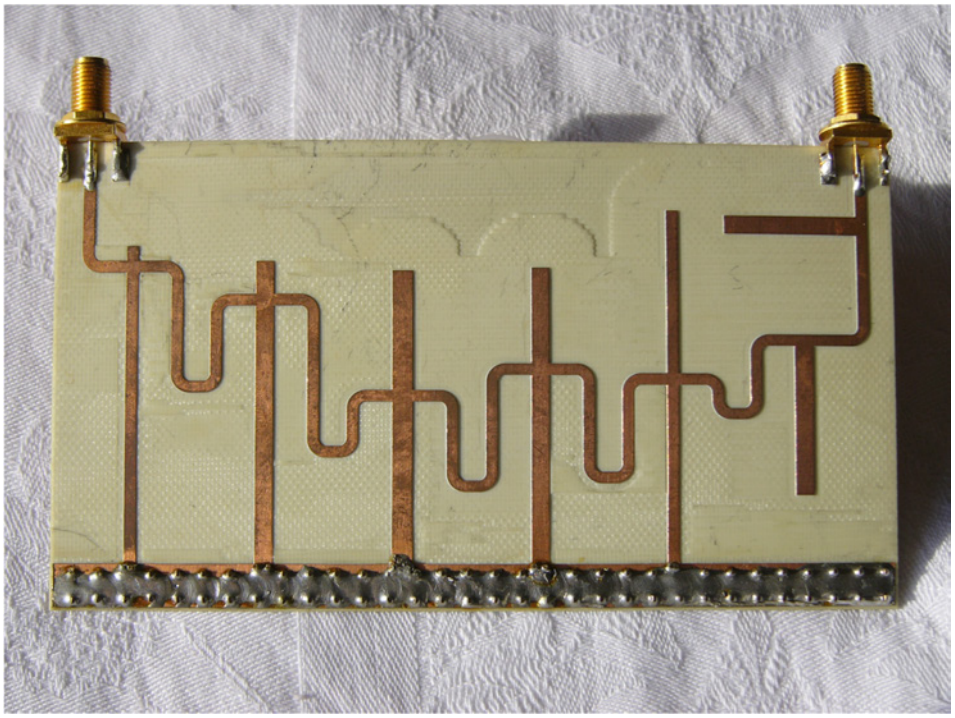


Figure 7.73. 750 MHz to 1250 MHz filter hardware.

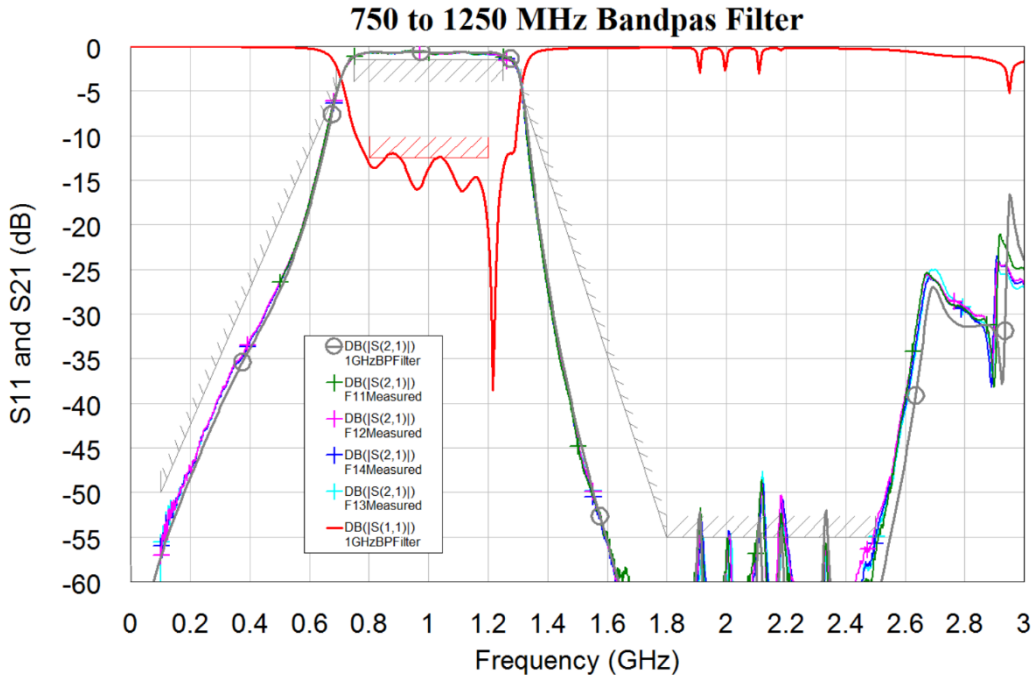



Figure 7.74. Frequency response of the filter of figure 7.73.

Figure 7.74 shows the frequency response of the final filter after optimisation, it also shows the final optimisation limits used. To determine the reliability of the design technique, four filters were constructed. The measured frequency response of those filters is also shown in figure 7.74. It can be seen that the design technique results in highly repeatable filters, whose measured performance agrees remarkably with the results from computer simulation. The agreement between the measured and simulated results for these filters is much better than those for the hairpin filter of figure 7.46, or the interdigital filter of figure 7.65 and 7.66. It should be noted that the right most resonator is significantly larger than the other resonators. This is required to compensate for the effects of the harmonic stubs on the passband response.

## Microstrip Filter Comparison

When designing a Microstrip Bandpass filter, it can be designed as: an interdigital filter, a Combline Filter, a hairpin filter or a direct-coupled resonator filter [14]. Each of these filters have advantages and disadvantages. To highlight the comparative performance of these filters, a 5-resonator filter with a centre frequency of 1 GHz and a 70 MHz bandwidth was designed as using each of these four filter types. The filters were optimised using the same optimisation limits. Each filter has 10 mm tracks connecting to the tapping point to allow a connector to be soldered to that track. The same RO4003 substrate was used and all resonators are 3 mm wide. For each of the filter types, a simple test circuit like those shown in figures 7.60, 7.61 or 7.68 is used. The tapping and coupling test circuit for the Combline filter, is shown in figure 7.75 and that for the hairpin filter is shown in figure 7.76.

The input tapping for all these four circuits is adjusted to obtain frequency responses like figures 58 and 59, but with the bandwidths as per equations 29 and 30 for the relevant filter. Since the centre frequency, bandwidth and the number of resonators for these filters is the same as those of figures 58 and 59, exactly the same responses should be obtained. The coupling tuning, can be done most accurately when the end resonator loading is reduced as done in figures 7.75 and 7.76.

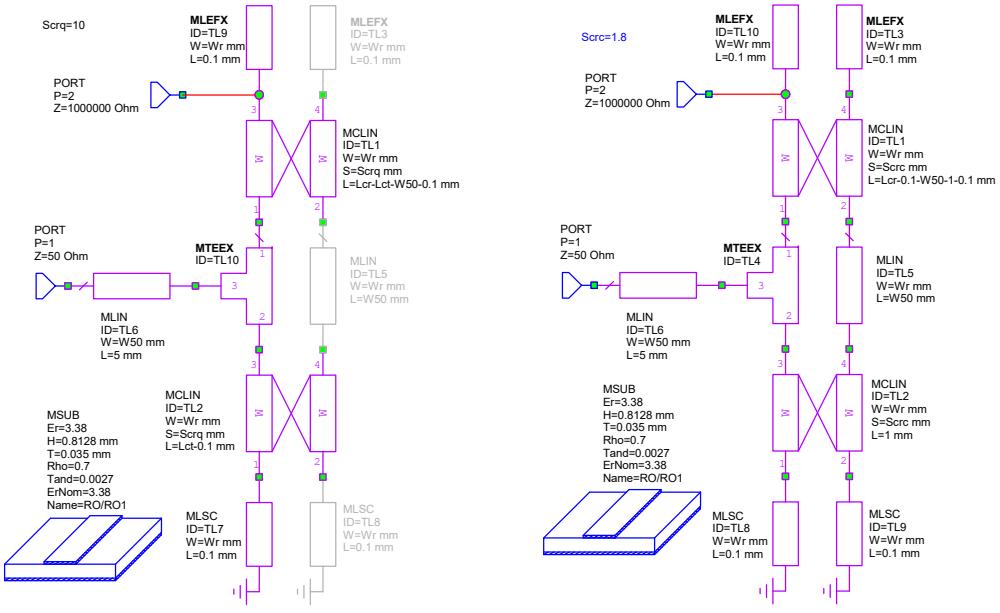



Figure 7.75. Resonator loading and coupling test circuit for Combline filters.

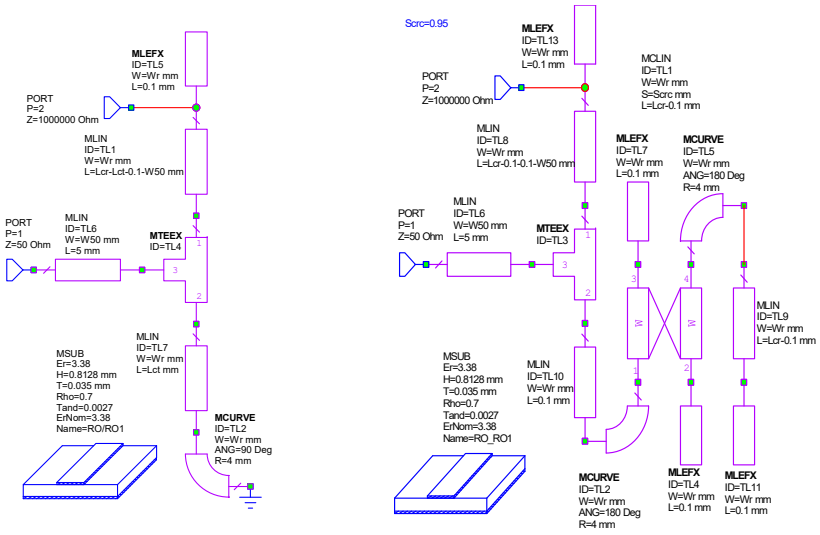



Figure 7.76. Resonator loading and coupling test circuit for hairpin filters.

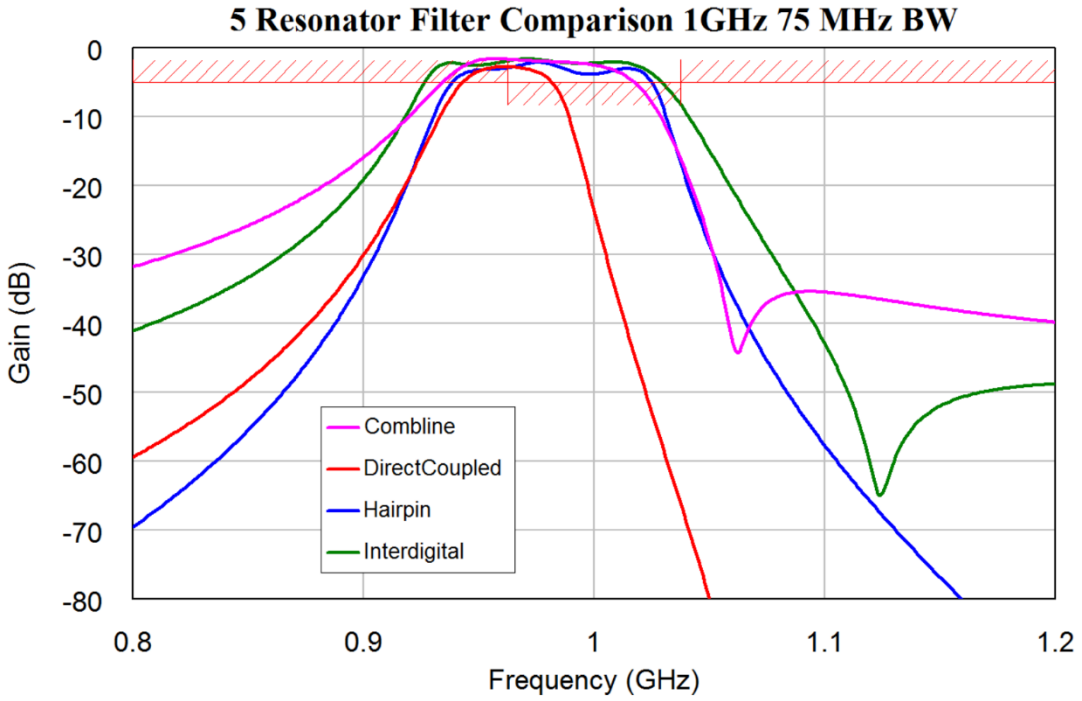



Figure 7.77. Filter performance with parameters as calculated.

Figure 7.77 shows the initial frequency response of the four 5-resonator filters, when the tapping and coupling gaps are set to those calculated using the test circuits.

The performance of all these filters is close enough that the specifications can be met using some simple optimisation. The tuning and optimisation is best done in three stages: Firstly adjust the resonator length using manual tuning, to give the correct centre frequency. The second step is to fine-tune the coupling gaps and tapping points using optimisation, to get as close to the requirements as possible. The final step is to allow the individual resonator lengths to be optimised as well as further minor optimisation of the coupling gaps and resonators. Since there is a significant interaction between the parameters to be optimised, the local random optimisation is most likely to result in the best optimisation. If the optimisation gets stuck, changing the weight of the worst error may get the optimisation out of the local minima and thus result in lower error costs.

Figure 7.78 shows the final performance of the filters after optimisation. The hairpin filter has a good symmetrical filter response and has good stopband attenuation. The direct-coupled resonator filter has a better higher frequency attenuation, but a poorer lower frequency attenuation. The interdigital filter has a poorer attenuation characteristic, compared with the other filters. In particular, the attenuation near 1 GHz is only 50 dB. The Combline filter has the worst close-in stopband attenuation of these filters. Combline filters are used less often than interdigital filters.

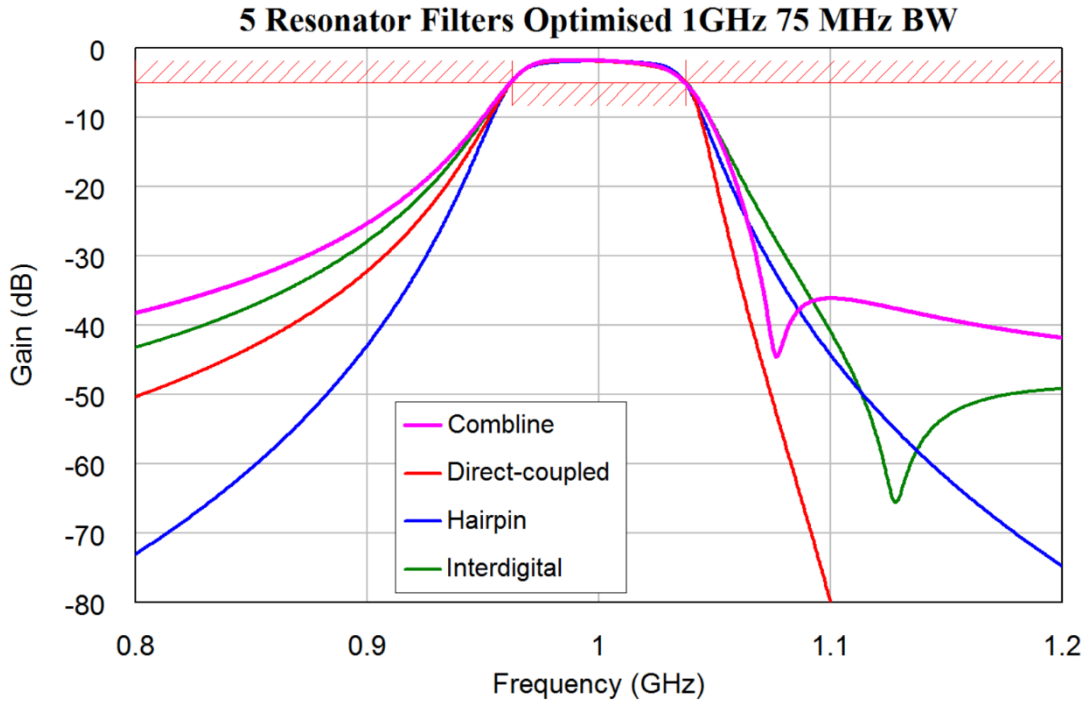



Figure 7.78. Frequency response of three 5-resonator filters.

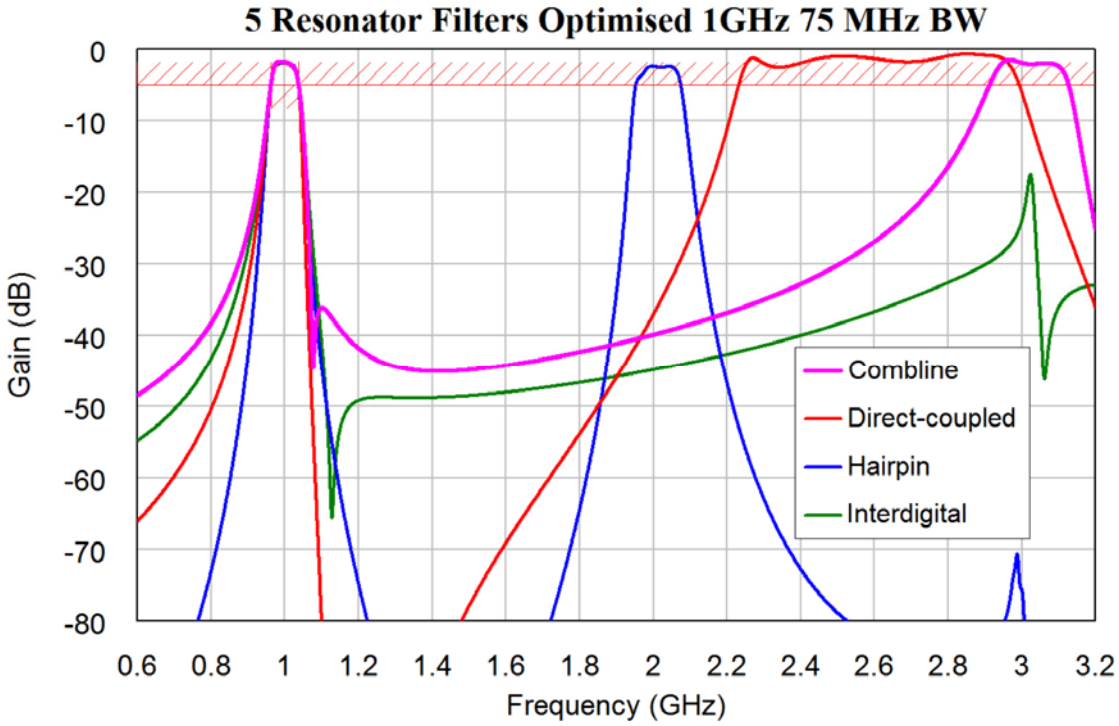



Figure 7.79. Harmonic response of the filters of figure 7.73.

Figure 7.79 shows the frequency response of the four filters at the harmonics of the 1 GHz passband. For the direct-coupled resonator filter the lengths of the coupling lines was 12.5% of a wavelength, which is half of the length of the coupling lines used for the filter in figure 7.73. This resulted in a lower harmonic attenuation. The direct-coupled filter has the best close-in stopband attenuation, but the worst stopband attenuation above 2 times the centre frequency. The second harmonic response from the hairpin filter is significant, but can be removed using harmonic stubs. The interdigital filter does not have a significant harmonic response, but it does not have a very good stopband attenuation either. The stopband attenuation for interdigital filters does not significantly improve with filter order. The Combline filter is the smallest, occupying 41 x 60 mm. The interdigital filter is slightly larger occupying 42 x 60 mm. The direct-coupled resonator filter, occupies 75 x 60 mm and the hairpin filter is the largest, occupying 78 x 68 mm.

Figures 7.80 to 7.81 show the hardware of the four filters, approximately to the same scale. The Combline filter is slightly smaller than the interdigital filter, but in most instances, there is not enough space saving to warrant the worse stopband attenuation.

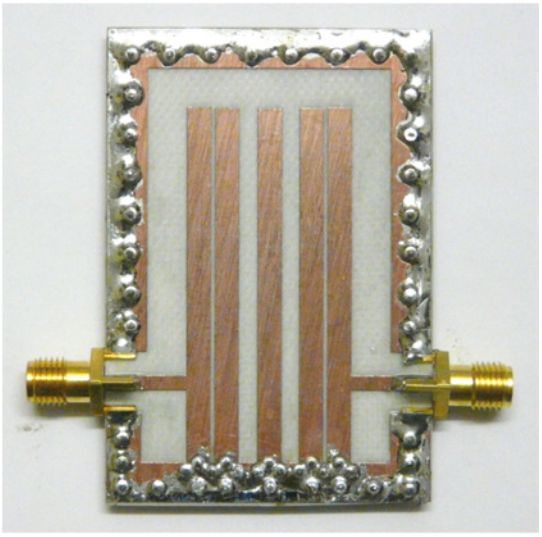


Figure 7.80. Interdigital filter hardware.

(42x60mm)

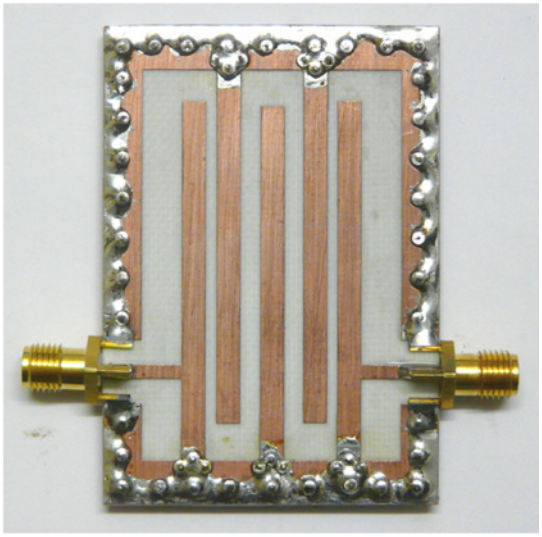


Figure 7.81. Combline filter hardware.

(41x60mm)

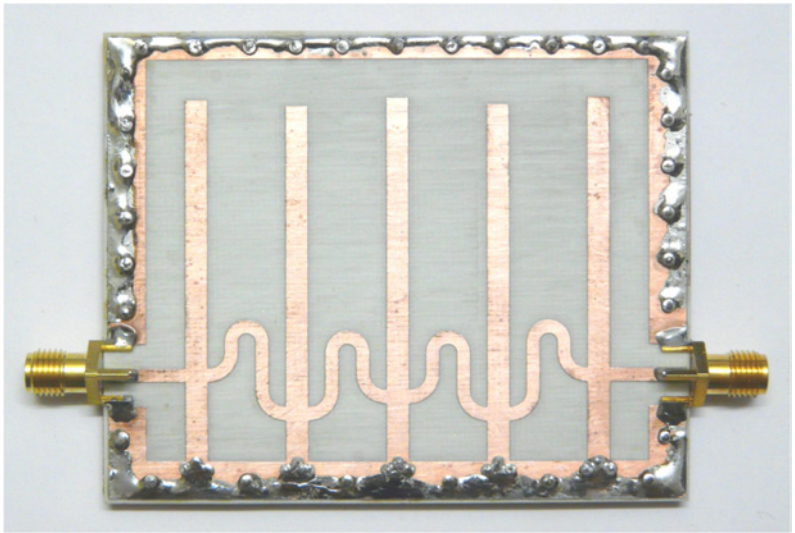


Figure 7.82. Direct-coupled filter hardware. (75x60mm).

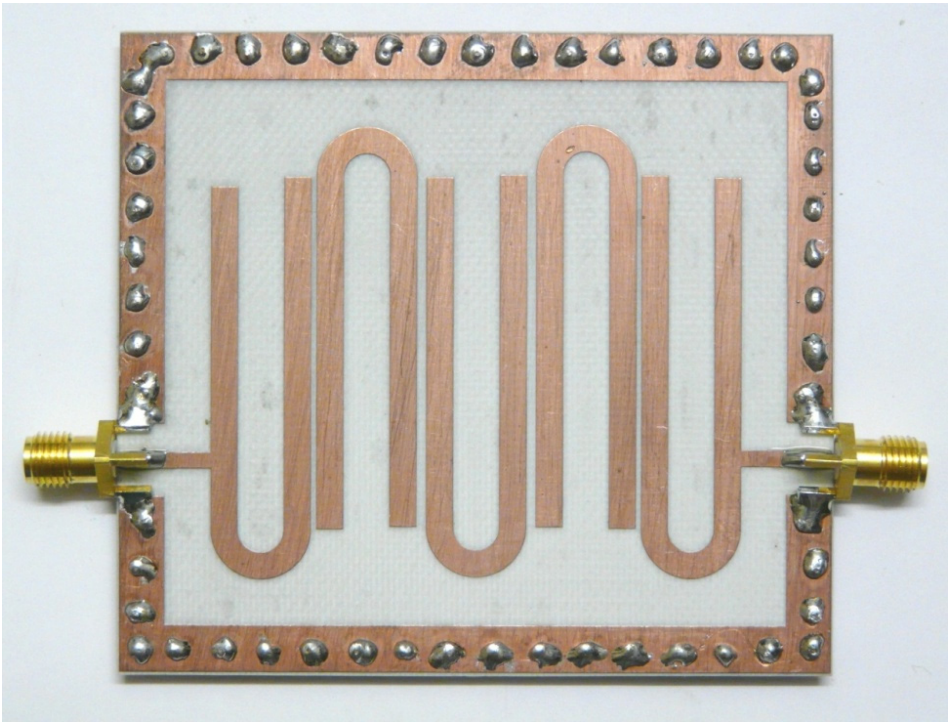


Figure 7.83. Hairpin filter hardware. (78x68mm).

Figures 7.84 to 7.87 show the measured frequency responses of the filters. Comparing these with figures 7.78 and 7.79, shows the remarkable agreement between the calculated and measured results. The passband of the interdigital, combline, and direct-coupled filters are a few percent lower than calculated. The difference matches the length of the pins used in connecting the grounded end of the resonators to the ground-plane on the bottom of the PCB. This can be taken into consideration in the second iteration of the filter designs if needed.

The hairpin filter has a measured centre frequency that is very close to the desired 1 GHz centre frequency. This is due to no ground connections being required, thus removing an uncertainty of pin or via placement from the design. From the measured passband responses, hairpin filters have a better close in stopband attenuation and a more accurate centre frequency are thus a good choice for one off designs, where the performance has to be correct first time. The frequency error between the measured and calculated centre frequency for the interdigital, combline and direct-coupled filters, closely responds to the resonator length equal to the thickness of the substrate.

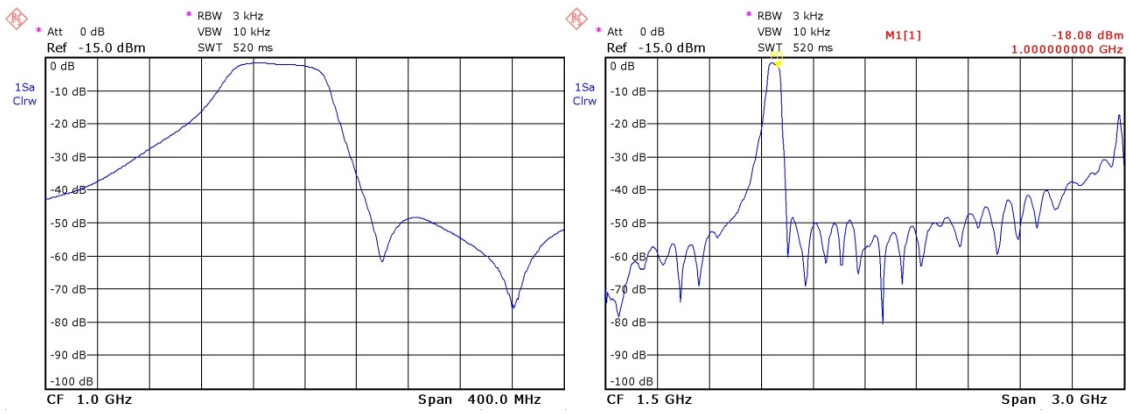



Figure 7.84. Measured frequency response of interdigital filter.

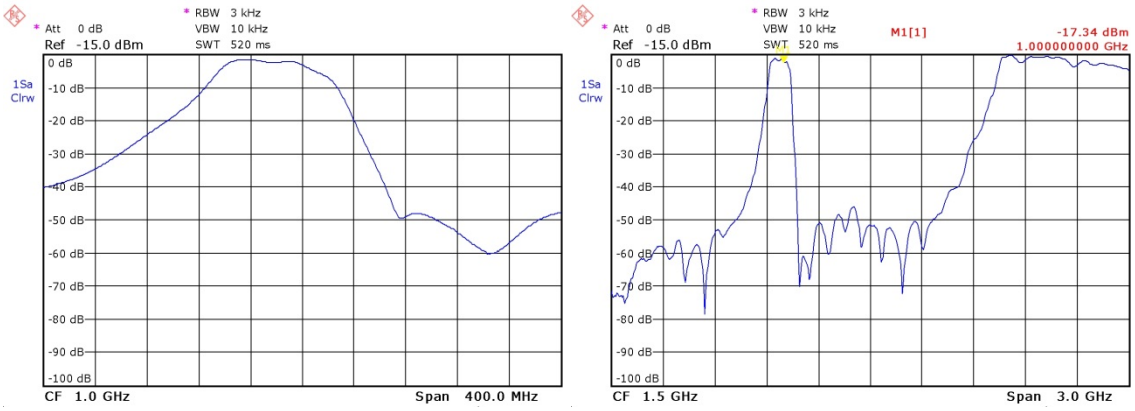



Figure 7.85. Measured frequency response of combline filter.

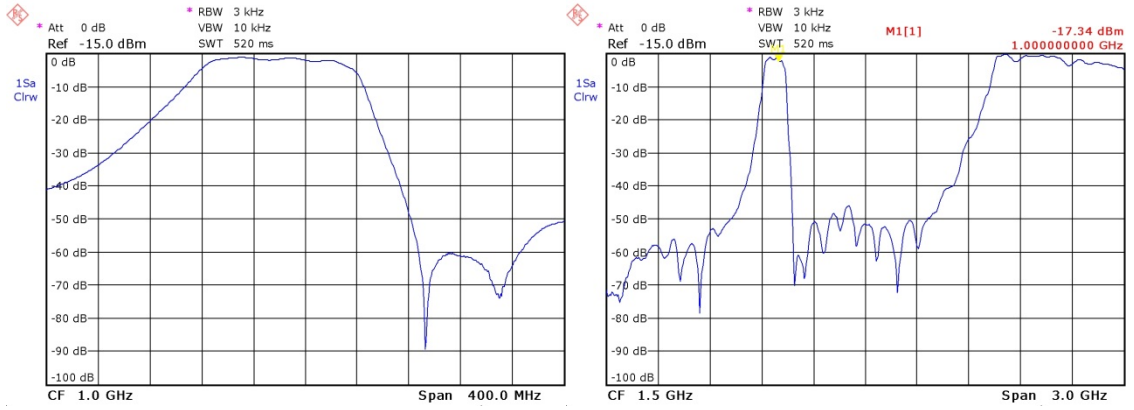



Figure 7.86. Measured frequency response of direct-coupled filter.

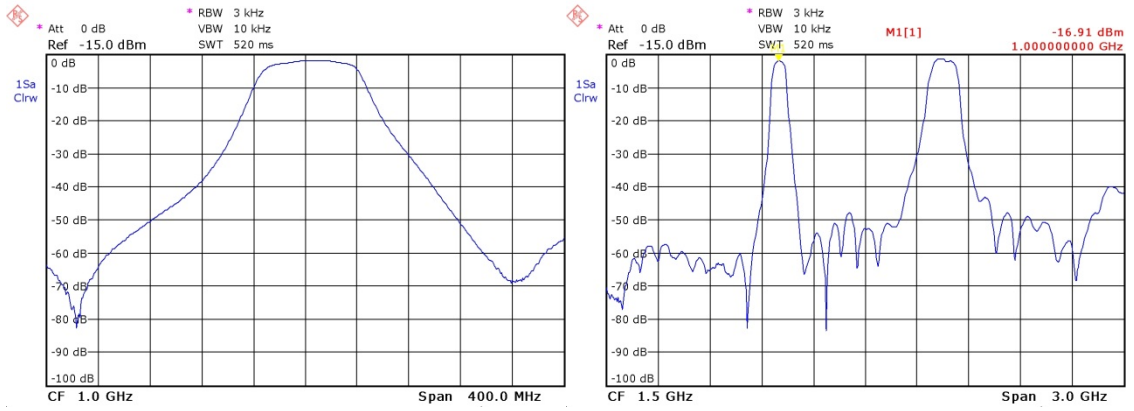



Figure 7.87. Measured frequency response of hairpin filter.

# EM Simulation

Prior to Cadence AWR DE Version 10, it was very time consuming to prepare a circuit, like the hairpin filter in figure 7.83, for an EM simulation. In version 10, *circuit extraction* was introduced. That allows the simple conversion of the circuit to an EM model for EM simulation to be carried out. The EM simulation speed improved significantly in version 13, making it now practical to use EM simulations as part of the design process.

The hairpin filter of figure 7.83, was designed and optimised using circuit simulation only. To minimise the effect of frequency response changes when this circuit is mounted

in an enclosure, a grounded track, connected with vias to the ground-plane was included in the PCB layout as shown in figure 7.83. EM simulation allows the designer to ensure that the grounded ring around the circuit does not cause any unwanted changes to the circuit's performance, by including an analysis of the coupling between the filter and the grounded ring. To illustrate the process, an EM simulation of the hairpin filter of figure 7.83 is now described.

The first step is to ensure that all circuit elements can be EM extracted. Select each element in turn and select *Properties* ⇒ *Model Options* and ensure a "✓" is placed in the *Enable* checkbox of the *EM EXTRACT Options* window. Add the *EXTRACT* element to the circuit diagram, by selection *Draw* ⇒ *More Elements* ⇒ *Extraction Control Block,* or *CNTRL-L* and place the Extract element on the circuit schematic, as shown in figure 7.88.

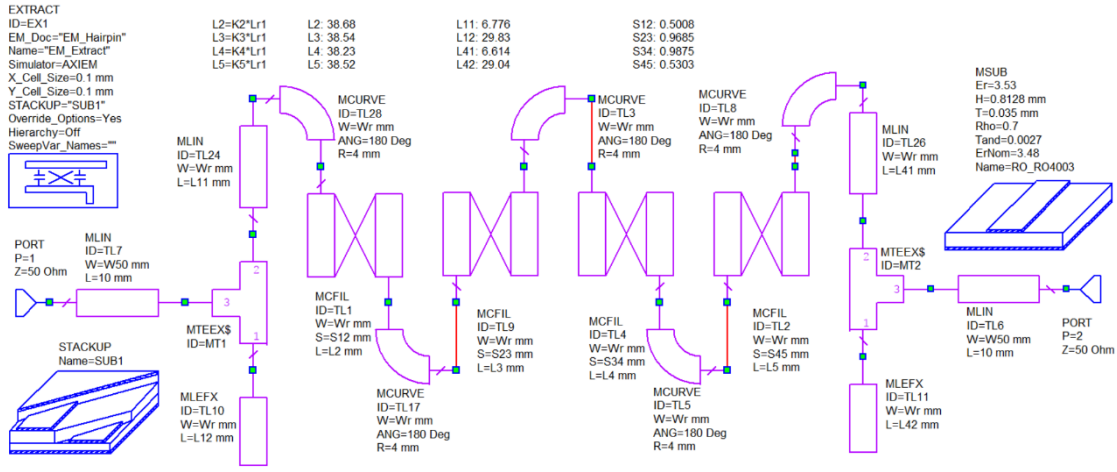



Figure 7.88. Hairpin filter circuit with EM control elements added.

There are several different EM simulators available, as can be seen from the drop-down selection for the simulator in the EXTRACT element. Analyst allows arbitrary 3-dimensional components to be simulated. In this case, a much simpler 3D planar EM analysis is required. The hairpin circuit is fairly complex, as a result AXIEM is used in this example. It is gives good results and is much faster than EMSight. Select AXIEM in the Simulator dropdown box of the EXTRACT control element. Right clicking on EXTRACT shows which circuit elements are included in the extraction, by highlighting them in red. Ensure that all circuit elements are included.

From the circuit element catalogue select *Substrates* ⇒ *STACKUP* and add the Stackup element to the circuit diagram and give that a suitable name if required. Add the Stackup circuit element name to EXTRACT using the STACKUP dropdown box in the EXTRACT element. Left click on the STACKUP element and set $E_r$ and other the material definitions and other properties to match the substrate and conductors to be used. For the *Line Type* property, select *Initialise* to match the *Line Type* used to the circuit diagram layers. The Line Type of *Top Copper* and the Material Name *Copper,* is used in the circuit of figure 7.88. Repeat this process for any other circuits to be simulated at the same time. Initially use the default settings for the EXTRACT element. Since the EM simulation can take a reasonable time, for the initial EM simulation, set the X and Y cell sizes to 1 mm, until the simulation completes without errors after which the cell sizes can be reduced. Reducing cell sizes will increase the accuracy and the time required to complete the simulation. For example, simulation of one of the enclosures used in the

AWR DE files for figures 7.88 to 7.94, on a modern laptop, takes about 9 minutes using a 1 mm cell size, 25 minutes using a 0.1 mm cell size and more than 5 days using a 0.01 mm cell size. Before starting an EM simulation, make sure that all the elements in the layout are snapped together. The first time the simulation is run, the EM structures corresponding to the STACKUP element are created. Check that there are no errors, which could affect the accuracy of the simulation. After the first simulation, right click on the enclosures in the *EM Structures* and ensure that the materials are defined correctly and that the layers are set up correctly, if not correct those in the STACKUP element.

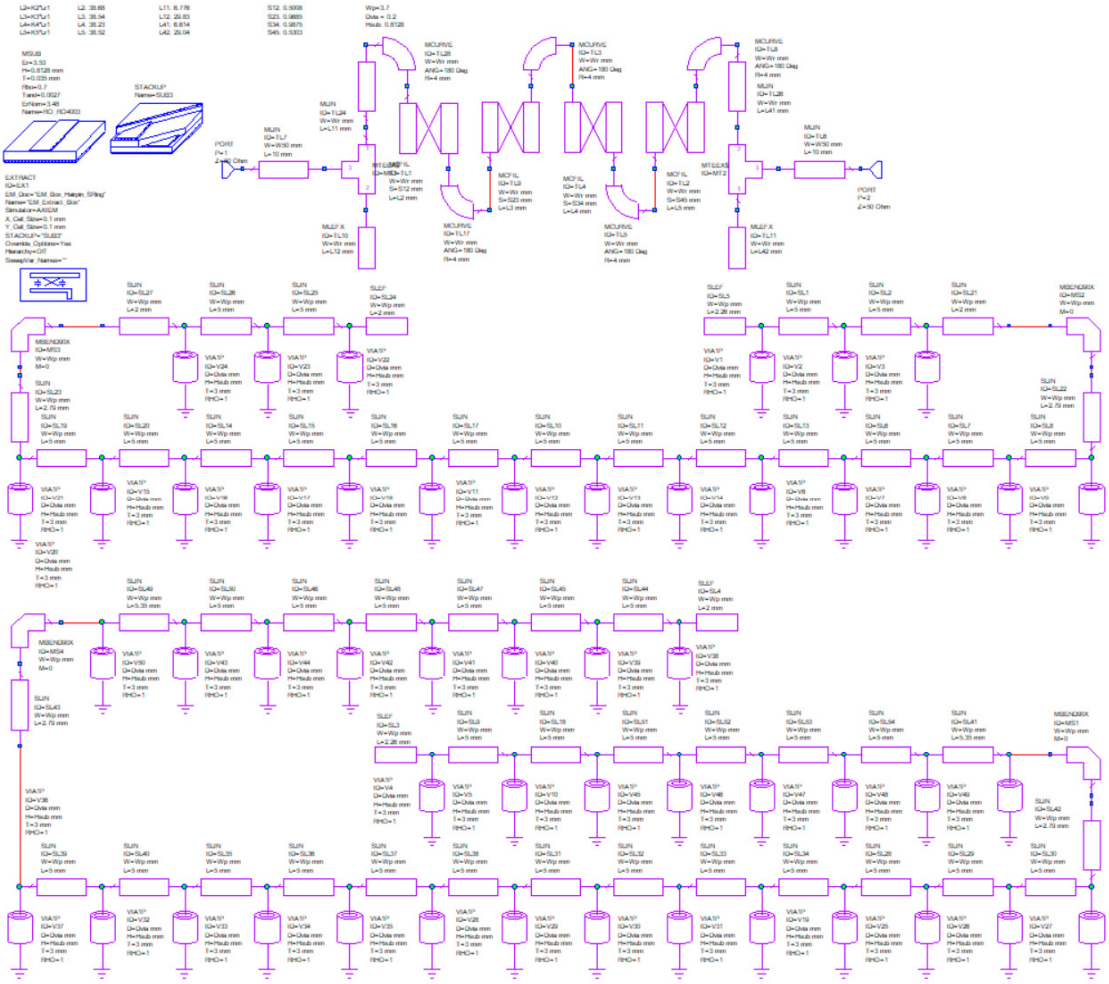


Figure 7.89. Hairpin filter circuit with EM control elements and shielding ring added.

The Cadence AWR DE project file for the comparison between the circuit and EM simulation of the hairpin filter, as presented in figures 7.88 - 7.94 has 5 circuits in it. The numbers in the labels in figures 7.94 and 7.95 correspond to the numbers for the circuits in the following descriptions. The first circuit (1_Hairpin Circuit) is the hairpin circuit schematic used to produce figure 7.83, including the grounded ring, which surrounds the PCB, made using the MCFIL element for the coupling of the resonators. The second circuit (2_Hairpin EM) is an EM simulation of the filter circuit only, without the PCB border.

The third circuit (3_Hairpin EM PCBRing) is the same as the first circuit, but with the grounded PCB border ring made up from transmission lines with vias spaced approximately 5 mm apart, added, as shown in figure 7.89. The EM simulation of

figure 7.89 includes the coupling between the hairpin filter and the grounded PCB border ring. Comparing the EM simulation of the hairpin only circuit with the EM simulation of the hairpin with the PCB border, allows the effect of the PCB border to be evaluated.

The fourth circuit (4_Hairpin EM Box_PCBRing) is the same as the third circuit, except that copper walls are used for the EM structure in STACKUP and a copper top boundary is used 25 mm above the circuit board. That matches a typical mounting of the circuit board in a metal box enclosure. Varying the height of the top boundary above the circuit board will allow the smallest enclosure size to be determined. Note that AXIEM ignores the sidewall boundary conditions, however the PCB border shown on figure 7.83 minimises any fields at the side boundaries, so that there is no practical difference between having no sidewall or a copper sidewall.

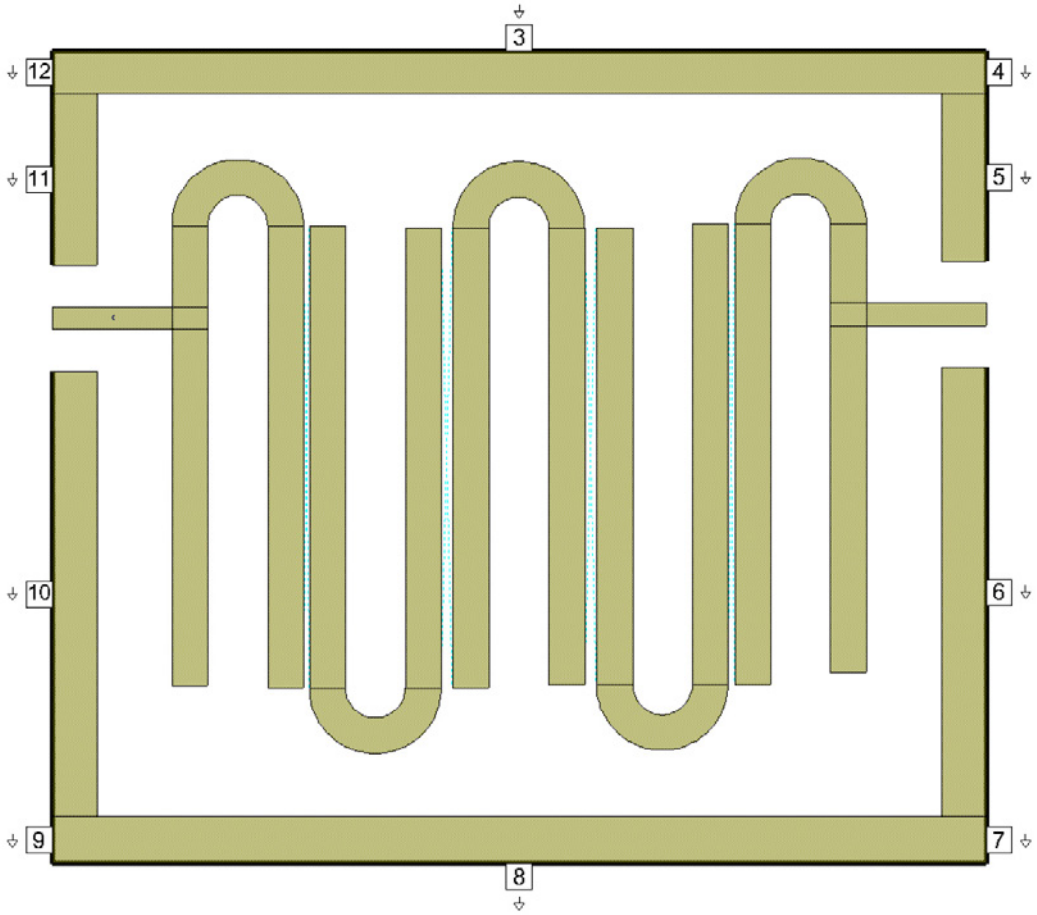



Figure 7.90. PCB border simulation using grounded extraction ports.

The fifth circuit (5_Hairpin EM EPort_PCBRing) uses the layout of the first circuit and places Extraction Ports on the outer edges of the shapes making up the PCB border. This is done by selecting one of the shapes, *Selecting Draw* ⇒ *Extraction Port* and placing the port on the outside edge of the board. Then select the properties of the extraction port by double clicking on it. Use the *Explicit Ground Reference* dropdown window to set the port to *"Connect to lower"*. That will then earth the shape and show a ground symbol on the layout. Right-click on the shape and select *Shape Properties*. Enable EM extraction and set the group name to the name of the EM Extraction element on the circuit schematic. This process is repeated for all the shapes. The resulting layout is shown in figure 7.90. It should be noted that circuit 1, 3, 4 and 5 all have exactly the same layout, but that the PCB border is treated different in their simulation.

This technique of using extraction ports on the PCB border was used for including the PCB border shown in figure 7.46 in the EM simulations shown in figures 7.51 and 7.52.

Since the layouts for each of the EM simulations are different, a different extraction name needs to be used for each of the EM simulations. To produce the circuit schematic for circuit 4, the schematic for circuit 3 (3_Hairpin EM PCBRing) was duplicated and renamed "hairpin EM Box_PCBRing". The extraction *Group Name* of each of the elements then needs to be changed from: *EM_Extract* to *EM_Exctract_Box*. This is done by viewing the layout of circuit 5, selecting all and then selecting Element Properties and in the *Model Options*, change the *Group Name* to EM_Extract_Box. That will change all the elements at once.

Before any EM simulation is carried out check that all the elements are linked to the EXTRACT element in the schematic, by left clicking on it. All the linked elements show up in red. While keeping the EXTRACT element selected, select *View* ⇒ *View Layout*. All the elements to be included in the EM simulation, should be shown in red and should all be joined correctly.

All the 5 circuits can then be simulated. If the EM simulation fails, some Extraction Control Block Properties may need to be changed. Firstly ensure the values are set to their default values, as V13 has different simulation settings to earlier versions. This is done by right clicking on the "extract element". Then selecting properties and in the *Extraction Control Block Properties* window, select *AXIEM* and click *reset defaults*. If this fails to resolve the problem, change the parameters that caused the simulation failure as shown in the status window.

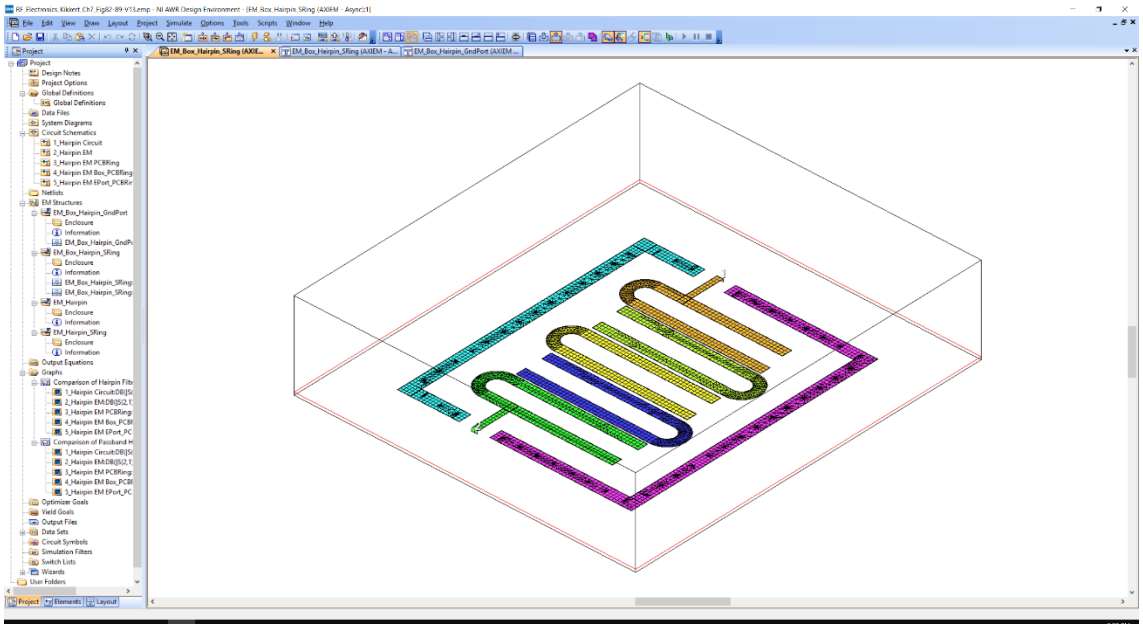


Figure 7.91. 3D Layout of hairpin filter of figure 7.89 with mesh shown.

AXIEM produces a mesh for the circuit layouts and uses those meshed elements to perform the EM analysis. To see the mesh, select the relevant structure in *EM Structures* such as: *EM_Box_Hairpin_SRing* of figure 7.91, right click on that structure and select *Mesh*. Selecting *View* and *View EM Layout*, will show the 2D mesh, as shown in figure 7.92. Note the way that the meshing is performed in the bends of the hairpin filter. Figure 7.93 shows a close-up of the meshing applied to the bends of the hairpin filters for the AXIEM simulation (left) and the EMSight simulation (right). It can be seen that

AXIEM uses less mesh elements and models the shape of the bend more accurately than EMSight. Requiring more mesh elements results in a slower simulation. Using a cell size of 0.1 mm and a typical computer, both circuits of figure 7.88 and 7.89 take 25 minutes to complete using AXIEM, but the circuit of figure 7.88 alone took more than 2 days to complete using EMSight and gave several warnings about convergence, thus producing an incorrect result. EMSight will be more accurate than AXIEM to use on simple couplers, like the one shown in figures 4.39 to 4.45.

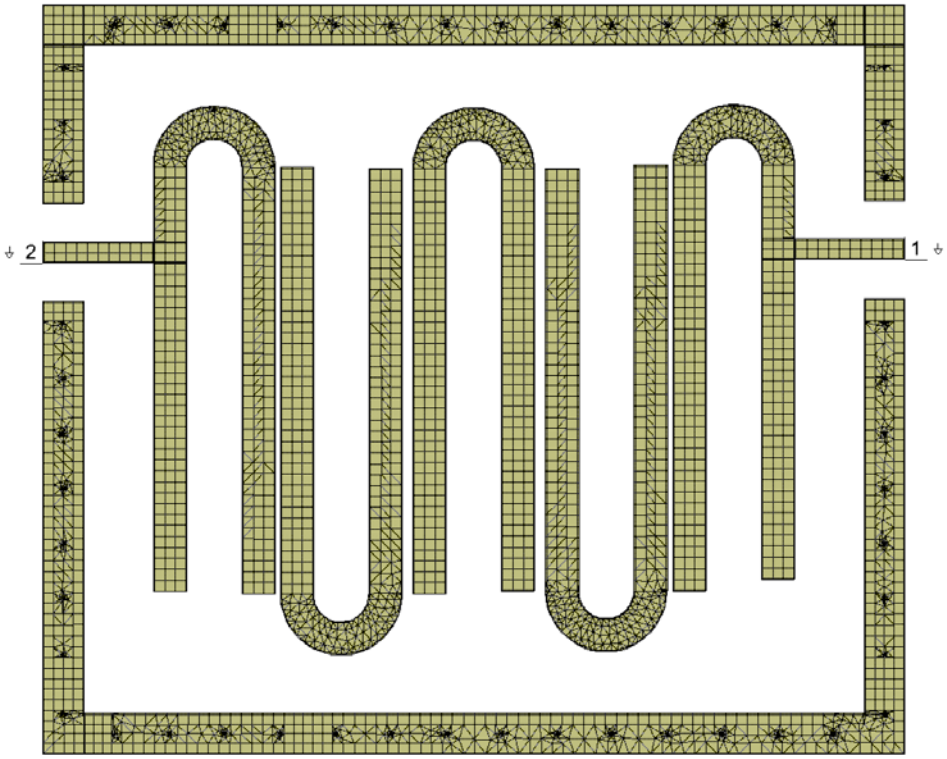



Figure 7.92. 2D Layout of hairpin filter of figure 7.89 with mesh shown.

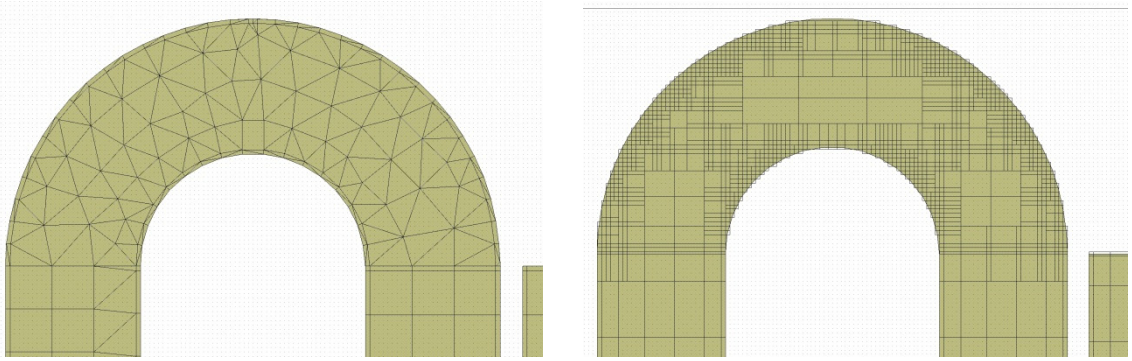


Figure 7.93. Close up of meshing applied by AXIEM (Left) and EMSight (Right).

For the filter design and optimisation, circuit simulation with $E_r$=3.38 and $E_{rNom}$=3.38 was used. Rogers in their datasheet [16] for R04003 specify $E_r$ =3.38 and suggest that $E_r$ = 3.55 is used for simulation. The circuit and EM simulation shown in figures 7.51 and 7.52 used $E_r$ = 3.38 for all simulations and the EM simulations are very close to the measured results. For the filter of figure 7.83, the circuit simulation shown in figures 7.94 and 7.95 with $E_r$=3.38 gives the desired 1 GHz centre frequency and $E_r$ = 3.53 gives the desired 1 GHz centre frequency for the EM simulation.

A Change of $E_r$ from 3.38 to 3.53 gives a 2% change in centre frequency. The circuit and EM simulations centre frequencies will thus differ by 2%, as shown in figure 7.51 (for same $E_r$) and figure 7.94 (different $E_r$). The difference between the desired and measured centre frequency of the circuit in figure 7.46 is 30 MHz (3%), as shown in figure 7.51. For the filter in figure 7.83, it is 5 MHz (0.5%), as shown in figure 7.87. The filter in figure 7.46 uses 1.75mm wide resonators and the filter in figure 7.83 uses 3mm wide resonators. The wider resonators result in a lower insertion loss and less impedance errors due to inaccuracies in milling or etching of the PCB.

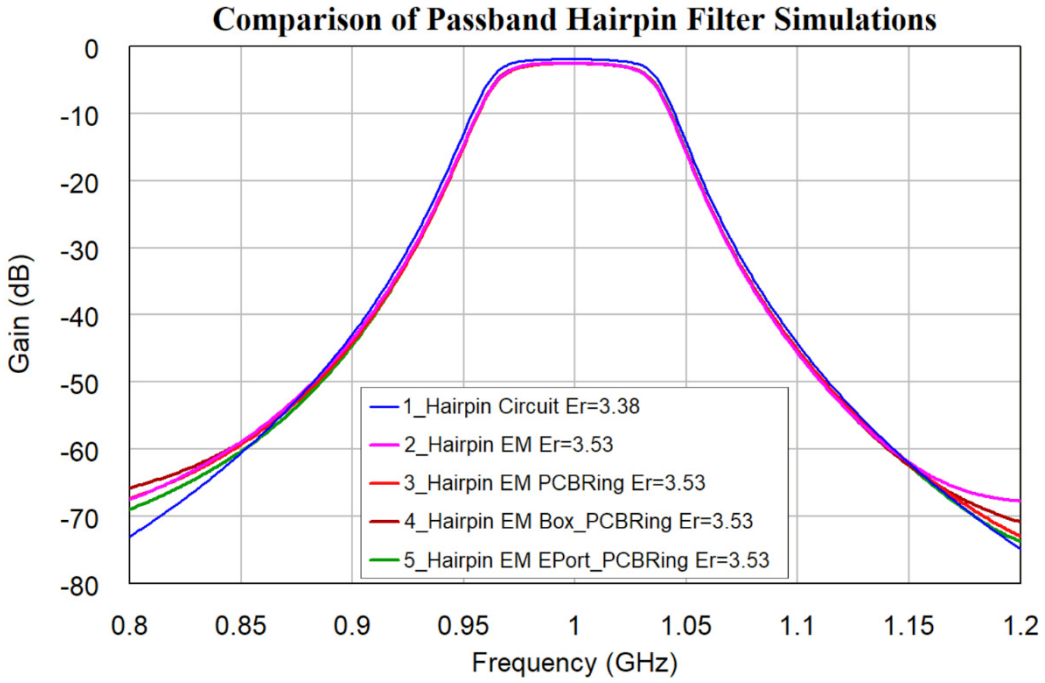



Figure 7.94. Passband Frequency response of Circuit and EM simulations of the hairpin filter.

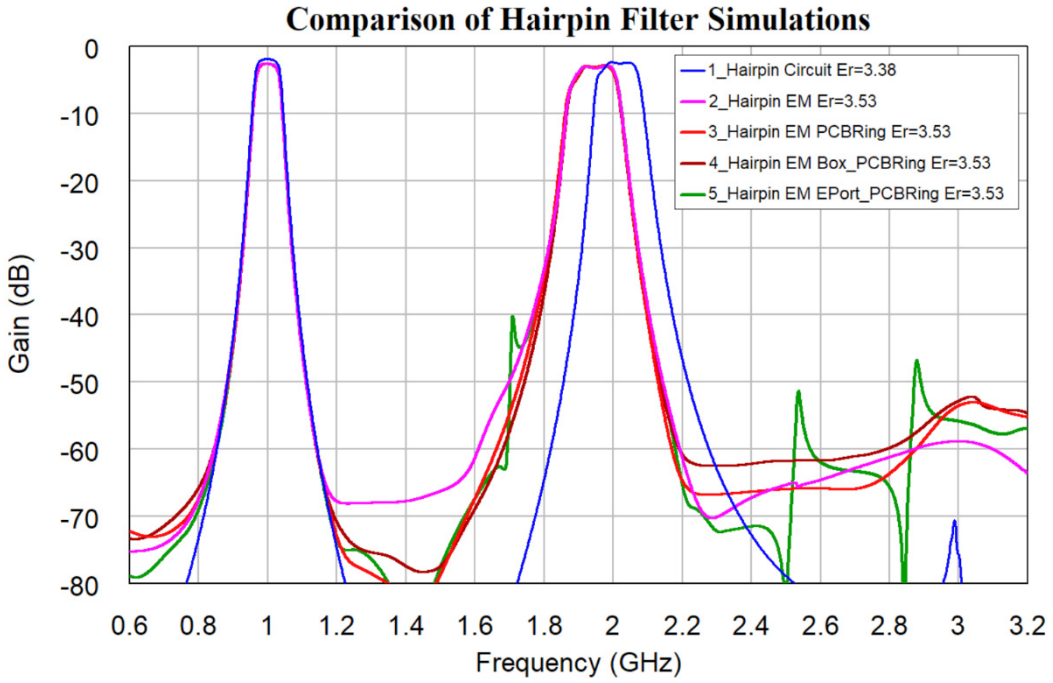



Figure 7.95. Passband Frequency response of Circuit and EM simulations of the hairpin filter.

Figure 7.94 shows a very good agreement in the passband for the 4 different EM filter simulations. That also shows that the screening ring or the top boundary conductor does not affect the passband response.

Figure 7.95 shows the harmonic response of the 5 filter simulations. The EM simulation of circuits 3, 4 and 5, those with the boundary ring, show a lower attenuation in the 500 MHz to 750 MHz frequency regions.

The second harmonic response of the filter is shifted in the EM simulation compared to the circuit simulation. The measured frequency of the second harmonic response on figure 7.87 exactly matches the second harmonic response from the EM simulation in figure 7.95. This shows that EM simulation is required, to determine the frequency response of a filter accurately. As expected figure 7.87, shows less stopband attenuation, due to leakage between cables used in the measurement setup

Since Cadence AWR DE V10, the ability to use the Extraction control block with AXIEM has made it feasible to obtain accurate EM simulations of RF designs, including the effect of any screening ground-planes on the top layer. Prior to the Extraction being available, EM simulation required a significant effort without a guaranteed useful result.

## Coaxial Filters

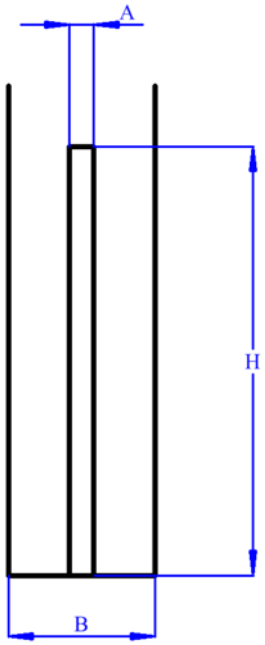



Figure 7.96. Coaxial cavity dimensions.



Figure 7.97. Coaxial cavity diplexer for 80 MHz (UM).

Coaxial filters are similar in principle to helical filters, except that the resonator is a straight rod, rather than a wound helix as shown in figure 7.96. The length of the centre rod is a quarter wavelength. For the highest Q values, the ratio of the centre rod diameter to the inner diameter of the cavity is such that the characteristic impedance of the coaxial line forming the resonator is 77 Ω. The equation for the characteristic impedance of a coaxial transmission line is:

$$Z_c = \frac{1}{2\pi}\sqrt{\left(\frac{\mu_0}{\varepsilon_0}\right)}\ln\left(\frac{B}{A}\right) = \frac{60}{\sqrt{\varepsilon_r}}\ln\left(\frac{B}{A}\right) \qquad \text{Eqn. 7.30}$$

So that the maximum Q is obtained when B/A = 3.6.

Typical Q values are in the range of 2000 to 10000. Because cavity filters have such a high Q, they are used in many applications requiring a low insertion loss. Air filled coaxial filters have a high power handling capability are typically used for filters and combiners for radio and TV transmitters and in mobile radio and mobile phone base stations.

Figure 7.97 shows a typical coaxial filter used in a mobile radio talk-through repeater operating at 80 MHz. The total height of the filter is 1.2 m and the cavities are 200 mm in diameter. The cavities used in this filter have a Q of 5000. The round cylinders at the top of the cavities are isolators, which ensure that the input impedance to the filter is perfectly matched over the entire bandwidth of the transmitter.

Some coaxial cavities are much smaller. Older mobile (cell) phones contain diplexers with ceramic filled coaxial resonators. Figure 7.98 shows a surface mount, ceramic 3-resonator coaxial filter for such applications. Using a high dielectric constant material for the cavity gives a significant reduction in filter size. The centre frequency of this filter is 881 MHz. The filter is 14 mm long.

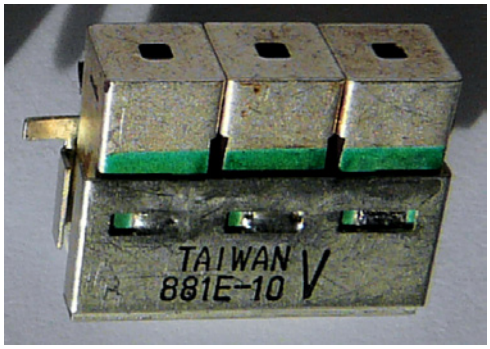



Figure 7.98. Coaxial cavity filter (UM).




Figure 7.99. Cavity filter diplexer for mobile radio applications [17].

For mobile radios, used by trucks or taxis to talk to their base, a coaxial diplexer is often used to provide isolation between the transmitter and the receiver in their mobile radio. Figure 7.99 shows a typical coaxial diplexer. Hills Industries [17] was sold and no longer make RF products. However figures 7.99 and 7.100, are a good illustration of the construction and operation of a diplexer. The receive frequency is 450.625 MHz and the transmit frequency is 460.125 MHz. These radios typically have a transmission power level of 25 W (43.98 dBm). The receiver typically has signals of -60 dBm applied to it, so that the difference between the transmitted and received signal is more than 100 dB. Connecting the transmitter directly to the receiver will result in severe damage to the input circuitry, but the diplexer prevents this.

As shown in Figure 7.100, at the receiver frequency of 450.625 MHz, the diplexer of figure 7.99 causes a less than 1 dB loss between the antenna and the receiver ports and more than 60 dB isolation between the antenna and the transmitter ports, thus protecting the input from any spurious signals generated by the transmitter at the receiver frequency.

At the transmitter frequency of 460.125 MHz, the diplexer provides less than 1 dB loss between the transmitter port and the antenna port, so that virtually all the 25W output signal is transmitted. At this frequency, there is more than 60 dB isolation between the antenna and receiver ports, thus protecting the input from the high power levels generated by the transmitter.

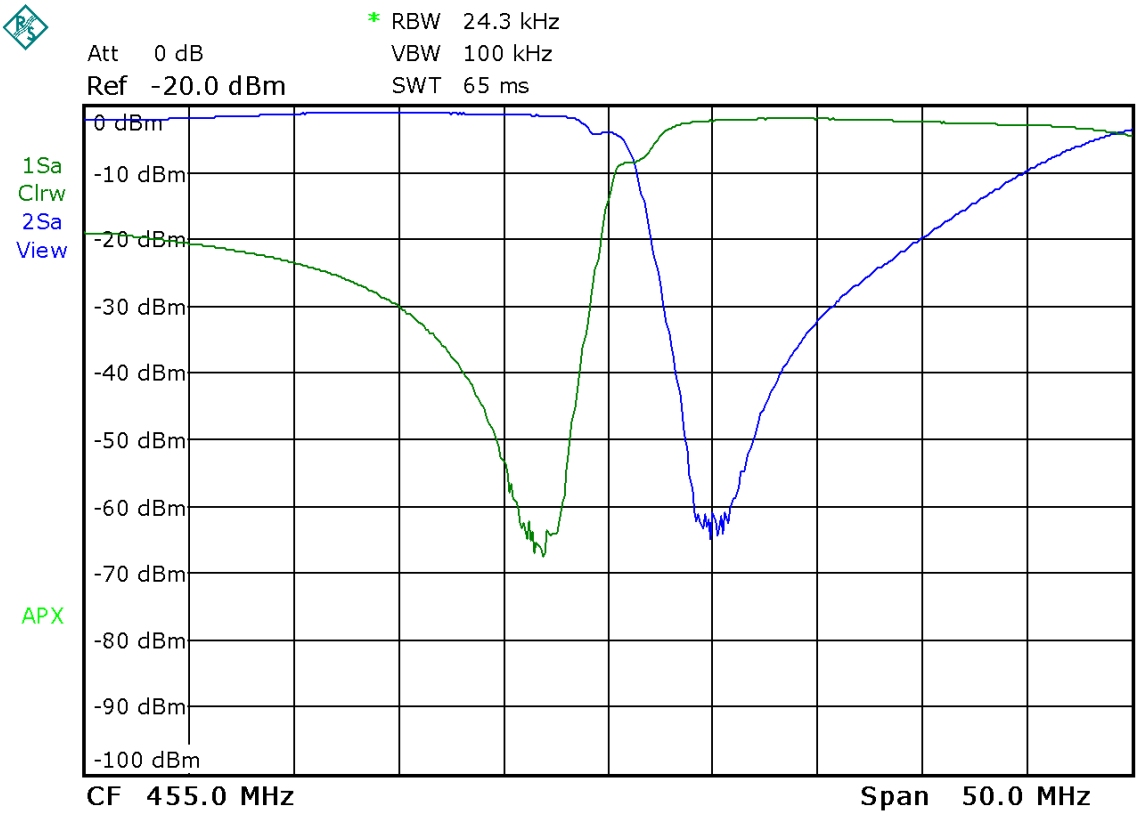



Figure 7.100. Frequency response of the diplexer of figure 7.99.

For low loss, high power microwave filters; it is often convenient to mill the whole filter out of a solid block of aluminium, as shown in figure 7.101. Martin [18] provides design tools for this. By including coupling between non-adjacent cavities, zeros of transmission can be included. In the filter of figure 7.101, non-adjacent cavity coupling has been applied to the first and last resonator.

These filters are tuned by capacitive top loading on each resonator. Each of the resonators is thus a fraction shorter than a quarter wavelength, with the required top-loading capacitance making up this shortfall.

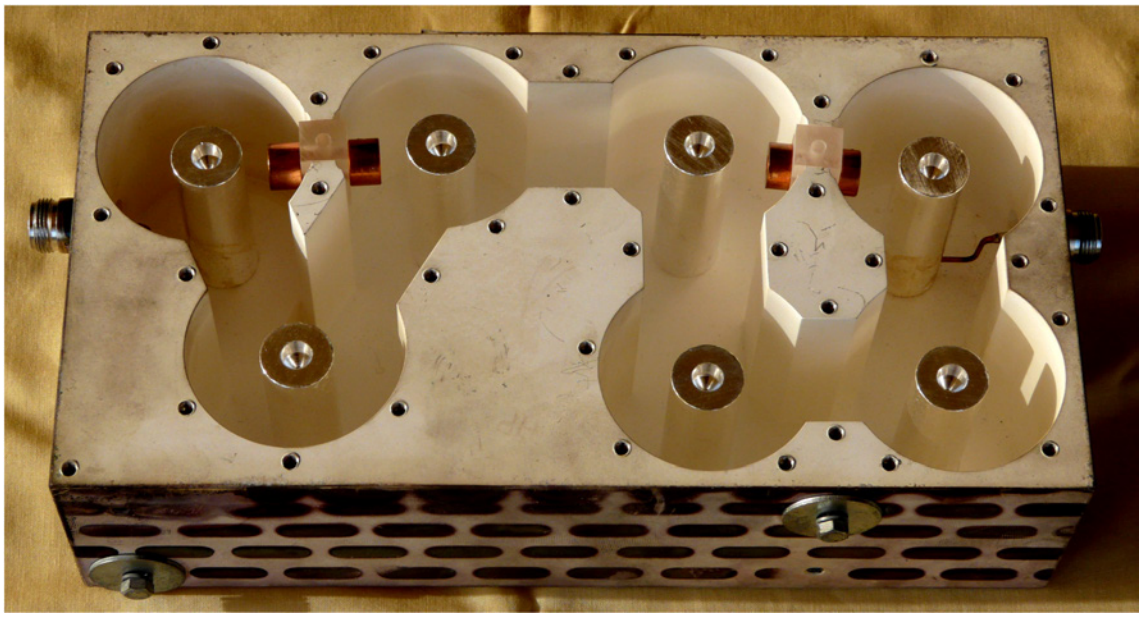


Figure 7.101. 1.8 GHz Coaxial Cavity Filter.

## Ceramic Filters

For many consumer applications IF filters are required at only a few specific frequencies. For example, all FM radios have an IF of 10.7 MHz. All AM radios use a 455 kHz IF. As a result, commercial filter manufacturers like Murata have a wide variety of low cost filters available for those frequencies. To achieve small size, low cost and freedom from microphony, ceramic materials are used for the resonators. Two typical 10.7 MHz ceramic IF filters are shown in figure 7.102. Many of the latest versions are surface mount instead of the through-hole filters shown in figure 7.102. The right hand filter contains two filters like the left hand one, inside the one casing and is used to provide more filtering of unwanted signals. Most of the FM IF filters are designed to provide a flat group delay over the passband. This minimised the distortion caused by the IF filter to the demodulated audio signals.




Figure 7.102. 10.7MHz ceramic IF filters [19].

In addition there are many filters available for specific IF applications, such as 5.5 MHz and 6 MHz for analogue TV sound IF, 38.9 MHz for Digital Audio Broadcasting (DAB), 44 MHz for digital TV receivers etc.

Ceramic resonator filters are also used for RF filtering. The Murata Gigafil range for instance contains many different RF filters covering the 800 to 950 MHz mobile phone band and the 1.4 to 2.4 GHz mobile phone and WLAN bands.

Since these ceramic filters are mass-produced, their cost is very low and it may be worthwhile to modify one's design to be able to incorporate these filters.

## SAW Filters

The resonators considered so far have electromagnetic or acoustic resonances with the resonator being a quarter wavelength. Voltages across an input transducer on the surface of a piezo-electric substrate, causes an acoustic wave to travel along the surface of the substrate. These travelling waves then induce voltages on a second transducer, which is used as an output transducer. By correctly designing the shape of these transducers, filtering can be achieved, with independent control over both the amplitude and group delay. Surface Acoustic Wave (SAW) filters are thus normally used for analogue TV IF filters, IF filters for radars and other applications where sharp filtering is required and where the group delay must be absolutely flat.

Since the input transducer generates a travelling wave in the direction of the output transducer as well as one in the opposite direction, which must be absorbed, SAW filters have a high insertion loss, typically 12 dB for devices with a centre frequency of 70 MHz and 4 dB for devices operating at 2 GHz [20]. Because of their low cost, small size and good performance, SAW filters are used in many consumer devices. The design of SAW filters is outside the scope of this book.

## References


1. A. I. Zverev, *Handbook of Filter Synthesis*, Wiley, 1967, Helical Filters pp 499-521, k and q Filter Tables, p 341, Eqn. 9.4.3 pp 517.
2. G G. Matthaei, L. Young, and E. M. T. Jones, *Microwave Filters, Impedance-Matching Networks, and Coupling Structures*. Boston, MA: Artech House, 1980. pp.583-650.
3. D. Pozar, *Microwave Engineering* , Third Edition, Wiley, 2005. pp. 416-438.
4. Kikkert C. J, "The Effect of Amplifier Distortion and Filter Type on BER of WCDMA-UMTS Mobile Radio Systems", 2nd International Conference on Signal Processing and Communication Systems (ICSPCS 2008), Gold Coast, Australia, 15-17 December 2008, ISBN: 978-0-9756934-6-9.
5. Mini-Circuits, Reflectionless Filters. https://www.minicircuits.com/pdfs/XHF-23+.pdf
6. Pairing Mixers with Reflectionless Filters to Improve System performance, Mini-Circuits AN-75-007, https://www.minicircuits.com/app/AN75-007.pdf
7. Morgan M. A. and T. A. Boyd, Synthesis of a New Class of Reflectionless Filter Prototypes, National Radio Astronomy Observatory. https://arxiv.org/ftp/arxiv/papers/1008/1008.3502.pdf
8. Microwaves 101, Reflectionless filters. https://www.microwaves101.com/encyclopedias/reflectionless-filters
9. Temwell Corporation, http://www.temwell.com.tw/

10. Temwell, “Toko 7H filter replacements”, https://www.temwell.com/category-toko-alternative-filter.html
11. M. Dishal, “A Simple Design Procedure for Small Percentage Bandwidth Round Rod Interdigital Filters” MTT, Vol 13, No5, Sep 1965, pp 696 – 698.
12. K&L Microwave, 9IR20-7500/X2000-O/O Wide Band Interdigital Filter Datasheet, https://klmicrowave.nyc3.digitaloceanspaces.com/products/attachments/_plk50_1_9IR20.pdf
13. Kikkert, C. J. “Designing Low Cost Wideband Microstrip Bandpass Filters”, IEEE Tencon ’05, Melbourne, Australia, 21-24 November 2005.
14. Kikkert, C. J. “A Design Technique for Microstrip Filters” ICECS 2008, St Julians, Malta, 31 Aug.-3 Sep. 2008.
15. Codan, http://www.codan.com.au/
16. Rogers, R04000 Data. https://rogerscorp.com/advanced-electronics-solutions/ro4000-series-laminates
17. Hills Communications, part of Hills Ltd, http://www.hills.com.au
18. P. Martin, “Designing Microwave Band Pass Filters”, 19 Mar 2011. Available: https://awrcorp.com/download/kb.aspx?file=EC_Mstrip_BPFilter.pdf
19. Murata Manufacturing Co, Ceramic Filters http://www.murata.com/en-global/products/filter/cerafil
20. Murata Manufacturing Co, SAW Based Components, https://www.murata.com/en-global/products/saw

# Chapter 8

# Amplifiers: Stability, Noise and Gain

## Introduction

A few years ago, if one had to use an RF or IF amplifier, one had to design it using individual transistors and associated passive components. Now for many commercial RF frequency bands there are low cost IC's available, which perform as well or better than discrete transistor designs. For example, Analog Devices HMC8410 low noise amplifier has a 10 MHz to 10 GHz bandwidth and a noise typical figure of 1.4 dB. The Mini-Circuits PMA-5043+ is an Enhancement-mode Pseudomorphic High Electron Mobility Transistor (E-PHEMT) MMIC amplifier with a 50 MHz to 6 GHz bandwidth and a typical 0.9 dB noise figure (NF) at 2 GHz. Many other manufacturers have similar devices.

Operational amplifiers with gain-bandwidth products >>1 GHz are readily available. Chapter 10 discusses the use of Operational amplifiers for RF applications in more detail. For IF amplifiers at HF frequencies it is now thus possible to use these high speed operational amplifiers, resulting in IF strips that have an excellent linearity and very low intermodulation distortion. VHF cable TV repeaters can be used for medium power amplifiers. There are also many amplifier modules available with a very high linearity, particularly for the frequency bands used by mobile phones, wireless LAN, Bluetooth and other high volume consumer frequencies.

The principles for obtaining stability and low noise, outlined in this chapter, apply to any amplifier, including Microwave Monolithic ICs (MMIC) and individual BJT or FET devices, such as High Electron Mobility Transistors (HEMT).

### *MMIC*

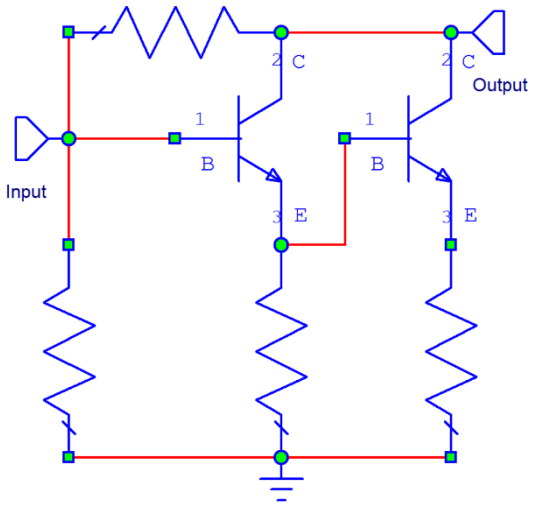



Figure 8.1. Typical Mini-Circuits MMIC circuit diagram.

Several IC manufacturers like Keysight (←Agilent), Mini-Circuits and NXP (←Freescale ←Motorola), Qorvo (←Triquint ←WJ) and others produce general purpose Microwave Monolithic Integrated Circuits (MMIC): These can be used as general-purpose amplifier blocks and can be used at frequencies from DC up to 50 GHz.

Some MMIC's are made using InGaP HBTs (indium gallium phosphide Heterojunction Bipolar Transistors). Mini-Circuit's MAR, ERA, Gali and Lee series of amplifiers are examples of this and they require a constant current source and have a typical circuit diagram as shown in figure 8.1. The Mini-Circuits [1] ERA-3+ amplifier has a bandwidth of DC to 3 GHz, and a 21 dB gain and NF of 2.6 dB at 1 GHz and operates using a 35 mA supply with a typical device voltage of 3.2V. The constant current supply is typically obtained using a series resistor in series with an inductor, as shown in figure 8.2.

A suitable constant supply is obtained, by using a resistor to set the current supplied to the MMIC as shown in figure 8.2. The RF loading of that resistor is minimised by having a large inductor in series with the resistor. Since the resistor is typically, 600 Ω for a 12 Volt supply voltage, in many applications, a slightly reduced gain can be tolerated and the inductor can be removed. This series resistor, together with the DC feedback resistor, between the collector and base of the transistor in figure 8.1, result in a stable quiescent current as the temperature changes.

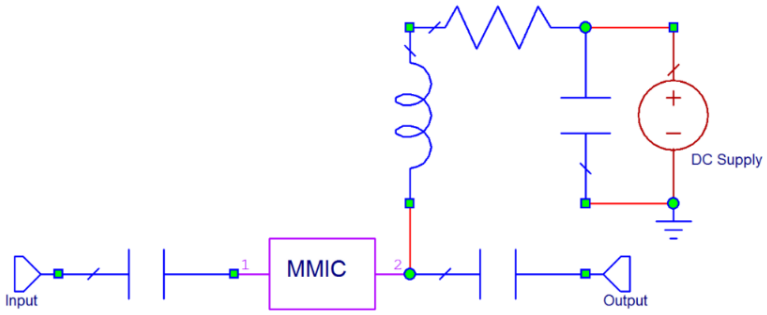



Figure 8.2 Typical connection requirement for an MMIC.

Other MMIC's are made using GaAs e-pHEMTs (Gallium Arsenide Enhancement Mode Pseudomorphic High Electron Mobility Transistors). A typical example of this is Mini-Circuit's PMA-5453+ [2] amplifier, which has a bandwidth of 50 MHz to 6 GHz and a 19.3 dB gain, a NF of 0.7 dB and IP3 of 35 dB at 1 GHz. It operates using a fixed 3 V supply. The typical MMIC connection is similar to Figure 8.2 with the resistor in the power supply replaced by a short circuit, to provide a constant DC voltage at the MMIC output, but not cause any RF loading due to the power supply.

Other manufacturers have devices with a similar performance to the above examples and there are hundreds of different commercial MMIC's available. In addition to low power MMIC's many manufacturers also produce high lower amplifier modules.

Most MMIC devices are unconditionally stable. However, since these devices have very wide bandwidths, microwave layout techniques must be used to ensure that the devices remain stable. As a typical example it is essential that the inductance of the ground pin connections of the MMIC are kept as low as possible. This is achieved by ensuring that the earth pins of the MMIC are soldered to a large ground plane and that a via connecting the top ground-plane to the bottom ground-plane is very close to the earth pin of the MMIC in the Microstrip PCB layout. Like the ground planes of figures 6.44, 7.67 or 9.59.

These amplifier modules and MMIC's can now be used for the majority of RF and microwave designs. There are applications, such as ultra-low noise amplifiers, millimetre wave amplifiers and high power amplifiers, where amplifier modules and MMIC's cannot be used for either performance or economic reasons. For such designs, a knowledge of amplifier stability, NF and gain circles, which are described in this chapter. is essential.

## Requirement for Stability

For power amplifier design, a single power transistor, or several combined in parallel, are used to provide the required amplification at the required frequency, with the required linearity. The amplifier should be stable and not oscillate at any frequency under normal operating conditions. Amplifier stability and matching of input and output, ensuring that the highest power output is obtained, are the most critical parameters in a power amplifier design.

## Smith Chart Revision

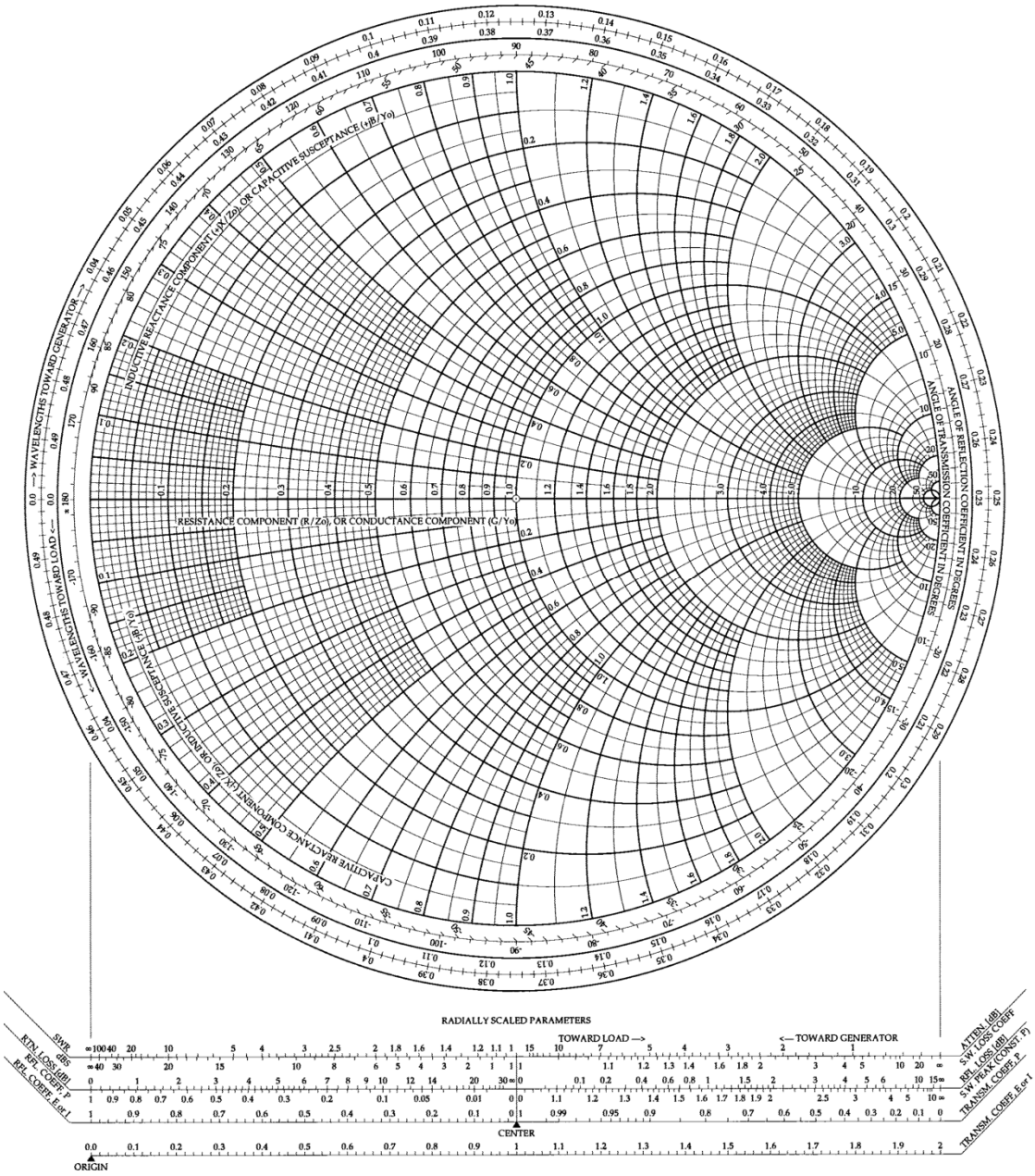



Figure 8.3. Smith Chart; a plot of the normalised reflection coefficient, Γ.

To ensure that the amplifier is matched at the input and output, normally the return loss $S_{11}$ at the input and $S_{22}$ at the output of the amplifier is measured. In order to be able to

adjust these reflection coefficients correctly, it is desirable to know both their magnitude and phase at different frequencies. The Smith Chart is a polar plot of reflection coefficient and allows both the magnitude and phase of the reflection coefficient to be plotted versus frequency. Such plots are very useful in visualising: the behaviour of the reflection coefficient, so that suitable action may be required to improve the matching of the devices. As shown later in this chapter, the Smith Chart is very useful in visualising the stability of amplifiers.

The Smith Chart was developed by P. Smith [3, 4] in 1939. It is a polar plot of the reflection coefficient superimposed with circles for real and reactive normalised impedances. It allows a good visualisation of the impedance of RF networks as the frequency changes. Some prior knowledge of the Smith Chart is presumed here and only the equations 8.1 and 8.2 governing the Smith chart are stated here, for a more detailed discussion on the Smith chart please refer to D. M. Pozar [5] or similar books. The copyright of the Smith Chart has been released into the public domain by the copyright holder. The normalised reflection coefficient Γ and the normalised impedance $Z_L$ of a network are related by:

$$\Gamma = \frac{Z_L - 1}{Z_L + 1} = |\Gamma| \angle e^{j\theta} = \Gamma_r + j\Gamma_j \qquad \text{or} \qquad Z_L = \frac{1+\Gamma}{1-\Gamma} = R_L + jX_L \qquad \text{Eqn. 8.1}$$

The Smith chart is a plot of $|\Gamma| \angle e^{j\theta}$ and this also represents $Z_L$ and we can plot contours of $Z_L = R_L + jX_L$. Solving for $R_L$ and $X_L$ gives:

$$R_L = \frac{1 - \Gamma_r^2 - \Gamma_j^2}{(1-\Gamma_r)^2 + \Gamma_j^2} \quad \text{and} \quad X_L = \frac{2\Gamma_j}{(1-\Gamma_r)^2 + \Gamma_j^2} \qquad \text{Eqn. 8.2}$$

$R_L$ and $X_L$ form a family of circles, which are also plotted on the Smith Chart. Γ = 0 is the centre of the Smith Chart. The Smith chart is a very useful tool for showing impedance values versus frequency.

Paper versions of the Smith Chart are now seldom used for design calculations, but the Smith chart is an integral part of modern computer based design tools. Cadence AWR DE allows the results of the RF network simulation to be plotted on a Smith Chart, as well as rectangular and polar charts. In Cadence AWR DE, the centre part of the Smith chart can be expanded or compressed, by right clicking on the smith chart of the project file of figure 8.6 and selecting *Options* ⇒ *Grid* and setting the *Size* to *Normal, Expanded* or *Compressed*. *Compressed* shows more of the area outside the Γ = 1 region on the Smith Chart and is useful for plotting stability circles. *Expanded* provides a close up of the centre of the Smith Chart and is useful for visualising impedance matching.

## Scattering Parameters Revision

Pozar [5] provides a more detailed description of S parameters than is presented here.

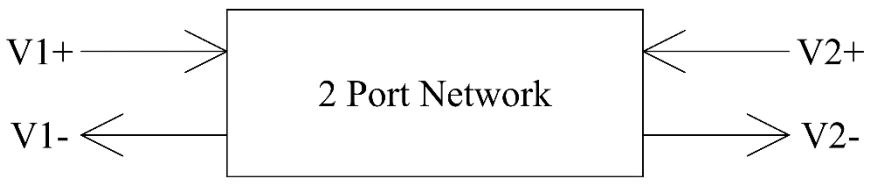



Figure 8.4. S parameter definitions.

$$\begin{bmatrix} V_1^- \\ V_2^- \end{bmatrix} = \begin{bmatrix} S_{11} & S_{12} \\ S_{21} & S_{22} \end{bmatrix} \begin{bmatrix} V_1^+ \\ V_2^+ \end{bmatrix} \qquad \text{Eqn. 8.3}$$

$S_{11} = \left.\frac{V_1^-}{V_1^+}\right|_{V_2^+ = 0}$ i.e. reflection coefficient at port 1, with port 2 matched.

$S_{22} = \left.\frac{V_2^-}{V_2^+}\right|_{V_1^+ = 0}$ i.e. reflection coefficient at port 2, with port 1 matched.

$S_{21} = \left.\frac{V_2^-}{V_1^+}\right|_{V_2^+ = 0}$ i.e forward gain, with port 2 matched.

$S_{12} = \left.\frac{V_1^-}{V_2^+}\right|_{V_1^+ = 0}$ i.e reverse gain, with port 1 matched.

An amplifier is unilateral if $S_{12} = 0$, i.e. the reverse gain is zero. That applies to many amplifiers, particularly operational amplifiers and other ICs where the output is well separated from the input.

The input reflection coefficient is:

$$\Gamma_{in} = S_{11} + \frac{S_{12}S_{21}\Gamma_{load}}{1 - S_{22}\Gamma_{load}} \qquad \text{For a unilateral amplifier } \Gamma_{in} = S_{11} \qquad \text{Eqn. 8.4}$$

$$\Gamma_{out} = S_{22} + \frac{S_{21}S_{12}\Gamma_{source}}{1 - S_{11}\Gamma_{source}} \qquad \text{For a unilateral amplifier } \Gamma_{out} = S_{22} \qquad \text{Eqn. 8.5}$$

The Available Power Gain ($G_A$) is the ratio of the maximum available power at the load to the maximum available power at the source. It is the amplifier gain under ideal conditions as it assumes conjugate input and output matching. $G_A$ is defined as:

$$G_A = \frac{Power\ available\ from\ network}{Power\ available\ from\ source} = \frac{|S_{21}|^2(1 - |\Gamma_{source}|^2)}{|1 - S_{11}\Gamma_{source}|^2(1 - |\Gamma_{out}|^2)} \qquad \text{Eqn. 8.6}$$

The Transducer Power Gain ($G_T$) is the ratio of the actual power at the load to the maximum available power at the source. It is the amplifier gain under actual load conditions. It assumes a conjugate input match, but uses the actual output match. $G_T$ is defined as:

$$G_T = \frac{Power\ delivered\ to\ the\ load}{Power\ available\ from\ source} = \frac{|S_{21}|^2(1 - |\Gamma_{source}|^2)(1 - |\Gamma_{load}|^2)}{|1 - \Gamma_{source}\Gamma_{in}|^2 |1 - S_{22}\Gamma_{load}|^2} \qquad \text{Eqn. 8.7}$$

There are measurement functions for $G_A$ and $G_T$ in Cadence AWR DE.

Under ideal conditions, $\Gamma_{source} = 0$ and $\Gamma_{load} = 0$ so that

$$G_A = G_T = |S_{21}|^2 \qquad \text{Eqn. 8.8}$$

An amplifier includes input and output matching circuits as shown in figure 8.5. The input match provides maximum power when $\Gamma_{in} = \Gamma_{source}^*$ so that the gain of the input matching network is $G_S = 1$. Similar when the output has a conjugate match so that $\Gamma_{out} = \Gamma_{load}^*$, then $G_L = 1$.

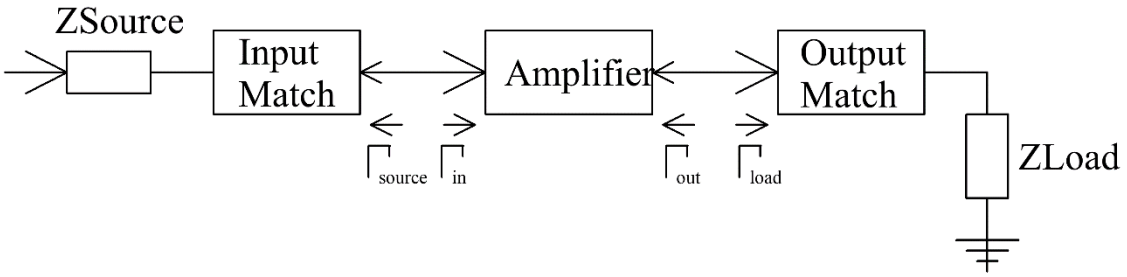



Figure 8.5. Amplifier block diagram.

In general:

$$G_S = \frac{1-|\Gamma_{source}|^2}{1-\Gamma_{in}\Gamma_{source}} \quad \text{Eqn. 8.9}$$

$$G_0 = |S_{21}|^2 \quad \text{Eqn. 8.10}$$

$$G_L = \frac{1-|\Gamma_{load}|^2}{1-\Gamma_{out}\Gamma_{load}} \quad \text{Eqn. 8.11}$$

The gain of the whole amplifier is:

$$G_T = G_s * G_0 * G_L \quad \text{Eqn. 8.12}$$

Under ideally matched conditions $G_S = 1$ and $G_L=1$ so that the gain is thus:

$G_T = |S_{21}|^2$, as was obtained before in equation 8.8

## Stability

Oscillations will occur if $G_S \rightarrow \infty$ or $G_L \rightarrow \infty$

For oscillations due to the input, $G_S \rightarrow \infty$ so that from equation 8.9, $\Gamma_{in}*\Gamma_{source} = 1$ result in oscillations. $\Gamma_{in}$ and $\Gamma_{source}$ are both complex variables. Oscillators often are designed by deliberately making $\Gamma_{in}*\Gamma_{source} = 1$. Equation 8.4 shows how $\Gamma_{in}$ depends on other parameters, including $\Gamma_{load}$ , which together with $\Gamma_{source}$ can be manipulated to ensure that $\Gamma_{in}*\Gamma_{source} = 1$ is only satisfied at one frequency, thus ensuring stable oscillations. The amplifier is stable if $\Gamma_{in} < 1$ for all values of $\Gamma_{load}$ , since for a passive source $|\Gamma_{source}| < 1$, so that $\Gamma_{in}*\Gamma_{source}$ is always <1.

Similarly, for oscillations due to the output, $G_L \rightarrow \infty$ so that from equation 8.11, $\Gamma_{out}*\Gamma_{load} = 1$. For oscillator design, equation 8.5 shows how $\Gamma_{out}$ depends on other parameters, including $\Gamma_{source}$ , which together with $*\Gamma_{load}$ can be manipulated to ensure that $\Gamma_{out}*\Gamma_{load} = 1$ is only satisfied at one frequency, thus ensuring stable oscillations. The amplifier is stable if $\Gamma_{out} < 1$ for all values of $\Gamma_{source}$ , since for a passive load $|\Gamma_{load}| < 1$, so that $\Gamma_{out}*\Gamma_{load}$ is always <1. For unilateral amplifiers $S_{12} = 0$, so that $\Gamma_{in} = S_{11}$ and $\Gamma_{out} = S_{22}$. This makes it relatively easy to ensure that the amplifier is stable. However many amplifiers are not unilateral, making it more difficult to determine the load and source conditions where the amplifier is stable.

## Stability Circles

Setting $|\Gamma_{in}| = 1$ in equation 8.4, allows it to be solved for the values $\Gamma_{load}$ that form the border between stable and unstable regions of the amplifier operation. When plotted on the Smith Chart, this border forms a circle, which shows the output impedances that cause the instability. This is called the Output Stability Circle [5, 6].

It has a centre $$c_L = \frac{(S_{22} - \Delta S_{11}^*)^*}{|S_{22}|^2 - |\Delta|^2}$$ Eqn. 8.13

And a radius $$r_L = \left| \frac{(S_{12}S_{21})}{|S_{22}|^2 - |\Delta|^2} \right|$$ Eqn. 8.14

Where $$\Delta = S_{11}S_{22} - S_{12}S_{21}$$ Eqn. 8.15

Similarly, Setting $|\Gamma_{out}| = 1$ in equation 8.5 allows it to be solved for the values $\Gamma_{source}$ that form the border between stable and unstable regions of the amplifier operation. When plotted on the Smith Chart, this is a circle and is called the Input Stability Circle [5, 6].

It has a centre $$c_s = \frac{(S_{11} - \Delta S_{22}^*)^*}{|S_{11}|^2 - |\Delta|^2}$$ Eqn. 8.16

And a radius $$r_s = \left| \frac{(S_{12}S_{12})}{|S_{11}|^2 - |\Delta|^2} \right|$$ Eqn. 8.17

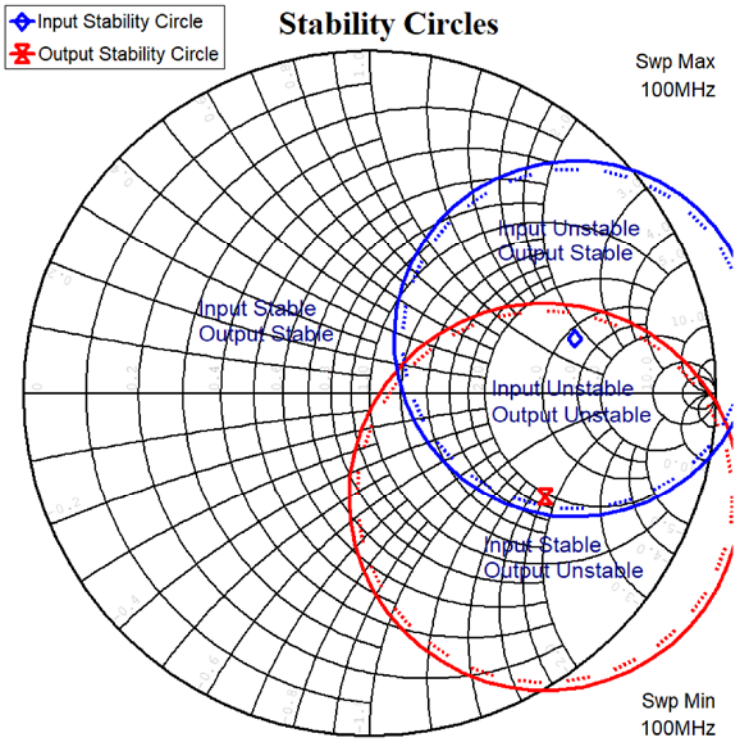



Figure 8.6. Input and output stability circles.

These stability circles show the border between stable and unstable regions. Depending on the values of the s parameters, the centre of these stability circles can be inside or outside the unit circle. For the input Stability Circle, if $S_{22}$ is <1, then the outside of the Stability Circle is stable. If $S_{22}$ is >1, then the inside of the Stability Circle is stable. However, that corresponds to reflection from port 2 to be larger than the incident voltage and that is unlikely in practical cases. Similarly, for the output Stability Circle, if $S_{11}$ is >1, then the inside of the Stability Circle is stable and if $S_{11}$ is <1, then the outside of the Stability Circle is stable.

Cadence AWR DE allows stability circles to be plotted. Figure 8.6 shows the input and output stability circles for the following S parameter values: $S_{11} = 0.96 - j0.26$, $S_{21} = 0.34 - j0.06$, $S_{12} = 0.58 + j0.28$ and $S_{22} = 0.84 + j0.5$. The blue circle is the Input Stability Circle and the Red circle is the Output Stability Circle. For Input Stability Circles if $|S_{22}| > 1$, then the area outside the Input Stability Circle is unstable. If $|S_{22}| < 1$, the area inside the Input Stability Circle is unstable. For the Input Stability Circle of figure 8.6, $|S_{22}| = 0.978$ so that the inside of the circle is unstable. Similarly for the Output Stability Circle of figure 8.6, $|S_{11}| = 0.989 < 1$ and the unstable region is inside the Output Stability Circle. In figure 8.6, the different regions are labelled as *Stable* or *Unstable*. The region outside both circles, where both the input and output are stable covers most of the Smith Chart with $|\Gamma|<1$. Stability circles will thus allow the input and output matching to be arranged to ensure that an amplifier is stable under normal operation.

## Unconditional Stability

An amplifier is unconditionally stable if $|\Gamma_{in}| < 1$ and $|\Gamma_{out}| < 1$, for all passive load and source impedances. For many MMIC's, measured S parameter are provided and those can be used to determine the stability of those devices. If the stable region of the Input and Output Stability Circles cover the whole Smith Chart with $|\Gamma|<1$, then the device is unconditionally stable.

## Conditional Stability

An amplifier is conditionally stable if $|\Gamma_{in}| < 1$ and $|\Gamma_{out}| < 1$, only for certain load and source impedances. As an example, the early version of the MAR8 amplifier was only conditionally stable and both input and output reflection coefficients had to be less than 0.5. For conditional stability, unstable regions of either or both the input and output stability circles partially lie inside the region of the Smith Chart with $|\Gamma|<1$.

## Stability Factors: Measures of Stability

When wide-band operations are required, as shown in figures 8.9, 8.23 and 8.29a, it is sometimes difficult to see if an amplifier is stable at a specified frequency. Stability factors provide a simple indication of an amplifier's stability versus frequency. There are different stability factors the as shown below.

The **Rollet's stability factor,** K is defined as:

$$K = \frac{1 - |S_{11}|^2 - |S_{22}|^2 - |\Delta|^2}{2|S_{12}S_{21}|} \qquad \text{Where } |\Delta| = |S_{11}S_{22} - S_{12}S_{21}| \qquad \text{Eqn. 8.18}$$

In addition, the auxiliary stability factor is defined as:

$$B = 1 + |S_{11}|^2 - |S_{22}|^2 - |\Delta|^2 \qquad \text{Eqn. 8.19}$$

For unconditional stability K > 1 and B > 0. Both equations involve the input and the output equally, so the Rollet's stability factor applies to the whole amplifier.

The **Geometric Stability Factor**, μ is defined as:

$$\mu_1 = \frac{1-|S_{22}|^2}{|S_{11}-\Delta S_{22}^*|+|S_{12}S_{21}|} \qquad \text{Eqn. 8.20}$$

$\mu_1$, measures the distance from the Smith Chart centre to the nearest unstable point of the output load plane, corresponding to the output stability circle.

$$\mu_2 = \frac{1-|S_{11}|^2}{|S_{22}-\Delta S_{11}^*|+|S_{12}S_{21}|} \quad \text{Eqn. 8.21}$$

$\mu_2$, measures the distance from the Smith Chart centre to the nearest unstable point of the source load plane, corresponding to the input stability circle.

For unconditional stability, $\mu > 1$. In addition, the larger the value of $\mu$, the more stable the amplifier.

The Rollet's stability factors K and B and the Geometric Stability Factors for both the input and output of an amplifier are available as measurements in Cadence AWR DE, so that an amplifier's stability can easily be determined at any frequency. It is important that the stability of an amplifier is determined at all possible frequencies, since if the device is unstable it will likely oscillate. If the designer only measures the performance of the amplifier in the operating band and it is oscillating at a frequency far removed from the operating frequency, the designer will be at a loss to explain the very poor amplifier performance, until a spectrum analyser is used to check for oscillations over a wide frequency range. Note that the possibility of oscillations of an amplifier determined by these stability factors are not the only ones that cause oscillations. The lack of power supply decoupling, poor circuit layout and ground-plane integrity and EM coupling between the output and input circuits and leads are common causes of oscillation. Sometimes these oscillations can be cured by using shielding and microwave absorbers [7] in strategic places. Figure 7.59 shows a good layout to avoid coupling between different parts of the hardware.

If the amplifier is not unconditionally stable, then the source and load must be carefully controlled to ensure that the amplifier is stable under normal operating conditions.

### *Design for Maximum Gain*

To design an amplifier for maximum gain, the input matching network and the output matching network are both designed to provide a conjugate impedance match at the operating frequencies, thus making $G_S = 1$ and $G_L=1$, as outlined above. Since the power gain depends on the impedance match at the input, one can plot constant gain circles on the Smith Chart, to show how the gain varies with the matching impedance. Designing an amplifier for maximum power gain may result in unstable operation. Often there is a compromise between stability and gain.

## Amplifier Noise Figure

If an amplifier is used at the input of a receiver, then the amplifier should be designed for the lowest possible NF. In addition, a good linearity (High third order intercept ($OIP_3$)) is required, so that unwanted signals do not degrade the reception of the wanted signal. The input matching conditions for the lowest NF are different from those for a high power gain, so that a reduced gain is obtained from the amplifier when one designs it for low noise performance. In addition, the match for best noise may make the amplifier only conditionally stable.

This section gives a brief overview of NF, noise power and equivalent temperature. Pozar [5] gives a detailed description of these concepts. The NF (or F) of a circuit block or amplifier is defined as the ratio of the actual noise at the output of the circuit, over the

noise that will be obtained if the circuit is noiseless. If $N_a$ is the noise power at the amplifier output, and $N_i$ is the noise power at the input and G is the power gain of the amplifier. Often the noise is referred to the input. $N_e$ is the noise power of the amplifier output, referred to the input of the amplifier. The NF is thus:

$$NF = \frac{N_a}{GN_i} = \frac{GN_e}{GN_i} = \frac{N_e}{N_i} \quad \text{Eqn. 8.22}$$

For an resistor of R Ω, at an absolute temperature (K) of $T_0$, has a noise voltage of:

$$V_n = \sqrt{4kT_0BR} \quad \text{Eqn. 8.23}$$

Since $P=V^2/R$, the thermal noise power ($N_0$) produced is independent of R:

$$N_0 = kT_0B \quad \text{Eqn. 8.24}$$

The NF can thus also be written as:

$$NF = \frac{T_0+T_e}{T_0} \quad \text{Eqn. 8.25}$$

where $T_e$ is the equivalent noise temperature of the amplifier and is the additional noise temperature, referred to the input, that is caused by the amplifier and $T_0$ is the ambient temperature of the input of the amplifier. The noise performance of an amplifier is either; specified as a NF or as an equivalent noise temperature. Equation 8.25 allows the conversion from one to the other.

Often amplifiers are used in cascade, with the output of one amplifier driving another. If the first amplifier has a noise figure of $NF_1$ and a gain of $G_1$ and for the amplifier that follows it is $NF_2$, and $G_2$ and so on. Then for that system, the total NF and noise temperature can be shown to be:

$$NF_{total} = NF_1 + \frac{NF_2-1}{G_1} + \frac{NF_3-1}{G_1G_2} + \frac{NF_4-1}{G_1G_2G_3} + \cdots \quad \text{Eqn. 8.26}$$

$$NF_{total} = T_1 + \frac{T_2}{G_1} + \frac{T_3}{G_1G_2} + \frac{T_4}{G_1G_2G_3} + \cdots \quad \text{Eqn. 8.27}$$

These are known as Friis formulas for noise factor and noise temperature, after Harald T Friis [8]. They show that the NF of the first amplifier in a chain is the most critical. The NF of a Low Noise Block downconverter (LNB), such as shown in figure 11.4 [9], which are mounted at the focal points of satellite dishes and convert the satellite signal to signals around 1 GHz with a gain of more than 60 dB, is typically 0.6 to 0.9 dB. The NF of the LNB is the most critical parameter for these devices. It is difficult to design an amplifier, which has a very low NF and is stable.

## *Examples*

The theory outlined above will now be applied to three different devices to illustrate the different ways that stability and noise information is obtained using AWR DE.

### Example 8.1: BGB707 MMIC

The first example uses an Infineon BGB707L7ESD, Silicon Germanium Carbon Bipolar MMIC. The IC is designed as a low noise front-end amplifier for a wide range of applications like GPS, WLAN, LTE, WiMAX. The IC has a bandwidth of 50 MHz to 10 GHz, operates at 1.8V to 4V, has a minimum NF of 0.6 dB, has Electro Static Discharge (ESD) protection on all pins and is a relatively low cost device. The supply current and can be adjusted using a resistor from 2 mA to 10 mA, resulting in a different noise

performance, transducer gain and Output 1 dB compression ($OP_{1db}$) and third order intercept (OIP3) power levels. The simulation models for the MMIC can be obtained from Infineon [10], or from within AWR DE by selecting *Elements* ⇒ *χ Libraries* ⇒ χ * AWR web site ⇒ *Parts by Vendor* ⇒ Infineon ⇒ Data ⇒ MMIC ⇒ General Purpose MMICs and FM Radio LNAs ⇒ BGB707L7ESD. The element can then be placed in a circuit as shown in figure 8.7. The MMIC requires external coupling capacitors and biasing inductors. These are normally realised using biasing Tees. By incorporating those in the schematic, the effect to these biasing networks on the stability and amplifier performance can be investigated. For a 6 mA supply current, the best amplifier stability occurs when coupling capacitors C1 = 2 nF. When the capacitance is increased, the input stability circle becomes slightly closer to the centre of the Smith Chart, but the amplifier remains stable when matched to a 50 Ω source and load. A biasing inductances of 1 µH, result in a low corner frequency of 13.5 MHz, which is suitable for most applications. However, an input biasing inductance of 10 µH results in a slightly better stability. As a result, the values of C1 = C4 = 2 nF and L1 = L2 = 10 µH are used in this example. Capacitors C2 and C3 are not required in the hardware but mimic the AC impedance at the power supply and the bias output (pin2) of the MMIC.

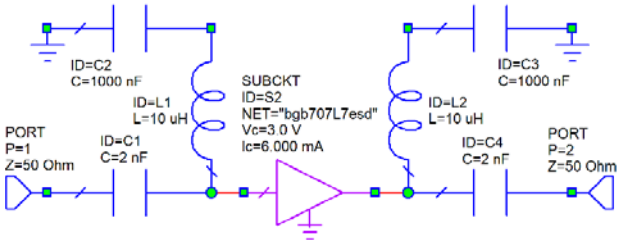



Figure 8.7. BGB707 model used in a circuit schematic.

The model used is a linear model based on S parameter and noise measurements made at different supply voltages and currents. By double clicking on the voltage or current value, different values can be selected.

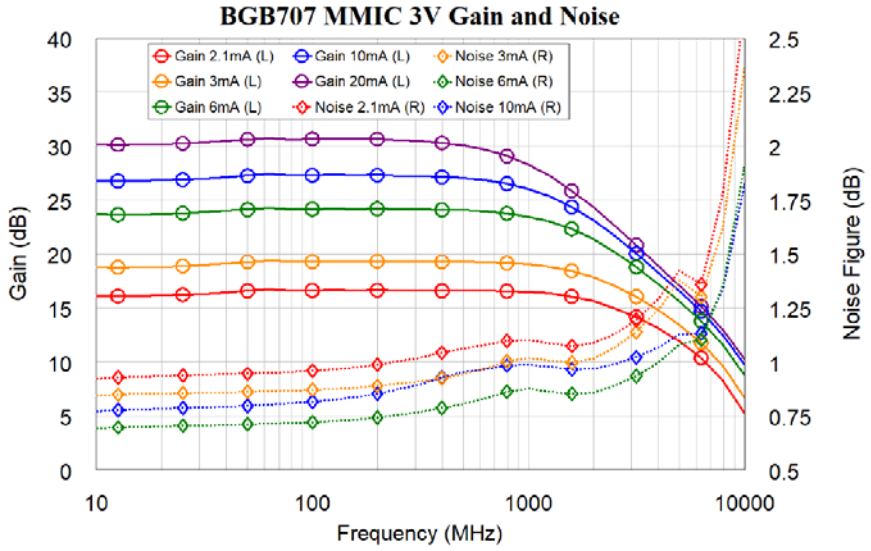



Figure 8.8. BGB707 MMIC gain and NF performance.

Figure 8.8 shows the different gain and NF values for a 3 V supply voltage and with different supply currents. Below 50 MHz the NF rises. That is due to the effect of the

input biasing impedance. Changing L1 to 10 uH results in a flat NF frequency response below 100 MHz. However increasing inductance L1 may result in a lower impedance at high frequencies due to the inductor having a lower self-resonance. That would then increase the NF at higher frequencies. Figure 8.8 shows that the gain increases with supply current, but that for a 3 V supply, the NF is best at 6 mA supply current. The manufacturer's measured data used for figure 8.8 does not include noise figure measurements above 10 mA, so the noise figure for 20 mA cannot be plotted.

The stability of the amplifier can now be determined. Figure 8.9 shows the input and output stability circles for a 3 V supply and 6 mA current, corresponding to the best NF in figure 8.8. The frequency increment is 10 steps per decade (10spd), to show the individual circles. The side of the circles marked with dots is unstable, so for a perfect 50 Ω source and load termination (the centre of the Smith Chart), the amplifier is stable. Figure 8.9 includes a green circle with a VSWR = 1.2. The top part of that circle is inside the unstable region of the input stability circle for frequencies between 57 MHz to 437 MHz. This can be verified by running the accompanying Ch8-Fig7-13.emp AWRDE project file and changing the *BGB 707 Stability Circles 50 Ohm* measurements shown in figure 8.9, by changing both the *SCIR1* and *SCIR2* measurements from *sweep frequency > Use for x-axis* to *select with tuner*. Then do the simulation with *Simulate > Tune* and change the frequency pointer using the *Tuner*. A VSWR of 1.2 is only a small mismatch, so that the amplifier is not very stable.

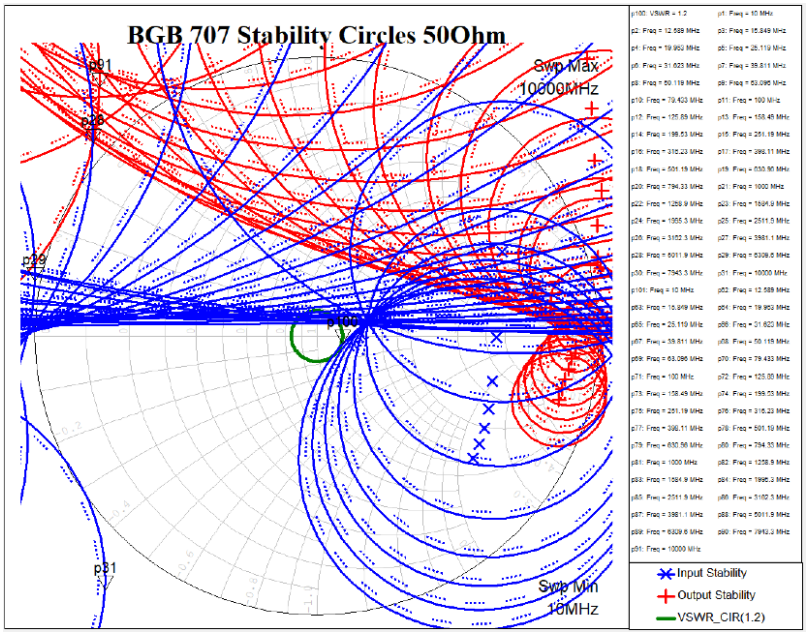



Figure 8.9. Stability circles for the BGB707 MMIC at 3 V and 6 mA.

Figure 8.10 shows the stability factors for this BGB707 MMIC. For unconditional stability K>1, B>0, MI1>1 and MU2>1. To provide smooth plots, the frequency increment is 50 steps per decade (50spd). It can be seen that none of the stability conditions are satisfied and that great care must be taken in the input and output matching to keep the amplifier stable. Despite this, the amplifier has a wide bandwidth a low NF and a low cost. Figure 8.11 shows the input and output impedances, plotted on a Smith Chart. They can also be produced as a table, by simply duplicating the graph as a Tabular Graph. Alternately, the data on the graph can be exported by selecting *Graph ⇒ Export Trace Data* and then specifying the file name for the data to be saved. The resulting data can then be used if needed to design matching networks as described in Chapter 9.

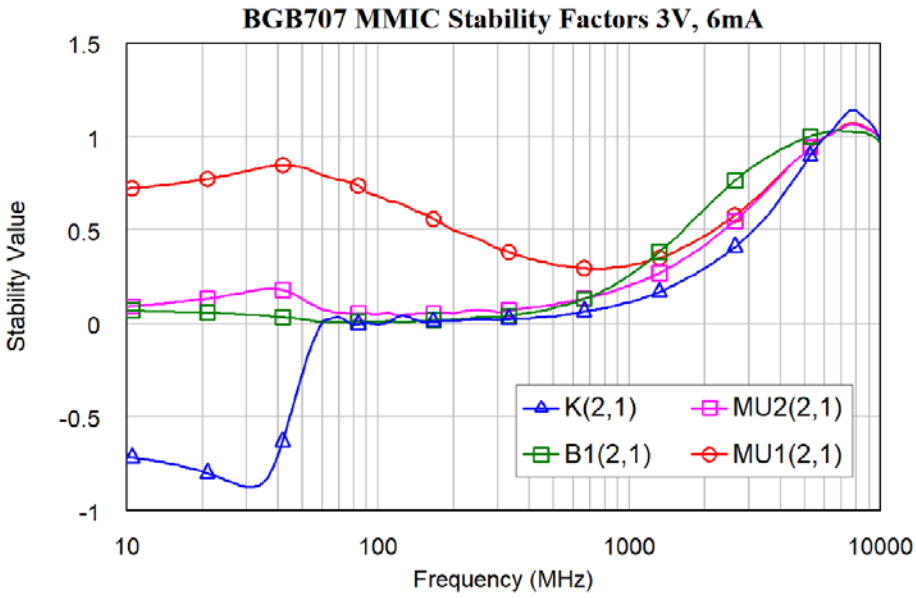



Figure 8.10. Stability factors for the BGB707 MMIC at 3 V and 6 mA.

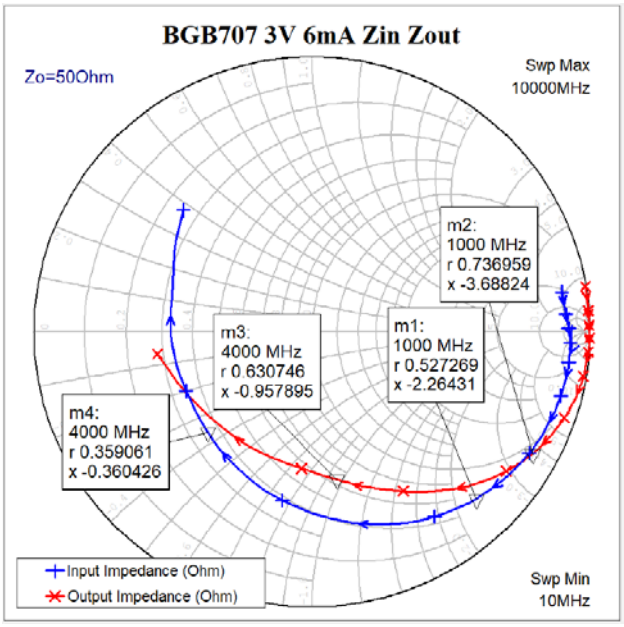



Figure 8.11. Zin and Zout for the BGB707 MMIC at 3 V and 6 mA.

The Gain and NF will vary with the input source impedance. That variation can be plotted on the Smith Chart as shown in figure 8.12. In that figure five NF Circles, being contours of constant NF are plotted as the green circles. The difference between each of the contours is 0.1 dB. That plot shows that the NF at 25.12 MHz can be improved by 0.4 dB by matching the input for optimum NF rather than 50 Ω. The first circle (p1) has a NF 0.1 dB above the minimum NF. Contour p4 nearly passes through the Smith Chart origin (50 Ω) and is 0.4 dB above the minimum NF. Figure 8.12 also plots the input and output stability circles and they show that the input impedance location for minimum noise is inside the unstable region of the input stability circle. To prevent oscillations with the minimum NF, the source used in figure 8.7 must be selected to correspond to the minimum NF and the load impedance must be selected for stable operation and prevent oscillations. Figure 8.12 shows the Gain, NF and stability at 25.12 MHz. To prevent oscillations, the same evaluation needs to be done over a wide range of frequencies.

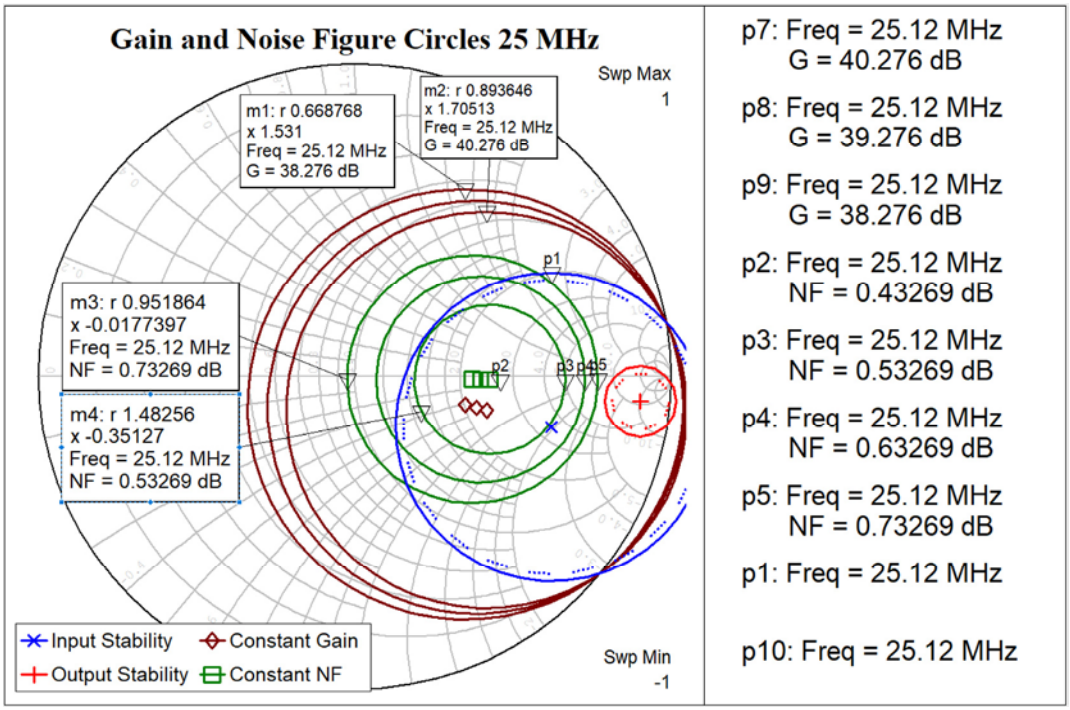



Figure 8.12. Gain and NF Circles for the BGB707 MMIC at 3 V and 6 mA.

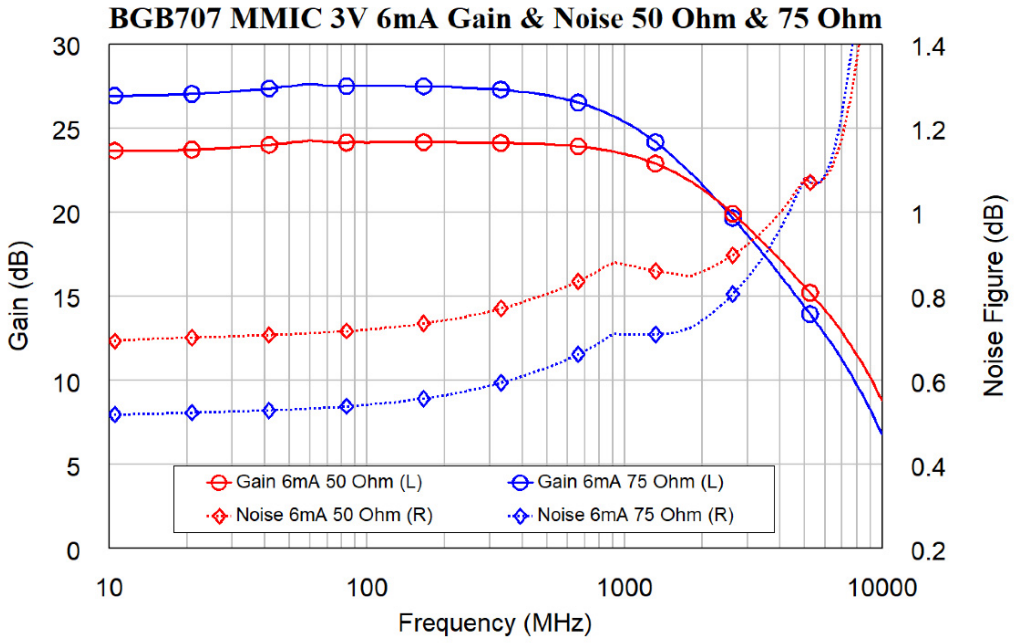



Figure 8.13. Gain and NF for the BGB707 MMIC at 3 V and 6 mA.

The most power can be transmitted using 50 Ω transmission lines, but 75 Ω transmission lines have the lowest loss, so that 75 Ω impedance levels are used for many receiver antennae and front-end amplifiers. Figure 8.13 shows a comparison of the gain and noise performance of the BGB707 MMIC for 75 Ω and 50 Ω terminations at both the input and output. It can be seen that the 75 Ω terminations give a higher gain and a lower NF. However, for frequencies below 40 MHz, the Smith chart centre is inside the unstable regions of the input stability circles, so the amplifier is less stable than the one using 50 Ω terminations. Later in this chapter, techniques to improve the stability are described.

## Example 8.2: PMA-5453 MMIC

The second example uses a Mini-Circuits PMA-5453+ E-PHEMT MMIC. The IC is designed as a low noise front-end amplifier for a wide range of applications like Cellular Radio, Mobile Phone, and WLAN. The IC has a bandwidth of 50 MHz to 6 GHz, operates at 3 V, has a NF of 0.6 dB, and is a relatively low cost device. This amplifier draws a lot more supply current than the BGB707, but it has a 9 dB higher 1 dB compression ($OP_{1db}$) power output and 20 dB higher third order intercept (OIP3) power level than the BGB707. The supply current can be set between 30 mA to 80 mA (@25°C) by varying a bias resistor. That will vary the RF performance. Mini-Circuits provides typical S parameter and measured performance data at different supply voltages, currents and temperatures. However, Mini-Circuits does not provide an AWRDE linear model like the one for the BGB707. The S Parameter data can be imported into AWR DE to plot stability.

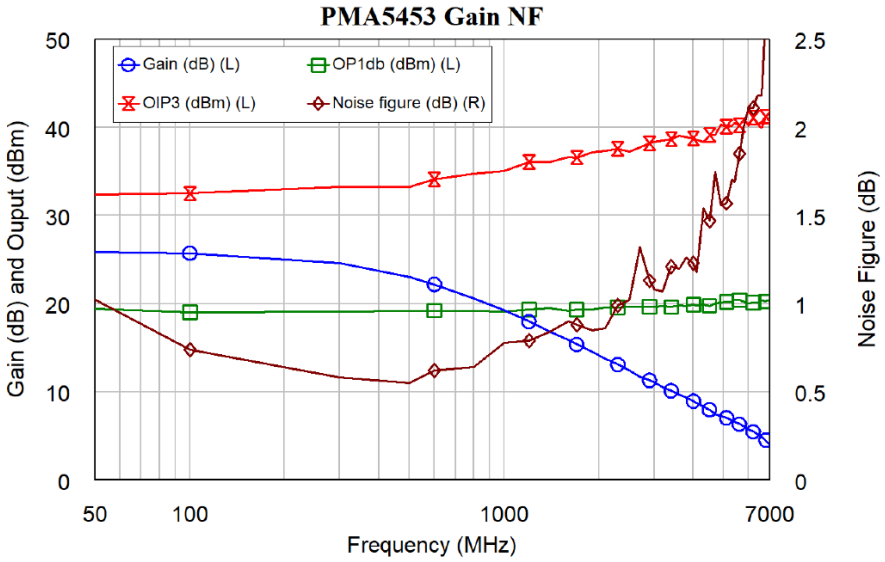



Figure 8.14. PMA5453 MMIC gain, power output and noise performance.

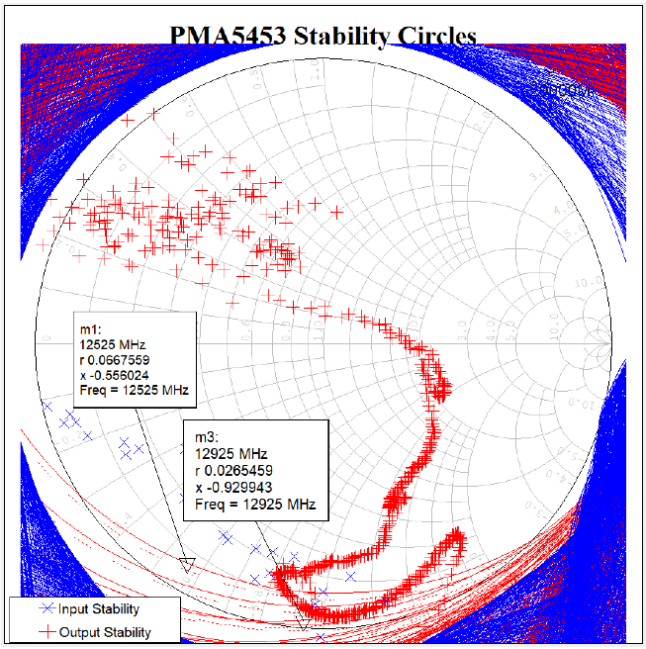



Figure 8.15. Stability circles for the PMA5453 MMIC.

Figure 8.14 shows the performance data of the PMA5453 obtained from [2] and then selecting View Data to download the pdf file containing tables of measured data. Comparing figures 8.8 and 8.14 shows that the BGB707 has a flatter frequency response to 1 GHz, but a slightly worse NF between 100 MHz and 1 GHz, than the PMA5453. Figure 8.14 shows that the amplifier has a very good linearity with an output IP3 level greater than 30 dBm (1W).

Figure 8.15 shows that the amplifier is unconditionally stable apart from the frequency region from 12.5 GHz to 12.9 GHz. Figure 8.16 shows the corresponding stability factors. For unconditional stability K>1, MU1>1 and MU2>1 and B>0. It can be seen that K, MU1 and MU2 are >1 and B>0 for all measured frequencies, apart from a small dip in MU1 at 12.5 to 12.9 GHz. As a result, the amplifier is unconditionally stable over its normal operating range of 50 MHz to 6 GHz.

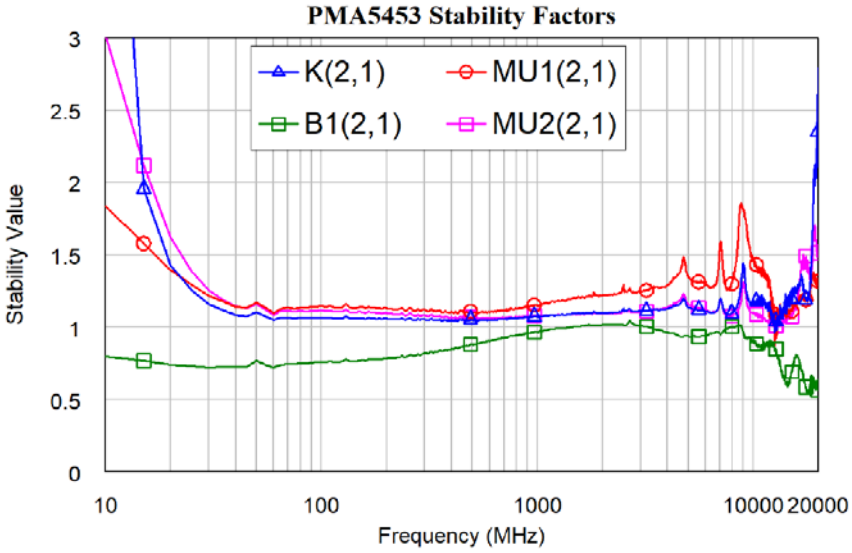



Figure 8.16. Stability factors for the PMA5453 MMIC

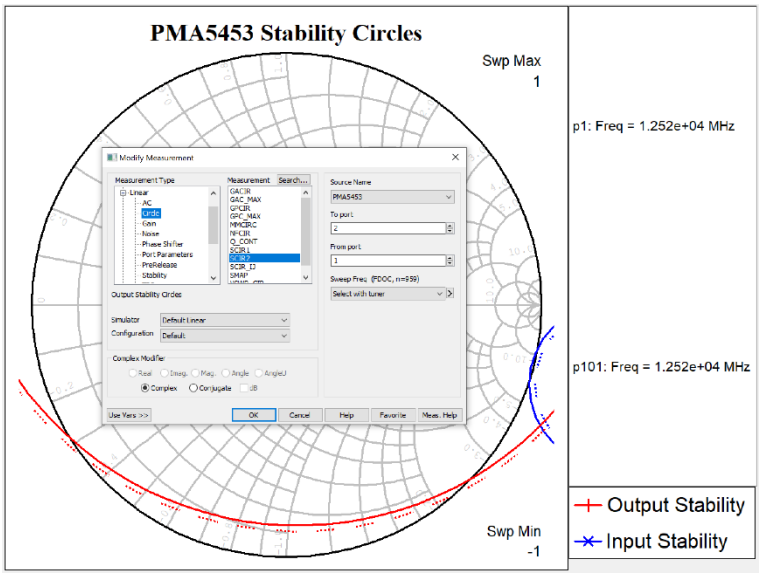



Figure 8.17. Tuning stability circle frequency to verify stability.

There reduced stability from 12.5 to 12.9 GHz, can be investigated further by plotting the stability circles when tuning the operating frequency, as shown in figure 8.17. This shows

that the amplifier is conditionally stable at 12.525 GHz for both the input and output stability circles. This shows that it is important to measure an amplifier's stability outside the normal 50 MHz to 6 GHz operating frequency region, since an amplifier may oscillate at a frequency outside the normal operating range. If an amplifier exhibits less gain or output power capability than expected, or it runs hotter than expected, then it is a good idea to use a spectrum analyser to check if it is oscillating outside the normal frequency region. The PMA5453 is much more stable than the BGB707 but it requires a supply current of 40 to 60 mA, compared to 6 mA for the BGB707.

## Example 8.3: Bipolar Transistor

The interaction between stability factors, noise factors and gain are illustrated using the design of a low noise amplifier using a Infineon BFP540 [11] low noise silicon NPN transistor. The typical specifications of that transistor are: NF = 0.9 dB, at $I_C$ = 5 mA, $V_{ce}$ = 2 V, f = 1.8 GHz. Gain = 21.5 dB and OIP3 =24.5 dBm at $I_C$ = 20 mA, $V_{ce}$ = 2 V, f = 1.8 GHz. The models for the BFP540 transistor are available from the *Elements* ⇒ *χ Libraries* ⇒ χ * AWR web site ⇒ *Parts by Vendor* ⇒ Infineon. The linear model, is available at ⇒ *Data* ⇒ *RF Bipolar Transistors* ⇒ *Low Noise Si Transistors up to 5 GHz* ⇒ *BFP540.* The nonlinear Spice model is at ⇒ *Nonlinear* ⇒ *RF Bipolar Transistors* ⇒ *Low Noise Si Transistors up to 5 GHz* ⇒ *BFP540.* In the first example, the linear model, based on S parameters is used. In this example, the Spice based model is used. There are different versions of the BFP540 family. The BFP540 has a slightly lower NF than the BFP540FESD. However, the BFP540FESD has ESD protection, which will protect the transistor from Electro Static Charges, which could be induced on the input.

When importing the model into a circuit schematic, a four terminal block is used. That can be changed to a dual emitter transistor symbol. However, that requires the pin numbers in the Spice files to be changed slightly as follows:

Original: DEF4P 2 1 3 4 "BFP540FESD"

Changed to: DEF4P 1 2 3 4 "BFP540FESD"

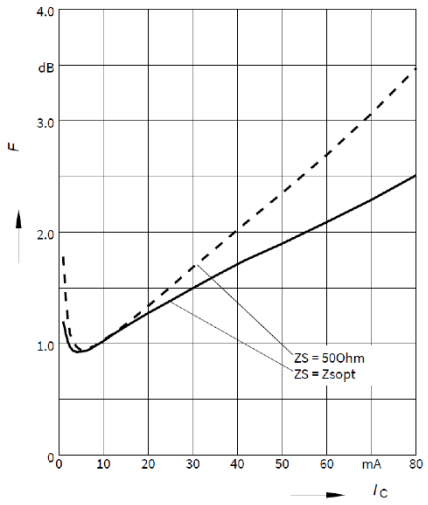



Figure 8.18. NF versus collector current at 1.8 GHz [Figure 14 of 11].

The NF will vary with frequency and collector current. At < 1MHz the noise rises due to 1/f noise at a rate of 20 dB per decade. This 1/f noise is not normally included in the model for the transistor, since external components such as coupling capacitors are likely

to dominate the NF at those frequencies. At high frequencies the noise rises because of changes in the transistor parameters. The NF in these the regions rises at 40 dB per decade. In addition the noise voltage changes with collector current and voltage across the transistor. The NF for the transistor is shown in figure 8.18. Coleman [12] shows how the NF relates to different transistor parameters.

To start the design, a basic amplifier as shown in figure 8.19 is used. That circuit uses the dual emitter transistor symbol for the BFP540. The transistor is designed to have the emitter device pins connected to ground. The design uses the 5 mA collector current and a $V_{ce}$ = 2 V corresponding to the values for which the NF is specified in the device data sheet [11]. Note that the resulting NF is worse at 1 GHz than shown in figure 8.18.

The NF and gain can now be calculated using computer simulation and they are shown in figure 8.20. The rise in NF at low frequency is due to the input coupling capacitor causing an impedance mismatch at low frequency. The rise in NF at high frequency is due to changes in transistor parameters and corresponds to a drop in gain. The supply voltage, emitter resistor and bias resistor values are tuned, to obtain the best NF. The values shown in figure 8.19 correspond to the lowest NF consistent with a high power gain.

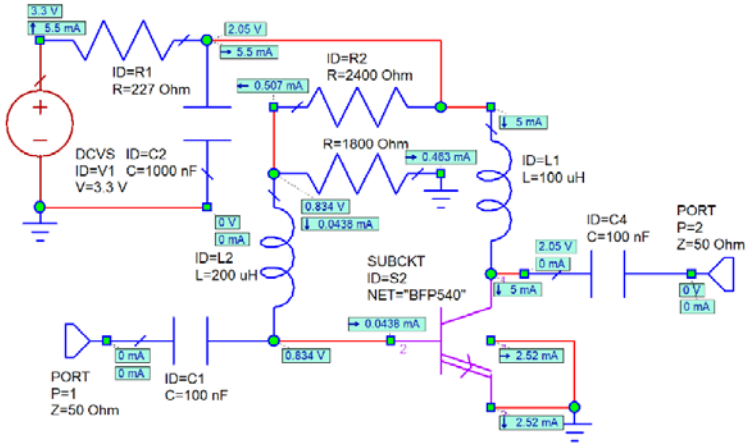



Figure 8.19. Basic low noise amplifier.

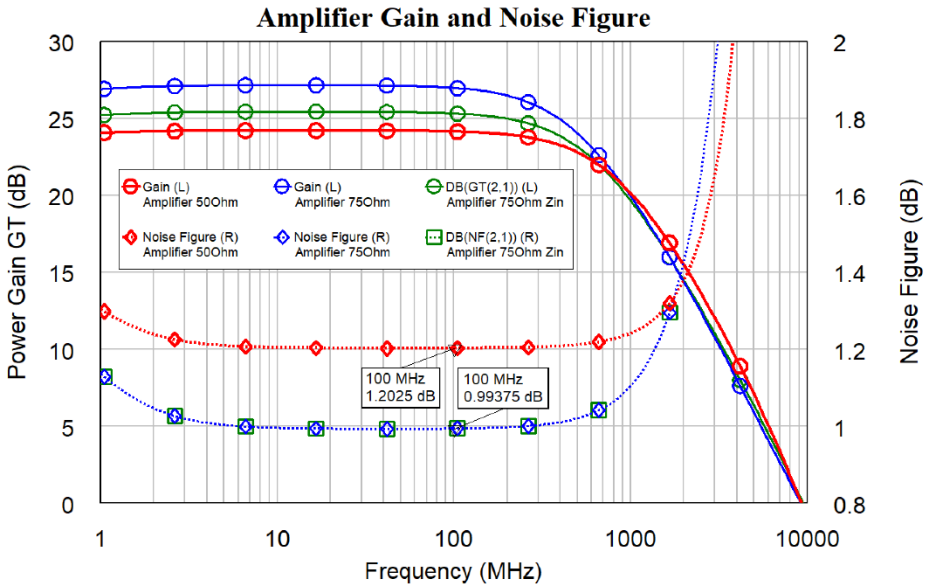



Figure 8.20. NF and gain of the amplifier.

Figure 8.21 shows a plot of K, B and Input μ and Output μ stability factors. For unconditional stability K>1, MU1>1 and MU2>1 and B>0. It can be seen that in the region of 3.5 MHz to 3 GHz, the amplifier is only conditionally stable. The amplifier is stable with a 50 Ω source and load impedance as shown in the gain plot of figure 8.20. Figure 8.22 shows the input and output stability circles plotted at 1 GHz, confirming that the BFP540 amplifier is only conditionally stable, but is stable for an input and output VSWR better than 2.5:1. The corresponding BFP540FESD (Electro-Static Protected) amplifier is stable for an input and output VSWR better than 3:1. However, the BFP540FESD has a 0.15 dB worse NF. To investigate the difference in performance between the BFP540 and the BFP540FESD simply change the linked netlist in the Circuit Schematics in the Ch8-Fig 19-24 AWR DE project file accompanying this book. The Input Stability Circle is shown in blue and the Output Stability Circle is shown in red.

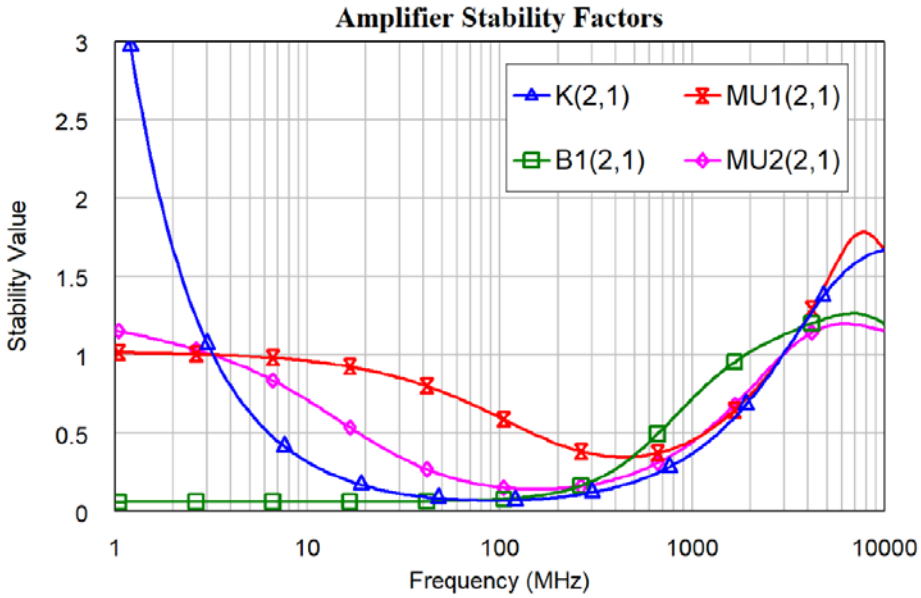



Figure 8.21. Stability factors for the basic amplifier.

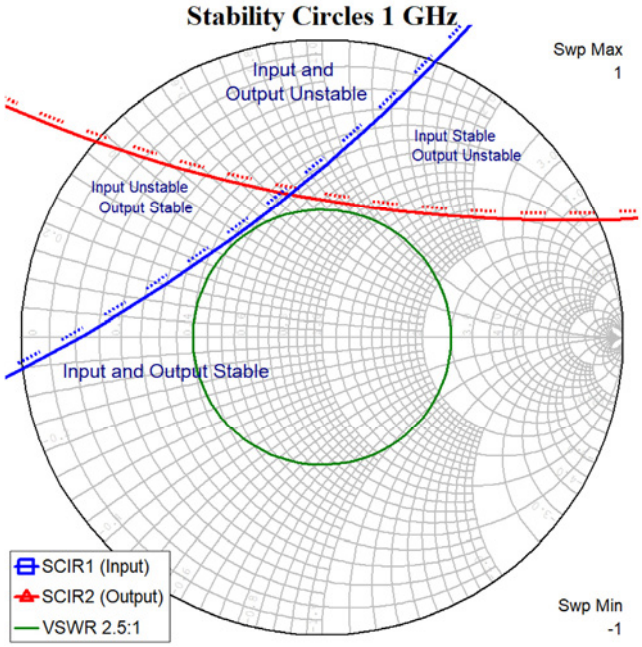



Figure 8.22. Stability input and output circles at 1GHz.

Figure 8.23 shows the input and output stability circles over a 10 MHz to 10 GHz sweep, and includes VSWR circles for VSRW ratios of 1.3:1, 1.5:1 and 2:1. For an unconditionally stable amplifier, the entire inside of the Smith Chart will be clear of any stability circles. From the input stability circles, the amplifier with 50 Ω termination is stable if the input has a VSWR less than 1.3. By disabling the SCIR1 (input) stability circle measurements, the output stability circles can clearly be seen and from them the amplifier is stable if the output has a VSWR less than 2:1.

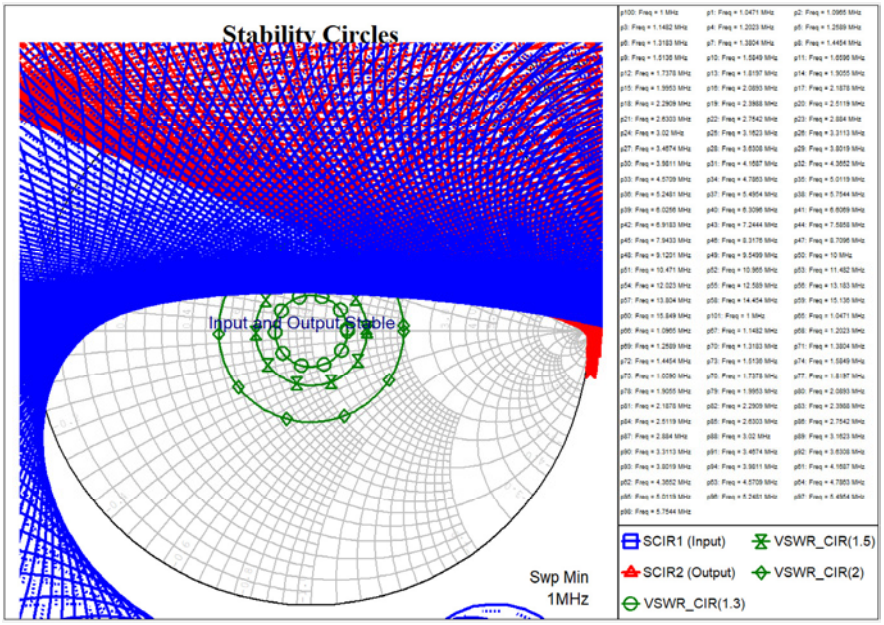



Figure 8.23. Stability input and output circles over 10MHz -10 GHz.

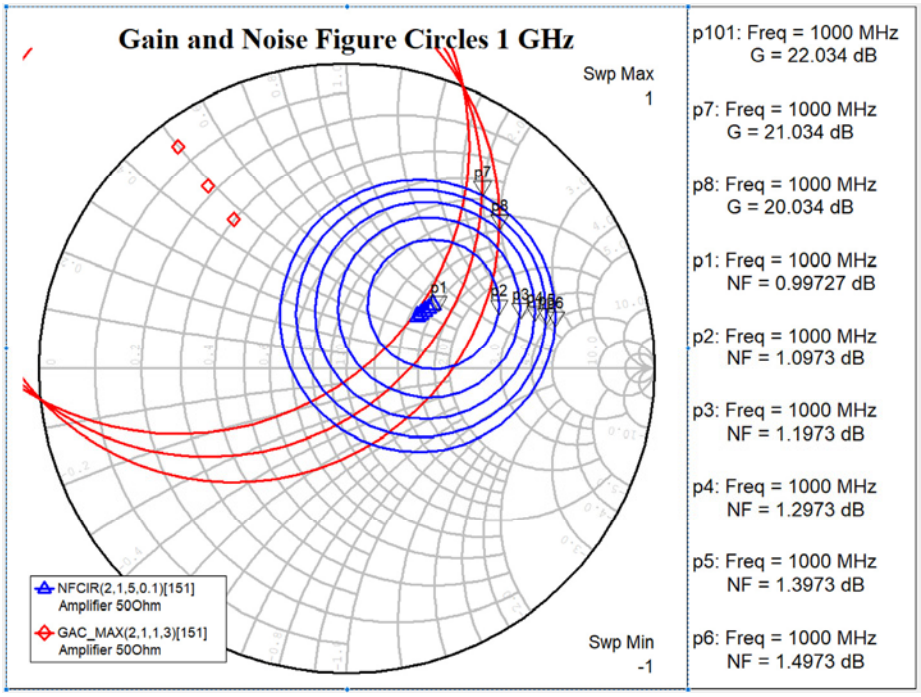



Figure 8.24. Constant gain and NF circles at 1 GHz.

Figure 8.24 shows the amplifier's constant gain and NF circles. Matching the amplifier input impedance to the centre of the constant noise circles, results in the lowest NF. Matching the input impedance of the amplifier to the centre of the available gain

(GAC_MAX) circles results in the highest amplifier gain. The circles show a constant NF contour or a constant gain contour. The spacing for the NF circles is 0.1 dB and the gain circles is 1 dB.

Figure 8.24 shows that matching the input of the amplifier to 75 Ω results in a normalised impedance of 1.5 (=75/50) on the Smith Chart. That gives a NF of 0.1 dB (Inner circle) below the optimum value and a 2 dB (second circle) below the optimum gain value. From figure 8.22 is can be seen that the location of the centres (Δ) of the NF circles is in a stable input region of the stability circle at 1 GHz, so that the optimum NF can be obtained at that frequency, by suitably matching the input. Changing the input and output impedances of the amplifier of figure 8.19, to 75 Ω, and retuning R1 and R2 to obtain a low NF as well as a good gain, results in R1=209 Ω and R2=2670 Ω. The blue curve in figure 8.20 shows that an improvement of 0.2 dB in the NF is obtained. The stability circles for the amplifier with 75 Ω input and output impedances is very similar to those shown in figure 8.23, for the amplifier with 50 Ω impedances. Changing the output impedance to 50 Ω, does not change the input stability circles, but makes the amplifier output slightly more stable and reduces the gain as shown in the green curves of figure 8.20. Changing the output impedance does not change the NF.

Figure 8.24 shows that a match for optimum noise performance will not result in the optimum gain. The centres (◊) of the constant gain circles of figure 8.24 lie in the unstable input region of the input stability circle at 1 GHz on figure 8.22, so that the optimum gain cannot be obtained, but 1 dB less gain will result in a stable amplifier. Normally the first stage of a low noise amplifier is matched for the lowest NF and the second stage is matched for the highest power gain, since equations 8.26 and 8.27 show that the NF of the first stage is critical, but the NF of later amplifier stages have much less effect.

## Improving Amplifier Noise Figure and Stability

The techniques described in this section can be used to improve amplifier noise figure and stability either singly or in combination. Depending on the amplifier some will be more effective than others.

### *Bandwidth Limiting using Reflectionless Filters*

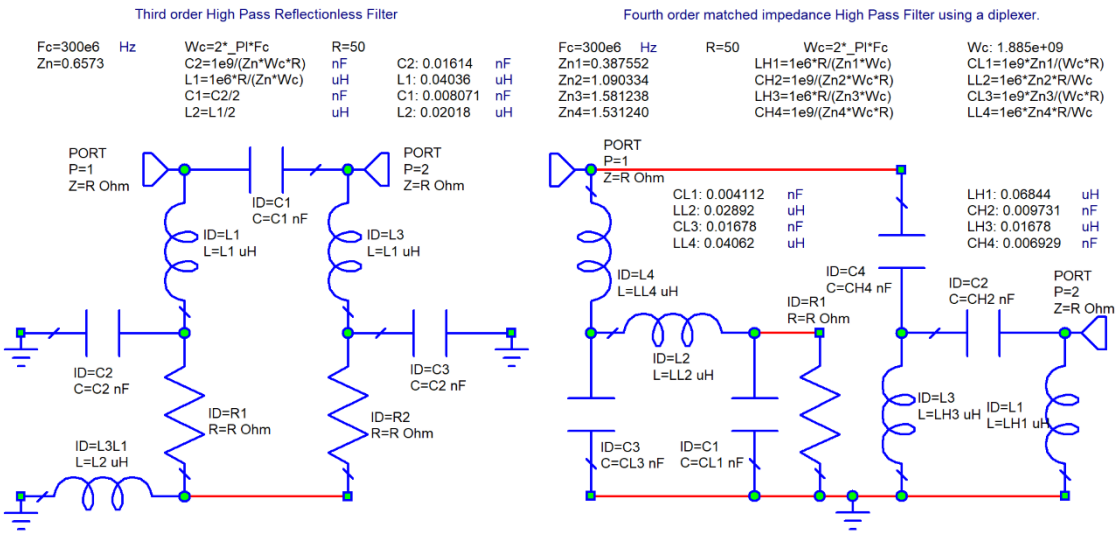



Figure 8.25. Reflectionless (L) and Diplexer (R) high pass filters with Fc = 300 MHz.

In many cases, the amplifier may be conditionally stable outside the operational frequency range. If the low noise amplifier is used at the input of a receiver, filters may be required to prevent unwanted input signals from passing through the filter. Using conventional filters is likely to make the amplifier less stable. However using reflectionless filters, as described in chapter 7, or diplexers as used in example 2.2, to the input and/or output may make the amplifier more stable. The impedance looking into port 1 for both the circuits in figure 8.25 is exactly 50 Ω at all frequencies. The BGB707 MMIC at 3 V and 6 mA of figure 8.7, 8.9 and 8.10, for frequencies between 57 MHz and 457 MHz, is only stable if the input VSWR is <1.2. If this amplifier is to be used above 500 MHz, then a reflectionless high pass filter or diplexer with a 300 MHz cut off frequency will ensure signals above 500 MHz are passed amplified without loss and will have the same NF.

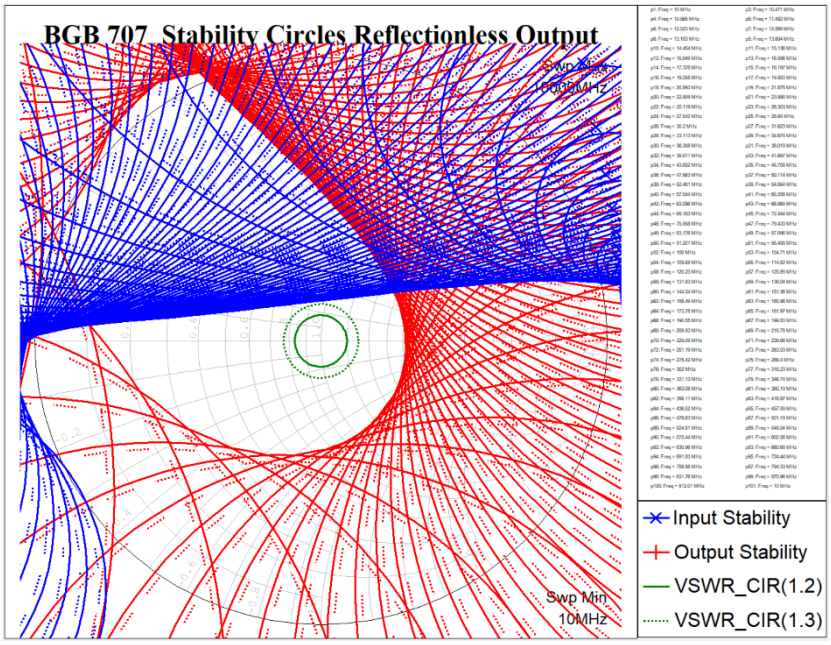



Figure 8.26. Stability circles with a reflectionless filter at the output.

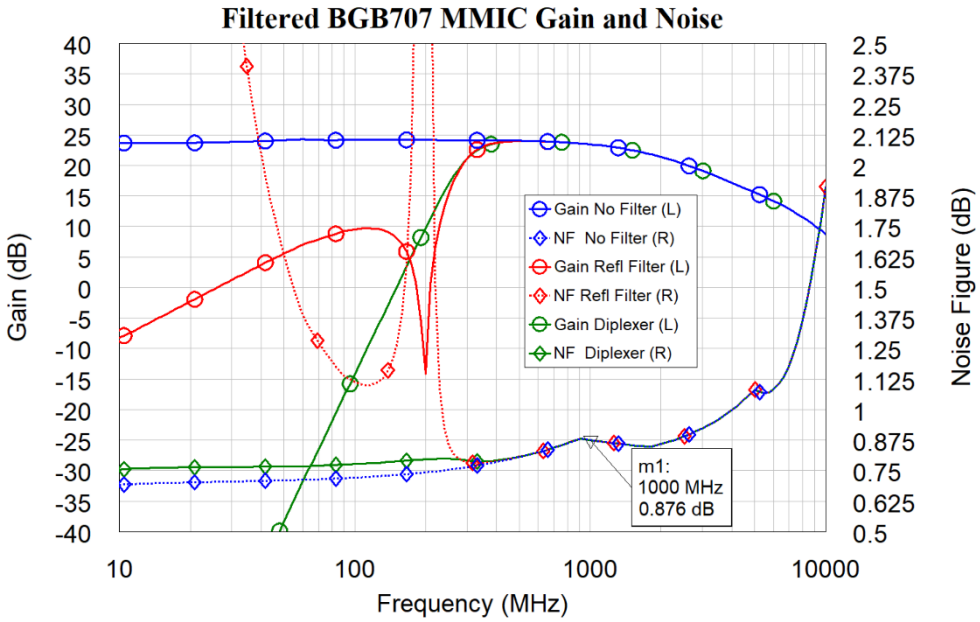



Figure 8.27. Gain and NF of amplifier with reflectionless filters.

For the BGB707 MMIC at 3 V and 6 mA, figure 8.9 shows that the input stability circles dominate the amplifier's stability. A reflectionless filter or diplexer at the output affects those input stability circles. Applying a reflectionless filter at the input does not have much effect of the stability. Figure 8.26 shows the stability circles of the BGB707 MMIC amplifier of figure 8.7, with the reflectionless filter of figure 8.25 at the amplifier's output. Comparing this with the performance of the amplifier alone, as shown in figure 8.10, shows that the amplifier stability is improved.

Figure 8.27 shows the resulting gain and NF of the amplifier, with and without the reflectionless filter or diplexer at the output. Above 500 MHz, the filters have little effect on the amplifier performance. The diplexer uses more components but gives a higher out of band attenuation and a better out of band noise figure. Reflectionless filters or diplexers can thus be used to stabilise low noise amplifiers and prevent them being overloaded by out-of-band signals, without affecting the NF and gain of the amplifier in the desired frequency band.

## *Resistors at Output*

Provided an amplifier has a reasonable stability, like the amplifiers in the three examples in this chapter, then the amplifier's stability can be improved by adding a resistive attenuator at the output. For an amplifier with a 50 Ω output impedance, a 250 Ω load corresponds to a 5:1 VSWR. Placing a 3 dB (50 Ω) attenuator in-between the amplifier and the 50 Ω load reduces the VSWR that the amplifier sees, to < 2:1. Similarly, a bigger mismatch can be handled by a bigger attenuation. Adding an attenuator to the output of an amplifier normally has little effect on the NF. Provided the amplifier's gain is much larger than the attenuation inserted, the loss of gain can be made up with little change in NF by adding additional amplifier stages. Generally, if one adds resistors at the input, then the NF of an amplifier will increase, however the stability can be improved. So adding resistors at the amplifier output is preferred.

There are three possible ways to add resistances to the output:

1) In series with the output, thus increasing the impedance that the amplifier sees.

2) As a shunt across the output, thus decreasing the impedance that the amplifier sees.

3) As a T or Pi Pad, thus keeping the amplifier's load impedance at its designed value.

It is also possible to use either a combination of 1) and 2) or using 3) to have a different load and amplifier impedances.

For the first stability improvement, a resistor is placed in series or parallel with the amplifier output and the impedance is tuned, to implement 1) and 2) above. To illustrate this, this technique is used on the BGB707 MMIC of the first example in this chapter. Figure 8.9 shows that this amplifier is conditionally stable and that an input VSWR of 1.2 results in instability. Figure 8.13 shows that having a 75 Ω input and output impedance results in a higher gain and lower noise, however for frequencies below 40 MHz, the Smith chart centre is inside the unstable regions of the input stability circles.

Changing the output impedance to 50 Ω as shown in figure 8.28a, results a slightly improved stability with the centre of the Smith Chart to be just inside the stable regions of the stability circles as shown in figure 8.29a. In addition, that reduces the gain from the 27.52 dB at 100 MHz for the blue curve in figure 8.13, to 25.77 dB for the blue curve in figure 8.30. Placing a 46 Ω resistor in parallel with the 50 Ω amplifier output load, as shown in figure 8.28b, makes the amplifier unconditionally stable, but reduces the gain

to 19.4 dB at 100 MHz and slightly increases the NF, as shown in the brown curves of figure 8.30. Figure 8.29 b) shows that adding the 46 Ω resistor, makes the amplifier unconditionally stable.

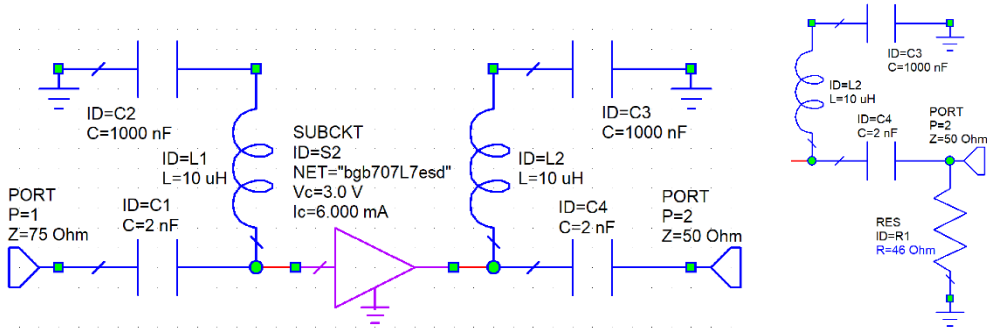



Figure 8.28. Circuit Schematic of: a) Basic bgb707 amplifier. b) Output change for stability.

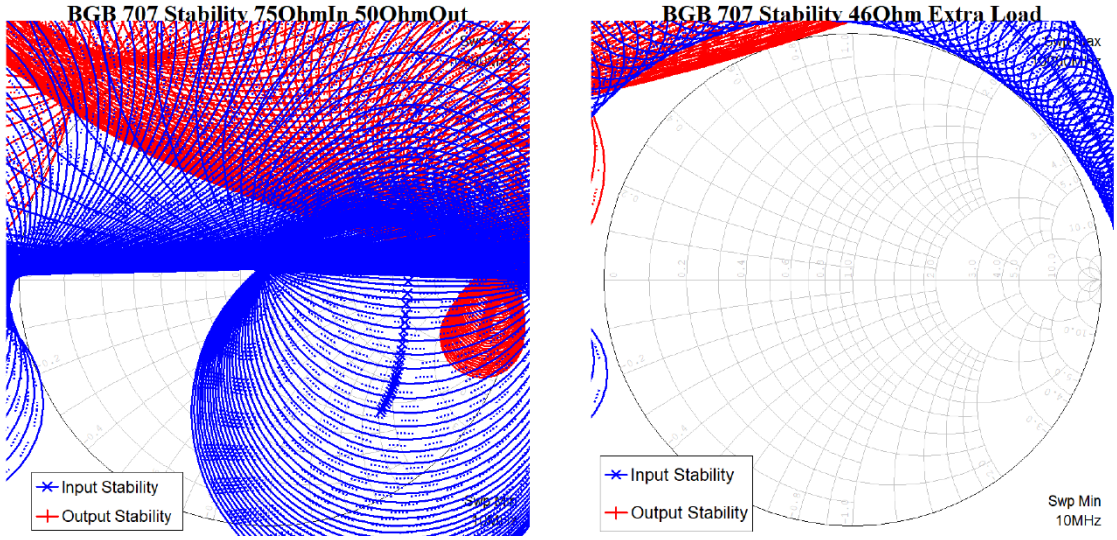



Figure 8.29 Stability circles of a) amplifier of figure 8.28a. b) with output change of figure 8.28b.

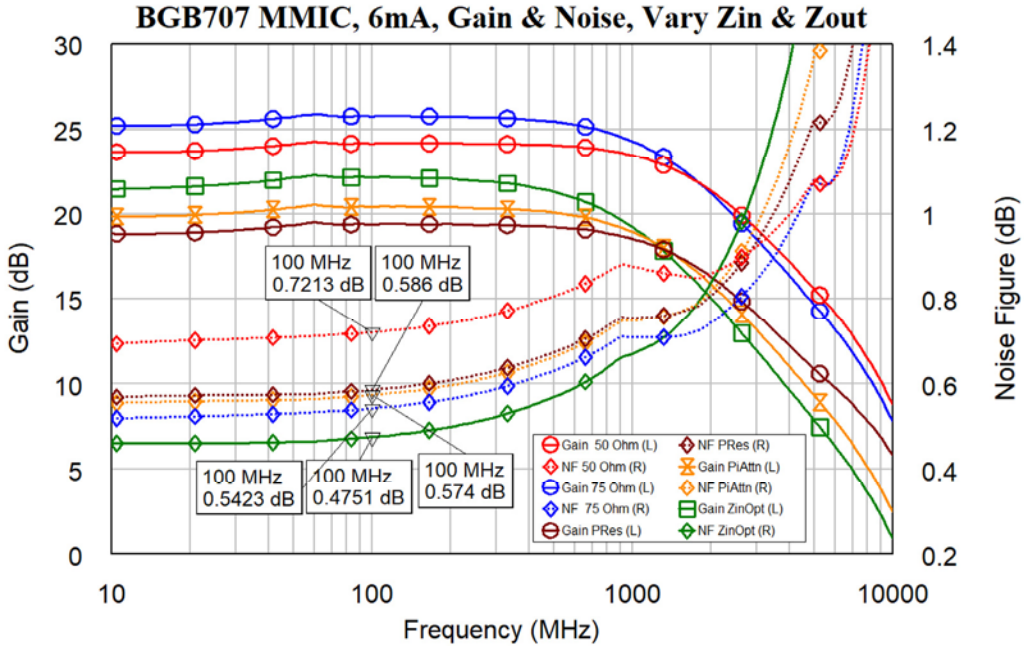



Figure 8.30 Gain and NF Stability

It is also possible to make the amplifier unconditionally stable by placing a 50 Ω, 5.35 dB attenuator between the amplifier output and the load. That results in a slightly higher gain of 20.42 dB at 100 MHz and a lower NF than the amplifier output of figure 8.28b, as shown in the orange (PiAttn) curves of figure 8.30.

Finally, the NF of the amplifier can be reduced by tuning the input impedance, Rin and Xin. Changing the input impedance will change both the NF and the gain of the amplifier. A low NF together with a good gain occurs when Zin =121 + j0 Ω, as shown in the green (ZinOpt) curves of figure 8.30. Changing the input impedance required the attenuation to be changed to 5.4 dB for unconditional stability. The corresponding stability circle plots look very similar to that of figure 29b. They can be obtained from the accompanying Ch8_Fig28-33 AWR DE project files. The 121 + j0 Ω input impedance is close to the impedance of the centre of the green 25 MHz NF circles in figure 8.12. Figure 8.31 shows the corresponding circuit and that includes an attenuator. Comparing the green curves in figure 8.30 for the amplifier of figure 8.31, with the red curves for the amplifier of figure 8.7 ($Z_{in} = Z_{out} = 50$ Ω), shows that by optimising the input impedance and placing a 5.4 dB attenuator before the output, the amplifier's performance is improved. The amplifier of figure 8.31 has a gain of 22.15 dB and a NF of 0.475 dB at 100 MHz and is unconditionally stable.

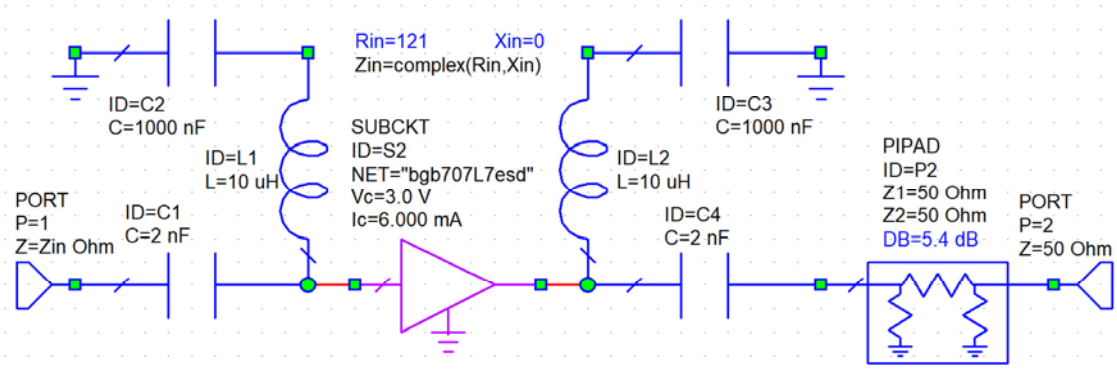



Figure 8.31 Tuning input impedance to obtain optimum NF.

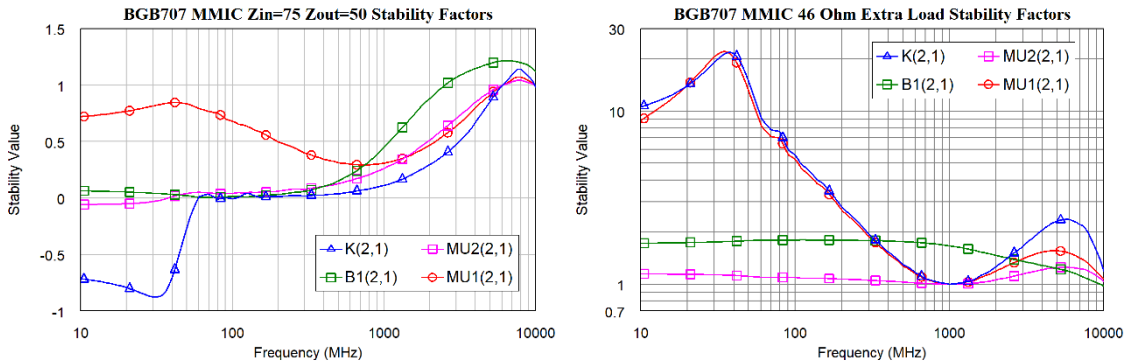



Figure 8.32 Stability Factors: a) Amplifier of figure 8.28a. b) Amplifier of figure 8.28b

Figures 8.32 and 8.33 show the stability factors of the above amplifiers. Figure 8.32a shows the stability factors of the amplifier of figure 8.28a with the 75 Ω input impedance. That amplifier is only conditionally stable, with both K and Mu2 being <0. Figure 8.32a is very similar to the stability factors of this amplifier with a 50 Ω input impedance as shown in figure 8.10. The amplifier of figure 8.28b with the 46 Ω additional load resistance, and the amplifiers of figure 8.33 with an attenuator before the output are all unconditionally stable.

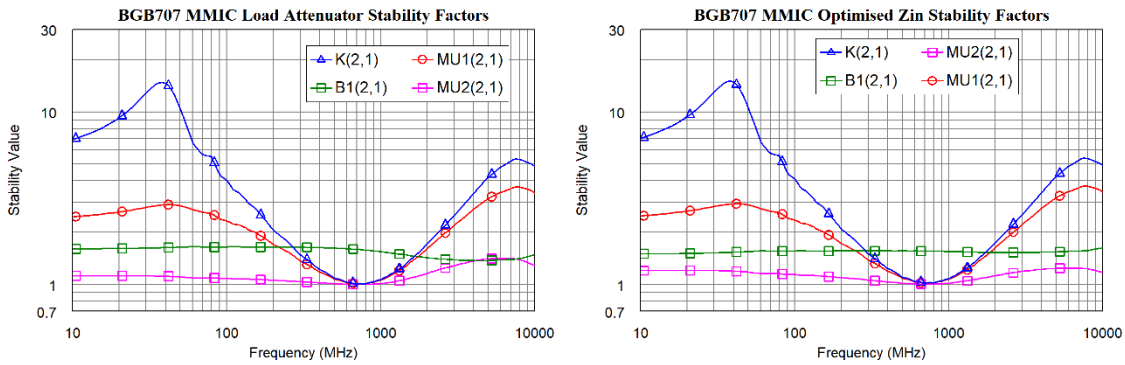



Figure 8.33 Stability Factors: a) Amplifier with attenuator. b) Amplifier with optimised Zin.

The technique of inserting an attenuator to make an amplifier unconditionally stable can also be applied to the BFP540 transistor amplifier of figure 8.19 used in example 3 above. Using a 50 Ω output impedance, inserting an attenuator and tuning the attenuation and resistors R1 and R2 results in the circuit of figure 8.34.

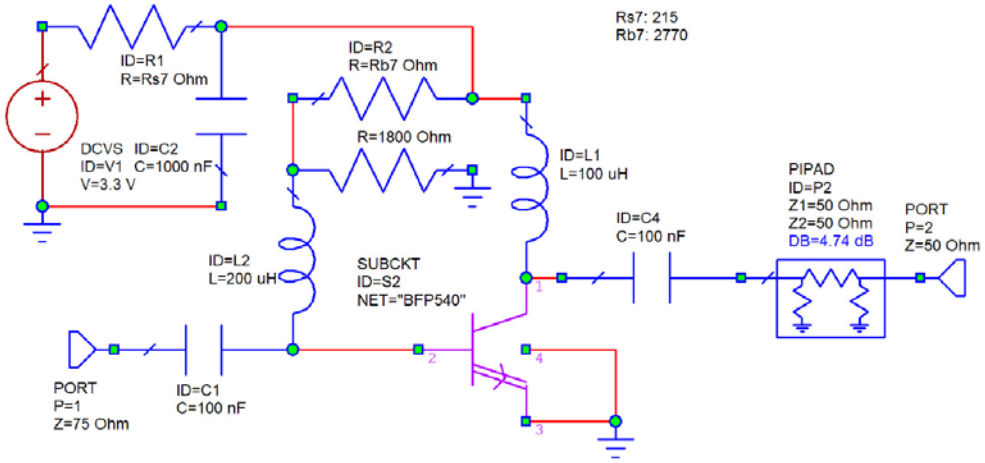



Figure 8.34. BFP540 amplifier after tuning to obtain optimum NF and unconditional stability.

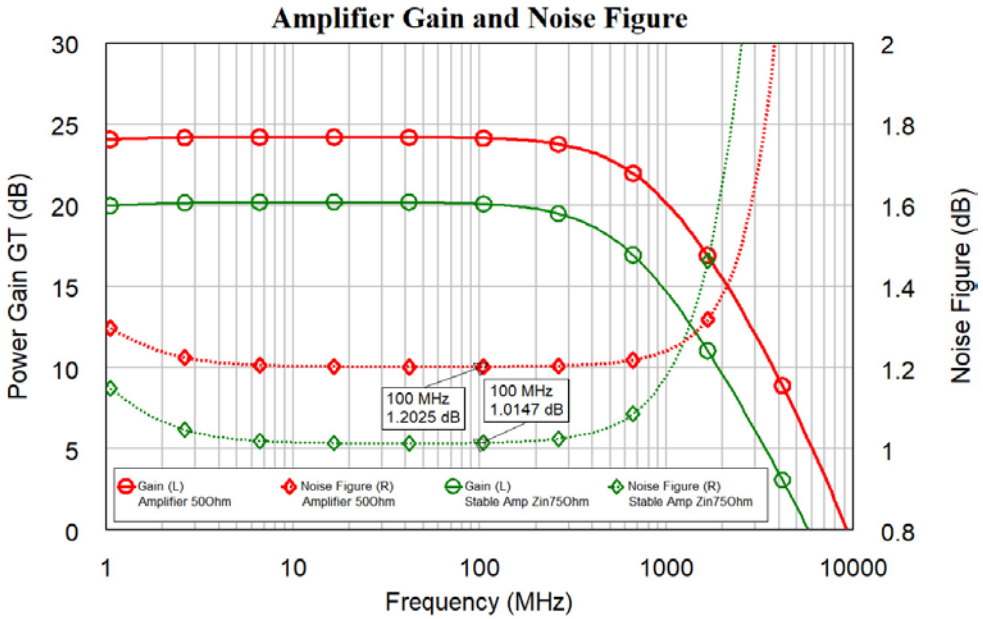



Figure 8.35. Gain and NF of amplifier of figure 8.34.

Figure 8.35 shows the corresponding gain and NF. Comparing the green curves of figures 8.34 with those of figure 8.20, shows that the stability has been obtained at just a 0.02 dB increase in NF, but that the gain has been reduced by slightly more than the 4.74 dB of the attenuator.

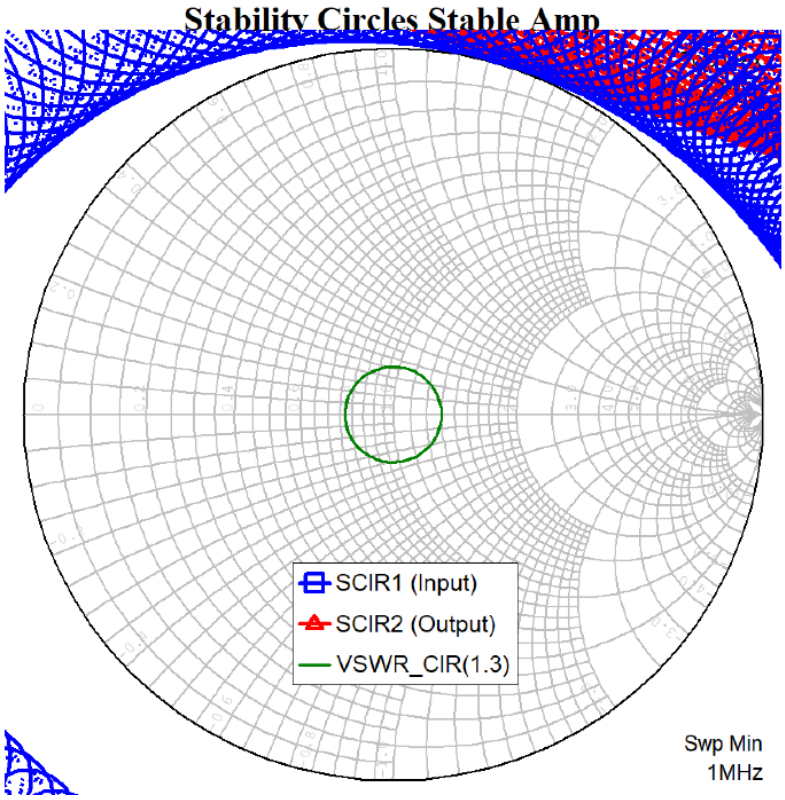



Figure 8.36. Stability circles of amplifier of figure 8.34.

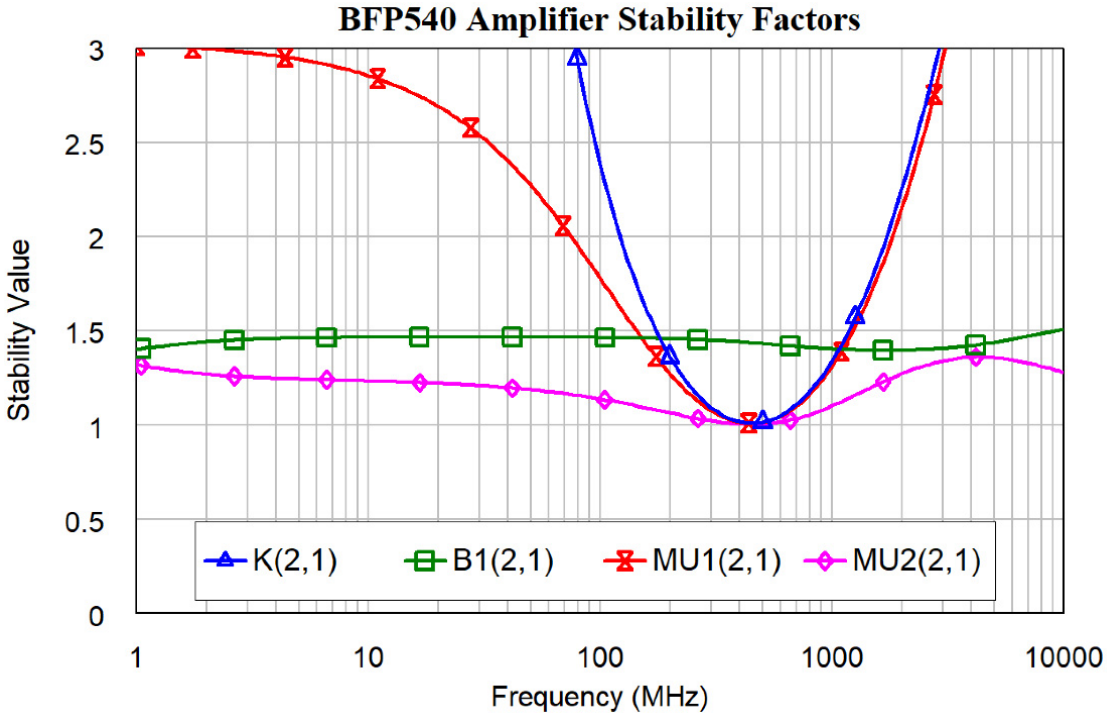



Figure 8.37. Stability factors of amplifier of figure 8.34.

Figure 8.36 shows the stability circles of the amplifier of figure 8.34. Figure 8.37 shows the corresponding stability factors. The worst stability is in the region of 300-500 MHz. Comparing these figures with figures 8.23 and 8.21, shows that the amplifier stability has been improved enormously by simply inserting an attenuator at the amplifier output. This has made a negligible difference in the NF.

## Conclusion

This chapter has described factors involved in amplifier stability. It was shown that selecting the correct input impedance will result in an optimum noise factor, but may affect amplifier stability. In many cases, the amplifier can be made unconditionally stable by changing the load applied to the amplifier or placing an attenuator in between the amplifier and its output terminals.

## References

Note: all web addresses were checked in September 2021.


1. Mini-Circuits, ERA-3+, https://www.minicircuits.com/WebStore/dashboard.html?model=ERA-3%2B
2. Mini-Circuits, PMA-5453+, https://www.minicircuits.com/WebStore/dashboard.html?model=PMA-5453%2B
3. Smith, P. H. “Transmission Line Calculator”, Electronics, Vol. 12, No. 1, pp 29-31, January 1939.
4. Smith, P. H. “An Improved Transmission Line Calculator”, Electronics, Vol. 17, No. 1, p 130, January 1944
5. D. M. Pozar, “Microwave Engineering” 3rd Edition, Wiley, 2005, Section 4.3 and Chapter 11. ISBN 0 471 44878 8
6. R. Gilmore, “Practical RF Circuit Design for Modern Wireless Systems”, Artech House, 2003.
7. Ecosorb Microwave absorber. https://www.laird.com/tool-bar?q=eccosorb
8. Harald T Friis Biography http://ethw.org/Harald_T._Friis
9. NORSAT Ku band LNB, http://www.norsat.com/solutions/microwave-products/lnb-ku-band/
10. Infineon bgb707L7ESD LNA MMIC, https://www.infineon.com/cms/en/product/rf-wireless-control/low-noise-amplifier-lna-ics/general-purpose-lnas/bgb707l7esd/
11. Infineon BFP540, https://www.infineon.com/cms/en/product/rf-wireless-control/rf-transistor/low-noise-si-transistors-up-to-5-ghz/bfp540/
12. C. Coleman; An introduction to Radio Frequency Engineering, Cambridge University Press, 2004. ISBN 0 521 83481 3.


## Abbreviations

| | |
|---|---|
| dBm | dB with respect to 1 mW. |
| E-PHEMT | Enhancement-mode Pseudomorphic High Electron Mobility Transistor. |
| ESD | Electro Static Discharge. |
| $G_A$ | Available Power Gain. |
| $G_T$ | Transducer Power Gain. |
| HEMT | High Electron Mobility Transistors. |
| InGaP | HBTs Indium Gallium Phosphide Heterojunction Bipolar Transistors. |
| LNB | Low Noise Block downconverter. |

| | |
|---|---|
| MMIC | Microwave Monolithic ICs. |
| $N_0$ | Thermal noise power. |
| NF | Noise Figure. |
| OIP3 | Third order Output intercept Point (power level). |
| $OP_{1db}$ | Output 1 dB compression power level. |
| $T_0$ | Ambient absolute temperature [K]. |
| $T_e$ | Equivalent noise temperature of an amplifier [K]. |

# Chapter 9

# Power Amplifier Design

## Introduction

In order to obtain the most power from a bipolar or field effect transistor, the input and output impedances of the device must be matched to that of the circuit in which it is placed. Similarly, if an antenna is to be driven effectively, the antenna needs to be matched. For the maximum power transfer, the source impedance and the load impedance must be a conjugate match, that is the resistive parts must be the same and the imaginary parts must be the same magnitude but opposite polarity.

### *RF Power Device Impedances*

In order to design a power amplifier and obtain the correct output using typical 50 Ω source and load impedances, the required input and output impedances of the transistor must be known. For maximum output power from a generator or a transistor, the load impedance should be, the complex conjugate of the output impedance of the generator. That results in the same power being dissipated in the load as is dissipated in the generator. For high power applications, the output impedance of the source should be much lower than the load impedance, so that most of the available power is dissipated in the load. The mains power network is one example where the desired generator's output impedance is much smaller than the loads applied. Similarly, the output impedance of an RF transistor should be much lower than the load impedance, to minimise the transistor's dissipation. The impedance that the source or load matching networks should present at the transistor are thus not the impedances of the transistor, but they are the impedances that must be presented in order to obtain the desired output power at a specified frequency and transistor quiescent currents. For an RF transistor operating at a supply voltage of $V_{cc}$, the collector or drain is normally connected to the supply voltage through an inductor. The output voltage can thus vary from close to $2*V_{cc}$ to $V_{sat}$. The maximum peak voltage is thus ($V_{cc}$-$V_{sat}$), where $V_{sat}$ is the saturation voltage of the device. The corresponding RMS output voltage is:

$$V_{rms} = \sqrt{V_{cc} - V_{sat}} \qquad \text{Eqn. 9.1.}$$

The load resistance for an output power of P is thus:

$$R_L = \frac{{V_{rms}}^2}{P} = \frac{(V_{cc} - V_{sat})^2}{2P} \qquad \text{Eqn. 9.2.}$$

Similarly, the required input matching impedance of a transistor used for RF power amplifiers is not the complex conjugate input impedance of the device. It is the impedance corresponding to the base or gate voltage and the base or gate current, which produces the desired output power from the device, whilst ensuring that the circuit is stable.

NXP's (Freescale ←Motorola) AN1526 [1] and AN282A [2] are good background documents that describes how these desired impedances are measured using test fixtures, and how the subsequent analysis of the impedance matching networks then results in the desired matching source and load impedances to obtain the desired output power from the transistor.

### *Large Signal Parameters*

For linear devices and small signals, S parameters are useful to determine input and output impedances and thus design complex conjugate matching networks to provide the maximum output power from those devices. S parameters also characterise forward and reverse gain and those are useful in determining the gain and stability of an amplifier. For power transistors, by performing measurements using test fixtures, the large signal input and output impedances and the corresponding forward and reverse gain parameters can be measured. From those, large-signal S parameters can be obtained. They are very different from the small signal impedances and small signal S parameters. For a given transistor, small signal parameters should only be used for small input signals, so that the device behaves in a linear manner, i.e. the superposition and scaling of signals is valid. The large-signal parameters should be used for the same device, if the magnitude of the input signal is such that, the device no longer behaves in a linear manner. The large-signal S parameters for the same device will differ depending on the biasing, modulation method and drive signal level. The large-signal S parameters are thus different for a Class AB amplifier for OFDM transmission for mobile phones, DAB and TV broadcasting compared to those for a class C amplifier for FM broadcasting. The large-signal S parameters or large signal source and load impedances can be used to design suitable impedance matching networks. However, in many cases, the parameters for the required operating conditions are not available and the optimum impedance matching needs to be determined experimentally.

### *Types of Matching*

**Transformer Matching:** RF Transformers can be used for wideband impedance-matching. The main limitations are the restricted range of available impedances (due to the turns-ratios being limited) and the frequency limitations on transformers.

**LC Matching:** Inductors and capacitors are used to provide the impedance transformation. LC matching results in a relatively narrow bandwidth match. LC matching is very practical at frequencies up to 1 GHz. Above 1 GHz, transmission-line matching is more economical. LC matching permits easy tuning of the match to allow for device variations.

**Transmission-Line Matching:** A transmission-line of a required length and Characteristic Impedance is used to obtain the required composite match. Such a match tends to be of a broader frequency range than LC matching and can be applied at frequencies above 100 MHz. Below 100 MHz the transmission-lines required tend to be too long to be practical. It is difficult to tune the length and characteristic impedance of a transmission-line once constructed.

For each application, each of the above matching techniques must be evaluated against the design criteria and the most appropriate technique selected.

## Choice of Components and Q Value

It is very important that the value of capacitors and inductors used be measured at the operating frequency. Many capacitors are not suitable for RF applications, as their self-resonance frequency is below the required operating frequency, or their losses are too high. For power applications, inductors need to be selected for the required current carrying capability and inductors with ferrite cores may not be suitable as their losses may be too high.

For a simple parallel tuned network, like the Pi network, the circulating current in a resonator is approximately Q times the external load current. For a 50 Watt amplifier, driving a 50 Ω load, the load current is 1 Amp. For Q = 10, the current circulating in the Pi network is thus of the order of 10 Amps. This can cause significant heating and failure of the components. For some networks like both the T networks and the Bandpass L network, very high voltages can be experienced at some nodes and this can lead to voltage breakdown of components. The higher the Q, the higher the stress on the components. A high Q value can also cause the matching network to drift out of match as the components change due to temperature. In general a Q value as low as possible is desirable, as this will give the widest bandwidth match and the lowest component stress. If the network is to be used as an output-matching network of an amplifier and harmonics are to be filtered as well, a higher Q value can be considered, since the higher the Q, the higher the attenuation at the amplifier harmonics. For amplifier output networks, where harmonic filtering is required, cascaded matching networks are preferred as a means to achieve the required harmonic attenuation. To obtain a wide bandwidth and use a low Q, successive impedance transformations are normally used, as described in this chapter, in the section on broadband matching.

Since the current and voltage limits in the output-matching networks are very important, a trade-off between the Q value and the order of the filter will need to be considered, in order to achieve the required harmonic attenuation and bandwidth, as well as desirable voltage and current levels.

## LC Matching

In LC matching, inductors and capacitors are used to obtain the required conjugate impedance match. The equations for calculating the components required are contained in NXP (Motorola) Application Note AN267 [1]. LC matching is very practical for power amplifiers up to 1 GHz. A good indication of the suitability of LC matching for a transistor can be obtained by noting the type of matching used for test circuits in the manufacturer's data sheet for the transistor.

Because it is easy to tune the matching network using variable capacitors, these LC matching networks are normally used by the manufacturers to determine the input and output impedance of the devices. The device is placed in a test jig and the matching network is adjusted to obtain the required output power at a good efficiency, a low input return loss and amplifier stability. The values of the resulting LC matching components are then used to determine the input and output impedance of the device.

AN267 describes 4 types of matching networks. In all the equations used in this chapter, the device impedance is $R_d+jX_d$ and the load impedance is $R_L$. That notation is different from AN267, where $R_l$ and $R_L$ can readily be confused, particularly if a lowercase L is used. In the equations presented here, it is not assumed that the device is capacitive, so that $X_d$ is used for the reactive part of the device impedance, instead of $-X_{cout}$, as in AN267. For the Pi Network, in AN267, the reactive part of the device impedance must manually be included in the matching network capacitance. The reactive part is included in equation 9.3.

In AN267, different expressions for A and B are used for the bandpass T and the lowpass T networks. In this book, consistent expression for A and B are used. In AN267, the term A for the bandpass T network is wrong. The LC matching equations 9.3 to 9.19 presented in this book are consistent and correct.

In the designs presented here, the equations for the matching networks are evaluated inside Cadence AWR DE. This allows design parameters to be changed or optimised and allows the effect of such design parameters changes to be observed.

## Pi Network

The Pi matching network is very useful for matching high impedance sources to 50 Ω loads. Pi matching is normally used in valve, or tube, amplifiers. For high power solid-state devices, the impedance values become impractical with very large capacitors and very small inductors being required. Figure 9.1 shows the Pi network used for matching.

To obtain the component values, firstly decide on a Q value for the matching network. The Q value will affect the bandwidth, harmonic attenuation and component stress. For the Pi network, the input impedance needs to be a parallel network, so that a series to parallel transformation may need to be applied before the network evaluation as shown in equation 9.3, which transforms the device impedance of RD+jXD into RP in parallel with XP. The equations for the Pi network in AN267 assume that the device is resistive and that any reactive impedances are compensated for after the Pi network is designed.

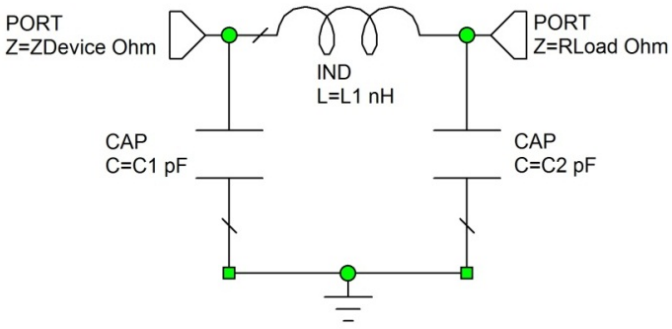



Figure 9.1. Pi matching network.

The equations in the included MWO files handle reactive parts correctly. The complete equations for the Pi matching network are as follows:

$$R_p = \frac{R_D{}^2 + X_D{}^2}{R_D} \qquad X_p = \frac{R_D{}^2 + X_D{}^2}{X_D} \qquad \text{Eqn. 9.3}$$

$$Y_{C1} = \frac{1}{X_{C1}} = \frac{Q}{R_P} + \frac{1}{X_P} \qquad \text{Eqn. 9.4}$$

$$X_{C2} = R_L \sqrt{\frac{\frac{R_P}{R_L}}{(Q^2+1) - \frac{R_P}{R_L}}} \qquad \text{Eqn. 9.5}$$

$$X_L = \frac{QR_P + (\frac{R_P R_L}{X_{C2}})}{Q^2+1} \qquad \text{Eqn. 9.6}$$

Note that $Q^2 + 1$ must be larger than $R_P/R_L$ for $X_{C2}$ to be valid, so that there is a minimum Q value for a given impedance transformation ratio.

## Lowpass T Network

The Lowpass T network is very good for use as an output-matching network for a power amplifier stage, where the amplifier is to be connected to an antenna. Having a series inductor (L1) as the element connected to the device results in an open circuit to the second harmonic currents, resulting in a reduced current flow through the transistor and resulting in a higher efficiency. However, since the output voltage is more distorted a higher inter-modulation distortion may result. For more severe filtering of harmonics, a cascaded set of Lowpass matching networks is desirable.

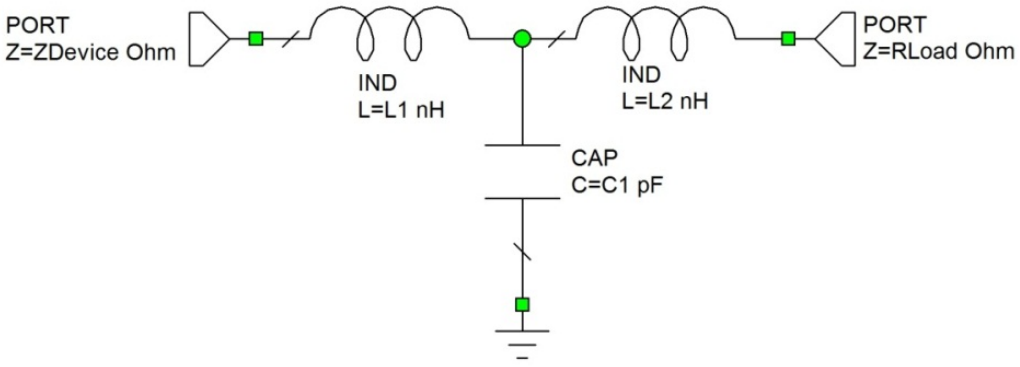



Figure 9.2. T matching network.

The equations for the Lowpass T network are as follows:

$$X_{L1} = QR_D - X_D$$ where $R_D + jX_D$ is the device impedance Eqn. 9.7

$$X_{L2} = R_L A$$ Eqn. 9.8

$$X_{C1} = \frac{B}{Q + A}$$ Eqn. 9.9

where

$$A = \sqrt{\left[\frac{R_D(1+Q^2)}{R_L}\right] - 1} = \sqrt{\left[\frac{B}{R_L}\right] - 1}$$ Eqn. 9.10

$$B = R_D(1+Q^2)$$ Eqn. 9.11

Note this network clearly shows that the Q used in the matching network relates to the impedance transformation ratio. The minimum Q occurs when $A_1=0$, so that

$$Q_{\min} = \sqrt{\frac{R_L}{R_D} - 1}$$ Eqn. 9.12

## Bandpass L Network

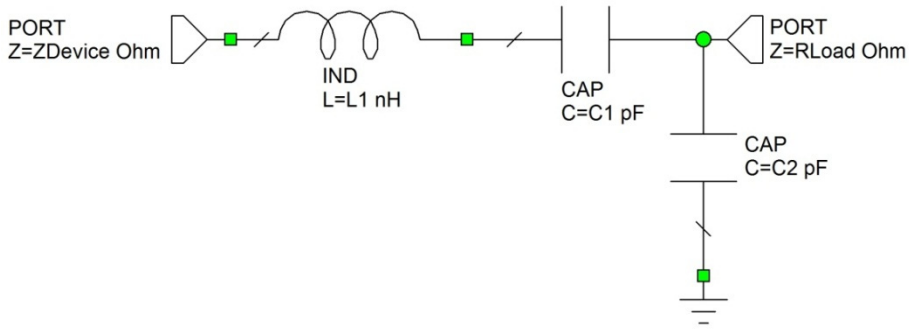



Figure 9.3. Bandpass L matching network.

The bandpass L network is often used as test circuit by semiconductor manufacturers. It incorporates a DC block (C1), to allow biasing to be set up for the input of transistors and to prevent any DC supply from appearing on the output of an amplifier stage. Normally C1 and C2 are adjustable, making it very easy to tune the amplifier for either a peak of output for an output-matching network or for the best input match for an input matching network.

The equations for the band pass L network are as follows:

$$X_{C1} = QR_D$$ where $R_D + jX_D$ is the device impedance Eqn. 9.13

$$X_{C2} = R_l\sqrt{\frac{R_d}{R_l - R_d}}$$ Eqn. 9.14

$$X_{L2} = X_{C1} + \left(\frac{R_D R_L}{X_{C2}}\right)$$ Eqn. 9.15

The device reactance $X_D$ is incorporated in either $C_2$ for capacitive device impedances or into $L_2$ for inductive device impedances. In the equations of figures 9.7 and 9.8, this is incorporated by having $X_{pd} = X_d$ and $X_{md} = 0$ if $X_d > 0$ and having $X_{pd} = 0$ and $X_{md} = X_d$ if $X_d < 0$. This will ensure the lowest Q of the network and thus the widest bandwidth. This network can only be used if $R_D < R_L$, since the parts under the square root sign

## Bandpass T Network

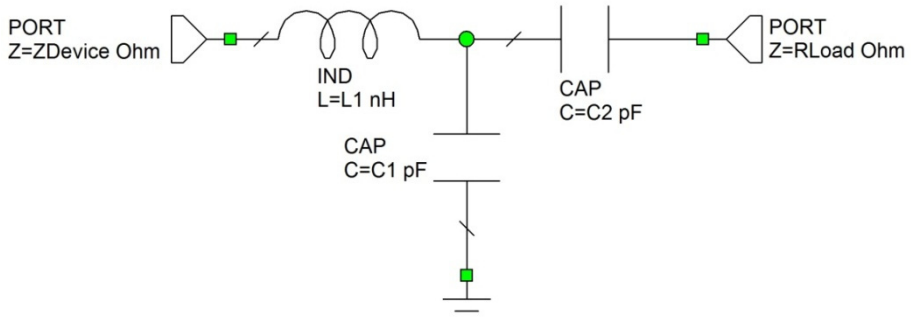



Figure 9.4. Bandpass T matching network.

The equations for the band pass T network are as follows:

$$X_{L1} = QR_D - X_D \qquad \text{where } R_D + jX_D \text{ is the device impedance} \qquad \text{Eqn. 9.16}$$

$$X_{C2} = A\ R_L \qquad \text{Eqn. 9.17}$$

$$X_{C1} = \frac{B}{Q - A} \qquad \text{Eqn. 9.18}$$

Where A and B and the minimum Q are as before:

This network can only be used if $R_D < R_L$ , since otherwise negative values for $C_1$ result.

**Important notes:**

1 Some of the equations for the Pi network are different since the reactive parts of the device are handled in the equations presented here and in the global variables panel of the AWR DE files for figures 9.9 to 9.19, while they are not in included in AN267 [1].

2 In these notes A and B are kept the same in these notes, while A and B are swapped and changed in AN267.

3 In AN267 the term A for the Bandpass T is wrong. AN267 uses:

$$A_{267} = \sqrt{\left[\frac{R_D(1+Q^2)}{R_L}\right]} - 1 = \sqrt{\left[\frac{B}{R_L}\right]} - 1 \qquad \text{Eqn. 9.19}$$

That will not give a correct match, as can be verified by using AWR DE. The square root should be extended to cover the –1 term as shown in the expression for A in equation 9.10.

## *Capacitive Impedance Transformer*

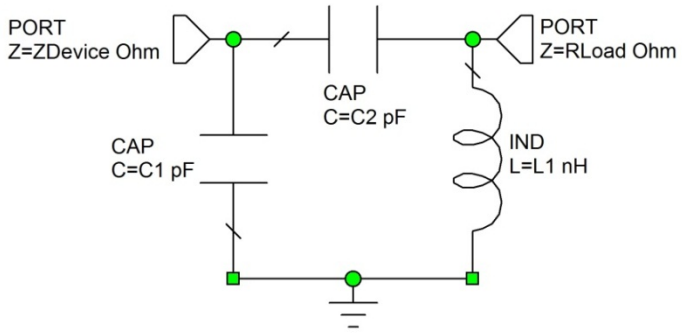



Figure 9.5. Capacitive Impedance Transformer matching network.

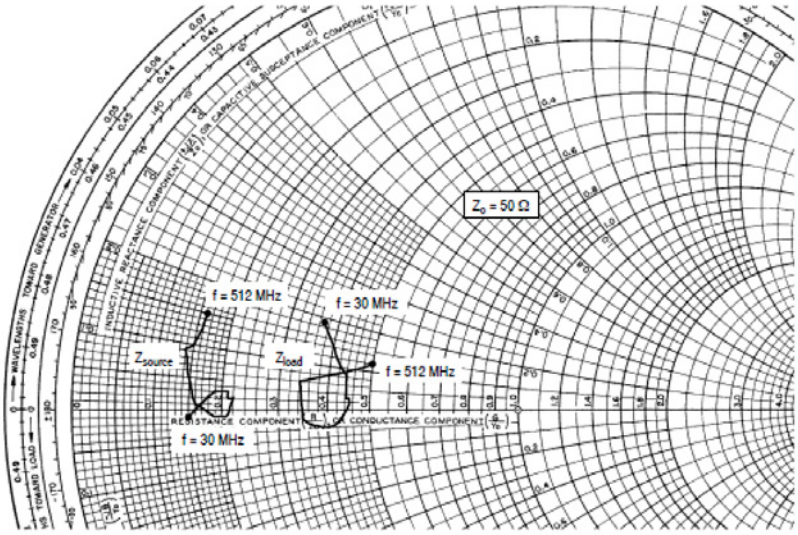
The capacitive transformer is not included in AN267, but this network can be quite useful and give very realisable components in inter-stage matching networks. The network is thus used to match the output impedance of one transistor to the input impedance of another transistor. The circuit is related to the lowpass Pi network, except the ground and the input port are changed. For this network, the output impedance at port 2 is always larger than that at port 1.

For a non-reactive device, the equations for the component values are the same as those for the Pi network, with the input impedance being the same (at port 1), but the reference

impedance 50 Ω now being the same as ($R_l$ - $R_{device}$) used in the Pi network. So instead of $R_l$, the value $R_l$ - $R_{device}$ is used in the equations. However if the source or load impedance of the matching network has a reactive part, then the Pi network equations no longer apply. For simplicity in the following example, the capacitance C1 in figure 9.5 is the same as C1 in figure 9.1. The impedances of $C_2$ and $L_1$ are tuned to obtain a correct device match at the correct frequency, using variables Xcct and Xlct, in figures 9.7 and 9.8. These variables can be tuned manually, or they can be tuned by optimisation.

## *Example 9.1: 100 MHz, 25 W Amplifier*

To illustrate the design process, the above equations are applied to an MRFE6VS25N [3], 1.8-2000 MHz, 25 W, 50V, laterally-diffused metal-oxide semiconductor (LDMOS) FET to obtain a suitable match. This FET is suitable for wide variety of applications handling a wide variety of modulated signals from FM to OFDM. For this example, the LDMOS FET is used to obtain a 25W output in the FM 88-108 MHz band.




$V_{DD}$ = 50 Vdc, $I_{DQ}$ = 25 mA, $P_{out}$ = 25 W CW

| f MHz | $Z_{source}$ Ω | $Z_{load}$ Ω |
|---|---|---|
| 30 | 7.60 - j0.40 | 18.3 + j9.40 |
| 64 | 9.30 + j1.40 | 21.9 + j4.00 |
| 88 | 10.3 + j1.40 | 22.2 + j1.90 |
| 98 | 10.6 + j1.20 | 22.2 + j1.40 |
| 100 | 10.7 + j1.20 | 22.3 + j1.30 |
| 108 | 10.9 + j0.90 | 22.5 + j0.50 |
| 144 | 10.7 - j0.40 | 21.2 - j1.50 |
| 170 | 9.70 - j0.60 | 19.8 - j1.80 |
| 230 | 8.10 + j0.30 | 17.4 - j0.80 |
| 352 | 7.20 + j4.30 | 17.0 + j2.80 |
| 450 | 7.40 + j5.00 | 21.3 + j4.60 |
| 512 | 8.10 + j7.60 | 25.2 + j5.90 |

$Z_{source}$ = Test circuit impedance as measured from gate to ground.

$Z_{load}$ = Test circuit impedance as measured from drain to ground.

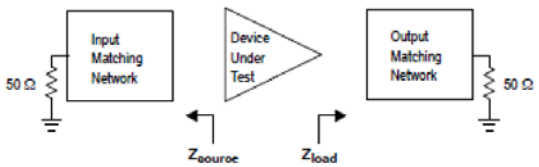



Figure 9.6. Part of datasheet showing large signal input and output impedances [3].

Figure 9.6, shows the impedances of the input and output matching networks, required at different frequencies to produce a 25W CW output. It should be noted that these values do depend on individual device and the quiescent current, so that in practice the actual values may be slightly different. Equation 9.2 shows that for a 50V supply, $V_{sat}$ = 0, and a 25W output, then $R_L$=50 Ω. That agrees with figure 20 of the MRFE6VS25N [3] datasheet, which shows that $R_L$ is close to 50 Ω from 1.8 MHz to 30 MHz. Figure 31 of this datasheet, shown in figure 9.6, uses a different test circuit to obtain a value of $R_L$ that is close to 20 Ω from 30 MHz to 512 MHz.

Figure 9.6 shows that the input and output impedances do not vary significantly over the 30 to 512 MHz frequency range. At 100 MHz $Z_{source}$ = 10.7 +j1.2 Ω and $Z_{load}$ = 22.3 + j1.3 Ω. The input impedance of the FET is the complex conjugate of these impedances, i.e. $Z_{in}$ = 10.7 -j1.2 Ω and $Z_{out}$ = 22.3 - j1.3 Ω. Those impedances are the impedances that the matching networks must provide to produce 25W from the MRFE6VS25N, using sufficient input power. The input impedance of the FET is the complex conjugate of these impedances, i.e. $Z_{in}$ = 10.7 - j1.2 Ω and $Z_{out}$ = 22.3 - j1.3 Ω. Motorola AN267 uses the device input and output impedances, so that $Z_{in}$ = 10.7 - j1.2 Ω and $Z_{out}$ = 22.3 - j1.3 Ω must be used to calculate the input matching components using equations 9.3 to 9.20. The equations and frequency responses are shown in figures 9.7 to 9.22. At out of band frequencies some networks have very low input impedances and others have very high input impedances. As a result, some matching networks may cause the amplifier to be unstable out of band. If that is the case, then other matching can provide stability.

For the Cadence AWR DE project files for figures 9.9 to 9.20, equations 9.3 to 9.20 are included as part of the "Global Variables". Those equations are shown in figures 9.7 and 9. For a Pi network, AN267 does not include the device reactance as part of C1. Equation 9.4 includes any device reactance as part of C1. Including any device reactance as part of C1 results in a lower effective Q and thus gives a wider bandwidth for the matching network.

The Q value to be selected for the matching network is a compromise. For a wide bandwidth, a low Q is required and the Q is normally selected to be as low as possible. However, the desired matching may not be possible at low Q values. For this FET for the Lowpass T and Bandpass T networks, the minimum Q is 1.916. For this example, a Q value of Qt = 2.5 is used for the Lowpass T and Bandpass T networks as shown in figure 9.7. The Q value of the Pi and bandpass L matching networks are then chosen to make the S11 bandwidth of the different matching networks similar, by tuning Qp. That results in Qp = 0.65. The same bandwidth for matching will thus require very different Q values of the matching networks for the same device resistance and reactance to be matched.

These matching network equations produce components values. That does not mean that these network can be realised and one may need to change Q values or select specific networks to ensure that realisable components are obtained. In this example, all of the component values are practical. For the output matching, the voltage and current ratings and possible resistive losses of these matching network components must be considered, to ensure that the matching components do not overheat and fail. The higher the Q, the higher the circulating currents and the higher the voltages across the components. The choice of network to be selected then depends on the frequency response and the component values for the different networks.

In order to have an exact source impedance of 10.7 - j1.2 Ω, it is convenient to make a complex input variable Zin, using Zin = complex (Rd, Xd) = complex (10.7,1.2). Note that if Rd < $R_L$), the matching network will have a voltage gain, since there is an

impedance transformation. A passive network cannot have a power gain. Figures 9.9 to 9.20 show that the bandwidth over which a good match is obtained is smaller than the bandwidth obtained with transformer matching and transmission-line matching, which are described later in this chapter. The impedance match and insertion loss versus frequency for the different types of matching network and matching to the large signal input impedance of the MRF1535NT1 MOSFET is shown in figures 9.9 to 9.20.

Matching Network Equations.
Fm Matching Frequency in MHz, Rd real part of device impedance, Xpd positive device reactance
Xmd negative device reactance. use either Xpd or Xmd. If Xd = -5 then Xpd=0 and Xmd = -5
Change Fm or Q and simulate to view their effect
Transistor MRFEVS25NR1 at 100 MHz, Large signal parameters, Input Match

| | | | | |
|---|---|---|---|---|
| Fm=100 | | | Set Kp and Kt for correct bandwidth to match Bandpass L | |
| Rl=50 | | | TwoPi=4*Acos(0) | |
| Rd=10.7 | Xpd=1.2 | Xmd=-0.0 | Xd=Xpd+Xmd | Xd: 1.2 |
| Wm=TwoPi*Fm*1e6 | | | Zin=complex(Rd,Xd) | Zin: (10.7,1.2) |
| Qmin=sqrt(Rl/Rd-1) | | For Lowpass T and bandpass T | | Qmin: 1.916 |
| Qt=2.5 | | For Lowpass T and bandpass T | | |
| Qp=0.65 | | For other networks (pi, bandpass L and Cap TF, can be lower then Qmin | | |

Pi Matching

| | | |
|---|---|---|
| Rp =( Rd * Rd + Xd * Xd ) / Rd | Rp: 10.83 | |
| Xp = (Rd * Rd + Xd * Xd ) / Xd | Xp: 96.61 | |
| Yp=1/Xp | | |
| Ycp1= (Qp/Rp +Yp) | | |
| Xcp1= (1/Ycp1) | Cp1= 1/(Wm*Xcp1) | Cp1: 1.12e-10 |
| Xcp2=Rl*(sqrt((Rp/Rl)/((Qp*Qp+1)-(Rp/Rl)))) | Cp2=1/(Wm*Xcp2) | Cp2: 7.509e-11 |
| Xlp=(Qp*Rp+(Rp*Rl/Xcp2))/(Qp*Qp+1) | Lp=Xlp/Wm | Lp: 3.647e-08 |

Low Pass T

| | | |
|---|---|---|
| Xllt1= (Rd*Qt - Xd) | Llt1=Xllt1/Wm | Llt1: 4.066e-08 |
| A2=((Rd*(1+Qt*Qt)/Rl) -1) | A=Sqrt(A2) | A: 0.7426 |
| B=Rd*(1+Qt*Qt) | | B: 77.57 |
| Xllt2=Rl*A | Llt2=Xllt2/Wm | Llt2: 5.91e-08 |
| Xclt=B/(Qt+A) | Clt= 1/(Wm*Xclt) | Clt: 6.653e-11 |

Band Pass L

| | | |
|---|---|---|
| Xcbl1= Rd*Qp + Xmd | Cbl1= 1/(Wm*Xcbl1) | Cbl1: 2.288e-10 |
| Xcbl2=Rl*sqrt(Rd/(Rl-Rd)) | Cbl2= 1/(Wm*Xcbl2) | Cbl2: 6.1e-11 |
| Xlbl=Xcbl1 - Xd+ (Rd*Rl/Xcbl2) | Lbl=Xlbl/Wm | Lbl: 4.18e-08 |

Band Pass T

| | | |
|---|---|---|
| Xlbt= (Rd*Qt - Xd) | Lbt=Xlbt/Wm | Lbt: 4.066e-08 |
| Xcbt2=Rl*A | Cbt2= 1/(Wm*Xcbt2) | Cbt2: 4.286e-11 |
| Xcbt1=B/(Qt-A) | Cbt1= 1/(Wm*Xcbt1) | Cbt1: 3.605e-11 |

Capacitive Transformer
Tune Xcct and Xlct for correct match at required centre frequency

| | | |
|---|---|---|
| Cp1 as for Pi Match | | Cp1: 1.12e-10 |
| Xcct=13.02 | Cct=1/(Wm*Xcct) | Cct: 1.222e-10 |
| Xlct=21.19 | Lct=Xlct/Wm | Lct: 3.372e-08 |

Figure 9.7. Input matching component values for example 9.1.

## Pi Network

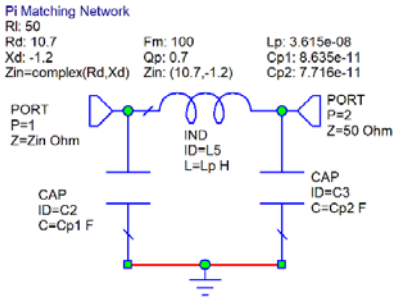



Figure 9.8. Values for the Pi matching network.

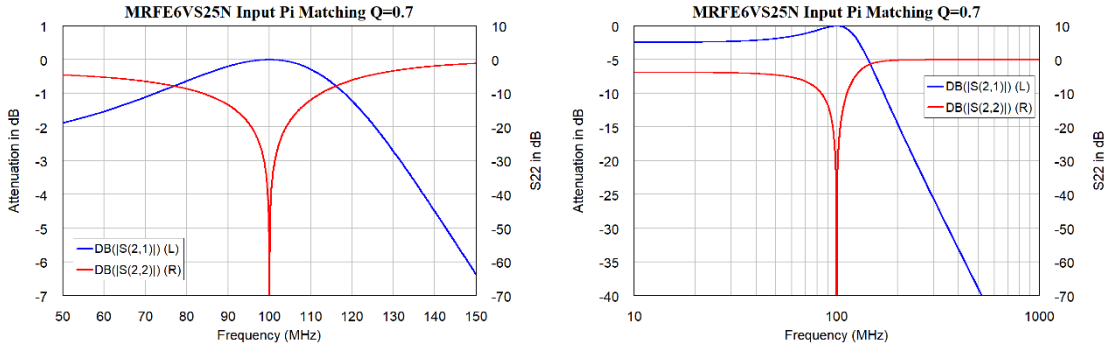



Figure 9.9. Frequency response of the Pi matching network.

## Lowpass T Network

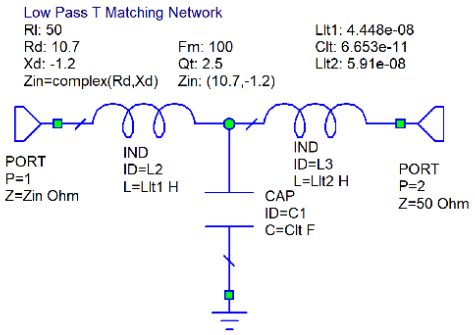



Figure 9.10. Values for the lowpass T matching network.

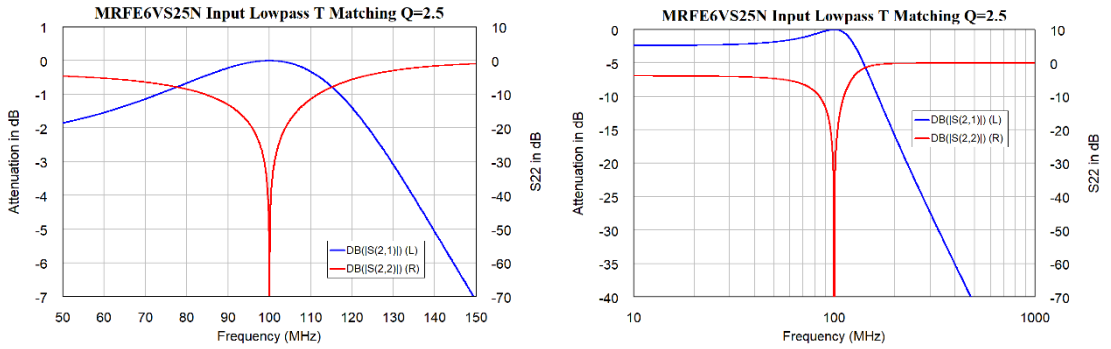



Figure 9.11. Frequency response of the lowpass T matching network.

## Bandpass L Network

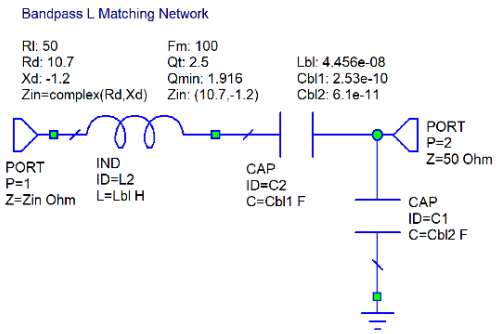



Figure 9.12. Values for the bandpass L matching network.

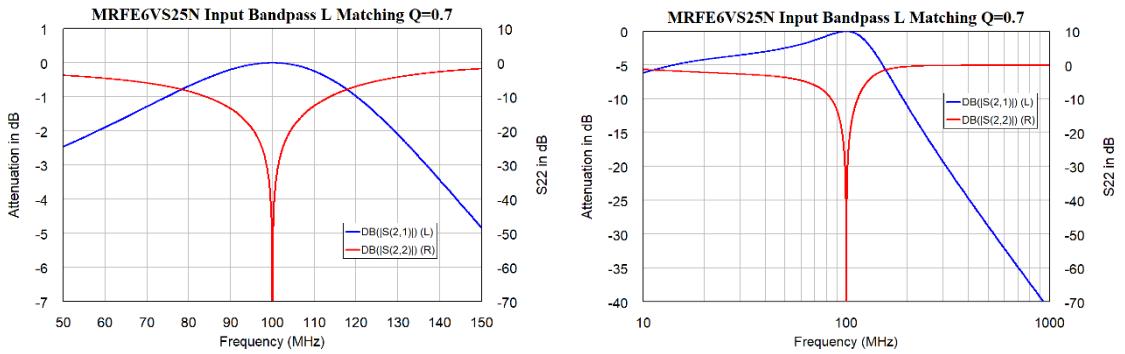



Figure 9.13. Frequency response of the Bandpass L matching network.

## Bandpass T Network

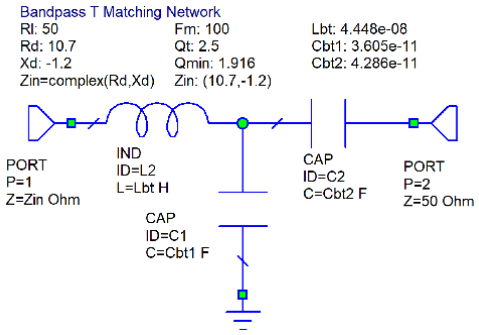



Figure 9.14. Values for the bandpass T matching network.

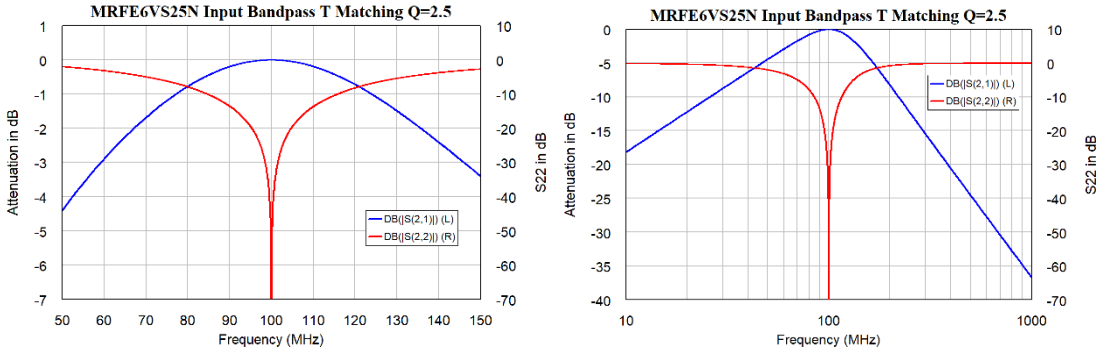



Figure 9.15. Frequency response of the bandpass T matching network.

## Capacitive Transformer Network

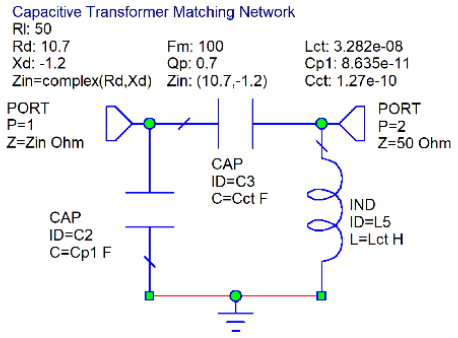



Figure 9.16. Values for the Capacitive Transformer matching network.

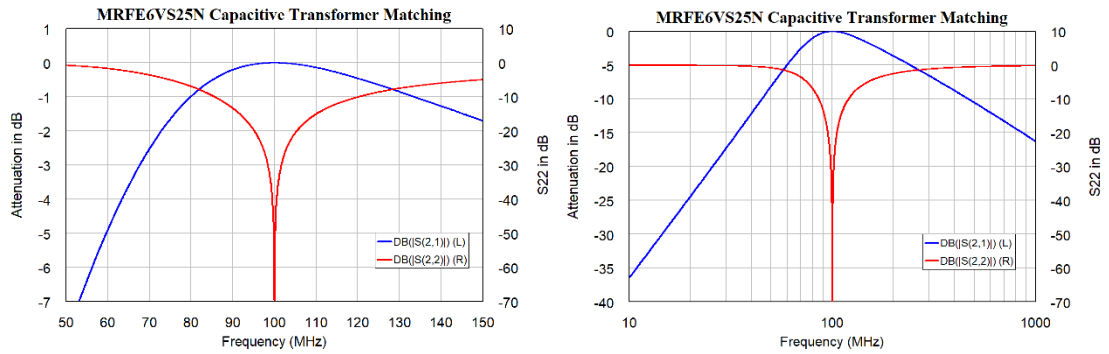



Figure 9.17. Frequency response of the capacitive transformer-matching network.

Comparing the attenuation of the networks in figures 9.17, 9.15, 9.13, 9.9, 9.11 and 9.18 at 125 MHz, shows a progressive reduction in attenuation. The Pi network and Lowpass T are thus the best networks to be used if harmonics of the source are to be filtered out.

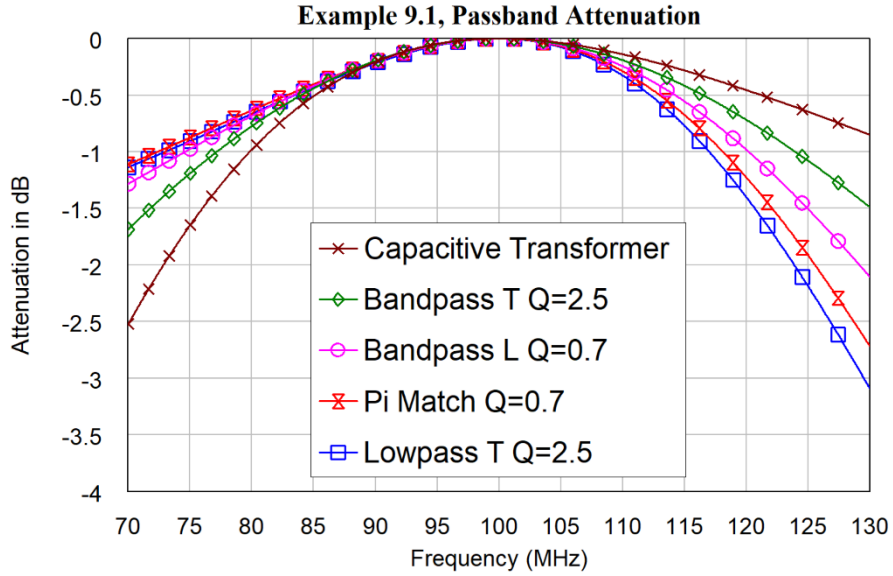



Figure 9.18. Comparison of LC matching networks.

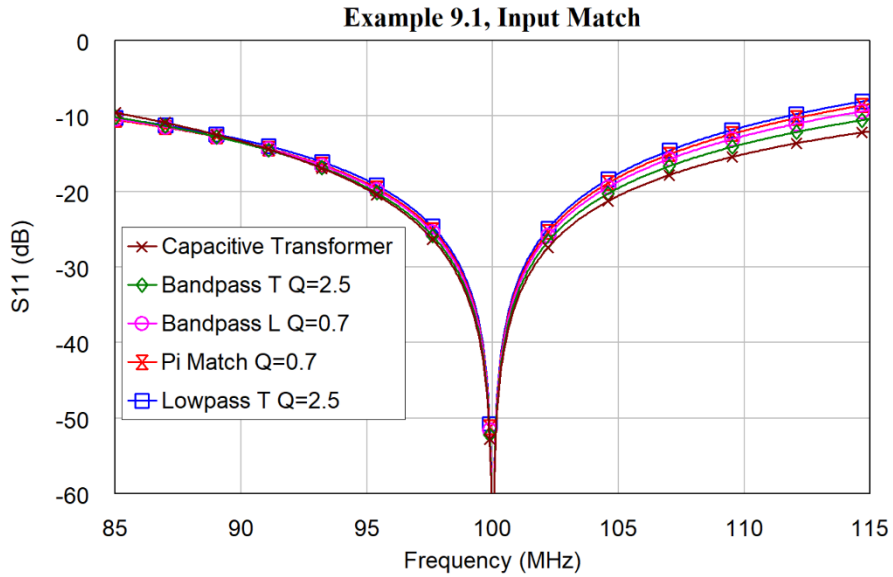



Figure 9.19. Comparison of LC matching networks.

Figures 9.18 and 9.19 show a comparison of the impedance matching performance of the LC networks of figures 9.8 to 9.16. The Pi matching network has the lowest bandwidth, but it does not have a minimum Q and its Q can be adjusted to make the bandwidth comparable to the other networks if needed.

The lowpass T, the bandpass T and the bandpass L networks, all present a high impedance at the second harmonic of the input frequency. This results in smaller second harmonic currents to flow in the bipolar transistor or FET and this slightly increases its efficiency. These networks will however result in higher peak voltages, due to the device impedance at the second harmonic being close to an open-circuit. This may then exceed the voltage breakdown ratings of the device or the components used in the matching network. The Lowpass networks are also good for filtering out harmonics produced by the amplifier. Bandpass T, bandpass L and the capacitive transformer networks all have a capacitance in series with the input to output path. This avoids the need for an additional coupling capacitor to set the bias levels correctly.

If the required bandwidth or the required harmonic attenuation cannot be obtained, several matching networks can be cascaded, allowing the impedance transformation ratios to be reduced, thus increasing the bandwidth. Cascading several Lowpass networks significantly increases the harmonic attenuation.

## Transformer Matching

In transformer matching, an RF transformer, as described in Chapter 3 of this book is used to provide the impedance transformation required. RF transformers can be used for impedance matching at HF and VHF frequencies. Since the number of turns used must be an integer and the impedance transformation is the turns-ratio squared, the impedance transformation ratios are limited to the square of simple fractions. For the matching of the LDMOS FET in this example, a 10.7 +j1.2 Ω impedance is required. The ideal turns ratio required is √(50/10.7) = 2.16. This can best be approximated by a 2:1 turns-ratio transformer, giving a 4:1 impedance transformation, so that a 50 Ω source is transformed into a 12.5 Ω impedance, which is sufficiently close to 10.7 - j1.2 Ω for most of the power to be transferred effectively.

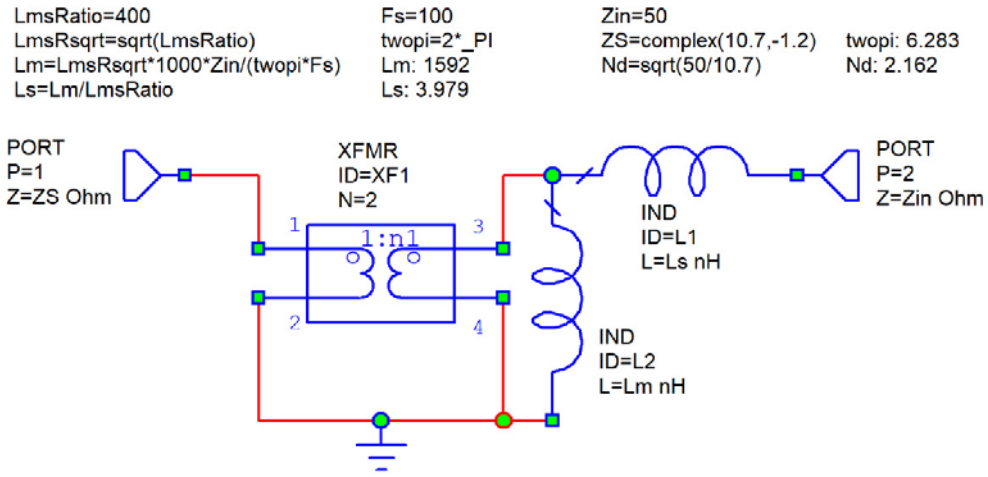



Figure 9.20. Values for the Transformer matching network.

A practical RF transformer can be represented by an ideal transformer, with a magnetising inductance in parallel with it and a leakage inductance in series with it, as shown in figure

9.20. The magnetising and leakage inductances are chosen to give a centre frequency of 100 MHz. The 400:1 ratio between Lm and Ls is on the low side of the typical range, so that the bandwidth typically will be larger than what is shown here.

In this example, the impedance to be matched is assumed to be constant at 10.7 – j1.2 Ω. In practice the device impedance changes significantly over the typically three decades of bandwidth of the RF transformer, thus limiting the frequency range over which the device is properly matched. FET amplifiers that are well matched up to 100 MHz can easily be designed, as is evident from many power FET manufacturers' application notes. The performance obtained by the transformer-matching network is shown on figure 9.21.

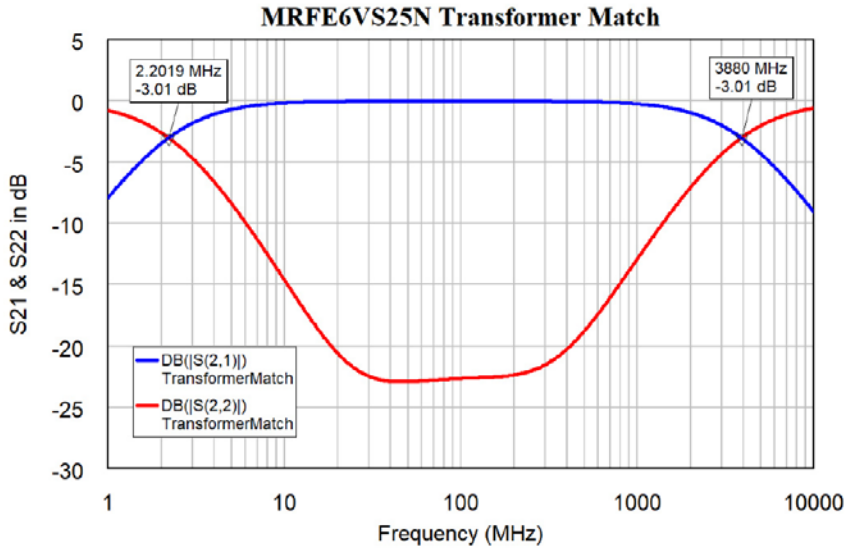



Figure 9.21. Frequency response of transformer matching network with and without reactive tuning capacitor.

If needed, the reactive part of the input can be resonated out, using a capacitance across pin 1 and 2 of the transformer in figure 9.20. This capacitor can be tuned to provide an optimum match at 100 MHz. Note that adding the capacitance will reduce the upper corner frequency of the transformer-matching network. In this case, such a capacitance is not needed and a good match is obtained over a wide range of frequencies. Due to the turns-ratio of the transformer being limited to integer values, the impedance match is not as good as that of the LC networks or that of the transmission-line networks described later. The model of figure 9.20 does not contain all the parasitic elements encountered in a practical transformer circuit, and the actual FET characteristics may be slightly different from the values given in the data sheet. The value of any tuning capacitance required is thus best determined experimentally, using the value obtained by the computer simulation of figures 9.20 and 9.21, as a starting point.

## Transmission-Line Matching

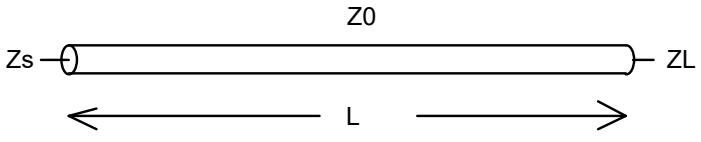



Figure 9.22. Transmission-line sending and load impedances.

For a transmission-line of characteristic impedance $Z_0$ and length L, shown in figure 9.23, the impedance looking into a transmission-line that is terminated in a load $Z_L$ is:

$$Z_s = Z_0 \frac{Z_L + jZ_0 \tan(\beta l)}{Z_0 + jZ_L \tan(\beta l)} \qquad \text{Eqn. 9.20}$$

By substituting $Z_S=R_S+jX_S$ and $Z_L=R_L+jX_L$ and then solving for $Z_0$ and the transmission-line length $\theta=\beta l$ as an electrical length, one obtains the following equations:

$$Z_0 = \sqrt{\frac{R_s|Z_L|^2 - R_L|Z_s|^2}{R_L - R_s}} \qquad \text{Eqn. 9.21}$$

$$\theta = Arc\tan\left(\frac{Z_0(R_s - R_L)}{R_s X_L + R_L X_s}\right) \qquad \text{Eqn. 9.22}$$

This assumes that $Z_0$ is real and tan(βl) is real. These equations do not always give a match, but if no match is possible, shifting the impedance by using a short length of transmission-line will always result in a match. Equations 9.20 to 9.22 are included in the AWR DE project file for the transmission-line matching network. For matching a 10.7 - j1.2 Ω impedance, being the same impedance match as is used in figures 9.8 to 9.20, these equations give $Z_0$ = 23.09 Ω and $\theta$ = 93.78 degrees and this can be included in the AWR DE circuit diagram as the variables shown in figure 9.23.

Figure 9.24, shows the frequency range of the resulting impedance match. It can be seen that transmission-line matching gives a broadband impedance match. The only limitations are that firstly, it is difficult to tune the matching impedances to allow for device variations and secondly the line lengths can physically become too large. This is why this technique is predominantly used above 100 MHz. Transmission-lines can replace the inductors used in the LC matching. This will then allow for some tuning of the matching network by changing the values and locations of capacitors. The replacement of the inductors used in Lowpass T matching networks of figure 9.11, with transmission-lines is often done in commercial applications above 100 MHz.

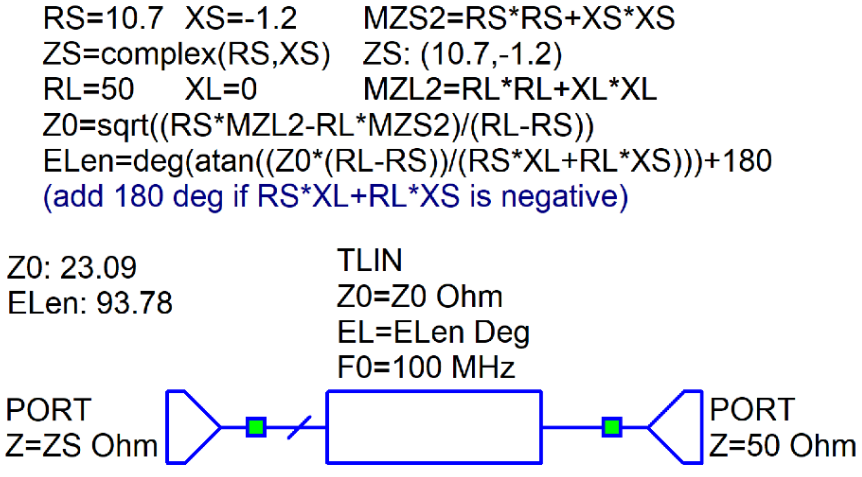



Figure 9.23. Values for the transmission-line matching network.

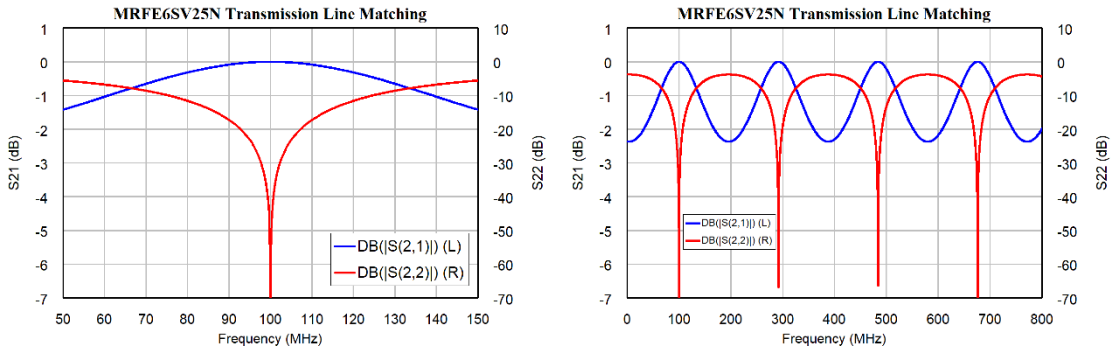



Figure 9.24. Frequency response of the transmission-line matching network.

## Broadband Matching

Sometimes a wideband match is required. This can be a wideband match into an active device, or a passive device, like an antenna. If a wideband match into an active device is required then, either the device impedance must be known at different frequencies, or it must be able to be represented by a simple circuit, containing resistors, capacitors and inductors. Often, small or large signal S parameter data, or manufacturers device models are used. Since AWR DE is good at optimising networks, it is often the easiest to design a first-guess of the matching network by cascading a succession of simple matching networks and then improve the performance by optimisation.

```
MRFE6VS25N Broadband Input Match 250-500 MHz, Geometric Mean 354 MHz
Zsource = 7.2 +j4.3. Zload = 17.0 + j2.8 at 352 MHz, Vdd 50V, IDQ 25mA, 25W CW, fig 31 data sheet
    R0=7.2      X0=-4.3                 Desired Load Impedance of matching network. This is the
                                        complex conjugate of the desired source impedance.
    If nonzero X0 then enable:            If X0 = 0 then enable:
      Rp =( R0 * R0 + X0 * X0 ) / R0        Rp=R0                              Rp: 9.768
      Xp =(R0 * R0 + X0 * X0 ) / X0         Xp=1e9                             Xp: -16.36
    RL=50                                                                    RL: 50
    KR1=1                 KR2=1                        For optimising transformation ratios
    Rt=pow((RL/R0),(1/3))                                                    Rt: 1.908
    R1d=R0*Rt                           R2d=R1d*Rt
    R1=KR1*R1d                                                 R1: 13.74     R1d: 13.74
    R2=KR2*R2d                          R3=RL                  R2: 26.21     R2d: 26.21
    Qmin=-Rp/Xp                                                              Qmin: 0.5972
    Fm=353                              Wm=2*_PI*Fm*1e6                      Wm: 2.218e+09
    Q1=0.6                              Wm1=2.218e9
    Q2=0.6                              Wm2=2.218e9
    Q3=0.6                              Wm3=2.218e9

Pi Match 1
    Yp = 1/Xp                                  Cp= -1e12/(Wm1*Xp)          Cp: 27.57
    Ycp11= (Q1/Rp +Yp)                                                     Ycp11: 0.0002844
    Xcp11= (1/Ycp11)                           Cp11= 1e12/(Wm1*Xcp11)      Cp11: 0.1282
    Xcp12=R1*(sqrt((Rp/R1)/((Q1*Q1+1)-(Rp/R1)))) Cp12=1e12/(Wm1*Xcp12)     Cp12: 31.35
    Xlp1=(Q1*Rp+(Rp*R1/Xcp12))/(Q1*Q1+1)       Lp1=Xlp1*1e9/(Wm1)          Lp1: 5.036

Pi Match 2
    Ycp21= (Q2/R1)
    Xcp21= (1/Ycp21)                           Cp21= 1e12/(Wm2*Xcp21)      Cp21: 19.69
    Xcp22=R2*(sqrt((R1/R2)/((Q2*Q2+1)-(R1/R2)))) Cp22=1e12/(Wm2*Xcp22)     Cp22: 21.72
    Xlp2=(Q2*R1+(R1*R2/Xcp22))/(Q2*Q2+1)       Lp2=Xlp2*1e9/(Wm2)          Lp2: 8.483

Pi Match 3
    Ycp31= (Q3/R2)
    Xcp31= (1/Ycp31)                           Cp31= 1e12/(Wm3*Xcp31)      Cp31: 10.32
    Xcp32=R3*(sqrt((R2/R3)/((Q3*Q3+1)-(R2/R3)))) Cp32=1e12/(Wm3*Xcp32)     Cp32: 11.39
    Xlp3=(Q3*R2+(R2*R3/Xcp32))/(Q3*Q3+1)       Lp3=Xlp3*1e9/(Wm3)          Lp3: 16.18

Combine C's
    Cp1=Cp11                                                               Cp1: 0.1282
    Cp2=Cp12+Cp21                                                          Cp2: 51.05
    Cp3=Cp22+Cp31                                                          Cp3: 32.05
    Cp4=Cp32                                                               Cp4: 11.39
```

Figure 9.25. Global definition equations for the initial broadband matching network.

As an example, consider the impedance matching of the input of an MRFE6VS25N LDMOSFET over a 250MHz to 500MHz range. The geometric mean frequency if that range is 354 MHz. At 352 MHz the MRFE6VS25N datasheet gives a large signal source impedance of 7.2 +j4.3 Ω. The device impedance is the complex conjugate of that and is thus 7.2 -j4.3 Ω. That is equivalent to 9.77 Ω in parallel with -j16.36 Ω. The reactive impedance corresponds to a capacitance of 27.57 pF at 353 MHz. An impedance transformation from 50 Ω to 7.2 Ω is thus required. That can be achieved by cascading three pi networks with impedance transformations of 1.908:1. The impedance levels are thus 7.2 Ω, 13.74 Ω, 26.21 Ω and 50 Ω. The match is required for the 250MHz to 500MHz range and provide a return loss of less than –20 dB. Figure 9.25 shows the equations used to calculate the initial element values. Figure 9.26 shows the circuit of the resulting matching network.

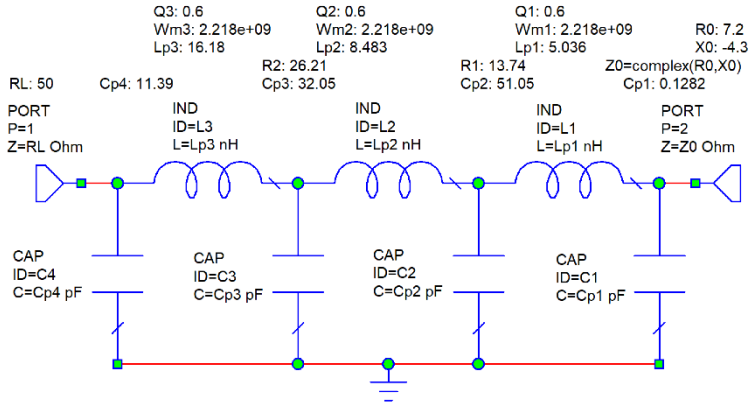



Figure 9.26. Initial broadband match schematic.

For a wideband match, a low Q is used. Figure 9.25 shows that for the required X0=-4.3, a minimum Q for the Pi section closest to the FET is 0.5972. A lower Q will result in a negative Cp1 in figure 9.26. As a result Q = 0.4 is used in figures 9.25 to 9.28. That results in practical components for the Pi networks. If X0 = 0, then Xp becomes infinite and the expression for Xp must be disabled and the equation Xp = 1e9 must be enabled. The equations in figure 9.25 can accommodate any impedance level. They can also be extended to include more sections.

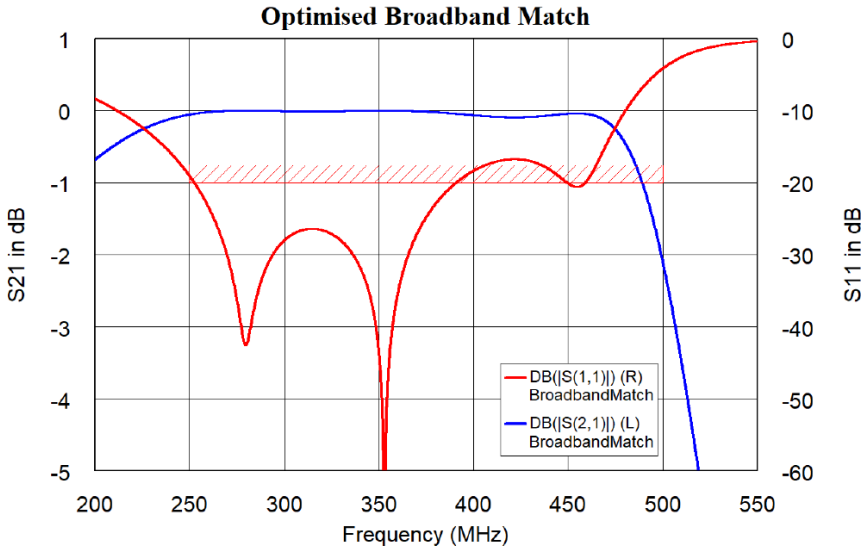



Figure 9.27. Starting broadband match $S_{21}$ and $S_{22}$.

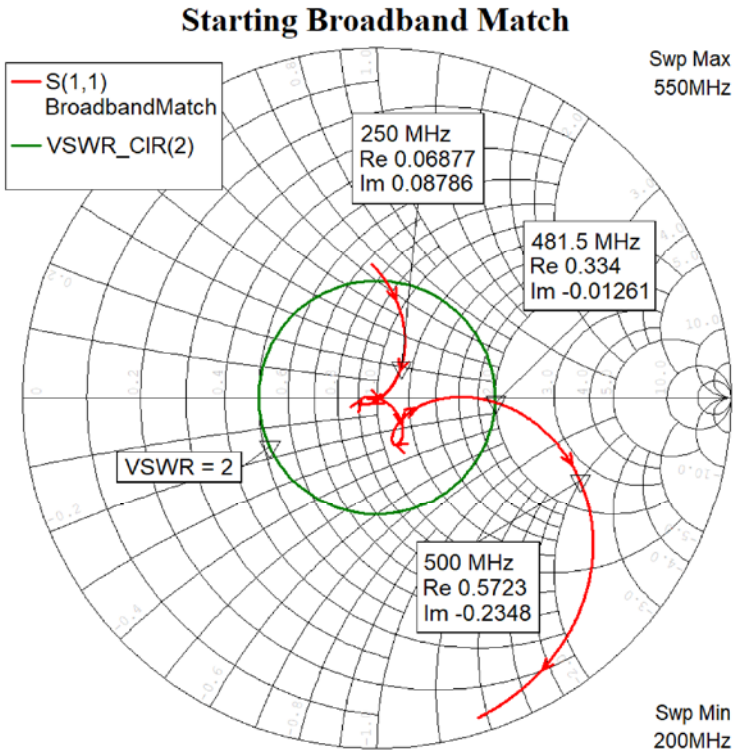



Figure 9.28. Starting broadband match $S_{11}$ and $S_{22}$ on a Smith Chart.

Figures 9.27 and 9.28 show the frequency response and return loss of the initial design, obtained from the equations in figure 9.25. It can be seen that simply using 3 Pi matching sections is a good starting point for the design. Figure 28 shows $S_{11}$ plotted on a Smith Chart. It can be seen that a good match is obtained over a wide frequency range.

The impedance match for the initial matching network of figure 9.25 does not meet the required $S_{11} < -20$ dB over the 250 MHz to 500 MHz bandwidth as shown in figure 9.27. The -20 dB limit can be obtained by optimising the network. There are different ways of optimising this circuit. Firstly, the individual elements can be optimised, by simply replacing the variables for the component values figure 9.26 with the calculated values that can be optimised. The calculated component values in figure 9.25 are used as the starting values for the element values in figure 9.26. Alternately one can keep using the equations in figure 9.25, in the *Global Definitions* of the AWRDE project, but allow the Q values, centre frequencies and impedance transformation ratios (KR) for each of the three matching sections to be optimised. Q1 has a minimum value of 0.5972, a lower value will result in a negative Cp11. For a broadband match, low Q values are required As a result Qmin is used for Q1, resulting in Cp11 = 0, and requiring some minor changes to the equations used in the *Global Definitions*, as can be seen by comparing figure 9.25 and 9.29. The initial values for Q2 and Q3 are the design value Q = 0.6 used in figure 9.27 and the initial values for Wm1, Wm2 and Wm3 are the design value $Wm = 2\pi \times 353e6 = 2.218 \times 10^9$.

As part of the optimisation, the normalised impedance transformation ratios for the first two sections are optimised (KR1 and KR2) and the transformation ratio for the third section is calculated to obtain the total transformation ratio required for the input match. The Q, Wm and KR optimisation results in the final values shown in figure 9.30. The optimisation limits for Q and KR need to be set carefully otherwise simulation errors with inductors or capacitors with imaginary values result. There is no unique optimum match for the network of figure 9.30 and neither of the element or the Q, Wm and Impedance

Ratio optimisations will achieve a perfect optimisation. Depending on the optimiser and the starting conditions used, different final component values are obtained.

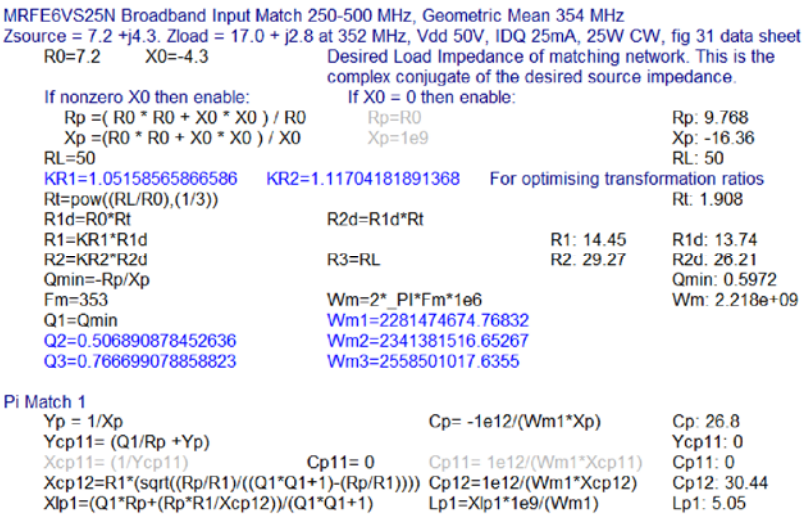



Figure 9.29. Final broadband match schematic.

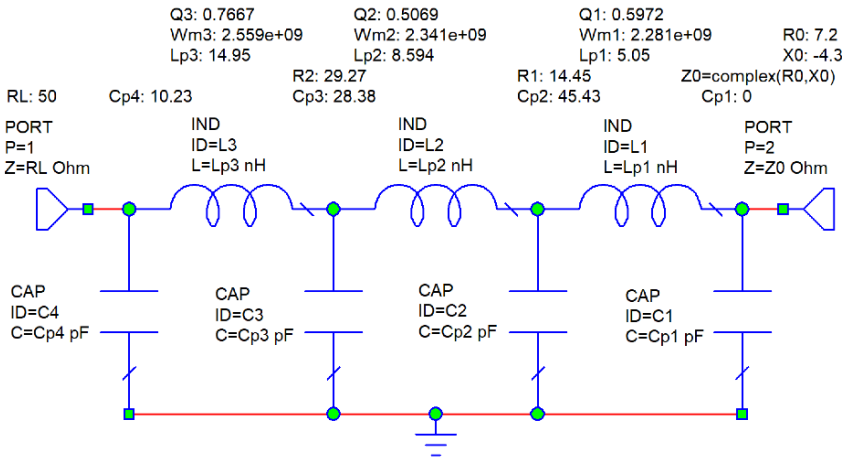



Figure 9.30. Final broadband match schematic.

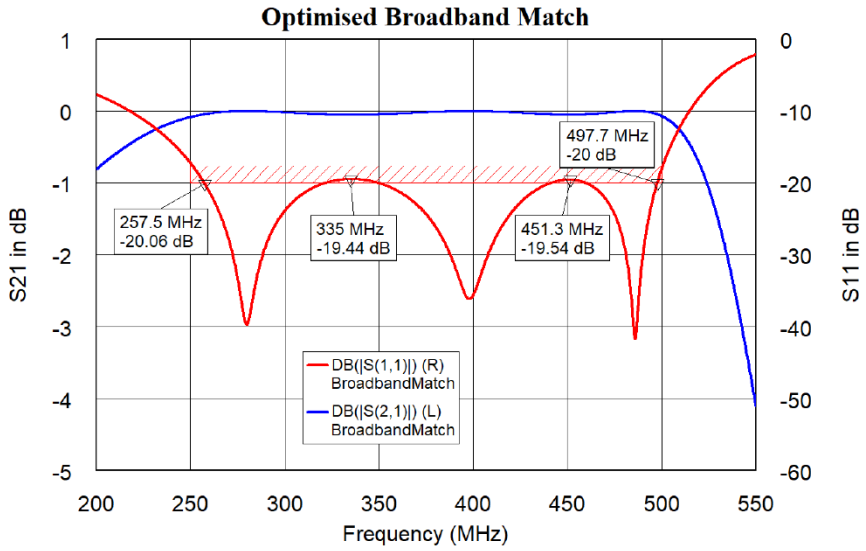



Figure 9.31. Final broadband match $S_{21}$ and $S_{22}$.

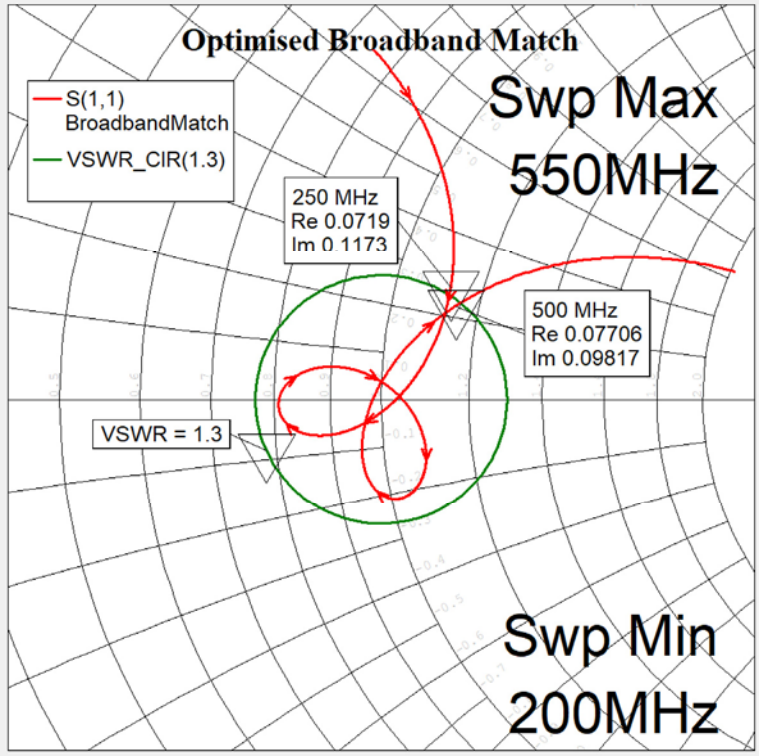



Figure 9.32. Final broadband match $S_{11}$ and $S_{22}$ on a Smith chart.

Figure 9.32 shows that $|S_{11}|$ is now less than -20 dB for virtually the entire 250 – 500 MHz frequency range. The curve for $|S_{11}|$ is identical to that for $|S_{22}|$. Figure 9.32 shows of $S_{11}$ of the network plotted on a close up of the centre of the Smith chart. It can be seen that a good match over the entire 250 to 500 MHz bandwidth is obtained, with the magnitude of the reflection coefficient being less than 0.14 and the VSWR being less than 1.3 from 250 to 500 MHz. A better match can be obtained by using more Pi sections. At frequencies above 100 MHz it is advantageous to replace the inductors in the Pi section with transmission lines. Similar optimisation techniques as described above can be applied to those networks.

For impedance matching of the output of transistors or FET's, it is desirable to make the first section a lowpass T network, to reduce harmonic currents and thus increase the amplifier's efficiency. In addition, a bandpass T or L section provides the DC isolation required for biasing. By selecting a suitable Q for one or more lowpass Pi sections, sufficient harmonic filtering of the output can be achieved. Suitable matching networks are thus an essential part of an amplifier design.

## *Example 9.2: Broadband Amplifier Using S Parameters*

This example uses S parameters and broadband complex conjugate matching, to produce an amplifier. Applying broadband matching to a transistor or FET results in additional problems. Since the device is not normally unilateral, there is an interaction between the input and output matching. As an example consider the MRFE6VS25N LDMOSFET that we used in example 9.1. From the manufacturer's data sheet, the S parameters at a drain current of 2 Amp is shown in table 9.1, where the lines beginning with '!' are comments. The line: '# hz S ma R 6.8', indicates that the frequency in the following file is in Hz, it is an S parameter file and the values are magnitude and phase in degrees, and that the reference impedance is 6.5 Ω.

Table 9.1. Small signal S parameter data for the MRFE6VS25N LDMOSFET [4].

```
! Copyright - Freescale Semiconductor, Inc., 2012
! 06/05/2012
! Rev. 0
! MRFE6VS25NR1 S-Paraneters
! Vdd = 50 Vdc, Idq = 150 mA
# hz S ma R 6.8
!
! freq          magS11  angS11  magS21  angS21  magS12  angS12  magS22  angS22
2.000E+08       0.9588  -24.15  3.9246  148.64  0.0050  64.44   0.9219  -20.86
2.050E+08       0.9589  -24.74  3.9198  148.14  0.0051  63.54   0.9212  -21.64
2.100E+08       0.9574  -25.36  3.9118  147.68  0.0052  63.28   0.9204  -22.38
2.150E+08       0.9577  -25.94  3.9024  147.12  0.0054  63.06   0.9200  -23.15
2.200E+08       0.9586  -26.54  3.9027  146.67  0.0055  62.06   0.9214  -23.84
2.250E+08       0.9588  -27.04  3.8941  146.08  0.0056  62.31   0.9223  -24.59
2.300E+08       0.9593  -27.52  3.8839  145.59  0.0056  60.79   0.9230  -25.15
2.350E+08       0.9606  -28.03  3.8837  145.11  0.0057  60.66   0.9245  -25.85
2.400E+08       0.9602  -28.55  3.8761  144.57  0.0059  60.43   0.9247  -26.36
2.450E+08       0.9601  -29.03  3.8684  143.98  0.0060  59.64   0.9254  -26.88
+ Many more lines, with the last lines:
1.090E+09       0.8987  -129.90 2.4501  44.61   0.0034  86.22   0.8218  -124.10
1.095E+09       0.8985  -130.50 2.4388  44.04   0.0035  88.73   0.8214  -124.67
1.100E+09       0.8986  -131.09 2.4267  43.49   0.0036  88.85   0.8210  -125.26
```

The frequency steps are 5 MHz, from 200 MHz to 1.1 GHz, except for a gap from 500 to 650 MHz. This can now be used as a sub-circuit in Cadence AWR DE.

For this example, an amplifier with a bandwidth of 300MHz to 400MHz is required. An input matching network will consist of a coupling capacitor followed by a Pi section and a lowpass T section. Having the lowpass T section at the input of the MOSFET provides a lower Q match for the input capacitance of the MOSFET than a Pi network. At the output, a lowpass T section is used to provide a high amplifier efficiency, by having an inductor in series with the output and minimising the RF harmonic currents flowing through the FET. This is followed by a Pi section in order to obtain good harmonic filtering. To determine the components of the matching networks the input and output impedances of the MOSFET is required. The centre of the 300 MHz to 400 MHz frequency band is 350 MHz, for which the S parameter data are given.

From equation 8.4, for an amplifier with a perfect output match, $\Gamma_{in} = S_{11}$ and from equation 8.5, for an amplifier with a perfect input match, $\Gamma_{out} = S_{22}$, so that from equation 8.1:

$$Z_{in} = Z_0 \frac{1 - S_{11}}{1 + S_{11}} \qquad \text{Eqn. 9.23}$$

$$Z_{out} = Z_0 \frac{1 - S_{22}}{1 + S_{22}} \qquad \text{Eqn. 9.24}$$

However, the S parameter data in table 9.1 is for a reference impedance of 6.8 Ω. The reference impedance of the S parameter data will thus first need to be changed. The easiest way to do this is to use the S parameter file MRFE6VS25R1 of figure 9.1 as a sub-circuit as shown in figure 9.33, by creating a new *Graph* → *Tabular*, and then using that to display Z(11), Z(22) and if needed the S parameters with a 50 Ohm reference. Those values can then be exported by selecting the tabular graph and then selecting *Graph* → *Export Trace Data*. Then save the tabular graph to a file.

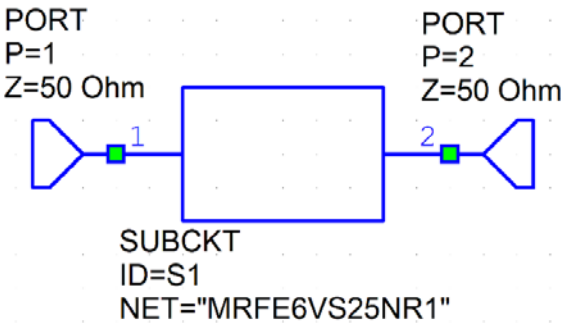



Figure 9.33. S parameter sub-circuit for determining $Z_{11}$ and $Z_{22}$.

For 350 MHz, that results in:

$Z_{in}$= 2.9313 -j17.968 Ω and $Z_{out}$= 4.2667 – j20.314 Ω Eqn. 9.25

NXP's AN721 [5] and AN1526 [6] and equation 9.2 show that the empirical load resistance for a power transistor at maximum power is:

$$R_L = \frac{(V_{cc}-V_{sat})^2}{2P_{out}} \quad \text{Eqn. 9.2}$$

Assuming a 50V supply, $V_{sat}$, = 0.3 V, for $P_{out}$ = 30W, gives $R_L$ = 41 Ω. Which is much larger than the small signal output impedance shown in shown in equation 9.25.

This amplifier design example involves three steps. The first step is to independently design and optimise the input and output impedance matching networks. The schematic for the matching networks is shown in figure 9.34 and the FET subcircuit is disabled to prevent interaction between the matching networks due to $S_{12}$ and $S_{21}$ of the FET. To allow optimisation of the individual components, the component values are calculated using the equations shown in figure 9.35, with the constants K1 to K12 as optimisable multipliers.

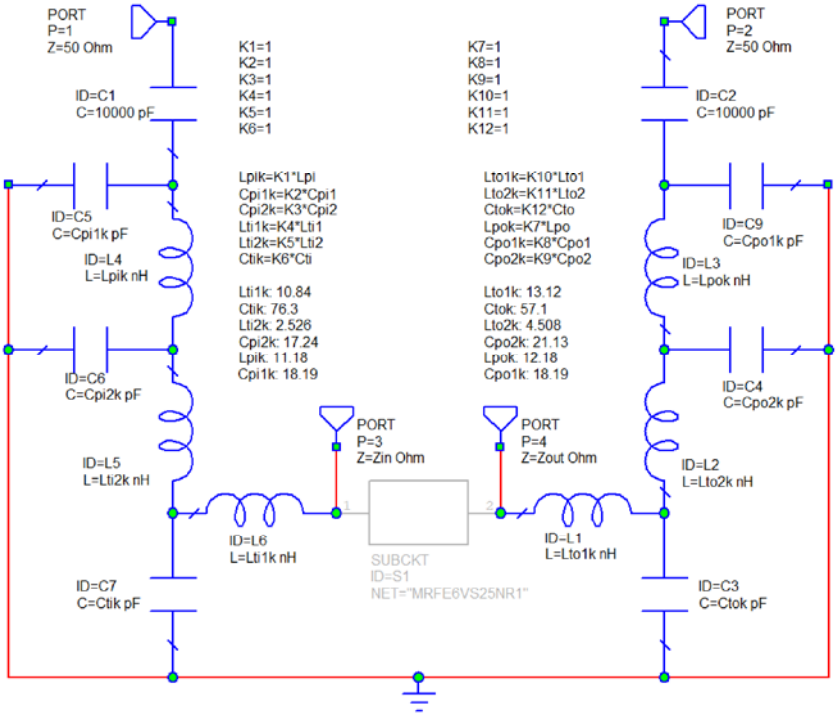



Figure 9.34. Initial Amplifier S parameter subcircuit and matching network.

Since the input and output impedances are much smaller than 50 Ω, having the coupling capacitors at the 50 Ω end of the matching networks result in smaller coupling capacitors. Since the output voltage can be larger than the FET supply voltage, this does however place an extra DC voltage on the capacitors of the output-matching network and high voltage, low loss capacitors may need to be used.

MRFE6VS25NR1 LDMOSS FET
S parameters at 350MHz, Rref=6.8Ohm S11=0.94051078 Ang -41.3599815, S21=3.68957525 Ang 133.784136,
S12= 0.00705502623 Ang53.0341365, S22=0.920112316 Ang-36.579586
From Tabular Graph Z11 = 2.9307 -j17.968 and Z22 = 4.2667 - j20.314

| | | | |
|---|---|---|---|
| Zin=complex(2.9307,-17.968) | Rin=real(Zin) | Xin=imag(Zin) | Zin: (2.931,-17.97) |
| Zout=complex(4.2667,-20.314) | Rout=real(Zout) | Xout=imag(Zout) | Zout: (4.267,-20.31) |
| Ri1=50 Rin: 2.931 | Xin: -17.97 | | |
| Ri2=sqrt(Ri1*Rin) | | | Ri2: 12.11 |
| Ro1=50 Rout: 4.267 | Xout: -20.31 | | |
| Ro2=sqrt(Ro1*Rout) | | | Ro2: 14.61 |
| Freq=350e6 | Wm=2*_PI*Freq | | Wm: 2.199e+09 |
| Qi=2 | | | |
| Qo=2 | | | |

Pi Match input

| | | |
|---|---|---|
| Ycpi1= (Qi/Ri1) | Qipmin=sqrt(Ri1/Ri2) | Qipmin: 2.032 |
| Xcpi1= (1/Ycpi1) | Cpi1= 1e12/(Wm*Xcpi1) | Cpi1: 18.19 |
| Xcpi2=Ri2*(sqrt((Ri1/Ri2)/((Qi*Qi+1)-(Ri1/Ri2)))) | Cpi2=1e12/(Wm*Xcpi2) | Cpi2: 17.24 |
| Xlpi=(Qi*Ri1+(Ri1*Ri2/Xcpi2))/(Qi*Qi+1) | Lpi=1e9*Xlpi/(Wm) | Lpi: 11.18 |

LowPassT Match input

| | | |
|---|---|---|
| Xlit1= (Rin*Qi - Xin) | Lti1=1e9*Xlit1/Wm | Lti1: 10.84 |
| Ai2=((Rin*(1+Qi*Qi)/Ri2) -1) | Ai=Sqrt(Ai2) | Ai: 0.4588 |
| Bi=Rin*(1+Qi*Qi) | | Bi: 14.65 |
| Qitmin=sqrt(Ri2/Rin-1) | | Qitmin: 1.769 |
| Xlit2=Ri2*Ai | Lti2=1e9*Xlit2/Wm | Lti2: 2.526 |
| Xcit=Bi/(Qi+Ai) | Cti= 1e12/(Wm*Xcit) | Cti: 76.3 |

Pi Match output

| | | |
|---|---|---|
| Ycpo1= (Qo/Ro1) | Qopmin=sqrt(Ro1/Ro2) | Qopmin: 1.85 |
| Xcpo1= (1/Ycpo1) | Cpo1= 1e12/(Wm*Xcpo1) | Cpo1: 18.19 |
| Xcpo2=Ro2*(sqrt((Ro1/Ro2)/((Qo*Qo+1)-(Ro1/Ro2)))) | Cpo2=1e12/(Wm*Xcpo2) | Cpo2: 21.13 |
| Xlpo=(Qo*Ro1+(Ro1*Ro2/Xcpo2))/(Qo*Qo+1) | Lpo=Xlpo*1e9/(Wm) | Lpo: 12.18 |

LowPassT Match output

| | | |
|---|---|---|
| Xlot1= (Rout*Qo - Xout) | Lto1=1e9*Xlot1/Wm | Lto1: 13.12 |
| Ao2=((Rout*(1+Qo*Qo)/Ro2) -1) | Ao=Sqrt(Ao2) | Ao: 0.6787 |
| Bo=Rout*(1+Qo*Qo) | | Bo: 21.33 |
| Qotmin=sqrt(Ri2/Rin-1) | | Qotmin: 1.769 |
| Xlot2=Ro2*Ao | Lto2=1e9*Xlot2/Wm | Lto2: 4.508 |
| Xcot=Bo/(Qo+Ao) | Cto= 1e12/(Wm*Xcot) | Cto: 57.1 |

Figure 9.35. Equations for initial values of matching networks.

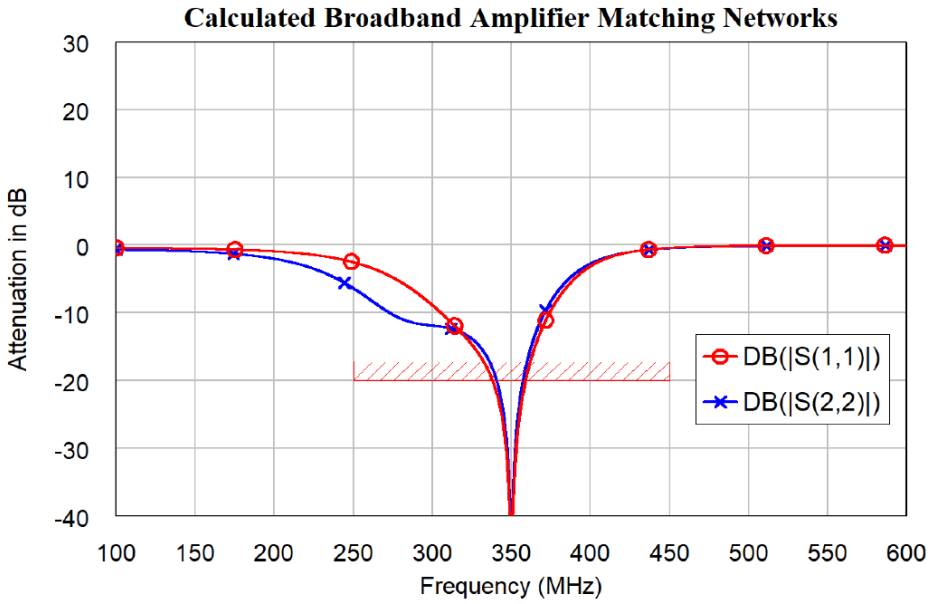



Figure 9.36. Frequency response for initial values of matching networks.

Figure 9.35 shows the equations for AWR DE to calculate these matching circuit component values using the manufacturers S parameters as a starting point. The initial component values for the input and output matching networks are calculated at 350 MHz, using a progressive impedance transformation and a lowpass T section at the amplifier terminals and a Pi section at the input and output terminals. These networks are then connected as shown in figure 9.34. The resulting $S_{11}$ and $S_{22}$ frequency response is shown in figure 9.36.

It can be seen that this simple matching procedure provides a reasonable input and output match at 350 MHz, but the matching network parameters need to be optimised to provide a good match over the 300 to 400 MHz band. Performing an optimisation of the constants K1 to K12 results of figure 9.34 results in the frequency response shown in figure 9.37.

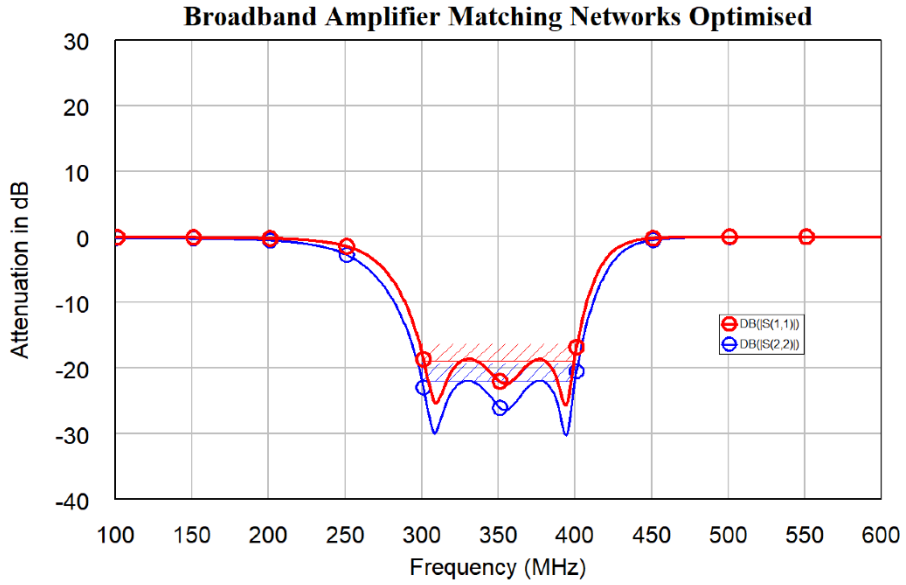



Figure 9.37. Optimised broadband matching network end of step 1.

A bigger impedance transformation ratio is required for the input matching, compared with the output matching. As a result, a slightly better match can be obtained for the output matching-network, as shown in figure 9.37. The resulting element modification constants are shown in figure 9.38. It can be seen that some significant changes from the starting values have occurred.

| | |
|---|---|
| K1=0.840936280654581 | K7=0.880139177836916 |
| K2=1.20238934788103 | K8=1.05256806419861 |
| K3=8.99057775160543 | K9=5.29922754729421 |
| K4=0.824491185056474 | K10=0.789083983335624 |
| K5=0.873044663554417 | K11=0.689966118305472 |
| K6=2.95975133760051 | K12=2.72442313452321 |

Figure 9.38. Element modification constants for figure 9.37.

The second step in the amplifier design is to disable ports 2 and 4 and enable the FET subcircuit, as shown in figure 9.41. Enabling the amplifier activates the transfer impedances S21 and S12, causing significant changes in the frequency response. The circuit of figure 9.41, with the constants of figure 9.38 is then optimised, to obtain good matching for both the input and output. In the optimisation for $S_{11}$ and $S_{22}$, the default goal L value must be disabled and L changed to 3, so that bigger errors have a much higher penalty. Figure 9.39 shows the resulting frequency response after this optimisation.

The resulting element modification constants are shown in figure 9.40. $S_{11}$ and $S_{22}$ are now only -5 dB and the amplifier gain between ports 1 and 2 is much higher than expected and oscillations are likely at 165 MH, 302 MHz and 395 MHz. Plotting the stability circles, shows a very unstable amplifier. K is less than 1 and B1 is negative between 260 and 300 MHz. The amplifier is thus unstable.

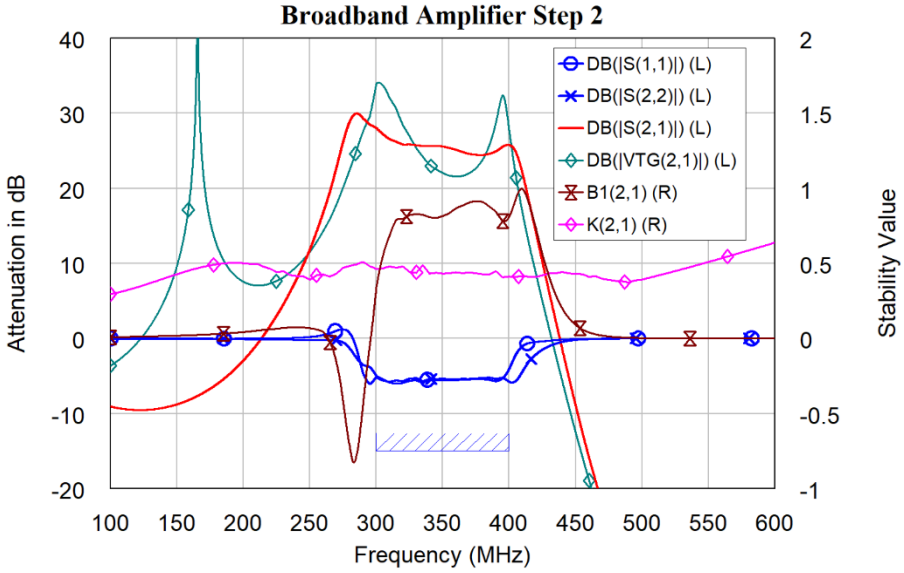



Figure 9.39. Broadband amplifier end of step 2.

K1=0.801940682496878
K2=1.26474946360482
K3=9.58291318913493
K4=0.800717750816016
K5=0.945212334469348
K6=2.38909409195089
K7=0.741206286719925
K8=1.27134043807916
K9=6.95607487816484
K10=0.766546877327417
K11=0.618185465362773
K12=2.46504608432839

Figure 9.40. Element modification constants for figure 9.39.

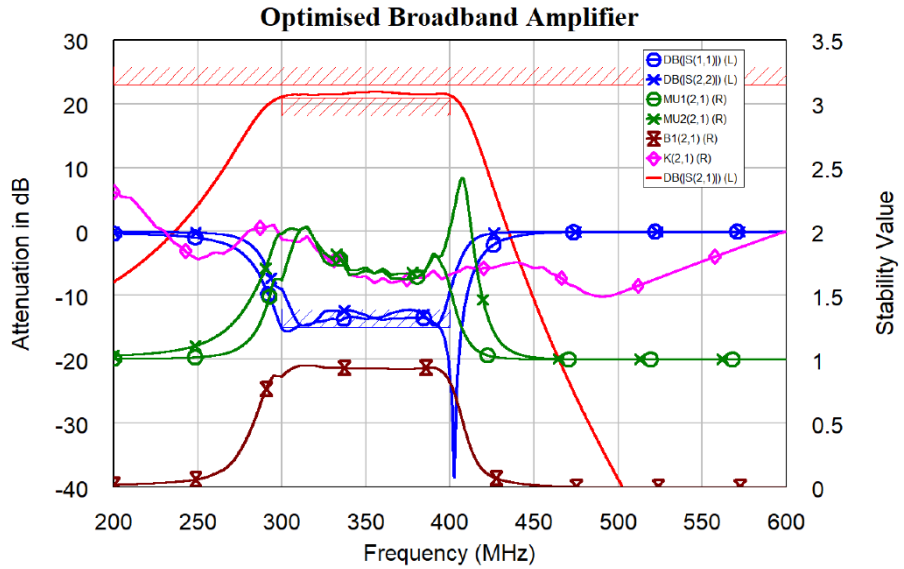



Figure 9.41. Final amplifier performance.

The third step is to make the amplifier stable. The FET input impedance is 4.26 –j17.97 Ω, corresponding to a Q = 6.1, for the input impedance. Reducing the input Q slightly by

placing a resistor at the input terminal of the FET will make the amplifier stable. Reducing the input coupling capacitor will improve the stability at 165 MHz. Placing optimisation constraints to ensure that the amplifier's gain (DB(|S2,1|)) is between 21dB and 23 dB enhances the stability and aims for a flat gain. The matching networks are then optimised again, to achieve a suitable amplifier performance. Figure 9.41 shows the amplifier's performance. Figure 9.42 shows the resulting circuit values, including the final element modification constants. The amplifier input match (blue curves) has been improved compared to figure 9.39. The stability factors show that the amplifier is unconditionally stable and the amplifier's gain is just over 21 dB from 300 MHz to 400 MHz.

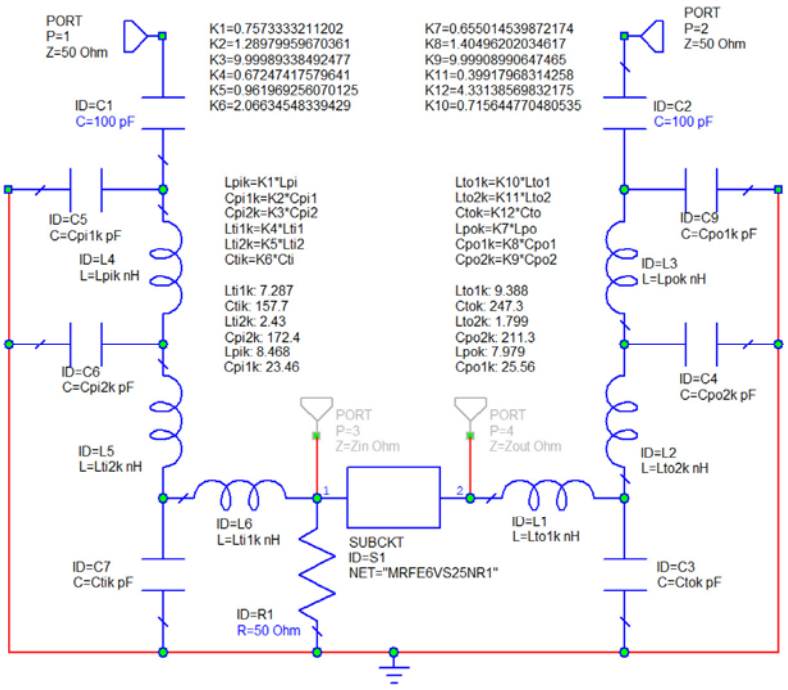



Figure 9.42. Final amplifier matching networks.

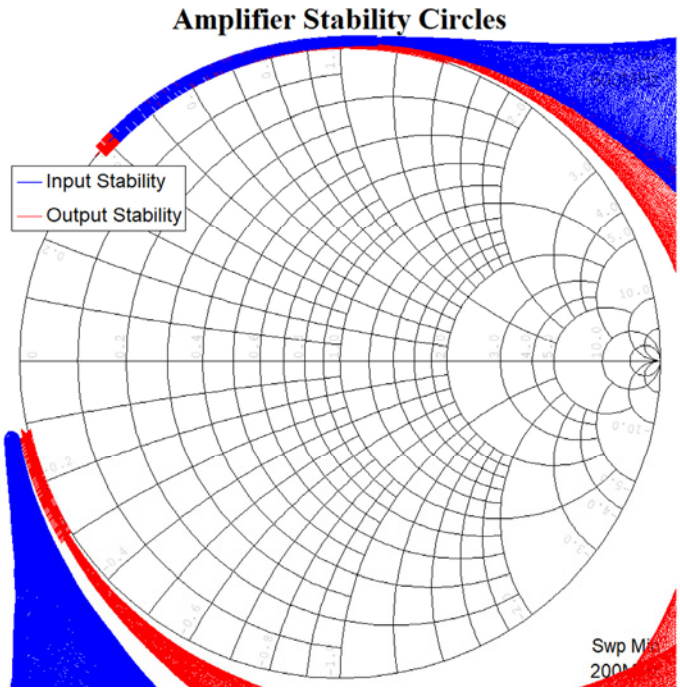



Figure 9.43. Final broadband amplifier stability circles.

Figure 9.43 shows the input and output stability circles for the 200 to 600 MHz frequency range and show that the amplifier is unconditionally stable. The amplifier has a gain of slightly more than 20 dB. The FET input impedance of 2.93 - j17.97 Ω is much smaller than the impedance of the 50 Ω stability resistor (R1), so most of the current flowing through the input matching network will flow into the FET. The S parameter file used contains small signal parameters, but even if the amplifier has a 25 W output, then the stability resistor will dissipate much less than 0.25W, which is negligible compared to the output.

To lower production costs at UHF and microwave frequencies, the inductors in matching networks like figure 9.30 can be replaced by Microstrip transmission lines, as shown in figure 7.16. That will change the input and output match slightly, so that further optimisation may be required. Figure 9.44 shows the schematic and figure 9.45 shows the PCB layout for the MRFE6VS25N 512 MHz test circuit used by NXP [3]. To accommodate slight FET variations, capacitor pads are normally included in the PCB layout. That allows the capacitors C6 to C10 in figure 44 to be varied if needed to tune the amplifier's performance.

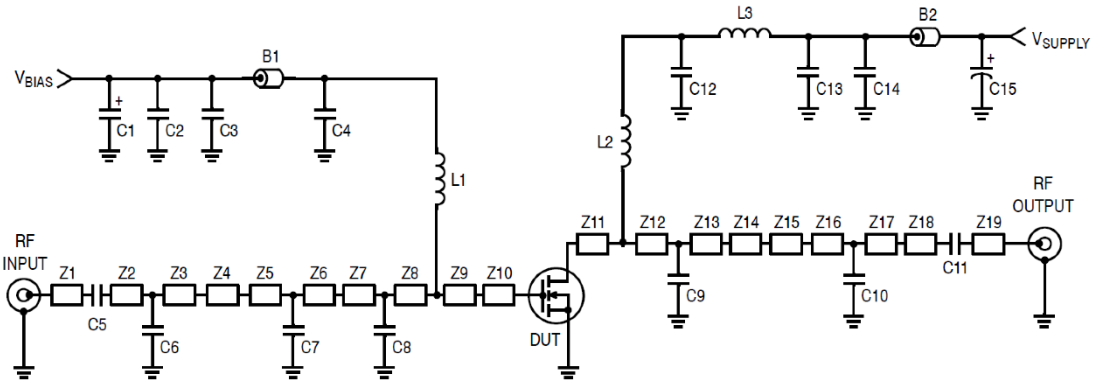



Figure 9.44. Schematic of 512 MHz amplifier from data sheet [3].

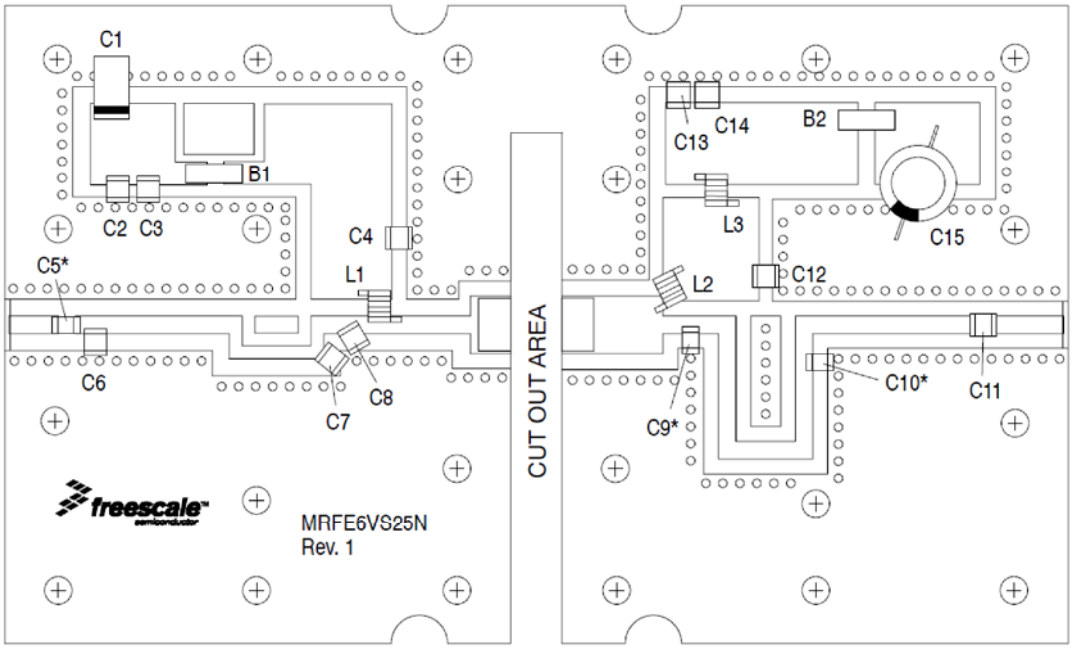



Figure 9.45. Manufacturer PCB from data sheet [3].

## *Example 9.3: Broadband Amplifier Using Device Models*

Typical UHF TV transmitters cover a wide bandwidth from 470 – 790 MHz [7, 8]. To minimise the transmitter running cost, the power consumption needs to be minimised and the power amplifier needs to be very efficient in terms of the amount of DC power required to produce the required RF power. The Power Added Efficiency (PAE) is the ratio of the effective RF output power ($P_{out}$ – $P_{in}$) over the DC supply power and is a measure of how efficient the amplifier is at converting DC power into RF energy. The power dissipated in the amplifier is (1 – PAE) and that heat needs to be removed to keep the amplifier operating reliably. A high PAE is thus desirable.

Just like audio amplifiers, for low RF frequencies, a Class A amplifiers can have a PAE up to 50% if transformer coupling is used. Class AB (push-pull) amplifiers can have a PAE up to 78%. An ideal Class C amplifier has a PAE of 100%. If maximum power transfer impedance matching is used, then the maximum PAE is half of those values. Equation 9.2 shows that maximum power matching is not always implemented in power amplifiers. At higher RF frequencies, the device losses tend to increase and lower PAE values result. Class C amplifier biasing is suitable for FM transmitters, which operate at a constant power.

Modern modulation methods, like OFDM, used for broadcasting or cellular radio have a large output peak power to average power ratio and require a linear voltage (or power) gain that can be obtained using Class A or Class AB operation. These amplifiers can use a single transistor or two transistors in a push pull operation. For a Class A or Class AB amplifier the PAE is proportional to the output power up to a power level when saturation occurs.

When the amplifier saturates, it generates harmonics that must be filtered out before transmission. Saturation also causes Intermodulation Distortion (IMD), which generally cannot be removed by filtering. Amplifier design is this a balance between power linearity, PEA, harmonics, saturation, bandwidth and amplifier stability. To estimate the PAE, amplifier saturation and IMD, a non-linear, power dependent model of the active device used is required. Most RF power device manufacturers now publish such nonlinear models for their devices.

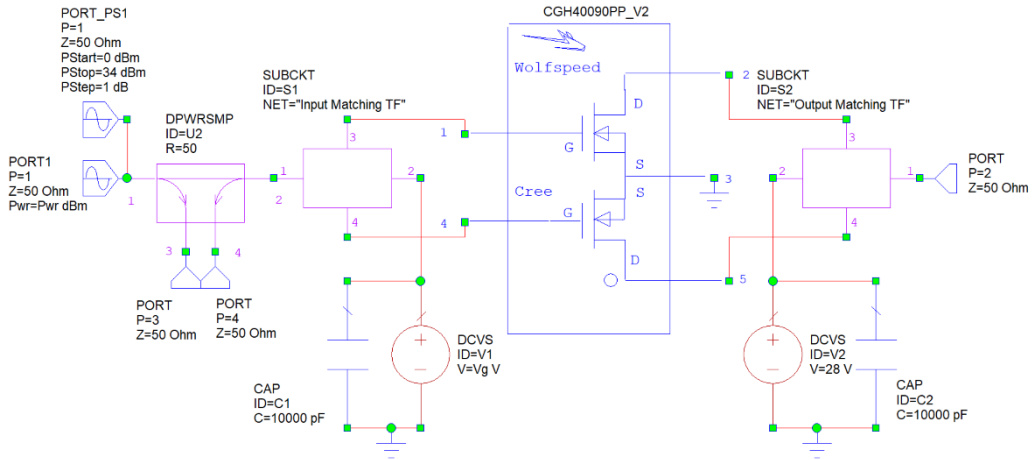



Figure 9.46. Basic Class AB power amplifier.

The amplifier in this example uses Class AB push pull operation, since that result in a lower harmonic level. The device used is a CGH40090PP, 4 GHz, 28V, 60W, GaN on SiC device [9]. That device contains 2 FET's in the one device, providing a thermal match

for both the Class AB push-pull devices, resulting in low even harmonic levels. The AWRDE nonlinear library and its installation instruction for their devices is available by application from Wolfspeed [10]. For this example, a wideband amplifier at 1 GHz with a good PAE and stability for an input and output VSWR of better than 6:1 is required. The basic AWR DE circuit schematic for the amplifier is shown in figure 9.46.

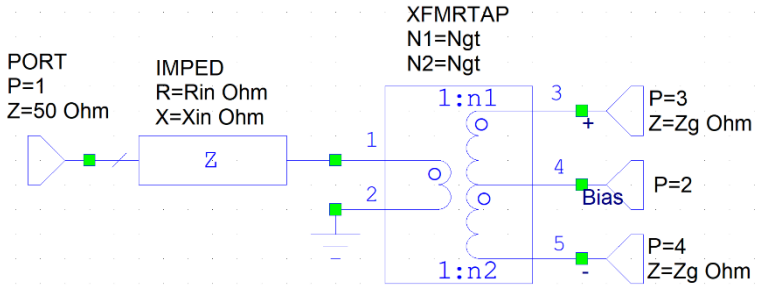



Figure 9.47. Tapped transformer Input Matching.

| | | |
|---|---|---|
| Vg=-2 | Pwr=20 | RL=28*28/90 RL for 90W at 28V |
| Zs=2.4 | Zg=2.4 | Ngt=sqrt(Zg/(2*50)) Ngt: 0.1549 |
| RL: 8.711 | Zl=8.7 | Ndt=sqrt(Zl/(2*50)) Ndt: 0.295 |
| Rin=25 | Xin=12 | Xout=0 |

Figure 9.48. Tuned parameters for the power amplifier with transformer matching.

The input matching circuit is shown in figure 9.47. A similar network is used for the output matching. The input network has a series resistance Rin and reactance Xin. The output network only has a series reactance Xout. Rin assists in providing stability. Rin, Xin, Xout, the turns-ratios Ngt for the input and Ndt for the output, and the bias voltage are all tuned to obtain a good PAE, bandwidth, stability and harmonic levels. Figure 9.48 show the resulting values. The resulting gain, PAE, output power at the fundamental and harmonics, versus input power is shown in figure 9.49. At a 1 dB compression, corresponding to an input of 26.81 dBm, the output power is 84.42W, the third harmonic output is 0.8W and the PAE is 44.68%.

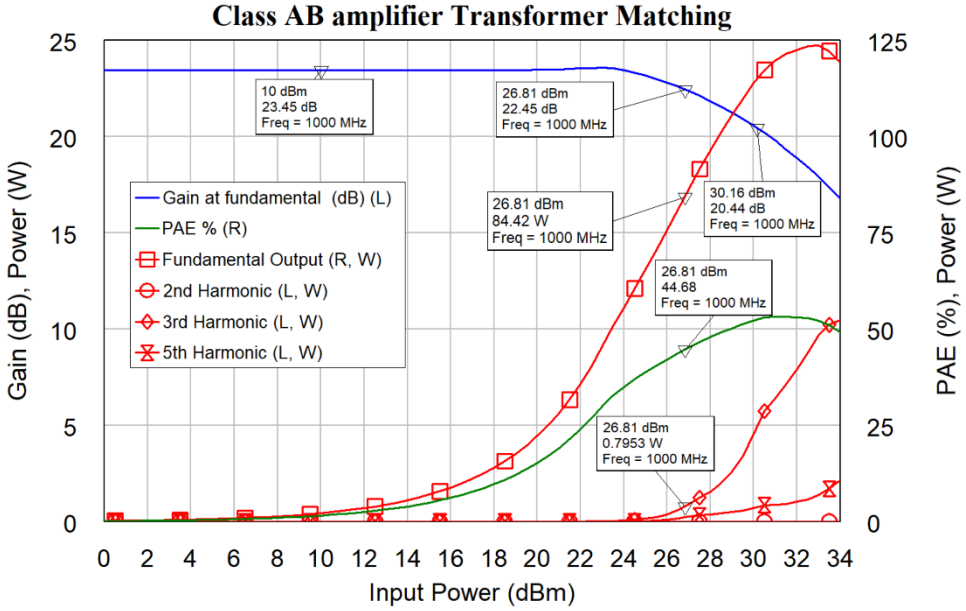



Figure 9.49. Output performance of the transformer matched power amplifier.

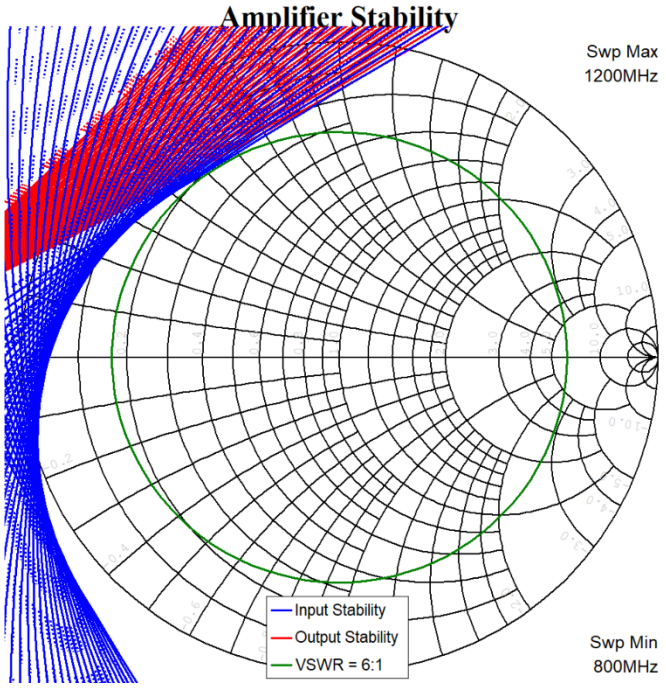



Figure 9.50. Stability of the transformer matched power amplifier, 0.8 -1.2 GHz.

Figure 9.50 shows the input and output stability circles for the 800 MHz to 1200 MHz frequency range. It can be seen that the amplifier is stable over this entire range, provided the input source impedance and output load have a VSWR less than 6:1. Figure 9.51 shows the corresponding amplifier frequency response at an input power level of 20 dBm. It shows that a good S11, good gain and flat frequency response is obtained.

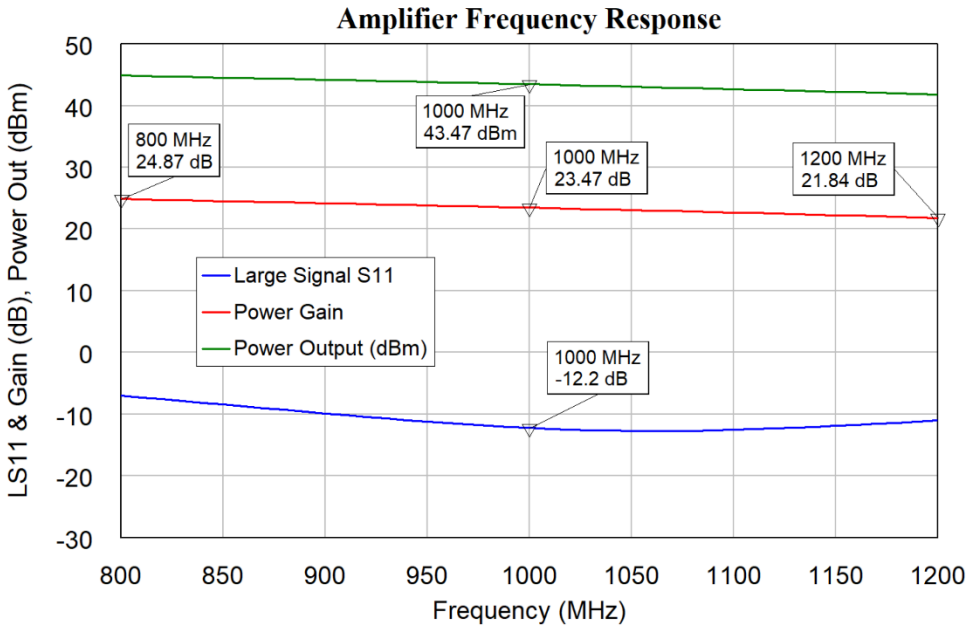



Figure 9.51. Frequency response of the transformer matched power amplifier.

Figure 9.52 shows the input and output stability circles for the amplifier over the 10 MHz to 2 GHz frequency range. It can be seen that the amplifier is borderline unstable below 100 MHz. To improve the stability, suitable filtering and frequency selective resistive loading needs to be included in either or both the input and output matching networks.

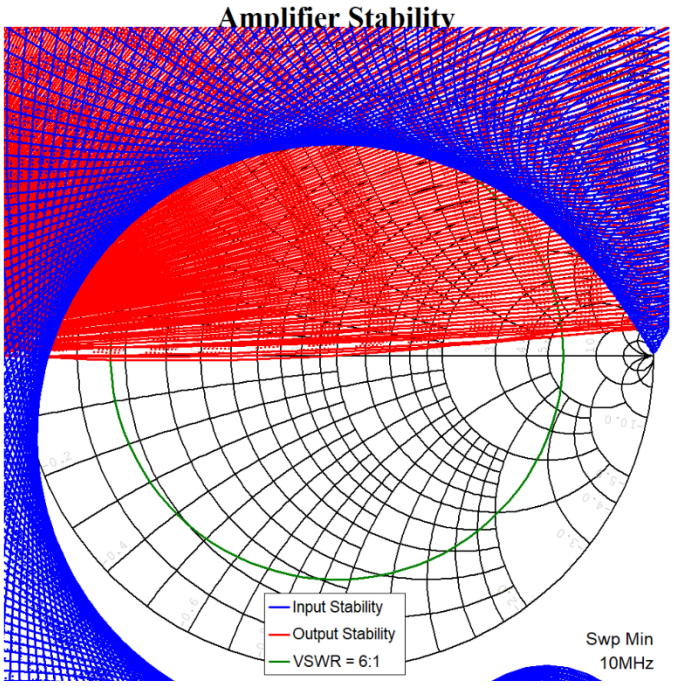



Figure 9.52. Stability of the transformer matched power amplifier, 10MHz - 2GHz.

The transformer matching is suitable for the first step in an amplifier design by using simulation to obtain the desired performance by determining optimum biasing and matching for the amplifier. For a practical amplifier at 1 GHz, it is difficult to realise transformers with the required turns-ratio, power handling capability and low losses. A 50 Ω floating coaxial-line-balun, as shown in figure 4.55, can be used to produce differential signals with a 25 Ω impedance. A Marchand Balun can also be used if desired. Figure 4.2 shows that a two-line impedance transformation can produce a flat impedance transformation over a wide bandwidth. Figure 9.52 shows how this is implemented in the design for the amplifier. For better stability, the stability resistors (Rin) are moved close to the Gate of the FET. That is a lower impedance, requiring Rin to be changed to 1 Ω. Resistors Rin2 have been added to provide stability at frequencies <100 MHz The output matching-network is the same but the resistors are not present.

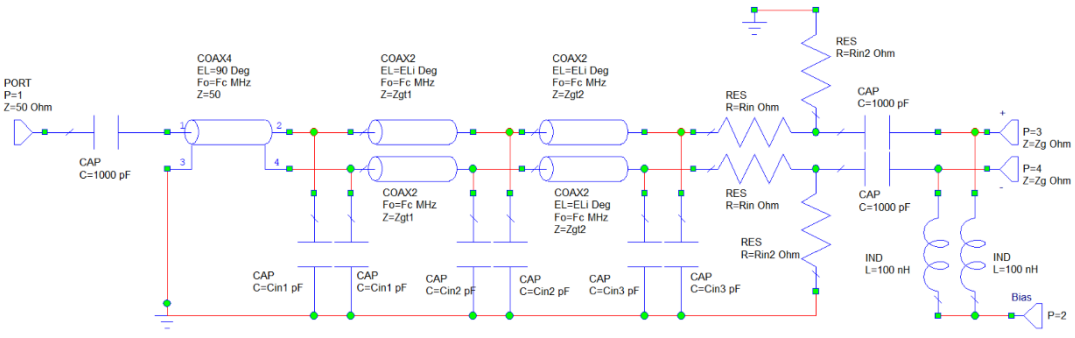



Figure 9.53. Transmission line based, input matching network.

In figure 9.53, Fc is the centre frequency for all the transmission lines, corresponding to the 90° electrical length. If needed, that electrical length of the individual lines in the input or output matching networks can be tuned, to obtain a better performance. Using the transformer-amplifier as a starting point, the input and output matching networks are tuned to obtain a good PAE, bandwidth, stability and harmonic levels. To be able to get

a fair comparison with the transformer-matched amplifier, the gate biasing is kept at -2V. Figure 9.54 shows the resulting values. The input and output impedances, Zg and Zl the same values as before. The resulting gain, PAE, output power at the fundamental and harmonics, versus input power is shown in figure 9.55. At an input of 27.31 dBm, the gain compression is 1 dB, the output power is 94.31W, the third harmonic output is 0.159 W and the PAE is 54.34 %. Those values are significantly better than those shown in figure 4.49.

| | | RL for 90W at 28V | |
|---|---|---|---|
| Vg=-2 | Pwr=20 | RL=28*28/90 | Fc=1000 |
| Zs=2.4 | Zg=2.4 | Kg1=sqrt(25/Zg) | Kg1: 3.227 |
| | Zg2=25/Kg1 | Zgt1=sqrt(25*Zg2) | Zgt1: 13.92 Zg2: 7.746 |
| ELi=90 | Zg3=Zg2/Kg1 | Zgt2=sqrt(Zg2*Zg3) | Zgt2: 4.312 Zg3: 2.4 |
| RL: 8.711 | Zl=8.7 | Kd1=sqrt(25/Zl) | Kd1: 1.695 |
| | Zd2=25/Kd1 | Zdt1=sqrt(25*Zd2) | Zdt1: 19.2 Zd2: 14.75 |
| ELo=90 | Zd3=Zd2/Kd1 | Zdt2=sqrt(Zd2*Zd3) | Zdt2: 11.33 Zd3: 8.7 |
| Rin=1 | Cin1=0 | Cout1=0 | |
| Rin2=27 | Cin2=0 | Cout2=0 | |
| | Cin3=0 | Cout3=0 | |

Figure 9.54. Tuned parameters for the power amplifier with transformer matching.

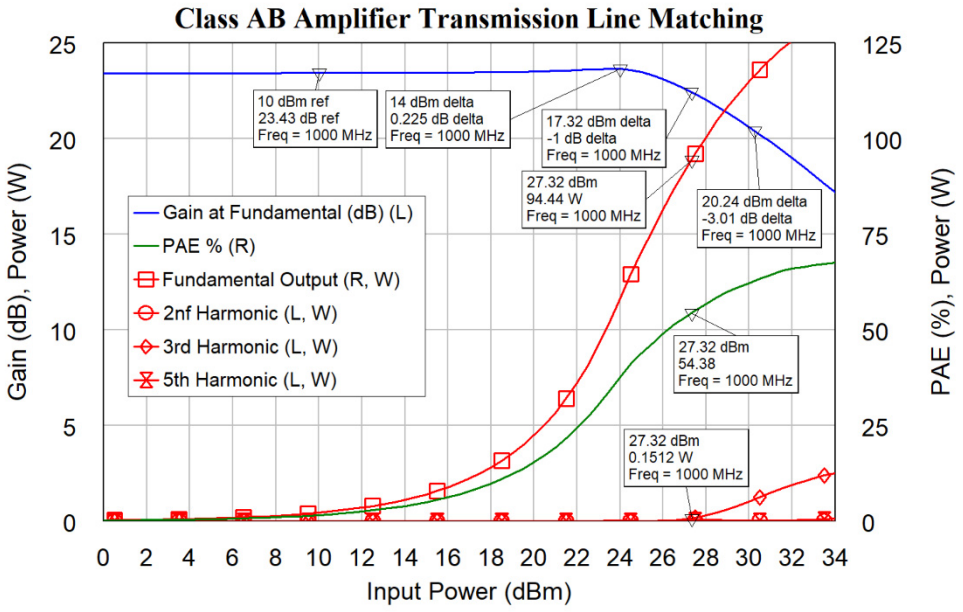



Figure 9.55. Output performance of the transmission line matched power amplifier.

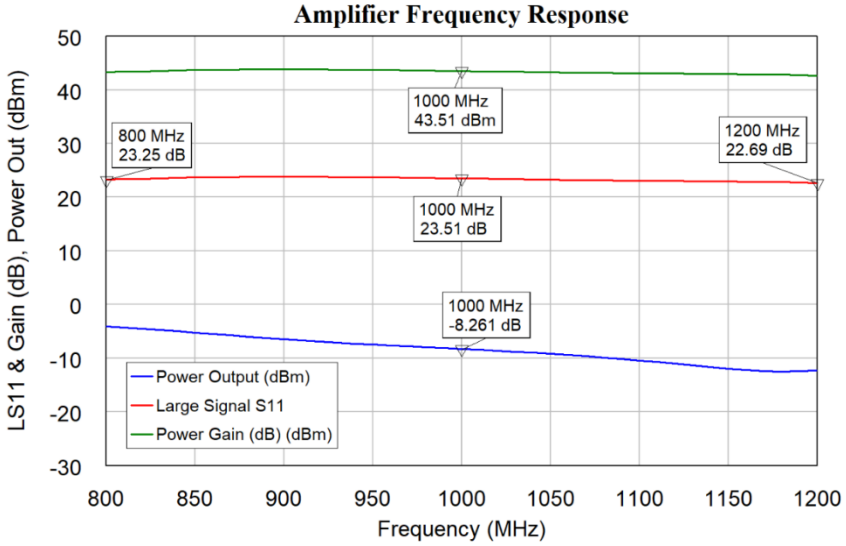



Figure 9.56. Frequency response of the transmission line matched power amplifier.

Figure 9.56 shows the amplifier's frequency response. The large signal S11 is not as good but the frequency response is flatter than the transformer-matched amplifier shown in figure 9.51. The gain is very similar. Using a one-line impedance transformation results in a higher gain at 1 GHz and a lower gain at 800 MHz and 1.2 GHz. At 1 GHz, for typical substrates, the 90 ° line length is 44 mm long, so that a two-line impedance transformation can easily be implemented. Figure 9.53 and 9.54 show input capacitors Cin1 to Cin3, and similarly Cout1 to Cout3, that can be inserted in the hardware to perform some fine-tuning in case the actual device is slightly different from the model used in the simulation.

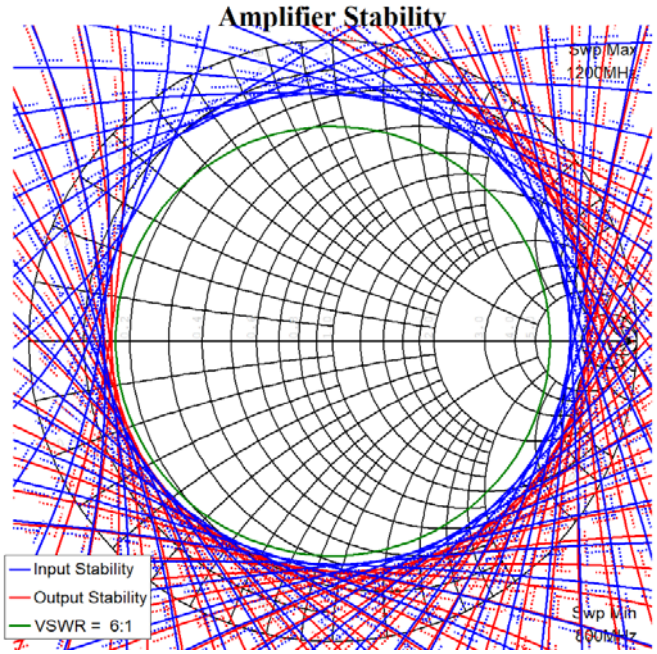



Figure 9.57. Stability of the transmission line matched power amplifier, 0.8-1.2 GHz.

Figure 9.57 shows that the amplifier is stable over the entire 600 MHz to 1400 MHz frequency range, provided the input and output have a VSWR less than 6:1.

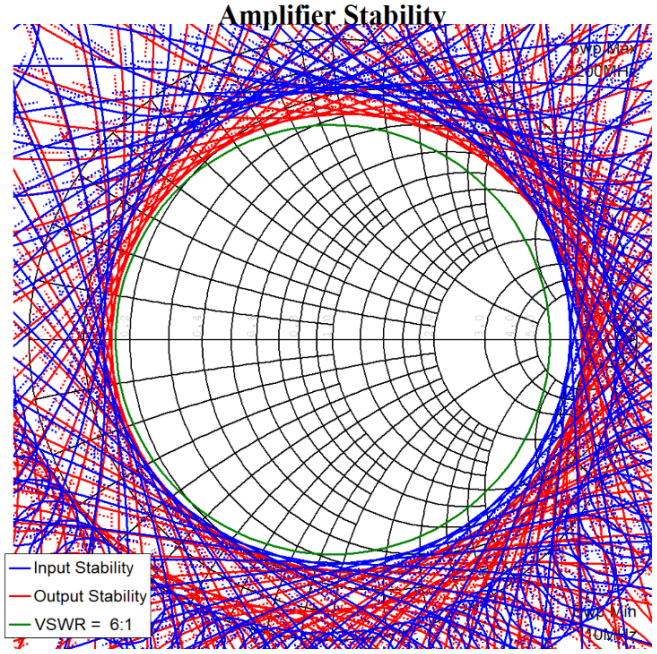



Figure 9.58. Stability of the transmission line matched power amplifier, 10 MHz - 2 GHz.

Figure 9.58 shows that the amplifier is also stable over the entire 10 MHz to 2 GHz frequency range. To achieve this stability, shunt resistors Rin2 needed to be added to the input matching network, as shown in figure 9.53.

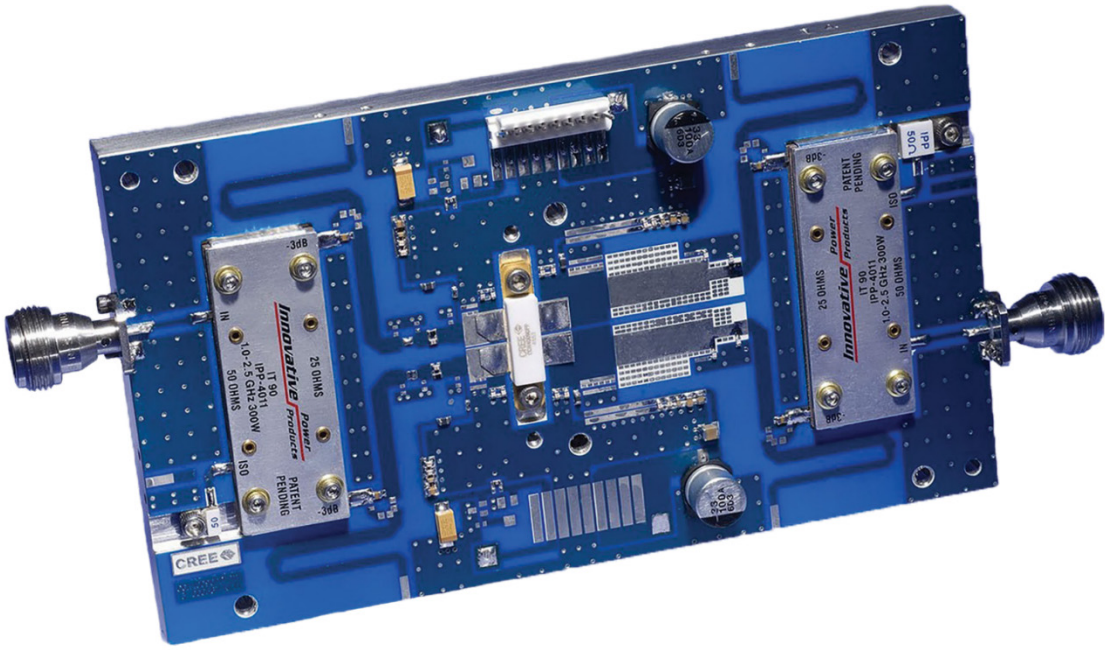



Figure 9.59. CGH40090PP-AMP demonstration amplifier [9].

Figure 9.59 shows the CGH40090PP-AMP demonstration amplifier, available from Wolfspeed. That amplifier has a PAE of typically 50% and an output of 50 dBm over a 0.5 GHz to 2.5 GHz bandwidth with a gain that varies between 12 and 18 dB. The circuit for this is more complex than the one shown in figures 9.46 and 9.53. The "Innovative Power Products" hybrids perform the same function as the coaxial Balun shown in figures 9.53 and 4.55. Notice how the low transmission-line impedances for the output matching result in very wide PCB tracks. The pads along the output transmission lines allow the tracks to be widened, or shunt capacitors to be placed to fine-tune the amplifier's performance. Black SMD components near the gate of the FET is a resistor, required for stability. In the CREE design that resistor has a capacitor in parallel with it to improve the high frequency performance. FET's in general, have better linearity than bipolar transistors and are thus preferred for applications requiring a low intermodulation distortion, such as mobile radio base-station amplifiers or DAB and TV transmitters. FET's have very high gains at low frequencies and are thus more susceptible to instability.

Most commercial VHF and UHF high power transmitters [6, 7] use Doherty amplifiers. These [11, 12] consist of a main amplifier that provides the average power and a peaking amplifier that provides the peak power levels. The design of Doherty amplifiers is beyond the scope of this book. David Vye [13] provides an excellent design tutorial on the design of a Doherty power amplifier using advanced transistor models.

Having an accurate non-linear model of the FET, allows the performance of the amplifier to be simulated accurately, thus reducing the number of iterations of a PCB that is required for producing a good RF power amplifier.

The Cadence AWR FAQ web site has useful additional information about Power Amplifier Design Flow [14], which covers information that is outside the scope of this book, but can assist the design of RF power amplifiers.

## References


1. F. Davis, Motorola (Freescale, NXP) Semiconductor Application Note AN267, "Matching Network Designs with Computer Solutions." 1993, https://www.nxp.com/docs/en/application-note/AN267.pdf
2. R Hejhall, Motorola (Freescale, NXP) Semiconductor Application Note AN282 "Systemising RF Power Amplifier Design." 1993, https://www.nxp.com/docs/en/application-note/AN282A.pdf
3. NXP Semiconductors, MRFE6VS25NR1 data sheet Rev2, March 2019, https://www.nxp.com/docs/en/data-sheet/MRFE6VS25N.pdf
4. NXP Semiconductors, Request download MRFE6VS25NR1 S parameters. https://www.nxp.com/webapp/sps/download/license.jsp?colCode=MRFE6VS25N_SP
5. B. Becciolini, "Motorola (Freescale, NXP) Semiconductor Application Note AN721, "Impedance Matching applied to RF Power Transistors", October, 2005. https://www.nxp.com/docs/en/application-note/AN721.pdf
6. A. Wood, B. Davidson, "Motorola (Freescale, NXP) Semiconductor Application Note AN1526, "RF Power Device Impedances: Practical Considerations", https://www.nxp.com/docs/en/application-note/AN1526.pdf
7. NEC DTU-H10/DTV-H20 Series: UHF and VHF Digital High Power TV Transmitters, https://www.nec.com/en/global/prod/nw/broadcast/products/dtu-h10_dtv-h20_series/index.html
8. Rohde & Schwarz, THU9evo liquid-cooled UHF Transmitter family, https://www.rohde-schwarz.com/us/products/broadcast-and-media/tv-transmitters/rs-thu9evo-liquid-cooled-uhf-transmitter-family_63493-313345.html
9. Wolfspeed CGH40090, 90W, 500 MHz-2.5 GHz, RF Power GaN HEMT, https://assets.wolfspeed.com/uploads/2020/12/CGH40090PP.pdf
10. Wolfspeed, Request Access to RF Portal models, to download models. https://www.wolfspeed.com/tools-and-support/rf/rf-portal-access
11. W. H. Doherty, "A New High Efficiency Power Amplifier for Modulated Waves," Proceedings of the IRE, Vol. 24, pp. 1163 – 1182, 1936.
12. Microwaves101.com, Encyclopedia, Doherty Amplifiers, https://www.microwaves101.com/encyclopedias/doherty-amplifiers
13. David Vye, High Efficiency GaN Doherty Power Amplifier Design Video, MTT IMS Conference 2020. 15 Jul 2020, https://resourcecenter.mtt.ieee.org/conferences/ims-2020/MTT2020IMS0030.html
14. Cadence AWR FAQ, Power Amplifier Design Flow, https://kb.awr.com/display/awrfaq/Power+Amplifier+Design+Flow

# Chapter 10

# Operational Amplifiers

## Introduction

Operational amplifiers (OpAmps) with 3 dB bandwidths larger than 1.5 GHz are now available. Such operational amplifiers are used in consumer applications like hard disk drives, computer monitors, industrial and medical applications, such as CAT scanners. In addition, one can use these operational amplifiers for IF amplifiers in many communication receiver applications.

These high-speed amplifiers fall into two categories [1, 2, 4]:

Voltage Feedback Amplifiers

Current Feedback Amplifiers

The Voltage Feedback amplifiers have the same properties as common operational amplifiers, such as the LF356 or LM741, used at low frequencies. The Voltage feedback amplifiers have lower noise, better dc performance and more freedom in feedback impedance selection.

The Current Feedback [3, 4] amplifiers on the other hand have faster slew rates and lower distortion, but have restrictions on feedback configurations.

### *Voltage Feedback Amplifier Theory*

If an operational amplifier has input voltages $V_1$ and $V_2$ at the input terminals, then for a voltage feedback amplifier the output voltage is:

$$V_{out} = A(s) * (V_1 - V_2) \qquad \text{Eqn. 10.1}$$

where A(s) is the open loop gain, which is frequency dependent. Consider the non-inverting amplifier configuration:

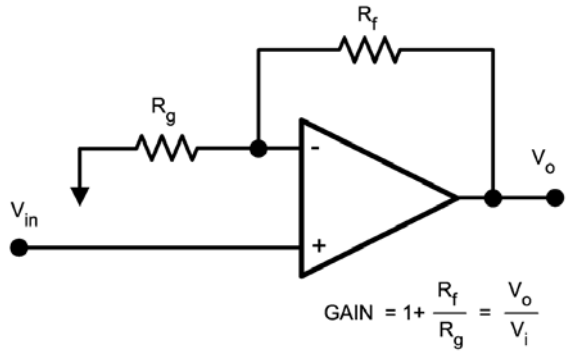



Figure 10.1. Non-inverting Amplifier [1]

If $$G = \frac{R_f + R_g}{R_g} \qquad \text{Eqn. 10.2}$$

Then $$V_{out} = V_{in}\left(\frac{G}{1+\frac{G}{A(s)}}\right) = V_{in}\left(\frac{G*A(s)}{A(s)+G}\right) \qquad \text{Eqn. 10.3}$$

When A(s) is very large, then the gain is approximately;

$$V_{out} = V_{in} * G \qquad \text{Eqn. 10.4}$$

When A(s) = G the gain will be 3 dB below the gain when A(s) is very large. The frequency when A(s) = G is thus the bandwidth of the amplifier. Since A(s) decreases with frequency as shown in figure 2, the bandwidth of the amplifier will depend on the gain as is also shown in figure 2.

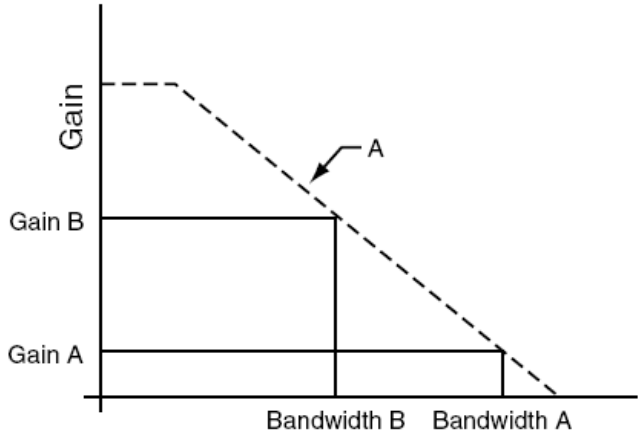



Figure 10.2. Open loop and Closed loop gain of Voltage Feedback Amplifier [1]

If *D* is the distortion introduced by the amplifier, the distorted gain *Ad(s)* is then;

$$\mathrm{Ad(s)} = \mathrm{A(s)} * (1 + \mathrm{D}) \qquad \text{Eqn. 10.5}$$

Then the gain of the amplifier can then be written as:

$$V_{out} = V_{in}\left(\frac{G}{1+\frac{G}{A(s)*(1+D)}}\right) \approx V_{in}\left\{G * \left(1 - \frac{G}{A(s)*(1+D)}\right)\right\} =$$

$$V_{in}\left\{G * \left(1 - \frac{G}{A(s)*(1+D)}\right)\right\} \qquad \text{Eqn. 10.6}$$

The larger A(s), the smaller the effect of the distortion *D*. OpAmps are thus very useful in producing low distortion amplifiers.

## *Current Feedback Amplifier Theory*

The Current feedback amplifier produces an output voltage proportional to an "Error current" $I_{error}$. The Current feedback amplifier "gain" is the transfer impedance Z(s).

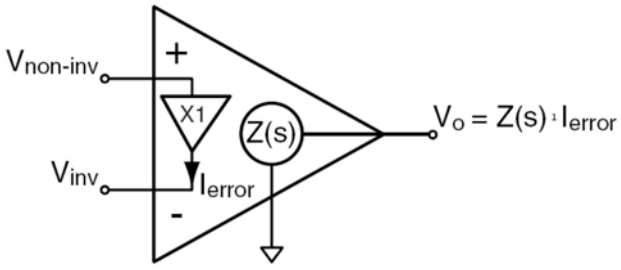



Figure 10.3 Current Feedback amplifier configuration [1]

For the inverting amplifier configuration of figure 10.1, the equations for the amplifier are:

$$i_{error} = \frac{V_{in} - V_o}{R_f} + \frac{V_{in}}{R_g} \qquad \text{Eqn. 10.7}$$

Since $V_o = Z(s)I_{error}$ , substituting for $I_{error}$ in the above equation after manipulation leads to:

$$V_o = \frac{\frac{R_g}{Z(s)+R_f}}{\frac{}{Z(s)}} V_{in} \qquad \text{Eqn. 10.8}$$

The current feedback amplifier will thus have a transfer function of:

$$V_o = \left[\frac{G}{1+\frac{R_f}{Z(s)}}\right] \qquad \text{Eqn. 10.9}$$

Compared with the transfer function of the voltage feedback amplifier of:

$$V_o = \left[\frac{G}{1+\frac{G}{A(s)}}\right] \qquad \text{Eqn. 10.10}$$

Where $G = \frac{R_f + R_g}{R_g}$ is the gain of an ideal amplifier Eqn. 10.11

The amplifier corner frequency is when $G/A(s) = 1$ or when $R_f/Z(s) = 1$. The way $G/A(s)$ and $R_f/Z(s)$ changes with frequency will thus result in a difference in the bandwidth of the amplifiers. Halving both $R_f$ and $R_g$, keeps the gain the same for both amplifier configurations. That will double the bandwidth of the current feedback amplifier, but not change the bandwidth for the voltage feedback amplifier. Halving $R_g$ and keeping $R_f$ the same, will increase the gain $G$, as per equation 10.10 for both amplifiers. According to figure 11.2, this will reduce the bandwidth of the voltage feedback amplifier by close to half. Changing $R_g$ will not change the bandwidth of the current feedback amplifier. The feedback resistor $R_f$ can only be varied over a small range. For example, the LMH6702 has been optimised for a 237 Ω feedback resistor. Using a lower value can lead to excessive ringing in a pulse response and a higher value will limit the bandwidth.

## *Current and Voltage Feedback Amplifier Comparison*

Voltage feedback (VFB) OpAmps, are normally used for teaching about OpAmps at universities and as a result, most engineers are very familiar with them. Voltage feedback OpAmps have high open loop gains, low offset voltage and low input bias currents. The +ve and –ve input circuit architectures are the same, so that input bias and noise currents for both inputs of VFB OpAmps are approximately equal. For FET input OpAmps the bias currents can be less than 1 pA. For low voltage power supplies, rail to rail inputs and outputs are required. The vast majority of rail-to-rail OpAmps are voltage feedback devices.

Current feedback OpAmps have a lower open loop gain and lower input impedances. That results in less gain accuracy. The +ve and –ve input circuit architectures are different, so that the input bias and noise currents are different for the +ve and –ve input. Current feedback amplifiers are thus not very suitable for integrators. Current feedback OpAmps, are optimised for a fixed feedback resistor and that makes it more difficult for them to be used for active filters. Current feedback amplifiers have larger bandwidths, higher slew rates and generally have a lower distortion than voltage feedback amplifiers, as can be seen in the table 10.1. The vast majority of high bandwidth, high output power OpAmps,

such as those used for xDSL drivers are current feedback amplifiers. For a fair comparison, the fastest commercial grade operational amplifiers from the same manufacturer, capable of operating from ±4V to ±6V supplies, are used in table 10.1. Some OpAmps require a minimum gain for them to be stable [4, 5].

Table 10.1. Current and Voltage Feedback performance comparison.

| | Current Feedback | Voltage Feedback |
|---|---|---|
| Device | LMH 6702 | THS4211 |
| 3dB Bandwidth (Gain = 2) | 1.7 GHz | 325 MHz |
| Slew rate | 3100 V/μs | 970 V/μs |
| Noise Voltage | 1.83 nV/√Hz | 7 nV/√Hz (1 MHz) |
| Noise Current | 18.5- 3.0+ pA/√Hz | 4 pA/√Hz (10 MHz) |
| Distortion (HD2) | -79 dBc (20 MHz, 2Vpp) | -68 dBc (30 MHz, 2Vpp) |
| Distortion (HD3) | -88 dBc (20 MHz, 2Vpp) | -80 dBc (30 MHz, 2Vpp) |
| Input Offset Voltage | 1 mV | 3 mV |
| Input Bias Current | 8 μA | 7 μA |
| Input Offset Current | | 0.3 μA |
| Load Resistor (test circuit) | 100 Ω | 499 Ω |
| Feedback Resistor (test circuit) | 237 Ω | 392 Ω |
| Feedback Resistor range | Narrow | Very wide |
| Supply Voltage | ±4 V to ±6 V | ±2.5 V to ±7.5 V |
| Supply Current | 12.5 mA | 19 mA |
| Output Current | 80 mA | 170 mA |
| Output Voltage ±5Vs | ±3.5V | ±5V |
| Input Impedance | 1.4 MΩ | 6 GΩ |
| Input Capacitance | 1.6 pF | 0.3 pF |

## Example 10.1: High Impedance 0.01-20 MHz Amplifier

As part of an On-Line Impedance Analyser [6], a Voltage Sensor is required, to measure Power Line Communication (PLC) signals, with frequencies from 10 kHz to 20 MHz, which are injected onto 240V, 50 Hz, mains voltage power lines. The PLC signals are much smaller than the mains voltage and the mains voltage must be filtered out, so that the PLC signals can be accurately measured. The input impedance of the circuit should be greater than 1 MΩ at all frequencies. The design of this Voltage Sensor shows how either current or voltage feedback amplifiers, best satisfy the requirements for different parts of the circuit. The PLC signals on the power line are about 1V, so that more than 60 dB mains voltage attenuation is required for a >12 dB signal to mains voltage ratio, to enable accurate signal detection. Filtering out the mains voltage and passing the PLC signals, requires a high pass filter with a 10 kHz cut off frequency. The whole circuit is to operate from ±5V supplies. OpAmps with a 12V total (±6V) supply voltage capability are used for reliability. AD8058 Dual OpAmps are used for the voltage feedback amplifiers and AD8017 Dual OpAmps are used for the current feedback amplifiers. Their *.cir* Spice models can readily be imported into Cadence AWR DE, to permit simulation.

Figure 10.4 shows the circuit diagram of the complete Voltage Sensor. The operational amplifiers A1 and A2 are a high impedance high pass buffer amplifier. The Cs = 15 pF series input capacitor and the 1.068 MΩ = Rs + Rp resistor to ground, form a passive high pass filter, that together with the active Sallen Key filter result in a 6th order Butterworth high pass frequency response of the whole circuit. Capacitor Cs, together with the potential divider consisting of the Rs = 1 MΩ and Rp = 68 kΩ resistors ensure that the mains voltage does not cause any damage to the OpAmps A1 and A2. For these values, a 240 $V_{rms}$ 50 Hz mains voltage, results in 217 $mV_{pp}$ at the input terminal of the OpAmp, which is quite safe. That potentiometer has a 24 dB voltage reduction at high frequency. This must be made up using gain in the other part of the circuit.

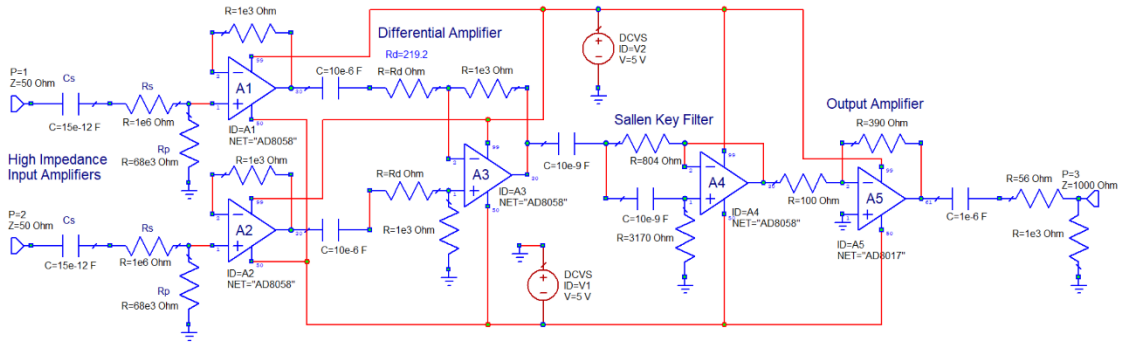



Figure 10.4. PLC Frequency Voltage Sensor.

The AD8057/8058 OpAmp has a 2 pF input capacitance (to ground) and that with the 68 kΩ resistor at the input pin of the OpAmp causes a 1.33 MHz low pass corner frequency, which is far less than the 20 MHz required upper frequency. Reducing the 68 kΩ resistor will increase the high frequency corner frequency, but reduces the output voltage of the circuit and will result in a higher output noise. For accurate differential input capability, it is important that both OpAmps A1 and A2 are matched as close as possible. This requires a Dual OpAmp package to be used, so that both A1 and A2 are well matched and operate at the same temperature. The THS4211 of table 10.1 has a lower input impedance, but it is only available as a single amplifier and will result in a poorer differential voltage accuracy.

## *High Impedance Input stage*

The design options for the high impedance input amplifiers in figure 10.4 will now be considered. A suitable circuit is shown in figure 10.5.

An input impedance > 1 MΩ is required, so that the amplifier does not load the circuit to be measured, Rs = 1 MΩ satisfies that requirement. With a 10V supply voltage. the OpAmp output should be less than $8V_{pp}$ to prevent distortion. Any mains voltages at the OpAmp output should be much less than 0.8 $V_{pp}$ to prevent that to cause intermodulation distortion with the PLC frequency signals to be measured. Figure 10.5 shows a first order passive high pass filter with a 10 kHz cut off frequency, consisting of CS = 15 pF, Rs = 1 MΩ and Rp = 68 kΩ. A 240 V 50 Hz mains voltage results in $3.42V_{pp}$ at the junction of CS and Rs, and 217 $mV_{pp}$ at the OpAmp input. A value of Rp = 250 k Ω results in a mains voltage of 0.8 $V_{pp}$ at the output of A1 or A2 in figure 10.4. Rp must thus be kept < 250 k Ω to prevent mains voltage overload.

Rs and Rp in parallel with the 2 pF input capacitance of the OpAmp form a low pass filter, limiting the high frequency response of the amplifier. A lower value of Rp results

in a higher bandwidth and less intermodulation due to mains voltages but requires more subsequent amplification, resulting in more noise at the output.

To investigate this the frequency response of the amplifier shown in figure 10.5 is plotted for Rs = 1 MΩ and Rp being 15 kΩ, 30 kΩ, 60 kΩ or 120 kΩ. Initially Rg in figure 10.5 is removed, so that the amplifier gain is determined by Rs and Rp only. When Rs = 1 MΩ and Rp = 120 kΩ the attenuation is calculated to be 19.4 dB and the 2 pF OpAmp input capacitance causes an upper corner frequency of 743 kHz. Rp = 60 kΩ causes an attenuation of 24.9 dB and a corner frequency of 1.41 MHz, Rp = 30 kΩ causes an attenuation of 30.7 dB and a corner frequency of 2.73 MHz, while Rp = 15 kΩ causes an attenuation of 36.6 dB and an upper corner frequency of 5.4 MHz. Figure 10.6 shows the corresponding frequency responses using a full Spice simulation of the circuit of figure 10.5. The simulated gains at 100 kHz are about 0.1 dB more than the calculated values and the corner frequencies are close to the calculated values shown above. The AD8058 voltage feedback OpAmp can be changed to an AD8017 current feedback OpAmp, to illustrate the difference between voltage and current OpAmps. For the current feedback OpAmp, Rs = 1 MΩ and Rp = 60 kΩ. Figure 10.6 shows that for this application, the current feedback amplifier has 6 dB less gain than the expected gain, which is shown by the gain of the voltage feedback amplifier. For the AD8017, the +input resistance is 50 kΩ, which is in parallel with Rp and will thus cause a significant gain reduction.

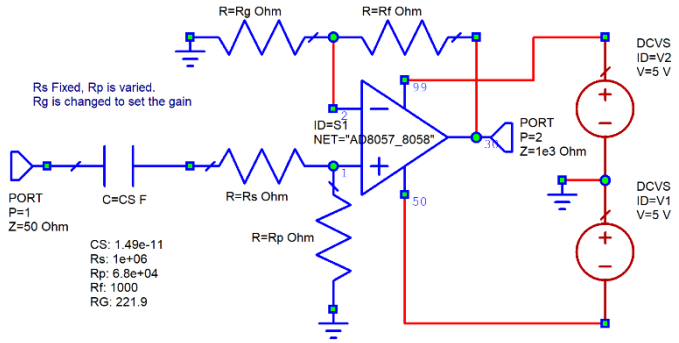



Figure 10.5. High impedance input amplifier.

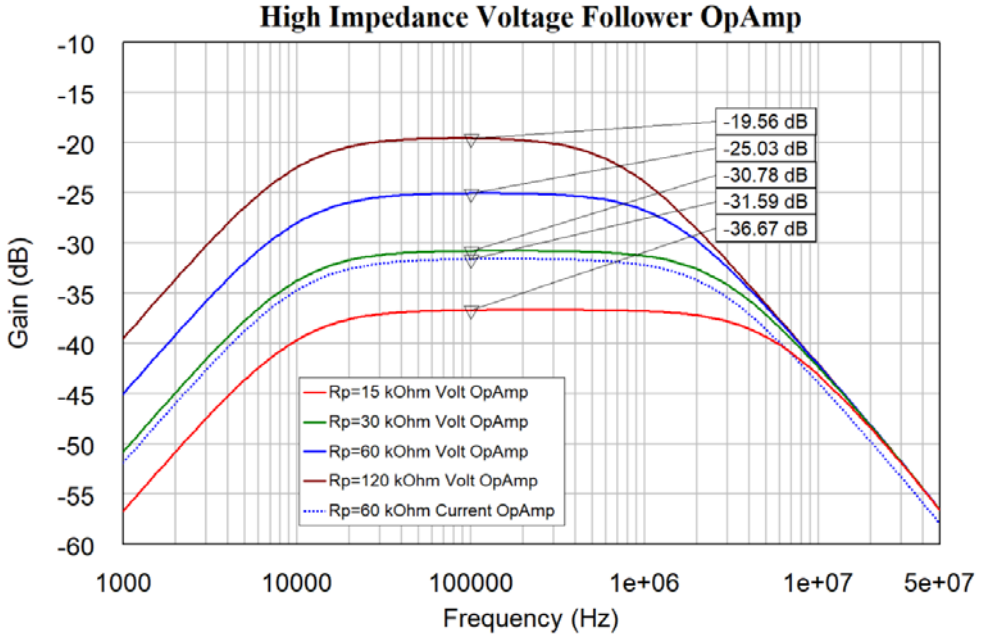



Figure 10.6. High input impedance operational amplifier frequency response.

Extending the frequency of figure 10.6 down to 50 Hz, shows that for Rp = 120 kΩ, at 50Hz, a 65.4 dB attenuation occurs. A 240 V mains voltage will thus cause a 384 $mV_{pp}$ at the output of the OpAmp. Halving the value of Rp, will also reduce the mains voltage at the output of the circuit of figure 10.5 by close to 6 dB. The values for Rp used above are thus unlikely to cause any intermodulation distortion in the OpAmp. The Sallen Key amplifier stage in figure 10.4 will attenuate this mains voltage further.

For a better comparison, the resistor Rg, shown in figure 10.5, is included in the circuit. For the value of Rg is changed, to ensure a -13 dB amplifier gain for all the different values of Rp. The resulting frequency responses are shown in figure 10.7. The corner frequencies shown are in good agreement with the calculated values shown above, except for Rp = 15 kΩ, where the high frequency response is limited by the characteristics of the OpAmp. To demonstrate this, the frequency response obtained from an ideal OpAmp with a 2 pF input capacitance, is included as the magenta curve in figure 10.7.

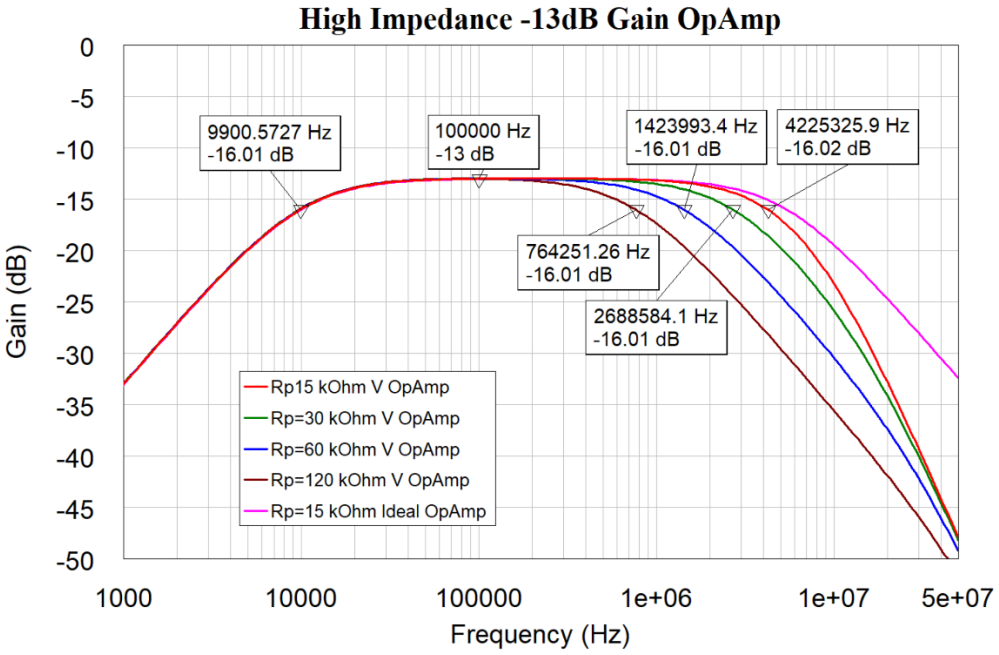



Figure 10.7. Amplifier circuits of figure 10.5 with same gain and Rs2 varied.

For the amplifiers shown in figure 10.7, with a 1 $V_{rms}$ PLC frequency input signal and using a 10 MHz noise bandwidth, the Signal to Noise Ratio (SNR) due to the OpAmps and the thermal noise of the resistors can be calculated as shown later in this chapter. For Rp = 15 kΩ the SNR is 47.4 dB, for Rp = 30 kΩ the SNR is 49.6 dB, for Rp = 60 kΩ the SNR is 51.0 dB and for Rp = 120 kΩ the SNR is 51.9 dB. Figure 10.7 shows that the lowest value of Rp has the widest bandwidth, but the noise calculations show that that also has the lowest SNR. The choice of Rp is thus a compromise.

## *Other OpAmp Stages*

The high input impedance amplifier stage of figure 10.5 involves the most compromises for the design of the circuit in figure 10.4. The final value used for Rp = 68 kΩ, and Rg is not used, resulting in a PLC frequency signal loss of 23.9 dB for the high impedance input stage. It is desired for the circuit of figure 10.4 to be able to handle PLC input signals up to 8 $V_{pp}$. Having a unity gain (0 dB) for the whole circuit satisfies this requirement. The remaining stages will this need to have a gain of 23.9 dB for Rp = 68 kΩ

The output stage of figure 10.4 is a current feedback OpAmp that has an output capability to drive 50 Ω loads. The gain of 3.9 for that amplifier is chosen to be close to 12 dB, being half the total gain required. Having a 56 Ω series resistor is used to prevent damage to the amplifier if the output is accidentally shorted. That also provides a good match when driving a 50 Ω load. A 1 kΩ resistor to ground is used to provide a DC path to ground for any output connection. The output amplifier gain of 3.9, will ensure that any clipping will occur in this amplifier, rather than the differential or the Sallen Key amplifier stages.

The 10 kHz high pass filter used to remove the mains voltages, consists of a first order high pass filter at the high input impedance amplifiers A1 and A2, together with a second order Sallen-Key high Pass filter for A4, to result in a third order Butterworth high pass frequency response. The required resistor values are 804 Ω and 3.17 kΩ, together with 10 nF capacitors. Those resistor values are more suitable for voltage feedback amplifiers. However, the impedance levels can be changed so that the feedback resistor, matches the required value for the current feedback amplifiers to be used. The AD8058 is a relatively low cost Dual OpAmp, one package can be used for both the differential amplifier and the Sallen-Key high Pass filter. The decision on whether to use voltage or current feedback amplifiers is thus mainly determined by cost and PCB area used, as well as the limitations outlined above and in [1-3].

The gain for the differential amplifier A3 is selected to produce the required Gain = 1 for the whole circuit, by changing resistors Rd for the differential amplifier in figure 10.4. Figure 10.8 shows the resulting frequency responses, for Rp = 15, 30, 60 and 120 Ω. The frequency response of an ideal 3rd order Butterworth high pass filter with a 10 kHz cut off frequency. The Voltage Sensor circuits match that response well below 200 kHz. Extending the frequency range down to 50Hz, shows that the whole circuit has 138 dB attenuation at 50 Hz, so that a 240$V_{rms}$ mains frequency input signal causes 30 μ$V_{rms}$ at the Voltage Sensor output.

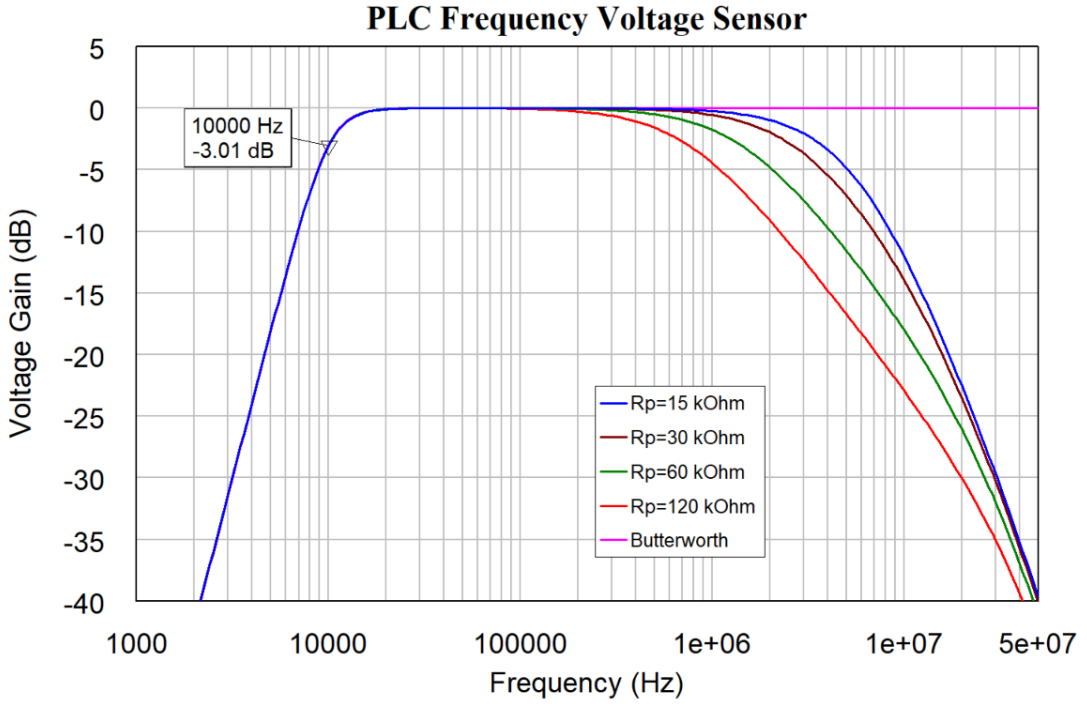



Figure 10.8. Frequency response of the whole circuit of figure 10.4.

## *Hardware Realisation*

These design simulations are only part of the story. The circuit of figure 10.5 with Rg removed, Rs = 1 MΩ and Rp = 100 Ωk, was used for an early version of this amplifier. The circuit used AD8045 OpAmps, which are single OpAmps with a 1.3 pF input capacitance. Figure 10.9 shows the measured frequency response of this circuit when different size surface-mount 1 MΩ, 1% tolerance, resistors are used for Rs. The SMD resistors have a very small capacitance and inductance associated with them and that changes the high frequency response. These effects can only be measured using actual hardware. Since the 3216 Metric SMD resistors have a good frequency response and a 200V rating, they were used in the hardware realisation of figure 10.11.

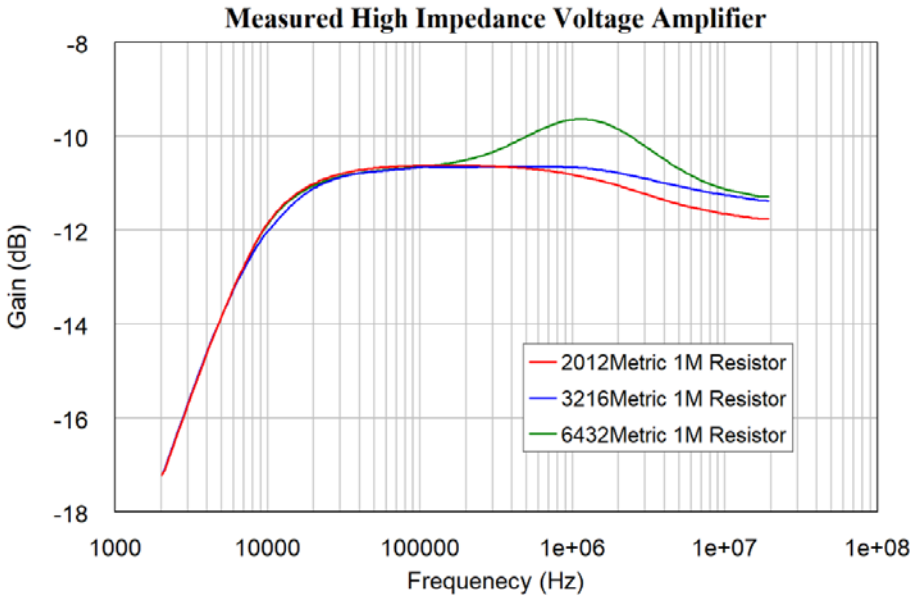



Figure 10.9. High input impedance OpAmp measured frequency response.

When building the full circuit of figure 10.4, it was found that the common mode input specification for the hardware, required a very good gain and phase match of OpAmps A1 and A2. This can only be obtained using Dual OpAmps. As a result, the AD8058, Dual OpAmp shown in figure 10.4 were used.

As part of this hardware, another amplifier was used to inject a PLC frequency onto the power line. The Voltage Sensor of figure 10.4 was then used to measure that PLC frequency voltage on that power line. Since there is some electromagnetic coupling between the PLC frequency signal generator and the Voltage Sensor, the attenuation due to Rp should be minimised, by keeping Rp as large as possible. For the hardware of figure 10.4, a satisfactory frequency response, noise performance and isolation between the different parts of the equipment was obtained using Rp = 68 kΩ.

This example shows that a high frequency OpAmp design involves many compromises to ensure that the components used and the OpAmp characteristics cause the least degradation in system noise and bandwidth performance.

Figure 10.10 shows the measured and simulated frequency response of the whole circuit. Even though both A1 and A2 are in the same package, the layout is made as symmetrical as possible and the matched resistors from the same batches are used, the frequency response of the +ve input (A1) and the –ve input (A2) are different. A prototype made with single AD8045 amplifiers had bigger differences between the inputs.

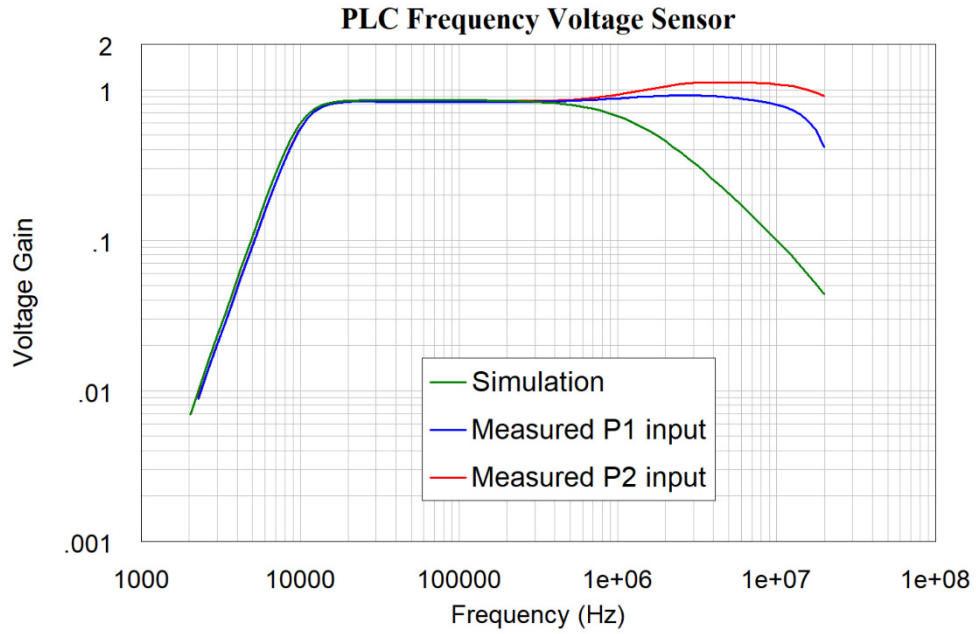



Figure 10.10. Measured and simulated frequency response of circuit of figure 10.4.

Figure 10.11 shows the final prototype hardware for the high impedance Voltage Sensor of figure 10.4. As part of the measurements, it was found that an AD8039 Dual OpAmp has a slightly better common mode performance, i.e. less difference between amplifier A1 and A2 in figure 10.4, than the same circuit with an AD8058 Dual OpAmp. Unfortunately, the Spice model for the AD8038/8039 OpAmp is based on the single AD8038, which has a "disable" input, and cannot be imported directly into Cadence AWR DE. The specified performance of the AD8039 and AD8057 OpAmps is very similar, however the quiescent current for the Dual AD8039 is 2 mA compared to 14 mA for the Dual AD5058, so that the hardware can run longer from a 12V battery.

The "*tuned*" value of 219.2 Ω for unity gain was changed to 330 Ω to prevent overloads due to the slight gain at higher frequencies as shown in figure 10.10. Figure 10.11 shows the resulting hardware. A simple heatsink is used to conduct the heat from the AD 8017 output amplifier to the PCB and the instrument case.

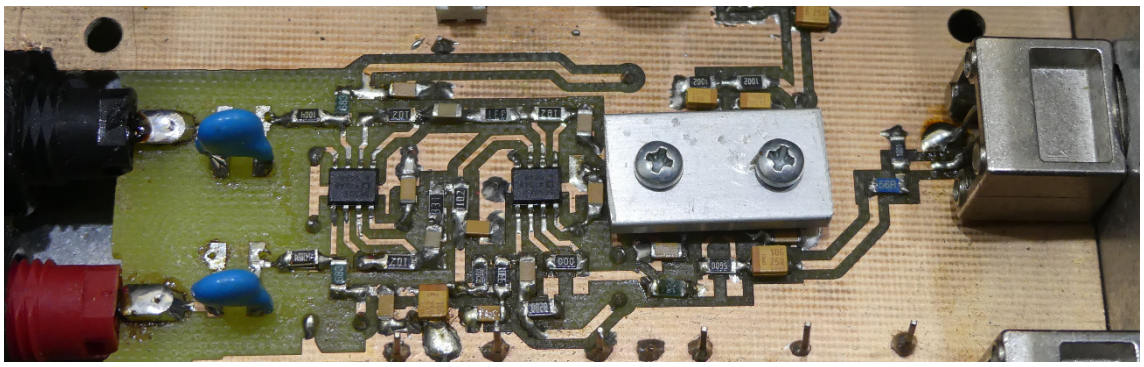


Figure 10.11. Hardware of circuit of figure 10.4.

## Amplifier protection

The OpAmps A1 and A2 of figure 10.4 operate from a ±5 V supply. The maximum voltage at the input can thus be 10 V. Any larger voltages can damage the OpAmps. Since

the potentiometer has a 23.9 dB attenuation, that corresponds to an input voltage of 78 $V_p$. If needed the OpAmps can be protected using RF Schottky barrier diodes connected between the input and the power supplies, as shown in figure 10.12. The input voltage should not exceed the supply voltages (±5 V). The MMSD301T1, RF Schottky barrier diodes used in the figure 10.12, have a maximum forward voltage of 0.6V at 10 mA. Thus 5.6 V at the junction of *Rs* and *Rsd*, will result in the diode conducting and ensuring the voltage there is clipped. Using the series resistor *Rsd* = 10 kΩ, results in the maximum voltage at the OpAmp input then being 4.88 V, so that the OpAmp input voltage can never exceed the supply voltage. The insertion of the resistor Rsd, requires Rd to be changed from 219.2 Ω to 217.2 Ω in order for the whole amplifier to have a 0dB gain.

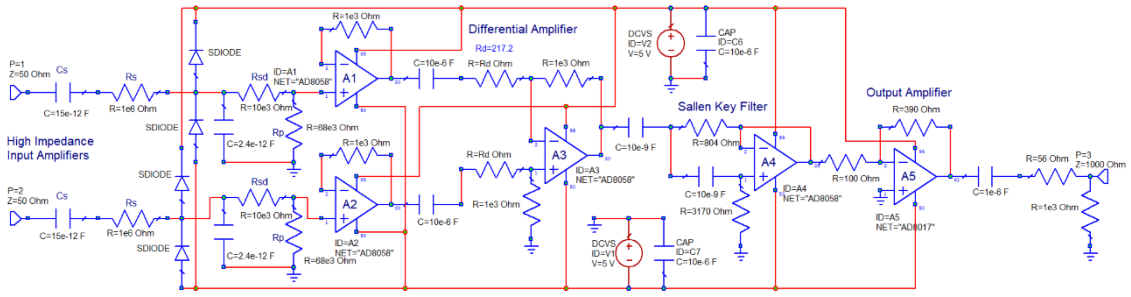



Figure 10.12. Voltage sensor circuit with input protection diodes.

The, MMSD301T1 [7] diode has a 200 mA current rating, a 30 V reverse voltage rating and a 1.2 pF diode capacitance at $V_r$ = 5 V. That capacitance is not properly included in the linear AWR DE simulation of figure 10.13, so that has to be added as a separate capacitance in figure 10.12. Figure 10.13 shows a comparison in the frequency response of the amplifier of figure 10.4 without the protection diodes and the amplifier of figure 10.12 which includes the protection diodes. The difference in gain is 6 dB at 2 MHz.

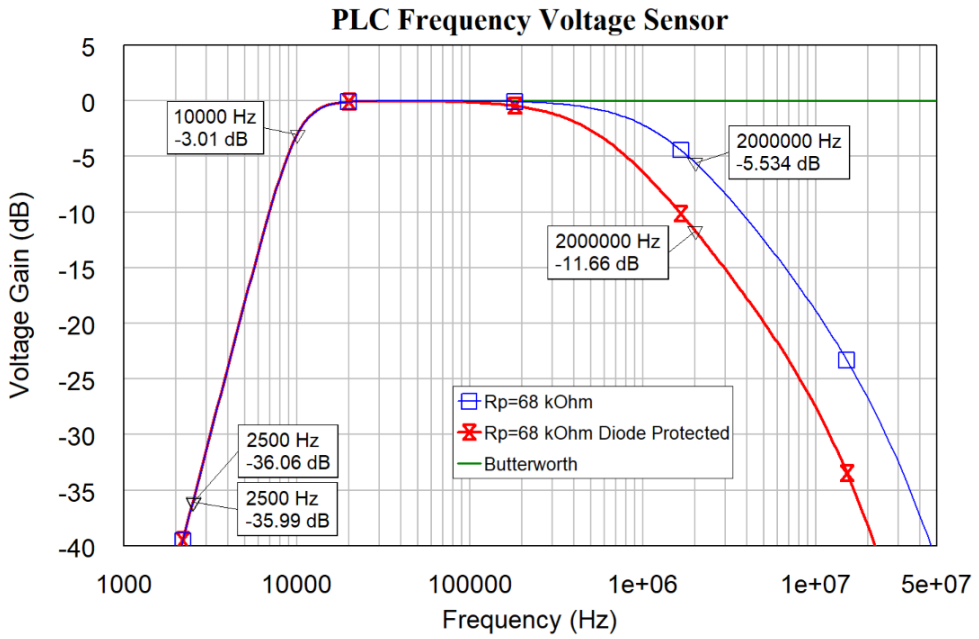



Figure 10.13. Comparison of amplifiers of figure 10.4 and 10.12.

Figure 10.13 shows that the input protection significantly affects the high frequency performance. For most RF amplifiers input protection is difficult. The cost of protection

needs to be balanced with the probability of the input being damaged and any reduction in performance caused by the inclusion of the protection devices. For many applications, the best option may be to design the front end, to enable easy replacement of the front-end devices if they are damaged by input surges.

## Low Noise Designs using Operational Amplifiers

The noise voltage associated with a resistor is;

$$E_{NR} = \sqrt{4kTBR} \qquad \text{Eqn. 10.12}$$

Where:

K = Boltzman's constant 1.38064852 x $10^{-23}$ Joules/Kelvin
T = Absolute temperature Kelvin
B = Bandwidth in Hz
R = Resistance in Ω

In a circuit each resistor is then associated with its own noise source which has a random noise voltage of $E_{NR}$. In addition the operational amplifier produces noise which can most accurately be represented as voltage ($e_{ni}$) and current noise sources ($i_{ni+}$ and $i_{ni-}$) at the inputs, as shown in figure 10.14.

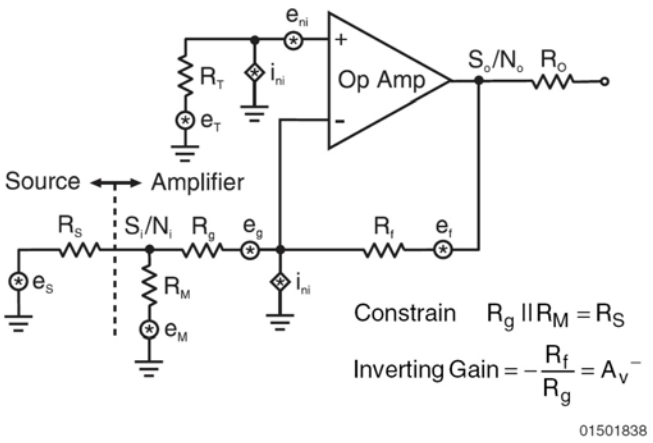



Figure 10.14 Noise sources in an operational amplifier configuration (Fig 29 of [4])

Table 10.2. Low Noise RF Operational Amplifiers.

| Manuf. | Part | Type | Vs | nV/√Hz | pA/√Hz | 1/f kHz | BW MHz |
|---|---|---|---|---|---|---|---|
| TI | LMH6629 | VFB | 5 | 0.69 | 2.6 | 5 | 900 |
| TI | OPA847 | VFB | 5 | 0.85 | 2.7 | 1 | 3500 |
| TI | THS4022 | VFB | ±5 to ±15 | 1.5 | 2 | 1.5 | 350 |
| Anal Dev | AD8000 | CFB | 4.5 to 12 | 4.3 | 26- 3.4+ | 0.3 | 1500 |
| Anal Dev | AD8099 | VFB | 5 to 12 | 0.95 | 2.6 | 10 | 510 |
| Anal Dev | ADA4898 | VFB | ±5 to ±16 | 0.9 | 2.4 | 0.02 | 65 |

The values for $e_{ni}$, $i_{ni+}$ and $i_{ni-}$ are normally obtained from manufacturer's data sheets. Table 10.2 shows the noise performance of some low noise amplifiers from different

manufacturers. The noise of operational amplifiers will rise at low frequency, as shown in figures 10.15, 10.16, 10.19 and 10.20, and is inversely proportional to frequency at low frequencies, due to flicker noise or 1/f noise. The corner frequency of that 1/f noise may be important in a design. For example if a microphone amplifier is required, the noise performance at <1 kHz is important and the ADA4898 has a better noise performance at those frequencies than the LMH6629, which has a better noise performance at higher frequencies.

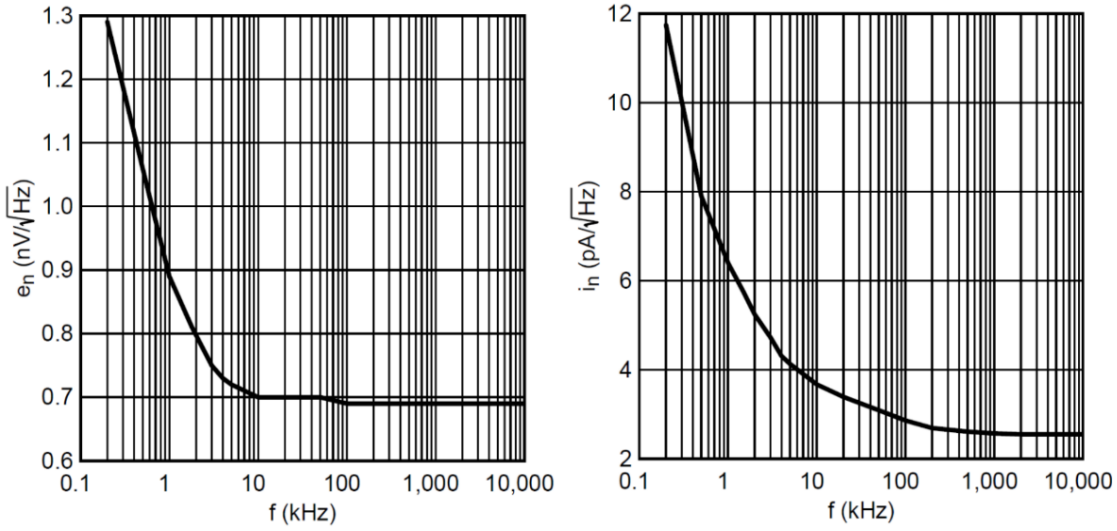



Figure 10.15. Noise of LMH6629 versus frequency [8]

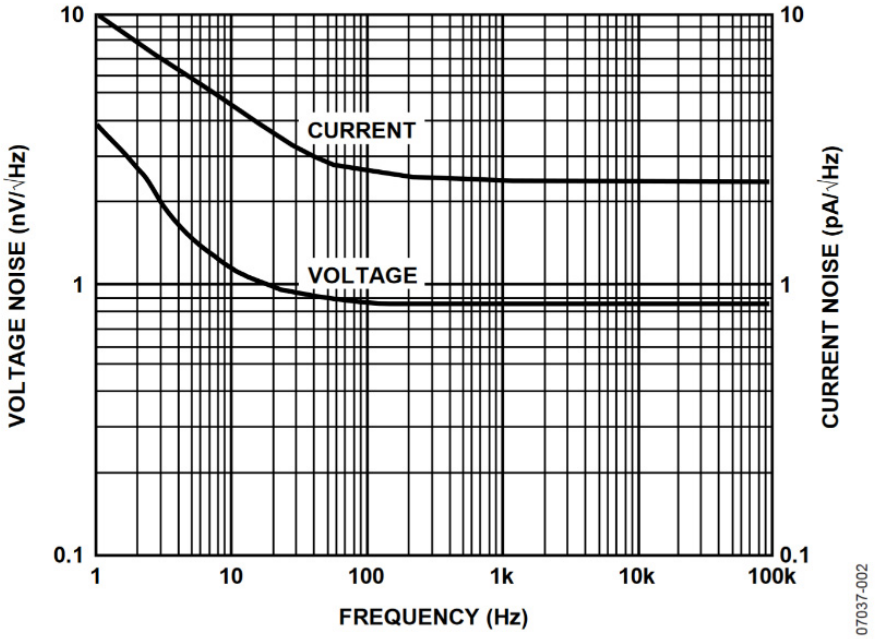



Figure 10.16. Noise and Distortion of ADA4898 [9]

Since the noise sources in the circuit are un-correlated, the total noise from the amplifier is obtained by adding the noise powers of those sources.

The amplifier configuration and the value of impedances used significantly affect the resulting noise performance of an amplifier as shown in the following example.

## *Example 10.2: Amplifier Design for Noise Performance.*

A microphone has a source impedance $R_s$ = 600 Ω and requires a load resistance larger than 1 kΩ for the microphone to operate correctly. The normal output from the microphone is 1mV. An amplifier with a voltage gain of close to 1000 is required. Figure 10.17 shows the circuit diagram of the non-inverting amplifier circuit. In practice, coupling capacitors are used at the input and output, to ensure that the amplifier output clips symmetrically and that no DC offset voltage occurs at the output. Rg should be such that it is much larger than the resistance of tracks used in the PCB or the resistance between the grounded side of Rg and the common ground point of the amplifier. Rg should be small to minimise the thermal noise of the resistor, which is amplified by the amplifier gain.

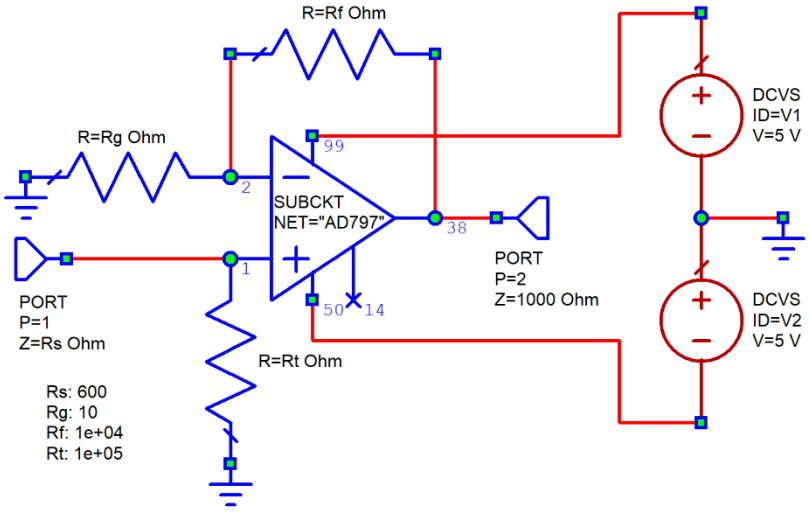



Figure 10.17. Non-inverting amplifier.

For the non-inverting amplifier, the noise power at the output of the OpAmp due to each component is evaluated using equations 10.13 to 10.20, [4, 10, 11]:

OpAmp noise voltage $$Pe_n = {e_n}^2 B \left(\frac{R_f+R_g}{R_g}\right)^2$$ Eqn. 10.13

OpAmp noise current +in $$Pi_{np} = (i_{np}\frac{R_s R_t}{R_s+R_t})^2 B \left(\frac{R_f+R_g}{R_g}\right)^2$$ Eqn. 10.14

OpAmp noise current -in $$Pi_{nn} = (i_{nn}\frac{R_g R_f}{R_g+R_f})^2 B \left(\frac{R_f}{R_g}\right)^2$$ Eqn. 10.15

Resistor *Rs* noise $$PR_s = 4kTBR_s \left(\frac{R_t}{R_s+R_t}\frac{R_f+R_g}{R_g}\right)^2$$ Eqn. 10.16

Resistor *Rt* noise $$PR_t = 4kTBR_t \left(\frac{R_s}{R_s+R_t}\frac{R_f+R_g}{R_g}\right)^2$$ Eqn. 10.17

Resistor *Rg* noise $$PR_g = 4kTBR_g \left(\frac{R_f}{R_g}\right)^2$$ Eqn. 10.18

Resistor *Rf* noise $$PR_f = 4kTBR_f$$ Eqn. 10.19

OpAmp Voltage Gain $$Gain_v = \frac{R_s}{R_s+R_t}\frac{R_f+R_g}{R_g}$$ Eqn. 10.20

For the non-inverting amplifier, Rg = 10 Ω is a good compromise. Rf sets the gain and Rf = 10 kΩ results in a gain of G = (Rf+ Rg)/ Rg = 1001. Some bias current needs to flow into the non-inverting OpAmp input, so that a resistor Rt is required. Rt should be large enough, not to load the input and small enough not to cause any DC offset voltage at the output due to the OpAmp bias current. Rt should be > 1 kΩ to prevent loading the microphone and small enough to ensure that the input bias current does not cause an offset voltage. The source impedance Rs and Rt form a potentiometer, which reduces the input signal. Rt = 100 kΩ results in a 0.6% voltage drop across this potentiometer and a total amplifier gain of 995, which is close enough to the desired gain. Equation 10.17 shows that the value of Rt has little effect on the amplifier noise output since Rs/(Rs+Rt) is very small.

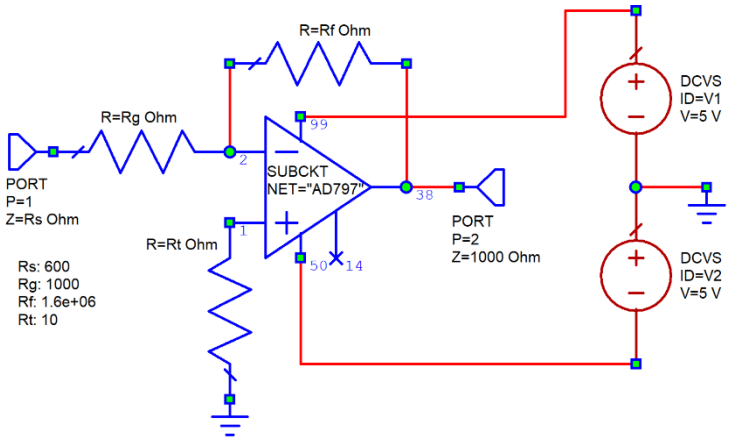



Figure 10.18. Inverting amplifier.

For the inverting amplifier, a minimum value of Rg = 1 kΩ, is required to prevent loading the microphone. Since Rs = 600 Ω and Rg = 1kΩ, for a gain G = Rf/ (Rs+Rg) = 1000, a value of Rf = 1.6 MΩ is required. Resistor Rt must now be small to not affect the noise at the output. Rt = 10 Ω is suitable. Figure 10.18 shows the resulting circuit. Equations 10.19 and 10.21 to 10.27 determine the noise contributions of each of the noise sources in the inverting amplifier. For the inverting amplifier, the noise power at the output of the OpAmp due to each component is as follows:

OpAmp noise voltage $$Pe_n = {e_n}^2 B \left(\frac{R_f+R_g+R_s}{R_g}\right)^2$$ Eqn. 10.21

OpAmp noise current +in $$Pi_{np} = (i_{np}R_t)^2 B \left(\frac{R_f+R_g+R_s}{R_g}\right)^2$$ Eqn. 10.22

OpAmp noise current -in $$Pi_{nn} = (i_{nn}\frac{(R_g+R_s)R_f}{R_g+R_s+R_f})^2 B \left(\frac{R_f}{R_g}\right)^2$$ Eqn. 10.23

Resistor $R_s$ noise $$PR_s = 4kTBR_s \left(\frac{R_f}{R_g+R_s}\right)^2$$ Eqn. 10.24

Resistor $R_t$ noise $$PR_t = 4kTBR_t \left(\frac{R_f+R_g+R_s}{R_g+R_s}\right)^2$$ Eqn. 10.25

Resistor $R_g$ noise $$PR_g = 4kTBR_g \left(\frac{R_f}{R_g+R_s}\right)^2$$ Eqn. 10.26

Resistor $R_f$ noise $$PR_f = 4kTBR_f$$ Eqn. 10.19

OpAmp Voltage Gain $$Gain_v = -\frac{R_f}{R_g+R_s}$$ Eqn. 10.27

These equations are included in the project files for figures 10.17 and 10.18. This allows the noise contribution of each noise source to be determined and component values to be tuned to minimise the noise, whilst maintaining practical component values. To compare the noise performance, these equations are also entered in a spreadsheet, the results of which are presented in table 3. For this example T = 290 Kelvin and the bandwidth B = 20 kHz. For Voltage feedback amplifiers, the +ve input noise current ($i_{np}$) is normally the same as the –ve input noise current ($i_{nn}$), however for current feedback amplifiers, they are normally different since the +ve and –ve input circuit architectures are different. Table 10.2 shows that for the AD8000, the –ve input current noise is 26 pA/√Hz and the +ve input current noise is 3.4 pA/√Hz. In figure 10.14, the +ve and –ve input current noise is assumed to be the same, ($i_{ni}$).

Table 10.3. Noise for inverting and non-inverting amplifier configurations.

| Operational amplifier Noise calculation | | | | | |
|---|---|---|---|---|---|
| Temperature | 290 | | | | |
| 4kT | 1.60E-20 | | | | |
| Bandwidth (Hz) | 20000 | | | | |
| Rs | Source resistance | | | | |
| Rt | Resistance to ground at non-inverting input | | | | |
| Rg | Input resistance series with inverting input | | | | |
| Rf | Feedback resistor | | | | |

| Op Amp | AD 797 | | | |
|---|---|---|---|---|
| | Non Inverting Op Amp | | Inverting Amp | |
| | Value | Output Noise | Value | Output Noise |
| en nV | 0.9 | 1.623E-08 | 0.9 | 1.620E-08 |
| in+ pA | 2.0 | 2.851E-08 | 2.0 | 8.000E-12 |
| in- pA | 2.0 | 8.000E-12 | 2.0 | 2.044E-07 |
| Rs | 600 | 1.903E-07 | 600 | 1.922E-07 |
| Rt | 1.00E+05 | 1.142E-09 | 1.00E+01 | 3.210E-09 |
| Rg | 10 | 3.203E-09 | 1.00E+03 | 3.203E-07 |
| Rf | 10000 | 3.203E-12 | 1.60E+06 | 5.125E-10 |
| Gain (FB) | 995 | | 1000 | |
| RInp (Rsn//Rtn) | 596.4 | | | |
| Ripp (Rgn//Rfn) | 9.99 | | 1.598E+03 | |
| Total Power/Hz | | 1.20E-11 | | 3.68E-11 |
| Total Noise Power | | 2.39E-07 | | 7.37E-07 |
| Noise Voltage mV | | 4.89E-01 | | 8.58E-01 |
| Signal In Out mV | 1 | 995 | 1 | 1000 |
| SNR | | 66.17 | | 61.33 |
| Noise figure dB | | 1.00 | | 5.84 |
| Noise figure | | 1.26 | | 3.83 |

The ADA4898 includes a power down switch, which causes simulation errors in Cadence AWR DE. So for the calculations in table 10.3 and simulation in figure 10.19, an AD 797 OpAmp is used, since it is suitable and its Spice model include input voltage and current

noise models. The Analog Devices AD797.cir can be directly imported as a netlist into Cadence AWR DE. At 1 kHz, that amplifier has an input noise voltage of 0.9 nV/√Hz and an input current noise of 2.0 pA/√Hz. Since this is a voltage feedback amplifier, this input current noise value applies to both the +ve and the –ve input terminals.

Table 10.3 shows that for the non-inverting amplifier, the dominant noise contribution is from the microphone source resistance Rs, and the second largest is due to the input current noise at the +ve input terminal. That current, flows through Rs in parallel with Rt and the resulting noise is thus directly related to Rs. All the other noise contributions are more than 10 times smaller than the noise power due to Rs. That is close to the best that can be achieved.

For the inverting amplifier, the noise caused by the 1 kΩ resistor Rg is the largest noise contributor. That resistor value is the lowest that can be used to load the microphone output. The input current noise at the -ve input terminal is the second largest noise contribution and this is mainly due to the value of Rf, which is limited by the gain required. The third largest noise contribution is due to Rs. The noise produced by Rs is thus not the dominant noise contribution. A non-inverting amplifier configuration is thus always preferred for low noise designs as it has a significantly higher signal to noise ratio and much lower noise figure than an inverting amplifier configuration. These calculations are for a microphone amplifier at audio frequencies, however the same principles apply for low noise operational amplifiers used in say MRI applications.

Figure 10.19 shows the Spice simulation of the amplifier. The 1.00 dB noise figure in table 3 for the non-inverting amplifier agrees closely with the 1.009 dB noise figure obtained for the simulation in figure 10.19. From table 10.2, using an ADA8099, OPA847 or LMH6620, OpAmp will achieve a much higher gain, lower bandwidth and similar noise performance to the MMIC and transistor amplifier design in figures 8.7, 8.8, 8.13, 8.19 and 8.20, so that low noise OpAmps can be used for receiver front end designs provided the required frequency is in the operational frequency range of the OpAmp.

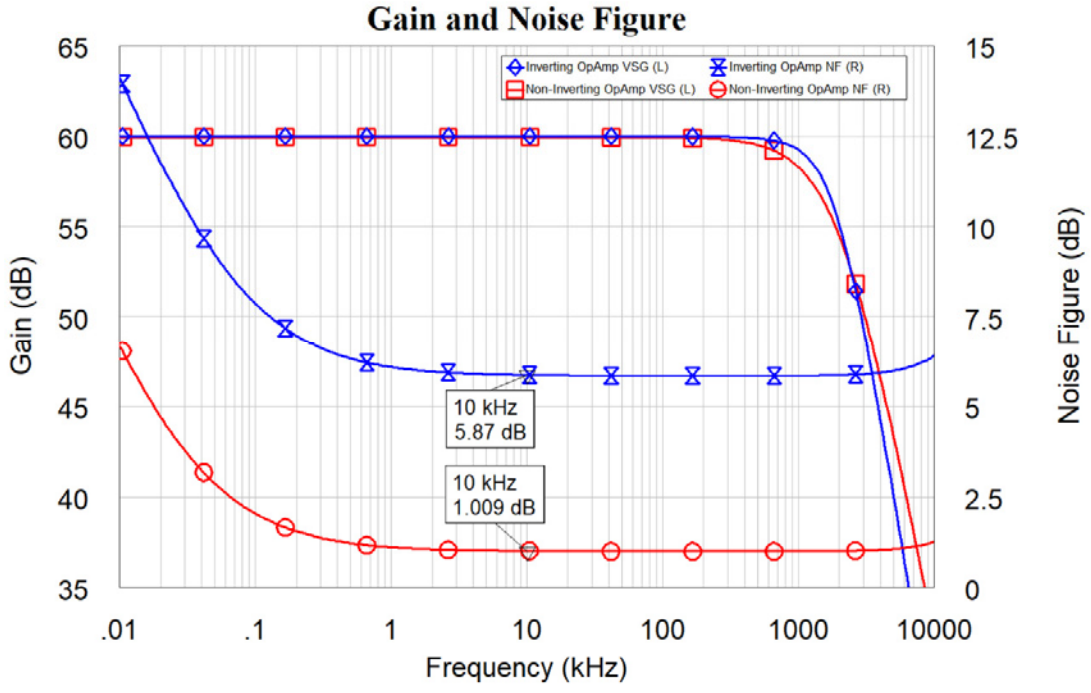



Figure 10.19. Gain and noise figure of amplifiers of fig. 10.17 and 10.18.

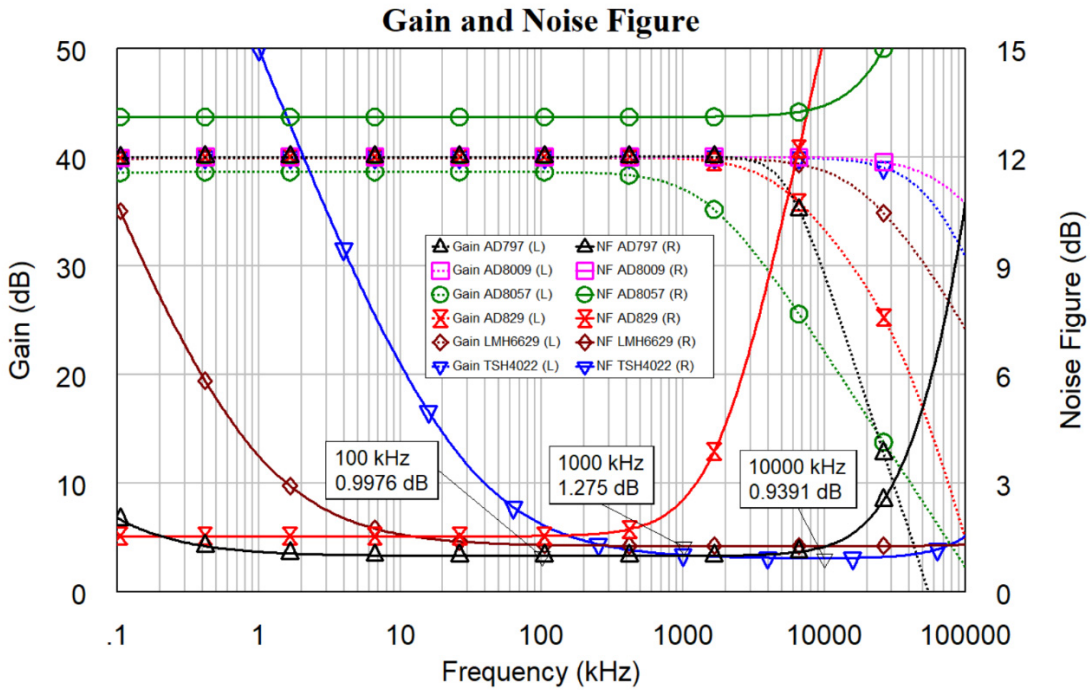



Figure 10.20. Gain and noise figure of different OpAmps.

Figure 10.20 shows the gain and noise figure performance for several high frequency low noise OpAmps from different manufacturers. The circuit used are the same as figure 10.18, but with *Rg* =10 Ω and *Rf* =1 kΩ, resulting in a 40 dB voltage gain, so that 3dB bandwidths in excess of 30 MHz can be obtained. In addition, the supply voltages are changed to match those used for the test circuits in the OpAmp data sheets. Figure 10.20 shows that noise figures of less than 1.5 dB can be obtained from 1 kHz to 100 MHz. In many cases, the Spice files will import directly. In some cases, the file extensions need to be renamed to *.cir* to allow Cadence AWR DE to convert the PSpice files. Several high frequency low noise amplifiers, like the AD8099, have power-down pins, which at this stage cause problems in importing the PSpice files into AWR DE.

## Oscillator using Operational Amplifiers

Since OpAmps can be used to frequencies above 100 MHz, OpAmps can be used for oscillators. Chapter 6 describes the design procedure for oscillators. A Colpitts resonator is slightly cheaper since only one inductor is used. In both the Colpitts or Hartley oscillators, one capacitor in the resonator can be replaced with a varactor diode, to produce a Voltage Controlled Oscillator (VCO). The correct DC biasing on the OpAmp pins is required and it is desirable not to have a short circuit path at DC between the output and ground, since any DC offset on the output will then cause current limiting or failure in the OpAmp.

To gain some understanding of the fundamental limitations, a linear OpAmp model (OPAMP) is used and output limiting is applied by using back to back diodes to clip the output. A Spice model SDIODE, which includes noise, is used. Figure 10.21 shows the circuits for two 10 MHz oscillators using this linear OpAmp model. A Hartley oscillator is shown on the left and a Colpitts oscillator is shown on the right. The *OSCTEST* element in the left circuit is used for the linear oscillator analysis to verify that the correct gain and phase shift occurs. The *OSCAPROBE* element in right circuit is used for the non-

linear oscillator analysis to determine the oscillating frequency, output spectrum, phase noise, and waveforms, as described in chapter 6.

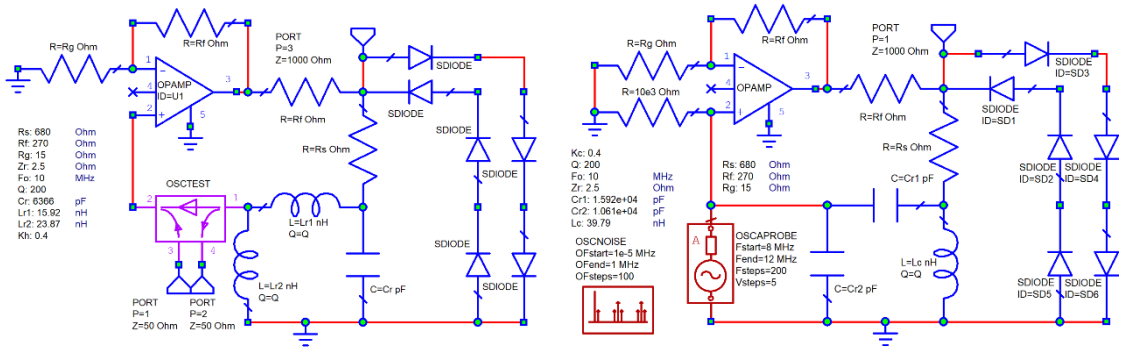



Figure 10.21. Circuits for 10 MHz oscillator, with ideal OpAmps.

The changes in performance can be investigated by changing the circuit gain (Rg), the resonator impedance (Zr), the voltage divider ratio Kh = Lr1/(Lr1 + Lr2) and the current limiting resistor (Rs). In some cases, the best performance is obtained with values that are limited by other constraints. For example, reducing the resonator impedance Zr, reduces the phase noise. Reducing Kh also reduces the phase noise. However, it is difficult to make inductors reliably when Lr1 ≤ 16 nH. Increasing the gain by reducing Rg, increases the output voltage and generally decreases the phase noise. In a practical OpAmp, that also decreases the bandwidth and may prevent oscillation. Optimising Zr, Kh, Rg and Rs to minimise the phase noise, while keeping Lr1 ≤ 16 nH, results in Zr = 2.5, Kh = 0.4, Rg = 15 Ω, Rs = 680 Ω. The same values, Zr = 2.5, Kc = Cr2/(Cr1 + Cr2) = 0.4, Rg = 15 Ω and Rs = 680 Ω are also used for the Colpitts oscillator. The circuit values shown in figure 10.21 correspond to these values. Figure 10.22 shows the linear Hartley oscillator OSCTEST loop gain versus frequency. The rate of change of the imaginary part of the gain is much higher than that shown in figure 6.9. This should result in a lower phase noise for the OpAmp based oscillators, but they are limited to lower frequencies.

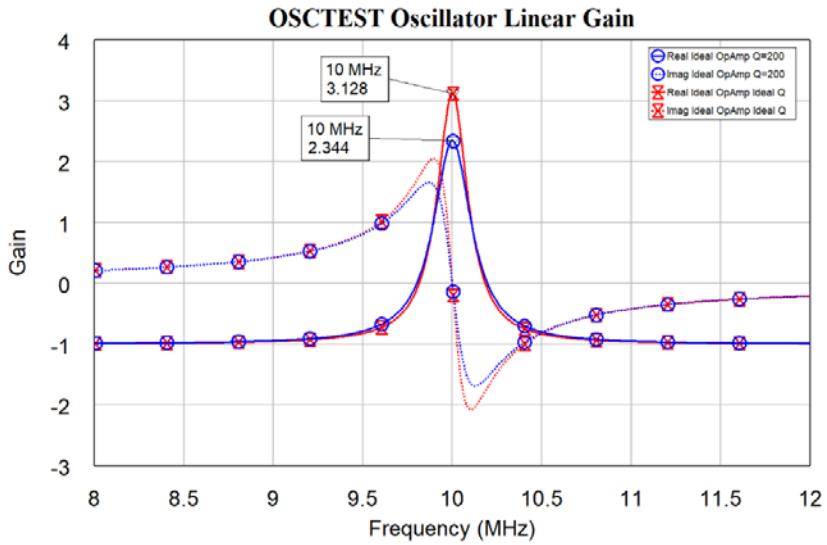



Figure 10.22. Linear 10 MHz OpAmp oscillator analysis.

The phase noise produced by the OpAmp oscillators depends on the diode models used. Using the MMSD301T1 RF Schottky diodes, results in a low phase noise and ensures that the diodes do not limit the phase noise. Using 3 diodes in series results in a similar

output voltage to that obtained from the LMH6629, so that a fair comparison to be made. Figure 10.23 shows the phase noise for the ideal OpAmp oscillators of figure 10.21, and the Spice simulations of the LMH6629 OpAmp oscillators, using the circuit values shown in figure 10.21.

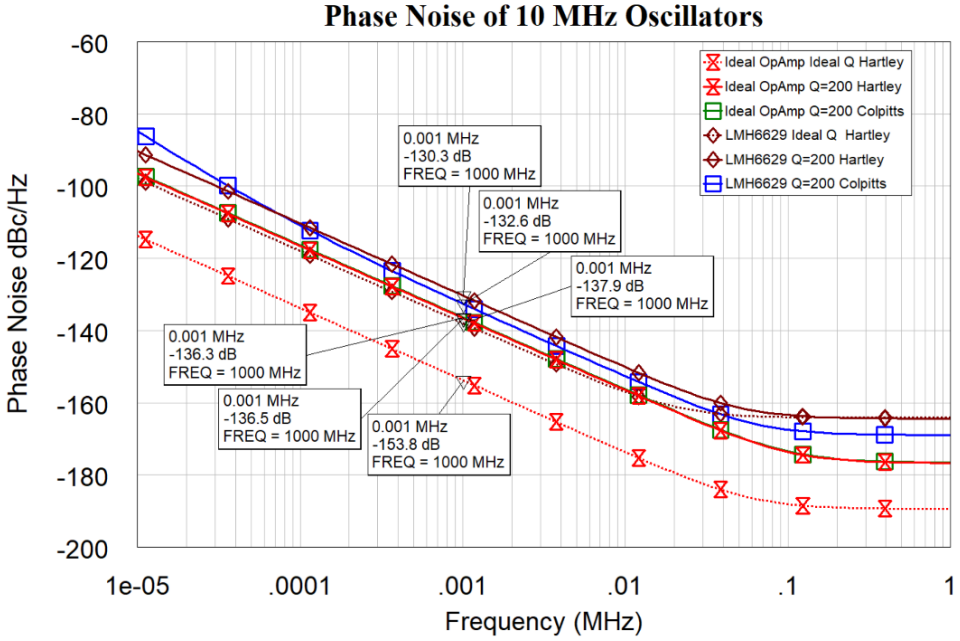



Figure 10.23. Phase noise for 10 MHz Hartley and Colpitts oscillators using OpAmps.

For ideal OpAmps, the Hartley oscillator with an ideal resonator (Q = 10000) has a phase noise of -153.8 dB. The same oscillator with a Q = 200 has a phase noise of -136.5 dB, and the corresponding Colpitts oscillator has a phase noise of -136.3 dB. For the LMH6629 OpAmp circuits with a Q = 200, the phase noise of the Hartley oscillator is -130.3 dB and the Colpitts oscillator is -132.6 dB. There is thus little difference between the phase noise of a Hartley and Colpitts oscillator.

For the ideal OpAmps, there is a 153.8 - 136.5 = 17.2 dB difference between the phase noise for the ideal resonator and the resonator with a Q = 200. For the LMH6629 oscillator the corresponding difference is 137.9 – 130.3 = 7.6 dB. The phase noise is thus dominated by the resonator Q.

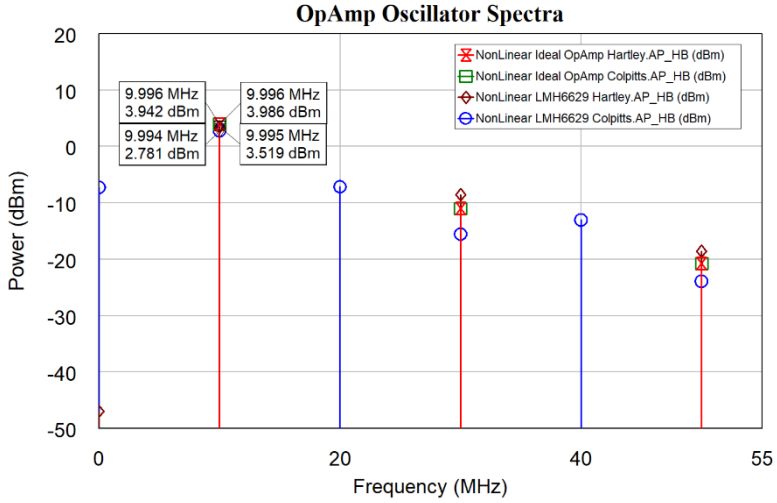



Figure 10.24. Spectra for 10 MHz Hartley and Colpitts oscillators using OpAmps.

Figure 10.24 shows the spectra for the Hartley and Colpitts oscillators with ideal OpAmps and LMH6629 OpAmps and using the same component values as shown in figure 10.19. For the ideal OpAmp and the LMH6629 OpAmp circuits, the fundamental output is nearly the same for the respective Colpitts and Hartley oscillators. The Hartley oscillators have a low even harmonic distortion. Figure 10.25 shows the corresponding waveforms. Using 3 diodes in series, results in a similar output from the ideal OpAmps compared with the LMH6629.

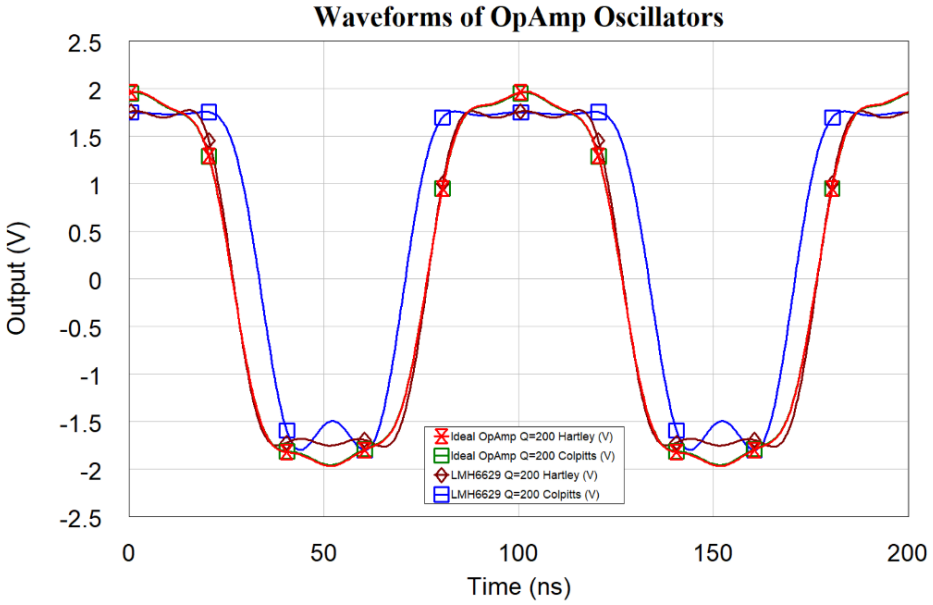



Figure 10.25. Waveforms of Hartley and Colpitts oscillators.

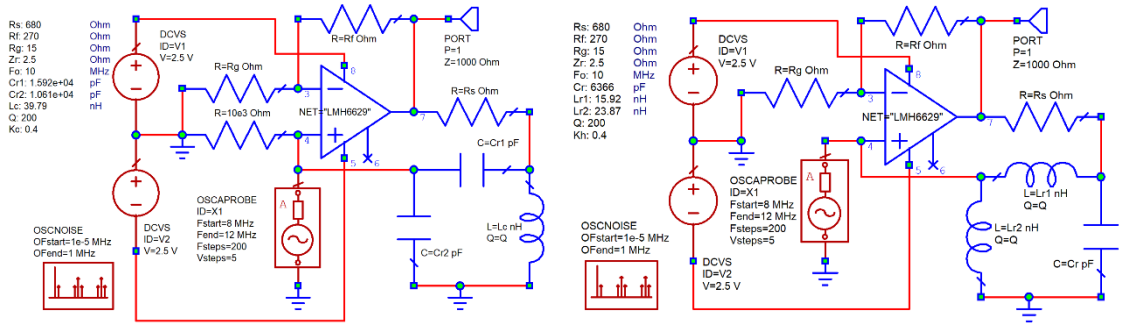



Figure 10.26. Circuit for 10 MHz oscillators, using LMH6629 OpAmp.

To compare the phase noise from oscillators using different OpAmps, the circuits of figure 10.26 are used, with the same component values but different OpAmps and supply voltages to match those required by the OpAmp. The circuits are the similar to figure 10.21. The resistor Rs prevents the low output impedance of the OpAmp from loading the resonator. For comparison, the values of Zr , Kh , Rg and Rs, are kept the same as for figures 10.21 to 10.26. Figure 10.24 shows the phase noise of these oscillators and as a reference the LMH6629 Hartley oscillator shown in figure 10.23 is again included. The AD829 and TSH4022 OpAmps are capable of operating at ±15 V. That then requires the secondary parameter VpMax of OSCAPROBE to be set to 15 V for the simulation to converge. The phase noise of the AD829 does not change much as the supply voltage changes. The TSH4022 gives a much lower phase noise at a ±5 V supply. As a result in figure 10.27, a ±5 V supply has been used for both the TSH4022 and AD829.

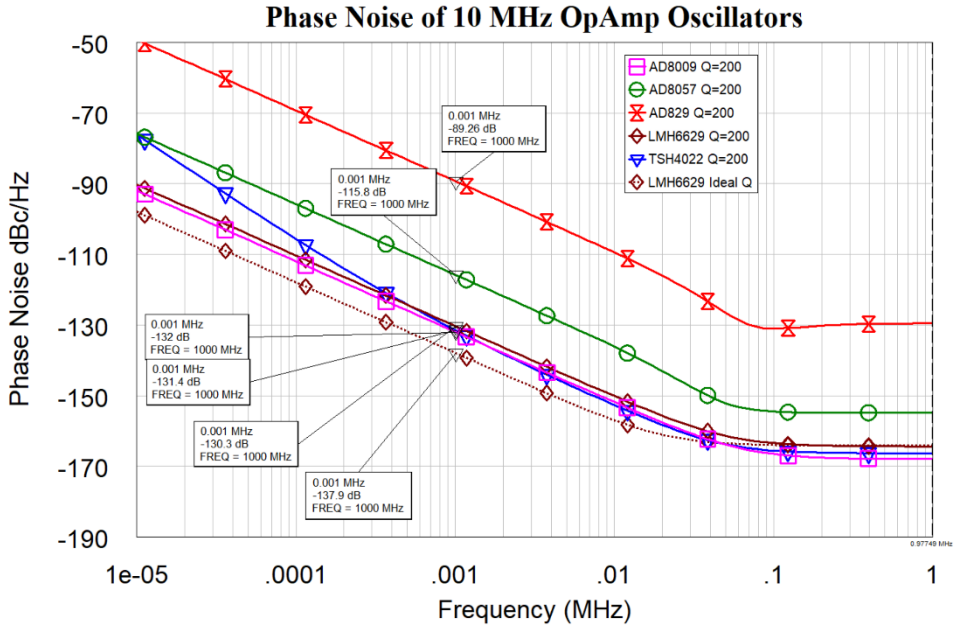



Figure 10.27. Phase noise for a 10 MHz oscillator using different OpAmps.

Comparing figures 10.23 and 10.27, show that for Q = 200, the ideal OpAmp Hartley oscillator at 1 kHz away from the carrier, produces a phase noise of -136.5 dB, compared with the best phase noise of -132 dB for the Spice models of the OpAmps. Figure 10.29 shows that the AD829 OpAmp slew rate limits and that results in a poor phase noise.

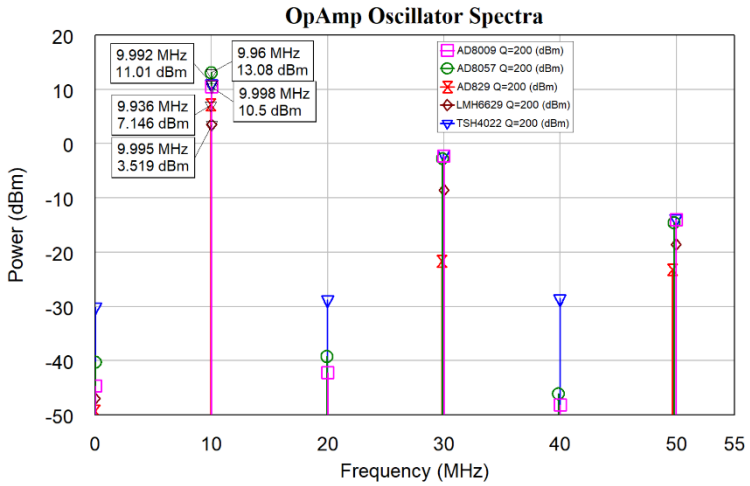



Figure 10.28. Output spectra for the oscillators of figure 10.23.

Figure 10.28 shows the output spectra of the different OpAmp oscillators operating at 10 MHz. Even though all the resonator components are identical, the oscillating frequency is slightly different due to differences in the input impedance and phase shifts of the active devices.

Figure 10.29 shows the output waveforms of the oscillators. The AD829, AD8009, AD8057 and the TSH4022 all have ±5 V power supplies and the LMH6629 has ±2.5 V power supplies. The AD829 circuit exhibits slew rate limiting. That is an explanation for the poor phase noise performance of the AD829 in figure 10.24. Figure 10.29 shows there is an error in the Spice model for the AD8057, the peak voltage in figure 10.29 is ±5.62 V. Since the circuit runs from a ±5 V power supply, the output cannot exceed ±5 V.

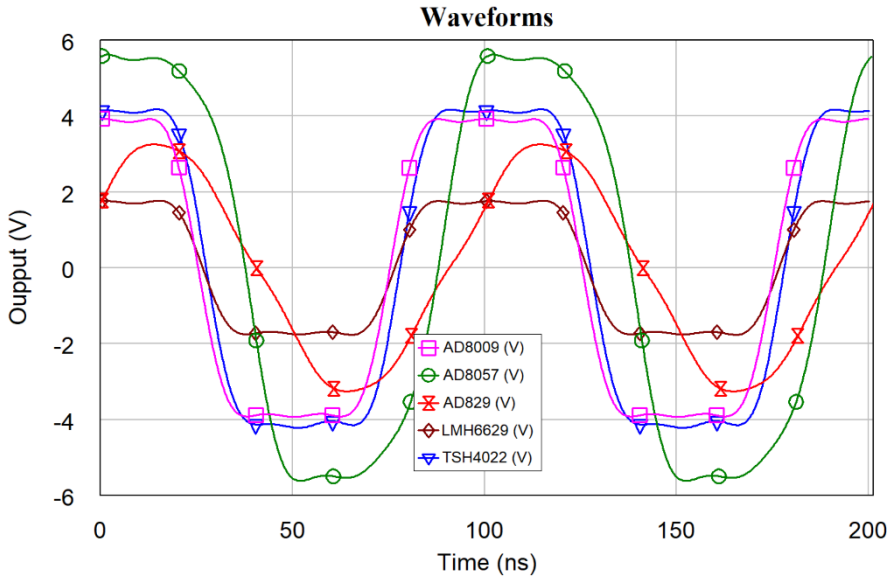



Figure 10.29. Waveforms of the oscillators of figure 10.23.

## Limitation of Simulations

Simulation can give a good indication of the expected performance of a circuit. However as indicated in figure 10.9, series inductance and parallel capacitance associated with many resistors can result in a measured hardware performance that is different from the simulation results.

It is also important to critically evaluate the simulated results. For example, figure 10.29 shows a peak output voltage of ±5.62 V for the AD8057 OpAmp oscillator. That voltage is larger than the ±5 V power supplies, and is thus not possible.

Some Spice diode models provided by manufacturers, do not include the diode capacitance when they are imported into AWR DE and used in linear simulations. That capacitance varies with the reverse voltage and when these diodes are used for input protection of RF circuits, the effect of that capacitance is critical. The MMSD301T1, RF Schottky barrier diodes, have a capacitance of 1.2 pF for a 5V reverse bias. Figure 10.13 shows that causes a significant gain reduction at high frequencies.

Sometimes the simulations raise questions that can only be answered by constructing the hardware and measuring the performance. For instance, in figure 10.20, the AD8057 has a lower bandwidth and poorer noise figure than the AD829. In figure 10.27 it is the other way around. In the light of the AD8057 simulation giving unrealistic output voltages, which one is right?

The simulated phase noise for the TSH4022 OpAmp with component values corresponding to figure 10.26, with an ideal resonator is worse than that with a Q of 200. That is not what one would expect. The phase noise of the TSH4022 oscillator in figure 10.27 has a different slope compared to the other oscillators. Are these correct results?

The nonlinear simulation using the AD797 OpAmp for figure 10.27, would not converge, even though the linear simulation shows a suitable gain and phase shift for oscillation and figure 10.20 shows nonlinear simulation using the AD797 OpAmp a that its bandwidth is larger than the AD8057. Will this AD797 circuit oscillate or is the expected 10 MHz output frequency beyond its capabilities?

The PSpice simulation models are very complex and may not necessarily accurately include all the parameters needed for a particular simulation. The simulation accuracy should improve over time. One should remember that a model will always only be an approximation of the actual hardware, and can help us understand the operating principles of the circuit to be designed, so that the best performance can be obtained from a design.

## References


1. Brandenburg D "Current vs. Voltage Feedback Amplifiers" National Semiconductor Application Note OA-30, Jan 1998, http://cas.ee.ic.ac.uk/people/dario/files/E416/OA-30.pdf
2. Analog Devices "Choosing between Voltage Feedback (VFB) and Current Feedback (CFB) Op Amps", Tutorial MT-60, www.analog.com/media/en/training-seminars/tutorials/MT-060.pdf
3. Texas Instruments, OA Current Feedback Op Amp Applications Circuit Guide, April 2013, http://www.ti.com/lit/an/snoa365c/snoa365c.pdf
4. Texas Instruments OA11 "A Tutorial on Applying OpAmps to RF Applications", http://www.ti.com/lit/an/snoa390b/snoa390b.pdf
5. Three common questions when designing with high-speed amplifiers, https://e2e.ti.com/blogs_/b/analogwire/posts/3-common-questions-when-designing-with-high-speed-amplifiers
6. Kikkert, C. J. and S Zhu, Resistive Shunt Impedance Analyzer, 2016 International Symposium on Power Line Communications and its Applications, Bottrop, Germany, 20-23 March 2016. pp 150-155 ISBN 978-1-4673-6642-7
7. MMSD301T1 Low Capacitance, RF Schottky barrier diode. https://www.onsemi.com/pdf/datasheet/mmsd301t1-d.pdf
8. Texas Instruments, LM6626 Data sheet: "LMH6624/LMH6626 Single/Dual Ultra Low Noise Wideband Operational Amplifier", http://www.ti.com/product/LMH6626
9. Analog Devices ADA4898 https://www.analog.com/media/en/technical-documentation/data-sheets/ADA4898-1_4898-2.pdf
10. Texas Instruments, Noise Analysis in Operational Amplifier Circuits, 2007, http://www.ti.com/lit/an/slva043b/slva043b.pdf
11. Analog Devices, MT-49 Tutorial, Op Amp Tutorial Output Noise Calculations for Single –Pole System, 2009, https://www.analog.com/media/en/training-seminars/tutorials/MT-049.pdf

# Chapter 11

# Circuit Manufacture

## Introduction

Once the design of the electronic circuit is complete, the circuit has to be produced. The fabrication method used will depend on: 1) The frequency at which the circuit operates, 2) Whether it is a prototype or a full production design and 3) The type of market the circuit is designed for. Low cost consumer circuits require very different manufacturing techniques compared with military or space electronics, to achieve the required electrical, mechanical, thermal and reliability performance. The most common technique for manufacturing a circuit is to use a printed circuit board (PCB). A PCB consists of an insulating material forming the PCB substrate onto which conductive tracks are placed. Components forming the circuit are connected to those tracks. There are two basic ways of producing PCBs:

### *Subtractive Process: Conductive Layer Removal*

A conductive layer, like copper, covers one or both side of the PCB substrate and the conductive layer is removed where there are to be no tracks. The metal can be removed using chemical etching, milling or laser ablation.

Chemical etching of copper clad printed circuit boards is the most common PCB manufacturing technique. In that process, the whole PCB is covered with a thin layer of photo resist material, which hardens when exposed to UV light. For commercial PCB manufacture, a Laser plotter shines UV light on areas where tracks need to be. For non-commercial applications, a photographic transparency, with dark areas where the conductor is to be removed and clear areas where the track is to be, is produced. That is then placed on the PCB and exposed to UV light. The unexposed areas of photoresist are then washed away. The resulting exposed board is then etched to remove the unwanted copper as shown in figure 11.1. Note that there will be some undercutting of the copper tacks. These chemical techniques are used for producing most commercial PCBs.

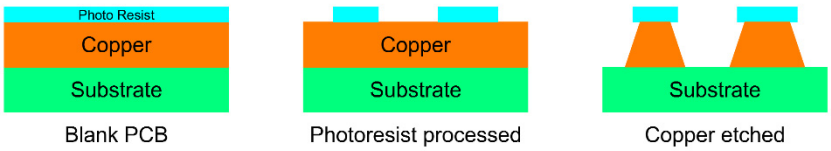



Figure 11.1. PCB Etching process

Including transport, it typically takes one week to produce an etched FR4 board and it takes slightly longer for an RF PCB. For prototypes, a faster turn-around time may be required. With in-house PCB milling or Laser ablation equipment, described later in this chapter, turnaround times of less than one hour are possible for FR4 or RF PCBs.

### *Additive Process: Depositing Tracks and Vias*

In this method, the conductive tracks are deposited onto the substrate. For thick and LTCC circuits, the conductive or dielectric tracks are printed on a bare substrate material and then fired to make them permanent. Such tracks have a higher resistance than the copper on etched PBCs.

Ceramic substrates are used for many RF circuits. This requires gold or copper conductor tracks to be deposited onto the ceramic. Those tracks are typically electro-plated. To ensure that all tracks have the same copper or gold thickness plated on them, all tracks must be electrically connected during the electroplating process. That requires a seed layer, of approximately 1 to 2 μm of conductive material, often copper or gold to cover the entire substrate before electro-plating. This is normally achieved by using a series of chemical baths, to coat the substrate with this seed layer. The seed layer can also be produced, by placing the ceramic substrates in a vacuum chamber and spluttering gold onto them.

The areas where no tracks are required are covered with a protective coating, using screen-printing or photoresist. Electroplating is then used to build up the tracks to the required thickness. The protective coating or photoresist is then removed, followed by and a light etch to remove the seed layer.

The additive process minimises the amount of copper that is to be etched away and thus results in less copper and etching waste that needs to be recycled. Additive processes are required to produce the vias in double and multi layered printed circuit boards.

# Printed Circuit Board Materials

- Most PCBs are made by having thin copper sheets glued to an insulating substrate material, called a laminate. The copper thickness depends on the applications. Typical thicknesses are 2, 1, ½ and 1/4 oz. copper per square foot, which corresponds to a copper thickness of 70 μm, 35 μm, 17 μm or 9 μm respectively. The copper thickness together with the track width must satisfy the current carrying capability and resistive loss requirements of the tracks. Subtractive processes are used to produce the required circuit boards.

Conventional PCB laminates consist of a filler or reinforcing material and a thermoset resin. These sheets are cured at high temperature and pressure. The mechanical and dielectric properties of the laminates depend on the composition of the laminate.

For very low cost and low frequency applications, paper pulp or cotton and epoxy resins are used. FR2 and FR3 boards are examples of this. For higher mechanical strength, woven fibreglass mats are used as reinforcement for the thermoset resins. The temperature range over which the board can be used, and the dielectric properties are governed by the type of resin used. By using resins containing Polytetrafluoroethylene (PTFE or Teflon®) and/or ceramics such as Alumina, PCBs with low losses at microwave frequencies can be obtained. In some applications, the fire retardant properties of the laminates must also be considered in the laminate selection process. The AWR DE *Libraries* ⇒ *AWR Web site* ⇒ *Parts by Type* ⇒ *Substrates* contain details of PCB substrates. The number of manufacturers of substrates has reduced during the last few years and the manufacture of RF PCB substrates is now dominated by the Isola Group [1], Rogers [2] and AGC Multi Material (Taconic) [3].

## *Conventional PCB Substrates*

### Paper and Resin Substrates; FR2 and FR3

FR2 and FR2 substrates consist of a mixture of paper pulp and a resin. Phenolic resin for FR2 and epoxy for FR3. They are mainly used in low cost consumer products, and are not normally used for multilayer boards. FR3 has a dielectric constant of approximately

2.3 but this is not controlled and the loss tangent is not specified. An advantage of FR2/3 and similar, paper based substrates are that holes and slots can be punched. This laminate is not recommended for RF designs. FR3 has a poor heat tolerance and scorches easily. FR3 is normally light brown with a smooth texture.

Figure 11.2 shows a typical low cost AM/FM radio manufactures using FR3 circuit board. The advantage of being able to punch out a particular shape can be seen.

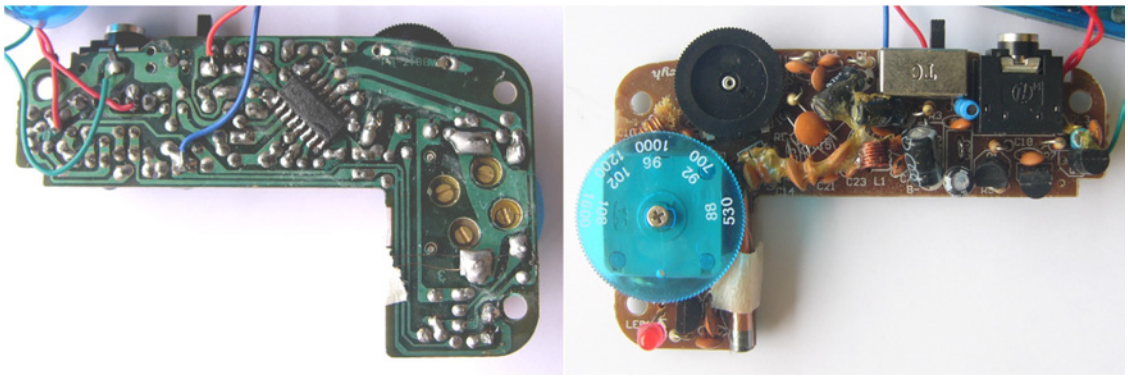


Figure 11.2. FR2/3 Printed Circuit Board for a low cost AM / FM radio. (Unknown manufacturer).

## Fibreglass and Epoxy Substrates; FR4, FR408, IS400

This is a substrate consisting of a mixture of fibreglass and epoxy. It is suitable for professional quality PCBs and has the following properties:

Table 11.1. FR4 Properties.

| | |
|---|---|
| Dielectric Constant | 4.7 at DC decreasing to 4.4 at 10 GHz. |
| Dissipation factor (Tan(δ)) | 0.014 |
| Q at 50 MHz | 95 |
| Max Temperature | 130 °C |

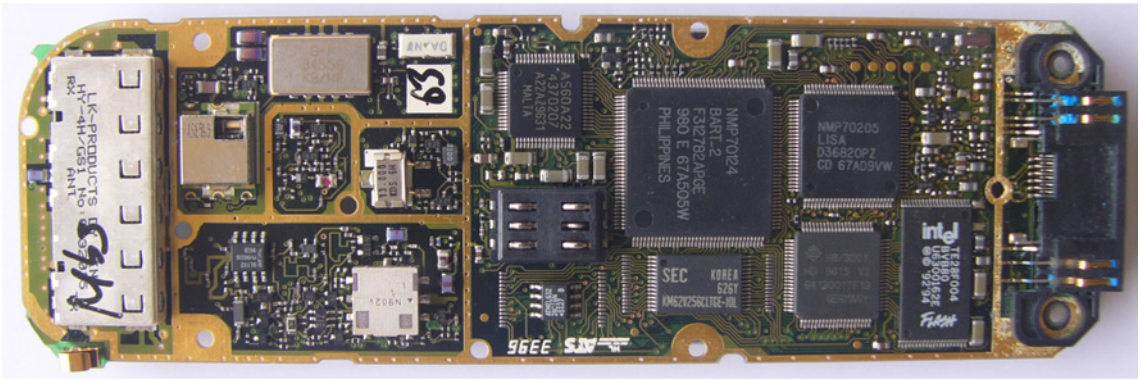


Figure 11.3. FR4 Multilayer Printed Circuit Board. (Nokia Mobile Phone).

At James Cook University, prototype boards are milled and as a result, we have been using FR3 for prototype PCBs since the fibreglass used in FR4 and many other PBCs is carcinogenic. Special precautions are required to ensure that the fine fibreglass particles produced by the PCB milling process are not inhaled. FR3 is safer in that respect, however

FR4 is a much better circuit board in that it has a better heat tolerance, is stronger and the dielectric constant is specified to 10 GHz.

FR4 PCB's can be made with many layers. Simpler PCBs have 4 layers, with one layer being earth, one layer being the supply voltage and the outer layers containing the tracks that are connected to the IC's and passive components. FR4 is normally light green and semi-translucent, often this can be seen at the left edge of the board as in figure 11.3. The dark green colour is due to the solder resist and not due to the laminate. The large component at the left edge of the board is a ceramic diplexer. Normally many printed circuits are etched together, on one sheet, or panel, as shown in figure 11.4. Cut-outs are provided to enable the individual circuits to be removed easily.

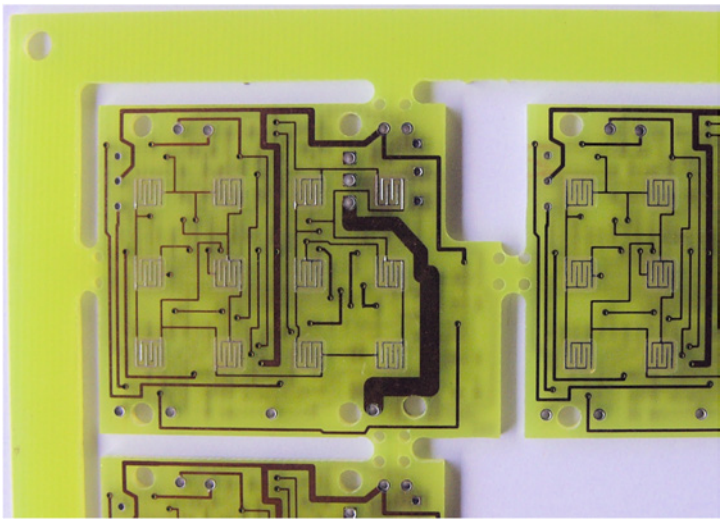


Figure 11.4. FR4 PCB showing cut-outs. (Layout by JCU).

FR3 and FR4 are ANSI terms, manufacturers such as Isola have fibreglass and epoxy products under names like FR408, IS400, IS410, and IS 420. Different resins used have different dielectric constants, typically ranging from 4.7 shown in table 11.1 to 3.67 for FR408.

## *Microwave and RF Printed Circuit Board Materials*

FR3 and FR4 can be used for PCBs to 1 GHz, however above these frequencies the losses may become significant. The laminate thickness for FR3 or FR4 is not tightly controlled, causing variations in impedance of Microstrip lines across the laminate and from batch to batch. That is not suitable for many RF designs.

The major laminate manufacturers make many different PCB laminates, especially for the RF and microwave frequency range. As an example several different laminates from Rogers Corporation, are described here, to illustrate that different applications require RF laminates with different properties.

### RT/duroid

RT/duroid are high frequency PTFE (Teflon) filled laminates for use in high reliability, aerospace and defence applications [4], with dielectric constants between 2.0 and 10.2. Some laminates are reinforced with glass fibres for strength. RT/duroid laminates were developed in the 1960's and are the oldest Rogers products. Others have a low weight or are dimensionally stable. RT/duroid 6010 has a high dielectric constant, which reduces the size of the circuit. For frequencies above 20 GHz, circuits with a high dielectric

constant become too small so that at these frequencies a low dielectric constant has to be used. Because of their low water absorption characteristics, RT/duroid 58X0 is good for applications in high moisture environments. The LNC of figure 11.5 is located at the focal point of antenna, which is sometimes very hot, sometimes very cold, and sometimes very wet. RT/duroid is thus a good choice for the PCB material. RT/duroid is flexible and thin laminates require care in mounting them securely. RT/duroid is normally brown and the woven glass mat can clearly be seen in figure 11.5. If the dielectric constant of the PTFE composite filling and the glass microfibers are slightly different then small local variations in dielectric constant will occur. Having a random orientation of the microfibers minimises that variation. The glass reinforcing provides an excellent strength and prevents tracks from cracking.

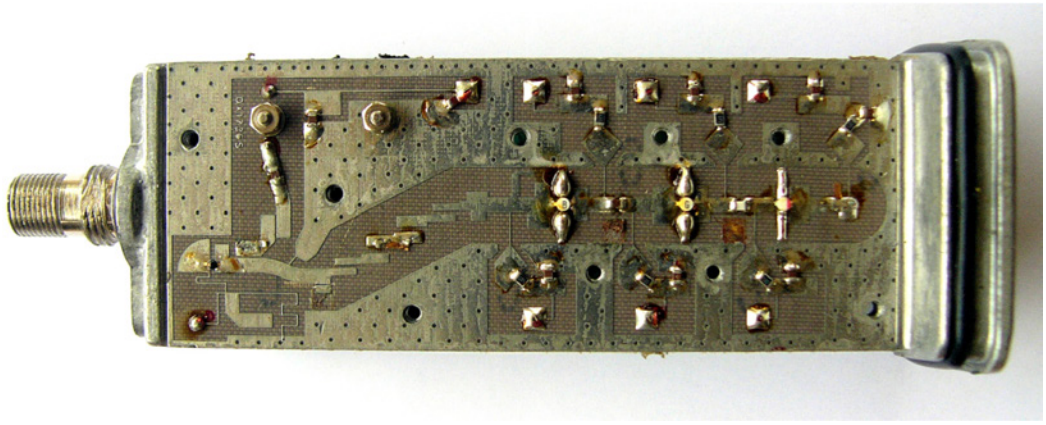


Figure 11.5. Ku band (12 GHz) low noise converter (LNC) using RT/duroid (Norsat).

The RT/duroid 6000 laminates have a thermal expansion coefficient of the laminate that matches that of copper. This product is ideal for applications in rapidly changing thermal environments such as space. Multilayer boards are possible with this laminate. RT/duroid 6000 is a military specified substrate and thus very expensive.

## RO3000 and RO3200 (PTFE/Ceramic Laminates)

The RO3000® laminates are aimed at a commercial market and are a lot cheaper than the corresponding RT/duroid 6000 laminates. Dielectric constants of 3.0 to 10.2 are available. The temperature coefficient of expansion matches that of copper and FR4 in the X-Y plane, so that multilayer RO3000/FR4 boards can easily be made. RO3003G2 is designed for 77/79 GHz auto radar applications.

## RO4000

The RO4000 series is a woven glass/ceramic loaded thermoset plastic resin laminate. This is a low cost commercial laminate, which is especially suited for multilayer boards using RO4000 and FR4. The boards have a glass transition temperature ($T_g$) > 280°C. They can thus be used with conventional PCB processing techniques, such as wave soldering and surface mount techniques. Unlike PTFE based microwave materials, no special through-hole treatments or handling procedures are required. Therefore, RO4000 material circuit processing and assembly costs are comparable to FR4 epoxy/glass laminates. Dielectric constants vary from 2.55 to 6.15. Prepreg sheets of matching dielectric constant are available to produce multilayer boards.

The Microstrip filters if figures 7.66, 7.73 and 7.80 to 7.83 have all been made by milling RO4003 substrates.

### Other Laminates

Rogers Corporation also have other RF laminates, some examples are: 92ML Laminates and 92ML Prepreg sheets. They have a high thermal conductivity, are flame retardant and are suitable for high temperature applications. XtremeSpeed RO1200 series are designed for digital signals to keep their pulse shape when using many layer boards. In addition there are many other laminates on their web site [2].

Other manufacturers have a similar range of RF and Microwave laminates to the Rogers products described above. For example, Isola have several RF and Microwave laminates, Astra MT77, I-Tera MT40 (RF/MW) and IS-680 AG are examples [1]. AGC Multi Material also has several RF and Microwave laminates [3]. RF-35 is a fibreglass and PTFE/Ceramic laminate, similar to RO3035. It also has a dielectric constant of 3.5. AGC Multi Material TLY laminates use fibreglass for mechanical reinforcement and increased dimensional stability. It is similar to RT-duroid 58X0. The TL series has dielectric constants from 2.17 to 3.2 and a loss tangent from 0.0009 to 0.003. Panasonic have Megtron6 R-5775(N) laminates and R5670 Prepreg sheets [5]. Those laminates have a similar performance as RO4003, but with a higher dissipation factor.

## Multilayer Boards

There are many applications where RF circuits require multilayer boards. One example is a Stripline RF circuit. Another is a multilayer board with an RF/Microwave substrate for an RF layout and an FR4 type substrate for power supply, control, and digital signal processing. A Prepreg sheet is a thin uncured sheet, containing fibreglass, thermoset resins, and fillers. The laminates are normally produced by gluing copper sheets to one or more Prepreg sheets, and curing them using pressure and heat.

For multilayer boards, jigs with locating pins are used to ensure that each of the boards making up the multilayer board are in perfect alignment. For a multilayer board, the inner layers are etched. The boards are stacked with Prepreg sheets between the multilayer boards, to form the multilayer board. In many cases, the same Prepreg sheets that are used to make the double-sided boards are used. That will space all the copper layers evenly, as shown in figure 11.6.

The vias in the boards are drilled and electro plated prior to the tracks being etched, so that all vias are connected together and electroplating of the vias is possible. The outer layers are then etched to produce the required tracks on them. The solder pads and solder mask are then applied, completing the PCB. It is possible to have vias on inner layers only. These are called blind or buried vias and are produced on a 2 or 4 layer board and then the location of these vias are not drilled in the outer copper layers. Buried vias offer space savings and provide some intellectual property protection by making it a little bit more difficult to trace the design, but they also make it more difficult to fault-find.

Several types of adhesives can be used depending on the laminates to be bonded. Figure 11.6 shows a typical construction requiring an RO4003 Stripline circuit bonded to an FR4 multilayer construction. For constructing the Stripline circuit, a high frequency bond-film like the RO4450 “Prepreg” sheet from Rogers is required. The bonding sheets are close to 0.1 mm thick and have dielectric constants from 3.3 to 3.54 at 10 GHz, matching the dielectric constants of the RO4000 series laminates. The loss tangent of the Prepreg bonding sheets of 0.004 at 10 GHz is close to the 0.0037 and 0.0037 for the RO4000 laminates, so that no sudden changes in dielectric occur in the multilayer board. Each

manufacturer has Prepreg sheets and bond sheets with properties that match their microwave laminates.

For a combination of microwave and FR4 boards, the inner layer of the microwave board should be a ground plane so that the dielectric properties of the Prepreg sheet joining the microwave and FR4 are not so important. A good low cost option is to use the standard bond films used for FR4 for making multilayer PCBs.

For bonding the laminates and Prepreg or bonding sheets are clamped at a pressure of typically 2.8 MPa and a temperature of typically 225°C for more than one hour. That temperature varies with the properties of the Prepreg sheets. Since air has an $\varepsilon_r = 1$, it is important to prevent air bubbles, particularly when high dielectric substrates or Striplines are used, since air-bubbles change the characteristic impedance of the Stripline at the point of the air-bubble and cause a discontinuity.

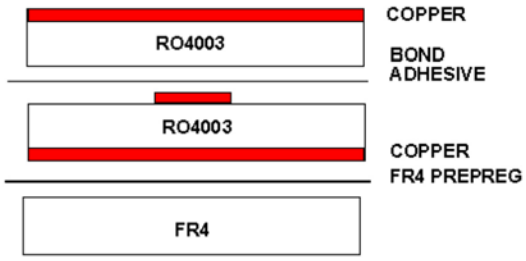



Figure 11.6. Bonding laminates to form a multilayer board [2].

# Non-Clad Substrates

During the 1980's the microwave PCB substrates were not readily available and many microwave circuits had to be produced on Alumina substrates using thin film techniques. These non-clad substrates are now only used for precision microwave circuits using thin film techniques and for low cost thick film circuits at both RF and low frequencies.

Companies such as Coors Ceramics [6] and Morgan Technical Ceramics [7] produce dielectric materials that can be used for such RF substrates. Ceramic substrates are used in many packaging applications. A paper by F. Bechtold [8] gives a good overview.

## *Alumina Substrates*

Alumina is the dominant substrate material for thick and thin film applications. The dielectric constant is close to 10, with both the dielectric constant and cost increasing with the purity of the substrate. For lower cost applications, thick film substrate materials with 85% to 95% purity are used. In many cases these substrates are used "as fired" for low frequency applications or ground flat for low cost microwave applications. For precision, low-loss microwave applications 99.5% to 99.8% purity substrates are used and these may be ground and polished in order to remove any surface irregularities and ensure a constant thickness of the entire substrate. Alumina is ideal for demanding low loss applications, such as substrates for thin film circuits.

Rogers Corporation [9] now have a range of metallised ceramic substrates in different substrate thicknesses. These are plated on both sides with copper, silver or gold. Their suggested applications are those involving high power. No RF properties of the substrates, like dielectric constant or the purity of the Alumina substrate, which affects the losses, is given. These substrates may possibly be used for RF applications.

### *Other Substrates*

Ceramic materials with higher dielectric constants are used to reduce the size and thus weight of resonators used for oscillators and filters. Dielectric resonator oscillators (DRO) [10, 11] are used in LNCs for satellite receivers. The LNC in figure 11.5 has a dielectric resonator oscillator mounted on the other side of the PCB shown in figure 11.5. The diplexer shown in the left of figure 11.3 and the cavity filters in figure 7.98 are examples.

## Manufacturing

RF printed circuit boards can be designed in a similar way to conventional PCBs, so that programs like Altium (formerly known as Protel) [12], Allegro [13] or Autodesk's (formerly CadSoft) Eagle [14] can be used to produce the circuit board layout. For circuits like Stripline filters, and other RF circuits, where the characteristics and lengths of transmission lines are critical, then software like Cadence AWR DE or Keysight is required. AWR DE can produce GDSII, DXF and Gerber plot files. GDSII file format is an industry standard file format for IC layout artwork and DXF is a vector file format developed by Autodesk (AutoCAD), for exchanging files between CAD software. Gerber ASCII vector files were initially developed by Gerber Systems Corp to drive their vector photo plotters. The Extended Gerber files include all the information, like board layer type, drill, solder mask and overlay detail, required to produce a complete PCB. They are the default file type used to produce prototype RF boards, either by commercial PCB manufacturers, or by the milling machines used by many universities for prototypes. The Gerber plot files can also be imported into most PCB layout software and Gerber plot files can be imported into AWR DE, to produce a combined RF and conventional PCB. Such technology is required for the multilayer boards shown in figure 11.6. Importing plot files into AWR DE allows those imported layers to be included in EM simulation.

Normal PCBs are protected using a solder-mask. Unless the thickness and the properties of the dielectric of the solder-mask is taken into account in designing the RF circuit, solder-masks should not be used for RF boards. Instead, to prevent corrosion, Gold plating is normally used on the RF circuits as shown in figure 7.67.

### *Layout Hints*

Many PCB manufacturers can etch to a specified accuracy. Typical values for the thinnest track widths and spacing that can be made on FR4 are 0.1 mm (0.004"). For High frequency laminates like RO4003C, track widths and spacing of 0.051 mm (0.002") are possible. Larger values > 0.15 mm are desirable and will reduce costs. [15, 16]. Ensure the tracks can handle the required current. Note 0.001" is called *thou* in the UK and other countries, and *mil* in the USA. In Europe *mil* is an abbreviation of a millimetre and it is also a measurement of angle. To avoid this confusion *mil* is not used in this book. Many of the modern ICs have 0.5 mm pitch of the leads on the IC. The 0.5 mm track pitch can easily be achieved using present day PCB manufacture.

The smallest drill size that can be used is typically 0.15 mm diameter. Drilling holes smaller than 0.3 mm increases the cost per hole. The smallest pad size for vias or leaded components, which should be used is the drill size plus 0.5 mm, however small pads will lift off easily when components are soldered to them. For through-hole components use a drill size that is approximately 0.1 mm larger than the lead size and use a pad that is approximately 1 mm larger than the drill size. The recommended hole size for a standard

leaded resistor or capacitor is 0.9 mm, with a pad size of 2 mm. To ensure that the circuit can be changed if needed, for prototyping boards a bigger pad size is advisable.

For milling of PCBs, the tolerances are slightly different. For a typical milling machine [17], the tool alignment has a ± 5 µm tolerance. Since 0.15 mm wide milling bits are the smallest commonly used, a minimum recommended track size is 0.5 mm, with a 0.15 mm minimum spacing between tracks. Having a 0.25 mm spacing ensures that 2 milling cuts are made, thus reducing the chance of short circuits. For short track lengths, track widths of 0.2 mm are possible, however such thin tracks should be avoided for long tracks since tracks may lift due to the mechanical friction of the milling bits. When milling circuit boards, as much ground-plane as possible should be left on the board, to minimise the amount of milling that has to be done and minimise the milling time and cost. In addition, the extra ground-plane provides some rigidity for thin boards to prevent them from curling. The ground plane can be used to provide a heat sink to remove heat from the circuit.

For RF boards the bottom conductor should be a high integrity ground-plane underneath any RF transmission lines to provide the correct Microstrip circuit configuration. Vias connected to tracks and leaded components affect the integrity of that ground-plane. As a result, surface mount components should be used in any RF design. If needed leaded components can be soldered onto pads on the top layer. To prevent performance changes as the RF circuit is mounted in an enclosure and to provide suitable mounting locations, it is desirable to provide an earthed strip around the RF board as shown in figures 7.66, 7.67 and 7.80 to 7.83. In figure 7.67, the big holes are used for mounting the board and the many small holes are vias, connecting the earthed area to the ground-plane. Note that this grounded area is also used to minimise EM coupling between the different parts of the circuit.

## *Etching*

Most commercial printed circuit boards are etched. There are many commercial PCB manufacturers that will etch prototype boards with a short turn-around time and low cost [18, 19, 20]. The turnaround times for PCBs using RF and Microwave substrates are normally longer than for FR4 substrates. The Gerber files generated by the designer are used to produce the PCB.

The laminate typically has rolled copper on both sides. Each side is then coated with Photo Resist and typically a laser plotter, operating on the Gerber file, shines a laser on the tracks and ground-plane where the copper needs to remain. That hardens the photoresist and the unexposed photo resist is washed off. The board is then placed in an etching acid, which removes the unprotected copper. The etching acid can be Ferric Chloride, Ammonium Persulfate, Sodium Persulfate or Cupric Chloride [21]. All of these are nasty chemicals since they must eat copper. For most, their fumes are toxic and their disposal is difficult. For multilayer boards, the inner layers are stacked and drilled. The holes for through hole pads and vias are electroplated to provide the connections between layers and then the top and bottom layers are etched.

A solder mask in normally applied to protect the copper tracks and prevent them from oxidation. The solder mask material is UV hardening like photoresist. A thin layer of the solder mask material is applied to the whole PCB and the areas that are to remain are exposed to UV light. The areas that are not exposed are then washed away to provide the areas for solder pads and mounting the required components. Overlay text and marks are

then printed on the board and finally the solder pads are dipped in solder for easy soldering of components onto the board.

For RF layouts the designer needs to be aware that the etching process will slightly undercut the tracks. The amount of undercut will depend on the copper thickness and the etching chemicals used. The manufacturer will supply details of the amount of undercut. If a solder mask is applied to protect the tracks, then the thickness, dielectric constant and dielectric losses need to be taken into account during the design process. If the losses are too high, the PCB may need to be gold plated to prevent oxidation.

### *Manufacturing using a PCB Milling Machine*

Many universities use a special PCB milling machine [17] to produce prototype PCBs. The ceramic filler used in RF substrates like RO4003 are much more abrasive than the epoxy, paper, and fibreglass used in FR3 and FR4 type substrates. As a result, the cost of milling bits is a major cost in the production of those boards. For milling the more flexible PTFE boards, like RT/Duroid, the substrate needs to be thick enough to be able to be held flat as part of the milling process, so that the more rigid RO4003 substrates are the best to use in PCB milling machines. Since the milling process can disperse copper and PCB substrate materials in the air, the appropriate workplace health and safety considerations must be considered. PCB milling allows a fast turn-around, for prototype RF boards needed for research and development, PCBs up to 229 x 305 mm can be accommodated. Typical position repeatability is ±5 μm when using the plotter's camera to detect registration marks. Tracks widths and spacing of 0.15 mm are possible.

### *Manufacturing using Laser Ablation*

PCB cutters can also use green or UV lasers to remove the copper from PCB laminates by laser ablation [22, 23]. The laser vaporises the copper or gold, where the metal needs to be removed. Minimum track widths of 50 μm and gaps between tracks of 15 μm are possible on ceramic substrates like RO4003. Trace widths of 75 μm are possible on FR4 or RT Duroid substrates. Since the heat absorption of ceramic substrates are different from FR4 or RT Duroid, the laser pulse duration is changed to ensure there is no heat damage to the substrate. The plotting accuracy is 2 μm. This accuracy is better than what can be achieved reliably with conventional etching or PCB milling. The UV laser plotters can also be used for inscribing, drilling or cutting the PCB. An A4 size PCB can be produced in about 20 minutes. The larger machines are fast enough for commercial production. Since no hazardous chemicals are used, this is a relatively environmentally friendly means of producing PCBs. However, since the ablation process vaporises copper and PCB substrate materials, the appropriate workplace health and safety considerations must be considered.

Some commercial PCB etching companies use these laser cutters to produce the masks used for putting solder paste onto conventional PCBs.

## Thin Film

The polished Alumina substrates, used for the thin film circuit boards, have a very low dielectric loss. The thin film substrates have less thickness variation than RF PCB material. As a result microstrip transmission lines have a better impedance accuracy, which may be critical in a design. Thin film circuits can be made to better accuracies, with smaller track and spacing sizes than etched PCB's.

Thin film circuits can be produced using semi additive processes, where a 1 to 2 μm seed-layer of gold is applied to an Alumina substrate. A photographic mask is then applied to the places where no track is required and the tracks are then electroplated to the correct thickness of several tens of μm. The photo-resist is then removed and a quick etch removes the seed-layer, where no tracks should be, but does not completely remove the tracks. The required solder-pads are then added, together with dielectric dams to prevent the lead from solder leaching into the gold.

Laser ablation can be used to remove metal cladding from Alumina substrates [23], so they can be used to produce thin film circuits.

Microfab [25] specialise in the design and production of thin film circuits, predominantly for space and military applications and use a subtractive process where the whole substrate is covered with copper or gold and then ion beam etching is used to remove the conductive layer as required. This process achieves etching tolerances of 0.2 μm, compared to 2 μm for PCB based technology.

The designer may have to adjust the track widths in the design, to compensate for the changes in track width caused by the production processes. For a 35 μm conductor thickness, corresponding to 1 oz. copper per square foot, then the additive process of depositing tracks will expand the tracks by tens of μm as plating will also occur on the sides of the tracks, where they are not confined by the photoresist. If subtractive processes are used then some etching on the sides will occur and the tracks will reduce in width by tens of μm in addition to the other manufacturing tolerances. Ion beam etching or laser ablation does not under-etch and will thus result in more accurate track widths. Once the amount of over-etching or under-etching is known, then the track widths can be adjusted to compensate for this. If the line widths are made as variables, then this correction factor can be set to zero for simulation and set for the required correction when the layout is exported to the plotter.

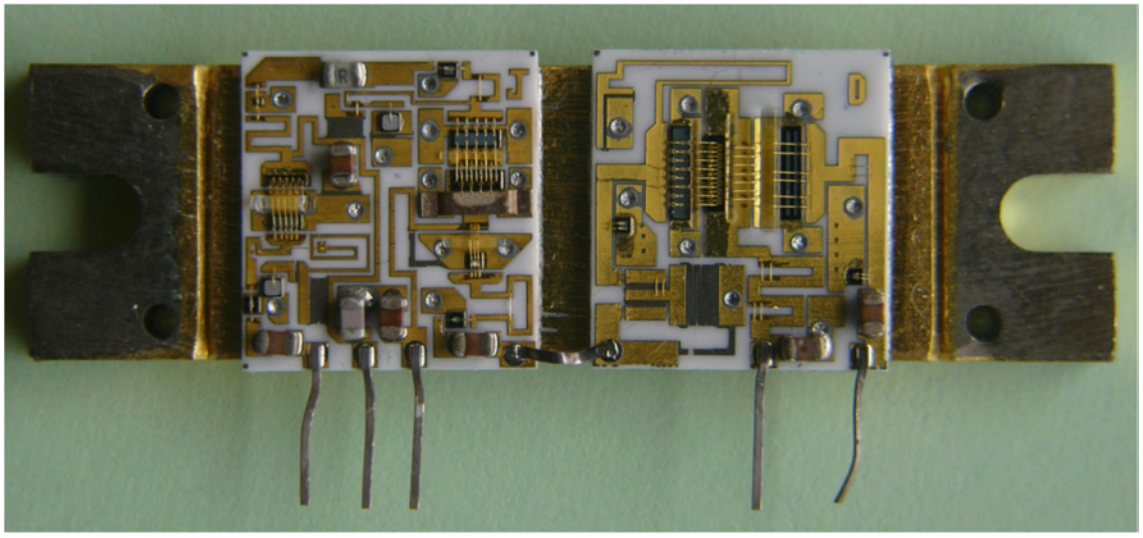


Figure 11.7. 20 W Class C amplifier hybrid MHW820 (Motorola).

Thin film circuits are much more expensive than RF and microwave PCB, circuits. Thin film circuits are firstly used where the accuracy and reliability requirements demand its use, such as military or space applications [25, 26]. Secondly, Alumina has a very good thermal conductivity. As a result, thin film techniques are often used for power applications, where the Alumina substrate is in contact with a heat-sink. A typical

example is the 20 W Class C 800-900 MHz amplifier hybrid, shown in figure 11.7. The whole circuit including heat sink is 56 mm long. The bond-wires for the large output transistor on the right can clearly be seen.

## Thick Film

Thick film techniques have a slightly higher circuit set up cost as several screen masks need to be made, but they have a lower increment cost as no etching or milling of the PCB's are required. In thick film techniques, a substrate, which normally is an Alumina substrate, has conductive, resistive or insulating inks applied to them using precision screen-printing technology. The substrate is then fired at typically 850 °C to harden the tracks and thus provide the correct circuit connections. Dielectric layers can be made, so that tracks can cross each other. For a multilayer track circuit, several separate firings may need to be made. Similarly, capacitors can be made by firstly using a conductive ink to form the one electrode and firing that. Then a dielectric layer is applied and fired, followed by another conductive layer for the other electrode. Resistors can be made using resistive inks and inductors can be made by printing conductive spirals. This results in a high-density circuit board of low cost. The low thermal coefficient of expansion (TCE) of ceramic materials guarantees mechanical stability and is closely matched to that of ICs for bare chip assembly.

The printing screen has a photographically produced mask applied to it, with the screen being open where the tracks need to go and being blocked everywhere else. The printing screen is placed in contact with the substrate and the ink pastes are applied with a squeegee to the screen. The inks can also be applied using other techniques, such as spraying, dipping using the appropriate screening techniques to ensure that the inks are only deposited where they are supposed to be.

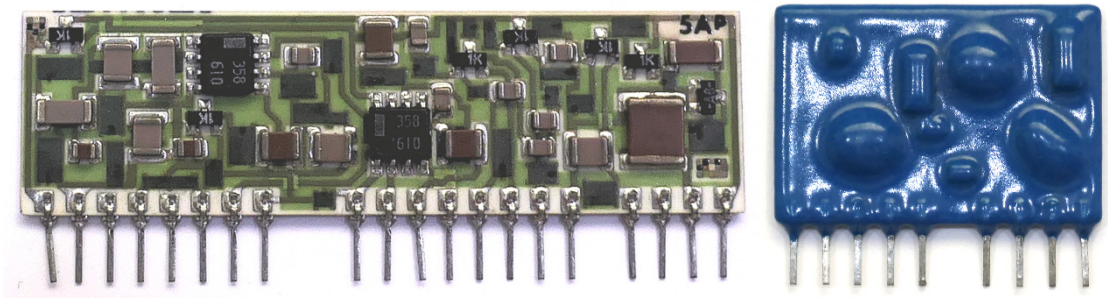


Figure 11.8. Thick film circuits before and after a protective coating has been applied.

Figure 11.8 shows some typical thick film circuits. The circuit on the left shows, that thick film circuits can have a high component density. After the circuit is tested, the whole circuit is protected with a protective coating as shown on the right of figure 11.8. This makes thick film circuits very suitable for hazardous or wet environmental conditions.

Many companies, such as [27, 29], specialise in the design and production of thick film circuits, or the supply of materials for them.

### *Printing Screens*

The ink is normally applied using a squeegee. When the ink is applied, the thickness of the ink is close to the thickness of the screen. By varying the thickness of the screen, the thickness of the tracks can be varied.

The screens used for the printing can be made from stainless steel, with a typical fibre diameter between 30 and 100 μm, a 50 to 224 μm mesh aperture and 65 to 220 μm mesh thickness with an aperture of 39 to 47%. Stainless steel screens are used for large production runs.

Screens can also be made from polyester. Polyester screens have a shorter life but are cheaper, and are thus used for smaller production runs. The screens have a typical fibre diameter between 35 and 110 μm, a 43 to 185 μm mesh aperture and 60 to 160 μm mesh thickness with an aperture of 30 to 40%.

## *Pastes (Inks)*

Conductivity: The conductivity of the pastes is given in terms of milliohm/square. The resistance of a printed conductor of 10 mm x 10 mm, is the same as the resistance of a conductor of 100 mm x 100 mm, as long as the thickness is the same.

Thick film inks [29, 30] contain precious metals, glass, and/or ceramic powders dispersed in an organic medium. Specialized compositions create conductors, resistors, and dielectrics for a variety of applications and operating environments. Table 11.2 shows the typical conductivity of various conductive inks. Copper inks are difficult to use since they require an oxygen free atmosphere in the ovens, to prevent oxidisation. The palladium inks are used for solder pads.

Table 11.2. Comparison of sheet resistance of conductive pastes.

| Conductor Material | Sheet resistance (mΩ/square) |
|---|---|
| Copper | 1.5 |
| Silver platinum | 2.0 |
| Gold | 3.0 |
| Silver palladium | 30 |
| Gold palladium | 30 |

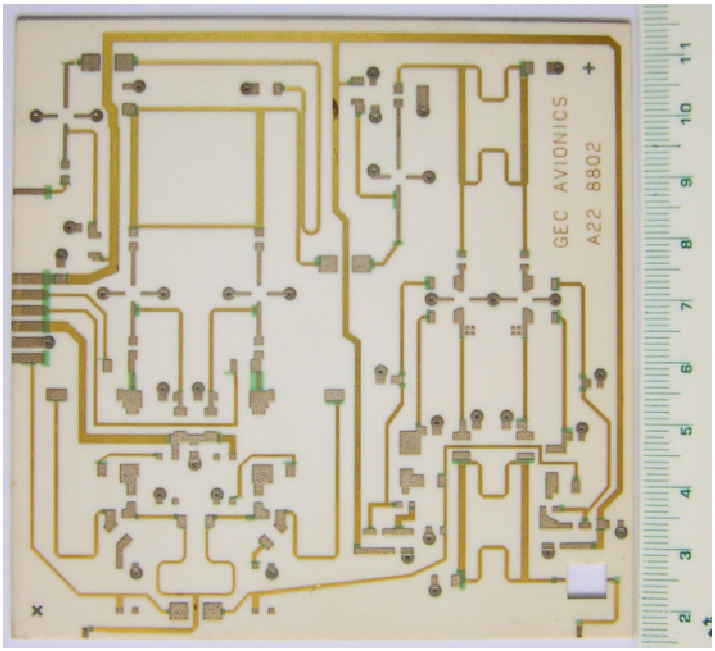



Figure 11.9. Thick film RF circuit on Alumina. (GEC Avionics, designer Kikkert).

### *RF Applications of Thick Film Circuits*

The Alumina substrate has a very low loss, and that is why it is used for thin film circuits. The application of the required tracks using thick film techniques is a lot cheaper than doing the same using thin film techniques. For accurate transmission line widths, fine screens need to be used and allowances need to be made for spreading of the inks. Figure 11.9 shows a circuit for a low noise amplifier and I-Q gain control circuit for a receiver beam steering application at 1.6 GHz. The circuit is 100 mm x 100 mm in size.

Thick film techniques are also used to produce patch antennae for mobile radio systems. In many cases, the antenna needs to be shaped to conform to the contours of the mobile phone. Thick film techniques are also used to coat the ceramic blocks of the dielectric filters used as a diplexer shown on the left of the mobile phone in figure 11.3.

## Manufacturing using 3D printing

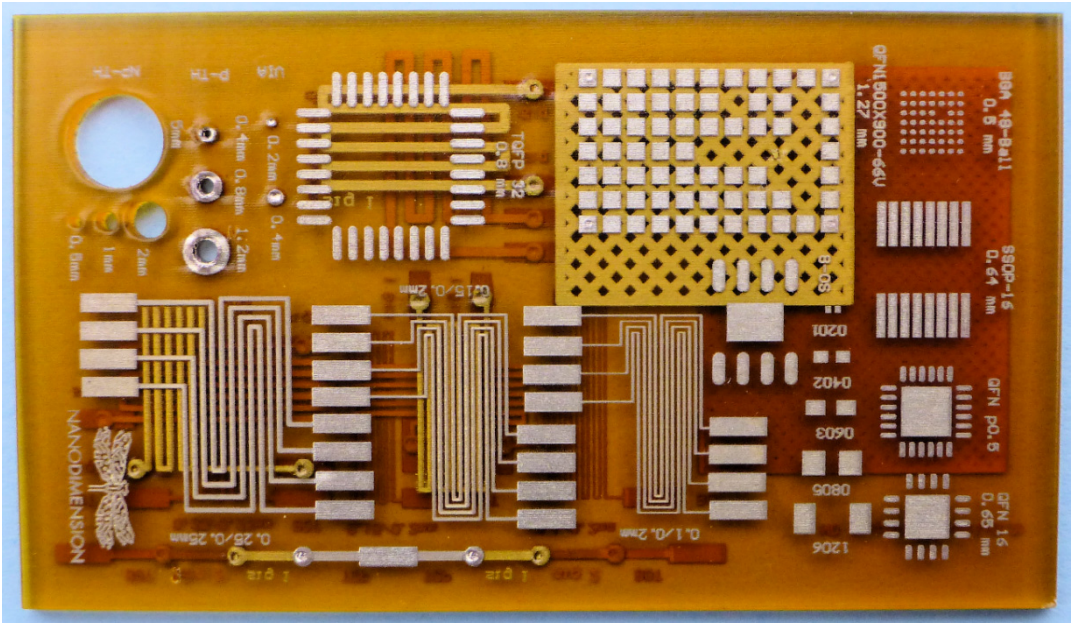



Figure 11.10. Multilayer 3D printed circuit board. [31]

Recently 3D printers capable of printing printed circuit boards have become available. [31 - 33]. The printer prints dielectric ink, or conductive ink in the location required in order to make the required printed circuit board. The dielectric ink from Nano Dimension [31] has a dielectric constant of 2.2 to 3.7 at 1 MHz. and a loss tangent of 0.02 to 0.04 at 1 MHz. Having such a wide range of dielectric constant makes it difficult to produce accurate transmission lines or accurate Stripline or Microstrip RF filters. The AgCite [31] conductive ink uses silver nanoparticles and has a conductivity up to 35 MS/m. Silver has a conductivity of 63 MS/m, Copper 59.6 MS/m, Gold 41 MS/m and Aluminium 35 MS/m. The inks thus have a similar conductivity to Aluminium. No ink is deposited where a hole is required and a pad is made by surrounding the hole with conductive ink. The inks use UV curing. A 200 x 200 mm printing area with a 3 mm thickness can be deposited. The smallest print trace width and pitch is 90 µm. Conventional thickness PCB's can be made and may contain many connector layers, so that very dense boards can be made. However, it is not possible to print on ceramic substrates, so the Nano Dimension's PCB printer has limited microwave application. Figure 11.10 shows a 4 layer 3D demonstration printed circuit board.

The Voltera PCB printer [32] is much lower in cost and can process a conventional 4″ x 5.3″ or 101 x 134mm FR4 substrate. It deposits silver nanoparticle inks to print tracks. No dielectric inks are available, so only 2 layer boards can be built. The inks use heat curing. The minimum track width is 0.2 mm. The datasheet gives no accuracy of the track widths and this may limit the accuracy of Stripline impedances. The cost of the inks is high, but since very little conductive ink is required for a typical board, this technology may soon be economical for RF circuit prototyping.

Sonoplot [34] have plotters that use ultrasonics to deposit fluid in a noncontact manner. The printed tracks can be 20 µm wide. A board size of 310 x 310 mm can be accommodated. After printing nanometalic silver ink tracks, they are annealed at 100 °C to transform the lines into solid tracks. The plotters have a position accuracy down to 5 µm.

The Optomec company [33], uses aerosol jet technology to spray conductive, resistive or dielectric inks onto a surface. Having an aerosol jet, removes the tight milling/printing head to PCB distance constraints and thus allows the inks to be deposited on curved surfaces. In one mass-production example, microwave 3D antennas are printed onto odd shaped surfaces for use inside smart phones. A minimum line thickness of 10 µm and a line spacing of 20 µm is possible, though a larger spacing is preferred. That is a 9 times thinner line width, than is possible for etched PCB's [12-14]. It is also possible to print semiconductors, so that advanced microwave electronic circuits can be fully printed on virtually any substrate. This may also lead to new sensors, which include the sensor, electronics, transmitter and antenna, as well as a battery and photovoltaic devices, all made using 3D printed technology. Electronic circuits, their antenna, as well as the leads connecting them can all be printed onto a contoured substrate.

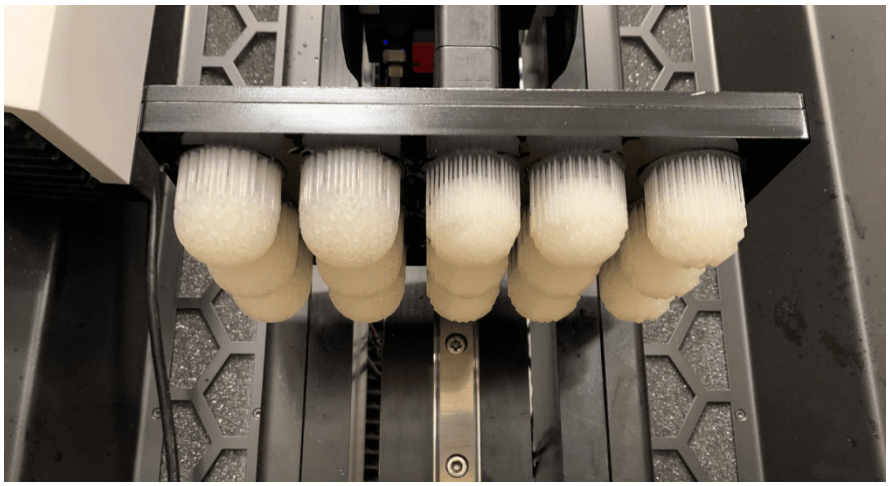


Figure 11.11. 3D lenses being printed. [36]

Rogers and Fortify [35, 36] have teamed up to produce RF photo polymer resin for 3D printing of dielectric lenses for antennae. Figure 11.11 shows the lens being printed and in figure 11.12 shows the cleaned up lens being tested.

Some of these printers are suitable for University prototyping and others are capable of producing 30 000 circuits per week and are used for consumer devices. Typical examples of applications and their resulting circuits are shown in *"Top10 Industrial Applications for Additive Manufacturing"* [37]. Due to the ability of being able to make the circuits in any shape, the 3D circuit board printing is also used for military and aeronautical applications. This technique will become more common in future.

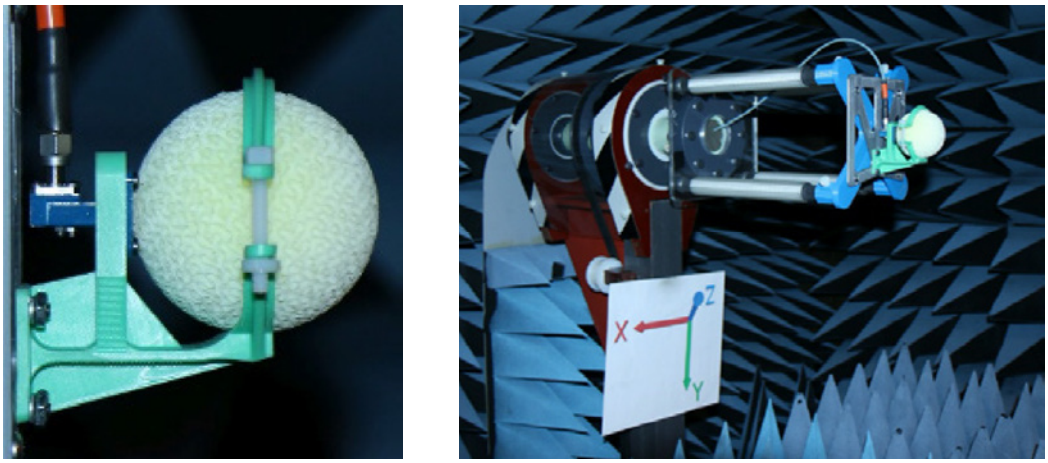



Figure 11.12. 3D lens mounted on waveguide (L) and being tested (R). [36]

The above show some examples of 2D and 3D PCB printers and printing materials. These techniques will continue to develop in performance, cost and accuracy and will become dominant for producing prototype PCBs.

## Low Temperature Cofired Ceramic (LTCC)

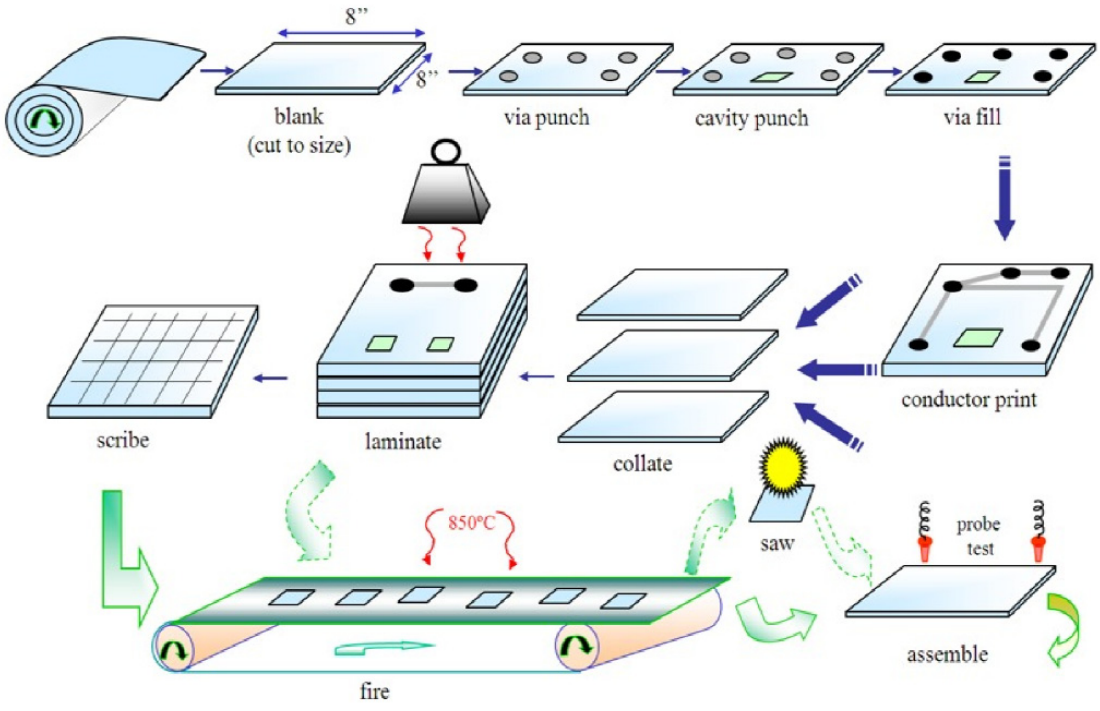



Figure 11.13. LTCC process flow. [38]

The Low Temperature Cofired Ceramic (LTCC) technology [38 - 41] is a means of producing small 3D and multilayer circuits at a relatively low cost. The technique is similar to thick film techniques, except many layers of ceramic are used, each of which has conductive, dielectric, and / or resistive pastes applied to them. The pastes are applied to ceramic sheets that have not yet been fired. These are called, ‘green-sheets’ and are normally supplied on a tape [41,42]. The printed sheets are then laminated together and fired in one process, resulting in structures as shown in figure 11.13 [38] and figure 11.14 [39, 40].

The low firing temperature for the ceramic green sheets allow low resistivity conductors like silver, gold, copper and alloys with palladium and platinum to be used [43]. The pastes are printed on the green-sheet using conventional thick film techniques. Special thick-film pastes must be used since the ceramic shrinks 10 to 15 percent in x/y-axis and about 10 to 45 percent in z-axis. If needed, shallow grooves, via holes or cavities can be milled in greentape and they can be cut using laser ablation cutters[44]. Shallow grooves allow thick tracks to be printed without any risk of air pockets resulting in surrounding areas. Any via holes are then filled with a gold based filler [45] that will then connect the required tracks on different layers.

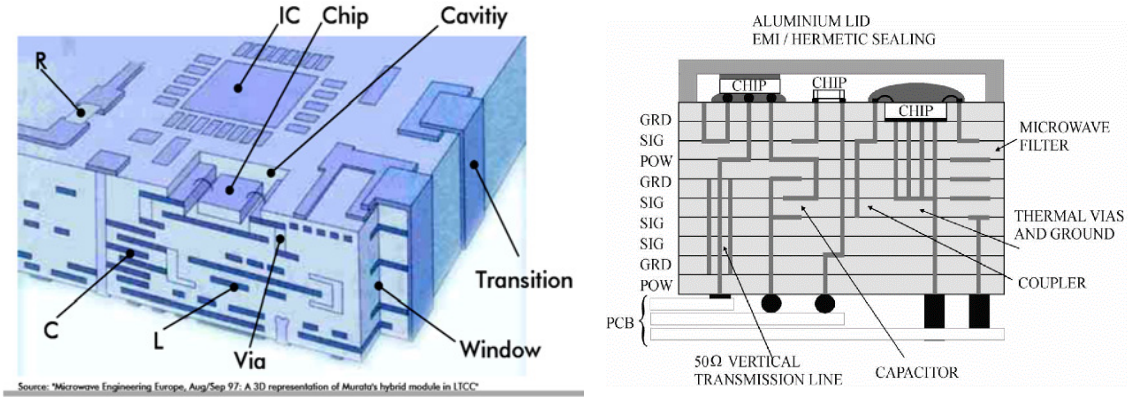



Figure 11.14. Typical LTCC structure [39,40].

It is also possible to integrate passive elements like resistors, capacitors, inductors, and transformers onto the substrate. Resistors are produced by printing tracks using resistive pastes of carefully controlled widths and lengths on the tape, just like conductor lines. Capacitors and inductors can be made by forming the conductive lines into plates or coils respectively. LTCC technology permits the construction of Stripline circuits, as opposed to Microstrip circuits. This reduces radiation and permits the construction of couplers with broadside rather than edge coupling, resulting in a high amount of coupling. Combining that with the ability to include active devices on the same small circuit opens up great possibilities.

Many LTCC mixers [46], filters [47] and directional couplers [48] are produced by Mini-Circuits. Many other manufacturers also use LTCC technology. The filters and couplers use the same principles as outlined in chapters 7 and 4 respectively of this book. LTCC allows 3 dimensional layouts, so that broadside coupled lines can easily be made. The high dielectric constant of the ceramic material used also results in small circuits. LTCC technology is also good for low cost reliable hardware required for the automotive industry [49].

## MMIC Fabrication

At mm-wave frequencies, the track lengths needed for couplers and hybrids become less than 1 mm. As a result different techniques need to be used to produce the circuits. The same techniques used to produce semiconductors, can also be used to produce Microstrip lines. The RF or Microwave design techniques for couplers, hybrids and filters, described in this book can thus all be implemented at mm-wave frequencies as a MMIC on silicon or gallium arsenide. AWR DE can produce GDSII files that can be sent to a foundry to produce the MMIC. Figure 4.65 shows an MMIC realisation of a Marchand Balun using

7 line Lange couplers with 5 µm tracks and spacing. Implementing the design on silicon or gallium arsenide, allows active devices to be incorporated in the same MMIC.

Figure 11.15 [50] shows a MMIC amplifier produced using a GaAs PHEMT 0.15 µm process. The amplifier is a 2 stage power amplifier where the input is split into 4 using 2 cascaded Wilkinson hybrids. Each signal is then amplified and 2 outputs are combined into one and impedance matching is applied. The resulting signal is then split into 4 and amplified. The outputs from the top 4 and the bottom 4 amplifiers are then combined using Wilkinson hybrids to produce a 27 dBm (0.5W) output at 35 GHz. The chip size is 2.45 x 2.95 mm.

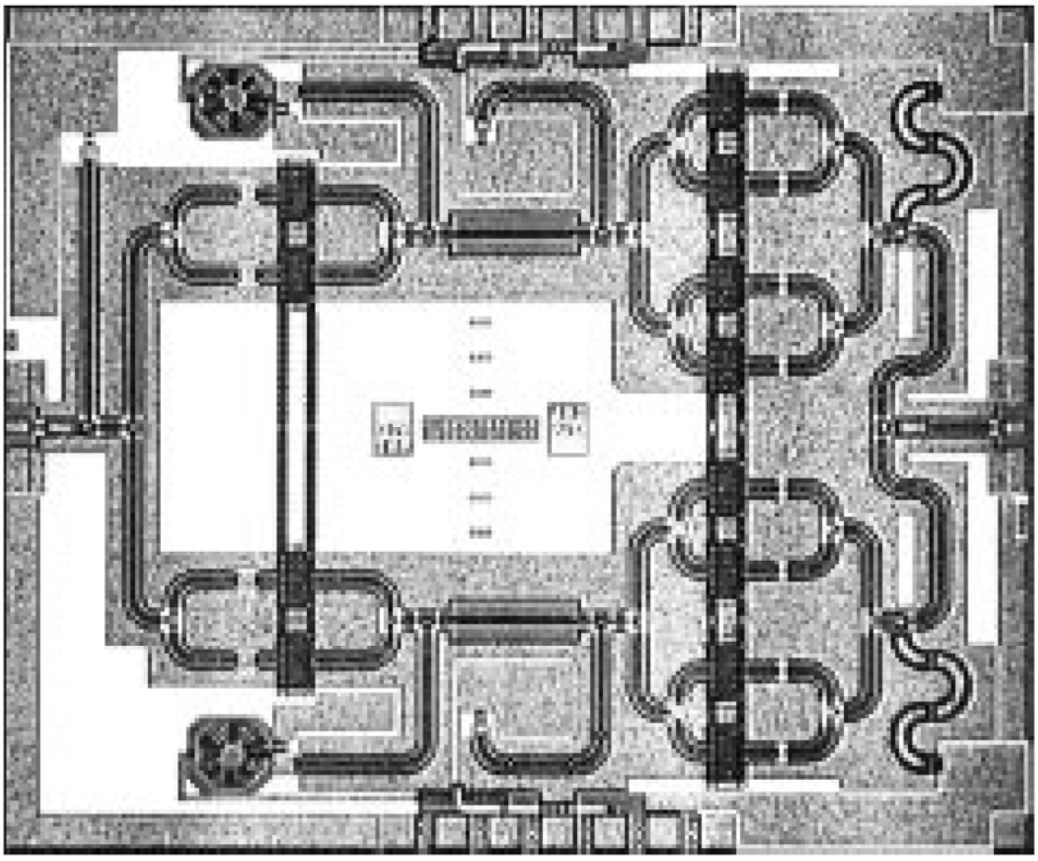


Figure 11.15. GaAs MMIC amplifier chip [50].

Figure 11.16 [51] shows a mm-wave power amplifier, made using 60 nm GaN on Si HEMT technology. The input is split into two, using a Lange coupler. Those signals are then amplified using 3 amplifier stages, their outputs are combined using another Lange coupler, to produce an output power of more than 26.5 dBm, from 88 to 93 GHz. The inter-stage matching networks can clearly be seen on figure 11.16. The size of the chip is 2.4 x 2.0 mm.

Since the 26-28 GHz band is used for 5G mobile phone communications and the 75-110 GHz frequency band is used for automotive cruise control radar, concealed weapon detection and satellite communications, the mm-wave frequency band is becoming very important for consumer applications.

The design techniques described in this book can thus be used to produce layouts for RF PCBs as well as MMICs.

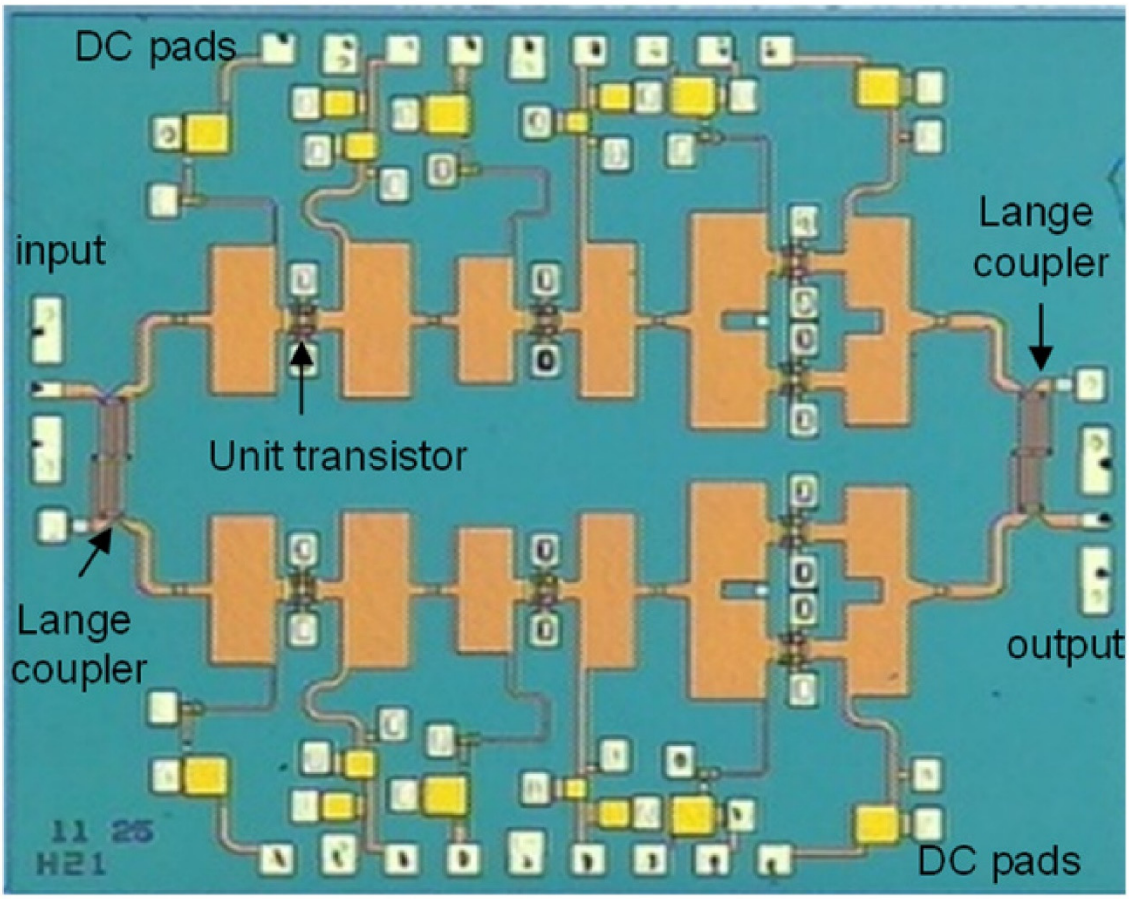



Figure 11.16. GaN MMIC amplifier chip, [51]

## References


1. Isola Group, http://www.isola-group.com/
2. Rogers Corporation, http://www.rogerscorporation.com/
3. AGC Multi Material, https://www.agc-multimaterial.com
4. Rorgers Corporation RT/duroid laminates, https://rogerscorp.com/advanced-electronics-solutions/rt-duroid-laminates
5. Panasonic Industry Circuit Board Materials, https://industrial.panasonic.com/ww/products/pt/megtron/megtron6
6. CoorsTek products: Ceramic Substrates, http://www.coorstek.com/resource-library/library/8510-1083_polished_substrates.pdf
7. Morgan Technical Ceramics, Technical Ceramics Products http://www.morgantechnicalceramics.com
8. Bechtold, F. "A Comprehensive Overview on Today's Ceramic Substrate Technologies", European Microelectronics and Packaging Conference, 2009. EMPC 2009. Rimini, Italy, 15-18 June 2009.
9. Rogers Corporation Ceramic Substrate, https://rogerscorp.com/advanced-electronics-solutions/curamik-ceramic-substrates
10. Miteq, Dielectric Resonator Oscillators. https://nardamiteq.com/docs/D210B.PDF
11. General Electronic Devices, Dielectric Resonator Oscillators, http://www.gedlm.com/DRO/DRO.asp
12. Altium http://www.altium.com/

13. Alegro PCB Editor https://www.cadence.com/ko_KR/home/tools/pcb-design-and-analysis/pcb-layout/allegro-pcb-designer.html
14. Autodesk Eagle PCB Design Software, https://www.autodesk.com/products/eagle/overview
15. PCBWay PCB Capabilities, https://www.pcbway.com/capabilities.html
16. JLC PCB Capabilities, https://jlcpcb.com/capabilities/Capabilities
17. LPKF Circuit Board Plotters for RF and Microwave, https://www.lpkf.com/en/industries-technologies/research-in-house-pcb-prototyping/products/lpkf-protomat
18. JLC PCB, https://jlcpcb.com/
19. PCBWay Printed Circuit Prototype, https://www.pcbway.com/pcb_prototype/Pinted_Circuit_Board_Prototype.html
20. NextPCB, https://www.nextpcb.com/service-type/pcb-prototype
21. PCBWay Etchants, https://www.pcbway.com/blog/Engineering_Technical/PCB_Etchant_Solutions.html
22. LPKF ProtoLaser ST, https://www.lpkf.com/en/industries-technologies/research-in-house-pcb-prototyping/produkte/lpkf-protolaser-st
23. LPKF ProtoLaser U4, https://www.lpkf.com/en/industries-technologies/research-in-house-pcb-prototyping/produkte/lpkf-protolaser-u4
24. PCB Design Guide and Manufacturing Input Requirement https://www.pcbpower.com/technology/design-guideline
25. MicroFab, Technology, https://microfabnh.com/technology/
26. BSC Filters, https://www.bscfilters.com/technologies/thin-film/
27. CMS Circuit Solutions, Facility, https://cmscircuitsolutions.com/facility/
28. Corintech Thick film Hybrid Boards https://www.corintech.com/electronics-manufacturing/thick-film-hybrids/
29. Dupont, Thick Film Hybrids Circuit Materials https://www.dupont.com/products/hybrid-circuit-materials.html
30. Koartan, Thick Film Conductor Pastes. https://www.inseto.co.uk/consumables/thick-film-materials-by-koartan/
31. NanoDimension, http://www.nano-di.com.
32. Voltera Circuit printing, https://www.voltera.io/product/pcb-printer
33. Optomec Aerosol Jet Core applications, https://www.optomec.com/printed-electronics/aerosol-jet-core-applications/
34. SonoPlot Microplotter Proto, https://www.sonoplot.com/microplotter-proto
35. Rogers corporation Radix Printeable Dielectric, https://rogerscorp.com/advanced-electronics-solutions/radix-printable-dielectric
36. Fortify 3D printed dielectic lens white paper, https://3dfortify.com/3d-printed-rf-devices/ and http://get.3dfortify.com/rf-white-paper/
37. Top 10 industrial applications for additive manufacturing, pdf available from https://www.optomec.com/additive-manufacturing/
38. Plextek RF Integration, Low Temperature Co—fired Ceramic (LTCC) white paper. https://www.prfi.com/wp-content/uploads/2021/05/LTCC_technology_overview.pdf
39. Maeder T, H Birol and P Ryser, “Integrated microfluidic devices based on low-temperature co-fired ceramic (LTCC) technology”, Semantic Scholar, 2004, Corpus ID 18282848.
40. H. Jantunen et al. “Design aspects of microwave components with LTCC technique”, Journal of the European Ceramic Society 23 (2003) 2541–2548.
41. Dupond Greentape LTCC, https://pdf4pro.com/cdn/dupont-greentape-28e403.pdf

42. Dupont Greentape 9K7, https://www.dupont.com/products/green-tape-9k7-ltcc-material-system.html
43. Dupont LL505 Co-fired wire bondable gold conductor, https://www.dupont.com/content/dam/dupont/amer/us/en/transportation-industrial/public/documents/en/LL505.pdf
44. LPKF Application Report Structuring and cutting LTCC carbon Tape, https://www.lpkfusa.com/products/pcb_prototyping/white_papers/structuring_and_cutting_ltcc_carbon_tape/
45. Dupont LL502 Co-fired Gold Via Fill, https://www.dupont.com/content/dam/dupont/amer/us/en/transportation-industrial/public/documents/en/LL500.pdf
46. Mini-Circuits, Low Cost Triple Balanced LTCC mixer http://www.minicircuits.com/pages/pdfs/tech4.pdf and http://www.minicircuits.com/app/AN00-002.pdf
47. Mini-Circuits, BFCN Series LTCC Band Pass Filters https://www.minicircuits.com/WebStore/RF-Filters.html
48. Mini-Circuits, Surface Mount LTCC Quadrature Splitters. http://www.minicircuits.com/pages/pdfs/tech2.pdf and http://www.minicircuits.com/app/AN10-005.pdf
49. Murata, High-Accuracy Automotive Circuit Boards Using LFC® Substrates, https://corporate.murata.com/more_murata/techmag/metamorphosis17/paper/01
50. A. Bessemoulin, H. Massler, A. Hulsmann and M. Schlechtweg, "Ka-band high-power and driver MMIC amplifiers using GaAs PHEMTs and coplanar waveguides," in *IEEE Microwave and Guided Wave Letters*, vol. 10, no. 12, pp. 534-536, Dec. 2000, doi: 10.1109/75.895094.
51. Jeong, J. et al, Design of W-Band GaN-on-Silicon Power Amplifier Using Low Impedance Lines, *Appl. Sci.* **2021**, *11*, 9017. Doi:10.3390/app1199017.

# Appendix 1

# Importing Local Vendor and Spice Files

## Local Vendor Libraries

AWR Design Environment contains component web based XML libraries using an industry standard format that can be accessed from the Cadence web site. The library contents are automatically retrieved when the relevant Element Browser area is selected. It may be desirable to download and install those libraries locally, and access the elements locally, rather than having to rely on internet access. At present, the AWR Design Environment support has moved from the awrcorp.com web site to the cadence.com online support system, so the vendor libraries available from the AWR download web site, only support vendor local files for AWR Design Environment up to V14. As a result, it is more desirable to use the components that are automatically downloaded from the AWR web site in the element browser, if they are suitable.

As part of this change, newer libraries have become available [1]. For example, the Wolfspeed (Cree) library was used in the power amplifier of Chapter 9, figures 46-53. That library can be accessed after applying for access to the Wolfspeed RF portal [2, 3]. The Ampleon MWO library can be downloaded direct from their web site [4] and their library will be used as an example, since no access permission is required. The installation process for this library is as follows:

1) Create a folder in a suitable temporary location like the desktop. This folder can be named *Ampleon*.
2) Download the library zip file, the manual and the example project file into that folder. Unzip the library. That will create an *AMP_Product_Lib_V15p00* folder in the *Ampleon* file. In that folder will then be an *AMP_Product* folder. In the C:Program Files(x86) there will be an *AWR* folder, where all the AWD software is located. In that folder, there may be a *Foundry* folder, if not, create it.
3) Copy the *AMP_Product* folder into the *Foundry* folder, as shown in figure A1.1. One may need to have administrator rights to place the the *AMP_Product* folder into the *Foundry* folder. (That is the reason for using the temporary *Ampleon* folder to unzip the files into). That *AMP_Product* folder will then contain all the required library files.

Figure A1.1 shows the resulting Ampleon Library folder files. The Cree Wolfspeed AWR Library has some additional files in it as shown in figure A1.2.

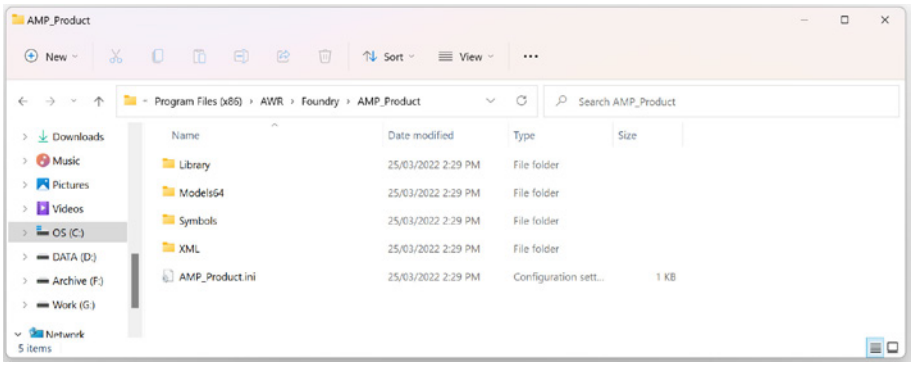



Figure A1.1 Ampleon Library folder structure.

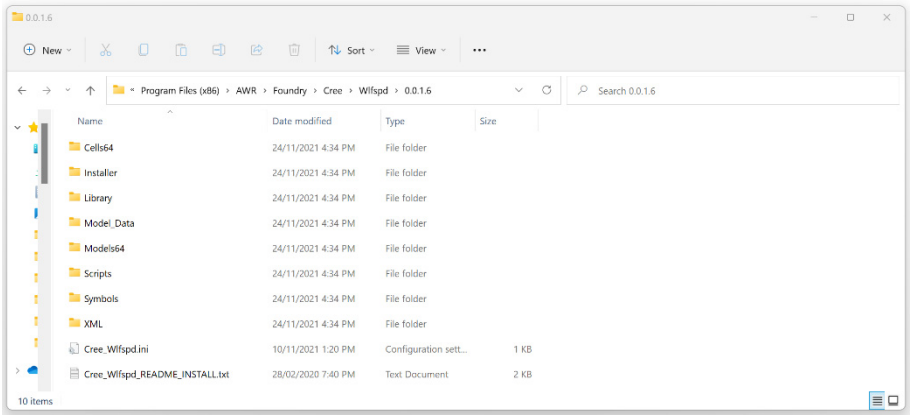



Figure A1.2 Cree Wolfspeed Library folder structure.

To use the library, open a project file and either start a *New With Library* project and select the appropriate library, or in an existing project select Project > Process Library > Add/Remove Library and select Add if the desired library is not shown, which will then show the AWM_Product library. Selecting that will include the Ampleon library in the project. The AMP_Product_Simulation_Example project can then be opened as shown in figure A1.3.

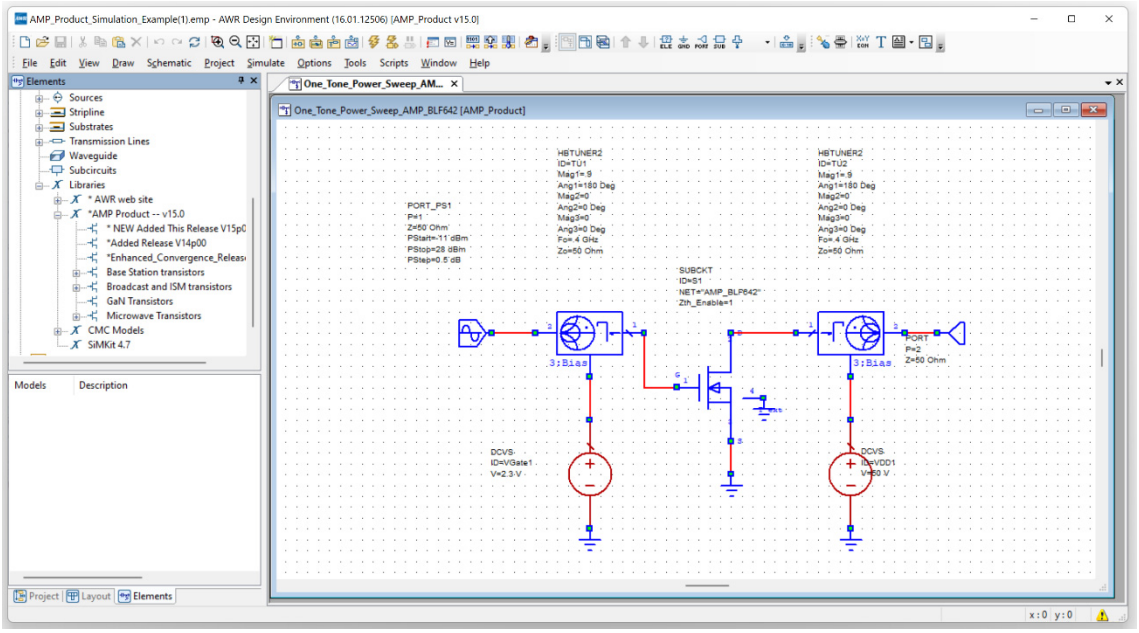



Figure A1.3. Ampleon Simulation Example.

Other libraries can be installed in a similar manner.

## Importing Spice Device Models

The process of importing Spice files is illustrated using some examples. Since chapter 10 uses Spice models of operational amplifiers (OpAmps), they are used to illustrate the process. Very useful information outlining this process is given in the help files, available from inside AWRDE by selecting *"Help ⇒ Help on Selected item"* and in the AWR Design Enviroment Help, type Pspice in the search text box and click on the first item in the list *"User Guide > Netlists > 5.3 Importing or Linking to a Netlist"*. As shown in

figure A1.4.The Spice files are text files, so one can use a standard text editor to inspect and edit the spice files if needed.

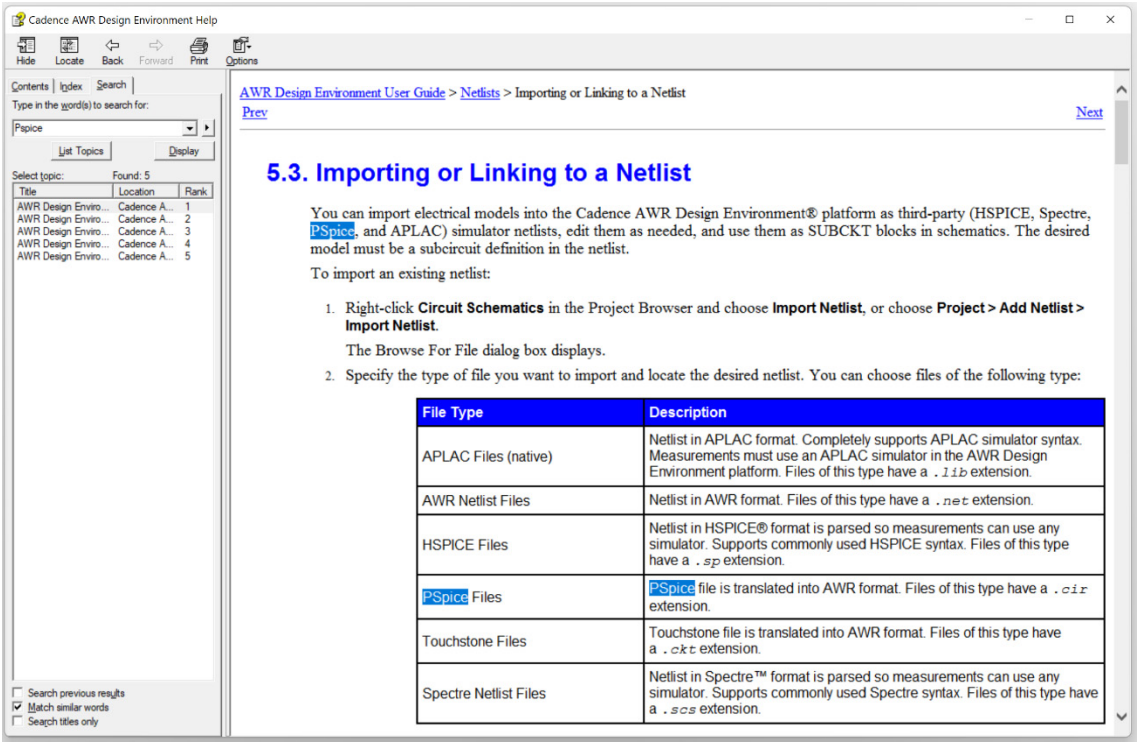



Figure A1.4. AWR DE help on importing PSpice files.

As an example of the process, the Spice model of an AD797 [5] operational amplifier is required. From the Analog Devices web site search for AD797, then select and download the spice model. That is a *.cir* file. In a Cadence AWR Design Environment project, select *Netlist ⇒ Import Netlist* and select the *ad797.cir* file to import. In a circuit Schematic, the spice file can then be added by *"Draw ⇒ Add Subcircuit"* and then selecting the AD797 element. It is desirable to change the square box *SUBCKT* symbol to one commonly used for OpAmps, by selecting *"Properties ⇒ Symbol"* and then selecting *OpAmp6@APLAC.syf* as the symbol to be used. That then allows a schematic like figure 10.17 to be produced.

The simulation will show some warnings where resistors R = 0 are replaced with small non-zero values. If it is desirable not to have errors, the netlist can be edited in a text editor to replace the zero ohm resistors with the suggested values, like R2 = 1e-6. That will then allow an easier identification of any other errors generated by the simulation.

The same process is used for importing Spice files for other devices such as transistors, or diodes.

The models for Texas Instruments devices are no longer directly available from their web site. The *PSpice for TI* [X] software by Cadence can be used for PSpice simulation of many of their devices. *PSpice for TI* can be downloaded and operated without cost. That software can be used to produce the required PSpice files for import into AWR DE. As an example, the PSpice file for the THS4021/4022 OpAmp used in figure 10.20 is generated. To create the PSpice file, run *PSpice for TI*. Create a design and place the desired component on the schematic page. In *PSpice Part Search*, select *Texas Instruments ⇒ Amplifiers ⇒ Operational Amplifiers ⇒ High Speed op amps*. Then place the THS4021 part on the schematic. Left click on the OpAmp to select it, then right click

and select *View Spice Model*. Select all the PSpice text and paste that into Notepad or similar plain text editor. Then save that text as THS4021.cir. To import it into AWR platform, in the *project browser*, select *Netlist* ⇒ *Import Netlist* as outlined above for the AD797. The simulation can then be carried, as has been done in the Figure 10.20 AWR Design Environment project file.

Sometimes the PSpice files produce simulation errors. For example using *PSpice for TI* for the THS4271 OpAmp, produces and error: *Node count error in element VCCS on line 111*. Other devices like the OPA691 [7] OpAmp or the have ADA4895 [8], have a disable pin. The associated switch description, at this stage does not import correctly into AWR Design Environment. It is possible to edit and correct the Spice files to eliminate errors and warnings that occur during importing of the Spice files. For example, the *'S_Device'* and *'vswitch'* descriptions in the ADA4895 Spice files can be modified, so that the enable pin is deleted and the OpAmp is always enabled. That will then overcome the errors during the importation of the files.

## References


1. Third Party Vendor Libraries. https://kb.awr.com/display/awrfaq/Third+Party+Vendor+Libraries
2. CREE Large Signal Models for GaN-based HEMTs, https://awrcorp.com/download/kb.aspx?file=/Questions/Cree_Portal_LS_Models.pdf
3. Request RF Portal access, https://www.wolfspeed.com/tools-and-support/rf/rf-portal-access/
4. Ampleon Model Libraries for Microwave Office, https://www.ampleon.com/support.html
5. Analog Devices, AD797, Ultralow Distortion, Ultralow Noise Op Amp. http://www.analog.com/en/products/amplifiers/operational-amplifiers/high-voltage-amplifiers-greaterthanequalto-12v/ad797.html
6. Texas Instruments PSpice for TI, https://www.ti.com/tool/PSPICE-FOR-TI
7. Texas Instruments, OPA691Wideband Current Feedback Operational Amplifier with Disable. http://www.ti.com/product/OPA691
8. Analog Devices, ADA4895-1, Low Power, 1 nV/√Hz, G ≥10 Stable, Rail to Rail Output Amplifier. http://www.analog.com/en/products/amplifiers/operational-amplifiers/low-noise-amplifiers-lessthanequalto-10nv/ada4895-1.html

# Appendix 2

# Producing Graphs using AWR Design Environment

## Generating Plots

AWR Design Environment is very good for producing graphs and plots to be used in technical articles, journal papers and seminars. The data to be plotted typically has the following form shown in table A2.1. Any line beginning with a "!" is a comment line. The data is in the form of columns or rows of data, typically as shown below for the monthly data of the South Australian electricity demand and price during 2021 [1].

Table A2.1. Data format for Plotting

! South Australian Wholesale Energy Cost and Demand, (Add 2000 to Year).

| ! Yr | Demand Ave | Max | Min | $ Ave | $ Max | $ Min |
|---|---|---|---|---|---|---|
| 21.375 | 1298.321 | 2122.8 | 521.21 | 72.99218 | 7038.75 | -170.08 |
| 21.458 | 1432.887 | 2241.37 | 668.47 | 84.38861 | 2348.71 | -183.33 |
| 21.542 | 1463.584 | 2483.73 | 669.47 | 91.18731 | 2102.13 | -269.95 |
| 21.625 | 1320.715 | 2227.62 | 371.49 | 43.43982 | 336.6 | -297.81 |

The plots of figures A2.1 and A2.3 were presented in a paper "A Phasor Measurement Unit Algorithm Using IIR Filters for FPGA Implementation" [2] by the author. A Phasor Measurement Unit (PMU), measures the Voltage, Phase, Frequency and Rate of Change of Frequency (RFE or ROCOF) of 3 phase mains supplies. The paper describes computer simulations produced by an algorithm that is suitable for implementation in an FPGA. Most of the plots presented in the paper were produced using AWR Design Environment. Each simulation as shown in figure A2.1 produces data with 200800 rows and 14 columns, the AWR project used for figures A2.1 to A2.4, contains 8 different simulations, so 2.6 million values. Figure A2.1 is the same as figure 10 of [2] and is a plot with 200000 of the 200800 simulation values plotted on the horizontal scale.

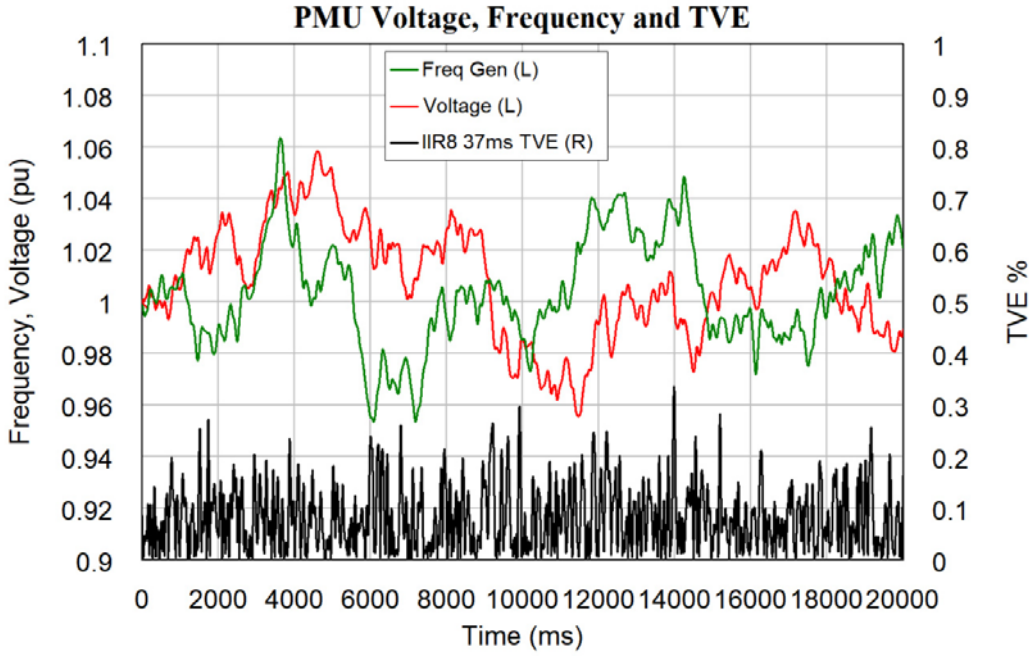



Figure A2.1. Plot with 200000 points on each trace.

This plot shows that when adding large random variations in mains amplitude and frequency the total vector error (TVE) of the algorithm is much less than the allowable 1% [3].

Figure A2.2 shows a plot of simulated ROCOF measurements and the corresponding errors, when using IIR or FIR filters. Figure A2.2 shows all the 200000 points covering 20 seconds, plotted for each of the 3 traces. By simply changing the horizontal and or vertical axis, different parts of the plot can be enlarged. Figure A2.3 shows the same plot with simply the horizontal axis changed to cover 4 to 5 seconds and contains 10000 points for each of the 3 traces and is the same as figure 12 in [2].

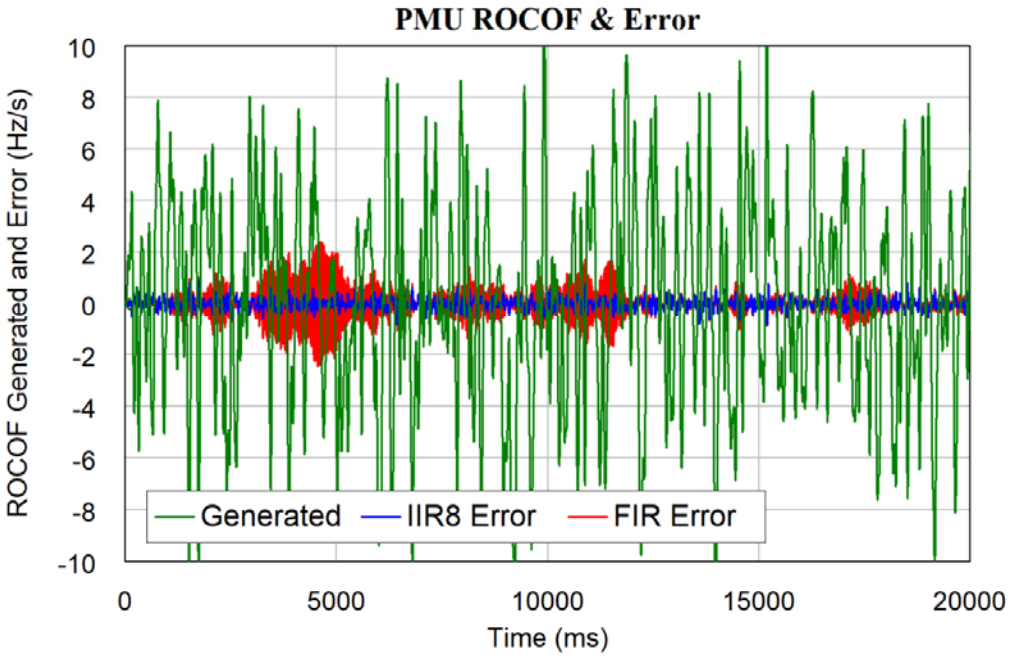



Figure A2.2. Plot of ROCOF with 200000 points on each trace.

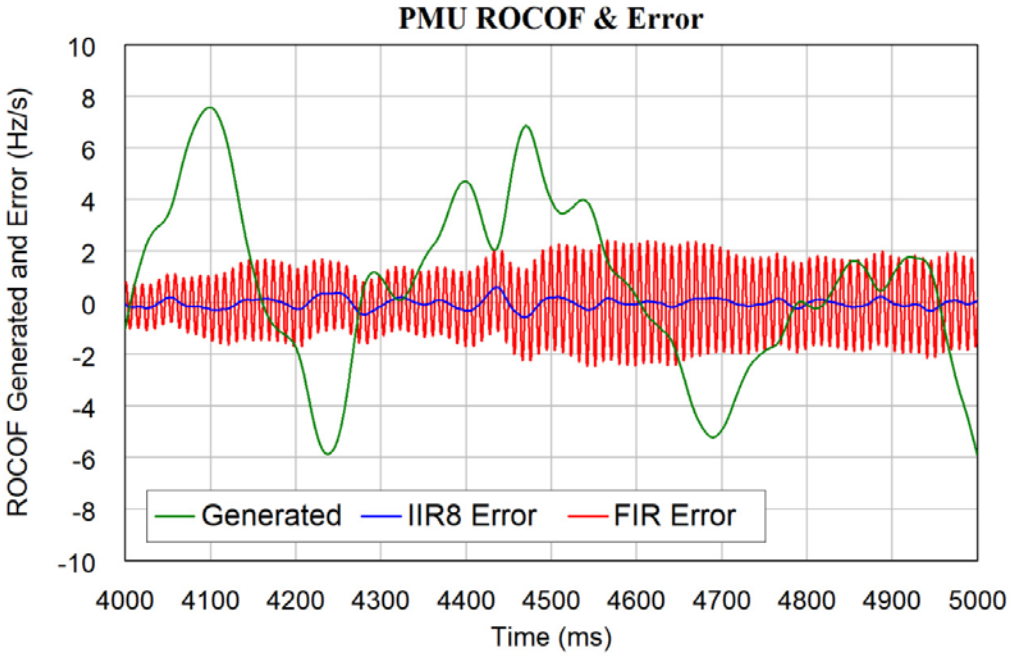



Figure A2.3. Close-up of Figure A2.2 with 10000 points on each trace.

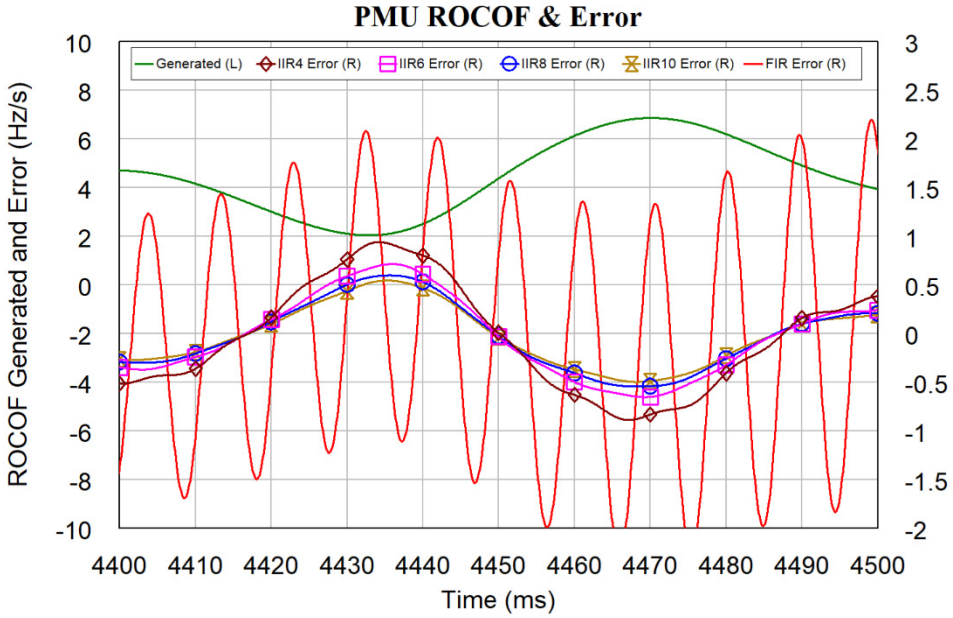



Figure A2.4. Further Close-up of Figure A2.3 with extra traces and 1000 points on each trace.

The project file used for these figures also contain simulations for different order IIR filters, so that the effect of filter order on the performance can be investigated. Figure A2.4 shows the resulting plot. The time axis has been reduced further to 1000 points. The same data file is used for figures A2.2 to A2.4, but by selecting a different horizontal axis, one can zoom in on part of a plot and by selecting additional columns, the behaviour of different filters can be investigated, to provide an understanding of different design options for the PMU.

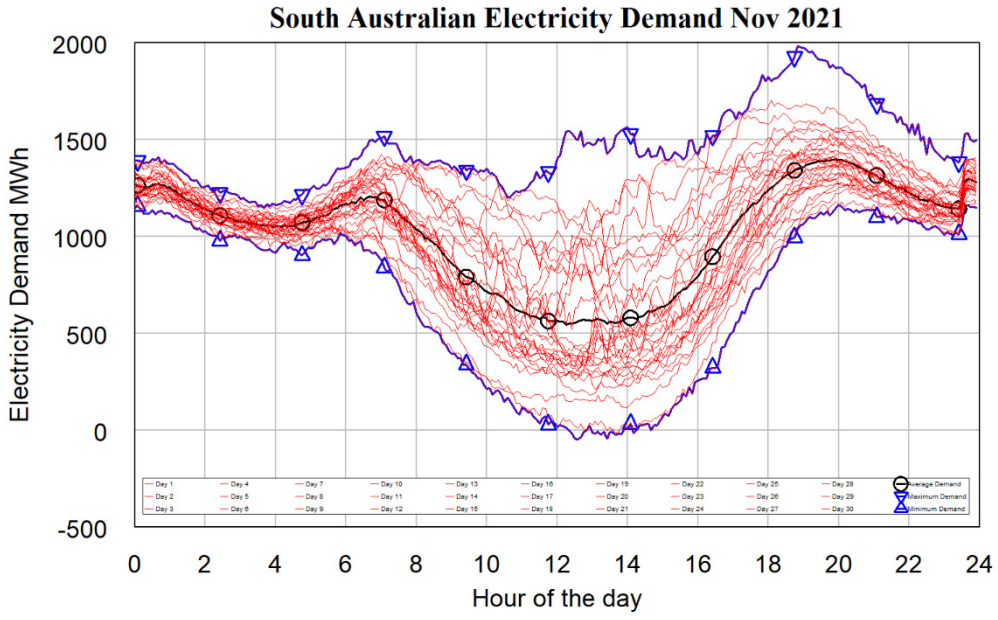



Figure A2.5. 5-minute electricity demand for November 2021 for South Australia.

Figure A2.5 shows the Electricity demand for the South Australia for 5-minute data intervals for the month of November 2021 [1]. The daily variation can be shown by plotting the data from each day as a thin line, with the same colour. Statistical data such

as average, maximum or minimum can be plotted in different colours and have markers. Individual days can still be investigated easily. Note, on November 21 and 27, rooftop solar generated more power than was needed by the whole state and a negative grid demand resulted. Close to 10000 data points are plotted in figure A2.5.

AWR DE is thus very useful for plotting data, to produce high quality and easy to understand graphs for many applications.

## References

1. AEMO Aggregated Electricity price and demand, download historical data, https://aemo.com.au/energy-systems/electricity/national-electricity-market-nem/data-nem/aggregated-data
2. Kikkert, C. J. "A Phasor Measurement Unit Algorithm Using IIR Filters for FPGA Implementation", *Electronics* 2019, Vol *8,* 12, 1523, pp1-18; https://doi.org/10.3390/electronics8121523
3. *IEC/IEEE Standard 60255-118-1:2018 Part 118-1: Synchrophasor Measurements for Power Systems*; IEEE STD23444; International Electrotechnical Commission: Geneva, Switzerland, 2018; ISBN 978-1-5044-5361-5.

Dr. Kikkert obtained his B.E. with first-class honors and his Ph.D. from the University of Adelaide and lectured there for three years before going to JCU, where he has taught communication systems principles and analog, digital, and RF electronics for over 37 years. In 2010, Dr. Kikkert retired from full-time teaching but continues to teach at different universities and is active in research and publishing in the area of electronic design for communication systems, using both computer simulation and hardware design and measurement techniques.



*Dr. Keith Kikkert, James Cook University*

cadence®

Cadence is a pivotal leader in electronic design and computational expertise, using their Intelligent System Design Strategy to turn design concepts into reality. Cadence customers are the world's most creative and innovative companies, delivering extraordinary electronic products from chips to boards to systems in the most dynamic market applications. **www.cadence.com**

© 2020 Cadence Design Systems, Inc. All rights reserved worldwide. Cadence, the Cadence logo, and the other Cadence marks found at www.cadence.com/go/trademarks are trademarks or registered trademarks of Cadence Design Systems, Inc. All other trademarks are the property of their respective owners. 08/22 PIP-KRT-RF/PDF